Mexican fossil ground sloths

A case study for Late Pleistocene megafaunal turnover in the Mexican Corridor

Zur Erlangung des akademischen Grades einer

DOKTORIN DER NATURWISSENSCHAFTEN (Dr. rer. nat.)

von der KIT Fakultät für

Bauingenieur-, Geo-, und Umweltwissenschaften

des Karlsruher Instituts für Technologie (KIT)

genehmigte

DISSERTATION

von

Sarah R. Stinnesbeck,

M. Sc. in Quartärforschung und Geoarchäologie

aus Bonn

Tag der mündlichen Prüfung: 24. November 2020

Referent: Prof. Dr. Eberhard Frey
Korreferent: Prof. Dr. Sebastian Schmidtlein

Karlsruhe 2020

Abstract

This dissertation summarizes the results of a long-term German-Mexican research project, on the megafauna, in particular the ground sloths, discovered in underwater caves of the state of Quintana Roo in south-eastern Mexico. Two new species of the new genus *Xibalbaonyx* (*X. oviceps* and *X. exinferis*) of Late Pleistocene to Early Holocene age are here documented and discussed from this area. Ground sloth bearing localities from north-eastern and west-central Mexico, as well as Guatemala were visited, and the respective fossil collections were revised. A third new species of *Xibalbaonyx* (*X. microcaninus*) was documented from a museum collection in Guadalajara. Collections housed in the Natural History Museum of New York, the Museum of Natural History and University of Florida in Gainesville (USA) and the State Museum of Natural History Museum in Karlsruhe (Germany) were used for anatomical comparison.

The palaeoecology of *Xibalbaonyx* and other ground sloths is discussed based on osteological observations and the analysis of associated fauna from the submerged caves of Quintana Roo. The functional morphology of *Xibalbaonyx* was interpreted based on osteological evidence. The animals were able to climb the steep slopes of karst sinkholes, and probably used the dry caves in search of water, as shelter and as nursing area. Congenital anomalies were detected repeatedly, including asymmetrical vertebral bodies. These pathologies suggest that either inbreeding and/or poor environmental conditions existed in the area at least intermittently.

A new genus and species of peccary (*Muknalia minima* gen. et sp. nov.) and a new species of jaguar (*Panthera balamoides* sp. nov.) were identified while analyzing the Pleistocene megafauna assemblage. The high number of endemism in this unique assemblage suggests a partial palaeogeographic and ecological isolation of the Yucatán Peninsula from the American continent. This scenario is also supported by anthropological data, indicating substantial morphological differences between the first settlers on the Yucatán Peninsula and other coeval hunter and gatherer populations in central Mexico. Human-megafauna interactions are documented for the Yucatán Peninsula for the first time in the region based on cut marks identified in a variety of megafaunal remains.

The correlation of datasets obtained through taxonomy, the survey of literature, the revision of museum collections, as well as fieldwork, provides insights on the ground sloth extinction on

the Yucatán Peninsula. Small populations of the terminal American megafauna persisted along the deep water-filled sinkholes (cenotes) and were isolated from each other by barren karst landscapes. Climatic variability across the Pleistocene-Holocene boundary may have supported the development of "biotic islands" on the north-eastern Yucatán Peninsula, triggering a rapid, but vulnerable diversification of Late Pleistocene ground sloths, especially Megalonychidae. These last highly endemic populations may have existed into the early Holocene on the north-eastern Yucatán Peninsula.

Zusammenfassung

Diese Dissertation ist Teil eines langjährigen deutsch-mexikanischen Forschungsprojektes über paläontologische und paläoanthropologische Funde aus den Unterwasserhöhlen im Bundesstaat Quintana Roo im Südosten Mexikos. Sie fasst dabei die Ergebnisse über spätpleistozäne Großsäuger, speziell Bodenfaultiere, zusammen. Zwei Arten der neuen Bodenfaultier-Gattung *Xibalbaonyx* werden im Untersuchungsgebiet neu beschrieben und in den Zeitraum des späten Pleistozän bis frühen Holozän datiert. Darüber hinaus wurden andere Lokalitäten im Nordosten, Westen und Zentralmexikos, sowie in Guatemala besucht und die fossilen Sammlungen der dortigen spätpleistozänen Megafauna dokumentiert und beschrieben, einschließlich einer dritten Art von *Xibalbaonyx* (*X. microcaninus*). Sammlungen aus dem Natural History Museum in New York und aus dem Museum of Natural History and University of Florida at Gainesville, USA, sowie die Sammlungen des Naturkundemuseums in Karlsruhe, Deutschland, dienten dem anatomischen Vergleich.

Auf Grundlage der osteologischen Beschreibung und paläontologischen Aufarbeitung der assoziierten Fauna aus den Unterwasserhöhlen Quintana Roos wurden Einblicke in die Paläoökologie von *Xibalbaonyx* und anderen Bodenfaultieren gewonnen. Die funktionsmorphologische Analyse legt nahe, dass *Xibalbaonyx oviceps* in der Lage war, die steilen Hänge der Dolinen zu erklimmen. *Xibalbaonyx* nutzte die trockenen Höhlensysteme zur Suche nach Wasser, als Zufluchtsort und zur Aufzucht der Jungen. Angeborene Pathologien wurden wiederholt bei den Bodenfaultieren festgestellt, einschließlich asymmetrischer Wirbelkörper. Diese Pathologien deuten darauf hin, dass es in dem Untersuchungsgebiet zeitweise zu Inzucht kam und vermutlich schlechte Umweltbedingungen vorlagen.

Eine neue Gattung und Art von Nabelschwein (*Muknalia minima* n. gen et sp.) und eine neue Art von Jaguar (*Panthera balamoides* sp. nov.) waren in Quintana Roo mit diesen Bodenfaultieren assoziiert. Die hohe Zahl an Endemismen in dieser einzigartigen Faunenvergesellschaftung belegen eine partielle paläogeographische und ökologische Isolation der Yukatan Halbinsel vom amerikanischen Kontinent und eine Verinselung des Untersuchungsgebietes. Diese Theorie wird auch durch anthropologische Untersuchungen untermauert, welche deutliche morphologische Unterschiede zwischen den ersten Jägern und Sammlern auf der Yukatan Halbinsel und anderen gleichaltrigen Populationen in

Zentralmexiko belegen. Menschliche Interaktionen mit der Megafauna sind durch Schnittspuren und weitere Befunde an Knochen belegt und werden erstmals für die Region beschrieben.

Die Klimaveränderungen am Pleistozän-Holozän Übergang könnten die Entwicklung von „Inselpopulationen" in der nordöstlichen Yukatan-Halbinsel unterstützt haben, die durch die Karstlandschaft zwischen den einzelnen Karstdolinen (Cenotes) voneinander getrennt existierten. Diese kleinen untereinander isolierten Populationen von Bodenfaultieren, insbesondere der Familie der Megalonychidae, diversifizierten schnell, waren aber gegenüber Umweltveränderungen anfällig.

Die hiervorgestellte vergleichende Auswertung taxonomischer Datensätze mit Literaturrecherche, Überarbeitung von Museumssammlungen, sowie Feldforschung liefert Hinweise auf das Aussterben der Bodenfaultiere auf der Yukatan Halbinsel zu Beginn des Holozäns.

Schlagwörter: Bodenfaultiere, Megafauna, Pleistozän, Mexiko

Table of Content

List of Abbreviations

Institutional

AMNH	American Museum of Natural History, New York, USA
CPC	Colección Paleontológica de Coahuila, at the Museo del Desierto (MUDE), Saltillo, Mexico
INAH	Instituto Nacional de Antropología e Historia, Mexico City, Mexico
IPA	Instituto de la Prehistoria de América, Playa del Carmen, Quintana Roo, Mexico
LEMA	Laboratorio de Espectrometria de masas con Aceleradores UNAM, Mexico City, Mexico
MICADAS	Klaus-Tschira-Archäometrie-Zentrum Mini Radiocarbon Dating System, Mannheim, Germany
MRG	Museo Regional de Guadalajara - Jalisco, Mexico
MPG	Museo de Paleontología de Guadalajara - Jalisco, Mexico
MUDE	Museo del Desierto, Saltillo, Coahuila, Mexico
MUSHNAT	Museo Nacional de Historia Natural de la Universidad de San Carlos, Guatemala City
SMNK	State Museum of Natural History Karlsruhe, Germany
UF	Museum of Natural History and University of Florida, Gainesville, Florida, USA
UNAM	Universidad Nacional Autónoma de México, Mexico City, Mexico

1   Introduction

Ground sloths were a highly diverse group of enigmatic placental mammals of the superorder Xenarthra. Xenarthrans are characterized by additional articulation processes between the vertebral joints, a unique anatomical feature only known in sloths, anteaters, armadillos, glyptodonts and pampatheres (Delsuc et al., 2001). Ground sloths evolved in South America around 60 million years ago (McKenna et al., 2006; Delsuc et al., 2019) and spread to North America and the Antilles during the Late Miocene (Hirschfeld and Webb, 1968), i.e. before the Great American Biotic Interchange (GABI) when the Isthmus of Panama connected North- and South America (Woodburne, 2010). They represent one of the most successful groups of the American Pleistocene megafauna. Nevertheless, more than 90% of all sloth species became extinct during the Pleistocene-Holocene transition (McKenna and Bell, 1997), with the tree sloth genera *Choloepus* and *Bradypus* as the only extant survivors (Steadman et al., 2005). Current hypotheses suggest that the cause for this selective extinction may have been a combination of rapid climate oscillations and human hunting pressure on the ground sloths (Martin, 1973; Gill et al., 2009; Johnson, 2009), but this remains to be a highly controversial debate (Sandom et al., 2014; Haynes, 2016).

The Pleistocene-Holocene boundary was a period of enormous climatic oscillations that coincides with the human settlement of the American continent. A combination of these two events likely triggered the Late Quaternary Extinction Event (LQE) of the Pleistocene megafauna (Koch and Barnosky, 2006; Barnosky and Lindsey, 2010). The LQE describes the disappearance of large herbivores of >45 kg (Barnosky et al., 2004; Koch and Barnosky, 2006), including proboscideans, giant armadillos, horses, and many others. The "Overkill-Hypothesis" established by Martin (1973) suggests systematic slaughtering of the megafauna by the first American settlers (Martin, 1973; Martin and Klein, 1984). In contrast to other large mammals, such as *Mammuthus*, *Mammut*, *Cuvieronius* and *Equus* (Surovell and Waguespack, 2008; Sanchez et al., 2014; Grayson and Meltzer, 2015; Waters et al., 2015), the interaction between humans and ground sloths is rarely discussed, and the exploitation of ground sloths by men has only been documented in a few rare cases in North- and South America (Steadman et al., 2005; Redmond et al., 2012; Politis et al., 2019).

Global climate and environmental changes across the Pleistocene-Holocene transition certainly also have contributed to the extinction of many megafaunal elements including ground sloths (Johnson, 2009; Rule et al., 2012). After the Last Glacial Maximum (LGM) the intervals between stadials and interstadials became increasingly shorter towards the beginning of the Holocene, resulting in rapid and dramatic fluctuations of plant communities (Beaudoin et al., 1996; Delcourt, 2005) and increased biomass burning (Marlon et al., 2009). It is not known to date, how and to what degree these environmental and vegetational changes affected the life, local diversification and distribution of ground sloths: Both their diet and habitat preferences are insufficiently known (Poinar et al., 1998; Hofreiter et al., 2000; Poinar and Kuch, 2003; McDonald, 2005; Bocherens et al., 2017).

1.1 Mexican Corridor

The concept of a "corridor" is used in biology and ecology to define habitat areas and routes used by animals (Rosenberg et al., 1997; Hilty et al., 2012). "Migration corridors" (Hilty et al., 2012) describe a natural, seasonal pathway used by animals, such as caribous, elephants, birds, fishes and insects (Joly et al., 2019), to reach summer and winter habitats, and for reproduction and resources.

Corridors are critical for the maintenance of ecological processes and the continuation of viable populations (Frankham, 2005). They prevent the negative effects of inbreeding and reduced genetic diversity (via genetic drift) that often occur within isolated populations. They may also help facilitate the re-establishment of populations that have been reduced or eliminated due to natural events such as fires or diseases.

Here, the term "Corridor" is used as rather discussed in biology and geoecology (Rosenberg et al., 1997), to interpret and discuss the habitat and possible connection routes used by the Pleistocene megafauna between North-, Central- and South America. Nevertheless, the terminology is rarely used and discussed in palaeontology, due to the limited knowledge on the palaeoecology and palaeobiogeography of the extinct megafauna (Wilson et al., 2009; Webb, 2013).

The Great American Biotic Interchange (GABI) describes one of the major faunal migration events between North- and South America (Marshall, 1988; Morgan, 2008; Woodburne, 2010). Here, the term "corridor" explains the terrestrial connection of North- and South America through the Isthmus of Panama, after an isolation of South America for >100 Million

years (Webb, 2006). The re-connection of North- and South America, about 3 Million years BP ago (Bacon et al., 2015; O'Dea et al., 2016), allowed North American fauna, such as proboscideans and horses, to migrate to South America, and South American fauna, like Xenarthrans, to disperse over North America (Marshall, 1988; Morgan, 2005; Cione et al., 2015). For example, the most southern migration of *Mammuthus* in Central American is coupled with the Pleistocene expansion of grassland described as a "savanna corridor" (McDonald and Dávila, 2017; Dávila et al., 2019). Therefore, the terminology has been mainly used in the context of proboscideans (Morgan, 2008; Mothé and Avilla, 2015), since seasonal migration routes of extant elephants are well-documented.

The term *Mexican Corridor* is here introduced to describe the biogeographical faunal connection and exchange between North- and South America during the Pleistocene (Stinnesbeck et al., 2018b). Climate, vegetation and geology are some of the main ecological factors that influence the migration of animal populations, or form palaeogeographical barriers.

1.2   Study objectives and concept of the dissertation

Pleistocene research in America is majorly limited to either the United States, while research in South America focuses on Argentina, Brazil and Chile. Mexico and Central America are understudied, mainly due to political circumstances in these countries and the lack of funding institutions, but also due to inadequate training of geoscientists, including palaeontologists (Lucas and Alvarado, 2016).

In consequence, Mexican research on the Pleistocene is rare. Field work and the revision of ground sloth material housed in museum collections has long been completely neglected. This contrasts with the research on proboscideans, e.g. mammoths (Arroyo-Cabrales et al., 2007; Mothé and Avilla, 2015; Prado et al., 2015), which apparently is more popular. Prior to this study, only few ground sloth remains were known from Central America (Webb and Perrigo, 1985; Cisneros, 2005) and Mexico (McDonald, 2002). Only a single paper summarized the literature on ground sloths from Mexico (McDonald, 2002).

Most published reports on ground sloth material from the region lacks information on the osteology, taxonomy and taphonomy of these animals. In most cases they refer to isolated teeth or bone fragments (McDonald, 2002; Ferrusquía-Villafranca et al., 2010). For instance, *Megalonyx jeffersonii* is only known from few bone fragments from two Mexican sites

(McDonald, 2002). In contrast, there are 152 North American sites, many of which have yielded complete specimens (McDonald et al., 2015; Hoganson and McDonald, 2007). *Glossotherium chapadmalense* is only represented in Mexico by isolated teeth and skull fragments from two sites (McDonald, 2002), whereas the remnants of this taxon are abundant throughout North America (Varela and Fariña, 2016). Even though McDonald (2002) listed numerous ground sloth reports from Mexico (Table 1), it now becomes evident that this database is out-dated and that the taxonomic assignation presented in this report requires substantial revision.

Mexican ground sloth fossils have never been documented in detail, nor have they been illustrated or described in terms of osteology. As a result, their status remains almost unknown, although the Central American as well as the *Mexican Corridor* are crucial for assessing palaeobiogeographic and palaeoecological relationships between North- and South American megafaunal assemblages, including ground sloths.

The osteology and taxonomy of Late Pleistocene ground sloths and associated megafaunal assemblage discovered by the German-Mexican team in the submerged caves of Quintana Roo on the Yucatán Peninsula (Figs. 1 and 2) presents the focus of this dissertation. In addition, an overview of Late Pleistocene ground sloth fossils is provided from other areas of Mexico (e.g. Jalisco, see Table 1) and an ecological comparison of these taxa with the faunal assemblage from the Yucatán Peninsula (Table 2).

The present dissertation thus also discusses the following fundamental questions:

a) How diverse was the ground sloth population of the *Mexican Corridor*?
b) What is the palaeogeographic and stratigraphic distribution of Mexican ground sloth taxa?
c) Which ecological factors may have influenced the geographic distribution of the Mexican ground sloth species?
d) Which environmental factors triggered ground sloth migration and local diversification in the *Mexican Corridor*?
e) What type of interaction existed between humans and ground sloths? Can an interaction be reliably reconstructed from the Mexican data?
f) Which factors may have influenced the extinction of ground sloths?

The correlation of taxonomy with palaeoenvironmental data leads to a discussion regarding the potential migration of the ground sloths, while the analysis of cut marks on some of the megafaunal bones suggests human interaction (e.g., hunting). The data collected here allows for an evaluation of factors that contributed to ground sloth extinction.

1.3 Study area: The Yucatán Peninsula

The Yucatán Peninsula (YP) separates the Gulf of Mexico from the Caribbean Sea and Central- from North America. It includes the Mexican states of Yucatán, Campeche and Quintana Roo, as well as Belize and north-eastern Guatemala. The northern YP consists of a 3000 m thick carbonate platform reaching back to the early Cretaceous (Ward et al., 1985).

The present dissertation focuses on the Mexican state of Quintana Roo (Fig. 1), located in the north-eastern part of the peninsula. This area (Fig. 1A) is characterized by flat-lying limestone of Mio-, Plio- and Pleistocene age (Ward et al., 1985; Weidie, 1985; Ward, 1997). During stadial periods of the Pleistocene the limestone bedrock was exposed, due to a sea-level of up to 120 m below present levels, leading to intensive karstification and the formation of one of the world's finest examples of karst landscape features, including caves, tunnels, subterranean water systems, dry valleys, sinkholes and poljes (Blanchon and Shaw, 1995; Moseley et al., 2015). This enormous karst system reaching to depths of >100 m is today covered by dense jungle vegetation growing either on thin soil layers or bare limestone rock.

During the Late Glacial Maximum (LGM) and across the Pleistocene-Holocene boundary the caves and tunnel systems were dry (Fig. 1B) and accessible to animals and humans (González González et al., 2008). The cave systems and sinkholes were ultimately flooded due to sea-level rise across the Pleistocene-Holocene boundary (Fig. 1C) and modern sea levels were reached between 6.000 and 4.500 cal BP (Smart et al., 2006; Smith et al., 2011; Grant et al., 2012; Moseley et al., 2015; Khan et al., 2017; Hering et al., 2018). In the cave system, the slow rise of water level has preserved a unique combination of climatic, archaeological and palaeontological archives (González González et al., 2008, 2013).
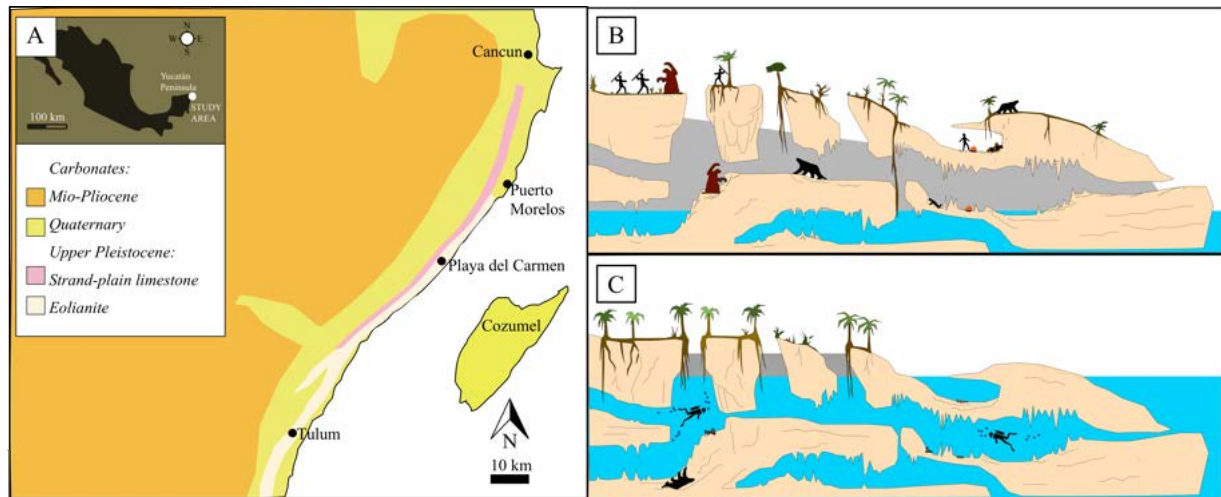
Fig. 1: (A) Schematic drawing of the geology in the study area on the north-eastern Mexican Yucatán Peninsula (modified after Ward et al. 1985, Ward 1997 and Weidie 1985). Intensive karstification of the study area formed cave systems and sinkholes, which were dry and accessible for man and megafauna during the Late Pleistocene (B). Early Holocene sea-level rise flooded the cave systems conserving anthropological and palaeontological evidence (C).

Numerous palaeontological and anthropological localities were reported from Quintana Roo, during the past 15 years (Fig. 2, Table 2). To date, ten human skeletons of Late Pleistocene to Early Holocene age have been discovered, among them some of the oldest human osteological remains of the American continent (Chatters et al., 2014; González González et al., 2013; Stinnesbeck et al., 2020, 2017). Several localities also contain human burials (Stinnesbeck et al., 2018a). Osteological remains of the Late Pleistocene fauna populating the area are also abundant, among them gomphotheres (*Cuvieronius hyodon*), horses (*Equus* sp.), camels (*Hemiauchenia* sp.), giant armadillos (*Glyptotherium* sp.), tapirs (*Tapirus bairdii*), felids (*Smilodon fatalis*, *Panthera onca, P. balamoides*), peccaries (*Tayassu pecari*, *Muknalia minima*). Some faunal bones exhibit cut marks (Stinnesbeck et al., 2017b; 2018b; 2020a) and have been discovered in hearths (Hering et al., 2018), suggesting hunting by the early human settlers. Ground sloths have been reported from 11 localities (Fig. 2) and make up for about 50% of the palaeontological material (Table 2).
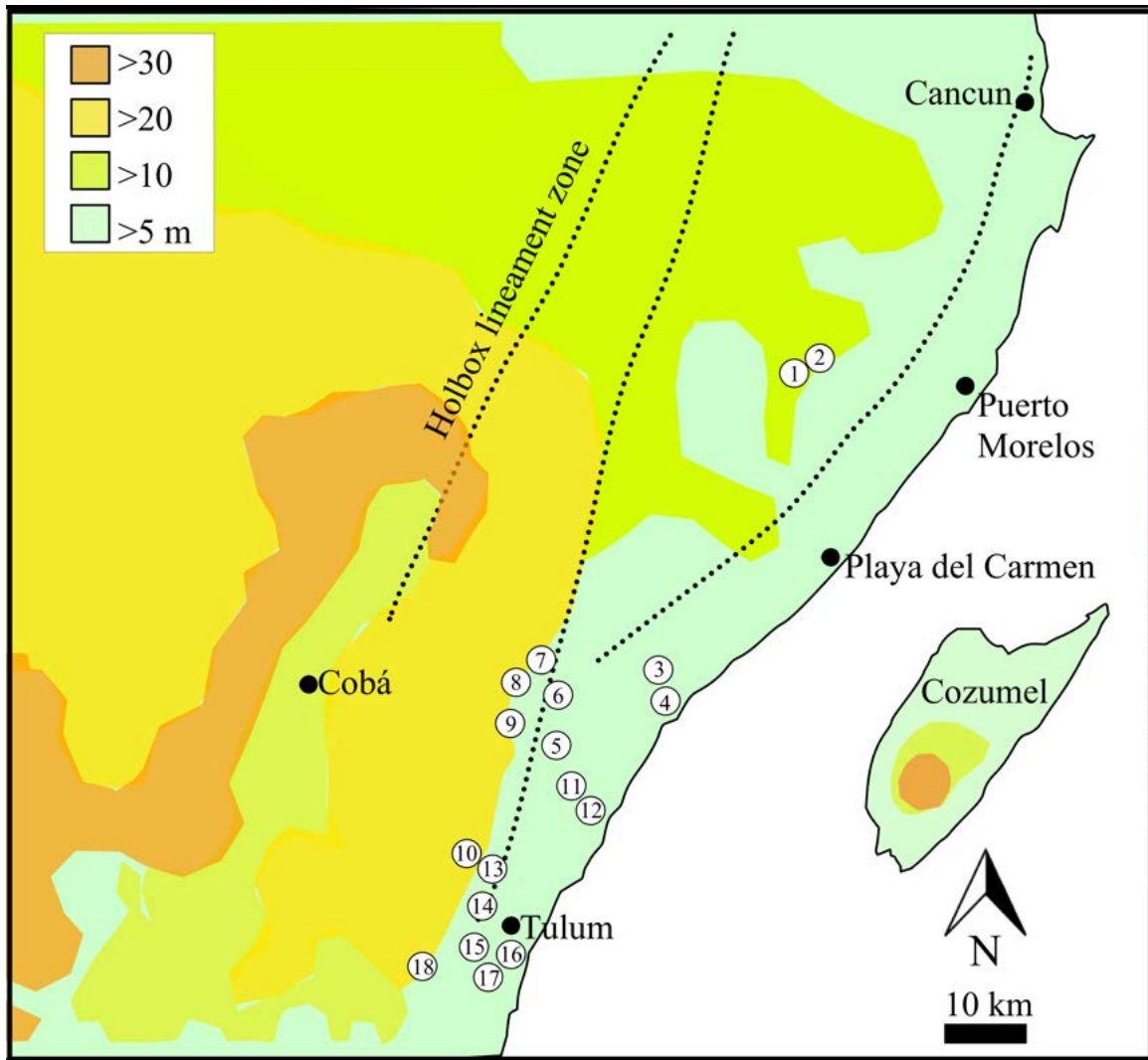
Fig. 2: Topography of the study area and distribution of the palaeontological and anthropological localities studied within the project. Note that all sites are sinkholes (spa. cenotes) or located in caves, which are today flooded by water. (1) El Zapote cenote, (2) cenote Tortugas, (3) Puntos de Luz, (4) La Chimenea, (5) El Pit, (6) Nai Tucha, (7) El Tigre, (8) Concha, (9) Hoyo Negro, (10) Kim Ha, (11) Toh, (12) El Templo, (13) Kalimba, (14) Naharon, (15) Caracoles y camellos, (16) Las Palmas, (17) Muknal, (18) Chan Hol. For further information about the faunal assemblage see Table 2.

2   Material and methods

2.1   Material

The fossil material on which this dissertation is based has been recovered during underwater palaeontological research from cenotes and submerged cave tunnels near Puerto Morelos and Tulum (Fig. 2, Table 2), as part of the DFG projects FR1314/26 to the State Museum of Natural History in Karlsruhe and STI128/28 to the University of Heidelberg, and in cooperation with the Museo del Desierto in Saltillo, Coahuila, Mexico. Further material has been reviewed within a DAAD scholarship (Kurzreisestipendium für Doktoranden 91683941).

The following ground sloth material has been documented, described and discussed within this dissertation:

Xibalbaonyx microcaninus (Stinnesbeck et al., 2018b) INAH-MRG-10-294922 (skull) and INAH-MRG-10-294923 (mandible), accessible at the MRG, Jalisco, Mexico.

Xibalbaonyx oviceps (Stinnesbeck et al., 2020a, 2017a) INAH Za2014-01 (skull and postcranial material) and INAH Za2014-131-02 (mandible), housed at the Museo Maya de Cancún y Zona Arqueológica de San Miguelito in Cancun, Quintana Roo, Mexico.

Xibalbaonyx exinferis (Stinnesbeck et al., 2020b) holotype CPC-2774 mandible, referred specimens CPC-2775 atlas and CPC-2776 humerus, housed at the IPA, Playa del Carmen, Quintana Roo, Mexico.

Scientific reference material was reviewed in the collections of the INAH in Mexico City, Villa de la Paz in San Luis Potosi, Mina in Nuevo León, MPG and MRG in Jalisco, the SMNK (Germany), AMNH (New York), the University of Florida at Gainsville and the MUSHNAT in Guatemala City.

The following type specimens of fossil ground sloths were included in the comparison and phylogenetic analysis:

Acratocnus odontrigonus, A. ye, A. antillensis (MacPhee et al., 2000; White and MacPhee, 2001).

Ahytherium aureum (Cartelle et al., 2008).

Australonyx aquae (De Iuliis et al., 2009, 2016).

Diabolotherium nordenskioldi (Pujos et al., 2007).

Megalocnus rodens, M. zile (de Paula Couto, 1956; MacPhee et al., 2000; White and

MacPhee, 2001).

Megalonyx jeffersonii (Leidy, 1855; Hirschfeld and Webb, 1968; McDonald, 1977).

Megistonyx oreobios (McDonald et al., 2013b).

Meizonyx salvadorensis (Webb and Perrigo, 1985) UF 27513 (for mandible) Florida Museum of Natural History, Gainsville, USA.

Neocnus gliriformis, N. major, N. comes, N. dousman, N. toupiti (MacPhee et al., 2000)

Nohochichak xibalbakah (McDonald et al., 2017) INAH-DP5832 (for skull and mandible), accessible at the INAH, Mexico City, Mexico.

Parocnus browni, P. serus (MacPhee et al., 2000).

Pliometanastes protistus (Hirschfeld and Webb, 1968).

Zacatzontli tecolotlanensis (McDonald and Carranza-Castañeda, 2017).

2.2 Methods

2.2.1 Underwater palaeontology and conservation

Cartography, underwater exploration and survey were developed by the Quintana Roo Speleological Survey (QRSS), a volunteer organization of underwater cave divers from the region. Most of the faunal material has been collected in >20 m and up to 60 m water depth and in tunnel systems reaching to >1000 m distance from the next entrance. Therefore, on-site documentation and collection was carried out by professional cave divers. Regarding the material discussed here, the dives were organized and directed by Jerónimo Avilés Olguín (MUDE). The fossils from the underwater caves and cenotes of Quintana Roo were brought to the IPA for conservation and further documentation. The IPA is a laboratory of the MUDE in Playa del Carmen.

Destructive samples for stable isotope analysis and ^{14}C dating were taken before conservation. The osteological remains were treated for several months with distilled water, since the bones were extremely brittle. For example, skull and mandible of *Xibalbaonyx oviceps* from El Zapote cenote were treated with distilled water for eight months and a combination of distilled water and polyvinyl acetate for one month for further handling and conservation. Further handling of all fossils for osteological documentation would therefore take weeks to months after collection of the material in the cave.

2.2.2 Fieldwork

Destructive samples of fossil bones for dating, isotope and geochemical analyses were taken from several ground sloths and other megafaunal fossils of the faunal assemblage of the MPG in Jalisco, west-central Mexico, as well as several museum collections in Guatemala.

Furthermore, sediment sections were measured and sampled in northern Mexico and Guatemala.

The Guatemala data has been documented in detail in Dávila et al. (2019), while the Mexican data still remains unpublished.

2.2.3 Taxonomy

The terminology used for the description of anatomical features is based on phylogenetic characters and anatomical terminology of both tree and ground sloths (Naples, 1982; Patterson et al., 1992; Gaudin, 1995, 2004; Adam, 1999; White and MacPhee, 2001; Hayssen, 2008, 2011; McDonald et al., 2013a).

To ensure a precise osteological description of the fossil material human-anatomical designations were maintained and partly reintroduced for the description of ground sloth morphology. In these cases, the nomenclature had to be supplemented by terms used in the current revision. New terms introduced here are based on the anatomical nomenclature for humans (Martin, 1914) and other mammals (Martin, 1914; Von den Driesch, 1976): The term "rhinion" describes the rostral-most point on the median line of the nasal bones (Martin, 1914).

The term "nasion" is often referred to as the point where the nasofrontal and internasal sutures meet (Groves, 2003), but also refers to the deepest depression on the nasal bridge (Martin, 1914). It has been used for *Australonyx* as a "depressed snout" (De Iuliis et al. 2009). The term "nasional impression" as a diagnostic feature of the genus *Xibalabonyx* has been introduced (Stinnesbeck et al., 2017a).

The acronyms "C" and "c" refer to the upper and lower caniniforms, "M" and "m" for upper and lower molariforms, respectively and does not refer to deciduous teeth, since there is no homology of the sloth dentition with other mammals (Mai et al., 2005; Ungar, 2010).

The basonasal length (BNL) is measured from the rhinion of the nasal to the caudal extremity of the occipital condyles (Gaudin, 2004). The maximum mandibular length (MML) is measured from the rostral tip of the mandibular symphysis or spout to the caudal edge of the

condyloid or angular process (Gaudin, 2004), depending which one is reaching further posterior.

2.2.4 Drawing documentation

Most drawings were created based on large format photos of the original material. The graphic representations are interpretations of these photographs.

The photographs were taken with a Panasonic Lumix, and a Canon EOS Rebel T4i with 10–22 mm zoom lens set at 22 mm; f 4.5, 1/80 – f 8, 1/20, using a tripod. The background of the photographs has been masked manually. All here presented photographs were taken by the author.

The schematic drawings and maps have been created by free-style drawing with the program "pixelmator". They are based on a compilation of published and unpublished Late Pleistocene vegetation and megafaunal data from Central American and free online and published maps. Modified maps based on literature are cited under the respective drawing. All drawings presented here and in all publications were created by the author.

2.2.5 Phylogenetic analysis

Phylogenetic analysis was performed to interpret the relationships of *Xibalbaonyx oviceps, X. microcaninus* and *X. exinferis* within Megalonychidae. The analysis was carried out using PAUP (version 4.0a 150 for Macintosh; Swofford, 2002). The methodology has been described in detail by several authors (Gaudin, 1995, 2004; Wible and Gaudin, 2004). The analysis is based on 80 cranial and mandibular features (McDonald et al., 2017). '?' represents missing data or characters that are inapplicable to a given taxon. The following symbols are used to represent character states in polymorphic taxa: a = {0, 1}; b = {1, 2}; c = {2, 3}; d = {0, 2}; e = {0, 1, 2}. A data matrix for all 18 megalonychids has been used (Stinnesbeck et al., 2018a, 2020b).

A phylogenetic analysis is today required by most scientific journals dedicated to vertebrate palaeontology.

The present work assumes that reconstructions of phylogenetic relationships between taxa using cladistic methods are purely theoretical, as anagenesis (development of traits) and phylogenesis (generation of species by species splitting) are not sufficiently correlated. Characteristics and their occurrence on individuals do not provide evidence for family relationships in the genealogical sense and for evolution (Peters, 1976; Neuchâtel, 1985). They can only be interpreted as the results of such operations. The cladistic method provides classification suggestions in the form of cladograms. These show similarity intervals of selected combinations of morphological features, which are considered synapomorph *sensu* (Henning, 1950). The present work follows the proposals of Patterson and Rosen (1977), according to which the alpha-taxonomy should first be resolved based on comparative osteology. Only in a second step, the cladistic method can then be used to determine morphological similarity distances with the help of the synapomorphies. These are then phylogenetically interpreted to identify sister groups under the axiomatic assumption that the distribution of characteristics is the result of genealogical processes.

However, while phylogenetic analysis is well accepted in palaeontology especially for dinosaurs (Wilson, 2002), the ground sloth data matrix is sparse and thus should be interpreted with care (Varela et al., 2019).

2.2.6 Isotope analysis

Isotope analysis on bones and teeth record a composition of information about the animal´s diet, physiology and mobility, as well as climate and environmental conditions.

Fossil samples of teeth were shipped to the Heidelberg University and Johannes-Gutenberg University in Mainz for isotope analysis. Several samples are still waiting to be analysed, the preliminary data is therefore unpublished but are mentioned in the text.

Sr-isotopes: The investigation of strontium isotope ratios in fossil tooth material is a powerful tool to determine provenance, mobility and migration of human and animal individuals and populations and is well-established in archaeological sciences (Ortega-Muñoz et al., 2019). Depending on the rubidium-strontium geochemistry, strontium isotopes develop specifically according to local condition in soils and bedrocks. The element strontium (Sr) is mobilized from these geological materials, is taken up via food chains and water, and is ultimately stored in the mineralized body tissues. The signature of Sr-isotopes in fossil teeth thus correlates with the specific geological composition of the geological surface of settlements; the

methodology thus allows to identify geographical areas where individuals developed their dentition during infancy and adolescence (Bentley, 2006), and non-locals and their provenance. It thus helps to elucidate the mobile behavior of individuals and groups (Price et al., 2008).

Stable Carbon and Oxygen isotopes: A small molar sample size (including ground sloth canini- and molariform) was drilled and transected following the crown to growth axis for further isotope analyses. The preference and availability of C_3 and C_4 plants in the faunal assemblage of the YP and Jalisco has been documented based on $\delta^{13}C$ analysis in enamel. C_3 plants, which include shrubs and trees, differ from C_4 plants, e.g. grasses, in their ^{13}C-isotope composition. Furthermore, the body water $\delta^{18}O$ value has been analyzed. $\delta^{18}O$ is discussed as a proxy of past climatic conditions such as ambient air temperature and aridity, but also water gained by the animal (e.g. drinking behavior) depending on available surface water and food source, including metabolic water from food processing.

Stable oxygen and carbon isotope samples were also measured and from speleothems (e.g. Chan Hol and El Zapote "Hells Bells"), to elucidate climatic conditions across the Pleistocene-Holocene transition. For further methodological information see Stinnesbeck et al. (2017) and Ritter et al. (2019).

2.2.7 Dating

Fossil samples of bones and teeth as well as charcoal and soot were sent for radiocarbon dating to the Curt-Engelhorn-Center of Archaeometry gGmbH (CEZA) at Mannheim, Germany, where they were analyzed with a MICADAS (Mini Carbon Dating System) AMS system, and to the Laboratorio de Espectrometría de Masas con Aceleradores of the Universidad Nacional Autónoma de México (UNAM), Mexico. Both charcoal and soot samples were prepared using a standard protocol including acid and base treatments to remove contaminants such as carbonate and humic acids (Lindauer et al., 2017). Charcoal associated with megafaunal bones has been found in several palaeontological localities on the YP (Stinnesbeck et al., 2017b). Soot patches were identified above illumination sites (Hering et al., 2018) and hearths for example at Muknal (Stinnesbeck et al., 2018a).

No data were obtained at MICADAS from several megafaunal samples due to insufficient collagen content (see Table 2), as collagen levels of underwater fossils from the system of submerged caves of the Yucatán Peninsula are extremely low (Burr et al., 2009; Taylor, 2009). Bone apatite ages are considered to be ambiguous, because of carbon interchange with the environment. Therefore, bone-based dating is difficult and resulting ages may not be accurate (Taylor, 2009).

All BP Radiocarbon years were calibrated with OxCal version 4.2.4 with the IntCal13 dataset (Reimer et al., 2013, Bronk Ramsey 2013). The calibrated ages are given as weighted mean and 1-sigma or 2-sigma standard deviations. The reference year for the age in this study is 1950 AD.

2.2.8   Microscopic analysis of cut marks

Cut marks were identified on ground sloth long bones and a peccary mandibular ramus. These were analyzed and photographed with a Keyence digital microscope VHX-5000. All modifications were examined under magnifications of 5-50x and 15x-200x using a VH-Z20R/W lens. Additional photos were taken with a resolution of 3200 x 2400 pixels. A high resolution three-dimensional model of each mark was created by the scan software of the Keyence VHX-5000, thus accurately representing the micromorphology of these modifications (Bello et al., 2009; Courtenay et al., 2017). Relief and depth of the cross-sections of the marks were measured perpendicular to the longitudinal axis of the modification and interpreted according to the attributes developed by Bello and Soligo (2008), Domínguez-Rodrigo et al. (2009), and Bello et al. (2011). They include cut mark length and depth, the opening angle of the mark, the shoulder height index and floor radius.

3   Results

The dissertation project was undertaken to improve the understanding of Mexican ground sloths. As a cumulative dissertation, each research paper was written to stand on its own as an independent publication (see Appendix). Repetitions in the respective introduction, material and method sections are therefore unavoidable. Osteological documentation and description of new ground sloth taxa forms the basis of this work. Other manuscripts presented here have focused on the identification of megafaunal taxa other than ground sloths and archaeological evidence. They are essential to understand the environmental conditions under which the ground sloths lived (e.g., palaeobiogeography, palaeoecology, palaeoenvironmental isolation of the region) and their potential interactions with humans. These publications are thus essential in the context of interpretation and discussion.

The following research papers form part of the cumulative dissertation (see Appendix). Personal achievements are presented for each paper listed below:

I. **Stinnesbeck, S. R.**, Frey, E., Olguín, J. A., Stinnesbeck, W., Zell, P., Mallison, H., González González, A., Aceves Núñez, E., Velázquez Morlet, A., Terrazas Mata, A., Benavente Sanvicente, M., Hering, F. Rojas Sandoval, C. (2017). *Xibalbaonyx oviceps*, a new megalonychid ground sloth (Folivora, Xenarthra) from the Late Pleistocene of the Yucatán Peninsula, Mexico, and its palaeobiogeographic significance. *Paläontologische Zeitschrift*, 91(2), 245-271.

The well-preserved skull and mandible of a ground sloth discovered in the El Zapote cenote near Puerto Morelos are here documented and described as a new genus and species of Megalonychidae named *Xibalbaonyx oviceps*. The genus is a composite of the Maya term *Xibalbá* for "underground" or "place of fear" and "ὄνυξ" (onyx), which is Greek for "claw" or "finger nail". The genus name is dedicated to the cave divers who dive into the Maya "underworld," the cenotes, and collect the fossils under risky conditions, but also in honor of the Yucatán Peninsula, which is also called the Maya region.

The holotype was a subadult individual, based on the degree of suture fusion in the skull, faint temporal lines, and the condition of the occlusion faces of the molariforms. *Xibalbaonyx oviceps* has a dental formula of 5/4 including a greatly enlarged caniniform tooth of triangular

cross-section. This caniniform is separated by a long diastema from the molariform tooth rows in both the lower and upper jaw. The molariform teeth show oval, rounded rectangular to reniform occlusal shapes with transverse crests. All teeth except for the upper caniniforms, show striations and apicobasal sulci that may be expressed as shallow grooves or deep sulci. The ascending process of the jugal is longer than the descending and middle process of the jugal. The pterygoids are inflated. The glenoid fossa is transversally widened. The skull is elongated and narrow, with a nasional impression. The temporal lines are widely separated and do not form a sagittal crest.

Fig. 3: Skull and mandible of *Xibalbaonyx oviceps* from El Zapote cenote in right (upper photograph) and left (lower photograph) lateral views.

Xibalbaonyx oviceps differs significantly from all hitherto known Megalonychidae including those from the Greater Antilles, North- and South America. The taxon suggests a local Caribbean radiation of ground sloths during the Late Pleistocene, which is consistent with the dispersal of the group along a Mexican Corridor.

contributed with a 3D-model of the fossil material for further research. PZ and FH helped with the manuscript layout und proof-reading. ATM and MBS contributed with ^{14}C-dating of the material. AVM, AGG and CRS were responsible for the Mexican on-site permits.

II. **Stinnesbeck, S. R.**, Frey, E., Avilés Olguín, J., González González, A. H., Velázquez Morlet, A., & Stinnesbeck, W. (2020). Life and death of the ground sloth *Xibalbaonyx oviceps* from the Yucatán Peninsula, Mexico. Submitted to *Historical Biology* in June 2020.

The paper describes hitherto unreported postcranial material from El Zapote cenote attributed to the holotype of *Xibalbaonyx oviceps*. The forelimbs had twice the length of hind limbs, as indicated by the short tibia. The anatomical proportions suggest a quadrupedal locomotion with facultative bipedalism. The forelimbs exhibited a great degree of liberty; this is typical for semi-arboreal to arboreal lever climbing animals, suggesting that *Xibalbaonyx* was capable to climb, as seen in large massive apes, or bears.

Furthermore, the pelvis, ulna and ribs exhibit cut marks and all long bones were fragmented and hollowed out. This suggests that the joints of the animal were deliberately broken to get to the medulla of the bones. This is the first published evidence, in Central America, for butchering of ground sloths by humans, and one of only five sites on the entire American continent.

SRS documented and interpreted the fossil material, visited museum collections for the comparison of postcranial elements, drew all figures and wrote the manuscript.

EF and WS provided conceptual help and contributed to the discussion and final version of the manuscript. JAO was responsible for the underwater survey, on-site photography, and documentation and collection of the material. AGG, CR and AM were responsible for the Mexican on-site permits.

III. **Stinnesbeck, S. R.**, Frey, E., & Stinnesbeck, W. (2018). New insights on the paleogeographic distribution of the Late Pleistocene ground sloth genus *Xibalbaonyx* along the Mesoamerican Corridor. *Journal of South American Earth Sciences*, 85, 108-120.

The manuscript describes the new ground sloth species *Xibalbaonyx microcaninus* from the Zacaoalco palaeolake in the federal state of Jalisco, based on a complete skull exhibited in the MRG. The specimen was here assigned to *Xibalbaonyx* from the Late Pleistocene of Quintana Roo in south-eastern Mexico (see I), based on a nasional impression level with the lacrimal and jugal constriction of the skull, the evenly convex dorsal skull surface of the skull roof, and the absence of a sagittal crest. Osteological differences, such as the temporal lines which merge with the nuchal crest, dentition, size and shape of the mandibular spout, are here interpreted to represent species-specific variations within the genus *Xibalbaonyx*. *X. microcaninus* is thus taxonomically separated from the coeval ground sloths from the Yucatán Peninsula, *X. oviceps, X. exinferis* and *Nohochichak xibalbahkah* from Quintana Roo in southern Mexico. The genus *Xibalbaonyx* thus had a wide geographic distribution ranging from central to southern Mexico.

The manuscript also gives an overview of the Late Pleistocene megafaunal assemblage and palaeoenvironments in the federal state of Jalisco in west-central Mexico.

SRS visited the museum collections, documented, described, illustrated and compared the presented fossil material and executed the phylogenetic analysis. She wrote the manuscript, interpreted and discussed all data.

EF and WS provided conceptual help and discussion and they contributed to the geology and revision of the faunal assemblage in Guadalajara. They were also responsible for the funding.

IV. **Stinnesbeck, S. R.**, Stinnesbeck, W., Frey, E., Avilés, J., & Gonzalez, A. (2020). *Xibalbaonyx exinferis* n. gen. et n. sp. (Megalonychidae), a new Pleistocene ground sloth from the Yucatán Peninsula, Mexico. *Historical Biology*, 1-13.

Xibalbaonyx exinferis n. sp. was discovered in a new fossil locality named cenote Tortugas, located west of Puerto Morelos in Quintana Roo. The taxon is based on a fragmentary left mandibular ramus. An atlas and a left humerus are also referred to this taxon. The new taxon is diagnosed by the presence of two mental foramina on the short symphyseal spout, a caniniform being the smallest mandibular tooth, and the anterolaterally directed aperture of the mandibular foramen on the lateral surface of the mandible. *Xibalbaonyx exinferis* is the third endemic megalonychid documented for the north-eastern Yucatán Peninsula and thus

provides increasing evidence for an ecological isolation of the area from the rest of Mexico during the Pleistocene.

The phylogenetic analysis suggests, that the ground sloths from the Yucatán Peninsula are more closely related to Mexican and South American ground sloths, than to sloths from the West Indies or North America, although these are geographically closer.

SRS visited all museum collections, documented, described and interpreted the fossil material. SRS did the phylogenetic analysis, drew all figures and wrote the manuscript.

EF and WS provided conceptual help and contributed to the discussion and final version of the manuscript. JAO was responsible for the underwater survey, on-site photography and documentation and collection of the material. AGG was responsible for the Mexican on-site permits.

V. **Stinnesbeck, S. R.**, Frey, E., Stinnesbeck, W., Avíles Olguín, J., Zell, P., Terrazas Mata, A. T., Benavente Sanvicente, M., González González, A., Rojas Sandoval, C. & Acevez Nuñez, E. (2017). A new fossil peccary from the Pleistocene-Holocene boundary of the eastern Yucatán Peninsula, Mexico. *Journal of South American Earth Sciences*, 77, 341-349.

The left mandibular ramus of a fossil peccary from the submerged Muknal cave northwest of Tulum, was assigned to a new genus and species of peccary termed *Muknalia minima*. The taxon differs significantly from all extant peccaries and their Pleistocene relatives by a concave notch at the caudal edge of the mandibular ramus and prominent ventrally directed angular process. These diagnostic osteological differences suggest that the masticatory apparatus differed from all other peccaries and may hint to an ecological isolation on the Late Pleistocene Yucatán Peninsula. This is also suggested by the low body mass of between 17 and 24 kg, which was certainly favorable in the shrub-dominated dry savannah that must then have covered the limestone plateau in northeastern Yucatán.

SRS documented, described and interpreted the fossil material and compared the fossil with extant peccaries housed in the SMNK. SRS drew all figures and wrote the manuscript.

EF and WS provided conceptual help and contributed to the discussion and final version of the manuscript. PZ helped with the visualization of several figures and editing. JA, AGG and EAN were responsible for the underwater survey, on-site photography and documentation and

collection of the material. ATM and MBS directed data curation and contributed to the original manuscript. CRS and AGG were responsible for the Mexican on-site permits.

VI. Stinnesbeck, S. R., Stinnesbeck, W., Frey, E., Avilés Olguín, J., Rojas Sandoval, C., Velázquez Morlet, A., & H. González, A. (2018). *Panthera balamoides* and other Pleistocene felids from the submerged caves of Tulum, Quintana Roo, Mexico. *Historical Biology*, 1-10.

A new species of a Pleistocene felid is based on the distal third of a right humerus from the submerged El Pit cenote (sinkhole) near Tulum in Quintana Roo. The new taxon, *Panthera balamoides* sp. nov., is characterized by a large entepicondylar foramen, a gracile and straight humeral shaft with a prominent supracondylar ridge with a small depression on the lateral epicondyle and a distal articular surface located medially with respect to the long axis of the shaft. Two felid clavicles from the same locality have been assigned to *Panthera atrox*, while a humerus fragment from the Kim Ha cave near Tulum likely corresponds to *Smilodon gracilis*. *Panthera balamoides* lines up with other likely endemic mammals in the region, which suggest that at least northern Quintana Roo, if not the entire Yucatán Peninsula, may have been ecologically isolated during the Pleistocene, due to the repeated expansion of grassland.

SRS documented, described and interpreted the fossil material and compared the fossil with bones of extant felids housed in the IPA, AMNH and SMNK. SRS drew all figures and wrote the manuscript.
JAO was responsible for the underwater survey, on-site photography and documentation and collection of the material. He also contributed to the anatomical comparisons of the fossil material with extant Mexican felids and to the original manuscript. He was also charge of the data curation. EF and WS provided conceptual help and contributed to the locomotion and palaeogeographic interpretation, discussion and final version of the manuscript. CRS, AVM and AGG were responsible for the Mexican on-site permits.

VII. Dávila, S. L., **Stinnesbeck, S. R.**, Gonzalez, S., Lindauer, S., Escamilla, J., & Stinnesbeck, W. (2019). Guatemala's Late Pleistocene (Rancholabrean) fauna: Revision and interpretation. *Quaternary Science Reviews*, 219, 277-296.

Guatemala is a key area along this Mesoamerican Corridor which acted as a palaeobiogeographic bridge and filter between North- and South America during both, the Plio- and Pleistocene. The Late Pleistocene fossil assemblages of Guatemala revised here thus add to the knowledge of faunal distribution in this poorly known region. The most fossiliferous localities in Guatemala, i.e. Chivacabe, Estanzuela, Ciudad Real and San Rafaelito, are all associated with reworked volcanic sediments (lahars) and thus provide evidence for high volcanic activity in the Late Pleistocene and early Holocene.

The Late Pleistocene fossil assemblages of Guatemala mostly consist of random findings of large herbivores, comparable to other fossil sites along the Mesoamerican Corridor. Although many of the findings have not been dated, due to significant mineralization of bones and the lack of stratigraphic context, an assignation of most localities to the Middle to Late Pleistocene (Rancholabrean) epoch is tentatively suggested by the faunal assemblages documented here. These are dominated by *Cuvieronius hyodon* and *Eremotherium laurillardi,* while *Glyptotherium* sp. is frequent and other taxa are surprisingly rare. For instance, *Equus* is under-represented in the faunal assemblages, and *Hemiauchenia* and *Mammuthus* have only been found as isolated fragments along the Motagua-Polochic fault-zone. *Bison*, cats and bears are totally absent to date, as are small faunal elements, although the latter is likely due to collection bias. In consequence, the faunal assemblages majorly consist of large herbivores, principally mesic-adapted browsers, e.g. *Cuvieronius* and *Eremotherium*. Their distribution within Central America is likely a result of adaptation to semitropical to tropical conditions (Prado et al., 2005) and forested areas with abundant precipitation. These animals are characteristically absent in Late Pleistocene sites in the arid southwest of North America. The presence of oak forests and *Eremotherium*, *Cuvieronius* and *Mixotoxodon* dating to the MIS 3 and 2, supports this scenario, as also the presence of *Glyptotherium* sp. which is well-known to have lived along water courses in moist, lowland tropical to subtropical habitats. The ages and finding localities of *Glyptotherium* sp. in Guatemala, however, reveal that this genus was highly adaptable and even reached high altitudes. *Mammuthus* findings from Guatemala, on the other side, appear to be stratigraphically unrelated to the above faunal assemblage. As *Mammuthus* is well known to be specialized to *Artemisia*-dominated grassland vegetation, a different stratigraphic interval, before or after MIS 3 and 2, is here suggested for the southward expansion of these large-sized grazers.

The survival of some megafaunal taxa beyond the Pleistocene-Holocene boundary has so far only been discussed for South America. Radiocarbon dates of *Cuvieronius hyodon* presented here for La Estanzuela in southern Guatemala, now suggest survival into the early Holocene

of these large gomphotheres in Central America. [14]C ages therefore suggest that survival of megafauna depended on refugial areas with suitable conditions. An early Holocene co-existence in Guatemala of man and megafauna therefore appears possible.

SRS documented, described and interpreted the fossil material and correlated all data. She drew all figures and wrote the original manuscript together with SLD. SRS also visited the museum collections in the AMNH, where most of the Guatemalan ground sloth fossils are housed.

VIII.   **Stinnesbeck, S. R.**, Stinnesbeck, W., Terrazas Mata, A., Avilés Olguín, J., Benavente Sanvicente, M., Zell, P., Frey, E., Lindauer, S., Rojas Sandoval, C., Velázquez Morlet, A., Acevez Nuñez, E. & González González, A. (2018). The Muknal cave near Tulum, Mexico: An early-Holocene funeral site on the Yucatán peninsula. *The Holocene*, 28(12), 1992-2005.

The Muknal cave contains substantial evidence for a burial site. A partial human skeleton, possible anthropogenic soot patches on the cave ceiling, and cut marks on the mandible of the extinct tayassuid *Muknalia minima*, were discovered in the submerged Muknal cave southwest of Tulum and are documented in this article. Osteological parameters have identified the human individual as a male based on cranial parameters, and the age at the time of death was estimated to between 40-45 years. The cranium corresponds to a mesocranial morphotype, with a narrow nose and low orbits; it presents significant dental pathologies. The Muknal skeleton is incomplete. Only the skull, mandible, right femur, right tibia, right and left humerus, right ulna, right radius, and right clavicule were found by us, despite repeated visits to the site and intensive search. Data on charcoal and soot patches as well as anthropogenic cut marks on the peccary mandible allowed us to propose that that the human bones have been brought to the cave not later than 8.600 yr BP (ca. 9.600 cal BP) and thus during the early Holocene, as a secondary burial of a partial skeleton, and that the peccary mandible was placed close to the burial site, possibly as part of a ritual. The Muknal cave therefore served as a place for funeral rituals.

The modified mandibular ramus of the extinct peccary *Muknalia minima* was placed at only 13 m distance from the human burial. It exhibits post-mortem cut marks on its medial and lateral surface, indicating removal of the masticatory muscles with a sharp, unretouched tool. This peccary bone was likely placed there in the context of the burial. Evidence for the early

Holocene age of the Muknal burial site comes from soot on the cave ceiling dated to 8.600 BP, indicating dry and accessible cave pathways to the 35m depth level. Nevertheless, the skeleton may be older, because the man-handled peccary mandibular ramus represents an element of the Pleistocene American fauna, which went extinct around the Pleistocene/Holocene boundary.

SRS wrote the original manuscript together with WS. SRS also analysed the cut marks on the peccary ramus. The anatomical description of the extinct animal, was already published by Stinnesbeck et al. (2017a). The archaeological interpretation as a secondary burial and visualization of the manuscript was also done by SRS.
ATM and MBS described the human osteology and pathologies and contributed to the archaeological interpretation. EF and WS provided conceptual help and contributed to the discussion and final version of the manuscript. JA, EAN and AGG were responsible for the underwater survey, on-site photography and documentation and collection of the material.
SL and PZ were responsible for the ^{14}C dating and contributed to the climatic data and discussion. CRS, AVM and AGG were responsible for the Mexican on-site permits.

IX. Hering, F., Stinnesbeck, W., Folmeister, J., Frey, E., **Stinnesbeck, S. R.**, Avilés, J., Aceves Núñez, E., González, A., Terrazas Mata, A., Benavente, M. E., Rojas, C., Velázquez Morlet, A., Frank, N., Zell, P. & Becker, J. (2018). The Chan Hol cave near Tulum (Quintana Roo, Mexico): evidence for long-lasting human presence during the early to middle Holocene. *Journal of Quaternary Science* 33(4), 444-454.

Charcoal accumulation sites from Chan Hol cave are interpreted as anthropogenic in origin and to represent illumination sites used by humans during cave exploration. The sites are ^{14}C age-dated by us to 9.122-7.951 cal a BP, indicating that the Chan Hol cave was repeatedly visited by man during at least 1.200 years, from the early Holocene to about the beginning of middle Holocene. At the time of the youngest charcoal datum, 7.951 cal a BP (7.177 ± 27 [14]C a BP), the cave was dry to 8 m bpsl., which concurs with global and regional sea-level curves. The charcoal data presented here not only extend the use of the Chan Hol cave from 13 ka BP to 7.177 a BP, and thus a period of 6.000 years. Moreover, they significantly narrow the present gap in the settlement history of the area, between this early phase of human settlement, and the Preclassic Period of Maya settlement at about 3.000 a BP.

SRS contributed to the writing, archaeological interpretation and visualization of the manuscript. SRS was also in charge of data curation.

X. Stinnesbeck, W., Becker. J., Hering, F., Frey, E., González, A., Fohlmeister. J., **Stinnesbeck, S. R.**, Frank, N., Terrazas Mata, A., Benavente, M. E., Avilés Olguín, J., Aceves Nuñez, E., Zell, P. & Deininger, M. (2017). The earliest settlers of Mesoamerica date back to the late Pleistocene. *PLoSOne* 12(8): e0183345.

Speleothem (U/Th) age data indicate that the Chan Hol underwater cave south of Tulum was accessed by humans during the Younger Dryas period, i.e. during the late Pleistocene. This is indicated by a minimum speleothem age of 11.377±370 y BP of a stalagmite encrusting and overgrowing the pelvic bone of an almost articulated human individual in this cave. The age was measured at 72 mm depth from the top of the CH-7 stalagmite, at about 21 mm above the pelvis and 33 mm above the base of the stalagmite, while ages in the immediate bone vicinity are altered due to uranium dissolution. 11.377±370 y BP is thus a minimum age for the skeleton. Based on a linear growth model and extension of growth rates from the well-dated upper part of the CH-7 stalagmite to its lower portion and base, the age of the Chan Hol II human rises to ~13 ky BP. The real age of the individual may even be substantially higher, because it must already have been completely decayed when the CH-7 stalagmite started to grow. The Chan Hol II skeleton thus represents one of the oldest directly dated osteological heritage of a human from the American continent. The age of the Chan Hol II human equals that of other skeletons in the Tulum cave system (e.g. Naia, Najaron), thus emphasizing the importance of these caves for early human settlement in the Americas

SRS contributed in the writing and conceptualization of the original draft and the visualisation of the taphonomic circumstances.

XI. Stinnesbeck, W., Rennie, S. R., Avilés Olguín, J., **Stinnesbeck, S. R.**, Gonzalez, S., Frank, N., Warken, S., Schorndorf, N., Krengel, Th., Velázquez Morlet, A., & González González, A. (2020). New evidence for an early settlement of the Yucatán Peninsula, Mexico: The Chan Hol 3 woman and her meaning for the Peopling of the Americas. *PLoSOne* 15(2): e0227984.

The article describes the Chan Hol woman, also named Ixchel, with a minimum age of 9.9±0.1 ky BP based on ^{230}Th/U-dating. This is the third Palaeoindian human skeleton with mesocephalic cranial characteristics documented in the cave, of which a male individual named Chan Hol 2 described here under X. is one of the oldest human skeletons found on the American continent. The new discovery emphasizes the importance of the Chan Hol cave and other systems in the Tulum area for understanding the early peopling of the Americas. Chan Hol 3, is a woman of about 30 years of age with three cranial traumas. There is also evidence for a possible trepanomal bacterial disease that caused severe alteration of the posterior parietal and occipital bones of the cranium. This is the first time that the presence of such disease is reported in a Palaeoindian skeleton in the Americas. All ten Late Pleistocene to early Holocene skeletons found so far in the submerged caves of the Tulum area have mesocephalic cranial morphologies, different to the dolicocephalic morphology for Palaeoindians from Central Mexico with equivalent dates. This supports the presence of two morphologically different Palaeoindian populations for Mexico, coexisting in different geographical areas during the Late Pleistocene-Early Holocene.

SRS contributed in the writing and conceptualization of the original draft, the formal anatomical analysis of the human skeleton and visualisation of the taphonomic circumstances.

4   Discussion

Ground sloths are classified into the families Mylodontidae, Megatheriidae, Nothrotheriidae and Megalonychidae, all of which occurred during the Pleistocene and Holocene in North-, Central- and South America, including the Caribbean islands. All four families are reported from Mexico (Fig. 4; Table 1), with evidence dating to the Middle, and more so, to the Late Pleistocene. Only a few fossil findings provide evidence for the presence of earlier ground sloths, i.e. of Late Miocene or Pliocene ages. These refer to *Thinobadistes* (Mylodontidae), *Pliometanastes* (Megalonychidae) and *Zacatzontli* (Megalonychidae).

During the Pleistocene, the giant Megatheriinae *Eremotherium laurillardi* had one of the widest geographical distributions of all North- and Central American sloths (Cartelle and De Iuliis, 2006; Dávila et al., 2019; Larmon et al., 2019). *Eremotherium* was a common faunal constituent in Mexico occurring along west-central Mexico (Fig. 4). Less common, the Mylodontidae *Glossotherium robustum, Paramylodon harlani* and the Megalonychidae *Megalonyx jeffersonii* (McDonald, 2002) had a similar west-central distribution along the Valley of Mexico (Fig. 1, Table 1). *Nothrotheriops shastensis* (Nothrotheriidae) has been reported from the United States, Mexico and Belize (De Iuliis et al., 2015), with a wide distribution along the Sierra Madre Oriental (Fig. 4).

The geographical distribution of ground sloths in Mexico correlates with the palaeoenvironment, i.e. habitat preferences and resources. There is a "palaeogeographical overlap", an area in which most ground sloth families co-occur, reaching from the Valley of Mexico across the federal state of Jalisco to the western lowlands. All ground sloth families (see Fig. 4 and Table 1), including the Pliocene Megalonychidae (*Pliometanastes* and *Zacatzontli*), were reported from the federal state of Jalisco (McDonald and Carranza-Castañeda, 2017; Stinnesbeck et al., 2018b). The Guadalajara basin, a depression surrounded by high volcanic mountain chains, exhibited gallery forests with lakes and extended river systems. Palaeolakes in the area include Zacoalco and Sayula, but also Lake Chapala was twice the size that it is today and connected to other lakes in Jalisco. Pleistocene fossil assemblages from the area are diverse and include proboscideans (*Mammuthus* sp., *Cuvieronius* sp., *Stegomastodon* sp.), capybaras (*Neochoerus* sp.), deers (*Odocoileus* sp., *Cervus* sp.), horses (*Equus* sp.), tapirs (*Tapirus* sp.), camels (*Hemiauchenia* sp., *Camelops* sp.) and Xenarthra (*Glyptotherium* sp., *Eremotherium* sp., *Megalonyx* sp., *Paramylodon* sp., *Nothrotheriops* sp.). The abundance of *Eremotherium laurillardi* in the fossil record of the

region is particularly notable (Lucas, 2008; Lucas and Sullivan, 2018; Stinnesbeck et al., 2018b).
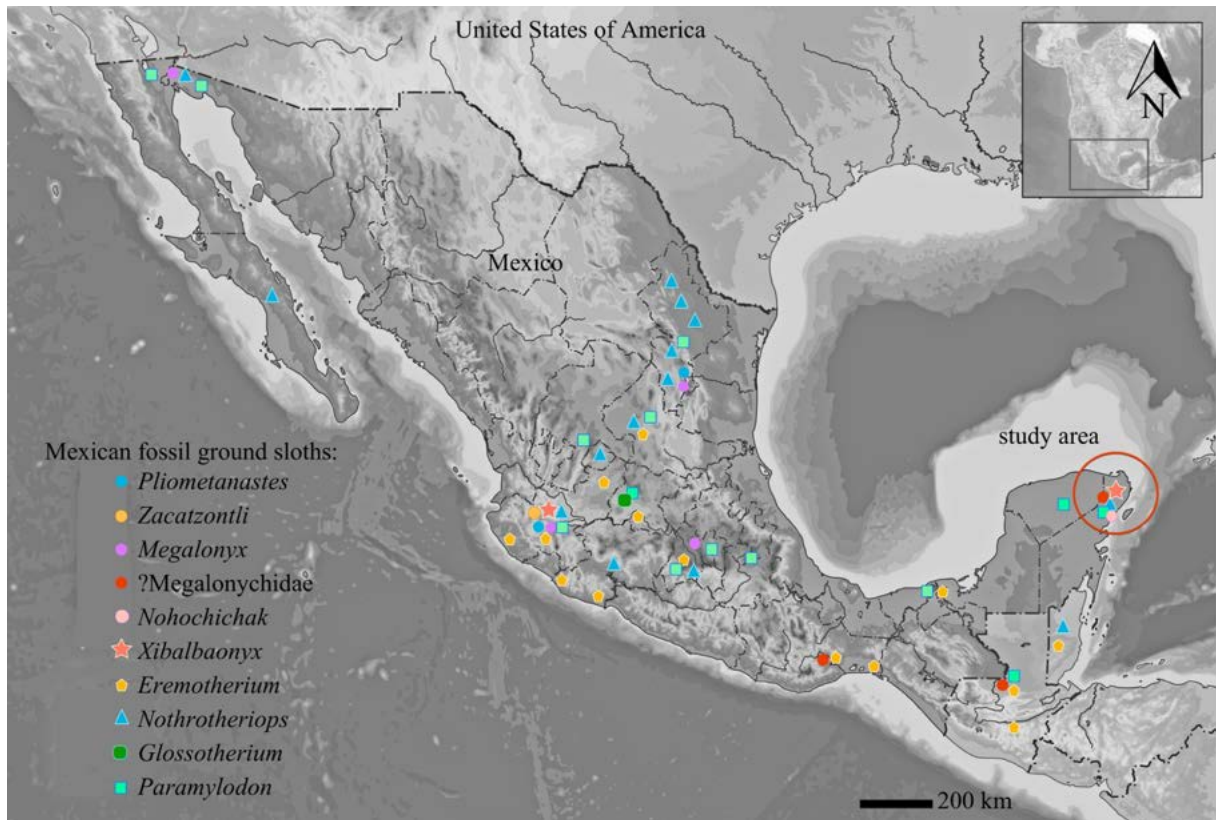

Fig. 4: Mexican ground sloth distribution. For exact location see Table 1.

Megalonyx, *Paramylodon* and *Eremotherium* inhabited riparian habitats (Hoganson and McDonald 2007). They favoured large gallery forests, with meandering river systems, with *Paramylodon* feeding on tussock and other grasses along the rivers, and *Eremotherium* and *Megalonyx* on deciduous trees, e.g. oak. Coprolites and isotope analyses from the US (Arizona, New Mexico) revealed that *Nothrotheriops shastensis* fed on xeric vegetation, such as *Yucca* sp. and other shrub land plants, suggesting an adaption to xeric environments (Poinar et al., 1998; Poinar and Kuch, 2003). This explains the explicit eastern distribution of the taxon along the Sierra Madre Oriental, close to the Mexican Gulf Coast and as far south as the Yucatán Peninsula.

4.1   Ground sloths on the Yucatán Peninsula

The Yucatán Peninsula exhibits a diverse ground sloth assemblage, with Megalonychidae and Nothrotheriidae being particularly abundant (Table 2). In the study area between Puerto Morelos and Tulum, ground sloths are now positively identified from at least 20 palaeontological localities (Fig. 5). Nothrotheriidae are represented by the Shasta ground sloth, *Nothrotheriops shastensis* and a yet undescribed species (Fig. 6). Two new genera and three species were documented and described within the family Megalonychidae, among them *Nohochichak xibalbakah* (McDonald et al., 2017), *Xibalbaonyx oviceps* (Stinnesbeck et al., 2017a) and *Xibalbaonyx exinferis* (Stinnesbeck et al., 2020b).
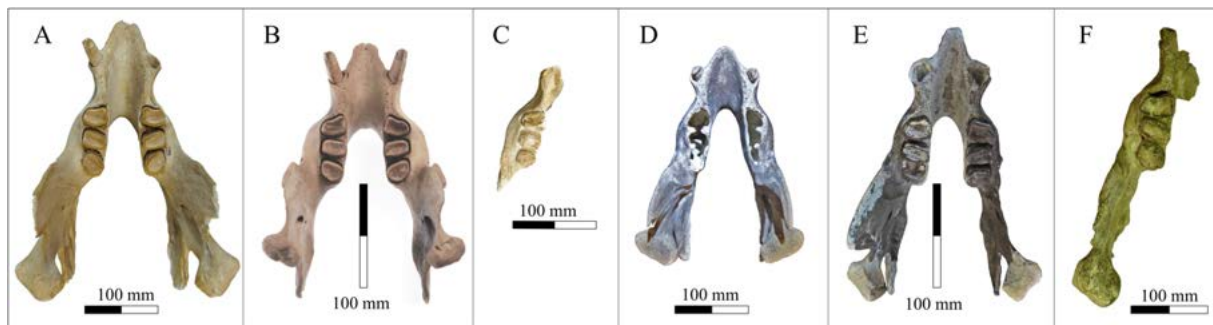

Fig. 5: Ground sloths from west-central and south-eastern Mexico and Central America. Mandibles in occlusal view: Unpublished adult individual from cenote Tortugas (A), *Xibalbaonyx oviceps* from El Zapote cenote (B), *X. exinferis* from cenote Tortugas, *X. microcaninus* from Jalisco (D), *Nohochichak xibalbakah* from Hoyo Negro (E) and *Meizonyx salvadorensis* from El Salvador (F). Note the overall similar morphology of the Mexican taxa (A-E), especially the ground sloths from the YP (A-C and E).

Nohochichak xibalbakah has been described based on the skull and mandible (Fig. 5E) from the sinkhole Hoyo Negro near Tulum (McDonald et al., 2017). The postcranial skeleton is still in the cenote and has not been published.

The original description of the megalonychid *Xibalbaonyx oviceps* (Fig. 3) was based on a complete skull and mandible (Fig. 5B) from the El Zapote cenote, located about 18 km west of Puerto Morelos (Stinnesbeck et al., 2017a). The postcranial skeleton, which has been documented recently, suggests that *Xibalbaonyx oviceps* was a medium sized animal of two metres length and approximately 200 kg weight (Stinnesbeck et al., 2020a submitted).

X. exinferis (Fig. 5C) from cenote Tortugas, only 2 km north-west of El Zapote cenote, has been described based on a fragmentary left mandibular ramus, humerus and an atlas (Stinnesbeck et al., 2020b).
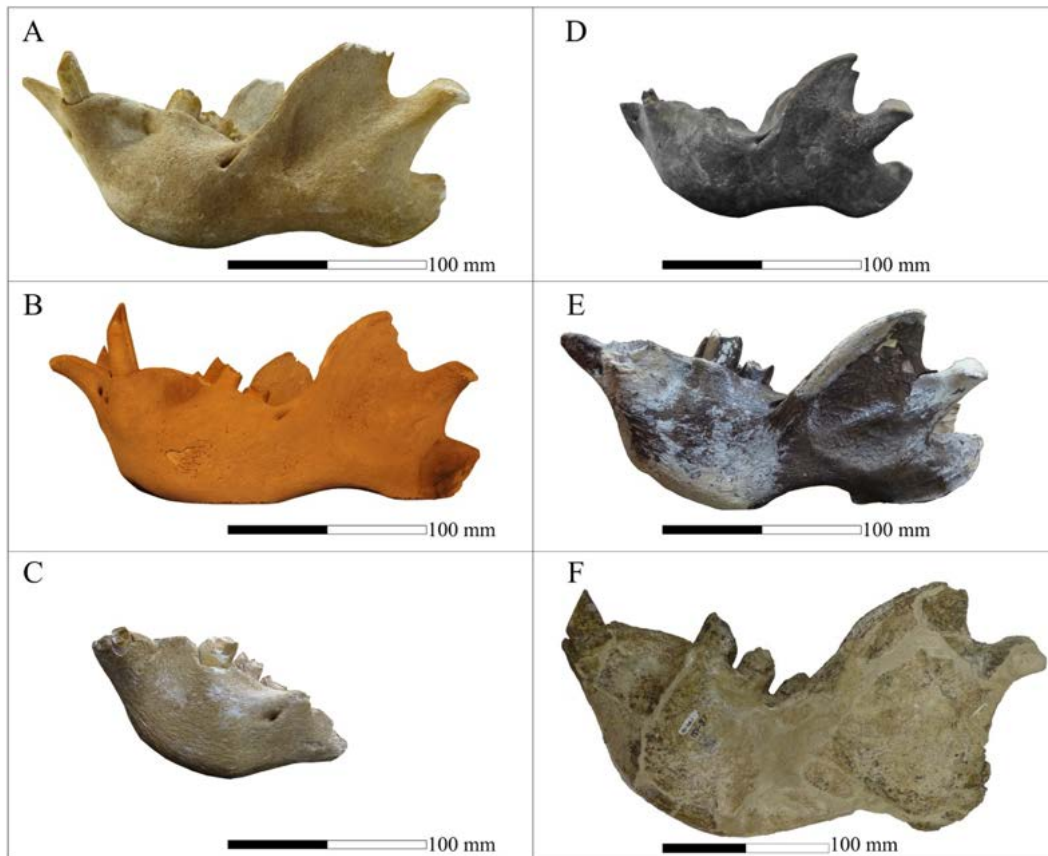

Fig. 6: Mandibles of Mexican and Central American ground sloths, all in lateral view. Unpublished adult individual from cenote Tortugas (A), *Xibalbaonyx oviceps* from El Zapote cenote (B), *X. exinferis* from cenote Tortugas, *X. microcaninus* from Jalisco (D), *Nohochichak xibalbakah* from Hoyo Negro (E) and *Meizonyx salvadorensis* from El Salvador (F).

According to the unfused cranial and postcranial sutures, both *Xibalbaonyx* species are interpreted as juvenile to subadult individuals (Stinnesbeck et al., 2020b, 2017a), while the Hoyo Negro individual (Fig. 6E) represents an adult specimen (McDonald et al., 2017). The ontogeny, sexual dimorphism and intraspecific diversity were discussed within the genus *Xibalbaonyx* and the ground sloths of the YP (Stinnesbeck et al., 2020b, 2017a). No sexual dimorphism was identified, while interspecific diversity is difficult to assess, since all collected specimens from the cenotes (Figs. 5, 6 and 7) represent new taxa. Although the overall cranial morphology of the Quintana Roo megalonychids is similar (Figs. 5 and 6),

generic and species differentiation is unequivocally possible based on the precise location and morphological shape of the mandibular foramen, the size of the caniniforms, and the number and location of mental foramina (Stinnesbeck et al., 2020b, 2018a). This osteological evidence is confirmed by the phylogenetic analysis (McDonald et al., 2017; Stinnesbeck et al., 2020b, 2018a). Based on the cranial features, a close relationship existed on the generic level between *Xibalbaonyx* and *Nohochichak* (Figs. 5 and 6).

It is important to note that abundant new postcranial material is now available from the cenotes El Zapote and Tortugas. Even though documentation of this material has not been completed yet, it becomes evident that, in addition to the above taxa of fossil ground sloths several other yet unpublished genera and species must have populated the area.
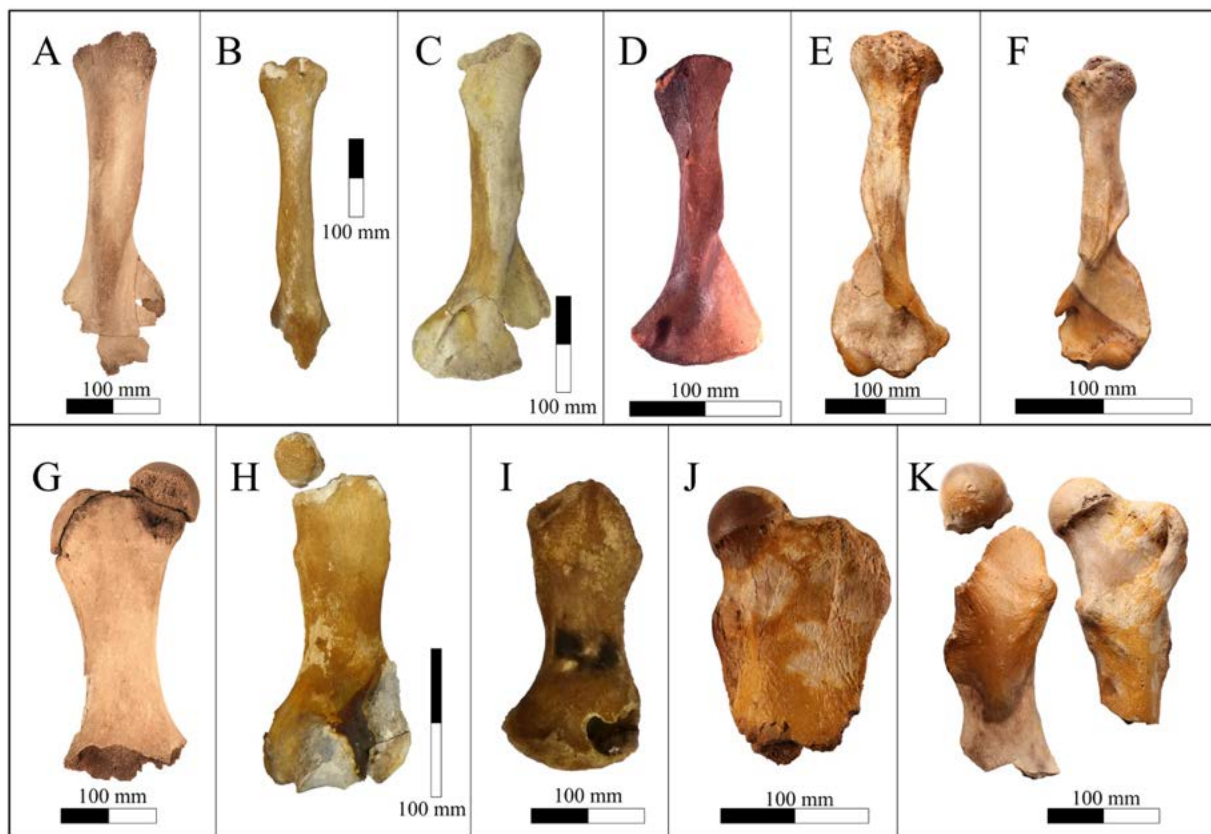

Fig. 7: Ground sloth humeri (A-F) and femora (G-K) of Megalonychidae from El Zapote cenote and cenote Tortugas (for exact location of the palaeontological sites see Fig. 2). *X. oviceps* (A, G), unpublished adult (B, H) and infant (I) individuals from El Zapote cenote. Unpublished infant (D), giant adult (E, J) and dwarf adult (F, K) individuals from cenote Tortugas. Note the strong morphological differences in the shape of the humeral and femoral diaphyses, processi, muscle attachment areas and body size.

For example, figure 7 shows five individuals of Megalonychidae recently collected from the El Zapote and Tortugas cenotes, based on a) the humerus (Fig. 7 upper row) and b) the femur (Fig. 7 lower row). The two localities are only separated by about 1 km distance (Fig. 2). The long bones of *X. oviceps* from El Zapote are illustrated in Fig. 7 (A: humerus and G: femur), one unpublished subadult to almost mature individual with slender fore- and hindlimbs (Fig. 7B, H) from El Zapote cenote, as also a femur from an infant from El Zapote cenote (Fig. 7I), humeri and femora of infant (Fig. 7D), juvenile (Fig. 7C) and mature (Fig. 7E and J) individuals from cenote Tortugas including *X. exinferis* (Fig. 7C). Among these specimens a mature specimen only reaches half the size of the juvenile *X. oviceps* and presents pronounced processes (Fig. 7F and K), whereas an infant individual (Fig. 7D) is characterized by different process developments along the long bones. Clearly, the long bones illustrated here from a single small cluster of cenotes represent a wide range in body sizes and distinct ontogenetic stages. More importantly, they also differ markedly in the development of muscle attachment areas (e.g. deltoid process) leading to different morphological shapes. This is reflected, among other features, by the development of the deltoid process and the deltopectoral plate, which range from faint muscle attachment areas to double crested diaphyses. The femura show a similarly wide morphological range. The unpublished specimens illustrated in Fig. 7F and K thereby indicate different types of locomotion and probably also feeding options, which are independent from ontogeny or gender. This suggests that the family Megalonychidae was extremely diversified on the north-eastern Mexican Yucatán Peninsula as a result of isolation and habitat splitting.

4.1.1   The ground sloth *Xibalbaonyx*: Anatomy, locomotion and behavioural interpretations

To date, the genus *Xibalbaonyx* is represented by three species, *X. microcaninus* (Stinnesbeck et al., 2018b) from the state of Jalisco in western Mexico, and two species from Quintana Roo: *X. exinferis* (Stinnesbeck et al., 2020b) and *X. oviceps* (Stinnesbeck et al., 2020a, 2017a).

X. microcaninus (Stinnesbeck et al., 2018b) is only known based on a skull and mandible (Figs. 5D, 6D); no postcranial material has yet been found. The species differs from *X. oviceps* in the small conical caniniforms (Fig. 6D), and temporal lines and nuchal crest which

are more pronounced in the Jalisco specimen. The temporal lines converge caudally and fuse with the nuchal crest in *X. microcaninus*, while they join with the dorsal margin of the zygomatic process of the squamosal in *X. oviceps,* running parallel to the nuchal crest (Stinnesbeck et al., 2018b). The coronoid process of the mandible is hook-shaped in *X. microcaninus* (Fig. 6D). This suggests a more powerful m. temporalis compared with that of *X. oviceps*, and likely a retraction movement of the mandible at the end of the occlusion phase. The pterygoids are ventrally elongated in *X. microcaninus*. The elongation serves to connect the m. pterygoideus medialis and m. pterygoideus lateralis with the condylar and angular processes of the mandible. These muscles, together with the m. masseter, are jaw adductors and provide lateral and longitudinal movements of the jaw for mastication. The functional-morphological differences of the caniniforms as well as the different spout size relative to the mandibular length suggest that *X. microcaninus* and *X. oviceps* differed from other megalonychids in the style of occlusion and thus food sources. The anatomical differences strongly support an allopatric specification of the genus *Xibalbaonyx* with respect to the vegetation, which differed between the Yucatán Peninsula and the Chapala basin of Jalisco (see above).

X. exinferis (Stinnesbeck et al., 2020b) has been described based on a fragmented mandibular ramus (Figs. 5C and 6C), and an associated atlas and humerus (Fig. 7C). *X. exinferis* differs from other megalonychid ground sloths by a mesiobuccally oriented lower caniniform of triangular occlusal shape and cross-section. The lower caniniform represents the smallest mandibular tooth, reaching about one fourth the size of m1. The symphyseal spout reaches less than 15% of the spout to tooth-row length (Fig. 6C). Two mental foramina are present on the rostral and lateral face of the symphyseal spout, one of which is located medially on the rostral surface of the spout; it is thus only visible in rostral view. The second foramen is located on the dorsolateral margin of the spout adjacent to the caniniform. The diastema reaches to 35% of the entire tooth-row length, including the caniniform. A mandibular foramen pierces the dorsolateral third of the mandibular ramus (Stinnesbeck et al., 2020b).

X. oviceps (Stinnesbeck et al., 2020a, 2017a) is the most complete ground sloth skeleton found in the area and has been described based on cranial (Figs. 3, 5B, 6B) and some postcranial material (Fig. 7A and G). *X. oviceps* was a medium-sized ground sloth of approximately 200 kg weight. The humerus is at least 10% longer than the humerus CPC-2776 assigned to *X. exinferis* (Figs. 7C). Both humeri belong to juvenile or subadult

individuals. However, *X. exinferis* is smaller and, according to the humerus, stouter than *X. oviceps*. Especially, the deltoid crest of the humerus is more prominent in *X. exinferis* than in *X. oviceps*, compared to the length of this bone, as preserved. Additionally, the pectoral tuberosity, in the latter taxon, almost lines up with the medial margin of the humeral shaft, while in *X. exinferis* the pectoral crest follows the long axis of the shaft and does not run medially.

X. oviceps exhibits pronounced pectoral and deltoid tuberosities or ridges suggesting powerful arm abductors. Also, features such as a teres major fossa reaching 8-10% of the scapular length and a posterior process of the scapular spine suggest additional adductor of the humerus and lateral rotator of the arm and therefore a highly mobile shoulder girdle. The scapula, humerus, radius and ulna suggest broad muscle attachment areas for manus and forearms with a high flexibility and wide range in motion, as often documented in semi-arboreal to arboreal animals (Stinnesbeck et al., 2020a).

The femur of *X. oviceps* is thus not only shorter but also more gracile than that of other adult Megalonychidae. The femoral head lacks a fovea capitis, suggesting that the teres femoris ligament was feeble. A weak teres femoris ligament, which is expressed by a small, shallow pit on the head of the femur, leads to a greater range in lateral femur motion. Owen (1842) already postulated that this feature could be an advantage in climbing sloths.

Compared to *Megalonyx*, the femur in *X. oviceps* is proximodistally and mediolaterally slender and consequently, the quadriceps muscle attachments are not as developed as in *Megalonyx jeffersonii*. The femoral strength coming from the vastus muscles (e.g. m. quadriceps) therefore plays a minor role in *X. oviceps*, as usually documented for ground sloths. The development of the m. quadriceps in *Megalonyx* supports a low gravity centre coupled with a femur showing anterolaterally, which gives the animal a wide stance. This morphological difference in the femur suggests that the centre of gravity was higher in *X. oviceps*.

The tibia is half the length of the femur, while in most other ground sloths this bone reaches three-fourths of the femur length. Although neither the distal end of the femur, nor is the proximal articular area of the tibia preserved, the compact and broad diaphysis of the tibia and the posterior convexity offer insertion surfaces for the m. tibialis posterior and for mm. flexores digitorium lateralis et medialis. These muscles are vital for stabilization and flexion of the knee joint, as well as plantar flexion of the pes.

The postcranial material of the holotype of *X. oviceps* provides evidence that the forelimbs were slightly longer than the hind limbs resulting in a caudally sloping position of the back.

This makes obligatory bipedalism impossible but does not hinder a rearing-up. *X. oviceps* had the ability to pull down branches to get in reach of leaves, fruits and inflorescences. However, the forearm musculature and hip joint indicate a significantly higher degree of liberty than usually seen in large terrestrial ground sloths (Stinnesbeck et al., 2020a).

The ability of grasping is documented for extant Xenarthra, such as armadillos, anteaters and sloths, although reflecting different behaviour patterns. For example, armadillos and anteaters use a hook-and-pull technique to excavate tubercles (Amson et al., 2015; Gaudin et al., 2018). The hook-and-pull digging-technique means that the animals hack with their long claws in a mound and pull the soil etc. towards their body (Straehl et al., 2013). The ability of grasping is therefore often connected with digging.

However, grasping is also needed for rearing of the young and has been documented in sloths and anteaters which cling on their mother's body (Gaudin et al., 2018; Grass, 2019). Nevertheless, *Xibalbaonyx* (both *X. exinferis* and *X. oviceps*) were large-sized animals with a body weight of 80-200 kg. They were too large and heavy for grasping on their parents. This would have been a possible behaviour for small-sized sloths, such as for the infant individuals from cenote Tortugas and El Zapote (Fig. 7D and I) reaching approximately 30-60 kg weight. Grass (2019) discusses the possibility that young ground sloths grasped on their mother´s abdomen or back, as is seen in juveniles of extant sloths and other Xenarthra. This scenario may also have been possible for infant *X. oviceps*, as suggested by the configuration of the shoulder musculature. This specimen was a subadult and it is therefore possible that the ability to climb was lost when the animal reached an adult stage, as interpreted for the terrestrial ground sloth *Megalonyx* (Holte, 2012). Clearly, the locomotion of *Xibalbaonyx* differed from that of extant sloths which are almost exclusively arboreal animals. Nevertheless, the bone reliefs and the reconstruction of muscle origin and insertion areas suggest that *X. oviceps* was capable to grasp and climb. Juvenile to subadult individuals probably used the well-developed forelimb to overcome steep slopes and perhaps even climb the rocky walls of cenotes (Stinnesbeck et al., 2020a).

Ground sloth fossils have often been found in caves, such as in Rampart Cave in Arizona, USA (Thompson et al., 1980; McDonald and Jefferson, 2008), San Josecito Cave in the state of Nuevo León in north-eastern Mexico (Stock, 1943), and the Cueva del Mylodon in southern Chile (Martin et al., 2013). Several authors have discussed the possibility that ground sloths used the caves as dens or shelters for protection against predators (McDonald,

1977; Holte, 2012), or to maintain their body temperature stable (Hansen, 1978; Vizcaíno et al., 2001; Toledo et al., 2017). Ground sloths have been interpreted as animals with a low metabolism rate, resembling their extant relatives (McNab, 1985; McDonald, 2005; Cliffe et al., 2015). The scenario that ground sloths passed part of their life in caves is supported by findings of complete and articulated skeletons in the cave systems of Quintana Roo, contrary to other megafaunal fossils which are all highly fragmented and only documented by single bone findings. These articulated ground sloth skeletons discovered in deep parts of the caves, hundreds of metres away from the next cenote entrance, suggest that these individuals died in situ.

The South American Mylodontidae have been interpreted as burrowers, and some authors even suggested that they dug long tunnels in Argentina and Brazil (Vizcaíno et al., 2001). This latter scenario can be excluded for *Xibalbaonyx* from Quintana Roo, due to the absence of soft sediment overlying the limestone bedrock in the area. Rather, it is thus likely that the YP ground sloths used the caves and sinkholes as dens, as water source, and as a save area to rear their babies.

A total of six infant and juvenile to subadult individuals were reported in 2 fossil localities (cenote Tortugas and El Zapote cenote) out of 20. Even though there are adult specimens among the findings, the fossils represent different ontogenetic stages at the time of death, with a dominance of juveniles. This suggests that the caves were likely used as a save nursery. At Tortugas, for example, two mature individuals were found in addition to several infant specimens and juveniles. At nearby El Zapote, an infant, a juvenile to subadult, and single bones of an adult individual were identified. For both cenotes, the use as a nursery is implied by mature individuals and their infants.

11 out of 20 palaeontological localities analysed here from Quintana Roo yielded ground sloth remains (Table 2). These animals are therefore over-represented in the megafaunal assemblage of the YP. In contrast to all other taxa identified from the area, they are often found in situ and skeletons are partially to fully articulated, different to proboscideans, equids, camelids, ursids, felids and tayassuids, which are majorly represented by single, isolated bones, mostly from wash-in events. The differences between single bones findings of other taxa and fully articulated skeletons of ground sloths, underlines the hypothesis that ground sloths actively used the caves and sinkholes as nurseries, or as dens.

4.1.2 Pathologies

Xibalbaonyx oviceps from El Zapote cenote exhibits an asymmetrical atlas, with the left wing differing strongly from the right one. In caudal view, the different inclination of the wings is well visible, as also the asymmetrical vertebral canal, suggesting irritation of the transverse nerves and vertical canal. Other vertebrae also seem to be affected by asymmetry, although their remains are too fragmented to allow for a final decision. A left/right asymmetry has also been documented in an atlas from cenote Tortugas, referred to *X. exinferis* (Stinnesbeck et al., 2020b). Pathologies such as joint diseases, and bone erosion, such as arthrosis and arthritis, have numerously been reported for ground sloths (de Souza Barbosa et al., 2016; Andrade et al., 2019). Left or right asymmetries are documented as a case of degenerative enlargement or bone spur, e.g. osteophytes (Andrade et al., 2019), but they are also known as inborn defects (Böhmer et al., 2018). In the El Zapote sloth, an erosive disease as a result of aging process is excluded, because the animal was subadult. Furthermore, preservation of the vertebrae is excellent, which would not be the case in bone diseases aligned with aging, trauma or other degenerative processes. It is therefore suggested that the pathology identified in the atlas of *Xibalbaonyx oviceps* represents a congenital anomaly of the cervical vertebrae (Stinnesbeck et al., 2020a). Congenital vertebral anomalies are often caused by genetics or environmental factors, such as stress, malnutrition, inbreeding etc. (Frankham, 2005; Reumer et al., 2014). Slight deformations of the atlas in extant tree sloths (Böhmer et al., 2018) appear to be a common feature and have been interpreted as a mutation (hox gene), which is detected not only in this group but also other Xenarthra, and more general, in mammals with a reduced number of vertebrae including manatees and dugongs (Varela-Lasheras et al., 2011; Böhmer et al., 2018).

Another ground sloth with evident pathologies is a yet unpublished nothrotheriid from cenote Tortugas (Fig. 6). The specimen was discovered as a partially articulated skeleton on the debris mount of the cenote, suggesting that the animal either fell into the sinkhole and died there, or that the carcass lying near the sinkhole opening was washed into the cenote prior to skeletonization. The skull is completely preserved but deformed. Frontals and parietals are strongly convex and protruding, a symptom of hydrocephalus. All cranial sutures are asymmetrical especially in the maxilla, the palatine, choanae, vomer and basioccipital, thereby indicating a congenital anomaly, probably during embryogenesis. The unfusing of cranial sutures during embryonic development often results in orofacial clefts. Clefts of lip and palate are one of the most common craniofacial disorders in humans, but they are also

well documented in domestic animals (Baker et al., 1961; Mulvihill, 1972; Moritomo et al., 1999; Jackling et al., 2011). Some exhibit a hydrocephalus (Robertson et al., 1966), but this latter pathology also stands by its own.

Fig. 8: *Nothrotheriops* sp. skull from cenote Tortugas (A) in lateral view, compared with a skull of *N. shastensis* from Rancho la Brea, Los Angeles, USA (B). Note the inflated cranium in the individual from cenote Tortugas (A).

Even though the nothrotheriid documented here does not show a cleft, this disturbance was probably the reason for the hydrocephalus development. Hydrocephalus is built-up during embryogenesis by fluid that normally surrounds and contains the brain. In this case, brain water builds up in the four inner cavities of the brain instead of flowing into the space between the meninges (subarachnoid space). Because the skull is still soft during embryogenesis, the head expands in order not to damage the nerves. This is the reason why adult animals will not exhibit a domed skull as seen in Fig. 6. The increased pressure causes the head to swell and damages brain tissue, which is extremely painful. Most humans and

animals affected by this pathology therefore show signs of neurologic dysfunction related to the dilated ventricles, e.g. ataxia.

Hydrocephalus has been reported in wild life animals (Kübber-Heiss et al., 2009), although the pathology is uncommon there, probably due to the neurological dysfunctions. The animals do not survive in the wild for long and juveniles are even abandoned by their mothers (Kübber-Heiss et al., 2009).

Congenital anomalies in the fossil record are scarce, but vertebral and genomic anomalies have been documented in small populations of Neanderthals (Ríos et al., 2019), mammoths (Reumer et al., 2014; Fry et al., 2020), horses (Griffin et al., 2016) and woolly rhinoceros (van der Geer and Galis, 2017). For example, the genome of latest mammoths from the North Sea suggests that hydrocephalus was a common pathology among these animals (Reumer et al., 2014).

Climatic oscillations leading to vegetation changes and subsequent habitat reduction have been identified as a main factor for megafaunal extinction towards the end of the Late Pleistocene. However, dynamics are difficult to verify in these late megafaunal populations and fossil evidence is sparse. It is evident that ecological changes often result in a reduction of the main population. This process is documented for fossil and extant island populations. For instance, dwarfism is proved for island populations of mammoths (Guthrie, 2006; Vartanyan et al 2008, van der Geer et al., 2018), woolly rhinoceroses (Stuart and Lister, 2012; Markova et al., 2013), and ground sloths (MacPhee, 2009). Recent research shows that not only body size changes, but also pathological deformations of the skeletons increase in number, probably due to inbreeding (van der Geer and Galis, 2017). In fact, the DNA of the last Wrangel Island (Siberia) mammoths shows a high degree of mutations (Vartanyan et al., 1993; Palkopoulou et al., 2013; Rogers and Slatkin, 2017; Fry et al., 2020), indicating that habitat reduction leading to small population sizes had a pronounced effect on the survival, and extinction, of this isolated population. When populations are already small, this leads to reduced genetic flux and, as noted by Rogers and Slatkin (2017), to "genetic meltdown". Faunal inbreeding is a problem frequently seen in captured animals, or small populations of wild life animals (Sacchei et al., 1998; Collevatti et al., 2007; Osborne et al., 2016); it has been also been discussed as a factor for Neanderthal extinction (Ríos et al., 2019).

In this case, the study area is part of the Mexican mainland and not an island, but the abundance of morphologically similar ground sloth species as well as pathological features as

discussed above, suggest that inbreeding was an important ecological factor in terminal ground sloth populations of north-eastern Yucatán Peninsula, as will be discussed below.

4.2   The Late Pleistocene palaeoenvironment of the north-eastern Yucatán Peninsula inferred from the faunal assemblage

The Late Pleistocene faunal assemblage in Quintana Roo (Table 2) includes the gomphotheriid *Cuvieronius hyodon*, horses (*Equus* sp.), tapirs (*Tapirus* sp.), llamas (*Hemiauchenia* sp.), peccaries (*Muknalia minima*, *Pecary tajacu*), cervids (*Odocoileus virginianus*, *Mazama* sp.), felids (*Smilodon fatalis*, *S. gracilis*, *Lynx rufus* and *Panthera balamoides*), canids, bears and ground sloths (*Nothrotheriops shastensis*, *Xibalbaonyx oviceps*, *X. exinferis, Nohochichak xibalbakah*) (Gonzalez et al. 2008; 2013; Chatters et al. 2014; McDonald et al. 2017; Stinnesbeck et al. 2017a, b, 2018).

Ground sloths have been reported from 11 out of 20 underwater localities in Quintana Roo and represent >50% of the faunal assemblage. Although taxonomic diversity is likely higher, four taxa have already been positively identified, among them the Shasta ground sloth, *Nothrotheriops shastensis*. This taxon was widely distributed throughout North America, including Mexico (McDonald, 2002) and Belize (De Iuliis et al., 2015). Its absence in Guatemala is noteworthy (Dávila et al., 2019) because it suggests that *Nothrotheriops* may not have entered Central America (Fig. 4). To date, there are no fossil findings of the taxon from this region, or further South (Dávila et al., 2019). The presence of seeds and leaves of *Yucca* in coprolites attributed to *Nothrotheriops shastensis* from Arizona suggests a dry xeric shrub habitat preference (Poinar et al., 1998; Hofreiter et al., 2000; Poinar and Kuch, 2003). Hansen (1978) stated that the Shasta ground sloth occupied a wide range of seasonal food and may therefore represent a browser to mix-feeder and not necessarily a specialist of semi-arid environments (Hansen, 1978). In Mexico, *N. shastensis* has been reported from north-eastern, central, west-central and south-eastern Mexico (e.g. Nuevo León, Jalisco, Quintana Roo, see Fig. 4 and Table 1).

Megalonychid ground sloths are represented by *Nohochichak xibalbakah* (McDonald et al., 2017), *Xibalbaonyx oviceps* (Stinnesbeck et al., 2020a, 2017a) and *X. exinferis* (Stinnesbeck et al., 2020b). As already noted in chapter 4.1, abundant unpublished ground sloth material is available from the Quintana Roo caves, which indicates that the diversity of megalonychid

sloths of this area was even notably higher than what is documented to date. In addition, the number of fossil individuals is also higher: Remnants of megalonychids outrange those of Nothrotheriidea by three times, but there are only three localities (yet), in which both families co-occur: Concha, Hoyo Negro and cenote Tortugas (Table 2). A similar numeric relation between *Nothrotheriops* and Megalonychidae has been documented previously for North American faunal assemblages, with *Megalonyx jeffersonii* as a counterpart to *N. shastensis*, e.g. during the Middle and Late Pleistocene. According to McDonald (2005), in the case of co-occurrence of *Nothrotheriops* and Megalonychidae, one of the taxa is often significantly more abundant than the other. This has been interpreted to be the result of similar nutritional needs. It has been suggested that both fed on the same plants, although on different parts (McDonald, 2005). In the case of Quintana Roo, *Xibalbaonyx* may have occupied a comparable ecological niche to that of *Megalonyx* in North America. *Xibalbaonyx* has been referred to as a browser (Stinnesbeck et al., 2018a, 2017a), as the Shasta ground sloth. This interpretation is based on similar dental features.

Other taxa are under-represented and most are only known from isolated findings (Table 2). Apart from ground sloths, *Equus* sp. is the most common taxon on the YP and is reported from five out of 20 sites, while *Hemiauchenia* is documented in three localities, Caracoles y Camellos, La Chimenea and Canún (Table 2). *Tapirus* sp. has only been found at Nai Tucha, and at Carcoles y Camellos (González González et al., 2013). The proboscid *Cuvieronius* is only reported by single findings of four out of 20 localities on the YP (González González et al., 2013; Chatters et al., 2014). Although, *Cuvieronius* had a wide geographic distribution reaching from the southern US (e.g., Florida) through the Veracruz coastal region of the Mexican Gulf coast plain, to Central America (e.g. Guatemala, El Salvador, Nicaragua, Costa Rica and Panama), and South to Ecuador, Bolivia and Peru in South America (Webb and Perrigo, 1984; Lucas et al., 1999; Cisneros, 2005; Mothé and Avilla, 2015; Dávila et al., 2019). *Cuvieronius hyodon* has been interpreted as a mixed feeder (Prado et al., 2005; Mothé and Avilla, 2015; Dávila et al., 2019) characterized by a dentition consisting of six pairs of upper and lower molars (Ferretti, 2008; Mothé et al., 2013).

Glyptotherium is a rare taxon in the study area and was only reported based on a single armor fragment from Canún in the federal state of Yucatán (Table 2). This rare occurrence on the YP contrasts with the abundant findings of *Glyptotherium* in western Mexico (e.g. Jalisco), Guatemala (Dávila et al., 2019), Honduras and El Salvador (Webb and Perrigo, 1984; Cisneros, 2005).

The cervid *Odocoileus virginianus* is only reported from one locality in Quintana Roo. This is surprising, since *Odocoileus* is numerically abundant in Guatemala (Dávila et al., 2019), El Salvador (Cisneros, 2005), Honduras (Webb and Perrigo, 1984), Panama and Nicaragua (Page, 1978; Lucas, 2014) and is also today a common taxon.

The faunal assemblage identified in the submerged caves of Quintana Roo is comparable to findings from Central America, for example Guatemala (Woodburne, 2010; Dávila et al., 2019). Nevertheless, different from Guatemala and other Central American countries, large carnivores are present on the Yucatán Peninsula, including *Protocyon*, *Smilodon*, *Arctotherium* and *Panthera balamoides* (Stinnesbeck et al., 2018c; Schubert et al., 2019), as well as middle to small-sized faunal elements, mostly peccaries (*Muknalia minima*, *Pecari tayassu*), bats and rodents. Therefore, a collection bias due to taphonomic circumstances etc. can be excluded for the study area, which is present and has been discussed for Central America, e.g. Guatemala (Webb and Perrigo, 1984; Lucas et al., 1997; Lucas, 2014; Dávila et al., 2019).

However, when compared to the faunal assemblage of central Mexico and Central America, certain taxa are absent in the study area, suggesting that the environmental circumstances were not suitable for every taxon. This is particularly striking in the case of the proboscideans. For example, *Mammuthus primigenius, M. columbi* or *Mammut americanum*, which had a wide distribution throughout North America, have not been reported from the YP, even though *Mammuthus primigenius* has even been reported from Central America, e.g. Guatemala, El Salvador, Nicaragua and Costa Rica (McDonald and Dávila, 2017; Dávila et al., 2019). Dentition, coprolite analyses and mummified corpses have indicated that *Mammuthus* was a highly specialized forb grazer, e.g. *Artemisia* (Kosintsev et al., 2012). *Mammut americanum* on the other hand, has been interpreted as mixed-browser (Pérez-Crespo et al., 2016).

The Panamerican giant ground sloth *Eremotherium* is another prominent taxon absent on the YP. *Eremotherium* had a wide distribution in west-central Mexico, Central- and South America (McDonald, 2002; Stinnesbeck et al., 2018b; Dávila et al., 2019; Larmon et al., 2019), but the taxon was a high browser (McDonald, 2005; Cartelle and De Iuliis, 2006) and the low xeric shrub on the YP was likely not a suitable food reservoir for these large-sized ground sloths. Other Xenarthra are extremely rare, such as the ground sloth *Paramylodon harlani* which has been reported so far only from the Loltún cave in Yucatán and Hoyo Negro

in Quintana Roo (Chatters et al., 2014), and the glyptodon *Glyptotherium* which has only been reported from a single locality in the federal state of Yucatán. *Glyptotherium* and *Paramylodon* likely populated water-rich areas, such as riparian forests and even swamps, rather than open grassland (Gillette and Ray, 1981).

The faunal composition detected in the cave system of northeastern Quintana Roo, allows for the following important conclusions:

(1) In contrast to south-central Mexico and Central America e.g. Guatemala and Belize, the faunal assemblage of the study area does not include specialized grazers and browsers, such as the proboscidean *Mammuthus primigenius* and the giant ground sloth *Eremotherium laurillardi*. Both taxa had a wide palaeogeographical distribution along the Mesoamerican Corridor and are well-known from west-central Mexico, Guatemala and Belize (Stinnesbeck et al., 2018b; Dávila et al., 2019; Larmon et al., 2019), but they are characteristically absent on the YP.

Grazers did occur in the area during the Late Pleistocene, such as *Equus* and *Hemiauchenia* (González González et al., 2008). However, they may have fed on a broader variety of plants than their modern equivalents and thus acted as generalists. *Hemiauchenia*, for instance, has been interpreted as an indicative element for xeric shrub environments (Yann et al., 2016). Nevertheless, Yann et al. (2016) documented that Pleistocene camelids were highly adaptable with regards to food, similar as coeval horses (Pérez-Crespo et al., 2018).

Unpublished ^{13}C analysis on teeth supports the interpretation that the faunal assemblage of the study area is characterized by opportunistic mix-feeders, including *Nothrotheriops shastensis*, *Equus* sp., *Tapirus* sp., *Hemiauchenia* sp. and *Cuvieronius hyodon*. These taxa are presently identified in 13 out of 20 palaeontological localities (Table 2). The analysis also suggest that *Xibalbaonyx* fed on C_3 plants. In fact, no evidence was yet detected in these Late Pleistocene taxa for the digestion of C_4 plants, suggesting a shrub- rather than grassland-dominated vegetation in the area.

A presence of opportunistic, mix-feeding taxa, rather than specialized grazers or browsers is well seen in the geographic distribution of *Nothrotheriops* and *Xibalbaonyx* in Mexico, which show overlaps with other ground sloth genera e.g. in Jalisco (McDonald, 2002;

Stinnesbeck et al., 2018b). In the study area of YP, however, ground sloths other than *Nothrotheriops* and megalonychids (e.g. *Xibalabonyx*, *Nohochichak*) are extremely scarce. The abundant and diverse fossil assemblage in the Chapala Lake area of Jalisco, west-central Mexico, on the other hand, includes a broad variety of proboscideans (e.g. *Mammuthus* sp., *Cuvieronius* sp., and *Stegomastodon* sp.), capybaras (*Neochoerus* sp.), armadillos and glyptodontids (*Glyptotherium* sp., *Dasypus* sp., *Holmesina* sp.), cervids (*Odocoileus* sp.), horses (*Equus* sp.), tapirs (*Tapirus* sp.), camelids (*Hemiauchenia* sp., *Lama* sp., *Camelops* sp.), and several members of North American ground sloths (*Eremotherium* sp., *Megalonyx* sp., *Paramylodon* sp., *Nothrotheriops* sp.). The abundance of *Eremotherium laurillardi* in the faunal assemblage suggests a rich arboreal vegetation (Lucas, 2008; Stinnesbeck et al., 2018b). The palaeoenviromental conditions in the Lake Chapala area of Jalisco must have been markedly different from those on the Yucatán Peninsula. The Chapala basin is surrounded by volcanic mountain chains of the Sierra Madre Occidental and the Neovolcanic belt. The palaeoenvironment was characterized by gallery forests with lakes, wide river systems with oxbows. Evidence for this large water areal, comes from the palaeolakes of the area, among them the predecessor of Lake Chapala, which was twice the size of the modern lake and was connected to other lakes in Jalisco (Schreiber, 2004).

On the other side, the low latest Pleistocene sea level, combined with extreme limestone karstification resulted in a dry surface and edaphic desert conditions on the northeastern Yucatán Peninsula with xeric shrub vegetation and reduced surface water availability. These palaeoenvironmental differences are mirrored by the cranial morphology of the ground sloths *X. microcaninus* from Jalisco and *X. oviceps* from Quintana Roo. The masticatory apparatus of *X. oviceps* and *X. microcaninus* suggests the presence of a strong m. masseter for the mediolateral and longitudinal mastication movements of the mandible. Different from *X. microcaninus*, however, a highly flexible muzzle and tongue is suggested based on the shape of the mandibular spout (Stinnesbeck et al. 2017). *X. oviceps* must therefore have been a more selective feeder, which probably used the muzzle and/or tongue to pick up fruits or leaves from xeric plants (Stinnesbeck et al., 2018b).

The faunal assemblage of the northeastern YP therefore includes opportunistic mix-feeders and excludes highly specialized taxa.

(2) The high percentage of endemic taxa.

The extraordinary high taxonomic diversity of megalonychid ground sloths in a small area reflects an extraordinary palaeoecological situation, as different species of ground sloths are rarely found in a single faunal assemblage, or small area (McDonald et al., 2013). Yet unpublished Sr-data indicate that these ground sloths did not migrate to Quintana Roo from other areas of the YP or central Mexico. Instead, they were born and passed their entire life in the region their skeletons were found. Based on the combination of low metabolism and slow absorption of nutrients, ground sloths probably had a small habitat radius when compared with proboscideans, equids, or bovids, which may migrate on a seasonally level and cover large habitat areas (McDonald and Pelikan, 2006).

Sympatric species, as seen in the diverse Megalonychidae of QR, did likely not use resources in the same way, because direct competition would result in the demise of both competitors (Guthrie, 2006). Rather, resource partitioning lowers competition among species sharing a habitat. It is therefore important to understand why the number of endemic ground sloth species is so high in this particularly small area.

4.3 Ecological factors which influenced ground sloth distribution, migration and local diversification in the Mexican Corridor

Periodic isolation of the Mexican YP is evidenced by a rapidly increasing number of endemic taxa documented from Quintana Roo. These include a small peccary, *Muknalia minima* (Stinnesbeck et al., 2017b), the megalonychid ground sloth taxa *Xibalbaonyx oviceps* (Stinnesbeck et al., 2020a, 2017a), *X. exinferis* (Stinnesbeck et al., 2020b) and *Nohochichak xibalbakah* (McDonald et al., 2017), and the extinct felid *Panthera balamoides* (Stinnesbeck et al., 2018c). Other new taxa have been discovered but are yet undescribed, such as the diverse material of megalonychid sloths from cenote Tortugas and El Zapote.

In addition to faunal endemism, skeletons of the first human settlers in the area also provide evidence for intermittent ecological separation of the north-eastern YP from the rest of the continent. Ten skeletons dating from the Latest Pleistocene to Early Holocene are presently known from the Tulum cave system (Fig. 2), and thus represent the largest assemblages of human skeletons of the American continent, including the oldest osteological human remains,

i.e. La Niña from Chan Hol 2, Eve of Naharon and Naia from Hoyo Negro (Chatters et al., 2014; González González et al., 2013; Stinnesbeck et al., 2017). The mesocranial skull morphology identified in these individuals (Hubbe et al., 2020; Stinnesbeck et al., 2020) differs significantly from that of coeval Palaeoindian skeletons from Central Mexico, e.g. the Peñon III Woman, the Tlapacoya Man, the Metro Man, the Chimalhuacan Man, and the North American Kennewick Man, which have been dated to between 12 to 7 ky BP and all present dolicocephalic morphologies (Hubbe et al., 2020; Stinnesbeck et al., 2020). The high degree of cranial morphological differences between the skulls from Central Mexico and Tulum has been interpreted as the result of a "local micro-evolutionary processes" by Stinnesbeck et al. (2020) and Hubbe et al. (2020). Long-term gene-flow barriers may thus have existed between the populations of the YP and those of central Mexico, established by palaeogeographical isolation and/or local processes of adaptation to different environmental conditions. This anthropological analysis, suggests that not only the megafauna of the YP was affected by at least intermittent isolation, but that "microevolution" due to isolation is also identified in the first human settlers (Stinnesbeck et al., 2020).

Adaptive radiation is one of the most fundamental processes producing bursts of species diversification, trait divergence, and niche evolution (Simpson, 1944; Schluter, 2000). Ecological opportunity, the abundance of available resources in a new environment with few competitors, has long been viewed as the primary force driving diversification through divergent selection on niche use, mediated by competition and predation (Schluter, 2000; Losos and Mahler, 2010; Pfennig and Pfennig, 2010). This relationship between new ecological space and divergent selection leading to reproductive isolation forms the basal concept of the Ecological Theory of Adaptive Radiation (Schluter, 2000; Losos and Mahler, 2010) and ecological speciation theories (McKinnon et al., 2004; Rundle and Nosil, 2005; Nosil, 2012).

The high degree of endemism of the Pleistocene megafauna identified on the northern-eastern Yucatán Peninsula contrasts with present day ecological interpretations of the area. According to a recent survey by Sosa-Escalante et al. (2013) about 28% (n=34) of the mammal fauna of the YP presents endemism (Sosa-Escalante et al., 2013; Martínez-Meyer et al., 2014), which was considered by the authors to be about average for this neotropical region, but notably lower than that of neighbouring regions (e.g. Chiapas, Veracruz, Oaxaca; Flores-Villela and

Fernández, 1994). The diversity of modern mammals is lower on the YP than in other regions of central and western Mexico, with a lower rate of endemic and geographically restricted species. Beta diversity is also low (Arita and Rodríguez, 2002), which was explained by the homogenous low-lying topography of the area (Figs. 1 and 2), the absence of natural barriers and the low heterogeneity of habitats (Vázquez-Dominguez and Arita, 2010). In addition, a notable "peninsular" gradient has been identified regarding the diversity of terrestrial mammals, with an increase from 90 species in the north to 130 in the south. Homogenous habitats and the absence of natural barriers leading to a low beta-diversity and lower than average endemism of the modern late Holocene mammal fauna of the YP have been attributed by Sosa-Escalante et. al. (2013) to the low elevation and flat topography of the region (see Fig. 2), features that result from the geological background conditions (Fig. 1), i.e. almost horizontally-lying limestone strata on a tectonically inactive carbonate platform (Ward et al., 1985; Weidie, 1985).

However, during the Late Glacial Maximum (LGM) of the Wisconsin Glacial stage, sea-level was 120 m below the average present level and the Neogene marine limestone bedrock that conforms the surface of the northern YP was widely exposed to intensive karstification (Blanchon and Shaw, 1995; Moseley et al., 2015). The region, especially the coastal stretch conforming the Riviera Maya, between Cancun and Tulum, likely was a hostile desert-like limestone plain during stadial periods of the Pleistocene, analogous to the extant Irish Burren landscape (Feehan, 2001). It was likely characterized by sparse shrub vegetation shrub, but almost no grass, because grass needs soil, and the latter is absent in the karstified study area (Figs. 1 and 2). This means that during a period of time in the past migration must have been possible between central Mexico and Central America and the YP (and vice versa), otherwise the faunal assemblage would not be present on the study area. But these intervals with faunal exchange alternated with periods in which the north-eastern YP was isolated, leading to local endemism in the study area.

Southern Mexico was ecologically connected to Central America (e.g. Guatemala) by the intermittent expansion of grassland (Dávila et al., 2019), but this vegetation corridor ended with karst-dominated water-less plains of the northern-eastern Yucatán Peninsula (Fig. 9).
The intermittent expansion of grassland may have favoured the isolation and formation of an ecological barrier between the north-eastern YP and south-central Mexico (Fig. 9), and thus the Mesoamerican Corridor (Stinnesbeck et al., 2018b). The Late Pleistocene savanna corridor extended from north-eastern Mexico (Nuevo León, San Luis Potosi) via southern

Mexico (e.g. Mexican Valley to Chiapas) to the lowlands of north-western Guatemala (Péten), along the river-systems of the Montagua-Polochic fault zone (Fig. 9) and further south to El Salvador, Nicaragua and Costa Rica (Dávila et al., 2019). Dry periods, in which the savanna corridor spread (Dávila et al., 2019), acted as a natural barrier on the YP (Fig. 9) due to the singular geology of the region as conformed by almost horizontally layered thick bedded limestone, not allowing for the development of soil (Fig. 1).
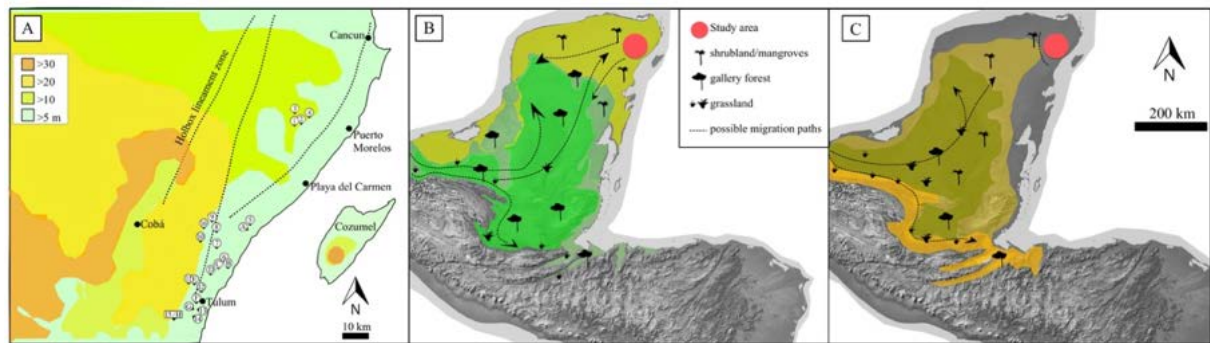
Fig. 9: A) Topography of the study area on the YP (for exact location and further information of the palaeontological sites see Fig. 2 and Table 2). Note that cave systems and sinkholes studied here are located along the north-eastern coast of the Mexican YP. This area is elevated to only 5-10 m above present day sea level and the thick-bedded limestone bedrock impedes the development of soil. Extant vegetation consists of xeric shrub and tropical depending on ground water supply. Sinkholes (spa. cenotes) form the only access to the extended system of submerged caves with phreatic levels. During stadial periods of the Late Pleistocene sea level was tens of metres below present day levels (Fig. 2B), and so were the phreatic water levels. Due to intense limestone karstification no surface water was available leading to a shrub or even semi-desertic landscape. B) Faunal migration in and out of the north-eastern YP was therefore restricted to periods of high precipitation and/or sea level leading to the propagation of vegetation. C) Low precipitation rates favored the expansion of grassland in south-central Mexico. Nevertheless, grassland was likely absent in the north-eastern YP, due to the absence of soil on the karstic bedrock. This schematic model of the isolation of the YP favored the development of endemic species as seen in Fig. 10.

Faunal exchange between south-central Mexico and the YP was therefore confined to moist periods (Fig. 9B), while small faunal populations were ecologically trapped on the YP during dry periods (e.g. the Younger Dryas see Fig. 9C; Stinnesbeck et al., 2018b). These small populations of e.g. ground sloths, were exposed to rapid local diversification. The repeated alternation between periods of isolation and dispersal may thus represent a viable mechanism to explain the remarkable diversification of megalonychid ground sloths in the area, because the dispersal abilities of these animals with reduced mobility were likely more restricted than those of e.g. large carnivores, equids, artiodactyls, or proboscideans.

Cenotes represent the only natural source of fresh water for humans and wildlife on the north-eastern YP, today and during the Pleistocene. Ecologically these water-filled karst sinkholes may thus be considered as islands of aquatic life. Cenotes are frequently surrounded by distinctive dense vegetation due to the presence of tall evergreen trees, such as *Ficus* spp., *Manilkara* and others (Guido et al., 1994). During times of significantly lower water levels, e.g. during stadial periods of the Pleistocene, the water-filled cenote sinkholes must have formed 'island habitats' within the ecologically isolated northern YP (Fig. 9).

Small ground sloth populations living next to specific cenote clusters may even have been isolated from populations living at close distance along other cenotes in the area, further triggering ecological isolation and evolutionary separation of taxa. Isolated from each other by the desert-like limestone karst landscape, each cenote, or cluster of cenotes, provided a life-giving oasis (Fig. 10) and wide ranges of habitats, including dense vegetation. Island biota are long known by evolutionists for their unique species, as refuges of extant, "relict" organisms, and most famously, for their display of adaptive radiation (Shaw and Gillespie, 2016). The importance of island habitats for our understanding of evolution, ecology, and biogeography can thus not be overstated (Warren et al., 2015). Although caution is necessary (Itescu, 2019), island biogeography theories may be applied to any kind of isolated habitat (MacArthur and Wilson, 1967; Warren et al., 2015). Consequently, small effective population sizes as well as geographical and ecological isolation of the 'island-like' cenote sites must have been essential factors to form unique and endemic Pleistocene megalonychids, while the limestone karst plain between individual cenotes must have formed effective ecological and thus biogeographic barriers for these species.

4.4   Human-environment interactions on the Yucatán Peninsula

The question of human impact on the megafauna is a strongly debated topic for the Americas, ranging from the hypothesis of an „overkill" by palaeoindians (Martin, 1973), habitat modification, or lethal diseases brought in by humans, or a combination of some or all of these issues (Barnosky et al., 2004; Haynes, 2016). Nevertheless, the archaeological evidence for human-megafauna interaction is surprisingly rare.

The human settlement of the YP initiates at about 13.000 BP (Stinnesbeck et al., 2017), but people repeatedly visited the caves of Tulum area for thousands of years, at least until the early mid-Holocene (Hering et al., 2018; Stinnesbeck et al., 2020). This long-term human settlement on the YP (González González et al., 2013) and Early Holocene ^{14}C data of faunal remains (e.g. *X. oviceps*, see Table 2) suggest a regional co-existence of man and megafauna for at least 2.000 to 4.000 years.

Isolated megafaunal bones with cut- and scratch marks have been documented from Muknal, where cut marks have been detected on the mandibular ramus of the endemic Pleistocene peccary *Muknalia minima* (Stinnesbeck et al., 2017b), the latter likely forming part of a burial context (Stinnesbeck et al., 2018).

In the Ilium cave near Tulum, three isolated fragments of *Equus* sp. with cut marks were found, but the data is still unpublished. The cut marks are straight, subparallel, with closed profiles of √- to V-shape and extensive shoulder effects, suggesting the use of a simple flake as a tool (Domínguez-Rodrigo et al., 2009). The color of all cut and scratch marks is identical with that of the bone surface and thus indicates a similar time of exposure to saltwater and erosion. A more recent application of the scratch and cut marks would have resulted in a significant color difference. Different to the peccary from the Muknal burial (Stinnesbeck et al., 2018a), no direct human presence or stone artifacts could yet be related to the fossils from Ilium.

The Toh locality near Tulum contains ground sloth long bones tentatively identified as *Nothrotheriops shastensis*. One of the long bones shows five parallel cut marks.

Anthropological handling is evident for the postcranial skeleton of the holotype of *Xibalbaonyx oviceps* collected from cenote El Zapote. This interpretation is supported by the identification of several small cut marks on ribs and ulna. The cut marks on the ulna only

reach to 20 mm length, but are pronounced (Stinnesbeck et al., 2020a). Moreover, all long bones of *X. oviceps* lack their proximal or/and distal epiphyses and all diaphyses, suggesting that the joints were intentionally broken. For example, epiphyses of the femora are intact, such as the femoral head and greater trochlea, but the distal epiphyses are missing. In the long bones (e.g. humeri, femura, ulnae, radii and tibiae), either the proximal, or distal epiphysis is broken, as is the corresponding end of the diaphysis. In these bones the medulla of the diaphysis is missing, suggesting that these bones were actively hollowed or scooped-out using scrapers, or other tools (Stinnesbeck et al., 2020a). The compacta is present only near the fragmented open ends of the bones; it is extremely thin there, due to the scooping out, while further away from the original break, the medulla is more complete and is still present, suggesting that the tools used to hollow the bone only reached to this depth. The medulla is therefore not absent due to dissolution, because this process would then also have produced a decay of the compacta of the long bones, as well as in other bones such as ribs, atlas, axis. However, these show an excellent preservation (Stinnesbeck et al., 2020a).

The El Zapote skeleton was dated to 9.305 ± 35 14C BP (10.647–10.305 cal BP) by the LEMA lab of the UNAM (Stinnesbeck et al., 2017a). The unusually young age of the skeleton, dating to the earliest Holocene, supports the scenario of a co-existence of *Xibalbaonyx oviceps* with humans in the area (González González et al., 2013; Stinnesbeck et al., 2020a).

To date, evidence for human interaction with ground sloths is surprisingly rare. There are only a few well-documented localities: Northern Ohio in the US (Redmond et al., 2012) and Campo Laborde in south-eastern Argentina (Politis et al., 2019). It is also known that some Caribbean ground sloths not only survived the end-Pleistocene mass extinction of American megafauna, but coexisted with humans even into the middle Holocene, e.g. *Neocnus* to about 4.391±42 ky BP in Cuba (Steadman et al., 2005; MacPhee et al., 2007).

Human interaction (e.g. hunting) with Pleistocene megafauna is better documented for proboscideans and bisons (Grayson and Meltzer, 2015; Meltzer, 2015; Waters et al., 2015). For instance, at Buffalo Jump in Alberta, Canada, bisons were chased by hunters across a cliff (Bamforth, 2011; Carlson and Bement, 2013), a scenario easy to imagine for the steep walls of the cenotes. In this case, however, hunters would then have had difficulties to climb down the vertical and even overhanging cliffs and bring the corpses back to the surface. The intentional fragmentation of long bone articular faces of the *Xibalbaonyx oviceps* holotype specimen rather indicates that the animal was butchered and dismembered on the surface

close to the cenote, and that leftovers were dropped into the sinkhole. The fractured pelvis also supports this scenario, because a pelvis is a massive structure, that would only break due to a trauma, such as the fall of a great height .

4.5 Which factors influenced the extinction of ground sloths on the Yucatán Peninsula?

Towards the end of the Wisconsin glaciation >35 taxa became extinct in North America (Barnosky et al., 2004; Koch and Barnosky, 2006; MacPhee, 2009; Meltzer, 2015; Seersholm et al., 2020). The scientific debate frequently focuses on large herbivores, but small mammals, reptiles and birds were also affected and many taxa did not survive into the Holocene (Brook and Bowman, 2002; Rule et al., 2012). The mass extinction was global but did take place in regionally asynchronous waves. In Australia, for example, the main extinction took place around 70.000 to 40.000 BP (Gill et al., 2009; Rule et al., 2012; Webb, 2013), while in some regions of South America and the West Indies species survived into the Holocene (Steadman et al., 2005; Hubbe et al., 2007, 2013; MacPhee et al., 2007; Barnosky and Lindsey, 2010). Nevertheless, the "extinction" of taxa has to be understood as a (slow or fast) shrinking of animal populations (Martin and Klein, 1984; Frankham, 2005). In this aspect, four main biological and physical factors triggered the end-Pleistocene extinction of populations:

I. Climate and vegetation change. Landscape and biotopes change, and as a result habitat shrink and original resources drop out.
II. "Non-adaptive evolution". The populations adapt to these environmental changes "too slowly" and can therefore not keep up and procreate.
III. Predators, diseases, etc. decimate these remaining megafaunal populations.
IV. Destruction of habitat and resources and/or hunting by humans.

In the case of North- and Central America a decrease of the megafaunal population has been documented for numerous taxa even to the time before the Last Glacial Maximum (LGM; 29.000-25.000 BP). The large Holarctic megafauna, such as *Bison*, *Ursus*, *Panthera* and *Mammuthus* etc., was particularly affected by rapid climatic changes (Cooper et al., 2015; Grayson and Meltzer, 2015). These megafaunal populations were already reduced strongly by

about 20.000 BP and trapped in Late Pleistocene refugial areas (Meltzer, 2009; Stuart, 2015). For example, *Mammuthus*, one of the best documented megafaunal taxon, is reported for this period only from specific areas (Haile et al., 2009; MacPhee, 2007), among them the Great Lakes in Utah, USA (Woodman and Beavan Athfield, 2009), but also from areas in central Mexico (Gonzalez et al., 2014) and Guatemala (Dávila et al., 2019). These youngest populations were isolated from each other.

The loss of resources, such as the Mammoth-Steppe, caused stress to the megafauna surviving in the refugial areas. The shrinking of suitable habitat also resulted in anatomical changes in the surviving mammals, such as as body size reduction in bison, musk ox, elk and caribou. In *Bison*, a progressive reduction in the size of foot bones was documented already for about the period of the LGM. Body size reduction correlates with the decrease of *Bison* populations at the end of the Pleistocene (Meltzer, 2009). This fits the observation that a mature dwarf ground sloth is identified in the unpublished ground sloth material from cenote Tortugas, (Fig. 7E, K). *X. oviceps* has been regarded as medium sized ground sloth with 2 m length (Stinnesbeck et al., 2020a), and therefore as "small" compared to co-eval ground sloths such as *Megalonyx* and *Paramylodon* (Pant et al., 2014), while *X. exinferis* was even smaller than *X. oviceps* (Stinnesbeck et al., 2020b). A decrease of body size, even to dwarfed specimens, is often correlated with a reduction of habitat size, as repeatedly documented in island-species such as the Wrangel mammoths and the Caribbean sloths (Vartanyan et al., 1993; Pant et al., 2014; Fry et al., 2020; Kirillova et al., 2020). The reduction in body size has also been documented in the endemic peccary *Muknalia minima*, and the felid *Panthera balamoides*. Both taxa were considerable smaller than extant peccaries and Pleistocene felids (Stinnesbeck et al., 2017b; Stinnesbeck et al., 2018b).

The diversity of taxa endemic to reduced habitats is noteworthy, because it supports the interpretation of periodic isolation of the study area. Under these conditions small ground sloth populations populated individual cenote clusters and diversified, a situation analogous to that of Darwin finches on the Galápagos Islands.

Late Pleistocene ground sloths diversified under the rapidly changing ecological conditions of the north-eastern YP, but recurrent long-lasting isolation and the scarcity of natural resources limited to cenote areas (Fig. 9) also caused stress and genetic stunt in these last populations with reduced habitats. These adverse ecological conditions must have favored negative inborn defects related to stress, malnutrition and inbreeding (Fig. 10). Low basal metabolism, long gestation periods, low growth rates, extended periods of parental care and small litter size

(McNab 1985), suggest that ground sloths were K-selected animals with an overall low rate of reproduction. They were therefore highly vulnerable to changes in the ecology, or hunting. The latter is evidenced by cut and butchering marks in the ground sloths from the El Zapote and Tortugas cenotes, which indicate that juvenile animals were probably preferentially hunted by humans.

The extinction of the ground sloths on the YP may thus have been triggered by several factors (Fig. 10):

➢ Habitat reduction.

Climatic oscillations during the Late Pleistocene led to vegetation changes and habitat reduction. The stable isotopic signature of a stalagmite from the Chan Hol cave near Tulum (Stinnesbeck et al., 2017) documents high precipitation rates before and after the Younger Dryas (YD; 12.900 cal BP / 11.900 BP), suggesting a northern shift of the Intertropical Convergence Zone (ITCZ). Conditions thus differed from the dry conditions of the Cariaco basin in Venezuela during the same period (Haug et al., 2001; Hodell et al., 2008). Higher precipitation rates before the YD have also been reported from the Petén region of northeastern Guatemala (Bush et al., 2009), there favoring the extension of *Quercus*–dominated forests (Dávila et al., 2019). This is also suggested by the presence of high specialized browsers in Guatemala, such as *Eremotherium*. Based on the faunal assemblage of Guatemala, in which the browser *Eremotherium* and the grazer *Mammuthus* are both present, although during different climatic periods (Dávila et al., 2019). This is supported by ^{14}C ages, indicating that *Mammuthus* migrated south during the Younger Dryas stadial, and therefore during a dry period, while *Eremotherium* populated the area during wet periods (Dávila et al. 2019).

Pollen evidence from Page Ladson in Florida also reflects dramatic vegetation changes leading to fluctuating herbivore populations (Perrotti et al., 2019). Between ca. 14.500 to 12.600 cal BP, an increase in hardwood forest and mesic plant taxa has been documented in Page Ladson, indicating an increase in both temperature and precipitation (Perrotti et al., 2019).

According to the similar habitat preferences, *Glyptotherium* and *Paramylodon* may thus have populated the YP only during short periods with abundant precipitation, and/or high water level before or after the Younger Dryas period.
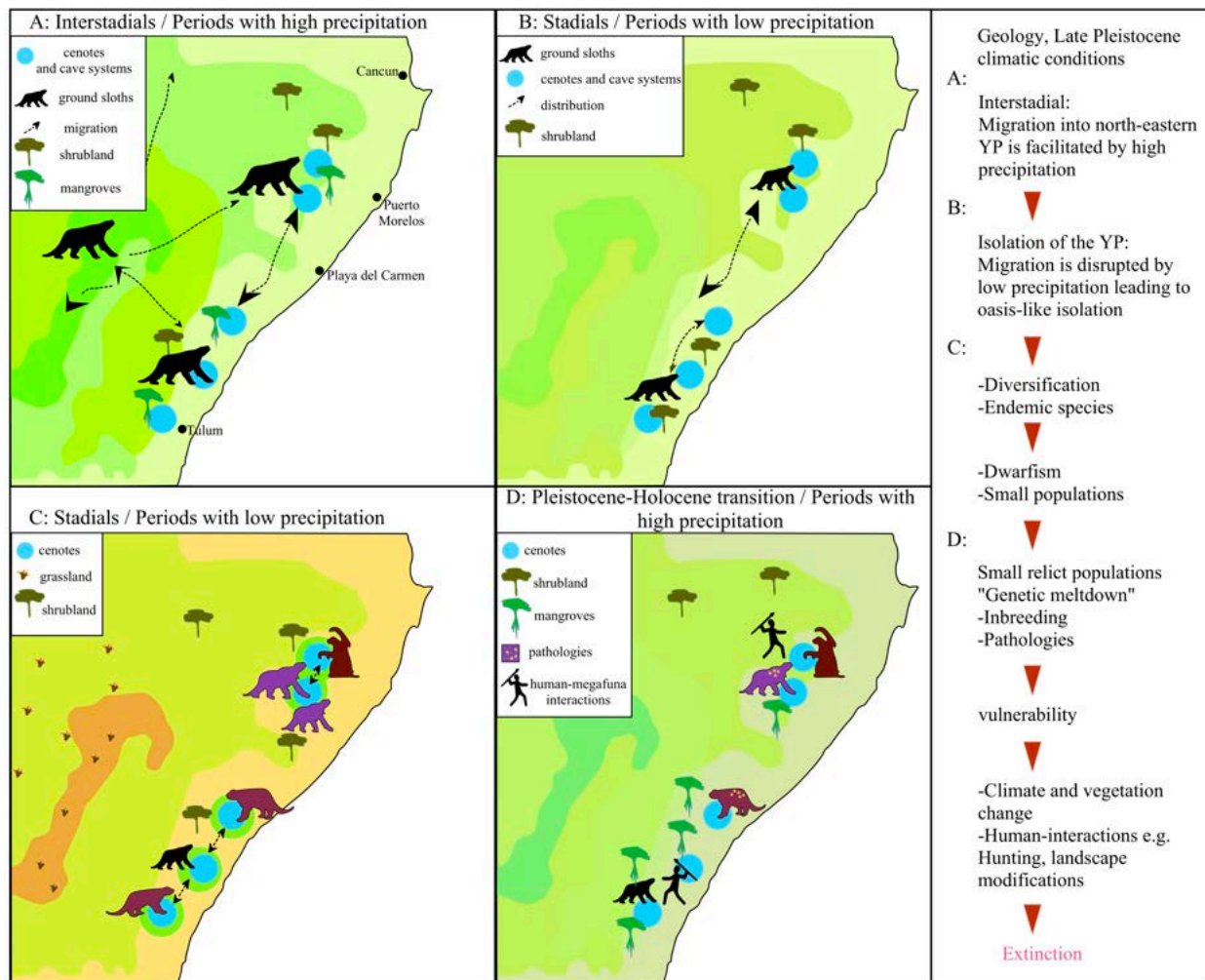
Fig. 10: Model of the „Oasis-theory" outlining an extinction scenario for the ground sloths on the YP. A) Migration of ground sloths to the YP was facilitated by high precipitation and the propagation of vegetation into the study area. B) Low precipitation rates cause a reduction of vegetation and ecological isolation of the study area, interrupting ground sloth migration and genetic exchange with south-central Mexico. Small ground sloth populations are trapped on the north-eastern YP. C) Ongoing habitat reduction and small areas of faunal interaction trigger the development of endemic species. D) Ecological stress and reduction in genetic flow lead to an increase in pathologies, indicating „genetic meltdown" of the ground sloth population. Early Holocene climatic and vegetation changes lead to a reduction of the original resources. Climatic and ecological factors, as well as ground sloth biological traits (slow-breeders etc.) and hunting by humans, cause the final decline in ground sloth population and extinction.

- Habitat reduction and isolation lead to small trapped populations (Figs. 9 and 10). The situation is evidenced by morphological changes (e.g. body size reduction) and appearance of new species of megalonychid ground sloths (e.g. *X. oviceps*, *X. exinferis*), but also seen in other taxa (e.g. *Muknalia minima*) and even humans.

- Sloths are slow-breeders. Extant sloths only have one baby at a time and these grow up slowly (McDonald, 2005). This low fertility rate had a negative effect to these late ground sloth populations already decimated by climatic and subsequent vegetational changes (Meltzer, 2009). The factor has been interpreted as a "vulnerability to extinction" by Meltzer (2009).

- ^{14}C dating suggests that the faunal assemblage on the YP (Table 2) conformed one of the latest megafauna populations in North America. Populations in this area may have survived the end-Pleistocene megafaunal mass extinction by at least a few hundreds of years, but likely longer. The small ground sloth population size led to a "genetic meltdown" reflected by negative inborn defects such as congenital anomalies (see chapter 4.1.2), as also documented for the mammoths from the North Sea (Reumer, 2007; Reumer et al., 2014; Fry et al., 2020) and some of human skeletons of the study area, such as the Klipple-Feile-Syndrom in the Eve of Naharon. The last ground sloths in the study area were likely highly vulnerable small populations (Fig. 10).

- Small ground sloth populations were hunted by humans, as evidenced by butchered animals at El Zapote cenote, Concha and Toh. In addition, Nickell and Moran (2017) discussed potential human-introduced diseases into the New World, which may have affected the megafauna (Nickell and Moran, 2017). These include anthrax (*Bacillus anthracis*), tuberculosis (*Myobacterium tuberculosis*), pertussis (*Bordetella pertussis, B. parapertussis* and *B. bronchiseptica*), rabies (*Lyssavirus*), syphilis (*Treponema pallidum*), giardia (Sarcomastigophora), hepatitis B (Orthohepadnavirus), herpes (Simplex virus) and polio (Enterovirus C), all of them highly contagious to both humans and animals and documented in pre-Columbian human skeletons (Ortner, 2003; Nickell and Moran, 2017). Even though human skeletal remains of Late Pleistocene age are highly scattered in the American continent, *Treponema* has been reported in one of the earliest human settlers of the peninsula, the Chan Hol 3 woman (Stinnesbeck et al., 2020). Also, bone lesions indicating tuberculosis, have been detected in *Mammut americanum* and *Bison antiquus* (Rothschild et al., 2001; Rothschild and Laub, 2006; Rothschild and Martin, 2006; Nickell

and Moran, 2017). It is therefore possible that the early settlers also brought new diseases to this area, which affected the faunal population.

➤ Habitat loss and destruction of resources.

Strong climatic oscillations are documented by isotope analysis (e.g. δ^{18}O) of stalagmites during the Early Holocene (Stinnesbeck et al. 2017, 2020). As a consequence to these perturbations an increase in forest fires is evidenced in QR by extraordinary amounts of charcoal dating to this period (9.000-7.000 BP) and washed into the caves such as Muknal and Chan Hol (Hering et al., 2018; Stinnesbeck et al., 2018). Higher precipitation rates at the beginning of the Holocene probably favored the development of mangroves and woodland. In fact, the early Holocene charcoal from Muknal and Chan Hol cave mostly represents mangroves (pers. comm. Dominguez-Vazquez). Also, the abundance increase of the cervid *Odocoileus* in the faunal assemblage towards modern times probably reflects its riparian habitat preference. Skeletal remains of *Odocoileus virginianus*, *Tapirus* sp., *Mazama* sp. and *Pecary tajacu* discovered in the QR cave system, might therefore rather represent modern than Pleistocene taxa (see Table 2).

This evidence presented above supports a scenario of a rapidly changing vegetation, due to warmer temperatures, a rise in phreatic levels and fast-changing conditions with low to high precipitation. The abundance of archaeological evidence, such as illumination sites, fireplaces and cut marks, also indicates a long co-existence of man and megafauna in the area during the Early Holocene (Stinnesbeck et al., 2020a).

Late Pleistocene to Early Holocene climatic oscillations suggest ongoing vegetation changes and a reduction of habitat and original resources around the cenotes. Along with ground sloth biological traits, such as small litter size, low metabolism, short extremities which prevent fast running and thus an escape from predators, the change in vegetation towards modern forest environments went along with a systematic shrinking of the already small populations and the final extinction of ground sloths on the YP (see Fig. 10).

5　Conclusions

The Late Pleistocene fossil assemblages of Quintana Roo majorly consist of large herbivores, comparable to other fossil sites along the Mesoamerican Corridor. Although many of the fossils have not been dated, due to a reservoir effect in the caves and the lack of stratigraphic context, an assignation of most localities to the Late Pleistocene (Rancholabrean) epoch is more than likely, due to the faunal assemblages documented here, but also by the few available ^{14}C analyses. Fossil assemblages are dominated by ground sloths, e.g., *Xibalbaonyx oviceps*, *X. exinferis*, *Nothrotheriops shastensis* and *Nohochichak xibalbakah*. Other taxa are under-represented and exceedingly fragmentary in the QR assemblages, such as the gomphotheres (*Cuvieronius hyodon*), horses (*Equus* sp.), tapirs (*Tapirus* sp.), llamas (*Hemiauchenia* sp.), peccaries (*Muknalia minima*, *Pecary tajacu*), cervids (*Odocoileus virginianus*, *Mazama* sp.), felids (*Smilodon fatalis*, *S. gracilis*, *Lynx rufus* and *Panthera balamoides*), canids (*Protocyon* sp.) and bears (*Arctotherium*). Although abundant elsewhere in Mexico and Central America, *Mammuthus* and *Eremotherium* remains are totally absent to date. In consequence, the faunal assemblages are dominated by principally opportunistic, xeric to mesic-adapted browsers.

The percentage of endemism is high in the Late Pleistocene faunal elements from QR. Among them the peccary *Muknalia minima* (Stinnesbeck et al., 2017b) and the felid *Panthera balamoides* (Stinnesbeck et al., 2018), as well as the numerically abundant megalonychid ground sloths, including the new genera *Nohochichak* (McDonald et al., 2017) and *Xibalbaonyx* (Stinnesbeck et al., 2020b, 2017a) and yet unpublished ground sloth species. The amount of endemic vertebrates in QR is remarkable and can only be explained by an intermittent isolation of the area, either geographically or ecologically, which lasted long enough to allow for a hitherto unexpected diversification of mammals. The precise intervals of isolation are unknown to date, because stratigraphic information is scarce.

Periods of habitat diversification may have altered during the Pleistocene with intervals of ecological isolation of the north-eastern YP. During stadial periods, dry, semi-desertic or even desertic conditions existed on the north-eastern YP. They were a consequence of the almost horizontally lying thick-bedded limestone base rock platform in this region and the extensive karstification due to repeated sea-levels changes, including lows of about 120 m below present day levels. Under these conditions, no soil developed on the carbonate platform and

rain water seeped away almost instantaneously. As phreatic levels only existed tens of meters below surface, beyond the reach of roots, no surface water existed and even the presence of extended grassland areas in the region appears unlikely. Mesic to xeric shrub environment could only exist in depressions, especially around the hundreds of sinkholes in the Tulum and Puerto Morelos areas.

Faunal exchange between south-central Mexico and the YP was likely restricted to humid periods. During dry periods, the browser habitats became patchy. During these intervals, small populations of herbivores depending on specific food sources became isolated. This ecological isolation boosted local diversification and not only caused endemism, but may evidently have created a biodiversity hotspot concerning ground sloths unknown elsewhere along the Late Pleistocene Mexican Corridor, and the Americas. The repeated changes of Late Pleistocene climatic conditions, followed by changes of vegetation on the YP, along with a geographic isolation of the north-eastern YP, likely formed an ecological barrier to the previously connected open habitat. The loss of migratory pathways to west-central Mexico and the resulting isolation of habitats during dry periods resulted in anatomical and genetic changes among the isolated ground sloths populating the peninsula.

The Early Holocene age dated for the holotype of *Xibalbaonyx* suggests a survival of megafauna on the YP and long-lasting co-existence of humans and megafauna during the Late Pleistocene and Early Holocene. Cut marks on ground sloth bones also suggest an active hunting of ground sloths by humans. A combination of small population numbers, rapid climatic oscillation with alternating high and low precipitation periods and associated vegetation changes across the Pleistocene-Holocene boundary, as well as human interactions, may thus have triggered the extinction of ground sloths on the Yucatán Peninsula.

Mexico played a crucial role in the migration of megafauna during the Great American Biotic Interchange (GABI) and since that event. Southern Mexico and Central America (e.g. Guatemala) are key areas along this Mesoamerican Corridor, which acted as a palaeobiogeographic bridge and filter between North- and South America during both the Plio- and Pleistocene. This is represented by the abundant presence of North American fauna in Central America, but under-representation of South American fauna (Dávila et al. 2019) in Central America, such as the canid *Protocyon* and tremarctine bear *Arctotherium* (Schubert et al. 2019).

The faunal assemblage of QR documented here is unique in comparison to central Mexico and other regions in Central America. In particular, the high diversity of megalonychid ground sloths is exceptional. The periodical isolation of the study area from the rest of Mexico and Central America, as indicated by faunal and anthropological data, shows the high potential of the study area as an periodically closed Late Pleistocene ecosystem, similar to the Galapagos Island. Due to its exceptional "insular" situation the study area does not form part of the Mesoamerican Corridor. Instead, it is important for the understanding of Late Pleistocene faunal migration and even early human settlement between Mexico and Central America, and in a greater scale between North- and South America.

6   References

Adam, P. J. 1999. *Choloepus didactylus*. *Mammalian Species*, 1–8.

Amson, E., C. Argot, H. G. McDonald, and C. de Muizon. 2015. Osteology and Functional Morphology of the Forelimb of the Marine Sloth *Thalassocnus* (Mammalia, Tardigrada). *Journal of Mammalian Evolution*, *22*(2):169–242.

Andrade, L. C., F. H. d. S. Barbosa, L. B. Melki, E. V. Oliveira, H. I. de Araújo-Júnior, and V. Maniesi. 2019. Revealing bone diseases in the Quaternary ground sloth *Eremotherium laurillardi* (Mammalia, Xenarthra). *Historical Biology*, 1–9.

Arita, H. T., and P. Rodríguez. 2002. Geographic range, turnover rate and the scaling of species diversity. *Ecography*, *25*(5):541–550.

Arroyo-Cabrales, J., O. J. Polaco, C. Laurito, E. Johnson, M. Teresa Alberdi, and A. L. Valerio Zamora. 2007. The proboscideans (Mammalia) from Mesoamerica. *Quaternary International*, *169*:17–23.

Bacon, C. D., D. Silvestro, C. Jaramillo, B. T. Smith, P. Chakrabarty, and A. Antonelli. 2015. Biological evidence supports an early and complex emergence of the Isthmus of Panama. *Proceedings of the National Academy of Sciences of the United States of America*, *112*(19):6110–6115.

Baker, M. L., L. C. Payne, and G. N. Baker. 1961. The Inheritance of Hydrocephalus in cattle. *Journal of Heredity*, *52*(4):135–138.

Bamforth, D. B. 2011. Origin stories, archaeological evidence, and Postclovis Paleoindian bison hunting on the Great Plains. *American Antiquity*, 76:24–40.

Barnosky, A. D., and E. L. Lindsey. 2010. Timing of Quaternary megafaunal extinction in South America in relation to human arrival and climate change. *Quaternary International*, *217*(1-2):10–29.

Barnosky, A. D., P. L. Koch, R. S. Feranec, S. L. Wing, and A. B. Shabel. 2004. Assessing the Causes of Late Pleistocene Extinctions on the Continents. *Science*, *306*(5693):70–75.

Beaudoin, A. B., M. Wright, and B. Ronaghan. 1996. Late Quaternary landscape history and archaeology in the "ice-free corridor": some recent results from Alberta. *Quaternary International*, *32*:113–126.

Bello, S. M., and C. Soligo. 2008. A new method for the quantitative analysis of cutmark micromorphology. *Journal of Archaeological Science*, *35*(6):1542–1552.

Bello, S. M., S. A. Parfitt, and C. Stringer. 2009. Quantitative micromorphological analyses of cut marks produced by ancient and modern handaxes. *Journal of Archaeological*

Science, *36*(9):1869–1880.

Bentley, R. A. 2006. Strontium isotopes from the earth to the archaeological skeleton: A review. *Journal of Archaeological Method and Theory*, *13*(3):135–187.

Blanchon, P., and J. Shaw. 1995. Reef drowning during the last deglaciation: evidence for catastrophic sea-level rise and ice-sheet collapse. *Geology*, *23*(1):4–8.

Bocherens, H., M. Cotte, R. A. Bonini, P. Straccia, D. Scian, L. Soibelzon, and F. J. Prevosti. 2017. Isotopic insight on paleodiet of extinct Pleistocene megafaunal Xenarthrans from Argentina. *Gondwana Research*, *48*:7–14.

Böhmer, C., E. Amson, P. Arnold, A. H. Van Heteren, and J. A. Nyakatura. 2018. Homeotic transformations reflect departure from the mammalian "rule of seven" cervical vertebrae in sloths: Inferences on the Hox code and morphological modularity of the mammalian neck. *BMC Evolutionary Biology*, *18*(1):1–11.

Bronk Ramsey, C. 2013. OxCal 4.2. Man. [online] available https//c14. arch. ox. ac. uk/oxcalhelp/hlp_contents. html (accessed 27/03/2013).

Brook, B. W., and D. M. J. S. Bowman. 2002. Explaining the Pleistocene megafaunal extinctions: Models, chronologies, and assumptions. *Proceedings of the National Academy of Sciences*, *99*(23):14624–14627.

Burr, G. S., J. W. Beck, T. Correge, G. Cabioch, F. W. Taylor, and D. J. Donahue. 2009. Modern and Pleistocene Reservoir Ages Inferred From South. *Radiocarbon*, *51*(1):319–335.

Bush, M. B., A. Correa-Metrio, D. A. Hodell, M. Brenner, F. S. Anselmetti, D. Ariztegui, A. D. Mueller, J. H. Curtis, D. A. Grzesik, C. Burton, and A. Gilli. 2009. Re-evaluation of climate change in lowland Central America during the Last Glacial Maximum using new sediment cores from Lake Petén Itzá, Guatemala. *In* F. Vimeux, F. Sylvestre, and M. Khodri (eds.), Past Climate Variability in South America and Surrounding Regions. Springer, Dordrecht, p. 113-128.

Carlson, K., and L. Bement. 2013. Organization of bison hunting at the Pleistocene/Holocene transition on the Plains of North America. *Quaternary International*, 297:93–99.

Cartelle, C., and G. De Iuliis. 2006. *Eremotherium laurillardi* (Lund) (Xenarthra, Megatheriidae), the Panamerican giant ground sloth: Taxonomic aspects of the ontogeny of skull and dentition. *Journal of Systematic Palaeontology*, *4*(2):199–209.

Cartelle, C., G. De Iuliis, and F. Pujos. 2008. A new species of Megalonychidae (Mammalia, Xenarthra) from the Quaternary of Poço Azul (Bahia, Brazil). *Comptes Rendus - Palevol 8*, *7*(6):335–346.

Chatters, J. C., D. J. Kennett, Y. Asmerom, B. M. Kemp, V. Polyak, A. N. Blank, P. a Beddows, E. Reinhardt, J. Arroyo-Cabrales, D. a Bolnick, R. S. Malhi, B. J. Culleton, P. L. Erreguerena, D. Rissolo, S. Morell-Hart, and T. W. Stafford. 2014. Late Pleistocene human skeleton and mtDNA link Paleoamericans and modern Native Americans. *Science*, *344*(6185):750–4.

Cione, A. L., G. M. Gasparini, E. Soibelzon, L. H. Soibelzon, and E. P. Tonni. 2015. The Great American Biotic Interchange A South American Perspective. Springer, Heidelberg, 97 p.

Cisneros, J. C. 2005. New Pleistocene vertebrate fauna from El Salvador. *Revista Brasileira de Paleontologia*, *8*(3):239–255.

Cliffe, R. N., R. J. Haupt, J. A. Avey-Arroyo, and R. P. Wilson. 2015. Sloths like it hot: ambient temperature modulates food intake in the brown-throated sloth (*Bradypus variegatus*). *PeerJ*, 3:e875.

Collevatti, R. G., K. C. E. Leite, G. H. B. de Miranda, and F. H. G. Rodrigues. 2007. Evidence of high inbreeding in a population of the endangered giant anteater, *Myrmecophaga tridactyla* (Myrmecophagidae), from Emas National Park, Brazil. *Genetics and Molecular Biology*, *30*(1):112–120.

Cooper, A., C. Turney, K. A. Hughen, B. W. Brook, H. G. McDonald, and C. J. A. Bradshaw. 2015. Abrupt warming events drove Late Pleistocene Holarctic megafaunal turnover. *Science*, *349*(6248):602–606.

Courtenay, L. A., J. Yvravedra, M. A. Mate-González, J. Aramendi, and D. González-Aguilera. 2017. 3D analysis of cut marks using a new geometric morphometric methodological approach. *Archaeological and Anthropological Sciences*, *11*(2):1–15.

Dávila, S. L., S. R. Stinnesbeck, S. Gonzalez, S. Lindauer, J. Escamilla, and W. Stinnesbeck. 2019. Guatemala's Late Pleistocene (Rancholabrean) fauna: Revision and interpretation. *Quaternary Science Reviews*, *219*:277–296.

De Iuliis, G., F. Pujos, and C. Cartelle. 2009. A new ground sloth (Mammalia: Xenarthra) from the Quaternary of Brazil. *Comptes Rendus - Palevol 8*, *8*:705–715.

De Iuliis, G., C. Cartelle, and F. Pujos. 2016. New Pleistocene remains of megalonychid ground sloths (Xenarthra: Pilosa) from the intertropical Brazilian region. *Journal of Paleontology*, *90*(3):578–587.

De Iuliis, G., H. G. McDonald, N. Stanchly, J. Spenard, and T. G. Powis. 2015. *Nothrotheriops shastensis* (Sinclair) from Actun Lak: First record of Nothrotheriidae (Mammalia, Xenarthra, Pilosa) from Belize. *Ameghiniana*, *52*(1):153–171.

de Paula Couto, C. 1956. On Two Mounted Skeletons of *Megalocnus rodens*. *Journal of Mammalogy*, *37*(3):423–427.

de Souza Barbosa, F. H., K. O. Porpino, L. P. Bergqvist, and B. M. Rothschild. 2016. Elucidating Bone Diseases in Brazilian Pleistocene Sloths Nothrotheriidae and Megalonychidae Families. *Ameghiniana*, *54*(3):331–340.

Delcourt, H. R. 2005. Prehistoric Native Americans and Ecological Change : Human Ecosystems in Eastern North America Since the Pleistocene. Cambridge University Press.

Delsuc, F., M. Kuch, G. C. Gibb, E. Karpinski, D. Hackenberger, P. Szpak, J. G. Martinez, J. I. Mead, H. G. McDonald, R. D. E. MacPhee, G. Billet, L. Hautier, and H. N. Poinar. 2019. Ancient Mitogenomes Revisit the Evolutionary History and Biogeography of Sloths the evolutionary history and biogeography of sloths. *Current Biology*, *29*(12), 2031-2042.

Delsuc, F., F. M. Catzeflis, M. J. Stanhope, and E. J. P. Douzery. 2001. The evolution of armadillos, anteaters and sloths depicted by nuclear and mitochondrial phylogenies: implications for the status of the enigmatic fossil *Eurotamandua*. *Proceedings of the Royal Society of London. Series B: Biological Sciences*, *268*(1476):1605–1615.

Domínguez-Rodrigo, M., S. de Juana, A. B. Galán, and M. Rodríguez. 2009. A new protocol to differentiate trampling marks from butchery cut marks. *Journal of Archaeological Science*, *36*(12):2643–2654.

Feehan, J. 2001. The Rocks and Landforms of the Burren. *In* J. W. O'Connell and A. Korff (eds.), The Book of the Burren. Tir Eolas, p. 14–23.

Ferretti, M. P. 2008. Enamel structure of *Cuvieronius hyodon* (Proboscidea, Gomphotheriidae) with a discussion on enamel evolution in elephantoids. *Journal of Mammalian Evolution*, *15*(1):37–58.

Ferrusquía-Villafranca, I., J. Arroyo-Cabrales, E. Martínez-Hernández, J. Gama-Castro, J. Ruiz-González, O. J. Polaco, and E. Johnson. 2010. Pleistocene mammals of Mexico: A critical review of regional chronofaunas, climate change response and biogeographic provinciality. *Quaternary International*, *217*(1-2):53–104.

Flores-Villela, O., and P. G. Fernández. 1994. Biodiversidad y conservación en México: vertebrados, vegetación y uso del suelo. Conabio y UNAM, 68–72.

Frankham, R. 2005. Genetics and extinction. *Biological Conservation*, *126*:131–140.

Franzen, J. L. 1993. Eine eiszeitliche Säugetierfauna aus Mina, NL Mexico. *Der Präparator*, *39*(2):67–72.

Fry, E., S. K. Kim, S. Chigurapti, K. M. Mika, A. Ratan, A. Dammermann, B. J. Mitchell, W. Miller, and V. J. Lynch. 2020. Functional Architecture of Deleterious Genetic Variants in the Genome of a Wrangel Island Mammoth. *Genome Biology and Evolution, 12*(3):48–58.

Gaudin, T. J. 1995. The ear region of edentates and the phylogeny of the Tardigrada (Mammalia, Xenarthra). *Journal of Vertebrate Paleontology*, 15(3):672–705.

Gaudin, T. J. 2004. Phylogenetic relationships among sloths (Mammalia, Xenarthra, Tardigrada): The craniodental evidence. *Zoological Journal of the Linnean Society, 140*(2):255–305.

Gaudin, T. J., P. Hicks, and Y. Di Blanco. 2018. *Myrmecophaga tridactyla* (Pilosa: Myrmecophagidae). *Mammalian Species, 50*(956):1–13.

Gill, J. L., J. W. Williams, S. T. Jackson, K. B. Lininger, and G. S. Robinson. 2009. Pleistocene megafaunal collapse, novel plant communities, and enhanced fire regimes in North America. *Science, 326*(5956):1100–1103.

Gillette, D. D., and C. E. Ray. 1981. Glyptodonts of North America. Smithsonian Institution Press, Washington D. C., 1–255 p.

González González, A. H., A. Terrazas Mata, W. Stinnesbeck, M. E. Benavente, J. Avilés Olguín, C. Rojas Sandoval, J. M. Padilla, A. Velázquez Morlet, E. Acevez Nuñez, and E. Frey. 2013. The First Human Settlers on the Yucatan Peninsula: Evidence from Drowned Caves in the State of Quintana Roo (South Mexico). *In* K. E. Graf, C. V. Ketron, and M. Waters (eds.), Paleoamerican Odyssey. Texas A&M University, p. 323–337.

González González, A. H., C. Rojas Sandoval, A. Terrazas Mata, M. Benavente Sanvicente, W. Stinnesbeck, J. Aviles Olguín, M. De los Ríos, E. Acevez Nuñez, J. Aviles O, M. De los Ríos, and E. Acevez. 2008. The Arrival of Humans on the Yucatan Peninsula: Evidence from Submerged Caves in the State of Quintana Roo, Mexico. *Current Research in the Pleistocene, 25*:1–24.

Gonzalez, S., D. Huddart, I. Israde-Alcántara, G. Dominguez-Vazquez, and J. Bischoff. 2014. Tocuila Mammoths, Basin of Mexico: Late Pleistocene-Early Holocene stratigraphy and the geological context of the bone accumulation. *Quaternary Science Reviews, 96*:222–239.

Grant, K. M., E. J. Rohling, M. Bar-Matthews, A. Ayalon, M. Medina-Elizalde, C. Bronk Ramsey, C. Satow, and A. P. Roberts. 2012. Rapid coupling between ice volume and polar temperature over the past 150,000 years. *Nature, 491*(7426):744–747.

Grass, A. D. 2019. Inferring differential behavior between giant ground sloth adults and

juveniles through scapula morphology. *Journal of Vertebrate Paleontology, 39*(1):1–15.

Grayson, D. K., and D. J. Meltzer. 2015. Revisiting Paleoindian exploitation of extinct North American mammals. *Journal of Archaeological Science, 56*:177–193.

Griffin, L. R., J. E. Rawlinson, H. G. McDonald, and C. Duncan. 2016. Mandibular osteopathy in a Hagerman horse, *Equus simplicidens* (Equidae, Mammalia), from Hagerman Fossil Beds National Monument (Idaho, USA). *International Journal of Paleopathology, 12*:41–45.

Groves, C. P. 2003. Morphology, morhometrics and taxonomy. *In* D. Curtis and J. Setchell (eds.), Field and laboratory methods in Primatology. Cambridge University Press, Cambridge, p. 140–157.

Guido, F., J. Salvador, and L. Espejel Carvajal. 1994. Tipos de Vegetación de La Península de Yucatán. Universidad Autónoma de Yucatán, Mérida, Yucatán, México, 135 p.

Guthrie, R. D. 2006. New carbon dates link climatic change with human colonization and Pleistocene extinctions. *Nature, 441*(7090):207–9.

Haile, J., D. G. Froese, R. D. E. MacPhee, R. G. Roberts, L. J. Arnold, A. V. Reyes, M. Rasmussen, R. Nielsen, B. W. Brook, S. Robinson, M. Demuro, M. T. P. Gilbert, K. Munch, J. J. Austin, A. Cooper, I. Barnes, P. Möller, and E. Willerslev. 2009. Ancient DNA reveals late survival of mammoth and horse in interior Alaska. *Proceedings of the National Academy of Sciences of the United States of America, 106*(52):22352–22357.

Hansen, R. M. 1978. Shasta ground sloth food habits, Rampart Cave, Arizona. *Paleobiology, 4*:302–319.

Haug, G. H., K. A. Hughen, D. M. Sigman, L. C. Peterson, and U. Röhl. 2001. Southward migration of the Intertropical Convergence Zone through the Holocene. *Science, 293*(5533):1304–1308.

Haynes, G. 2016. North American Megafauna Extinction: Climate or Overhunting? *Encyclopedia of Global Archaeology*, 5382–5390.

Hayssen, V. 2008. *Bradypus pygmaeus* (Pilosa: Bradypolidae). *Mammalian Species, 812*:1–4.

Hayssen, V. 2011. *Choloepus hoffmanni* (Pilosa: Megalonychidae). *Mammalian Species, 43*:37–55.

Henning, W. 1950. Grundzüge Einer Theorie Der Phylogenetischen Systematik. Berlin, 370 p.

Hering, F., W. Stinnesbeck, J. Folmeister, E. Frey, S. R. Stinnesbeck, J. Avilés, E. Acevez Nuñez, A. H. González, A. Terrazas Mata, M. E. Benavente Sanvicente, C. Rojas Sandoval, A. Velázquez Morlet, N. Frank, P. Zell, J. Becker, E. Aceves Núñez, A. H.

González, A. Terrazas Mata, M. E. Benavente, C. Rojas, A. Velázquez Morlet, N. Frank, P. Zell, and J. Becker. 2018. The Chan Hol cave near Tulum (Quintana Roo, Mexico): evidence for long-lasting human presence during the early to middle Holocene. *Journal of Quaternary Science, 33*(4):444–454.

Hilty, J. A., W. Z. Lidicker Jr., and A. M. Merenlender. 2012. Corridor Ecology: The Science and Practice of Linking Landscapes for Biodiversity Conservation. Island Press.

Hirschfeld, S. E., and S. D. Webb. 1968. Plio-Pleistocene megalonychid sloths of North America. *Bulletin of the Florida State Museum Biological Sciences, 12*(5):213–296.

Hodell, D. A., F. S. Anselmetti, D. Ariztegui, M. Brenner, J. H. Curtis, A. Gilli, D. A. Grzesik, T. J. Guilderson, A. D. Müller, M. B. Bush, A. Correa-Metrio, J. Escobar, and S. Kutterolf. 2008. An 85-ka record of climate change in lowland Central America. *Quaternary Science Reviews, 27*(11-12):1152–1165.

Hofreiter, M., H. N. Poinar, W. G. Spaulding, K. Bauer, P. S. Martin, G. Possnert, and S. Pääbo. 2000. A molecular analysis of ground sloth diet through the last glaciation. *Molecular Ecology, 9*(12):1975–1984.

Hoganson, J. W., and H. G. McDonald. 2007. First Report of Jefferson's Ground Sloth (*Megalonyx jeffersonii*) in North Dakota: Paleobiogeographical and Paleoecological Significance. *Journal of Mammalogy, 88*(1):73–80.

Holte, S. E. 2012. Description of Jefferson's Ground Sloth (*Megalonyx jeffersonii*) from ACb-3 Cave, Colbert County, Alabama, with Comments on Ontogeny, Taphonomy, Pathology, and Paleoecology. East Tennessee State University, 181 p.

Hubbe, A., M. Hubbe, and W. A. Neves. 2007. Early Holocene survival of megafauna in South America. *Journal of Biogeography, 34*(9):1642–1646.

Hubbe, A., M. Hubbe, I. Karmann, F. W. Cruz, and W. A. Neves. 2013. Insights into Holocene megafauna survival and extinction in southeastern Brazil from new AMS ^{14}C dates. *Quaternary Research, 79*(2):152–157.

Hubbe, M., A. Terrazas Mata, B. Herrera, M. E. Benavente, A. González González, C. Rojas Sandoval, J. Avilés Olguín, E. Acevez Nuñez, and N. Von Cramon-Taubadel. 2020. Morphological variation of the early human remains from Quintana Roo, Yucata´n Peninsula, Mexico: Contributions to the discussions about the settlement of the Americas. *PLoS ONE, 15*(1):e0227444.

Hunt, A. P., and S. G. Lucas. 2018. The Record of Sloth Coprolites in North and South America: Implications for Terminal Pleistocene Extinctions. *New Mexico Museum of Natural History and Science Bulletin*, *79*, 277-298.

Itescu, Y. 2019. Are island-like systems biologically similar to islands? A review of the evidence. *Ecography, 42*(7):1298–1314.

Jackling, F. C., J. L. Vaughan, M. E. Goddard, and B. R. Appleton. 2011. Genetic diversity in alpacas: Can inbreeding explain the high prevalence of congenital defects? Breeding Objectives: A New Paradigm. *Association for the Advancement of Animal Breeding and Genetics, 11*(2):10–14.

Johnson, C. N. 2009. Ecological consequences of Late Quaternary extinctions of megafauna. *Proceedings of the Royal Society B: Biological Sciences*, *276*(1667):2509–19.

Joly, K., E. Gurarie, M. S. Sorum, P. Kaczensky, M. D. Cameron, A. F. Jakes, B. L. Borg, D. Nandintsetseg, J. G. C. Hopcraft, B. Buuveibaatar, P. F. Jones, T. Mueller, C. Walzer, K. A. Olson, J. C. Payne, A. Yadamsuren, and M. Hebblewhite. 2019. Longest terrestrial migrations and movements around the world. *Scientific Reports, 9*(1):1–10.

Khan, N. S., E. Ashe, B. P. Horton, A. Dutton, R. E. Kopp, G. Brocard, S. E. Engelhart, D. F. Hill, W. R. Peltier, C. H. Vane, and F. N. Scatena. 2017. Drivers of Holocene sea-level change in the Caribbean. *Quaternary Science Reviews, 155*:13–36.

Kirillova, I. V., O. K. Borisova, O. F. Chernova, T. Van Kolfschoten, J. H. J. L. Van Der Lubbe, A. V. Panin, P. Pečnerová, J. Van Der Plicht, F. K. Shidlovskiy, V. V. Titov, and O. G. Zanina. 2020. 'Semi-dwarf' woolly mammoths from the East Siberian Sea coast, continental Russia. *Boreas, 49*(2):269–285.

Koch, P. L., and A. D. Barnosky. 2006. Late Quaternary Extinctions: State of the Debate. *Annual Review of Ecology, Evolution, and Systematics, 37*(1):215–250.

Kosintsev, P. A., E. G. Lapteva, S. S. Trofimova, O. G. Zanina, A. N. Tikhonov, and J. Van der Plicht. 2012. Environmental reconstruction inferred from the intestinal contents of the Yamal baby mammoth Lyuba (*Mammuthus primigenius* Blumenbach, 1799). *Quaternary International, 255*:231–238.

Kübber-Heiss, A., A. Zedrosser, G. Rauer, W. Zenker, P. Schmidt, and J. M. Arnemo. 2009. Internal hydrocephalus combined with pachygyria in a wild-born brown bear cub. *European Journal of Wildlife Research, 55*:539–542.

Larmon, J. T., H. G. McDonald, S. Ambrose, L. R. G. DeSantis, and L. J. Lucero. 2019. A year in the life of a giant ground sloth during the Last Glacial Maximum in Belize. *Science Advances, 5*(2):eaau1200.

Leidy, J. 1855. A Memoir on the Extinct Sloth Tribe of North America. Smithsonian institution.

Lindauer, S., G. M. Santos, A. Steinhof, E. Yousif, C. Phillips, S. A. Jasim, H.-P. Uerpmann,

and M. Hinderer. 2017. The local marine reservoir effect at Kalba (UAE) between the Neolithic and Bronze Age: An indicator of sea level and climate changes. *Quaternary Geochronology, 42*:105–116.

Losos, J. B., and D. L. Mahler. 2010. Adaptive Radiation: The Interaction of Ecological Opportunity, Adaptation, and Speciation. *In* J. S. Levinton, M. Bell, W. Eanes, and D. J. Futuyma (eds.), Evolution since Darwin: The First 150 Years. Palgrave Macmillan, p. 381–420.

Lucas, S. G. 2008. Late Cenozoic fossil mammals from the Chapala rift basin, Jalisco, Mexico. *Neogene Mammals: New Mexico Museum of Natural History and Science, 44*:39–49.

Lucas, S. G. 2014. Late Pleistocene Mammals From El Hatillo, Panama. *Revista Geológica de América Central, 50*:139–151.

Lucas, S. G., and G. E. Alvarado. 2016. Vertebrate palaeontology in Central America: a narrative and analytical history. *In* W. Mayer, R. M. Clary, L. F. Azuela, T. S. Mota, and S. Wołkowicz (eds.), History of. Geoscience: Celebrating 50 Years of INHIGEO., 442. Geological Society, London, p. 155–169.

Lucas, S. G., G. E. Alvarado, and E. Vega. 1997. The Pleistocene mammals of Costa Rica. *Journal of Vertebrate Paleontology, 17*(2):413–427.

Lucas, S. G., G. S. Morgan, J. W. Estep, G. H. Mack, and J. W. Hawley. 1999. Co-occurrence of the proboscideans *Cuvieronius*, *Stegomastodon*, and *Mammuthus* in the Lower Pleistocene of southern New Mexico. *Journal of Vertebrate Paleontology, 19*(3):595–597.

MacArthur, R. H., and E. O. Wilson. 1967. The Theory of Island Biogeography. Princeton University Press., New Jersey, 224 p.

MacPhee, R. D. E. 2007. Mammoths in the insular Nearctic? Some constraints on the existence of a Pleistocene megafaunal refugium in the Canadian Arctic Archipelago. *Quaternary International, 169–170*:29–38.

MacPhee, R. D. E. 2009. Insulae infortunatae: Establishing a Chronology for Late Quaternary Mammal Extinctions in the West Indies. *In* G. Haynes (ed.), American Megafaunal Extinctions at the End of the Pleistocene. Springer Science, p. 169–170.

MacPhee, R. D. E., J. L. White, and C. a. Woods. 2000. New Megalonychid Sloths (Phyllophaga, Xenarthra) from the Quaternary of Hispaniola. *American Museum Novitates, 2000*(3303):1–32.

MacPhee, R. D. E., M. A. Iturralde-Vinent, and O. J. Vázquez. 2007. Prehistoric sloth

extinctions in Cuba: Implications of a new "Last" appearance date. *Caribbean Journal of Science, 43*(1):94–98.

Mai, L. L., M. Young Owl, and M. P. Kersting. 2005. The Cambridge Dictionary of Human Biology and Evolution. Cambridge University Press, Cambridge & New York.

Markova, A. K., A. Y. Puzachenko, T. Van Kolfschoten, J. Van der Plicht, and D. V. Ponomarev. 2013. New data on changes in the European distribution of the mammoth and the woolly rhinoceros during the second half of the Late Pleistocene and the early Holocene. *Quaternary International, 292*:4–14.

Marlon, J. R., P. J. Bartlein, M. K. Walsh, S. P. Harrison, K. J. Brown, M. E. Edwards, P. E. Higuera, M. J. Power, R. S. Anderson, C. Briles, A. Brunelle, C. Carcaillet, M. Daniels, F. S. Hu, M. Lavoie, C. Long, T. Minckley, P. J. H. Richard, A. C. Scott, D. S. Shafer, W. Tinner, C. E. Umbanhowar, and C. Whitlock. 2009. Wildfire responses to abrupt climate change in North America. *Proceedings of the National Academy of Sciences of the United States of America, 106*(8):2519–2524.

Marshall, L. G. 1988. Land Mammals and the Great American Interchange. *American Scientist, 76*(4):380–388.

Martin, F., M. San Román, F. Morello, D. Todisco, F. J. Prevosti, and L. A. Borrero. 2013. Land of the ground sloths: Recent research at Cueva Chica, Ultima Esperanza, Chile. *Quaternary International, 305*:56–66.

Martin, P. S. 1973. The Discovery of America: The first Americans may have swept the Western Hemisphere and decimated its fauna within 1000 years. *Science, 179*(4077):969–974.

Martin, P. S., and R. G. Klein. 1984. Quaternary Extinctions: A Prehistoric Revolution. Tucson, Arizona.

Martin, R. 1914. Lehrbuch Der Anthropologie in Systematischer Darstellung Mit Besonderer Berücksichtigung Der Anthropologischen Methoden. Gustav Fischer Verlag, Jena.

Martínez-Meyer, E., J. E. Sosa-Escalante, and F. Álvarez. 2014. The study of the biodiversity in Mexico: A route with a course? *Revista Mexicana de Biodiversidad, 85*:1–9.

McDonald, H. G. 1977. Description of the osteology of the exctinct gravigrade edentate *Megalonyx* with observations on its ontogeny, phylogeny and functional anatomy. University of Florida, 328 p.

McDonald, H. G. 2002. Fossil Xenarthra of Mexico: A review. *Avances En Los Estudios Paleomastozoológicos*, 227–248.

McDonald, H. G. 2005. Paleoecology of Extinct Xenarthrans and the Great American Biotic

Interchange. B*ulletin of the Florida Museum of Natural History, 45*:313–333.

McDonald, H. G., and S. Pelikan. 2006. Mammoths and mylodonts: Exotic species from two different continents in North American Pleistocene faunas. *Quaternary International, 142–143*:229–241.

McDonald, H. G., and G. T. Jefferson. 2008. Distribution of Pleistocene *Nothrotheriops* (Xenarthra, Nothrotheridae) in North America. *In* Geology and Vertebrate Paleontology of Western and Southern North America, 41. Natural History Museum of Los Angeles County, Los Angeles, p. 313–331

McDonald, H. G., T. W. Stafford, and D. M. Gnidovec. 2015. Youngest radiocarbon age for Jefferson's ground sloth, *Megalonyx jeffersonii* (Xenarthra, Megalonychidae). *Quaternary Research, 83*(2):355–359.

McDonald, H. G., and O. Carranza-Castañeda. 2017. Increased xenarthran diversity of the Great American Biotic Interchange: a new genus and species of ground sloth (Mammalia, Xenarthra, Megalonychidae) from the Hemphillian (late Miocene) of Jalisco, Mexico. *Journal of Paleontology, 91*(5):1069–1082.

McDonald, H. G., and S. L. Dávila. 2017. Mammoths in Central America: New records from Guatemala. *Quaternary International, 443*:122–128.

McDonald, H. G., A. D. Rincón, and T. J. Gaudin. 2013a. A new genus of megalonychid sloth (Mammalia, Xenarthra) from the late Pleistocene (Lujanian) of Sierra de Perija, Zulia State, Venezuela. *Journal of Vertebrate Paleontology, 33*(5):1226-1238.

McDonald, H. G., R. G. Dundas, and J. C. Chatters. 2013b. Taxonomy, paleoecology and taphonomy of ground sloths (Xenarthra) from the Fairmead Landfill locality (Pleistocene: Irvingtonian) of Madera County, California. *Quaternary Research, 79*:215–227.

McDonald, H. G., J. C. Chatters, and T. J. Gaudin. 2017. A new genus of megalonychid ground sloth (Mammalia, Xenarthra) from the late Pleistocene of Quintana Roo, Mexico. *Journal of Vertebrate Paleontology, 37*(3):e1307206.

McKenna, M., A. R. Wyss, and J. J. Flynn. 2006. Paleogene Pseudoglyptodont Xenarthrans from Central Chile and Argentine Patagonia. *American Museum Novitates*, 1–18.

McKenna, M. C., and S. Bell. 1997. Classification of Mammals: Above the Species Level. New York, 486 p.

McKinnon, J. S., S. Mori, B. K. Blackman, L. David, D. M. Kingsley, L. Jamieson, J. Chou, and D. Schluter. 2004. Evidence for ecology's role in speciation. *Nature, 429*(6989):294–298.

McNab, B. K. 1985. Energetics, population biology, and distribution of xenarthrans, living and extinct. *In* G. G. Montgomery (ed.), The evolution and ecology of armadillos, sloths, and vermilinguas. Smithsonian Institution Press, Washington D. C., p. 219–232.

Meltzer, D. J. 2009. First Peoples in a New World: Colonizing Ice Age America. University of California Press, Los Angeles, 446 p.

Meltzer, D. J. 2015. Pleistocene Overkill and North American Mammalian Extinctions. *Annual Review of Anthropology, 44*(1):33–53.

Morgan, G. S. 2005. The great American biotic interchange in Florida. *Bulletin of the Florida Museum of Natural History, 45*(4):271–311.

Morgan, G. S. 2008. Vertebrate fauna and geochronology of the Great American Biotic Interchange in Northamerica. *Neogene Mammals: Bulletin 44*(44):93.

Moritomo, Y., T. Tsuda, and H. Miyamoto. 1999. Craniofacial Skeletal Abnormalities in Anomalous Calves with Clefts of the Face. *Journal of Veterinary Medical Science, 61*(10):1147–1152.

Moseley, G. E., D. A. Richards, P. L. Smart, C. D. Standish, D. L. Hoffmann, H. ten Hove, and O. Vinn. 2015. Early–middle Holocene relative sea-level oscillation events recorded in a submerged speleothem from the Yucatán Peninsula, Mexico. *The Holocene, 25*(9):1511–1521.

Mothé, D., and L. Avilla. 2015. Mythbusting evolutionary issues on South American Gomphotheriidae (Mammalia: Proboscidea). *Quaternary Science Reviews, 110*:23–35.

Mothé, D., L. S. Avilla, and M. A. Cozzuol. 2013. The South American Gomphotheres (Mammalia, Proboscidea, Gomphotheriidae): Taxonomy, Phylogeny, and Biogeography. *Journal of Mammalian Evolution, 20*(1):23–32.

Mulvihill, J. J. 1972. Congenital and Genetic Disease in Domestic Animals. *Science, 176*(4031):132–137.

Naples, V. L. 1982. Cranial osteology and function in the tree sloths, *Bradypus* and *Choloepus*. *Amerian Museum Novitates*, 2739.

Neuchâtel, R. J. 1985. Der Artbegriff in Zoologie, Phylogenetik und Biostratigraphie. *Paläontologische Zeitschrift, 59*(3-4):171–182.

Nickell, Z., and M. Moran. 2017. Disease Introduction by Aboriginal Humans in North America and the Pleistocene Extinction. *Journal of Ecological Anthropology, 19*:29–41.

Nosil, P. 2012. Ecological Speciation. Oxford University Press, New York, 279 p.

O'Dea, A., H. A. Lessios, A. G. Coates, R. I. Eytan, S. A. Restrepo-Moreno, A. L. Cione, L. S. Collins, A. De Queiroz, D. W. Farris, R. D. Norris, R. F. Stallard, M. O. Woodburne,

O. Aguilera, M. P. Aubry, W. A. Berggren, A. F. Budd, M. A. Cozzuol, S. E. Coppard, H. Duque-Caro, S. Finnegan, G. M. Gasparini, E. L. Grossman, K. G. Johnson, L. D. Keigwin, N. Knowlton, E. G. Leigh, J. S. Leonard-Pingel, P. B. Marko, N. D. Pyenson, P. G. Rachello-Dolmen, E. Soibelzon, L. Soibelzon, J. A. Todd, G. J. Vermeij, and J. B. C. Jackson. 2016. Formation of the Isthmus of Panama. *Science Advances, 2*(8):e1600883.

Ortega-Muñoz, A., T. D. Price, J. H. Burton, and A. Cucina. 2019. Population movements and identity in Postclassic Yucatan. Bioarchaeological analysis of human remains from the East Coast of the Yucatan peninsula. *Journal of Archaeological Science: Reports, 23*(8):490–500.

Ortner, D. J. 2003. Identification of Pathological Conditions in Human Skeletal Remains. Academic Press., San Diego, 645 p.

Osborne, A. J., S. S. Negro, B. L. Chilvers, B. C. Robertson, M. A. Kennedy, and N. J. Gemmell. 2016. Genetic evidence of a population bottleneck and inbreeding in the endangered New Zealand sea lion Phocarctos hookeri. *Journal of Heredity, 107*:392–402.

Owen, R. 1842. Description of the Skeleton of an Extinct Gigantic Sloth, *Mylodon robustus* Owen, with Observations on the Osteology, Natural Affinities and Probable Habits of the Megatherioid Quadrupeds in General. Royal College of Surgeons, London, 176 p.

Page, W. D. 1978. The geology of El Bosque Archaeological Site, Nicaragua. *In* A. L. Bryan (ed.), Early Man in America from a Circum-PacificPerspective., Occasional. University of Alberta, Alberta, p. 231–260.

Palkopoulou, E., L. Dalén, A. M. Lister, S. Vartanyan, M. Sablin, A. Sher, V. N. Edmark, M. D. Brandström, M. Germonpré, I. Barnes, and J. A. Thomas. 2013. Holarctic genetic structure and range dynamics in the woolly mammoth. *Proceedings of the Royal Society B: Biological Sciences, 280*: 20131910.

Pant, S. R., A. Goswami, and J. A. Finarelli. 2014. Complex body size trends in the evolution of sloths (Xenarthra: Pilosa). *BMC Evolutionary Biology, 14*(1):184.

Patterson, B., W. Segall, W. D. Turnbull, and T. J. Gaudin. 1992. The ear region in xenarthrans (=Edentata, Mammalia): Part II. Pilosa (sloths, anteaters), palaeanodonts, and a miscellany. *Geology, 24*:1–79.

Patterson, C., and D. E. Rosen. 1977. Review of Ichthyodectiform and Other Mesozoic Teleost Fishes and the Theory and Practice of Classifying Fossils. 358 p.

Pérez-Crespo, V. A., J. L. Prado, M. T. Alberdi, and J. Arroyo-Cabrales. 2018. Stable isotopes

and diets of Pleistocene horses from southern North America and South America: similarities and differences. *Palaeobiodiversity and Palaeoenvironments, 98*:663–674.

Pérez-Crespo, V. A., J. L. Prado, M. T. Alberdi, J. Arroyo-cabrales, and E. Johnson. 2016. Diet and Habitat for Six American Pleistocene Proboscidean Species Using Carbon and Oxygen Stable Isotopes. *Ameghiniana, 53*(1):39–51.

Perrotti, A. G., B. Winsborough, J. J. Halligan, and M. R. Waters. 2019. Reconstructing Terminal Pleistocene-Early Holocene Environmental Change at Page-Ladson, Florida Using Diatom Evidence. *PaleoAmerica, 6*(2):181–193.

Peters, D. S. 1976. Evolutionstheorie und Systematic. *Journal of Ornithologie, 117*:329–344.

Pfennig, D. W., and K. S. Pfennig. 2010. Character displacement and the origins of diversity David. *American Naturalist, 176*:26–44.

Poinar, H. N., M. Hofreiter, W. G. Spaulding, P. S. Martin, B. A. Stankiewicz, H. Bland, R. P. Evershed, G. Possnert, S. Pääbo, A. Stankiewicz, H. Bland, R. P. Evershed, G. Possnert, and S. Pääbo. 1998. Molecular coproscopy: Dung and diet of the extinct ground sloth *Nothrotheriops shastensis*. *Science, 281*(5375):402–406.

Poinar, H. N., and M. Kuch. 2003. Nuclear Gene Sequences from a Late Pleistocene Sloth Coprolite. *Current Biology, 13*:654–658.

Politis, G. G., P. G. Messineo, T. W. Stafford, and E. L. Lindsey. 2019. Campo Laborde: A Late Pleistocene giant ground sloth kill and butchering site in the Pampas. *Science Advances, 5*(3):1–11.

Prado, J. L., M. T. Alberdi, B. Azanza, B. Sánchez, and D. Frassinetti. 2005. The Pleistocene Gomphotheriidae (Proboscidea) from South America. *Quaternary Geochronology*, 21–30.

Prado, J. L., J. Arroyo-Cabrales, E. Johnson, M. T. Alberdi, and O. J. Polaco. 2015. New World proboscidean extinctions: comparisons between North and South America. *Archaeological and Anthropological Sciences, 7*(3):277–288.

Price, T. D., J. H. Burton, P. D. Fullagar, L. E. Wright, J. E. Buikstra, and V. Tiesler. 2008. Strontium isotopes and the study of human mobility in ancient Mesoamerica. *Latin American Antiquity, 19*(2):167–180.

Pujos, F., G. De Iuliis, C. Argot, and L. Werdelin. 2007. A peculiar climbing Megalonychidae from the Pleistocene of Peru and its implication for sloth history. *Zoological Journal of the Linnean Society, 149*(2):179–235.

Redmond, B. G., H. G. McDonald, H. J. Greenfield, and M. L. Burr. 2012. New evidence for Late Pleistocene human exploitation of Jefferson's Ground Sloth (*Megalonyx jeffersonii*)

from northern Ohio, USA. *World Archaeology, 44*:75–101.

Reimer, P. J., E. Bard, A. Bayliss, J. W. Beck, P. G. Blackwell, C. B. Ramsey, C. E. Buck, H. Cheng, R. L. Edwards, M. Friedrich, P. M. Grootes, T. P. Guilderson, H. Haflidason, I. Hajdas, C. Hatté, T. J. Heaton, D. L. Hoffmann, A. G. Hogg, K. A. Hughen, K. F. Kaiser, B. Kromer, S. W. Manning, M. Niu, R. W. Reimer, D. A. Richards, E. M. Scott, J. R. Southon, R. A. Staff, C. S. M. Turney, and J. van der Plicht. 2013. IntCal13 and Marine13 Radiocarbon Age Calibration Curves 0–50,000 Years cal BP. *Radiocarbon, 55*(4):1869–1887.

Reumer, J. W. F. 2007. Habitat fragmentation and the extinction of mammoths (*Mammuthus primigenius*, Proboscidea, Mammalia): Arguments for a causal relationship. *CFS Courier Forschungsinstitut Senckenberg*, *269*:279–286.

Reumer, J. W. F., C. M. A. ten Broek, and F. Galis. 2014. Extraordinary incidence of cervical ribs indicates vulnerable condition in late Pleistocene mammoths. *PeerJ*, *2*:1–9.

Ríos, L., T. L. Kivell, C. Lalueza-Fox, A. Estalrrich, A. García-Tabernero, R. Huguet, Y. Quintino, M. de la Rasilla, and A. Rosas. 2019. Skeletal Anomalies in The Neandertal Family of El Sidrón (Spain) Support A Role of Inbreeding in Neandertal Extinction. *Scientific Reports, 9*(1):1–11.

Ritter, S. M., M. Isenbeck-Schröter, C. Scholz, F. Keppler, J. Gescher, L. Klose, N. Schorndorf, J. Avilés Olguín, A. González-González, and W. Stinnesbeck. 2019. Subaqueous speleothems (Hells Bells) formed by the interplay of pelagic redoxcline biogeochemistry and specific hydraulic conditions in the El Zapote sinkhole, Yucatán Peninsula, Mexico. *Biogeosciences Discussions*, 1–35.

Robertson, J. M., L. Samankova, and T. H. Ingalls. 1966. Hydrocephalus and cleft palate in an inbred rabbit colony. *Journal of Heredity, 57*:142–148.

Rogers, R. L., and M. Slatkin. 2017. Excess of genomic defects in a woolly mammoth on Wrangel island. *PLoS Genetics, 13*(3):1–16.

Rosenberg, D. K., B. R. Noon, and E. C. Meslow. 1997. Biological corridors: Form, function, and efficacy. Linear conservation areas may function as biological corridors, but they may not mitigate against additional habitat loss. *BioScience, 47*(10):677–687.

Rothschild, B. M., and L. D. Martin. 2006. Did ice-age bovids spread tuberculosis? Die *Naturwissenschaften, 93*(11):565–569.

Rothschild, B. M., and R. Laub. 2006. Hyperdisease in the late Pleistocene: validation of an early 20th century hypothesis. *Die Naturwissenschaften, 93*(11):557–564.

Rothschild, B. M., L. D. Martin, G. Lev, H. Bercovier, G. K. Bar-Gal, C. Greenblatt, H.

Donoghue, M. Spigelman, and D. Brittain. 2001. *Mycobacterium tuberculosis* Complex DNA from an Extinct Bison Dated 17,000 Years before the Present. *Clinical Infectious Diseases, 33*(3):305–311.

Rule, S., B. W. Brook, S. G. Haberle, C. S. M. Turney, a. P. Kershaw, and C. N. Johnson. 2012. The Aftermath of Megafaunal Extinction: Ecosystem Transformation in Pleistocene Australia. *Science, 335*(6075):1483–1486.

Rundle, H. D., and P. Nosil. 2005. Ecological speciation. *Ecology Letters, 8*(3):336–352.

Sacchei, I., M. Kuussaari, M. Kankare, P. Vikman, W. Fortelius, and I. Hanski. 1998. Inbreeding and extinction in a butterfly metapopulation. *Nature, 392*(2):491–494.

Sanchez, G., V. T. Holliday, E. P. Gaines, J. Arroyo-Cabrales, N. Martínez-Tagüeña, A. Kowler, T. Lange, G. W. L. L. Hodgins, S. M. Mentzer, I. Sanchez-Morales, G. Sanchez, V. T. Holliday, G. W. L. L. Hodgins, T. Lange, I. Sanchez-Morales, N. Martinez-Taguena, E. P. Gaines, S. M. Mentzer, and A. Kowler. 2014. Human (Clovis)-gomphothere (*Cuvieronius* sp.) association 13,390 calibrated yBP in Sonora, Mexico. *Proceedings of the National Academy of Sciences, 111*(30):10972–10977.

Sandom, C., S. Faurby, B. Sandel, and J. C. Svenning. 2014. Global late Quaternary megafauna extinctions linked to humans, not climate change. *Proceedings of the Royal Society B: Biological Sciences, 281*(1787):20133254.

Schluter, D. 2000. The Ecology of Adaptive Radiation. Oxford University Press, Oxford, UK, 296 p.

Schreiber, H. D. 2004. Faunal characterisation of Neogene and Pleistocene localities of the State Jalisco, Mexico. *Carolinea, 62*:63–68.

Schubert, B. W., J. C. Chatters, J. Arroyo-Cabrales, J. X. Samuels, L. H. Soibelzon, F. J. Prevosti, C. Widga, A. Nava, D. Rissolo, and P. L. Erreguerena. 2019. Yucatán carnivorans shed light on the great American biotic interchange. Biology Letters, 15(5):13–15.

Seersholm, F. V., D. J. Werndly, A. Grealy, T. Johnson, E. M. Keenan Early, E. L. Lundelius, B. Winsborough, G. E. Farr, R. Toomey, A. J. Hansen, B. Shapiro, M. R. Waters, G. McDonald, A. Linderholm, T. W. Stafford, and M. Bunce. 2020. Rapid range shifts and megafaunal extinctions associated with late Pleistocene climate change. *Nature Communications, 11*(1):2770.

Shaw, K. L., and R. G. Gillespie. 2016. Comparative phylogeography of oceanic archipelagos: Hotspots for inferences of evolutionary process. *Proceedings of the National Academy of Sciences of the United States of America, 113*(29):7986–7993.

Simpson, G. G. 1944. Tempo and Mode in Evolution. Columbia University Press, New York, 1–237 p.

Smart, P. L., P. Beddows, J. Coke, S. Doerr, and F. F. Whitaker. 2006. Cave Development on the Caribbean coast of the Peninsula, Yucatan Roo, Quintana. *Geological Society of America Special Papers, 404*:105–128.

Smith, D. E., S. Harrison, C. R. Firth, and J. T. Jordan. 2011. The early Holocene sea level rise. *Quaternary Science Reviews, 30*:1846–1860.

Sosa-Escalante, J. E., J. M. Pech-Canché, M. C. Macswiney, and S. Hernández-Betancourt. 2013. Mamíferos terrestres de la península de Yucatán, México: Riqueza, endemismo y riesgo. *Revista Mexicana de Biodiversidad, 84*:i–xxi.

Steadman, D. W., P. S. Martin, R. D. E. MacPhee, A. J. T. Jull, H. G. McDonald, C. A. Woods, M. Iturralde-Vinent, and G. W. L. Hodgins. 2005. Asynchronous extinction of late Quaternary sloths on continents and islands. *Proceedings of the National Academy of Sciences of the United States of America, 102*(33):11763–11768.

Stinnesbeck, S. R., E. Frey, W. Stinnesbeck, J. Avíles Olguín, P. Zell, A. Terrazas Mata, M. Benavente Sanvicente, A. González González, C. Rojas Sandoval, and E. Acevez Nuñez. 2017a. A new fossil peccary from the Pleistocene-Holocene boundary of the eastern Yucatán Peninsula, Mexico. *Journal of South American Earth Sciences, 77*:341–349.

Stinnesbeck, S. R., E. Frey, J. A. Olguín, W. Stinnesbeck, P. Zell, H. Mallison, A. González González, E. Aceves Núñez, A. Velázquez Morlet, A. Terrazas Mata, M. Benavente Sanvicente, F. Hering, and C. Rojas Sandoval. 2017b. *Xibalbaonyx oviceps*, a new megalonychid ground sloth (Folivora, Xenarthra) from the Late Pleistocene of the Yucatán Peninsula, Mexico, and its paleobiogeographic significance. *Paläontologische Zeitschrift, 91*(2):245–271.

Stinnesbeck, S. R., W. Stinnesbeck, A. Terrazas Mata, J. Avilés Olguín, M. Benavente Sanvicente, P. Zell, E. Frey, S. Lindauer, C. Rojas Sandoval, A. Velázquez Morlet, E. Acevez Nuñez, and A. González González. 2018a. The Muknal cave near Tulum, Mexico: An early-Holocene funeral site on the Yucatán peninsula. *The Holocene*, *28*(12):1–14.

Stinnesbeck, S. R., E. Frey, and W. Stinnesbeck. 2018b. New insights on the paleogeographic distribution of the Late Pleistocene ground sloth genus *Xibalbaonyx* along the Mesoamerican Corridor. *Journal of South American Earth Sciences, 85*:108–120.

Stinnesbeck, S. R., W. Stinnesbeck, E. Frey, J. Avilés Olguín, C. Rojas Sandoval, A. Velázquez Morlet, and A. H. González. 2018c. *Panthera balamoides* and other

Pleistocene felids from the submerged caves of Tulum, Quintana Roo, Mexico. *Historical Biology, 00*:1–10.

Stinnesbeck, S. R., W. Stinnesbeck, E. Frey, J. Avilés Olguín, and A. González González. 2020a. *Xibalbaonyx exinferis* n. sp. (Megalonychidae), a new Pleistocene ground sloth from the Yucatán Peninsula, Mexico. *Historical Biology, 00*:1–12.

Stinnesbeck, S. R., E. Frey, J. Avilés Olguín, A. H. González González, A. Velazquez Morlet, and W. Stinnesbeck. 2020b. Life and death of *Xibalbaonyx oviceps*. *Historical Biology*, Submitted.

Stinnesbeck, W., S. R. Rennie, S. R. Stinnesbeck, J. Avilés Olguín, S. Gonzalez, N. Frank, S. Warken, N. Schorndorf, T. Krengel, A. Velázquez Morlet, and A. González González. 2020. New evidence for an early settlement of the Yucatan Peninsula, Mexico: The Chan Hol 3 woman and her meaning for the Peopling of the Americas. *Plos One, 15*:e0227984.

Stinnesbeck, W., J. Becker, F. Hering, E. Frey, A. H. González González, J. Fohlmeister, S. R. Stinnesbeck, N. Frank, A. Terrazas Mata, M. E. Benavente Sanvicente, J. Avilés Olguín, E. Aceves Núñez, P. Zell, and M. Deininger. 2017. The earliest settlers of Mesoamerica date back to the late Pleistocene. *Plos One, 12*:16–18.

Stock, C. 1943. The Cave of San Josecito, Mexico. *Engineering and Science, 6*:10–14.

Straehl, F. R., T. M. Scheyer, A. M. Forasiepi, R. D. MacPhee, and M. R. Sánchez-Villagra. 2013. Evolutionary Patterns of Bone Histology and Bone Compactness in Xenarthran Mammal Long Bones. *Plos One, 8*:1–19.

Stuart, A. J. 2015. Late Quaternary megafaunal extinctions on the continents: a short review. *Geological Journal, 50*:338–363.

Stuart, A. J., and A. M. Lister. 2012. Extinction chronology of the woolly rhinoceros *Coelodonta antiquitatis* in the context of late Quaternary megafaunal extinctions in northern Eurasia. *Quaternary Science Reviews, 51*:1–17.

Surovell, T. A., and N. M. Waguespack. 2008. How many elephant kills are 14?. Clovis mammoth and mastodon kills in context. *Quaternary International, 191*(49):82–97.

Swofford, D. L. 2002. PAUP: Phylogenetic Analysis Using Parsimony, Version 4.0b10. Sinauer Associates, Sunderland, Massachusetts.

Taylor, R. E. 2009. Six Decades of Radiocarbon Dating in New World Archaeology. *Radiocarbon, 51*(1):173–212.

Thompson, R. S., T. R. Van Devender, P. S. Martin, T. Foppe, and A. Long. 1980. Shasta ground sloth (*Nothrotheriops shastense* Hoffstetter) at Shelter Cave, New Mexico:

Environment, diet, and extinction. *Quaternary Research, 14*(3):360–376.

Toledo, N., M. S. Bargo, S. F. Vizcaíno, G. De Iuliis, and F. Pujos. 2017. Evolution of body size in anteaters and sloths (Xenarthra, Pilosa): Phylogeny, metabolism, diet and substrate preferences. *Earth and Environmental Science Transactions of the Royal Society of Edinburgh, 106*:289–301.

Ungar, P. S. 2010. Mammal Teeth: Origin, Evolution, and Diversity. John Hopkins University Press, Baltimore, Maryland, 304 p.

van der Geer, A. A. E., and F. Galis. 2017. High incidence of cervical ribs indicates vulnerable condition in Late Pleistocene woolly rhinoceroses. *PeerJ, 5*:3684.

van der Geer, A. A. E., G. A. Lyras, P. Mitteroecker, and R. D. E. MacPhee. 2018. From Jumbo to Dumbo: Cranial Shape Changes in Elephants and Hippos During Phyletic Dwarfing. *Evolutionary Biology, 45*(3):303–317.

Varela-Lasheras, I., A. J. Bakker, S. D. van der Mije, J. A. J. Metz, J. van Alphen, and F. Galis. 2011. Breaking evolutionary and pleiotropic constraints in mammals: On sloths, manatees and homeotic mutations. *EvoDevo, 2*(1):1–27.

Varela, L., and R. A. Fariña. 2016. Co-occurrence of mylodontid sloths and insights on their potential distributions during the late Pleistocene. *Quaternary Research, 85*(1):66–74.

Varela, L., P. S. Tambusso, H. G. McDonald, and R. A. Fariña. 2019. Phylogeny, Macroevolutionary Trends and Historical Biogeography of Sloths: Insights From a Bayesian Morphological Clock Analysis. *Systematic Biology, 68*(2):204–218.

Vartanyan, S. L., V. E. Garutt, and A. V. Sher. 1993. Holocene dwarf mammoths from Wrangel Island in the Siberian Arctic. *Nature, 362*(6418):337–340.

Vázquez-Dominguez, E., and H. T. Arita. 2010. The Yucatan peninsula: biogeographical history 65 million years in the making. *Ecography, 33*(2):212–219.

Vizcaíno, S. F., M. Zárate, M. S. Bargo, and A. Dondas. 2001. Pleistocene burrows in the Mar del Plata area (Argentina) and their probable builders. *Acta Palaeontologica Polonica, 46*(2):289–301.

Von den Driesch, A. 1976. A Guide to the Measurement of Animal Bones from Archaeological Sites. Peabody Museum Bulletin 1, Harvard, 137 p.

Ward, W. C. 1997. Geology of coastal islands, northeastern Yucatan Peninsula. *In* H. L. Vacher and T. M. Quinn (eds.), Geology and hydrogeology of carbonate islands., 54th ed. Elsevier, p. 275–298.

Ward, W. C., A. E. Weidie, and W. Back. 1985. Geology and Hydrogeology of the Yucatan and Quaternary Geology of Northeastern Yucatan Peninsula. Geological Society, New

Orleans, 95 p.

Warren, B. H., D. Simberloff, R. E. Ricklefs, R. Aguilée, F. L. Condamine, D. Gravel, H. Morlon, N. Mouquet, J. Rosindell, J. Casquet, E. Conti, J. Cornuault, J. M. Fernández-Palacios, T. Hengl, S. J. Norder, K. F. Rijsdijk, I. Sanmartín, D. Strasberg, K. A. Triantis, L. M. Valente, R. J. Whittaker, R. G. Gillespie, B. C. Emerson, and C. Thébaud. 2015. Islands as model systems in ecology and evolution: Prospects fifty years after MacArthur-Wilson. *Ecology Letters, 18*(2):200–217.

Waters, M. R., T. W. Stafford, B. Kooyman, and L. V. Hills. 2015. Late Pleistocene horse and camel hunting at the southern margin of the ice-free corridor: Reassessing the age of Wally's Beach, Canada. *Proceedings of the National Academy of Sciences of the United States of America, 112*(14):4263–4267.

Webb, S. 2013. Corridors to Extinction and the Australian Megafauna. Elsevier, London.

Webb, S. D. 2006. The Great American Biotic Interchange: Patterns and Processes. *Annals of the Missouri Botanical Garden, 93*(2):245–257.

Webb, S. D., and S. C. Perrigo. 1984. Late Cenozoic Vertebrates from Honduras and El Salvador. *Journal of Vertebrate Paleontology, 4*(2):237–254.

Webb, S. D., and S. Perrigo. 1985. New megalonychid sloths from El Salvador. *In* Montgomery (ed.), The evolution and ecology of armadillos, sloths, and vermilinguas. Smithsonian Institution Press, Washington & London, p. 113–120.

Weidie, A. E. 1985. Part I: Geology of Yucatan Platform. *In* W. C. Ward, A. E. Weidie, and W. Back (eds.), Geology and hydrogeology of the Yucatan and Quaternary geology of northeastern Yucatan Peninsula. Geological Society, New Orleans, p. 1–19.

White, J. L., and R. DE MacPhee. 2001. The sloths of the West Indies: a systematic and phylogenetic review. *In* Biogeography of the West Indies: Patterns and Perspectives. CRC Press, New York, p. 201–235.

Wible, J. R., and T. J. Gaudin. 2004. On the cranial osteology of the yellow armadillo *Euphractus sexcintus* (Dasypodidae, Xenarthra, Placentalia). *Annals Carnegie Museum Pittsburgh*, *73*:111–117.

Wilson, J. A. 2002. Sauropod dinosaur phylogeny: critique and cladistic analysis. *Zoological Journal of the Linnean Society, 136*(2):215–275.

Wilson, M. C., S. M. Kenady, and R. F. Schalk. 2009. Late Pleistocene *Bison antiquus* from Orcas Island, Washington, and the biogeographic importance of an early postglacial land mammal dispersal corridor from the mainland to Vancouver Island. *Quaternary Research, 71*(1):49–61.

Woodburne, M. O. 2010. The Great American Biotic Interchange: dispersals, tectonics, climate, sea level and holding pens. *Journal of Mammalian Evolution, 17*(4):245–264.

Woodman, N., and N. Beavan Athfield. 2009. Post-Clovis survival of American Mastodon in the southern Great Lakes Region of North America. *Quaternary Research, 72*(3):359–363.

Yann, L. T., L. R. G. DeSantis, P. L. Koch, and E. L. Lundelius. 2016. Dietary ecology of Pleistocene camelids: Influences of climate, environment, and sympatric taxa. *Palaeogeography, Palaeoclimatology, Palaeoecology, 461*:389–400.

7   Appendix

Table 1. Ground sloth localities in Mexico. *Hemphillian*, *Irvingtonian* and *Rancholabrean* are North American Land Mammal Ages. The *Hemphillian* is considered to overlap the Miocene-Pliocene transition from 10.3 to 4.9 million years BP. The *Irvingtonian* spans the Early to Middle Pleistocene, 1.9 million to 250.000 years BP, while the *Rancholabrean* period is set from 240.000 to 11.000 years BP. Note that most references are based on the listing by McDonald 2002 and these fossils have not been revised here. "?" indicates that a review is required. For an exact geographical distribution of the Mexican ground sloths see figure 4.

Taxa	Locality	Age	Reference
Megalonychidae			
Pliometanastes sp.	Nuevo León	Hemphillian	Carranza-Castañeda and Miller 2004.
Pliometanastes sp.	Río Virgenes, Tamaulipas	Hemphillian	McDonald 2002.
Megalonyx weatleyi	El Golfo, Sonora	Irvingtonian	Shaw 1981; McDonald 2002.
Megalonyx jeffersonii	San Josecito Cave, Nuevo León	Rancholabrean	Stock 1943; McDonald 2002; Ferrusquía-Villafranca et al. 2010.
Megalonyx jeffersonii	Valsequillo Reservoir, Puebla	Rancholabrean	McDonald 2002; Ferrusquía-Villafranca et al 2010.
Megalonychidae	Puebla	Rancholabrean	Unpub.
Zacatzontli tecolotlanensis	Jalisco	Hemphillian	McDonald and Carranza-Castañeda 2017.
Xibalbaonyx microcaninus	Lago Chapala, Guadalajara, Jalisco	Rancholabrean	Stinnesbeck et al. 2018.
Megalonychidae	El Pit, Quintana Roo	Rancholabrean	Unpub.
Megalonychidae	Caracoles y Camellos, Quintana Roo	Rancholabrean	Unpub.
Megalonychidae	Naitucha 1 und 2, Quintana Roo	Rancholabrean	Unpub.
Megalonychidae	Concha 1, Quintana Roo	Rancholabrean	Unpub.
Nohochichak xibalbakah	Hoyo Negro, Tulum Quintana Roo	Rancholabrean	Chatters et al. 2014.
Megalonychidae	El Tigre / Kóox Baal, Quintana Roo	Rancholabrean	Unpub.
Megalonychidae	Tortuga, Quintana Roo	Rancholabrean	Unpub.
Xibalbaonyx exinferis	Tortuga, Quintana Roo	Rancholabrean	Stinnesbeck et al. 2020.
Xibalbaonyx oviceps	El Zapote, Puerto Morelos, Quintana Roo	Early Holocene	González et al. 2008; Stinnesbeck et al. 2017.
Megalonychidae	El Zapote, Puerto Morelos, Quintana Roo	Rancholabrean	Unpub.
Nothrotheriidae			
Nothrotheriops shastensis	Comondu, Baja California Sur	Rancholabrean	Thompson et al 1980.
Nothrotheriops texanus	El Golfo, Sonora	Rancholabrean	Shaw 1981; McDonald 2002; McDonald and

			Jefferson 2008.
Nothrotheriops shastensis	Bustamante Cave, Nuevo León	Rancholabrean	McDonald 1985; McDonald 2002; Ferrusquía-Villafranca et al. 2010.
Nothrotheriops shastensis	Mina, Nuevo León	Rancholabrean	Franzen 1994; McDonald 2002.
Nothrotheriops shastensis	San Josecito Cave, Nuevo León	Rancholabrean	Stock 1943; McDonald 2002.
Nothrotheriops shastensis	Cerro de la Silla, Nuevo León	Rancholabrean	Furlong 1925; McDonald 2002; Ferrusquía-Villafranca et al. 2010.
Nothrotheriops shastensis/ N. mexicanum	Valley of Mexico, Mexico	Rancholabrean	Freudenberg 1921; McDonald 2002; Ferrusquía-Villafranca et al. 2010.
Nothrotheriops shastensis	Cedazo, Aguascalientes	Rancholabrean	Mooser & Dalquest 1975; McDonald 2002; Ferrusquía-Villafranca et al. 2010.
Nothrotheriops shastensis	Cueva de la Presita, San Luis Potosi	Rancholabrean	Polaco-Ramos & Butron 1997; McDonald 2002; Ferrusquía-Villafranca et al 2010.
Nothrotheriops shastensis	Lago Chapala, Jalisco	Rancholabrean	Downs 1958; McDonald 2002; Lucas 2008; Ferrusquía-Villafranca et al. 2010.
Nothrotheriops shastensis	Rancho de las Ollas, Michoacán	Rancholabrean	Silva-Bárcenas 1969; McDonald 2002.
Nothrotheriops shastensis	Valsequillo Reservoir, Puebla	Rancholabrean	Pichardo 1997; Ferrusquía-Villafranca et al. 2010.
Nothrotheriops shastensis	Hoyo Negro, Tulum, Quintana Roo	Rancholabrean	Chatters et al. 2014.
Nothrotheriops shastensis	Kalimba, Quintana Roo	Rancholabrean	Unpub.
Nothrotheriops shastensis	Concha 2, Quintana Roo	Rancholabrean	Unpub.
Nothrotheriops sp.	Tortugas, Quintana Roo	Rancholabrean	Unpub.
Nothrotheriops shastensis	El Pit 10 min, Quintana Roo	Rancholabrean	Unpub.; González et al. 2008.
Mylodontidae			
?Mylodon	Tequesquinahua, Mexico	Rancholabrean	Mones 1971; McDonald 2002.
?Mylodon	Valle de Bravo, Mexico	Rancholabrean	Villada 1903; McDonald 2002.
?Mylodon	Villa Gustavo Madero, Mexico	Rancholabrean	Muelleried 1934; McDonald 2002.
?Glossotherium sp.	El Ocote, Guanajuato	Irvingtonian	Carranza-Castaneda & Miller 2004.
Glossotherium chapadmalense	Arroyo El Tanque, Guanajuato	Irvingtonian	Montellano-Ballesteros & Carranza-Castañeda 1986.
Paramylodon harlani	Bustamente Cave, Nuevo León	Rancholabrean	McDonald 2002.
Paramylodon harlani	El Golfo, Sonora	Rancholabrean	Shaw 1981; McDonald 2002.
Paramylodon harlani	Cabo Colnett, Baja California Norte	Rancholabrean	McDonald 2002.
Paramylodon harlani	Zacoalco, Lago Chapala, Jalisco	Rancholabrean	Polaco-Ramos 1981; McDonald 2002; Lucas 2008.

Taxon	Locality	Age	Reference
Paramylodon harlani	El Cedral, San Luis Potosi	Rancholabrean	Polaco-Ramos 1981; McDonald 2002.
Paramylodon harlani	Arperos, Guanajuato	Rancholabrean	Dugés 1882; Mones 1973; Ferrusquia-Villafranca et al. 2010.
Paramylodon harlani	Arroyo Cedazo, Auguascalientes	Rancholabrean	Faith & Surovell 2009.
Paramylodon harlani	Tajo de Tequixquiac, Edo México	Rancholabrean	Freudenberg 1921; McDonald 2002.
Paramylodon harlani	Cueva Encantada, Morelos	Rancholabrean	Arroyo-Cabrales et al. 2004; Ferrusquia-Villafranca et al. 2010.
Paramylodon harlani	Aquiahua, Tlaxcla	Rancholabrean	Polaco-Ramos 1981; Ferrusquia-Villafranca et al. 2010.
Paramylodon harlani	Teapa, Tabasco	Rancholabrean	Polaco-Ramos 1981; McDonald 2002.
?Paramylodon harlani	Actun Spukil, Yucatán	Rancholabrean	Hatt 1953; McDonald 2002.
Megatheriidae			
Eremotherium laurillardi	Aguascalientes	Rancholabrean	Unpub.
Eremotherium laurillardi	Aguacate, Michoacán	Rancholabrean	McDonald 2002.
Eremotherium laurillardi	Arteaga, Michoacán	Rancholabrean	Polaco-Ramos 1981.
Eremotherium laurillardi	El Cedral, San Luis Potosi	Rancholabrean	Polaco-Ramos 1981.
Eremotherium laurillardi	Teapa, Tabasco	Rancholabrean	Polaco-Ramos 1981.
Eremotherium laurillardi	Tlatlalla, Mexico	Rancholabrean	Polaco-Ramos 1981.
Eremotherium laurillardi	Venustiano Carranza, Jalisco	Rancholabrean	Polaco-Ramos 1981.
Eremotherium laurillardi	Lago de Chapala, Zacoalco, Jalisco	Rancholabrean	Polaco-Ramos 1981, Stinnesbeck et al. 2018.
Eremotherium laurillardi	Arperos, Guanajuato	Rancholabrean	Dugés 1882; Monés 1973.
Eremotherium laurillardi	Etla, Oaxaca	Rancholabrean	Polaco-Ramos 1981.
Eremotherium laurillardi	Chiapas	Rancholabrean	Unpub.

Table 2: Palaeontological localities studied in Quintana Roo and Yucatán, south-eastern Mexico.

Locality	Cave system and state	Taxa	Age / Dating ^{14}C years BP	Comment	Reference
Canún	Yucatán	*Equus* sp.			Unpubl.
		Hemiauchenia sp.			
		Glyptotherium sp.			
		Tapirus sp.			
Caracoles y Camellos	Muknal, Quintana Roo	*Canis* sp.			Unpubl.
		Cuvieronius hyodon			
		Equus sp.	7.805 ± 30		
		Hemiauchenia sp.			
		Mazama americana			
		Tayassu tajacu			
		Tapirus bairdii			
		Odocoileus virginianus			
		Xibalbaonyx sp.			
La Chimenea	Taj Mahal system, Quintana Roo	*Hemiauchenia* sp.	8.896 ± 29	Fireplace	González et al. 2013.
Concha	Outland system, Quintana Roo	*Cuvieronius hyodon*			Unpubl.
		Nothrotheriops shastensis		Illumination sites	
		Xibalbaonyx sp.			
Dos Ojos cenote	Dos Ojos, Quintana Roo	*Tapirus* sp.		Cut marks	Unpubl.
Hoyo Negro	Dos Ojos, Quintana Roo	*Nohochichak xibalbakah*			McDonald et al. 2017.

		Nothrotheriops shastensis			Chatters et al. 2014.
		Paramylodon harlani			Chatters et al. 2014.
Kalimba	Sac Actun, Quintana Roo	*Nothrotheriops shastensis*			Unpubl.
Kim Ha		*Cuvieronius hyodon*		Cut marks	Unpubl.
		Equus sp.	13.138 ± 65	Cut marks	
		Tapirus sp.		Cut marks	
Muknal	Muknal, Quintana Roo	*Muknalia minima*		Cut marks, burial context	Stinnesbeck et al. 2017.
Nai Tucha	Tuhx Cubaxa system, Quintana Roo	*Cuvieronius hyodon*	20.860	Nai Tucha	Unpubl.
		Tapirus bairdii			
		Xibalbaonyx sp.			
Las Palmas	Muknal, Quintana Roo	*Equus* sp.		Cut marks	Unpubl.
Papakal	Yucatán	Camelidae			Unpubl.
El Pit cave 10	Dos Ojos, Quintana Roo	*Nothrotheriops shastensis*	14.093 ± 136		Unpubl.
El Pit cave 45	Dos Ojos, Quintana Roo	Megalonychidae			Unpub.
El Pit cenote	Dos Ojos, Quintana Roo	*Panthera balamoides*			Stinnesbeck et al. 2019.
		Panthera leo atrox			
Puntos de Luz	Taj Mahal system, Quintana Roo	*Tapirus* sp.			Unpubl.

Site	Location	Taxon			Reference
El Tigre	Sac Actun system, Quintana Roo	*Xibalbaonyx* sp.			Motycka et al. 2013
Toh	Quintana Roo	Megalonychidae		Cut marks?	Unpub.
Cenote Tortugas	Puerto Morelos, Quintana Roo	*Nothrotheriops* sp.		Pathologies	Unpubl.
		Xibalbaonyx exinferis			Stinnesbeck et al. 2020.
		Xibalbaonyx sp.	12.110 ± 40	Adult	Unpubl.
		Megalonychidae		Several new species, infant and mature individuals	
El Zapote cenote	Puerto Morelos, Quintana Roo	*Puma concolor*			
		Xibalbaonyx oviceps	9.305 ± 35	Cut marks	Stinnesbeck et al. 2017. Stinnesbeck et al. 2020, submitted.
		Megalonychidae	23.530 ± 290 (adult)	Infant and adult individuals	Unpubl.
		Nothrotheriops sp. ?		Adult individuals	Unpub.

8   Acknowledgements – Danksagung

bedanken für die uneingeschränkte und vielseitige Unterstützung. Seiner Geduld und seinem Verständnis konnte ich während der letzten Jahre immer gewiss sein.

Mein ganz besonderer Dank aber gilt meinen Eltern Lily und Wolfgang, die mir meinen bisherigen Lebensweg ermöglichten und immer hinter mir gestanden haben. Die zahlreichen Gespräche und der konstruktive Austausch haben mich stets ermutigt und motiviert. Vor allem meinem Vater Wolfgang, danke ich für die unerschöpflichen wissenschaftlichen Diskussionen, seinen Enthusiasmus, und dass ich Teil dieses wunderbaren Projektes werden durfte!

Herzlichen Dank Euch allen!   Karlsruhe, den 15. August 2020

9   Publications

The following research papers form part of the cumulative dissertation and were published in different scientific journals. Osteological documentation and description of new ground sloth taxa forms the basis of this work. Other manuscripts presented here have focused on the identification of megafaunal taxa other than ground sloths and archaeological evidence. They are essential to understand the environmental conditions under which the ground sloths lived (e.g., palaeobiogeography, palaeoecology, palaeoenvironmental isolation of the region) and their potential interactions with humans. These publications are thus essential in the context of interpretation and discussion. For further information about the author´s work within every paper listed below see the "results and methods sections".

Ground sloth taxonomy, ecological implications and Mexican radiation and diversification:

I.   **Stinnesbeck, S. R.**, Frey, E., Olguín, J. A., Stinnesbeck, W., Zell, P., Mallison, H., González González, A., Aceves Núñez, E., Velázquez Morlet, A., Terrazas Mata, A., Benavente Sanvicente, M., Hering, F. Rojas Sandoval, C. (2017). *Xibalbaonyx oviceps*, a new megalonychid ground sloth (Folivora, Xenarthra) from the Late Pleistocene of the Yucatán Peninsula, Mexico, and its palaeobiogeographic significance. *Paläontologische Zeitschrift*, 91(2), 245-271. https://doi.org/10.1007/s12542-017-0349-5

II.   **Stinnesbeck, S. R.**, Frey, E., Avilés Olguín, J., González González, A. H., Velázquez Morlet, A., & Stinnesbeck, W. (2020). Life and death of the ground sloth *Xibalbaonyx oviceps* from the Yucatán Peninsula, Mexico. *Historical Biology* 00:1-17. https://doi.org/10.1080/08912963.2020.1819998

III. **Stinnesbeck, S. R.**, Frey, E., & Stinnesbeck, W. (2018). New insights on the paleogeographic distribution of the Late Pleistocene ground sloth genus *Xibalbaonyx* along the Mesoamerican Corridor. *Journal of South American Earth Sciences*, 85, 108-120. https://doi.org/10.1016/j.jsames.2018.05.004

IV.   **Stinnesbeck, S. R.**, Stinnesbeck, W., Frey, E., Avilés, J., & Gonzalez, A. (2020). *Xibalbaonyx exinferis* n. gen. et n. sp. (Megalonychidae), a new Pleistocene ground

sloth from the Yucatán Peninsula, Mexico. *Historical Biology*, 1-13. https://doi.org/10.1080/08912963.2020.1754817

Faunal assemblage from Quintana Roo and palaeoenvironmental implications:

V.   **Stinnesbeck, S. R**., Frey, E., Stinnesbeck, W., Avíles Olguín, J., Zell, P., Terrazas Mata, A. T., Benavente Sanvicente, M., González González, A., Rojas Sandoval, C. & Acevez Nuñez, E. (2017). A new fossil peccary from the Pleistocene-Holocene boundary of the eastern Yucatán Peninsula, Mexico. *Journal of South American Earth Sciences*, 77, 341-349. https://doi.org/10.1016/j.jsames.2016.11.003

VI.   **Stinnesbeck, S. R.**, Stinnesbeck, W., Frey, E., Avilés Olguín, J., Rojas Sandoval, C., Velázquez Morlet, A., & H. González, A. (2018). *Panthera balamoides* and other Pleistocene felids from the submerged caves of Tulum, Quintana Roo, Mexico. *Historical Biology*, 1-10. https://doi.org/10.1080/08912963.2018.1556649

Faunal assemblage of Guatemala and Central America:

VII.   Dávila, S. L., **Stinnesbeck, S. R.**, Gonzalez, S., Lindauer, S., Escamilla, J., & Stinnesbeck, W. (2019). Guatemala's Late Pleistocene (Rancholabrean) fauna: Revision and interpretation. *Quaternary Science Reviews*, 219, 277-296. https://doi.org/10.1016/j.quascirev.2019.07.011

Archaeological and anthropological data:

VIII.   **Stinnesbeck, S. R.**, Stinnesbeck, W., Terrazas Mata, A., Avilés Olguín, J., Benavente Sanvicente, M., Zell, P., Frey, E., Lindauer, S., Rojas Sandoval, C., Velázquez Morlet, A., Acevez Nuñez, E. & González González, A. (2018). The Muknal cave near Tulum, Mexico: An early-Holocene funeral site on the Yucatán peninsula. *The Holocene*, 28(12), 1992-2005. https://doi.org/10.1177/0959683618798124

IX.   Hering, F., Stinnesbeck, W., Folmeister, J., Frey, E., **Stinnesbeck, S. R.**, Avilés, J., Aceves Núñez, E., González, A., Terrazas Mata, A., Benavente, M. E., Rojas, C., Velázquez Morlet, A., Frank, N., Zell, P. & Becker, J. (2018). The Chan Hol cave near Tulum (Quintana Roo, Mexico): evidence for long-lasting human presence during the early to middle Holocene. *Journal of Quaternary Science* 33(4), 444-454. https://doi.org/10.1002/jqs.3025

X. Stinnesbeck, W., Becker. J., Hering, F., Frey, E., González, A., Fohlmeister. J., **Stinnesbeck, S. R.**, Frank, N., Terrazas Mata, A., Benavente, M. E., Avilés Olguín, J., Aceves Nuñez, E., Zell, P. & Deininger, M. (2017). The earliest settlers of Mesoamerica date back to the late Pleistocene. *PLoSOne* 12(8): e0183345. https://doi.org/10.1371/journal.pone.0183345

XI. Stinnesbeck, W., Rennie, S. R., Avilés Olguín, J., **Stinnesbeck, S. R.**, Gonzalez, S., Frank, N., Warken, S., Schorndorf, N., Krengel, Th., Velázquez Morlet, A., & González González, A. (2020). New evidence for an early settlement of the Yucatán Peninsula, Mexico: The Chan Hol 3 woman and her meaning for the Peopling of the Americas. *PLoSOne* 15(2): e0227984. https://doi.org/10.1371/journal.pone.0227984

CrossMark

Xibalbaonyx oviceps, a new megalonychid ground sloth (Folivora, Xenarthra) from the Late Pleistocene of the Yucatán Peninsula, Mexico, and its paleobiogeographic significance

Sarah R. Stinnesbeck[1] · Eberhard Frey[1] · Jerónimo Avíles Olguín[2] ·
Wolfgang Stinnesbeck[3] · Patrick Zell[4] · Heinrich Mallison[5] · Arturo González González[6] ·
Eugenio Aceves Núñez[2] · Adriana Velázquez Morlet[7] · Alejandro Terrazas Mata[8] ·
Martha Benavente Sanvicente[8] · Fabio Hering[3] · Carmen Rojas Sandoval[7]

Abstract Here we describe a new genus and species of giant ground sloth, *Xibalbaonyx oviceps* (Megalonychidae, Xenarthra), from the drowned cave system of the northeastern Yucatán Peninsula. The specimen is Late Pleistocene in age and was discovered in the Zapote sinkhole (cenote) near Puerto Morelos in the Mexican state of Quintana Roo. *Xibalbaonyx oviceps* differs significantly from all hitherto known Megalonychidae including those from the Greater Antilles and South America. The new taxon suggests a local Caribbean radiation of ground sloths during the Late Pleistocene, which is consistent with the dispersal of the group along a Mexican corridor.

Keywords Ground sloths · Pleistocene · Yucatán Peninsula · Mexico

Kurzfassung Die Unterwasserhöhlen auf der nordöstlichen Halbinsel Yukatan zeigen eine artenreiche Ansammlung von Großsäugern aus dem späten Pleistozän und frühen Holozän. Hier beschreiben wir die neue Gattung und Art eines Riesenfaultiers, *Xibalbaonyx oviceps* (Megalonychidae, Xenarthra), aus der Zapote Doline (Cenote) in der Nähe von Puerto Morelos im mexikanischen Bundesstaat Quintana Roo. Das Exemplar unterscheidet sich signifikant von allen bisher dokumentierten Megalonychidae einschließlich derjenigen von den Großen Antillen und aus Südamerika. Das neue Taxon deutet auf eine lokale karibische Radiation von Bodenfaultieren währen des Spätpleistozäns hin, die mit der Ausbreitung der Gruppe entlang des mexikanischen Korridors übereinstimmt.

Schlüsselwörter Bodenfaultiere · Pleistozän · Yukatan Halbinsel · Mexiko

✉ Sarah R. Stinnesbeck
sarah.stinnesbeck@smnk.de

[1] Geowissenschaftliche Abteilung, Staatliches Museum für Naturkunde Karlsruhe, Erbprinzenstraße 13, 76133 Karlsruhe, Germany

[2] Instituto de la Prehistoria de América, Carretera federal 307, km 282, Solidaridad, 77711 Solidaridad, Quintana Roo, Mexico

[3] Institut für Geowissenschaften, Ruprecht-Karls-Universität Heidelberg, Im Neuenheimer Feld 234, 69120 Heidelberg, Germany

[4] Abteilung für Naturgeschichte, Hessisches Landesmuseum Darmstadt, Friedensplatz 1, 64283 Darmstadt, Germany

[5] Museum für Naturkunde – Leibniz-Institut für Evolutions- und Biodiversitätsforschung, Invalidenstraße 43, 10115 Berlin, Germany

[6] Museo del Desierto, Carlos Abedrop Dávila 3745, Nuevo Centro Metropolitano de Saltillo, 25022 Saltillo, Coahuila, Mexico

[7] Instituto Nacional de Antropología e Historia, Carretera federal 307, km 128, 77710 Tulúm, Quintana Roo, Mexico

[8] Área de Prehistoria y Evolución del Instituto de Investigaciones Antropológicas de la Universidad Nacional Autónoma de México, UNAM, 04510 Coyacán, Mexico

Introduction

The earliest fossil of a sloth is reported from the latest Eocene of Cerro Blanco, south Argentina (McKenna et al. 2006; Gaudin and Croft 2015). Ground sloths are widely known from the later Paleogene and Neogene of South America (Pujos et al. 2016), but must have reached North America by island-hopping about nine million years ago (Hirschfeld and Webb 1968; McDonald et al. 2013a). This arrival thus dates prior to the formation of the Isthmus of Panama (Woodburne 2010), although the timing of this land bridge is still under discussion (MacPhee and Iturralde-Vinent 1995, Montes et al. 2015). Evidence for island dispersal into North America comes from a Miocene site in the Antilles, where the palate of *Imagocnus zazae* (incertae sedis; MacPhee and Iturralde-Vinent 1994) was reported by MacPhee and Iturralde-Vinent (1994), whereas *Pliometanastes* (Hirschfeld and Webb, 1968), reported from Florida is the earliest known genus of Megalonychidae in North America (Hirschfeld and Webb 1968; Pujos et al. 2016). This latter specimen dates back to 9–8 million years (Hirschfeld and Webb 1968; Carranza Castañeda and Miller 2004; Morgan 2005). Webb and Perrigo (1985) suggested that the genus *Megalonyx* evolved from *Pliometanastes* 4.8 million years ago in North America (Hirschfeld and Webb 1968; McDonald 1977; Flynn et al. 2005; Morgan 2005). *Megalonyx* was a widespread genus and was present throughout North America as far north as the Yukon Territory in Alaska (Hirschfeld and Webb 1968; McDonald 1977; McDonald et al. 2000). Mexican reports exist from the States of Nuevo León, Sonora and Puebla (McDonald 1977, 2002). Four species have been described from Mexico, which differ in osteology, size, and their chronostratigraphic ranges (Hirschfeld and Webb 1968): *Megalonyx jeffersonii* (Desmarest, 1822; Harlan 1825), *M. wheatleyi* (Cope, 1871), *M. mathisi* (Hirschfeld and Webb, 1968), and *M. leptostomus* (Cope, 1893; Hirschfeld and Webb 1968; McDonald 1977).

Megalonychidae are a phenotypically diverse family of ground sloths, among them the arboreal, extant two-toed sloth (*Choloepus*), which is up to 0.7 m long and weighs 4–8 kg (Adam 1999; Hayssen 2011), as well as massive ground sloths like the North American *M. jeffersonii* (Desmarest, 1822), with an estimated mass of one metric ton and a length of 3 m (Steadman et al. 2005; Pant et al. 2014). Geographically, the extant two-toed sloths *C. didactylus* (Linnaeus, 1758) and *C. hoffmanni* (Peters, 1858) range from Honduras in Central America to Bolivia and Brazil in South America. The small extinct semiarboreal sloths *Acratocnus* and *Neocnus* (White 1993, 1997) from the Pleistocene–Holocene of the Antilles are close relatives of *Choloepus* (White and MacPhee 2001; Gaudin 2004).

Fossil sloths from the West Antillean islands (e.g., Cuba, Hispaniola, Puerto Rico, Curaçao and Grenada) show a wide morphological variation, hence all of them are referred to Megalonychidae (White and MacPhee 2001). The record from Cuba is particularly diverse and abundant (MacPhee et al. 2000). According to White and MacPhee (2001), Antillean megalonychid sloths are divided into two subfamilies: the large terrestrial Megalocninae (*Megalocnus* and *Parocnus*) and small semiarboreal sloths Choloepodinae (*Acratocnus*, *Paulocnus*, *Neocnus*). Fossil remains of the Megalocninae *Megalocnus* and *Parocnus* are mainly documented from Cuba and Hispaniola (Van der Geer et al. 2010).

Fossils of the subfamily Choloepodinae (i.e., *Acratocnus*, *Paulocnus*, and *Neocnus*) are presently restricted to Cuba, Hispaniola, Puerto Rico, and Curaçao, except for the extant two-toed sloth (White and MacPhee 2001).

Both groups range throughout the Pleistocene and Holocene (White and MacPhee 2001; Van der Geer et al. 2010). MacPhee et al. (2000) hypothesized that the Antillean sloths became extinct after human arrival on the islands during the Mid- to Late Holocene.

Imagocnus zazae (incertae sedis), from the Domo de Zaza Site in Cuba, is of Early Miocene age and thus reveals the long evolutionary history of West Antillean sloths.

The ground sloth record from South America has markedly expanded during the past decade (Cartelle et al. 2008; De Iuliis et al. 2009; McDonald et al. 2013b; Pujos et al. 2016). Megalonychidae are known from the Oligocene of Patagonia (*Deseadognathus* Carlini and Scillato-Yané, 2004) and Bolivia and the Early Miocene of Patagonia (*Eucholoeops* Ameghino, 1887; De Iuliis et al. 2014; *Megalonychotherium* Scott, 1904). Several genera, e.g. *Ortotherium* (Ameghino, 1885), *Pliomorphus* (Ameghino, 1885), *Torcellia* (Kraglievich, 1923a), *Paranabradys* (Scillato-Yané, 1980), *Megalonychops* (Kraglievich, 1930) were recorded from the Late Miocene of the Entre Ríos Province in Argentina (Ameghino 1885; Kraglievich 1923a; Brandoni 2011). Further records come from the Pleistocene of Venezuela (*Megistonyx*, McDonald et al. 2013b), Brazil (*Ahytherium*, *Australonyx*, De Iuliis et al. 2009; Cartelle et al. 2008), Peru, and Chile (*Diabolotherium*, Pujos et al. 2007).

The migration routes and evolutionary relationships among ground sloth species in North and South America are still poorly understood, due to possible geographical or habitat barriers and the scarcity of well documented fossil remains from Central America. Mexico may have formed a corridor between the two continents and thus played a crucial geographic role for migration, specification and the distribution of Neogene sloths in the Americas.

Nevertheless, the published database on ground sloths in Mexico is sparse and none of the species reported from the country has been documented osteologically (McDonald 1985, 2002; González González et al. 2008; Ferrusquía-Villafranca et al. 2010; Pujos et al. 2016). For instance, Megalonychidae, e.g., *Pliometanastes* Hirschfeld and Webb, 1968, *M. jeffersonii* Desmarest, 1822 and *M. wheatleyi* Cope, 1871, are known to have occurred in North Mexico (McDonald 2002; Ferrusquía-Villafranca et al. 2010), but *Nothrotheriops shastensis* Sinclair, 1905, *Eremotherium laurillardi* Lund, 1842, *Glossotherium* sp. and *Paramylodon harlani* Harlan, 1825 may also have inhabited large parts of Mexico during the Pleistocene, even though their record is extremely sparse when compared to North America (McDonald 2002). *Nothrotheriops shastensis* had the widest distribution across Mexico, ranging from the Federal States of Sonora, Nuevo León, Baja California, San Luis Potosí, Jalisco, Michoacán, to the Valley of Mexico and the Yucatán Peninsula (McDonald 2002; González González et al. 2008; Lucas 2008; Chatters et al. 2014; De Iuliis et al. 2015). Information on environmental and faunal changes in Mexico is also highly scattered and varies enormously depending on the region and author in terms of quantity, quality, chronologic position, geographic distribution, and statistical significance (Leyden et al. 1994; Bradbury 1997; Cervantes-Borja et al. 1997; Metcalfe et al. 2000; Brenner et al. 2002; Ferrusquía-Villafranca et al. 2009). Recent findings from the Yucatán Peninsula (Fig. 1) including those documented here demonstrate that ground sloths not only were common elements of the south Mexican megafaunal assemblage, but also showed a remarkable diversity (McDonald 2002; Ferrusquía-Villafranca et al. 2010).

The Yucatán Peninsula

The Yucatán Peninsula is today covered by tropical rainforest growing on limestone karst bedrock, with high levels of chemical erosion and weathering. Therefore, surface records of fossils from the Pleistocene are presently unknown from the region. Nevertheless, the drowned cave system has become a focus of investigation because of its abundant and diverse Pleistocene/Holocene fossil assemblage (e.g., González González et al. 2008, 2013; Chatters et al. 2014). In the Mexican State of Quintana Roo, for instance, the karst cave system is mostly submerged and has a presumed total extension of 7000 km, of which only 700 km are currently explored (Bauer-Gottwein et al. 2011). It is characterized by horizontally layered, thick bedded, shallow water carbonate bedrock of Mio-, Plio-, and Pleistocene age with karstification during cold periods of the Pleistocene (Ward et al. 1985; Weidie 1985; Lefticariu et al. 2006).

Sea level and hydrology changes during the Pleistocene–Holocene transition contributed to the development of the extant cave ecosystem. During the Last Glacial Maximum (LGM) large parts of the system were exposed due to a sea level up to 120 m below present levels (Blanchon and Shaw 1995; Moseley et al. 2013). The cave system was flooded during the Pleistocene–Holocene transition, reaching modern sea levels between 6000 and 4500 BP (Smart et al. 2006; Smith et al. 2011; Grant et al. 2012; Moseley et al. 2015), thereby preserving climatic, archaeological and paleontological evidence inside (González González et al. 2013). Ongoing investigation in water-filled sinkholes, locally known by the Maya term *cenote*, revealed numerous and diverse Pleistocene megafaunal elements, among them equids (*Equus conversidens* Owen, 1862, *E. occidentalis* Owen, 1863), camelids (*Hemiauchenia macrocephala* Cope, 1893), glyptodonts (*Glyptotherium* cf. *floridanum* Simpson, 1929), tapirids (*Tapirus bairdii* Gill, 1865), and gomphotheriids (*Cuvieronius* sp., Osborn 1923). Ground sloth remains are particularly abundant and well preserved. Fossil sloth material from the Tulúm area was given a preliminary assignment to *N. shastensis*, but there is also evidence for a new unnamed species of Megalonychidae (González González et al. 2008; Chatters et al. 2014).

The megalonychid ground sloth described here was discovered in the El Zapote cenote (Figs. 1A, 2) near Puerto Morelos, 36 km south of Cancún and 90 km north of Tulúm, in the Federal State of Quintana Roo, Mexico. The ground sloth was discovered by underwater cave explorer Vicente Fito in 2009 and reported to the Instituto Nacional de Antropología e Historía (INAH) Quintana Roo. The entrance to the El Zapote cenote is today a vertical chimney of 8.5–10 m diameter and a depth of 30 m, which opens to a wide bottle-shaped chamber (Fig. 3). The chamber reaches approximately 40 m in diameter and a depth of more than 60 m. In vertical line with the sinkhole entrance a debris mount of limestone blocks and organic matter is piled up on the cave floor (Figs. 2, 3). The skeleton was discovered at a water depth between 50 and 55 m on the debris mount.

The skull of the ground sloth and some postcranial bones (Fig. 2), among them fragmentary ribs and vertebrae, are spread over six bathymetric debris levels (Fig. 3). Each bathymetric level has a height of approximately 0.5–0.7 m. The bones have shifted laterally, but are still limited to a 3 m deep slope area. The cranium and mandible were articulated and deposited at a depth of 50 m. The skull was wedged in a niche between two rocks (Fig. 3). The depth of 62 m of the cenote suggests that the site was flooded at an early stage of sea level rise, likely during the latest Pleistocene or Early Holocene (Blanchon and Shaw 1995; Smart et al. 2006; Smith et al. 2011; Moseley et al. 2015).

Fig. 1 The Yucatán Peninsula
and localities with evidence of
ground sloths. (A) Cenote
Zapote/study site,
(B) Cementerio de Xenartros/
Tortugas, (C) Luum Balaam/
Toh, (D) Dos Ojos/Toh, (E) El
Pit, (F) Naitucha, (G) K'oox
Baal/El Tigre, (H) Concha,
(I) Kalimba, (J) Muknal/
Caracoles y Camellos,
(K) Vértebras/Chan Hol,
(L) Hoyo Negro (USGS 2015)
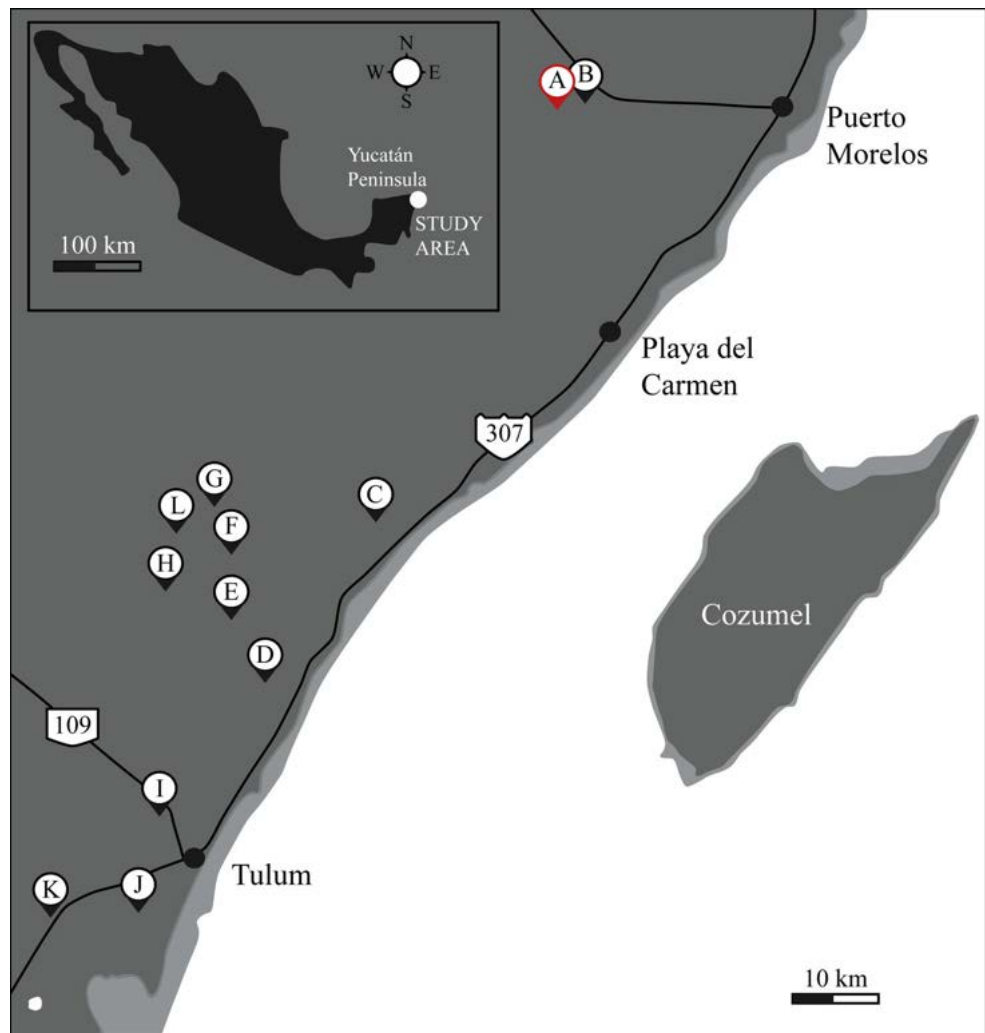
Materials and methods

For conservation and handling of the fragile fossil material,
discovered in the saltwater unit of the submerged Zapote
Cave, the skull and mandible were treated with distilled
water for 8 months and a combination of distilled water and
polyvinyl acetate for 1 month. For techniques used see
González González et al. (2008).

The skull of the Yucatán specimen is almost complete.
Fragments and holes seen on the photographs and inter-
pretive drawings (Fig. 4) result from the extremely brittle
skull bones including the mandible due to erosion and
dissolution in the cave water. Preservation of the left side
(Fig. 5) is better than of the right (Fig. 4). Both jugals and
the right zygomatic process broke off during recovery and
were reattached in the lab. The dorsal part of the left
jugal, which connects to the lacrimal and maxilla, also
broke off during recovery and could not be reattached
because of the extremely fragile bone consistency. The

dorsal surface of the braincase shows superficial abrasion
and is perforated by numerous holes with diameters of
2–20 mm (Fig. 6).

The skull and mandible are presently housed and
accessible in the Instituto de la Prehistoria de las
Américas (IPA) facilities at Playa del Carmen, Quintana
Roo, Mexico, under the INAH and Colección Paleon-
tológica de Coahuila (CPC) collection numbers Za2014-
01/CPC-1875 (skull) and Za2014-05/CPC-1879 (mand-
ible). In order to create a photogrammetric 3D model, the
specimen was placed on a turntable and a total of
768 photographs of the skull and mandible were taken
from a horizontal position at inclination angles of 15°,
30° and 90° (Mallison and Wings 2014). The
turntable was rotated by hand at increments of approx-
imately 10°–15°. From the images one of us (HM) cre-
ated high-resolution photogrammetric models of both the
skull and mandible in AgiSoft Photoscan Pro 1.2.0.
Because of the fragile nature of the specimen, the skull
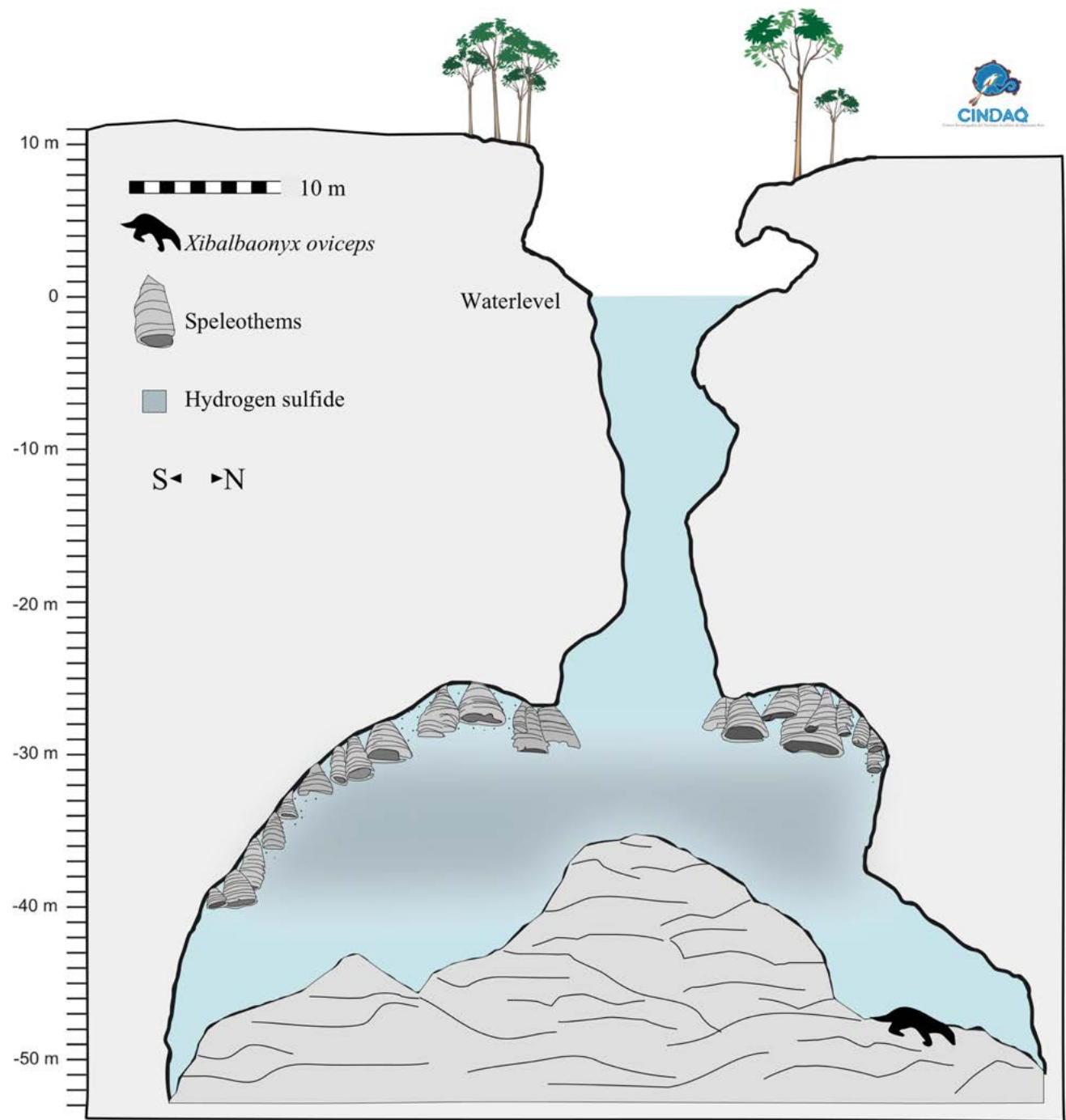
Fig. 2 Cross section of the Zapote Cave. Note that the disarticulated skeleton of *Xibalbaonyx oviceps* was discovered on the northern foot slope of the debris mount below the mouth of the Zapote cenote in a water depth of 50–55 m

could not be turned upside down, so that only a few images of the ventral side were taken with the specimen supported right side up by hand. On all images the background was manually masked. The model was scaled based on five measurements taken on the specimen. The 3D reconstruction of the skull is available at the Museum für Naturkunde (MfN) Berlin's 3D repository vc.mfn-berlin.de.

Recent photographic documentation was executed with a Canon EOS Rebel T4i with 10–22 mm zoom lens set at 22 mm; *f* 4.5, 1/80–*f* 8, 1/20 with tripod.

Anatomical nomenclature

The terminology used for the description of anatomical features of Za2014-01 (skull) and Za2014-05 (mandible)
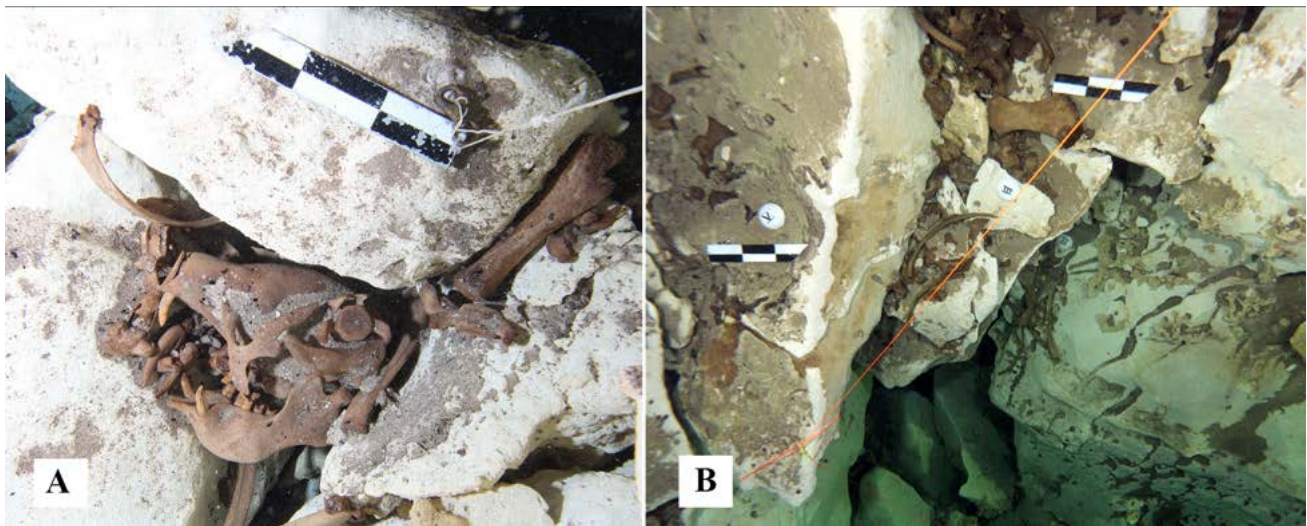
Fig. 3 *Xibalbaonyx oviceps* in situ within the Zapote cenote. (**a**) Skull and mandible (Za2014-01, -05) and (**b**) post-cranial skeleton

are based on phylogenetic characters of both tree and ground sloths according to references: Patterson et al. (1992), Adam (1999), Hayssen (2011), Gaudin (1995, 2004), Pujos et al. (2007), White and MacPhee (2001), and McDonald et al. (2013a, b).

New terms introduced here are based on the anatomical nomenclature for humans (Martin 1914) and other mammals (Martin 1914; Von den Driesch 1976): the term "rhinion" describes the rostral-most point on the median line of the nasal bones (Martin 1914).

The term "nasion" is often referred to as the point where the nasofrontal and internasal sutures meet (Groves 2003), but also refers to the deepest depression on the nasal bridge (Martin 1914), and it has been described for *Australonyx* as a "depressed snout" (De Iuliis et al. 2009). We here introduce the term "nasional impression" for this feature, which is an important diagnostic character of the new genus and species described here.

The acronyms "C" and "c" refer to the upper and lower caniniforms, "M" and "m" for upper and lower molariforms, respectively.

The basonasal length is considered and measured from the rostral edge, or rhinion, of the nasal bones, to the caudal edge of the occipital condyles (Gaudin 2004). The maximum mandibular length is measured from the rostral tip of the mandibular symphysis to the caudal edge of the condyloid process or angular process (Gaudin 2004).

Institutional abbreviations

CPC	Colección Paleontológica de Coahuila, at the Museo del Desierto (MUDE), Saltillo, Mexico.

INAH	Instituto Nacional de Antropología e Historia, Mexico City, Mexico.
IPA	Instituto de la Prehistoria de América, Solidaridad, Quintana Roo, Mexico.
LEMA	Laboratorio de Espectrometria de masas con Aceleradores UNAM, Mexico City, Mexico.
MICADAS	Klaus-Tschira-Archäometrie-Zentrum Mini radiocarbon Dating System, Mannheim, Germany.
MfN	Museum für Naturkunde Berlin, Germany.
MUDE	Museo del Desierto, Saltillo, Coahuila, Mexico.
UNAM	Universidad Nacional Autónoma de México, Mexico City, Mexico.

Dating

Samples for radiocarbon dating were sent to the Klaus-Tschira-Archäometrie-Zentrum Mini radiocarbon Dating System (MICADAS) at Mannheim, Germany and to the LEMA of the UNAM, Mexico.

No data were obtained at MICADAS from samples ZPT 1 and 3 of the Zapote sloth due to insufficient collagen content. However, LEMA bone sample 262.1.2/M15 ZP 2014 was dated to 9.305 ± 35 ^{14}C BP (10.647–10.305 cal BP) by the UNAM Lab. Radiocarbon years were calibrated with OxCal version 4.2.4 (Bronk Ramsey 2013). The calibrated age is given as a weighted mean and 2-σ standard deviation. The reference year for the age in this study is 1950 AD.

Nevertheless, the Early Holocene age of the Yucatán megalonychid must be treated with considerable caution, as
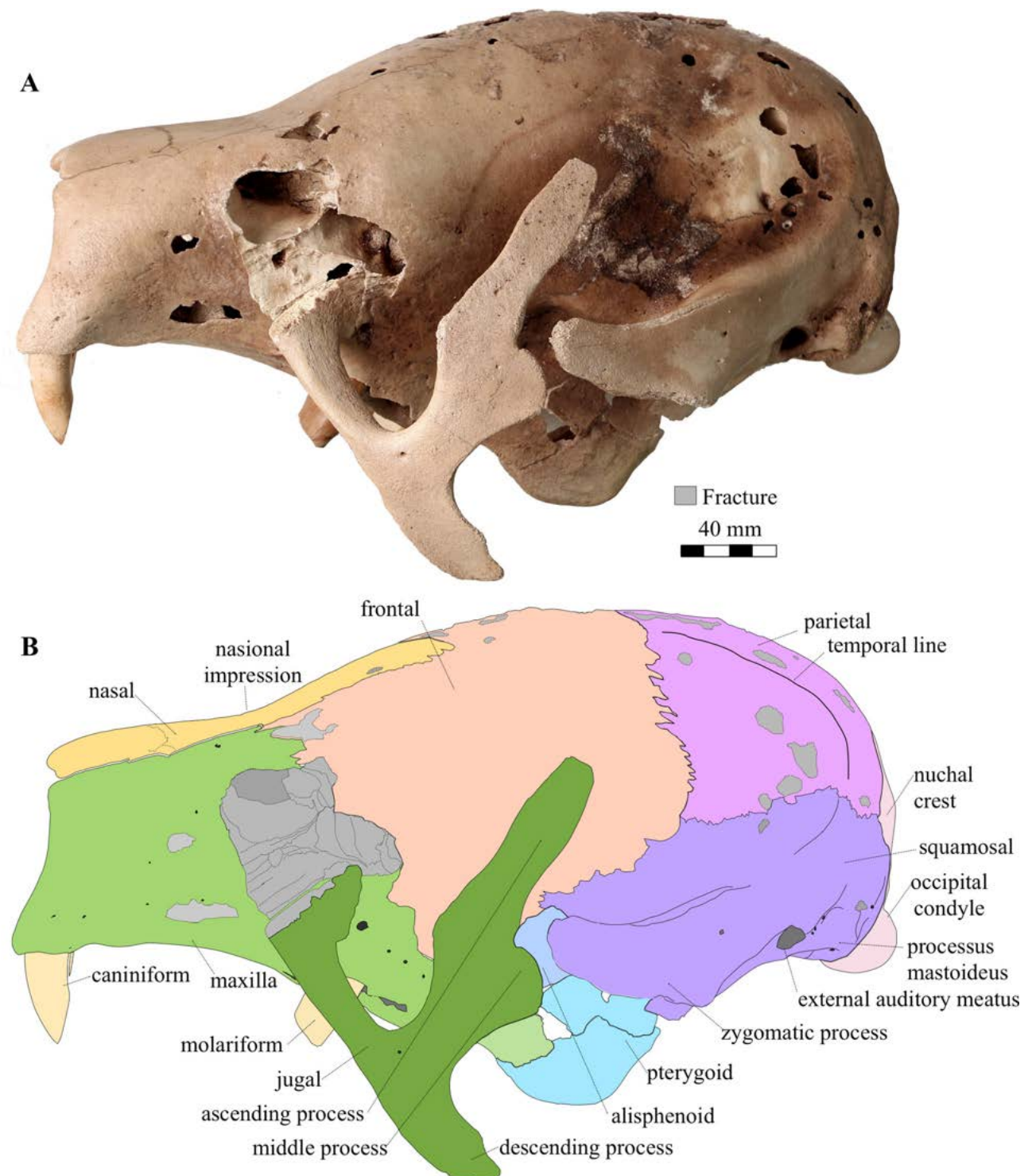
Fig. 4 *Xibalbaonyx oviceps* (Za2014-01) skull in lateral view (*left side*). **a** Photograph and **b** interpretive line drawing

collagen levels of underwater fossils from the system of submerged caves of the Yucatán Peninsula are extremely low (Burr et al. 2009; Taylor 2009). Bone apatite ages are considered to be ambiguous, because of carbon interchange with the environment. Therefore, bone-based dating is difficult and resulting ages may not be accurate (Taylor

2009). Independently, however, the taphonomic context also suggests a Late Pleistocene age for the Zapote ground sloth. Despite its disarticulation, completeness of the skeleton suggests an in situ decay and thus an originally dry environment, in which the animal died and decayed, prior to flooding. In that case, deep levels of the Zapote
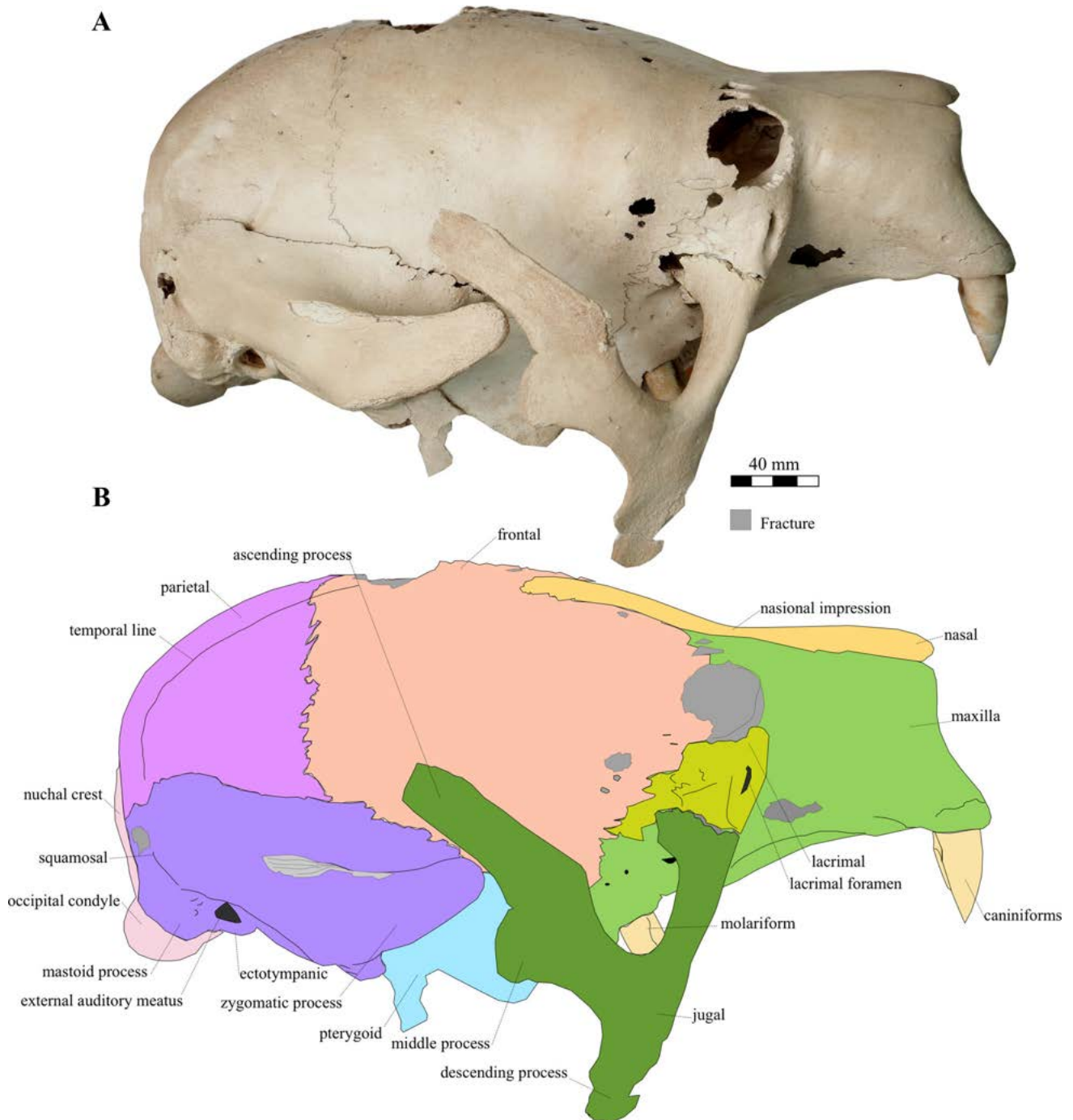
Fig. 5 *Xibalbaonyx oviceps* (Za2014-01) in lateral view (*right side*). **a** Photograph and **b** interpretative line drawing

Cave must have been flooded early during the early Holocene rise of sea level (Smart et al. 2006).

Systematic palaeontology

Superorder **Xenarthra** Cope, 1889
Order **Pilosa** Flower, 1883

Superfamily **Megatherioidea** Gray, 1821
Family **Megalonychidae** Gervais, 1855

Diagnosis of the family. Xibalbaonyx oviceps is identified as a member of Megalonychidae based on the following features: dorsal contour of skull evenly convex in lateral view. The glenoid fossa is mediolaterally widened, its posterior surface smooth and the fossa is well separated
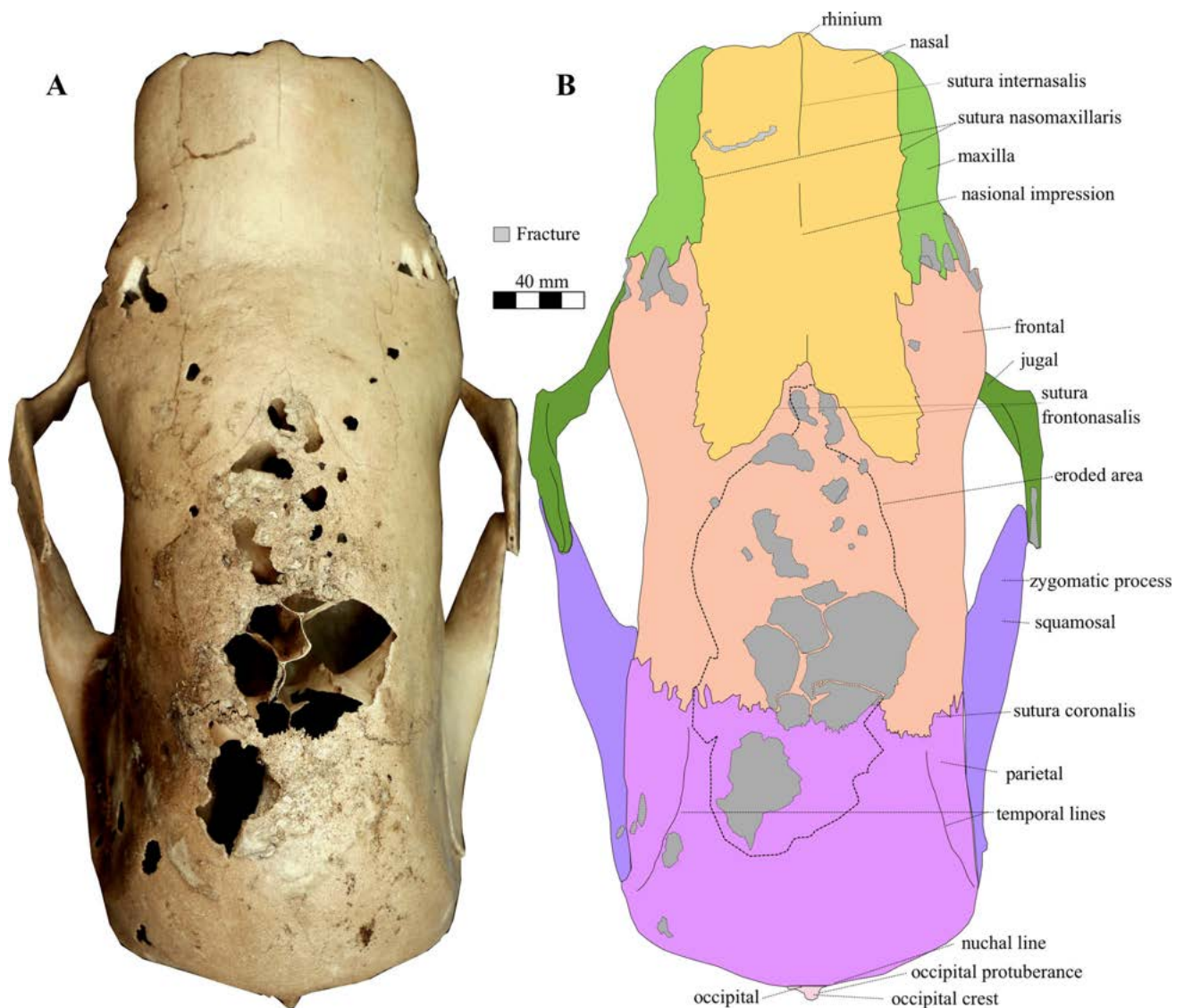
Fig. 6 *Xibalbaonyx oviceps* (Za2014-01) skull in dorsal view. **a** Photograph and **b** interpretive line drawing

from the porus acusticus. The lateral plate of the ento-tympanic is thin with a medial expansion and weak participation in the floor of the tympanic cavity. The paroccipital process is well developed (Patterson et al. 1992; Gaudin 1995, 2004; McDonald et al. 2013b).

Dental features of Megalonychidae seen in Za2014-01 and Za2014-05: the dental formula is C1/c1 M1 − 4/m1 − 3 for each side of the jaws 5/4. The total tooth count is 18. The pair of enlarged caniniforms (C1/c1) is separated from the molariform teeth by a diastema, which is about one fourth the length of the skull. The caniniforms are oblique with a nearly vertical wear facet and a triangular cross-section. Upper and lower caniniforms have an oval occlusal surface. The occlusal surface of m1 and m4 is oval, while the ones of m2 and m3 are rectangular with rounded borders, or reniform with

transversal crests and apicobasal sulci (Gaudin 1995, 2004; Pujos et al. 2007).

***Xibalbaonyx oviceps* gen. et sp. nov.**
Figures 4, 5, 6, 7, 8, 9, 10, 11, 12, 13.

Studied material. This study refers to the skull (Za2014-01) and mandible (Za2014-05) because the postcranial material is still in the Zapote cenote. It is planned to secure this material in 2017.

Etymology. For the genus: Xibalbá = Maya for "underground" or "place of fear," dedicated to the cave divers who dive into the "underworld," the cenotes, and collect the fossils under risky conditions, but also in honor of the Yucatán Peninsula, which is also called the Maya region; "ὄνυξ" (onyx) = Greek for "claw" or "finger nail;" for

the species: oviceps from ovum = Latin for "egg" and caput = "head," "egghead," referring to the regularly domed skull roof of the specimen.

Stratigraphic and geographic distribution. The Cenote Zapote 16 Q 0486971 UTM 2305968, Ruta de los Cenotes Puerto Morelos Quintana Roo, Mexico. Late Pleistocene and/ or Early Holocene (9.305 $\pm$ 35 ^{14}C BP, 10.647–10.305 cal BP).

Diagnosis of genus and species. The new genus *Xibalbaonyx* is defined by the following diagnostic features:

1. Large body size with respect to skull length.
2. Frontals and parietals form a regularly convex and smooth skull roof between nasal and occipital.
3. Blunt rhinion.
4. Strong nasional impression in the middle of the nasals.
5. Nearly horizontal rostral half of the nasals, which form one-fourth of the entire skull length.
6. Subparallel lateral margins of the parietals and frontals in dorsal view.
7. Jugal gracile with parallel ascending and middle processes proceeding dorsocaudally.
8. Ascending process narrow and elongated and dorsocaudally inclined.
9. Middle process inclined dorsocaudally with a blunt end and half as long as the ascending process.
10. Descending process is rostrolaterally convex, ventrally inclined; its ventral end is pointed and shows caudoventrally.
11. Ascending and descending processes of the jugal include an angle of 90°.
12. Jugal separated from the zygomatic process of the squamosal; zygomatic arch absent.
13. Zygomatic process separated from nuchal crest and rostral end of the process showing rostrodorsally.
14. Sagittal crest absent.
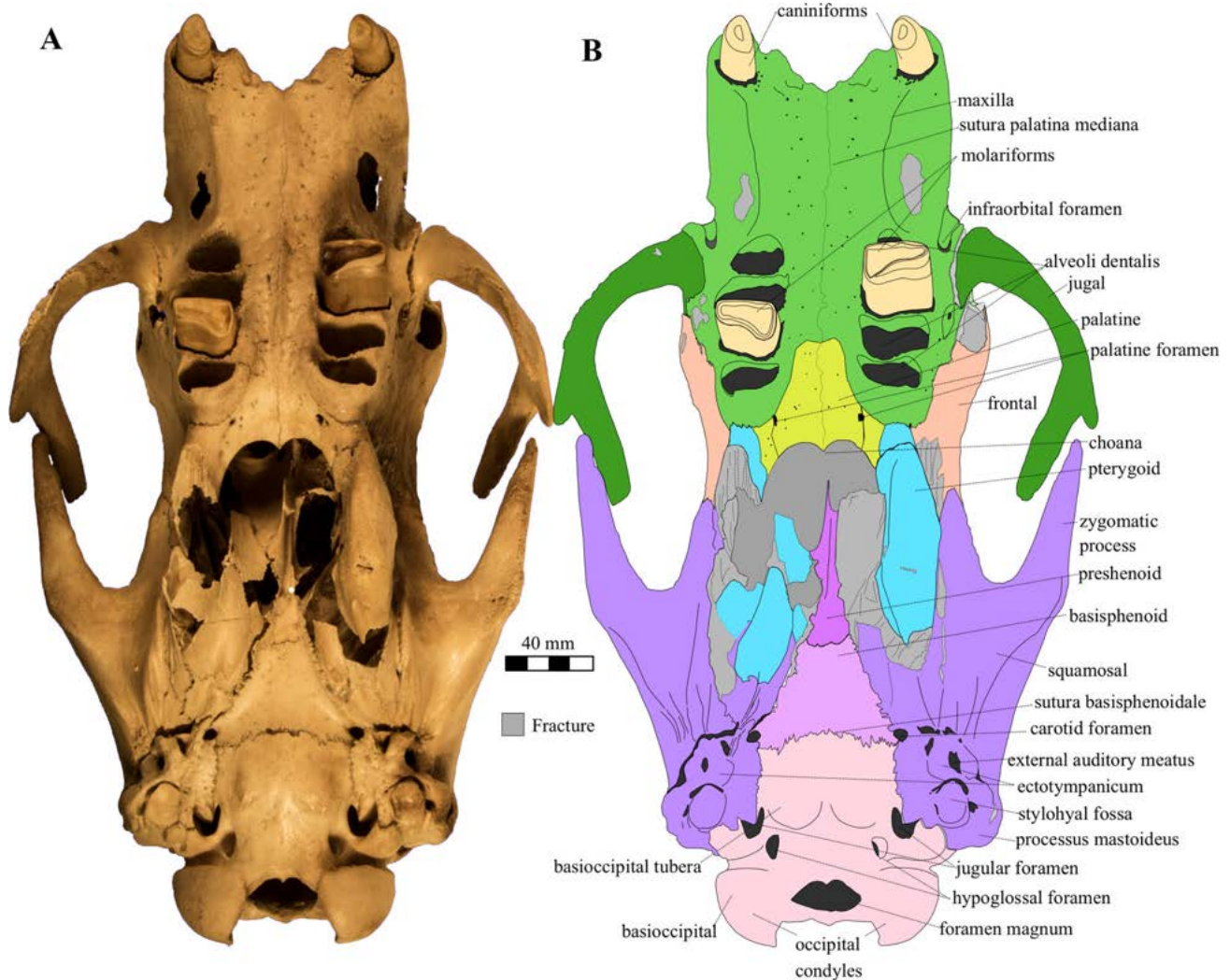
Fig. 7 *Xibalbaonyx oviceps* (Za2014-01) in ventral view. **a** Photograph and **b** interpretative line drawing
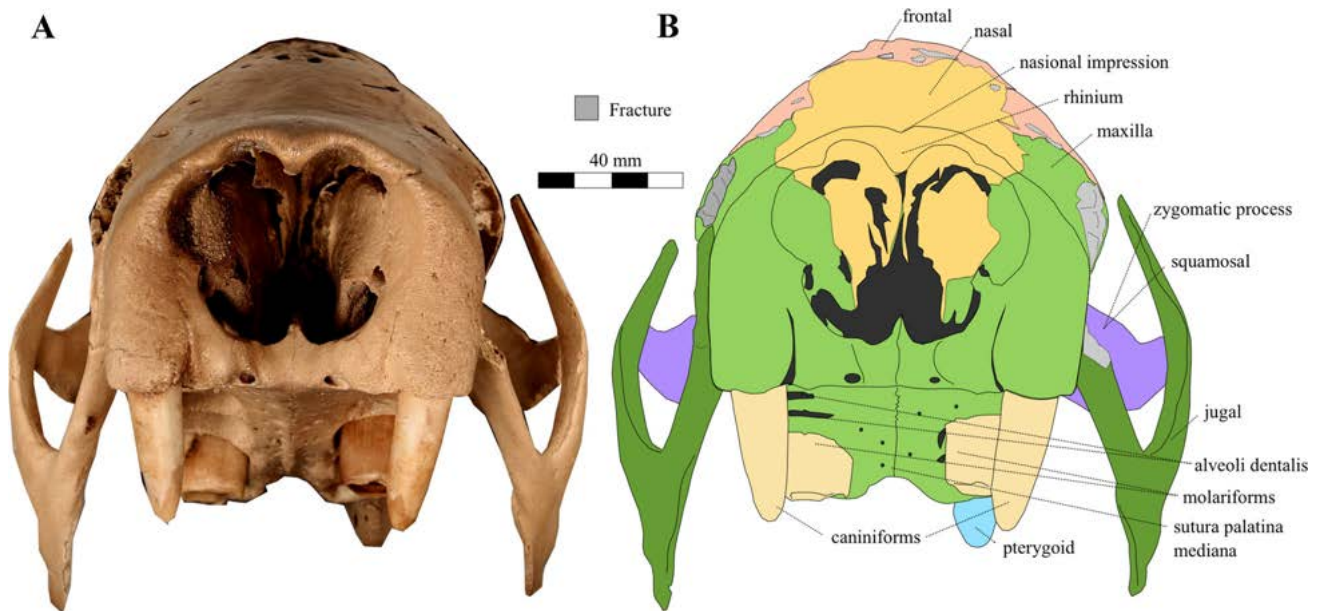
Fig. 8 *Xibalbaonyx oviceps* (Za2014-01) in rostral view. **a** Photograph and **b** interpretative line drawing

15. Temporal lines run parallel, curve caudoventrally, connecting to the dorsal margin of the zygomatic process.
16. Mandible hourglass shaped in lateral view.

Description. The skull has a maximum length of 390 mm (Figs. 4, 5; Table 1). The maximum cranial width of the postorbital constructions (without jugals) is 146 mm. The skull is characterized, in lateral view, by an evenly convex dorsal outline from the nasional impression to dorsal of the occipital condyles (Figs. 4, 5).

The slightly vaulted roof of the rostrum exclusively formed by the nasals terminates caudally level with the rostral half of the internasal suture in a nasional impression, with the deepest depression on the nasal bridge (Figs. 4, 5). The dorsal margin of the nasal bone and the frontal part of the braincase present an angle of about 165°. The rostrum comprises one fourth of the skull length. The dorsal surface of the skull is smooth, without a sagittal crest.

Maxilla

The maxilla articulates rostroventrally with the (missing) premaxilla, rostrodorsally with the nasal, caudodorsally with the lacrimal, jugal and frontal, caudoventrally with the pterygoid and palatine (Fig. 8).

In lateral view, the maxilla reaches approximately one half of the entire skull length and has a trapezoidal outline, in which the ventral margin, with a length of 190 mm, is twice as long as the dorsal part. In lateral view, the dorsal margin of the maxilla runs diagonally at an angle of 10° against the almost horizontal nasal. The ventral margin of the maxilla has a semi-circular shape in lateral view; the curvature increases caudally and is ventrally concave. In lateral view, the caudal half of the maxilla is ventrally convex. The serrated caudal margin of the maxilla runs diagonally, from rostrodorsally to caudoventrally.

The alveoli of the caniniforms are located at the rostral-most section of the maxilla, and rostral to the nasal. Two small foramina are located dorsal to the caniniforms and four foramina are located dorsal of M2 to M4.

In ventral view, the lateral margins of the maxilla are 190 mm long, while the sutura palatina mediana is 110 mm in length. The rostral maximum width of the maxilla is 72 mm. In ventral view, the rostral margin of the maxilla forms a rostrally open angle of 100°. The rostral suture has a wave shape, in which the rostrolateral margins converge mediocaudally. In rostral view (Fig. 8), two anterior palatal foramina of 1 mm diameter are present on each convex side. The rostral margins of the maxilla are sinusoid, being laterally concave and medially convex. The premaxilla is not preserved in Za2014-01. Rostrolaterally, the maxilla has a semi-circular convexity followed by an 80 mm long concave diastema. The rostral part of the maxilla, including the diastema, reaches to about 25% of the ventral side of the skull. The caudolateral margins become caudally wider, diverging slightly from each other. They run subparallel to each other, lateral of the alveoli. The caudolateral margins are convex, with a semi-circular outline. In ventral view, the caudal margins of the maxilla run around the alveoli of M4 and half of M3, and meet in the median line. This median part of the caudal margin of the maxilla is 12 mm wide.
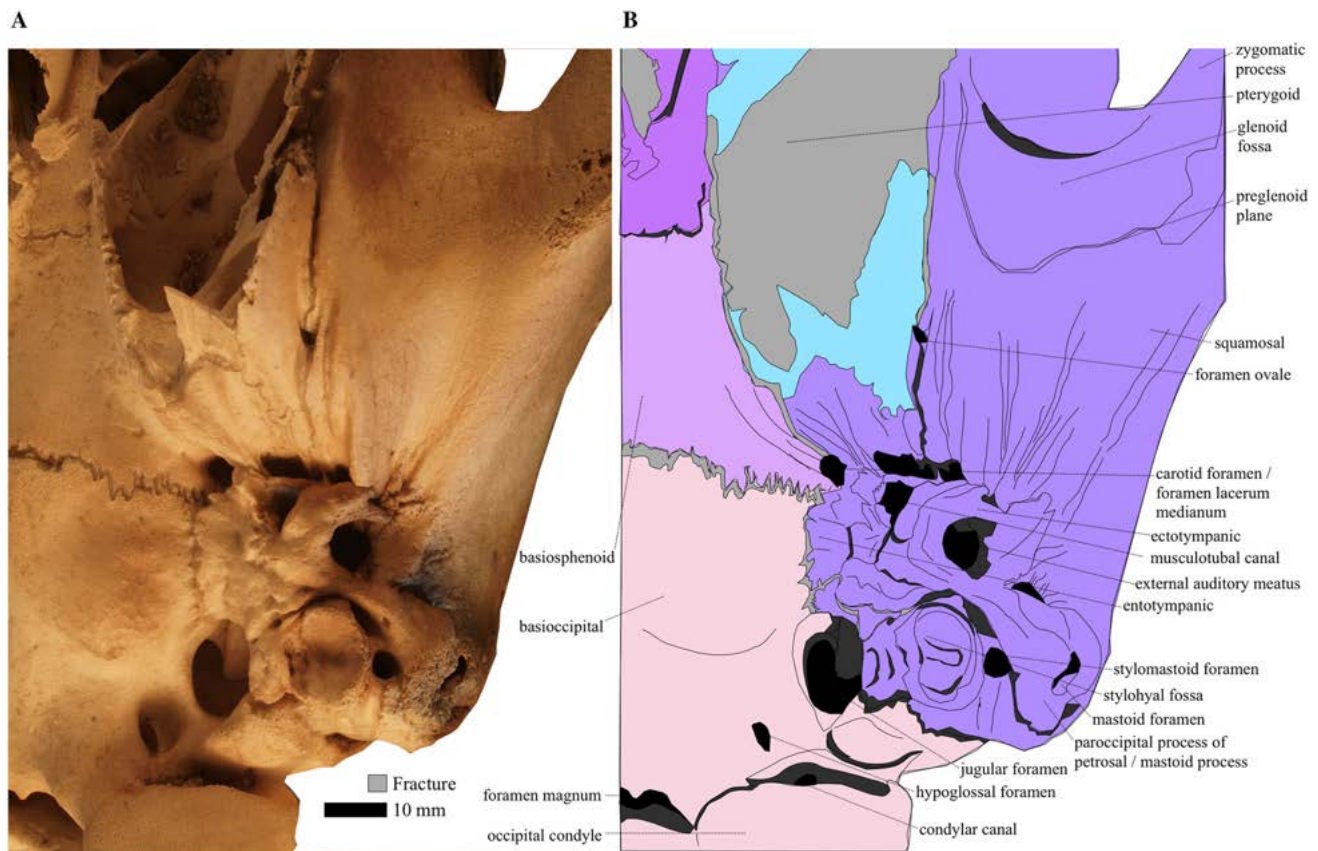
Fig. 9 *Xibalbaonyx oviceps* (Za2014-01) auditory region in ventral view. **a** Photograph and **b** interpretative line drawing

The maxilla is pierced by approximately 40 small foramina with diameters of between 0.2 and 1.5 mm. The sutura palatina mediana is visible.

Palatine

The palatine reaches to less than one eighth of the entire ventral length of the skull connecting rostrally to the maxilla and caudally to the presphenoid. The rostral margin of this bone is at the same height as the caudal part of M3. The rostral margin is transversely 6 mm long and strongly serrated. The rostrolateral margins diverge caudally for 25 mm. The lateral margins are concave, lunate-shaped and encircle the alveoli of M4 completely from rostromedial to caudal and lateral. The maximum length of the bone is 40 mm. The caudal margin is medially pointed in caudal direction and laterally concave. Two palatal foramina of 0.5 mm in diameter are piercing the palatinum on the caudolateral margin of the palatinum.

Nasal

The nasal is a little longer than one third of the entire skull length. The rostral part of the nasal is 80 mm long

and almost horizontal in lateral view. In dorsal aspect, the bone is trapezoidal in outline. The rostral margin of the bone is inclined at an angle of about 85° against the medial margin. The rostromedial corner is marked by a blunt process of the rhinium that protrudes from the median fourth of the rostral margin of the nasal. The rostrolateral corner is regularly rounded and confluent with the lateral margin that runs sub-parallel to the median margin of the bone. The lateral margin of the nasal is about one fourth longer than the medial one. In consequence, the caudomedial margin is inclined at an angle of about 45° against the lateral margin. The contralateral caudomedial margins meet medially at an angle of about 80° in a wide caudally open V (Fig. 6). The lateral part of the nasal sharply curves ventrally and forms the dorsal-most seventh of the lateral face of the rostrum.

The two contralateral suturae nasomaxillares are slightly serrated and reach from the margin of the naris caudally to the frontal, dorsally adjacent to the nasion. The sutura nasomaxillaris merges with the unregularly wavy sutura frontonasalis at an acute, caudally open angle of about 45° (Fig. 6). The margins of the naris are almost vertical in lateral view. The nasal aperture is 72 mm wide and 85 mm high (Fig. 8).

Fig. 10 *Xibalbaonyx oviceps* (Za2014-01) in caudal view. **a** Photograph and **b** interpretative line drawing
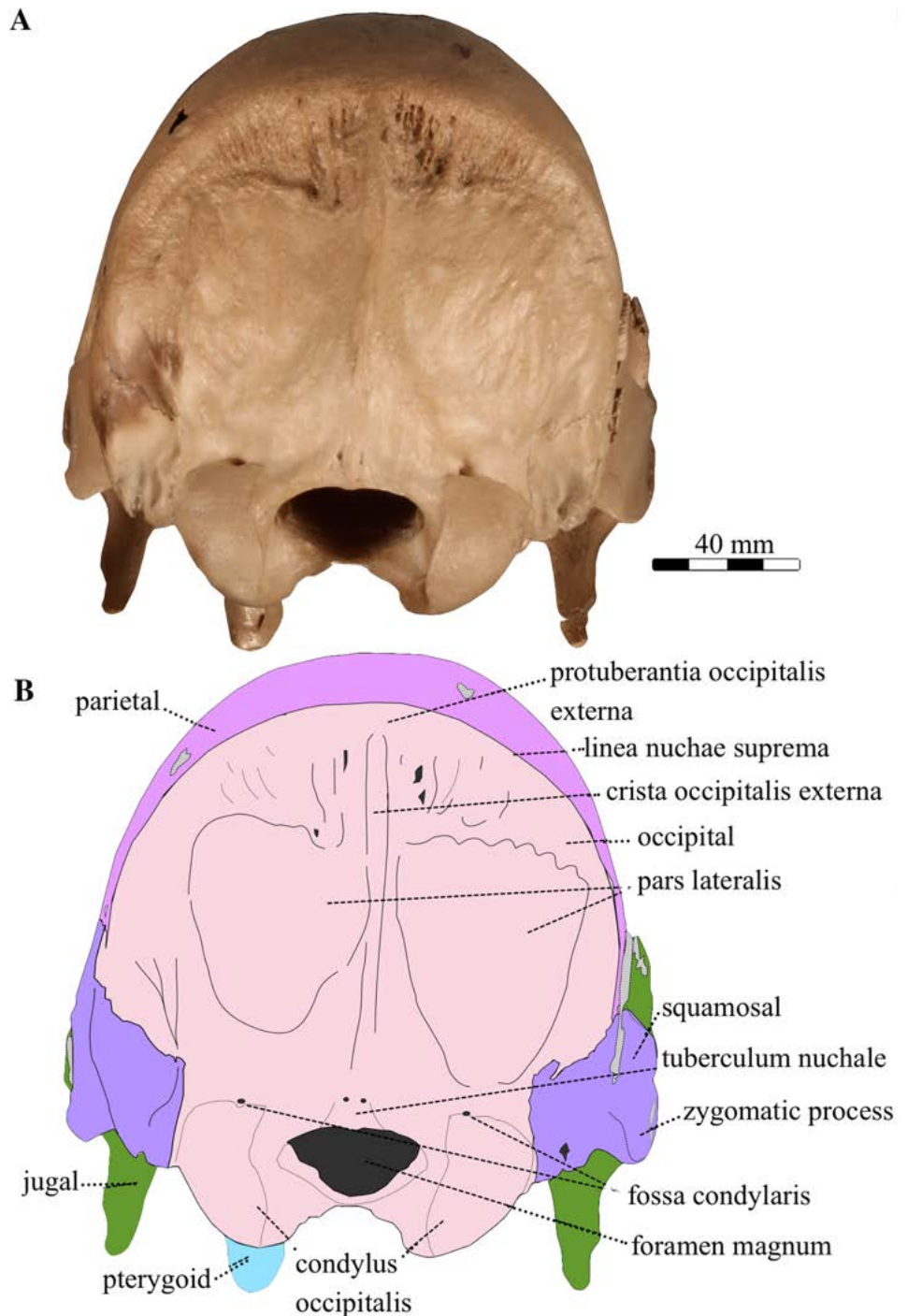
One third of the rostral part of the sutura internasalis is visible, while the caudodorsal two thirds are nearly fused and thus barely visible.

Frontal

The frontal reaches one third of the entire skull length. The dorsal face of the bone is vaulted and in rostral view slightly inclined to the left. In lateral aspect, the rostral, dorsal, caudal, and ventral margins have an almost quadrangular outline. The dorsal margin is convex, running rostrally to caudodorsally. After 30 mm the dorsal margin curves dorsally for 5 mm and then turns caudally, forming a convex outline. The rostral and ventral margins are strongly serrated and run subparallel to each other dorsally to ventrally, becoming ventrally slightly narrower. In lateral view, the ventral-most quarter of the frontal is triangular in outline pointing ventrally. The margin of the

Fig. 11 Photograph of the malleus of *Xibalbaonyx oviceps* in lateral view
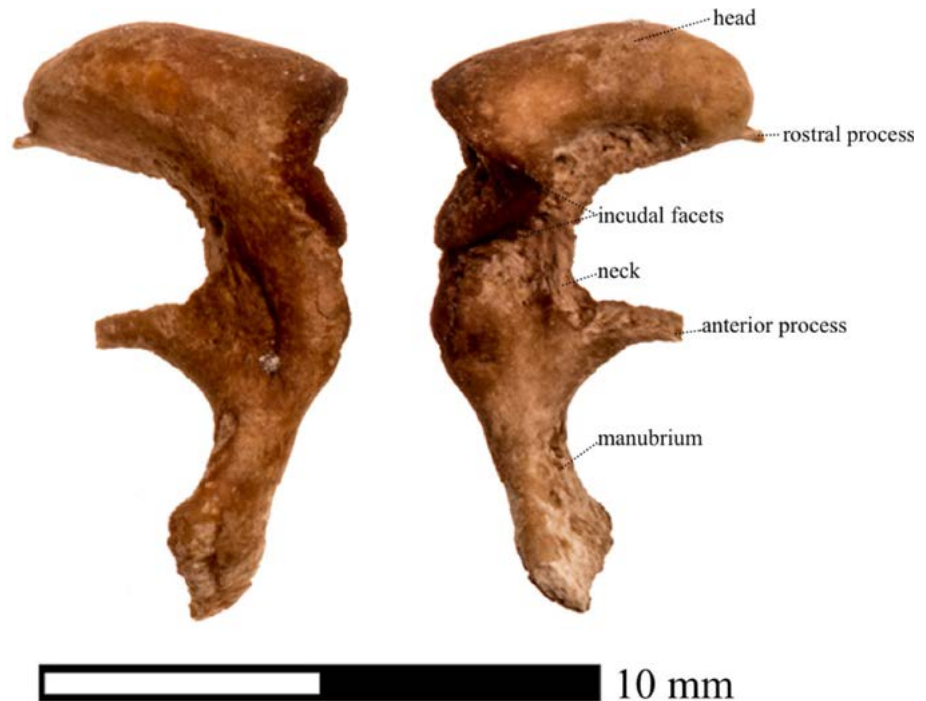
frontal connects rostrally to the nasal and jugal, rostro-ventrally to the maxilla, ventrally to the sphenoid and temporal, and caudally to the parietal. In dorsal view, the caudolateral two thirds of the lateral margins of the frontal run parallel to each other, becoming rostrolaterally convex in the caudal-most third. The rostrolateral margins of the frontal run medially for 43 mm. Before reaching the median line they run caudomedially for 30 mm and finally meet on the medial line. The rostral margins curve rostromedially in a caudally open angle of 40° and finally meet medially. In contrast, the caudal margins of each frontal are straight in dorsal aspect. The lateral margins are about one fourth longer than the medial ones. Because of the abrasion of both frontal bones the medial and caudal margins are only partially preserved, whereby the rostral part of the frontal is better preserved.

Parietal

In lateral aspect, the parietal forms half of the lateral skull wall and one third of the entire skull length. In dorsal and lateral view, the rostral margin of the bone is strongly serrated. In lateral view, the rostral margin of the parietal runs 70 mm vertically from dorsal to ventral. The caudal margin of the parietal is convex and fused with the occipital. The external face of the parietal is vaulted. The degree of convexity is longitudinally stronger than transversely. In dorsal view, the bone is roughly pentagonal in outline. The rostral two thirds of the exceedingly brittle bone broke off during transport. The lateral margins run

subparallel to each other, slightly diverging caudally. The rostral margin is almost completely abraded. The caudal margin is regularly convex with a low median protuberance on the linea nuchae suprema. The parietal rostrally connects with the frontal in an extremely serrated sutura coronalis, which in itself is irregularly wavy. Ventrally the parietal articulates with the squamosal and caudally with the occipital. The dorsolateral faces of the parietal contain the paired temporal lines. The latter ones are barely visible on the postorbital constriction, running from the dorsocaudal margins of the nasals, continue onto the dorsal part of the frontal (Figs. 4, 5). Here, the contralateral temporal lines parallel each other. From the caudal end of the frontal, the temporal lines diverge in caudal direction for 40 mm. The temporal lines continuing caudally onto the parietals. From the caudal-most part of the parietals, the temporal lines curve caudoventrally, merging with the caudodorsal margin of the zygomatic process of the squamosal. The temporal lines take a wide semi-circular course with a maximum prominence in their parietal parts. Caudal to the temporal maximum, the prominence of the temporal lines gradually taper. Between the temporal lines the skull roof is smooth.

Lacrimal

The lacrimal is only preserved on the right side (Fig. 5). It has a diameter of approximately 25–30 mm and is trapezoidal in outline. The rostral margin is medially convex. The ventral margin runs horizontally and is 5 mm longer
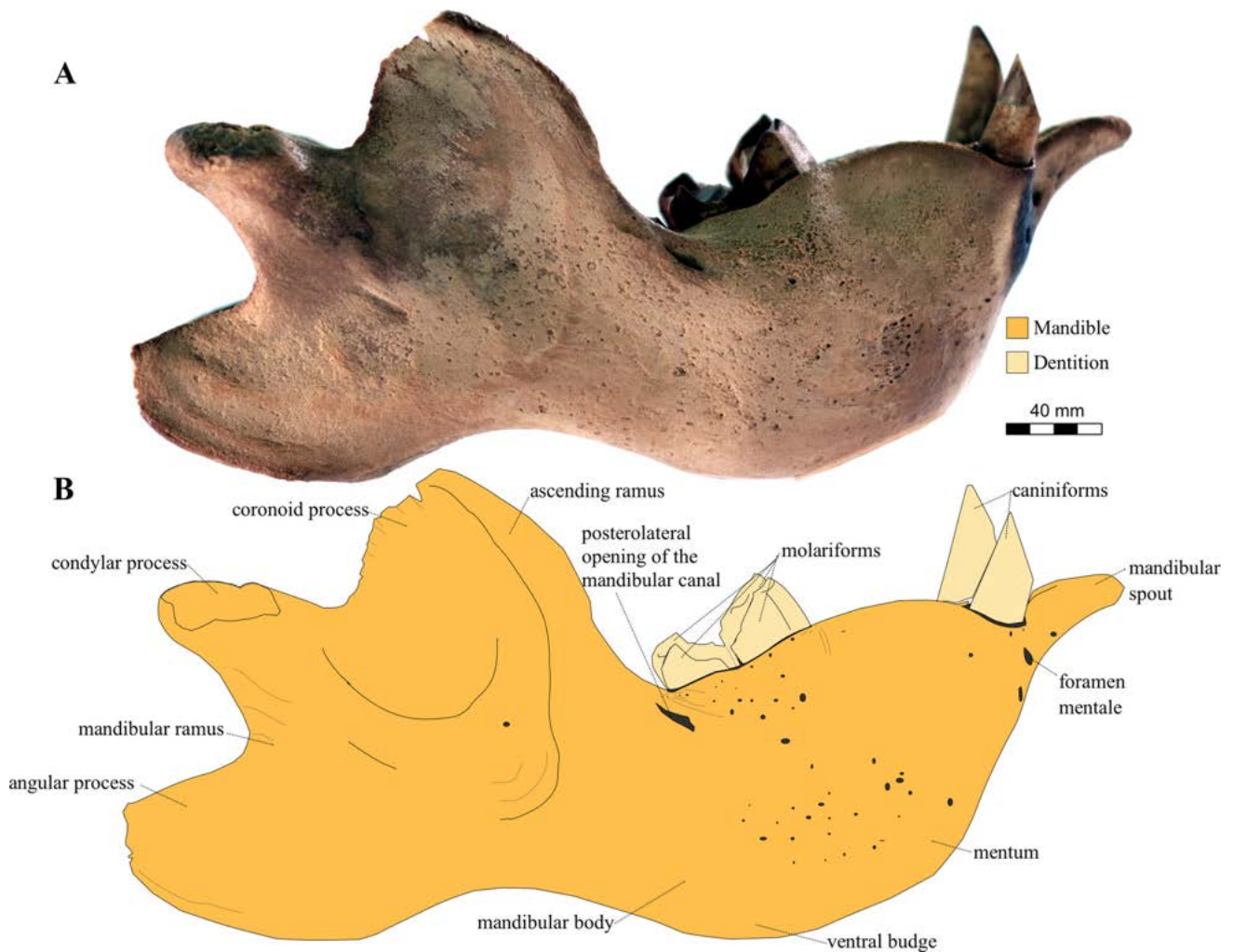
Fig. 12 *Xibalbaonyx oviceps* mandible (Za2014-05) in lateral view. **a** Photograph and **b** interpretative line drawing

than the dorsal one. The dorsal and caudal margins are strongly serrated. In rostral view, the lacrimal is oval, slightly reniform and has a 4 mm long lacrimal foramen, which opens rostrolaterally. Medially, the bone is connected to the maxilla and ventrolaterally to the jugal. It is located dorsal to the first upper molariform and dorsolateral to the foramen infraorbitale.

Jugal

The bone has a gracile, triangular body with three processes, the dorsocaudally oriented ascending, and middle process, and the caudoventrally oriented descending process. The ascending and descending processes form an angle of about 90°. With its rostral end, the 126 mm long ascending process articulates with the caudal third of the lateral face of the maxilla, forming a 43 mm long middle process that is angled caudally against the descending

process at about 100°. The middle process has one third the height of the caudal margin of the maxilla. The ventral and caudal margins of the sutura maxillojugalis are partially broken. The craniodorsal corner of the jugal is sharply rounded. The orbital area of the jugal has almost straight rostroventral and caudodorsal margins. The latter, together with the ascending and middle processes, form the cranial margin of the orbita. The ventral and caudal margins of the orbita are formed by the concave ventral third of the cranial margin. The orbita is formed by the jugal, especially the 87 mm long descending process and the 40 mm long middle process. The triangular meeting area of the processes forms the corpus of the bone. The dorsal two thirds of the ascending process are spatulate in outline when seen from laterally, with slightly convex rostral and caudal margins in the middle third. From these convexities the ascending process converges towards its dorsal terminus to half the maximum width at the convexity. The dorsal

Table 1 *Xibalbaonyx oviceps* measurements

	Millimeter
Skull (Za2014-01)	
Alveolar length of toothrow (C_1–M_4)	168
External naris width	60
External naris height	85
Bicanine width (maximum breadth of muzzle across caniniform alveoli)	104
Maximum cranial width (in dorsal view; maximum horizontal distance of the postorbital constrictions, without jugals)	146
Condylobasal length (alveolus of C_1 to condyles)	390
Basonasal length	353
Foramen magnum width	27
Greatest width across the nasals	60
Greatest length of the nasals	160
Maximum skull height	214
Mandible (Za2014-05)	
Alveolar length of toothrow (c1–m3)	131
Alveolar length of toothrow (m1–m3)	75
Width at caniniforms	85
Diastema length	49
Mandibular length	303
Maximum mandibular height; measured from the dorsal tip of the coronoid process to the ventral edge of the mandibular body	130
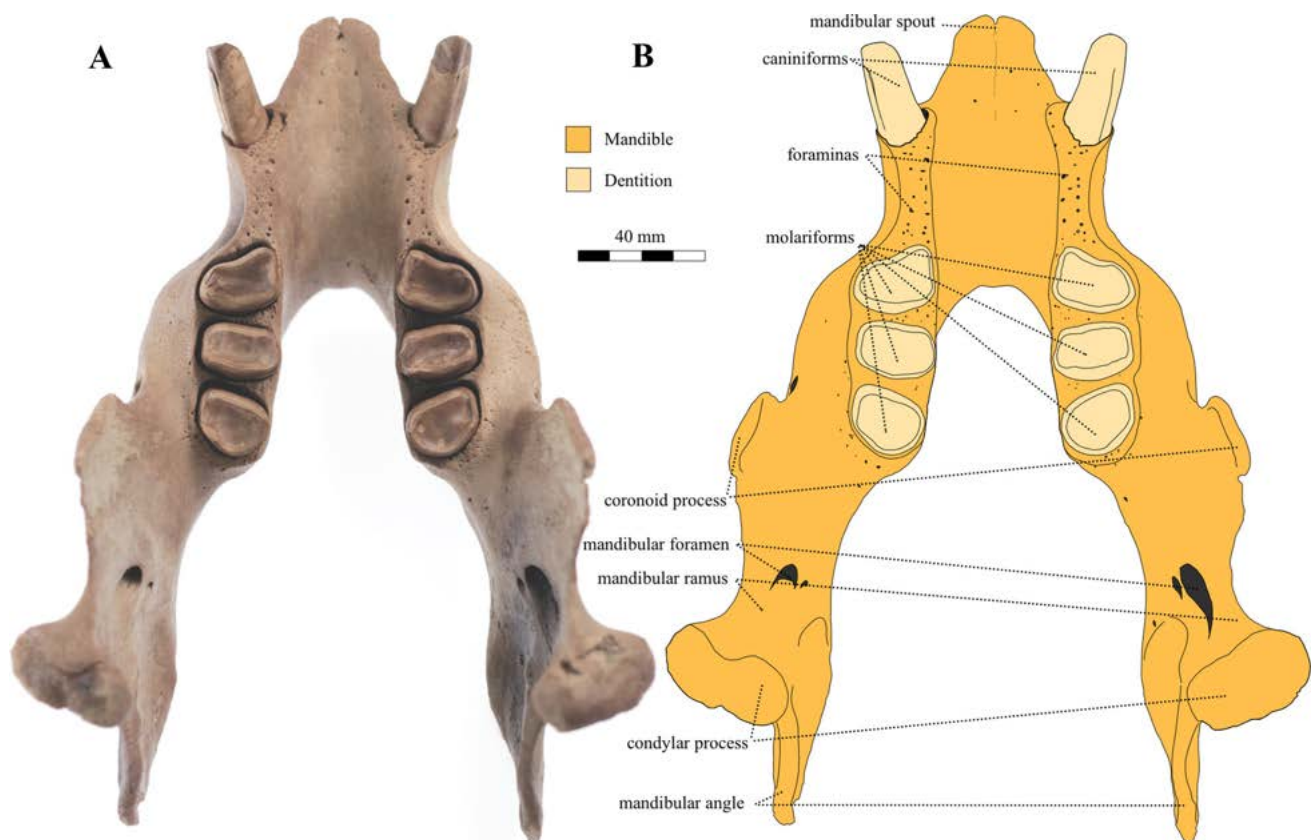
Fig. 13 *Xibalbaonyx oviceps* mandible (Za2014-05) in dorsal view. **a** Photograph and **b** interpretive line drawing

margin of the jugal is straight, with rounded rostral and caudal corners. Caudally, and opposite to the dorsal third of the orbital concavity of the ascending process, there is a dorsocaudally facing regularly rounded expansion of the caudal margin, the middle process. The latter lies ventrally adjacent to the rostral extremity of the zygomatic process, but without reaching bony contact. Ventral to the middle process, its caudal margin is concave. The narrowest longitudinal diameter of the base of the middle process is about one half its maximum width, immediately dorsal to the basal constriction. A descending process is present in prolongation of the ascending process caudoventrally to the corpus. It is about half the length of the ascending process but twice as wide. The rostral margin of the descending process is slightly convex, with a continuous increase of the curvature onto the ventral margin. The caudal margin is deeply concave, with a blunt convex elevation at the distal half of its middle third. The ventral apex is sharply rounded.

Squamosal

The lateral part of the squamosal measures about one fourth of the skull length, the ventral part almost one half. The paired bone connects rostroventrally with the pterygoid and alisphenoid, rostrally with the frontal, dorsally with the parietal, ventrally to the basisphenoid and the occipital. In lateral view, the squamosal has a pentagonal shape with irregular margins. Both the rostral and caudal margins of the temporal bone are approximately 40–55 mm long and diverge dorsally in a 45° angle. The rostrodorsal margin is 31 mm long, straight and serrated. The caudodorsal one is slightly convex and 9 mm longer, reaching to 40 mm. Both borders converge dorsally at an angle of 100°.

The zygomatic process is approximately 140 mm long, which is one third of the skull length. The medial margin of the zygomatic process forms a rostrally open angle of 20° with the lateral surface of the skull. The dorsal margin of the process connects dorsocaudally with the temporal line. In lateral aspect, the caudodorsal and caudoventral margins of the zygomatic process are 60 mm long and run subparallel to each other, diverging rostrally at an angle of 5° from each other. The zygomatic process has a maximum height of 42 mm. The rostrodorsal and rostroventral margins of the process are 80 mm long and converge rostrally from a width of 42 to 19 mm. The rostral margin of the process is convex. In ventral view, the glenoid fossa is shallow and rostrally separated from the auditory region. It is twice as wide as rostrocaudally long. The postglenoid surface is smooth. The postglenoid area is rostrally wider than caudally and rostrocaudally as elongated as it is rostrally wide. The median margin of the squamosal is straight. The rostroventral face of the squamosal is concave and smooth.

In ventral view, the auditory region is convex (Fig. 9) and strongly compressed at the most caudal part of the squamosal. In ventral view this region is rostrocaudally as long as the basioccipital area. Several foramina are at the same level of the basisphenoid–basioccipital suture: the carotid and musculotubal canal, but also the opening of the fenestra vestibuli and cochlea. The promontorium is rostrocaudally elongated, emerging from the postglenoid surface and adjacent to the rostrolateral border of the ectotympanic. The promontorium is an elongated bulge, which is rostrolaterally flat, while becoming caudally convex. The promontorium faces caudomedially and almost covers the opening of the fenestra cochleae, which is located caudoventrally to it. The carotid canal or foramen lacerum medium (Patterson et al. 1992; Gaudin 1995) opens medially and is located caudolateral to the basisphenoid, rostrolateral to the basioccipital and medial to the squamosal. Lateral to the carotid canal, the musculotubal canal is located medially to the ectotympanic. The ectotympanic is horseshoe-shaped in outline and its crus is convex. Its rostromedial crus is well pronounced and one half thicker than its caudal half. The ectotympanic ring and external auditory meatus are slightly laterally inclined. The medial border of the crus is connected to the entotympanic. The latter one lies level with the rostral margin of the crus of the ectotympanic. It extends rostrocaudally from the basisphenoid-basioccipital suture level with the carotid foramen to the rostral border of the stylohyal fossa and the rostral margin of the jugular foramen. It is rostrally wider than caudally and its sutures are strongly serrated. The caudal part of the ectotympanic crus contacts the stylohyal fossa. The latter one is oval and its caudomedial part is concave, almost funnel- or cup-shaped (Patterson et al. 1992). The external aperture of the fossa faces caudomedially. A big, oval stylomastoid foramen is located immediately laterally to the stylohyal fossa. The mastoid contacts the stylohyal fossa from laterally. Its mastoid process is located at the caudolateral-most edge of the skull in ventral view. The foramen mastoideum is located on the lateral surface of the squamosal. The stylohyal fossa has the same size as is the jugular foramen. The latter one is located between the squamosal and the basioccipital. The jugular foramen, or posterior lacerate foramen (Patterson et al. 1992; Gaudin 1995), is rostrocaudally oval and with a diameter of 16 mm the biggest foramen in the auditory region. The hypoglossal foramen is located medial to the jugular foramen and half the size of the jugular foramen. Caudal to the jugular foramen and the stylohyal fossa, the paracondylar process of the exoccipital extends caudally. The paracondylar process of the exoccipital is caudally twice as wide as rostrally and of trigonal shape.

Presphenoid

The presphenoid is strongly fragmented, especially its rostral part. It measures one fourth the ventral length of the skull. It is elongated, triangular in longitudinal direction, with the narrow tip facing rostrally. Lateral margins are concave. The caudal margin is convex and 10 mm wide.

Basisphenoid

The basisphenoid (Fig. 7) is transverse trapezoidal in outline, with the narrower end facing rostrally. The rostral margin of the basisphenoid is 10 mm wide and laterally concave, while it is rostrally pointed. The caudal margin measures 57 mm and is straight.

Alisphenoid and pterygoid

Both alisphenoids and the pterygoids are fragmented, but the left pterygoid has been reconstructed to a maximum width of 65 mm and a height of 40 mm. The margins of the alisphenoid are not clearly visible due to the fragmentation. The pterygoids are rostrocaudally elongated and inflated, which means, that they are hollow and ventrally convex. The outline of the bone is rhomboidal in lateral view. The rostral half of the ventral margin is convex, while the caudal one is straight. The rostrodorsal and caudodorsal margins are connected to the alisphenoid, frontal and squamosal. All respective sutures are strongly serrated. The optic canal and orbital fissure are located on the rostral suture of the alisphenoid connecting to the maxilla, while the foramen ovale is located on the caudal suture connecting the alisphenoid with the squamosal.

In ventral view, the pterygoid connects to the palatine and caudally to the basisphenoid and squamosal.

Occipital

The occipital (Fig. 10) is circular in caudal and rectangular in ventral view. In lateral aspect, its caudal margin is convex. Rostrally the occipital connects to the parietal, ventrally to the temporal and rostroventrally to the basisphenoid. In caudal view, the occipital is dorsally and caudally convex, with a pronounced supreme nuchal line (linea nuchae suprema; Fig. 10). The dorsal margin is fused with the parietal. In the median line of the nuchal line, the external occipital protuberance is located at the dorsal-most point of the occipital. It is convex and faces caudally. A supraoccipital crest with a length of 105 mm extends from the external occipital protuberance dorsally to the dorsal margin of the foramen magnum. Lateral to the occipital crest, the lateral parts of the occipital are convex

and have an almost triangular outline (Fig. 10). The lateral margins of the occipital are circular in caudal view. Only approximately 10 mm dorsal of the occipital condyles, the lateral margins bend back and are concave. In caudal aspect, the ventral margins of the occipital condyles include a ventrally open angle of 45°. The occipital condyles are convex, triangular, located ventral to the foramen magnum; they are caudally oriented. Two circular foramina are located adjacent to the foramen magnum (Fig. 10). The foramen magnum is oval, 38 mm wide and 30 mm high.

In ventral view, the rostral half of the basioccipital is rectangular in outline and with strongly serrated margins. The caudal half of the occipital is laterally convex. The basioccipital tubera are oriented rostrolaterally and slightly inflated. The foramen jugulare has a diameter of 16 mm. It is located on the lateral margin of the occipital caudolaterally to the basioccipital tubera. The foramen condylaris is located caudomedial to the foramen jugularis and rostral to the occipital condyle.

Malleus

The malleus (Za2014-02) of the left inner ear is preserved (Fig. 11). It is 12 mm high and 5–6 mm wide (Fig. 11). It has a rounded head on its dorsal end, which tapers to a narrow neck and manubrium on its ventral end. The head of the malleus is ovoid, rostrocaudally elongated, with a small rostral process. The articular facets cover the complete length of the neck and have the shape of an acute angle facing caudally. The neck of the malleus is slightly wider than the manubrium. Its rostral and caudal margins run subparallel to each other in ventral direction. The caudal margin of the neck is convex with a caudal crust, while the rostral margin is concave and smooth. The anterior process arises from the eminence ventral to the neck from the middle length of the malleus. The slightly broken lateral tip of the anterior process faces rostroventrally. The manubrium is orientated ventrally and decreases in size towards its ventral terminus. It is the most slender part of the ossicle and its ventral end curves slightly rostrally.

Mandible

The mandible (Za2014-05) is very well preserved (Figs. 12, 13). It has a maximum length of 300 mm and is 130 mm high. Its maximum width is 202 mm at the condylar processes. The dentition is restricted to the rostral half of the mandible. In ventral view, the body of the mandible is rostrally thicker than caudally. The rostral half of the mandible is approximately 40 mm thick, while the caudal half of the mandible gradually narrows transverse thickness of 10 mm.

In dorsal view, the rostrolateral margins of the mandible diverge caudolaterally for about 30 mm, forming an angle of 45° between each other (Fig. 12). The rostral-most 30 mm of the mandible conform the symphysis region, which is restricted to the mandibular spout. In dorsal view, the mandibular spout is triangular in outline. A small indentation is present medial to the rostral end of the mandible. The mandibular spout is caudally delimited by the alveoli of the caniniforms. In lateral view, the process is spout-shaped (Fig. 12) and presents a longitudinally concave ventral face (Fig. 12). The rostral terminus of the mandibular spout is oriented rostroventrally. The dorsal face of the mandibular spout is convex and its dorsal and ventral margins run subparallel to each other from rostrally to caudally; the caudal half of the mandibular spout becomes one half wider than rostrally. In rostral view, two circular foramina are located on the ventrolateral surface of the mandibular spout.

The lateral margins of the mandible are sinusoid. The caniniform-bearing part of the mandible is laterally convex. There is a 49 mm long diastema between the canini- and molariforms. The rostrolateral margins of the mandible are concave, while the median margins are almost parallel to each other. The dorsal surface of the mandible is pierced with approximately 12 small foramina. The tooth-bearing part of the mandible is laterally convex and its lateral and median margins run subparallel to each other. In the caudal half of the mandible, the median faces are concave. The caudolateral margins are sinusoid.

In lateral aspect, the mandible is hourglass-shaped. Its rostral half has a maximum height of about 100 mm caudally, followed by a 65 mm high constriction with concave dorsal and ventral margins. Caudal to this constriction, the height of the caudal half gradually increases to a maximum of 130 mm. The rostrolateral face of the mandible is perforated by a variety of small mental foramina of around 0.5 mm. The coronoid process is 69 mm wide and 50 mm high, and its dorsal end is dorsally pointed. In lateral view, the ascending ramus of the coronoid process covers the m3 completely. In lateral view, the condyloid process is triangular, pointing caudodorsally. The head of the condyloid process is convex in lateral view and hourglass shaped in dorsal view. The caudal margin of the condyloid process diverges from the dorsal margin of the angular process in a caudally open angle of 45°. The angular process has a blunt caudal end. It is located at the caudal-most extremity of the mandible and forms a rostral 45° angle with the ventral margin of the mandible.

The caudolateral (or posterolateral) opening of the mandibular canal is located ventrolaterally to the tooth row, between m2 and m3. The canal emerges on the notch of the dorsal margin of the horizontal ramus of the mandible and the bottom of the coronoid ramus. It is rostrocaudally elongate, oval with a length of approximately 10 mm and opens rostrodorsally (Fig. 12). The mandibular foramen is located on the medial side of the mandible, caudally of the mandibular notch between the coronoid and the condylar process (Fig. 13). Its ventral border lies level with the dorsal margin of the angular processes. The foramen opens dorsocaudally and is located dorsocaudally of the toothrow, approximately 40 mm from the caudal edge of m3. A small foramen, half the size of the mandibular foramen, is located ventral to the mandibular foramen, at the height of the dorsal margin of the mandibular angle.

Dentition

Upper caniniforms (C)

The crowns of the upper caniniforms are rostrocaudally curved, 34 mm long and slender compared to the molariforms. They show an ovate occlusal surface with an oblique, almost vertical wear facet, which is 20 mm long. The occlusal surface is inclined caudoventrally at an angle of about 90° with respect to the rostral face of the caniniform. In ventral view, the upper caniniforms are at the same height with the molariforms.

Upper molariforms (M)

M1, M3, and M4 on the left side, and M1, M2, and M4 on the right side of the maxilla are lacking (Fig. 7). The alveolar apertures of M1 and M4 are one third smaller than those of M2 and M3 (Table 2). The alveolus of M1 is 18 mm wide and rounded to triangular in outline. The lingual side of the alveolus is 19 mm wide and thus considerably wider than the buccal one, which has a length of 13 mm. The occlusal surface of the contralateral M2 is 28 mm wide and thus almost twice as wide as alveoli of M1 and 4. The alveolus of M2 indicates that M2 was the broadest upper molariform. The occlusal surface of the M2 alveolus is transversally elliptical, being lingually wider than bucally (16 mm lingual width and 9.5 mm buccal width). The occlusal surface of the right M3 has an elongated subtriangular outline, similar to molariforms described by McDonald et al. (2013a, b) as reniform. The occlusal surface is concave. The occlusal surface of M3 is lingually and distally lower than mesially and buccally. Furthermore, the occlusal surface of M3 is lingually wider (19 mm) than buccally (12 mm). The alveolar shape (right side) and occlusal surface (left side) of M2 suggest that this tooth was morphologically similar to M3. The distal and lingual edges of M3 are more worn down than the mesial

Table 2 *Xibalbaonyx oviceps* measurements

Dentition (Za2014-01 and Za2014-05)			Millimeter
C1: crown height			34
M3: crown height			30
c1: crown height right/left			18/21
C1 occlusal surface (mesiodistal diameter)			20
c1 occlusal surface (mesiodistal diameter)			18

	Buccolingual width	Mesiodistal width Lingual side	Mesiodistal width Buccal side
Upper alveoli of the M1	18	19	13
M2 (left side)	28	16	9
M3 (right side)	28	19	12
M4 (left side)	21	9	16
m1	25	16	13
m2	24	13	12
m3	23	14	10

ones, with a mesially maximum height of 30 mm. The buccal and distal surfaces of M3 and 4 have vertical striations. Distally, M3 has a vertically running apicobasal sulcus emerging on the occlusal surface. A well-developed apicobasal sulcus is also present on the buccal side, emerging from the concave margin of the occlusal surface of M3. The occlusal surface of M4, as well as the aperture of its respective alveolus are also triangular in outline, but the buccal side is 16 mm wide and thus 7 mm wider than the lingual one (9 mm). The distal faces of the left M4 are one fourth lower than the mesial ones. The distal surface of M4 is abraded to the level of the alveolar margin. The lingual and buccal sides of M4 are rounded and almost blunt.

Lower caniniforms (c)

The mandibular caniniforms (c1) are located caudolaterally to the mandibular spout. They are separated from the respective rows of molariforms by a 49 mm long diastema. The alveolar aperture of the caniniforms is transversely oval. The caniniforms are slightly higher than the molariforms. They are straight in lateral view and transversely oval to slightly triangular in cross-section. The occlusal surface faces rostrally and is 11.5 mm high. The right caniniform is worn down to a height of 18 mm, while the left one is 21 mm high. In lateral view both lower caniniforms have well-developed, vertical running apicobasal sulci on their buccodistal face. Compared to the premaxillomaxillary dentition, the outer surface of the mandibular dentition has vertical striations, including c_1.

Lower molariforms (m)

The molariform tooth rows are 78 mm long and range in width from 20 to 25 mm. Their lateral margins run subparallel to each other. The aperture of the alveoli is transversely oval with a length width ratio of the interalveolar width of 1–2 mm. All molariforms have well-developed and strongly worn down transversal crests of thin, light-colored laminations. The occlusal surfaces of m1–m2 are rounded rectangular in outline. M1 has a reniform outline. Its transversal crest is rostrolaterally slightly broken. The lingual face of m1 is one third wider than the buccal one. Its surface has vertical striations with deep pronounced apicobasal sulci on the mesiobuccal and lingual face of the tooth. The occlusal surface of m2 is rectangular in shape with rounded borders. Its transversal crest is laterally broken, and the mesiolingual crest of m2 is particularly worn off on the right side. M2 is the largest of the lower molars, with a buccal width of 13 mm and a mesiodistal width of 25 mm. Its lingual surface bears an apicobasal sulcus. M3 has a rounded pentagonal occlusal surface. The lingual and buccal sides are equally wide, but the mesiodistal width is 16 mm wide and therefore approximately 5 mm wider than the buccal or lingual margins. Its transversal crest is smooth, laminated and light-colored. Its surface has vertically striations as seen on the other molariforms. The occlusal surface of the molariforms is concave and completely worn. The wear facets of the lower molariforms are inclined buccally at an angle of about 45° against the vertical axis of the crown. This contrasts to the upper molariforms, where the wear faces are inclined lingually.

Comparative osteology

North and Central American Megalonychidae

Xibalbaonyx was approximately as big as the North American *Megalonyx*. *Megalonyx jeffersonii* is characterized by a massive, short skull with nearly horizontal skull roof, a sagittal crest and a closed zygomatic arch (Leidy 1855; Lindahl 1891). The skull is roughly cylindrical, lacking any vaulting of the skull roof or nasional impression seen in *Xibalbaonyx*. In *M. jeffersonii* the sagittal crest rostrally bifurcates into the temporal ridges (McDonald 1977), and the occipital crest is prominent (Leidy 1855). Furthermore, the jugal is connected to the zygomatic process of the squamosal forming a closed zygomatic arch (Leidy 1855), and the ascending process of the jugal extends caudodorsally at an angle of 45° against the descending process. In *Xibalbaonyx*, the ascending process is oriented caudodorsally at an angle of 60° against the

descending process and the jugal and zygomatic process of the squamosal are separated. Similar to *Xibalbaonyx* the caniniforms of *Megalonyx* are separated from the molariforms by a diastema, but the cross-section of caniniforms is trapezoidal in *Megalonyx* (McDonald 1977) and not triangular like in *Xibalbaonyx*. The caniniforms of *Megalonyx* are located ventral to the rostral margin of the nasals (Lindahl 1891), while they are placed rostral to them in *Xibalbaonyx*. The long caniniforms of *M. jeffersonii* have the same transverse diameter as the molars, with a horizontally orientated wear facet (Leidy 1855). In *Xibalbaonyx* the occlusal surface of the caniniforms faces caudally, due to the self-sharpening occlusion action, and thus differs strongly from that of the molariforms. The molariforms of *Megalonyx* resemble those of *Xibalbaonyx* in having a trapezoidal to triangular occlusal surface (McDonald 1977), but in *Xibalbaonyx* the occlusal surfaces of the molariforms are reniform and thus differ from *Megalonyx*. These differences in dental wear are suggestive for a different type of mastication of the two genera. The mandible of *Megalonyx* has a rounded chin and lacks the mandibular spout, which characterizes *Xibalbaonyx*.

Meizonyx salvadorensis (Webb and Perrigo, 1985) is known from Barranca del Sisimico, the Department of San Vicente in El Salvador. With approximately 262 mm the mandible is slightly smaller than that of *Xibalbaonyx*, which is 300 mm long, though it is also fragmented (Webb and Perrigo 1985). Webb and Perrigo (1985) describe a vestigial symphyseal spout, which is not depicted in the paper, because the symphyseal suture is broken. Therefore, this structure cannot be compared to that of *Xibalbaonyx*. The articular condyle in *M. salvadorensis* nearly reaches as far dorsal as the coronoid process. In *Xibalbaonyx* the condylar process extends dorsal. The notches between coronoid and condylar process and condylar process and mandibular angle are of nearly equal 45°. The notch between condylar process and mandibular angle in *Meizonyx* is broader and has a concave, semicircular margin, whereas this margin is cornered in *Xibalbaonyx*. Like in *Xibalbaonyx* the mandible of *Meizonyx* reaches a maximum height of 130 mm (Webb and Perrigo 1985). The mandibles of the two species differ in their hourglass shape, in which the ventral margin of the mandibular body is semicircular at the height of the ascending ramus of the coronoid process in *Xibalbaonyx*. In *Meizonyx* the narrowest height of the mandibular body is reached at the notch between condylar process and descending ramus of the coronoid process, at the same height of the mandibular foramen. There is only one mandibular foramen in *Meizonyx*, but two in *Xibalbaonyx*. The rostral two thirds of the ventral mandibular margin of *Meizonyx* run almost horizontally. In *Xibalbaonyx* the rostral first-third and the caudal third of the mandibular margin run horizontally,

while the second third, halfway of the mandibular body is semicircular. The caudal portion of the mandibular angle of *Meizonyx* is broken, but its stub faces caudoventrally. The angular process is orientated rostrocaudally in *Xibalbaonyx*. In *Meizonyx*, the recess between the mandibular angle and the condylar process is shallow with a rounded outline. In *Xibalbaonyx* it is V-shaped with a caudally open aperture angle of 45°. Furthermore, the shape of the head of the condylar process in *Meizonyx* is almost circular in lateral view. In *Xibalbaonyx* it is triangular. The overall shape of the caniniforms and molariforms of *Meizonyx* are similar to those of *Xibalbaonyx*. However, the caniniform of *Meizonyx* is characterized by a triangular occlusal surface. In *Xibalbaonyx* the occlusal surface of the caniniform is oval and presents a distal apicobasal sulcus. The m1 of *M. salvadorensis* is the largest one of the series, and the m1 and 2 are quadrangular in cross-section (Webb and Perrigo 1985). In both species, the ascending ramus covers m_3 laterally.

Meizonyx salvadorensis is reported from the Early to Middle Pleistocene. To date, *X. oviceps* is only known from the Late Pleistocene of the Yucatán Peninsula.

West Antillean Megalonychidae

The megalonychid subfamily Choloepodinae includes *Choloepus*, *Acratocnus*, *Paulocnus*, *Neocnus* (Gray 1821; White and MacPhee 2001) and is defined by the following diagnostic features: the rostrum is flared and the cranium domed without a trace of a nasional impression. The skull of *Xibalbaonyx* differs from this group in having an elongated postorbital skull roof, which is convex, but not domed. The strong nasional impression on the nasals is a diagnostic feature for *Xibalbaonyx*, which is absent or only weekly expressed in Choloepodinae. *Xibalbaonyx* does not present a sagittal crest. Sagittal crests occur in some genera of the subfamily, e.g., in *Acratocnus* and *Neocnus*. *Acratocnus* also presents a prominent postorbital constriction (MacPhee et al. 2000), which is absent in *Xibalbaonyx*. Furthermore, in the cranium of *Neocnus* with its low sagittal crest is dorsally flattened (MacPhee et al. 2000), while the skull roof of *Xibalbaonyx* is circular. All extant Choloepodinae are small compared to *Xibalbaonyx* and are semi-arboreal to arboreal.

The subfamily Megalocninae includes *Parocnus* and *Megalocnus* (Kraglievich 1923b; White and MacPhee 2001) and is characterized by the absence of a postorbital constriction, an elongated cranium of relatively uniform width with a flat-skull roof and an inflated pterygoid (White and MacPhee 2001). These features are also visible in *Xibalbaonyx*. However, the Cuban genus *Megalocnus* (Leidy, 1868; MacPhee et al. 2000) also differs by an expanded jugal, in which the ascending process is thin and

caudally curved converging to a slender spine, while the descending process is a short, flat plate with a wavy caudal margin (Matthew and De Paula Couto 1959), different from *Xibalbaonyx*. The paroccipital process is substantially enlarged and free standing (Gaudin 1995). The genus *Megalocnus* is further distinguished by its maxillary "pseudo-rodentiform" (White and MacPhee 2001) caniniforms, which are rostrocaudally compressed (White and MacPhee 2001; Van der Geer et al. 2010) instead of peg-like with a triangular cross-section as in *Xibalbaonyx*, and the caniniforms in the latter one are smaller in relation to the skull, as in *Megalocnus*.

The genus *Parocnus* (Miller, 1929) is characterized by enlarged, convergent temporal lines (Fischer 1971) also interpreted as a paired sagittal crest (White and MacPhee 2001), while the skull in *Xibalbaonyx* is smooth without a sagittal crest, and the temporal lines are separated. The two genera share a greatly elongated mandibular spout, but its margin is rostrodorsally convex and rostroventrally concave in *Xibalbaonyx*, while that of *Parocnus* is dorsally straight, almost horizontal. Further characteristics of *Parocnus* are triangular caniniforms, different from the oval occlusal surface of the caniniforms in *Xibalbaonyx*. A deep lingual groove caudal to the caniniforms is present in *Parocnus*, while this fossa is small and barely visible in *Xibalbaonyx*. Molariforms are subquadrate in *Parocnus* (White and MacPhee 2001), while the molariforms in *Xibalbaonyx* are reniform. Megalocninae are the only large-sized ground sloths known from the West Indies with an estimated weight of 150–270 kg (De Paula Couto 1979; MacPhee et al. 2000; Van der Geer et al. 2010); even though, they are smaller-sized than *Xibalbaonyx*.

South American Megalonychidae

Eucholoeops (Ameghino, 1887) is a megalonychid from the Early Miocene of Argentina. It is characterized by a convex cranium with a slight medial depression in dorsal view (De Iuliis et al. 2014). This differs from *Xibalbaonyx* where the postorbital cranium is of uniform width. In lateral view, the nasals of *Eucholoeops* differ from that of *Xibalbaonyx*, which has slightly concave nasals formed by a nasional impression. In dorsal aspect, the lateral and caudal margins of the nasals of *Eucholoeops* are concave. In *Xibalbaonyx*, the lateral margins are straight and the caudal margins converge in rostral direction when seen from dorsally, whereas those of *Eucholoeops* converge caudally (De Iuliis et al. 2014). The temporal lines in *Eucholoeops* curve caudomedially and merge to a low sagittal crest that reaches from frontal to the occipital (De Iuliis et al. 2014). The temporal lines in *Xibalbaonyx* are caudally pronounced, but do not approach one another and there is no sagittal crest. The prominent nuchal crest and

the incomplete zygomatic arch are shared characters in both *Eucholoeops* (De Iuliis et al. 2014) and *Xibalbaonyx*.

Pliomorphus is documented (Ameghino, 1885; Kraglievich 1923b) from the Miocene of Argentina, Uruguay, and Brazil (Brandoni 2011). Here we compare nearly complete skulls of *Pliomorphus ameghinoi* and *Pl. ameghinoi gracilis* lacking the teeth (Brandoni 2011). The skull of *Pliomorphus* differs from that of *Xibalbaonyx* in a circular dorsal margin from the nasal tip to the nuchal crest, reaching the highest point at the rostral margin of the parietal, without a nasional impression as in *Xibalbaonyx*. The caudally pointing ascending process of the jugal in *Pliomorphus* is dorsally convex and its end points caudally, while that in *Xibalbaonyx* is straight and points dorsally. In ventral view, the nasals and the caudal third of the maxilla become caudally narrower in *Pliomorphus*, which is not the case in *Xibalbaonyx* where the bones retain the same width along their entire extent. The occipital protuberance along with the nuchal crest are pronounced in *Pliomorphus*, which is not the case in *Xibalbaonyx*. Furthermore, the Miocene age and geographical distribution of *Pliomorphus* of southern South America precludes a close relationship with the Mexican Late Pleistocene *Xibalbaonyx*.

Megistonyx oreobios from the Cueva de los Huesos in the Zulia State of Venezuela is a massive Late Pleistocene (14.150 ± 50 BP, 17.385 ± 239 cal BP) ground sloth (McDonald et al. 2013b) that morphologically resembles the North American *Megalonyx* (Harlan, 1825; Leidy 1855) and the Brazilian *Ahytherium aureum* (Cartelle et al., 2008). The holotype of *M. oreobios* is an almost complete skull without basicranium, squamosal, caniniforms, and right toothrow. The species differs from *X. oviceps* by its extremely wide nasals (McDonald et al. 2013b), with caniniforms located in the rostrolateral extremities, protruding laterally beyond the rows of the molariforms (McDonald et al. 2013b). In ventral view, the maxilla of *Megistonyx* becomes caudally two thirds narrower compared to its rostral width (McDonald et al. 2013b). In *Xibalbaonyx* the maxilla is of uniform width. Therefore, the rostrum of *Xibalbaonyx* is more gracile and narrower compared to *Megistonyx*. In addition, the sagittal crest of *Megistonyx* is formed by the two converging temporal crests that arise from the postorbital processes of the frontal (McDonald et al. 2013b). *Xibalbaonyx* has neither a sagittal nor temporal crests and the temporal lines do not meet. A diastema between the caniniforms and first molariform is present in both species (McDonald et al. 2013b), but there is a shallow, barely visible fossa caudal to C1 in *Xibalbaonyx* which is missing in *Megistonyx* (McDonald et al. 2013b). The caniniforms of *Megistonyx* are missing, but McDonald et al. (2013b) report a triangular outline of the respective alveolar aperture similar to the Choloepodinae and *Australonyx* (De Iuliis et al. 2009). In *Xibalbaonyx* the

respective alveolar apertures are oval. M1 of *Megistonyx* is as wide as M2 and M3 and trapezoidal in cross section (McDonald et al. 2013b), whereas the alveolar aperture of M1 of *Xibalbaonyx* is oval and one third smaller than M2 and M3. The occlusal surface of the M2 of *Megistonyx* is trapezoidal (McDonald et al. 2013b), but reniform to rectangular in *Xibalbaonyx*. The separation of the zygomatic process from the jugal is a common character in both *Megistonyx* (McDonald et al. 2013b) and *Xibalbaonyx*.

Diabolotherium nordenskioldi (Kraglievich, 1926; Pujos et al. 2007) from the Pleistocene of Casa del Diablo Cave in the Peruvian Andes is a small ground sloth, similar in size to *Parocnus browni* from the West Indies (Pujos et al. 2007). *Diabolotherium* has no caniniforms (Pujos et al. 2007). This feature and the considerable difference in body size are sufficient to separate *D. nordenskioldi* from *Xibalbaonyx* and other Megalonychidae. A complete skull of *D. nordenskioldi* was reported by Shockey et al. (2009) from Peru, but has neither been described nor is it available to us. Based on the published fragmentary material (Kraglievich 1926; Pujos et al. 2007), however, the morphological differences are sufficient to exclude a close relationship between *D. nordenskioldi* and *Xibalbaonyx*.

Ahytherium aureum (Cartelle et al., 2008) was discovered in the flooded Poço Azul Cave in the municipality of Nova Redenção, Federal State of Bahia, Brazil (Cartelle et al. 2008; De Iuliis et al. 2009). The holotype of *A. aureum* comprises an almost complete skull with mandible and some postcranial elements (Cartelle et al. 2008). Its skull differs from that of *Xibalbaonyx* by a dorsally protruding frontal and short nasal (Cartelle et al. 2008). In dorsal view, the rostrum of *Ahytherium* is wider than the braincase, reaching one eighth of the entire skull length. In dorsal view, the rostrum in *Xibalbaonyx* is narrower than the rest of the skull, but of uniform width. The lateral margins of the caudal two thirds of the skull of *Ahytherium* become caudally concave and one fourth narrower than the rostral part. In dorsal view, the lateral skull margins of *Xibalbaonyx* run subparallel to each other, and are not convex like in *Ahytherium*. The jugal of *Ahytherium* is massive compared to that of *Xibalbaonyx*. In particular, the caudoventrally pointing descending process of the jugal reaches almost the same length as the ascending process (Cartelle et al. 2008). It is, therefore, twice the length of the respective processes of *Xibalbaonyx*. *Ahytherium aureum* has a closed zygomatic arch (Cartelle et al. 2008). This is not the case in *Xibalbaonyx*. In contrast to *Xibalbaonyx*, *Ahytherium* has an elongated sagittal crest, which is formed by the merging pair of temporal lines (Cartelle et al. 2008). The temporal lines in *Xibalbaonyx* do not merge dorsally and run far apart from each other. Only the shape of the caniniforms and the prominent external occipital crest are shared characters of *Xibalbaonyx* and *Ahytherium* (Cartelle et al. 2008), although the occipital crest is more prominent in

Ahytherium than in *Xibalbaonyx*. The mandible of the holotype of *Ahytherium* is 210 mm long and has a rostral width of 66 mm (Cartelle et al. 2008). The mandible of *Xibalbaonyx* is significantly more massive, with a length of 300 mm, of which the rostral part reaches approximately 100 mm in width. *Australonyx aquae* (De Iuliis et al. 2009, 2016) was discovered at the same location as *A. aureum*, in the Poço Azul Cave in the Federal State of Bahia, Brazil, and as the latter one, also dates back to the Pleistocene (De Iuliis et al. 2009). The skull of *A. aquae* is 15% smaller (De Iuliis et al. 2009) than that of *Xibalbaonyx*. In lateral view, the dorsal faces of the frontals, parietals and nasals of *Australonyx* are flat and run horizontally with a sharp bend towards caudal at the orbital constriction. This differs from *Xibalbaonyx*, in which the frontals and parietals are dorsally convex, while the dorsal margin of the skull roof rostral to the orbital constriction is concave. In dorsal view, the rostral margins of the nasal of *X. oviceps* are straight, with the exception of the median nasion process or rhinion. In *A. aquae* the median rhinion of the nasal is rostrally pointed (De Iuliis et al. 2009). In dorsal view, the rostrum of *Australonyx* is twice as narrow as the braincase, whereas the rostrum of *Xibalbaonyx* has nearly the same width as the braincase. The skull of *Australonyx* has a well developed postorbital constriction in dorsal view and the braincase is hourglass-shaped, while the skull of *Xibalbaonyx* is longitudinally oval. The area rostral to the postorbital constriction of *Australonyx* is laterally convex, while both the parietal and squamosal are concave in dorsal view. The skull roof of *Australonyx* is marked by a low sagittal crest on the frontal and parietal, formed by the medially merging, prominent temporal lines (De Iuliis et al. 2009). Furthermore, in *Xibalbaonyx* the temporal lines are only visible on the caudal part of the skull. *Xibalbaonyx* also shows a short and narrow nuchal crest, different from the dorsally expanded crest of *Australonyx*. In both *Australonyx* and *Xibalbaonyx* the nuchal crest continues ventral to the paroccipital process of the petrosal.

In lateral view, the rostrolateral face of the maxilla of *Australonyx* is characterized by a massive line, which begins rostral to the upper caniniforms and ends rostral to the postorbital constriction. This line is absent in *Xibalbaonyx*. The preserved part of the zygomatic process of *A. aquae* suggests that this bone was dorsoventrally narrow in lateral aspect and may thus have resembled that of *X. oviceps* (De Iuliis et al. 2009). The mastoid process of *A. aquae* is laterally pointed and big (De Iuliis et al. 2009), while that of *Xibalbaonyx* is rounded and smaller. The mandible of *Xibalbaonyx* is one-third longer than that of *Australonyx*. In lateral view, the mandible of *Australonyx* presents a 90° angle between its ventral edges, including the angular processes and the caudal-most point of the condyloid processes (De Iuliis et al. 2016). This is not the case in *Xibalbaonyx*. The degree between the heads of the

condyloid and coronoid processes is 45° in *Xibalbaonyx*, while that in *Australonyx* is wider (De Iuliis et al. 2016).

The malleus of *Xibalbaonyx* has an extremely elongated and gracile head, ventrally followed by a neck and an elongated manubrium. The body of the malleus of *A. aquae* is twice as big and there is no neck between head and manubrium (De Iuliis et al. 2009). On the other side, the manubrium of the malleus of *Xibalbaonyx* is twice as wide as the one in *Australonyx*. In *Xibalbaonyx*, a small caudally pointing process is seen on the ventral part of the head of the malleus but is apparently absent in *Australonyx* (De Iuliis et al. 2016). A close relationship between both genera is, therefore, excluded here.

The Zapote ground sloth is characterized by a dental formula of 5/4, including a large caniniform tooth with a triangular cross section. The caniniforms are separated from the molariform toothrow by a diastema in both the upper and lower jaw. The occlusal rims of the molariforms are either oval, rounded rectangular, or kidney-shaped with transverse crests (McDonald et al. 2013b). All teeth bear deep striations and apicobasal sulci, with the exception of the upper caniniforms. The ascending process of the jugal is longer than the descending and middle process. The pterygoids are inflated and hollow. The glenoid fossa is mediolaterally twice as wide than rostrocaudally long. Autapomorphies of the Zapote ground sloth that justify the erection of a new genus and species comprise the nasional impression of the nasal, an elongated uniform shape of the skull in dorsal view, the absence of a sagittal crest and the evenly smooth skull roof.

Several cranial characters of *X. oviceps* exclude a close relationship with Late Miocene *Pliometanastes* and *Eucholoeops*, but also with Plio- to Pleistocene ground sloths such as *Megalonyx*, *Megistonyx*, *Diabolotherium*, and *Ahytherium*. *Xibalbaonyx oviceps* shares many anatomical features with *A. aquae*, suggesting a close relationship between the two Late Pleistocene species (De Iuliis et al. 2009). Nevertheless, osteological differences are sufficiently significant to separate the genera. There are also striking similarities between *Xibalbaonyx* and the Pleistocene megalonychid sloths from the West Indies, but a direct terrestrial connection between the Yucatán Peninsula and the West Indies, which would have been fundamental for genetic interchange, did not exist (MacPhee and Iturralde-Vinent 2005; Montes et al. 2015). *Xibalbaonyx* may thus be the result of megalonychid microevolution on the Yucatán Peninsula.

Discussion

The ontogenetic stages of ground sloths and their individual osteological development are not fully understood (Cartelle and De Iuliis 2006). However, Cartelle and De Iuliis (2006) documented ontogenetic stages of *Eremotherium laurillardi* (Megatheriidae) based on the skull and occlusal surfaces of the molariforms. The authors suggest that the closure of basicranial sutures is suggestive of a subadult stage (Cartelle and De Iuliis 2006).

The occipital area of *Xibalbaonyx* is fused, which confirms that the parietal and occipital are among the first cranial bones to fuse during ontogeny (Cartelle and De Iuliis 2006; Pujos et al. 2007). The supraoccipital crest of *Xibalbaonyx* is well developed, which implies a late ontogenetic stage and a subadult to adult ontogenetic stage of the basicranium. Other sutures, especially in the rostral, basisphenoid/basioccipital and jugal areas, are still open, which implies that Za2014-01/-05 is a subadult individual.

The absence of a sagittal crest in *Xibalbaonyx* may also be suggestive of a subadult age of Za2014-01/-05. Pujos et al. (2007) and De Iuliis et al. (2009) suggested that a prominent sagittal crest, as seen in *D. nordenskioldi* and *A. aquae*, characterizes an adult individual. However, the temporal lines in *Xibalbaonyx* are so faint and so far from each other that the formation of a sagittal crest in a fully grown individual appears highly unlikely. It thus appears likely that Za2014-01/-05 was a subadult.

Conclusions

The well-preserved skull and mandible of a ground sloth discovered in the Zapote cenote Cave near Puerto Morelos on the northeastern Yucatán Peninsula of Mexico is here described as a new genus and species of Megalonychidae. The individual, here named *Xibalbaonyx* oviceps, has a dental formula of 5/4 including a greatly enlarged caniniform tooth of triangular cross-section. This caniniform is separated by a long diastema from the molariform tooth rows in both the lower and upper jaw. The molariform teeth show oval, rounded rectangular to reniform (McDonald et al. 2013b) occlusal shapes with transverse crests. All teeth except for the upper caniniforms, show striations and apicobasal sulci that may be expressed as shallow grooves or deep sulci. The ascending process of the jugal is longer than the descending and middle process of the jugal. The pterygoids are inflated. The glenoid fossa is transversally widened. The skull is elongated and narrow, with a nasional impression on the nasals. The temporal lines are widely separated and do not form a sagittal crest. The skull is narrow and gracile compared that of other Megalonychidae of similar size, such as *Megalonyx* or *Ahytherium*. The Zapote ground sloth was a subadult individual, based on the degree of suture fusion in the skull, faint temporal lines and the condition of the occlusion faces of the molariforms. To present knowledge *Xibalbaonyx* appears to have been endemic on the Yucatán Peninsula,

suggesting a local microevolution on this karst desert during the Late Pleistocene.

References

Adam, P.J. 1999. *Choloepus didactylus*. *Mammalian Species* 621: 1–8.

Ameghino, F. 1885. Nuevos restos de mamíferos fósiles Oligocenos recogidos por el Profesor Pedro Scalabrini y pertenecientes al Museo Provincial de la ciudad del Paraná. *Boletín de la Academia Nacional de Ciencias* 8: 1–205.

Ameghino, F. 1887. Enumeración sistemática de las espécies de mamíferos fósiles coleccionados por Carlos Ameghino en los terrenos Eocenos de la Patagonia austral y depositados en el Museo de La Plata. *Boletin del Museo de La Plata* 1: 1–26.

Bauer-Gottwein, P., B.R.N. Gondwe, G. Charvet, L.E. Marín, M. Rebolledo-Vieyra, and G. Merediz-Alonso. 2011. Review: The Yucatán Peninsula karst aquifer, Mexico. *Hydrogeology Journal* 19: 507–524.

Blanchon, P., and J. Shaw. 1995. Reef drowning during the last deglaciation: Evidence for catastrophic sea-level rise and ice-sheet collapse. *Geology* 23: 4–8.

Bradbury, J.P. 1997. Sources of glacial moisture in Mesoamerica. *Quaternary International* 43: 97–110.

Brandoni, D. 2011. The Megalonychidae (Xenarthra, Tardigrada) from the Late Miocene of Entre Ríos Province, Argentina, with remarks on their systematics and biogeography. *Geobios* 44 (1): 33–44.

Brenner, M., M.F. Rosenmeier, D.A. Hodell, and J.H. Curtis. 2002. Long-term perspectives on interactions among climate, environment, and humans. *Ancient Mesoamerica* 13: 141–157.

Bronk Ramsey, C. 2013. *OxCal 4.2 manual*. https://c14.arch.ox.ac.uk/oxcalhelp/hlp_contents.html. Accessed 27 March 2013.

Burr, G.S., J.W. Beck, T. Correge, G. Cabioch, F.W. Taylor, and D.J. Donahue. 2009. Modern and Pleistocene reservoir ages inferred from South Pacific corals. *Radiocarbon* 51 (1): 319–335.

Carlini, A.A., and G.J. Scillato-Yané. 2004. The oldest Megalonychidae (Xenarthra: Tardigrada); phylogenetic relationships and an emended diagnosis of the family. *Neues Jahrbuch für Geologie und Paläontologie, Abhandlungen* 233: 423–443.

Carranza Castañeda, O., and W.E. Miller. 2004. Late Tertiary terrestrial mammals from central Mexico and their relationship to South American immigrants. *Revista Brasileira de Paläontologie, Abhandlungen* 7: 249–261.

Cartelle, C., and G. De Iuliis. 2006. *Eremotherium laurillardi* (Lund) (Xenarthra, Megatheriidae), the Panamerican giant ground sloth: Taxonomic aspects of the ontogeny of skull and dentition. *Journal of Systematic Palaeontology* 4: 199–209.

Cartelle, C., G. De Iuliis, and F. Pujos. 2008. A new species of Megalonychidae (Mammalia, Xenarthra) from the Quaternary of Poço Azul (Bahia, Brazil). *Comptes Rendus - Palevol* 8 (7): 335–346.

Cervantes-Borja, J.F., G. Meza-Sánchez, and M. Alfaro-Sánchez. 1997. Sedimentological characterization of palaeo-soils in the northern part of the Basin of Mexico. *Quaternary International* 43: 75–86.

Chatters, J.C., D.J. Kennett, Y. Asmerom, B.M. Kemp, V. Polyak, A. Nava Blank, P. Beddows, E. Reinhardt, J. Arroyo-Cabrales, D.A. Bolnick, R.S. Malhi, B.J. Culleton, P.L. Erreguerena, D. Rissolo, S. Morell-Hart, and T.W. Stafford Jr. 2014. Late Pleistocene human skeleton and mtDNA link Paleoamericans and modern Native Americans. *Science* 344: 750–754.

Cope, E.D. 1871. Preliminary report on the vertebrata discovered in the Port Kennedy Bone Cave. *American Philosophical Society* 12: 73–102.

Cope, E.D. 1893. A preliminary report on the vertebrate paleontology of the Llano Estacado. In *4th annual report on the Geological Survey of Texas*, 136.

De Iuliis, G., F. Pujos, and C. Cartelle. 2009. A new ground sloth (Mammalia: Xenarthra) from the Quaternary of Brazil. *Comptes Rendus - Palevol* 8 (8): 705–715.

De Iuliis, G., F. Pujos, N. Toledo, M.S. Bargo, and S.F. Vizcaíno. 2014. *Eucholoeops* Ameghino, 1887 (Xenarthra, Tardigrada, Megalonychidae) from the Santa Cruz Formation, Argentine Patagonia: Implications for the systematics of Santacrucian sloths. *Geodiversitas* 36: 205–255.

De Iuliis, G., H.G. McDonald, N. Stanchly, J. Spenard, and T.G. Powis. 2015. *Nothrotheriops shastensis* (Sinclair) from Actun Lak: First record of Nothrotheriidae (Mammalia, Xenarthra, Pilosa) from Belize. *Ameghiniana* 52: 153–171.

De Iuliis, G., C. Cartelle, and F. Pujos. 2016. New Pleistocene remains of megalonychid ground sloths (Xenarthra: Pilosa) from the intertropical Brazilian region. *Journal of Paleontology* 90: 578–587.

De Paula Couto, C. 1979. *Tratado de Paleomastozoologia*. Academia Brasileira de Ciências.

Desmarest, M.A.G. 1822. *Mammalogie ou description des espèces de Mammifères. 2e partie*. Paris: Agasse.

Ferrusquía-Villafranca, I., M.R. Easton, and D.E. Owen. 2009. Do GSSPs render the dual time-rock/time classification and nomenclature systems redundant? *Stratigraphy* VI: 135–169.

Ferrusquía-Villafranca, I., J. Arroyo-Cabrales, E. Martínez-Hernández, J. Gama-Castro, J. Ruiz-González, O.J. Polaco, and E. Johnson. 2010. Pleistocene mammals of Mexico: A critical review of regional chronofaunas, climate change response and biogeographic provinciality. *Quaternary International* 217: 53–104.

Fischer, K. 1971. Riesenfaultiere (Megalonychidae, Edentata, Mammalia) aus dem Pleistozän der Plio-Domingo-Höhle in Kuba. *Wissenschaftliche Zeitschrift, Humboldt-Universität, Mathematisch-Naturwissenschaftliche Reihe* 20 (4–5): 609–673.

Flynn, J.J., B.J. Kowallis, C. Nuñez, O. Carranza Castañeda, W.E. Miller, C.C. Swisher III, and E. Lindsay. 2005. Geochronology of Hemphillian-Blancan Aged Strata, Guanajuato, Mexico, and implications for timing of the Great American Biotic Interchange. *The Journal of Geology* 113: 287–307.

Gaudin, T.J. 1995. The ear region of edentates and the phylogeny of the Tardigrada (Mammalia, Xenarthra). *Journal of Vertebrate Paleontology* 15: 672–705.

Gaudin, T.J. 2004. Phylogenetic relationships among sloths (Mammalia, Xenarthra, Tardigrada): The craniodental evidence. *Zoological Journal of the Linnean Society* 140: 255–305.

Gaudin, T.J., and D.A. Croft. 2015. Paleogene Xenarthra and the evolution of South American mammals. *Journal of Mammalogy* 96: 622–634.

González González, A.H., A. Terrazas, W. Stinnesbeck, M.E. Benavente, J. Avíles, J.M. Padilla, A. Velásquez, E. Aceves, and E. Frey. 2013. The first human settlers on the Yucatan Peninsula: Evidence from drowned caves in the State of Quintana Roo (south Mexico). In *Paleoamerican Odyssey, Center for the Study of the First Americans*, eds. K.E. Graf, C.V. Ketron, and M. Waters, 323–338. Texas A&M University.

González González, A.H., C. Rojas, A. Terrazas, M. Benavente Sanvicente, W. Stinnesbeck, J. Aviles, M. De los Ríos, and E. Acevez. 2008. The arrival of humans on the Yucatan Peninsula: Evidence from submerged caves in the State of Quintana Roo, Mexico. *Current Research in the Pleistocene* 25: 1–24.

Grant, K.M., E.J. Rohling, M. Bar-Matthews, A. Ayalon, M. Medina-Elizalde, C. Bronk Ramsey, C. Satow, and A.P. Roberts. 2012. Rapid coupling between ice volume and polar temperature over the past 150,000 years. *Nature* 491: 744–747.

Gray, J.E. 1821. On the natural arrangement of vertebrose animals. *London Medical Repository* 15: 297–310.

Groves, C.P. 2003. Morphology, morhometrics and taxonomy. In *Field and laboratory methods in primatology*, ed. Debbie Curtis, and Jo Setchell, 140–157. Cambridge: Cambridge University Press.

Harlan, R. 1825. *Fauna americana: Being a description of the mammiferous animals inhabiting North America*. Philadelphia.

Hayssen, V. 2011. *Choloepus hoffmanni* (Pilosa: Megalonychidae). *Mammalian Species* 43: 37–55.

Hirschfeld, S.E., and S.D. Webb. 1968. Plio–Pleistocene megalonychid sloths of North America. In *Bulletin of the Florida State Museum Biological Sciences* 12, 213–296.

Kraglievich, L. 1923a. Un nuevo representante de la subfamilia "Ortotherinae" en la Formación Entrerriana de las Barrancas del Río Paraná "*Torcellia paranense*" n. gen. n. sp. *Comunicaciones de Historia Natural de Buenos Aires* 2: 1–8.

Kraglievich, L. 1923b. Descripción de dos cráneos y otros restos del género *Pliomorphus* Ameghino procedentes de la Formación Entrerriana de las barrancas del río Paraná. *Anales del Museo Nacional de Historia Natural de Buenos Aires* 33: 1–56.

Kraglievich, L. 1926. Notas sobre gravigrados du Sud America. *Anales del Museo Argentina Ciencias Naturales "Bernardino Rivadavia"* 34: 21–36.

Kraglievich, L. 1930. Nuevos megalonícidos gigantescos de los géneros *Megalonychops* Kragl. y *Diheterocnus* Kragl. *Revista del Museo de La Plata* 32: 9–21.

Lefticariu, M., E.C. Perry, W.C. Ward, and L. Lefticariu. 2006. Post-Chicxulub depositional and diagenetic history of the northwestern Yucatan Peninsula, Mexico. *Sedimentary Geology* 183: 51–69. doi:10.1016/j.sedgeo.2005.09.008.

Leidy, J. 1855. *A memoir on the extinct sloth tribe of North America*. Smithsonian Institution.

Leidy, J. 1868. Notice on some vertebrate remains from the West Indian Islands. *Proceedings of the Academy of Natural Sciences of Philadelphia* 20: 178–180.

Leyden, B.W., M. Brenner, D.A. Hodell, and J.H. Curtis. 1994. Orbital and internal forcing of climate on the Yucatan Peninsula for the past ca. 36 ka. *Palaeogeography, Palaeoclimatology, Palaeoecology* 109: 193–210.

Lindahl, J. 1891. Description of a skull of *Megalonyx* Leidyi, n. sp. *Transactions of the American Philosophical Society* 17: 1–10.

Linnaeus, Carl. 1758. *Systema Naturæ*. Stockholm: Lars Salvius.

Lucas, S.G. 2008. Late Cenozoic fossil mammals from the Chapala Rift Basin, Jalisco, Mexico. In *Neogene mammals*: *New Mexico, USA*, 39–49. New Mexico: New Mexico Museum of Natural History Bulletin.

MacPhee, R.D.E., and M.A. Iturralde-Vent. 1994. First Tertiary land mammal from Greater Antilles: An Early Miocene sloth (Xenarthra, Megalonychidae) from Cuba. *American Museum Novitates*: 1–13.

MacPhee, R.D.E., and M.A. Iturralde-Vent. 2005. The interpretation of Caribbean paleogeography: Reply to hedges. In *Proceedings of the international symposium "Insular Vertebrate Evolution*: *The Palaeontological Approach"*, eds. J.A. Alcover and P. Bover, 175–184. Monografies de la Societat d'Historia Natural de les Balears.

MacPhee, R.D.E., and M.A. Iturralde-Vent. 1995. Origin of the Greater Antillean land mammal fauna, 1: New tertiary fossils from Cuba and Puerto Rico. *American Museum Novitates* 3141: 1–31.

MacPhee, R.D.E., J.L. White, and C. Woods. 2000. New Megalonychid sloths (Phyllophaga, Xenarthra) from the Quaternary of Hispaniola. *American Museum Novitates* 3303: 1–32.

Mallison, H., and O. Wings. 2014. Photogrammetry in paleontology—A practical guide. *Journal of Paleontological Techniques* 12: 1–31.

Martin, R. 1914. *Lehrbuch der Anthropologie in systematischer Darstellung mit besonderer Berücksichtigung der anthropologischen Methoden*. Jena: Gustav Fischer Verlag.

Matthew, W.D., and C. De Paula Couto. 1959. The Cuban edentates. *Bulletin of the American Museum of Natural History* 117: 1–104.

McDonald, H.G. 1977. *Description of the osteology of the extinct gravigrade edentate Megalonyx with observations on its ontogeny*, *phylogeny and functional anatomy*. University of Florida.

McDonald, H.G. 1985. The Shasta ground sloth *Nothrotheriops shastensis* (Xenarthra, Megatheriidae) in the Middle Pleistocene of Florida. In *The evolution of armadillos, sloths, and vermilinguas*, ed. G.G. Montgomery, 95–104. Washington, DC: Smithsonian Institution Press.

McDonald, H.G. 2002. Fossil Xenarthra of Mexico: A review. In *Avances en los estudios paleomastozoológicos: México*, Serie Arqu, 227–248. DF: Instituto Nacional de Antropología e Historia.

McDonald, H.G., C.R. Harington, and G. De Iuliis. 2000. The ground sloth *Megalonyx* from Pleistocene deposits of the Old Crow Basin, Yukon, Canada. *Arctic* 53: 213–220.

McDonald, H.G., R.G. Dundas, and J.C. Chatters. 2013a. Taxonomy, paleoecology and taphonomy of ground sloths (Xenarthra) from the Fairmead Landfill Locality (Pleistocene: Irvingtonian) of Madera County, California. *Quaternary Research (United States)* 79: 215–227.

McDonald, H.G., A.D. Rincón, and T.J. Gaudin. 2013b. A new genus of megalonychid sloth (Mammalia, Xenarthra) from the Late Pleistocene (Lujanian) of Sierra de Perija, Zulia State, Venezuela. *Journal of Vertebrate Paleontology* 33: 1226–1238.

McKenna, M., A.R. Wyss, and J.J. Flynn. 2006. Paleogene pseudoglyptodont Xenarthrans from central Chile and Argentine Patagonia. *American Museum Novitates*: 1–18.

Metcalfe, S.E., S.L. O'Hara, M. Caballero, and S.J. Davies. 2000. Records of Late Pleistocene–Holocene climatic change in Mexico—A review. *Quaternary Science Reviews* 19: 699–721.

Miller, G.S. 1929. *Mammals eaten by Indians*, *owls*, *and spaniards in the coast region of the Dominican Republic*: (*with two plates*). The Smithsonian Institution.

Montes, C., A. Cardona, C. Jaramillo, A. Pardo, J.C. Silva, V. Valencia, C. Ayala, L.C. Pérez-Angel, L.A. Rodriguez-Parra, V.

Ramirez, and H. Niño. 2015. Middle Miocene closure of the Central American Seaway. *Science* 348: 226–229.

Morgan, G.S. 2005. The Great American Biotic Interchange in Florida. *Bulletin of the Florida Museum of Natural History* 45: 271–311.

Moseley, G.E., P.L. Smart, D.A. Richards, and D.L. Hoffmann. 2013. Speleothem constraints on marine isotope stage (MIS) 5 relative sea levels, Yucatan Peninsula, Mexico. *Journal of Quaternary Science* 28: 293–300.

Moseley, G.E., D.A. Richards, P.L. Smart, C.D. Standish, D.L. Hoffmann, H. ten Hove, and O. Vinn. 2015. Early–Middle Holocene relative sea-level oscillation events recorded in a submerged speleothem from the Yucatán Peninsula, Mexico. *The Holocene* 25: 1511–1521.

Pant, S.R., A. Goswami, and J.A. Finarelli. 2014. Complex body size trends in the evolution of sloths (Xenarthra: Pilosa). *BMC Evolutionary Biology* 14: 184.

Patterson, B., W. Segall, W.D. Turnbull, and T.J. Gaudin. 1992. The ear region in xenarthrans (=Edentata, Mammalia): Part II. Pilosa (sloths, anteaters), palaeanodonts, and a miscellany. *Geology* 24: 1–79.

Peters, W. 1858. *Naturwissenschaftliche Reise nach Mossambique, auf Befehl seiner Majestät des Königs Friedrich Wilhelm IV. in den Jahren 1842 bis 1848 ausgeführt*. Berlin: Reimer.

Pujos, F., G. De Iuliis, and C. Cartelle. 2016. A paleogeographic overview of tropical fossil sloths: Towards an understanding of the origin of extant suspensory sloths? *Journal of Mammalian Evolution*: 1–20.

Pujos, F., G. De Iuliis, C. Argot, and L. Werdelin. 2007. A peculiar climbing Megalonychidae from the Pleistocene of Peru and its implication for sloth history. *Zoological Journal of the Linnean Society* 149: 179–235.

Scillato-Yané, G.J. 1980. Nuevo Megalonychidae (Edentata, Tardigrada) del "Mesopotamiense" (Mioceno tardío-Plioceno) de la Provincia de Entre Ríos. *Ameghiniana* 17: 193–199.

Scott, W.B. 1904. Mammalia of the Santa Cruz beds, Part 1. Edentata. *Report of Princeton University Expedition to Patagonia* 5: 161–364.

Shockey, B.J., R. Salas-Gismondi, P. Baby, J.-L. Guyot, M.C. Baltazar, L. Huamán, A. Clack, M. Stucchi, F. Pujos, J.M. Emerson, and J.J. Flynn. 2009. New Pleistocene cave faunas of the Andes of central Peru: Radiocarbon ages and the survival of low latitude, Pleistocene DNA. *Palaeontologia Electronica* 12: 15p.

Smart, P.L., P. Beddows, J. Coke, S. Doerr, and F.F. Whitaker. 2006. Cave development on the Caribbean Coast of the Peninsula, Yucatan Roo, Quintana. *Geological Society of America Special Papers* 404: 105–128.

Smith, D.E., S. Harrison, C.R. Firth, and J.T. Jordan. 2011. The Early Holocene sea level rise. *Quaternary Science Reviews* 30: 1846–1860.

Steadman, D.W., P.S. Martin, R.D.E. MacPhee, A.J.T. Jull, H.G. McDonald, C.A. Woods, M. Iturralde-Vinent, and G.W.L. Hodgins. 2005. Asynchronous extinction of Late Quaternary sloths on continents and islands. *Proceedings of the National Academy of Sciences of the United States of America* 102: 11763–11768.

Taylor, R.E. 2009. Six decades of radiocarbon dating in new world archaeology. *Radiocarbon* 51: 173–212.

USGS. 2015. *The national map viewer*. Topographic map of Mexico. http://viewer.nationalmap.gov/viewer/. Accessed 7 Dec.

Van der Geer, A.L., J. De Vos, and M. Dermitzakis. 2010. The West Indies. In *Evolution of island mammals: Adaptation and extinction of placental mammals on islands*, ed. George Van der Geer, Alexandra Lyras, John De Vos, and Michael Dermitzakis. Oxford: Wiley-Blackwell.

Von den Driesch, A. 1976. *A guide to the measurement of animal bones from archaeological sites*. Harvard: Peabody Museum Bulletin 1.

Ward, W.C., A.E. Weidie, and W. Back. 1985. *Geology and hydrogeology of the Yucatan and Quaternary geology of northeastern Yucatan Peninsula*. New Orleans: Geological Society.

Webb, S.D., and S. Perrigo. 1985. New megalonychid sloths from El Salvador. In *The evolution and ecology of armadillos, sloths, and vermilinguas*, ed. G.G. Montgomery, 113–120. Washington, DC: Smithsonian Institution Press.

Weidie, A.E. 1985. Part I: Geology of Yucatan platform. In *Geology and hydrogeology of the Yucatan and Quaternary geology of northeastern Yucatan Peninsula*, ed. W.C. Ward, A.E. Weidie, and W. Back, 1–19. New Orleans: Geological Society.

White, J.L. 1993. Indicators of locomotor habits in xenarthrans: Evidence for locomotor heterogeneity among sloths. *Journal of Vertebrate Paleontology* 13: 230–242.

White, J.L. 1997. Locomotor adaptations in Miocene xenarthrans. In *Vertebrate paleontology in the neotropics. The Miocene fauna of La Venta*, ed. R.F. Kay, R.H. Madden, R.L. Cifelli, and J.J. Flynn, 246–264. London: Smithsonian Institution Scholarly Press.

White, J.L., and R.D.E. MacPhee. 2001. The sloths of the West Indies: A systematic and phylogenetic review. In *Biogeography of the West Indies: Patterns and perspectives*, 201–235. New York: CRC Press.

Woodburne, M.O. 2010. The Great American Biotic Interchange: Dispersals, tectonics, climate, sea level and holding pens. *Journal of Mammalian Evolution* 17: 245–264.

Taylor & Francis
Taylor & Francis Group

Check for updates

ARTICLE

Life and death of the ground sloth *Xibalbaonyx oviceps* from the Yucatán Peninsula, Mexico

Sarah R. Stinnesbeck[a], Eberhard Frey[a], Jerónimo Avilés Olguín[b], Arturo González González[b], Adriana Velázquez Morlet[c] and Wolfgang Stinnesbeck[d]

[a]Abteilung Geowissenschaften, Staatliches Museum für Naturkunde Karlsruhe, Karlsruhe, Germany; [b]Department of Palaeontology, Museo del Desierto, Saltillo, Mexico; [c]Instituto Nacional de Antropología e Historia, CINAH, Campeche, Mexico; [d]Institut für Geowissenschaften, Ruprecht-Karls-Universität Heidelberg, Heidelberg, Germany

ABSTRACT

Ongoing investigations in submerged cave systems of Quintana Roo in south-eastern Mexico reveal a rich Late Pleistocene megafaunal assemblage, among them the megalonychid ground sloth *Xibalbaonyx oviceps*. The taxon has been described based on a complete skull and mandible from El Zapote cenote west of Puerto Morelos. We here add hitherto unreported postcranial material from El Zapote, attributed to the holotype. This new material allows us to reconstruct unexpected locomotion capabilities for *Xibalbaonyx oviceps* including steep slope and rock climbing. This may have enabled the ground sloth to use the sinkholes and underground caverns as water resource and shelter. The Late Pleistocene age of the fossil allows for a co-existence with early human settlers on the Yucatán Peninsula.

Introduction

The extant two- and three-toed sloth genera *Choloepus* and *Bradypus* inhabit the tropical jungle of Central- and northern South America and are today the only remnants of the formerly diverse Folivora, a group of mammals of South American origin (Adam 1999; Steadman et al. 2005; Presslee et al. 2019), which flourished during the Plio- and Pleistocene. Their hook-like claws enable extant tree sloths for an upside-down suspensory locomotion mode in the jungle canopy (Nyakatura 2010, 2012). In contrast, the fossil relatives of all extant sloths were terrestrial animals, including rare semi-arboreal and even semi-aquatic taxa (Bargo et al. 2000; White and MacPhee 2001; McDonald 2007; Laurin et al. 2014). Their locomotor options ranged from quadrupedalism, facultative bipedalism to even swimming (White 1993; de Muizon and McDonald 1995; Pujos et al. 2007; Amson et al. 2015). This remarkable range of locomotor modes allowed the group to successfully populate a wide range of habitats throughout the Americas (McDonald et al. 2000; White and MacPhee 2001; McDonald 2005; De Iuliis et al. 2009; Pujos et al. 2016; McDonald and Carranza-Castañeda 2017; Stinnesbeck et al. 2018a).

Xibalbaonyx oviceps Stinnesbeck et al. (2017a) inhabited the north-eastern coastal area of the Mexican Yucatán Peninsula (YP). Today, this region is covered by tropical forest but a xeric shrub steppe environment likely prevailed during the Late Pleistocene (González González et al. 2013; Stinnesbeck et al. 2018b). The geology of the area is characterised by horizontally layered thick-bedded limestone of Neogene age. This calcareous basement rock is today affected by intensive karstification (Blanchon and Shaw 1995; Moseley et al. 2015), which developed from Pleistocene conditions of repeatedly oscillating sea levels. Large parts of the extensive cave system and sinkholes (locally called cenotes) were dry and accessible during the Last Glacial Maximum (Late Pleistocene). The cave systems were flooded during the early Holocene sea-level rise due to global warming. The abundant megafaunal remains in the area including remnants of humans remained in place (González González et al. 2013; Stinnesbeck et al. 2017a, 2017b, 2018c; Stinnesbeck et al., 2020).

Xibalbaonyx oviceps Stinnesbeck et al. (2017a) has been described as a new genus and species of megalonychid ground sloth based on an almost complete skull and mandible from the El Zapote cenote, located about 18 km west of Puerto Morelos. Here we present hitherto unreported remains of the postcranial skeleton of the holotype, reconstruct the locomotor options based on anatomical evidence of this endemic ground sloth, and we discuss the interaction with early inhabitants of the YP based on possible cut marks. Missing epiphysis suggests gnawing by carnivores.

Material and methods

Institutional abreviations: CPC – Colección Paleontológica de Coahuila; INAH – Instituto Nacional de Antropología e Historia, Mexico City, Mexico; IPA – Instituto de la Prehistoria de América, Solidaridad, Quintana Roo, Mexico; LEMA – Laboratorio de Espectrometria de masas con Aceleradores UNAM, Mexico City, Mexico; MUDE – Museo del Desierto, Saltillo, Coahuila, Mexico; UNAM – Universidad Nacional Autónoma de México, Mexico City, Mexico.

El Zapote cenote

El Zapote cenote is a water-filled karst sinkhole located 36 km south of Cancun and 90 km north of Tulum in the Mexican state of Quintana Roo, along the east-west directed 'Ruta de los Cenotes' that connects Puerto Morelos with Valladolid (Figure 1). The sinkhole opening is 8.5 to 10 m in diameter with vertical walls forming a 30 m deep chimney. Beyond 30 m water depth, the chimney opens into a wide bottle-shaped chamber 40 m wide and up to 60 m deep (Figure 1). A regularly cone-shaped 29 m high debris mount piles up below the cenote opening.
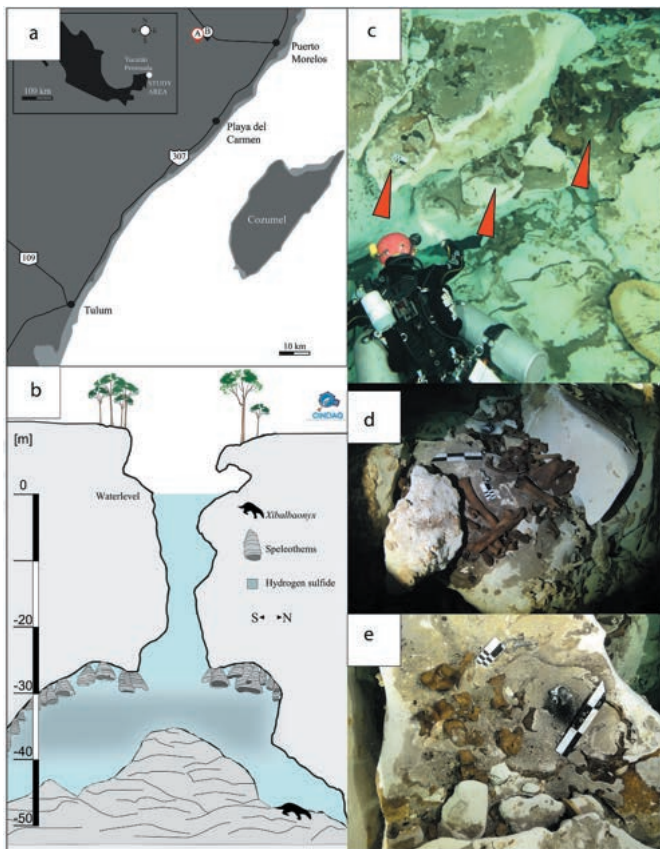
Figure 1. Study area on the Mexican Yucatán Peninsula and finding situation of the postcranial ground sloth material. a) Location of the El Zapote cenote (a) and cenote Tortugas (b) on the Ruta de los Cenotes, close to Puerto Morelos in Quintana Roo. b) Cross-section of the El Zapote cenote and finding situation of *Xibalbaonyx oviceps* (modified after Stinnesbeck et al., 2017a). c, d and e) Distribution of the postcranial material of *Xibalbaonyx oviceps*, over several depth levels on the debris mount in the El Zapote cenote.

The bones described as new genus and species of giant ground sloth, were found in the El Zapote cenote in 2009 by local cave diver Vicente Fito and his team (Stinnesbeck et al., 2017a). They reported the discovery to the INAH Tulum and to the IPA in Playa del Carmen, Quintana Roo.

The skull and postcranial bones documented here were secured in 2014 by both institutions as part of a rescue campaign (Oficio 401. tf(4) | 9.2014/36/0601), resulting in the description of *Xibalbaonyx oviceps* Stinnesbeck et al. (2017a), based on the near-complete skull and mandible only. The collection of further bone material was impossible due to closure of the site by the land-owners, the rejection of further permissions by the local INAH, and financial problems related to the dives of 50 to 60 m depth, which require expensive gas mixtures. We are aware that more postcranial bone material of *Xibalbaonyx oviceps*, as well as other megafaunal remains, still await collection on the spoil heap of the cenote, but for the moment there is no chance for recovery.

All bones collected have been treated with distilled water and polyvinyl acetate at the IPA for several months, because the bone substance is extremely fragile and thus subject to abrasion. Almost all epiphyses of the long bones were disconnected, supporting the assumption of a juvenile individual based on the skull (Stinnesbeck et al. 2017a). Most of the long bones are broken at one end, and the spongiosa is excavated. Except for the fragmented areas, the external face of the bones is well preserved. Approximately 20% of the postcranial skeleton is documented here including atlas, axis, ulnae,

left radius, humeri, femora and tibiae, three ribs, digits, claws, calcanei and astralagi. All elements were found clustered on several levels on the debris mount (Figure 1). The postcranial material, contrary to skull and mandible, was not anatomically articulated, but preservation and colouration of the bones make an identification of the same individual possible. However, several vertebrae, ribs and digits cannot be referred to an exact anatomical position.

The material was photographed with a Panasonic Lumix G9 and a Canon EOS Rebel T4i camera using 10–22 mm zoom lens sets at 22 mm, f 4.5, 1/80 – f 8, 1/20 with tripod. The background of the pictures has been masked manually.

Anatomical terminology is based on phylogenetic characters of both tree and ground sloths. Furthermore, descriptive comparisons with North-Central- and South American Megalonychidae and other families are based on the original descriptions and fossil material of e.g. *Ahytherium aureum* (Cartelle et al. 2008; De Iuliis et al. 2009), *Australonyx aquae* (De Iuliis et al. 2009), *Megalonyx jeffersonii* (Leidy 1855; Hirschfeld and Webb 1968; McDonald 1977), *Pliometanastes* sp. (Hirschfeld and Webb 1968) and *Diabolotherium* sp. (Pujos et al. 2007).

All fossils are housed and available in the INAH facilities of the Museo Maya de Cancún y Zona Arqueológica de San Miguelito in Cancun. Treatment of the fossil bones took place at the IPA in Playa del Carmen, a dependence facility of the MUDE. All fossils are available under the INAH number Za2014-01.

Systematic palaeontology

<div align="center">

XENARTHRA Cope, 1889
PILOSA Flower, 1883
MEGATHERIOIDEA Gray, 1821
MEGALONYCHIDAE Gervais, 1855

Xibalbaonyx Stinnesbeck et al. 2017a
X. oviceps Stinnesbeck et al. 2017a
(Figures 2–4, Table 1)

</div>

Atlas

In cranial view, the atlas (Figure 2(a-e)) is rhombical. The aperture of the vertebral canal is rounded quadrangular in outline. The dorsal arch is one-third thicker than the ventral one. A bulgy protuberance is present on the rostrodorsal surface of the dorsal atlas arch. The articular surfaces for the occipital condyles are concave, twice as high than wide, and of reniform outline. Their dorsal margin is twice as wide as the ventral one. In the dorsal third of the articular surfaces, an oval imprint is pressed into the surface (Figure 2(c)). The surface of the articular facets is pierced by several small foramina of 0.5 mm diameter. In dorsal view, the atlas is trapezoidal in outline, with a 25% shorter cranial border compared to its ventral side. The dorsal protuberance faces cranially and is half the length of the dorsal arch. A 90 mm large, cranioventrally expanded, elliptic intervertebral foramen (=anterior superior orifice of canal, after Owen, 1842) is laterally present. The posterior superior (Figure 2(a)) and inferior (Figure 2(b)) orifice of canal are one-half smaller than the anterior superior orifice of canal (=intervertebral foramen). Nevertheless, the lateral wings are asymmetrical (Figure 2(a)): While the right wing exhibits a straight lateral margin, the left wing is not completely closed at the height of the intervertebral foramen. In ventral view, the ventral arch is narrowest at midline and has the shape of a biconcave rectangle, in which cranial and caudal margins are concave. The caudal articular surfaces are smooth, concave, and their ventral borders merge in the median line.
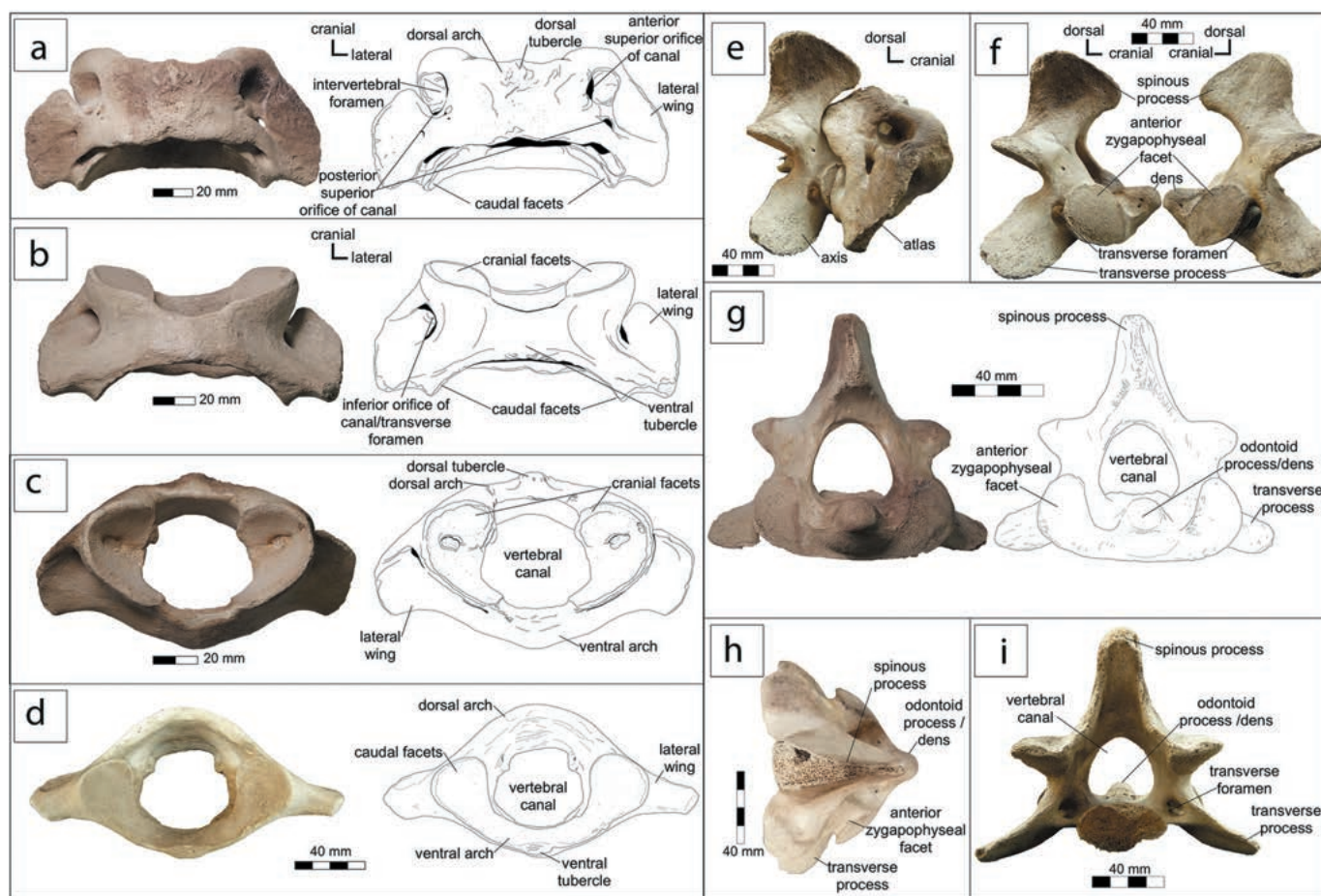
Figure 2. Atlas and axis of *Xibalbaonyx oviceps* from El Zapote cenote. Photograph and interpretative line drawing of the atlas a) in dorsal, b) ventral, c) cranial and d) caudal view. e) Photograph of articulated atlas and axis in right lateral view. Photograph of the axis in f) right and left lateral views, g) cranial view including interpretative line drawing, h) axis in dorsal and i) caudal view.

Table 1. *Xibalbaonyx oviceps* postcranial measurements in millimetres (mm).

Description	mm
Humerus	
Length of the left humerus as preserved	328
Maximum proximal diaphysal width as preserved	87
Mediolateral width of the diaphysal shaft	49
Maximum distal width, measured at the epicondyles	102
Ulna	
Total length of the left ulna as preserved	324
Anteroposterior width measured at the coronoid process	93
Radial notch width	39
Maximum height of the radial notch	70
Anteroposterior width measured at the ulnar tuberosity	46
Radius	
Total radius length as preserved	333
Mediolateral width of radial head	52
Mediolateral width of distal end as preserved	63
Femur	
Right femur length as preserved including femoral head	323
Anteroposterior diameter of the femoral head	72
Mediolateral width of the femoral head	81
Maximum proximal width of the right femur, measured at the femoral head	155
Smallest mediolateral width of the diaphysis	75
Maximum width of the distal diaphysis as preserved	133
Tibia	
Maximum length as preserved	165
Maximum proximal width	106
Smallest width of the diaphysis	62
Maximum width of the distal end	94

Axis

In cranial view, the axis is of triangular outline (Figure 2(f-i)), with a thick and wide centrum, which reaches one-fourth of the complete height and three-fourths of the width of the bone. The vertebral canal has the shape of a rounded isosceles triangle in cranial view.

The articular facets for the atlas are flattened, only slightly convex and dorsally rounded to oval shaped. They merge ventral to the odontoid process (=dens). The process is a short craniodorsally oriented nodular bulge. A short but deep suture is visible on the anterior articular dens of the axis (Figure 2(h)). The transverse processes are roughly horizontal in cranial view and twice as long than wide.

In lateral view, the spinous process is fan-shaped (Figure 2(f)). The process is cranioventrally oriented and its dorsal margin is 25° anteriorly inclined, so that the caudal half is twice as high as the cranial one. Its dorsocaudal margin is convex. The cranial and caudal margins of the spinal process converge ventrally becoming half as wide at its ventral base dorsal to the aperture of the vertebral canal.

The transverse foramina are only visible in lateral and caudal views (Figure 2(f)). They are craniodorsally oriented and completely covered by the anterior zygapophyseal.

Cervical vertebrae

Two fragmentary cervical vertebra have been collected (Figure 3 (a)). We hypothesise that these may correspond to C5 (Figure 3
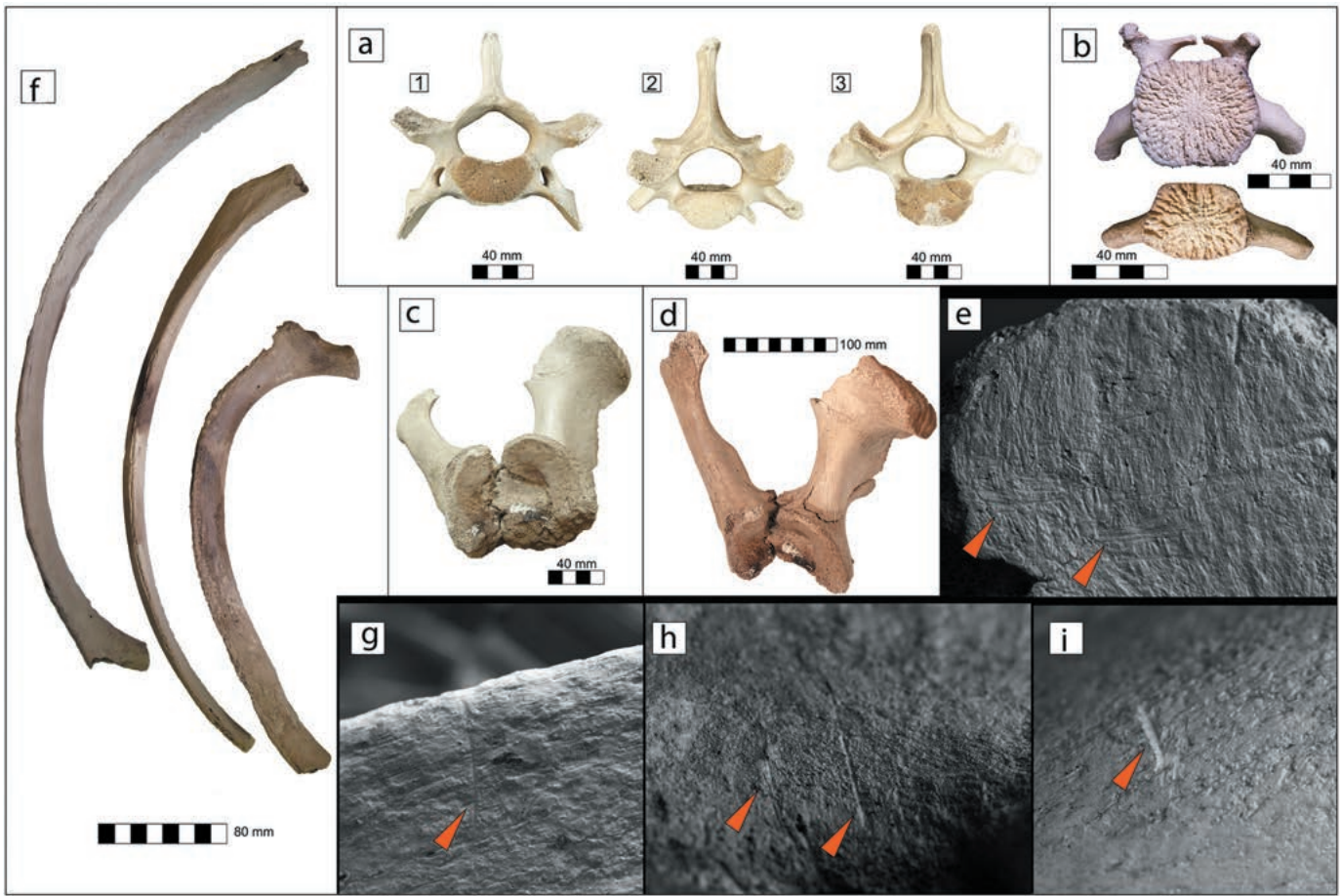
Figure 3. Photographs of vertebrae, ribs and fragmented pelvis, including acetabulum of *Xibalbaonyx oviceps* from El Zapote cenote. Cervical (a1-2), thoracic (a3) and caudal vertebrae (b) in cranial view. Photographs of the acetabulum (c), pelvis (d) and scratch marks on the pelvis fragment (e). Photograph of the collected ribs (f) and close-ups of the potential cut marks (g, h, i).

(a-1)) and to C6 (Figure 3(a-2)). This interpretation is based on the long and narrow spinous process in both, reaching half of the dorsoventral height of the entire bone.

C5 (Figure 3(a-1)): The lateral faces of this process run parallel to each other. The cranial margin of the neural spine forms a sharp vertical running crest. The latter bifurcates at its base to form the contralateral cranial margins of the neural arch that merge with the anterior margins of the transverse processes. Immediately adjacent to the bifurcation point, there is a triangular shelf forming the central fourth of the roof of the anterior aperture of the neural canal. The centre of this shelf is marked by a semicircular, cranially pointing protuberance. In C5 the articular facets of the prezygapophyses are rough, concave, of elliptical shape, mediolaterally twice as wide as high and inclined in a 95° angle against the long axis of the bone, showing cranioventrally. Their cranial margins are sharp and projecting. In caudal view, the facets of the postzygapohyses are convex. Their lateral margins are triangular and point dorsolaterally. Their caudal margins are sharp merging dorsally with the base of the spinous process. The posterior face of the spinous process is marked by a median sulcus.

The transverse processes are of uniform width; however, their ends are not preserved. The transverse foramen is elliptical in cross-section, twice as high than wide (Figure 3(a-1)). The centrum of the vertebra is semi-circular in dorsal direction, in cranial and trapezoidal in caudal view. The vertebral foramen has the shape of a rounded rhomboid (Figure 3(a-1)).

C6 (Figure 3(a-2)): In cranial view, the vertebra has the shape of an inverted kite with concave margins. The spinal process reaches almost the height of the rest of the bone. The cranial margin of the spinous process forms a sharp crest running along the midline of the long axis (Figure 3(a-2)). Also, the caudal side forms a deep sulcus. Its lateral faces run parallel to each other diverging in the ventral half of the process and merge with the bases of the pre- and postzygapophyses. The latter are of semi-circular shape ventrally oriented. In cranial view, the craniodorsal articular surface of the prezygapophysis is rough and concave, with ventrolaterally semi-circular, thickening margins. The postzygapophysis has a rough and almost flat articular surface, and is only visible in caudal view. The transverse processes are almost horizontal. However, in caudal view, a small asymmetry is visible with respect to their orientation (Figure 3(a-2)). The right process rotates cranially so that the lateral margin runs obliquely to the longitudinal axis, while the left process is ventrolaterally directed without any twist. The ventral fourth of the vertebra is not preserved. It can therefore not be decided whether an oval transverse foramen is present. The centrum of the bone is almost rectangular, with rounded borders.

Thoracic vertebra

One thoracic vertebra has been collected (Figure 3(a-3)). However, the bone could also represent C7, as in some *Choloepus* individuals

the cervical vertebrae C6 and C7 present shapes similar to the thoracic ones (Buchholtz and Stepien 2009).

The vertebra exhibits a rhomboidal shape in cranial view (Figure 3(a-3)), of which the spinous process reaches the dorsal half of the height of the entire vertebra. The lateral faces of the spinous process run parallel to each other. The prezygapophyses are concave. Their lateral borders are bulge-like, becoming laterally twice as thick as the median side and of semi-circular shape facing cranioventrally. Their articular surface is rough when compared to the surface of the peduncle, which is smooth. The transverse processes are almost horizontal. Their dorsal and ventral margins diverge laterally, becoming one-third thicker than at their base. They are ventro-caudally inclined, reaching approximately a 95° angle against the horizontal plane of the bone. The articular facets of the postzyga-pophysis are flat and elliptical. Their caudal borders connect dor-sally to the lateral faces of the spine. In caudal view, the vertebral foramen is rounded. The centrum of the vertebrae is rectangular with rounded borders, twice as wide as high.

Caudal vertebrae

Two fragmented caudal vertebrae were collected (Figure 3(b)). In cranial view the upper caudal vertebra in Figure 3(b) is trapezoidal in outline. Due to its fragmentation in the dorsal portion of the bone a precise assignation of its anatomical position cannot be given. The neural arch is medially thin and splits laterally into the prezygapo-physal processes. In dorsal view, the margins of each process run parallel to each other facing cranially, ending as a knob. The vertebral canal is semi-circular and has one-third the height of the centrum.

The caudolaterally facing transverse processes are dorsoventrally flat and strongly fragmented. They are medially connected to the slightly rounded isosceles trapezoidal centrum in cross-section.

The second preserved caudal vertebra (Figure 3(b), lower row) consists of a centrum and transverse processes which are caudo-ventrally oriented by about 25° against the long axis of the bone. The transverse processes are one-third shorter than the centrum is long. The centrum is of isosceles trapezoidal outline in cranial view and oval in caudal view, twice as wide as it is high.

Ribs

Three ribs were recovered (Figure 3(f)). The smallest pictured is probably the 5th or 6th left rib. Only one rib preserves the articulation facet to the sternum. The articular areas of the other two ribs are fragmented. The angle of the complete rib is strongly curved to 95°.

The curvature of the larger ribs is less pronounced, reaching 120°. Both are one-eighth longer than the short and most complete one. All are of uniform width.

Scapula

Both scapulae were collected, but the right one is severely damaged and thus will not be described here (Figure 4). In lateral view, the left scapula is almost circular in outline as preserved (Figure 4(a,b)). The lateral fourth of the acromion process that curves towards the coracoid is not preserved. In ventral view, the glenoid cavity is oval in outline and twice as wide as long (Figure 4(c)). The area anterior to the glenoid fossa (Figure 4(d)) suggests that the coracoid process was unfused. This area has been described as 'procoracoid' (Rose and
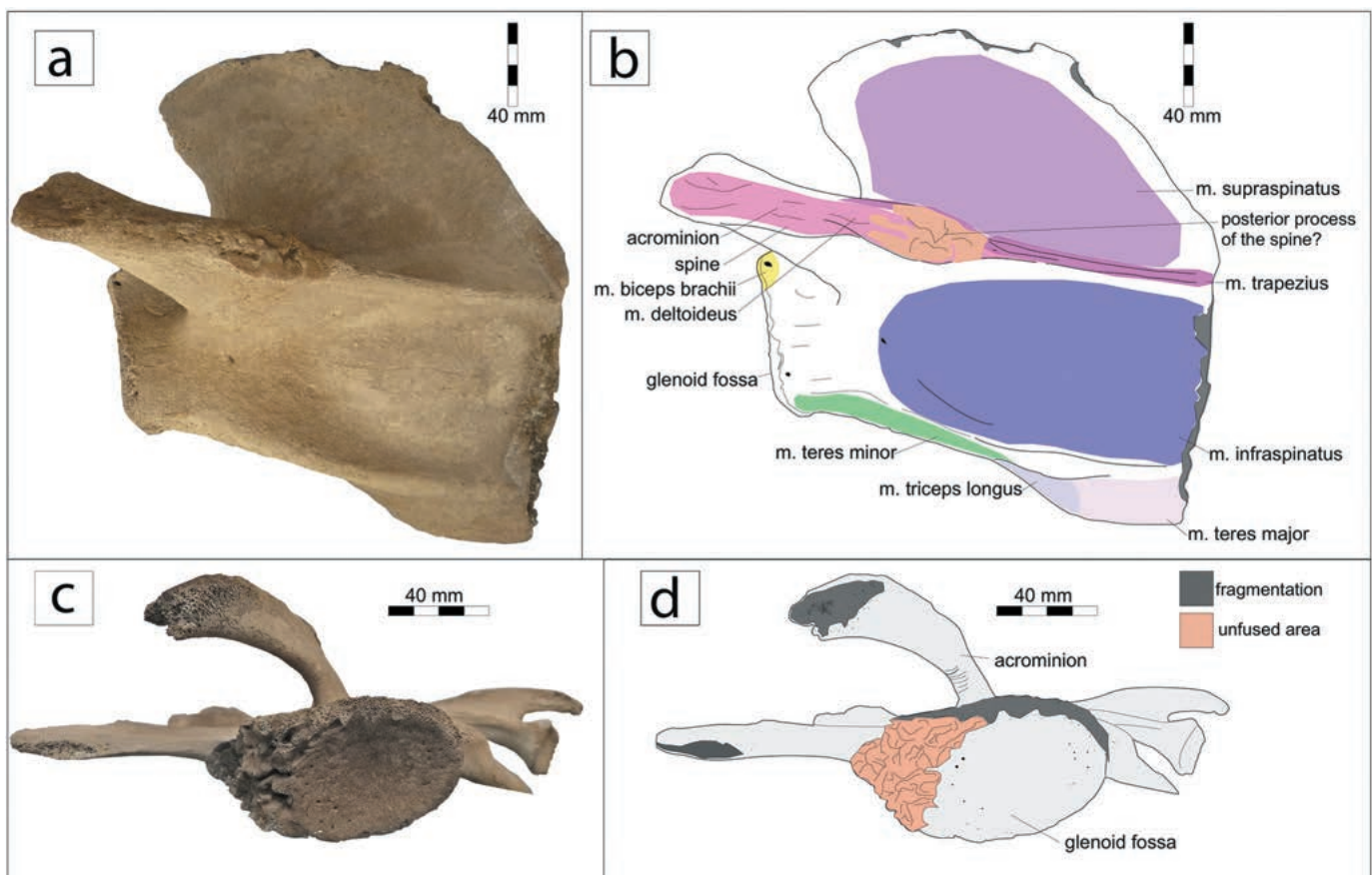
Figure 4. Photographs and interpretative line drawings of the left scapula of *Xibalbaonyx oviceps* from El Zapote cenote in lateral (a, b) and ventral view (c, d).

Emry 1993; Hildebrand 1985), which forms part of the coracoacromial arch originating anterior of the glenoid fossa. The anterior border and coracoacromial arch broke off. However, the coracoscapular foramen is semi-circular in outline, suggesting a rounded shape. The foramen reaches about 20% of the overall height of the scapula as preserved. It is located dorsal to the anterior and posterior borders of the glenoid fossa, level with the mid-length of the scapular spine. In lateral view, the primary spine arises ventrally from the acrominion process. The dorsal and ventral margins of the spine run parallel to each other until mid-length. At mid-length, the dorsal and ventral margins of the spine converge, fading to a low but pronounced crest extending along the entire dorsal half of the bone length. An unossified bony structure at mid-length of the spine suggests the presence of another process, probably the posterior process of the spine (Figure 4(b)).

The primary spine separates the scapula into two areas, the supraspinous and infraspinous fossae. Both fossae have smooth surfaces and are flat. The supraspinous fossa is about 5% larger than the infraspinous fossa (Figure 4(b)).

Posterior to the infraspinous fossa, a secondary scapular spine arises from the posterodorsal margin of the glenoid fossa and runs along the posterior border of the scapula. The secondary spine is of uniform width and beaded-shaped. Its anterior and posterior margins merge at the dorsal-most fourth of the bone. Along the posterodorsal margin of the scapula the postscapular fossa diverges dorsally, reaching twice the size of its ventral half and almost 10% of the anteroposterior extension of the bone, as preserved.

Humerus

Both humeri (Figure 5) are preserved but incomplete, with the proximal and distal epiphyses missing in both bones, as well as the proximal and distal diaphyseal margins. The description is based on the left humerus, which is the more complete (Figure 5).

The diaphysis reaches two-thirds of the bone length as preserved (Figure 5(e)). In anterior view, the median and lateral borders of the diaphysis converge distally reaching the length of the entire bone as preserved. They diverge at the metaphysis by one-third of the maximum width of the diaphysis. The proximal three-fourths of the deltopectoral plate are flat and reach almost the width of the diaphysis, converging distally at its last fourth along the metaphysis. The deltoid and pectoral tuberosities proceed distally and merge to a deltopectoral tuberosity at the long axis of the humerus along the proximal half of the metaphysis. The surface of the diaphysis is laterally smooth, while deltoid and pectoral areas are strongly rugose, as is the medial side of the diaphysis. These rugose areas of the humerus are marked by numerous vertically running scars, which are indicative for the attachment of massive muscles. The pectoral tuberosity parallels the medial margin of the diaphysis and reaches from the distal two-thirds of the diaphysis to the proximal half of the metaphysis. The deltoid ridge marks the lateral border of the diaphysis and is most prominent at about middle of the preserved bone. The metaphysis is distally one-third wider than the proximal end of the diaphysis and longitudinally flattened in its distal third. The entepicondylar foramen is mediodistally oriented. Its entepicondylar bridge is flat and covers the opening in anterior view. A small and rounded foramen is located 5 mm proximal to the entepicondylar foramen.

Although the distal epiphysis is preserved, the attachment areas on both capitulum and trochlea are highly damaged (Figure 5(d)). Consequently, a secure assignation to either the left or right humerus is not possible. Capitulum and trochlea (Figure 5(f)) are of the same size as the metaphysis, thus suggesting that the distal meta- and epiphysis were approximately 15% to 20% wider than the maximum width of the shaft.

Ulna

Both ulnae were collected (Figure 6(a,b)), but both are highly fragmented and appear to have been damaged on purpose. Here we will only describe the left ulna, which is the more complete (Figure 6(b)-f)), although the epiphyses are missing. The bone is four times longer than wide (Figure 6(b)). The shaft decreases gradually in diameter distally by about 20% until the distal third of the bone. From there, the lateral and medial faces of the ulna are straight and parallel each other. This leads to a transversally expanded diaphysis. The latter configuration is also supported by a pronounced supinator crest running diagonally from the proximoposterior side of the trochlear and radial notches. The supinator crest merges with the interosseous crest at the anterodistal border of the bone. The bone is slightly curved, and the anterior face markedly concave.

The proximal half of the olecranon process is strongly damaged. In posterior view (Figure 6(f)), the olecranon process, as preserved, is twice as wide as the ulnar shaft. The fossa for the m. anconeus is particularly deep resulting in a notable expansion of the lateral proximal third of the bone as preserved (Figure 6(b)). In posterior view, the ulnar shaft is of uniform width with a convex lateral face and a concave medial one.

The medial surface of the bone is smooth. A deep fossa for the flexor digitorum profundus muscle extends from the medial extension of the olecranon, distal to the trochlear notch, to about half the length of the preserved bone.

The trochlear notch is well visible in proximal and lateral view (Figure 6(b,d)). In lateral view, the trochlear notch is anteroproximally oriented and wide, opening to a 120° angle between the anconeal and coronoid processes (Figure 6(b)). In lateral view, the trochlear notch is twice as high as wide. Its surface is concave and smooth. The coronoid process is twice as pronounced than the anconeal one, which is barely visible as a small crest, almost merging with the olecranon. The coronoid process contacts the head of the radial notch distally. This area is slightly fragmented and, in consequence, delimitations of the bone remain unclear.

The radial notch is located at midline of the long axis of the ulna (Figure 6(b)). It is rounded and its articular facet is laterally oriented. In proximal and posterior views, the radial notch is anteroproximally oriented. Its posterior and distal borders form a small but marked crest, while merging with the supinator crest. The surface of the radial notch is highly rugose.

Between coronoid process and radial notch, a small ulnar tuberosity is identified for the insertion of the brachialis muscle.

Radius

Only the left radius is present (7A-E) with its distal eight missing. The distal epiphysis may have been removed on purpose and the shaft was damaged. The diaphysis was hollowed as seen in all other long bones of the individual. The radius is six times longer than wide. Its neck is cylindrical, as is the proximal fourth of the diaphysis. The radial tuberosity is rugose and slightly convex. The distal three-fourths of the shaft curve posteriorly, and the shaft diverges distally by about 30%. In anterior view, the shaft is laterally flexed (Figure 7(b)). The rugose part of the interosseous ligament area reaches half the length of the shaft. The diaphysis is mediolaterally one-fourth as narrow as anterioposteriorly broad. The proximal articular face is circular and concave. The head is anteriorly inclined and its anterior face has twice the width of the posterior one (Figure 7(d)).

Ungual phalanges and manus

A total of 10 ungual phalanges were collected (Figure 7(f,g)). Seven of the ungual phalanges appear to be contralateral pairs but cannot
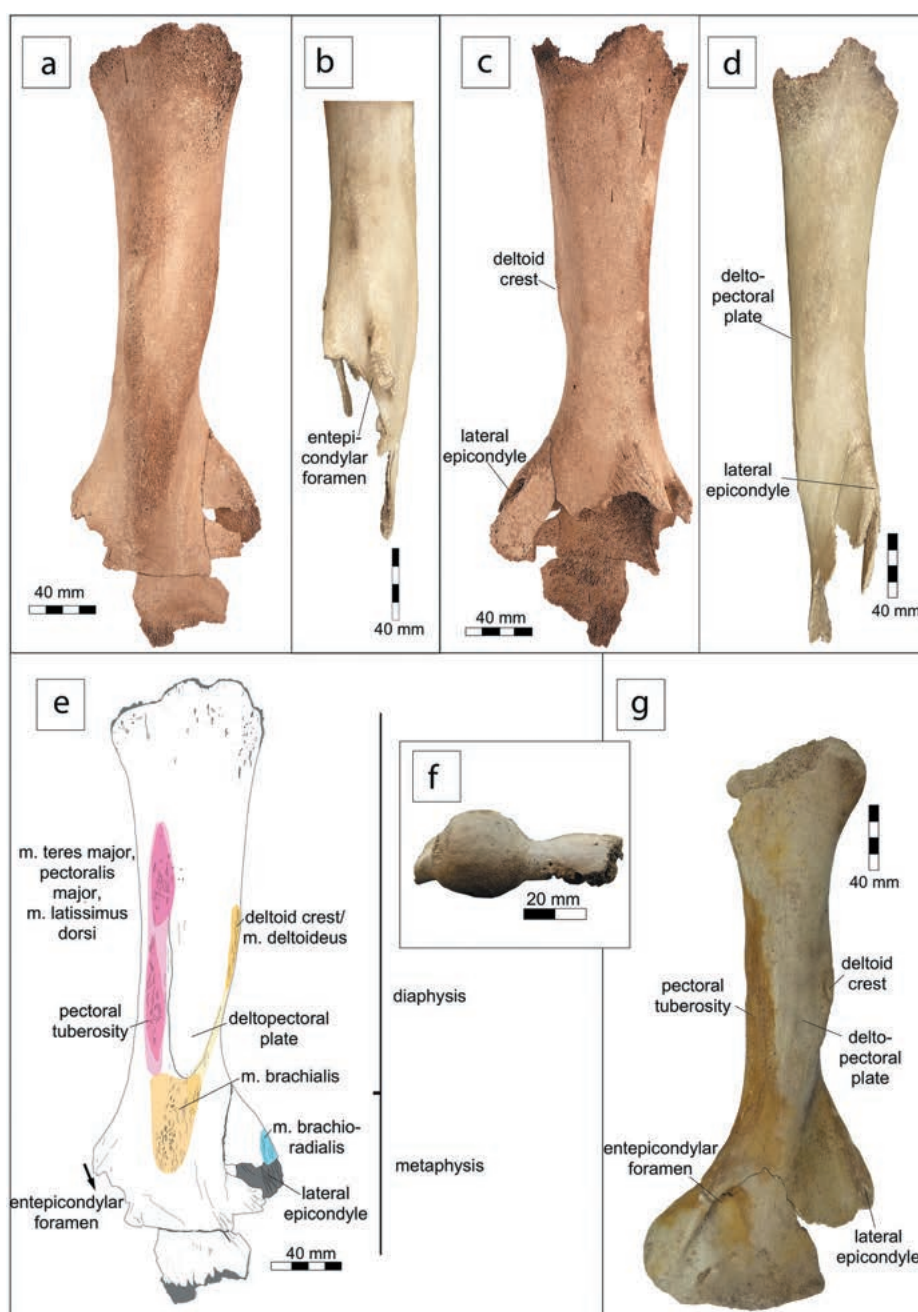
Figure 5. Photographs of the left humerus of *Xibalabonyx oviceps* from El Zapote cenote in anterior (a), medial (b), posterior (c) and lateral view (d). Interpretative line drawing of the left humerus in anterior view (e) and photograph of the fragmented distal epicondyle of the humerus (f). A left humerus from cenote Tortugas referred to *X. exinferis* (g) for direct comparison.

be assigned to the respective digits. All ungual phalanges are nearly bilaterally symmetrical. Only the largest ungual digits are slightly concave along their medial curvature, indicating that they correspond to the right/left manus. All exhibit a similar morphology, three times longer than high, with the shape of a scalene triangle in cross-section. The tips never pass the ventral base of the claw.

Two ungual phalanges were collected still articulated with their corresponding phalanges. Only one of them exhibits a three phalanx combination including the metacarpal, suggesting that this combination represents the third digit, because the ungual phalanx is one of the largest of the present ones and almost bilateral symmetrical along its base. In cross-section, the claw has the shape of an irregular acute-angled triangle. The claw is three-fourths longer than high. The largest claws reach approximately 115 mm in length,

the smallest ones are 40% shorter. Phalanx 2 is only two-thirds longer than high. The metacarpal is twice as long than high.

The remaining ungual phalanges were found scattered and the pes/manus assignation; therefore, remains unclear.

Femur

Both femora were collected. Here we describe the right femur (Figure 8(a-f)), which only lacks its distal epiphysis. The head of the femur and greater trochanter are unfused, suggesting a juvenile to subadult age. The diaphysis is twice as long than wide. The diaphysis is elliptic in cross-section and twice as broad, as also anterioposteriorly flattened. Across the femoral head and towards the greater trochanter the femur has its maximum width. From there the bone tapers 51% distally, reaching the narrowest area at
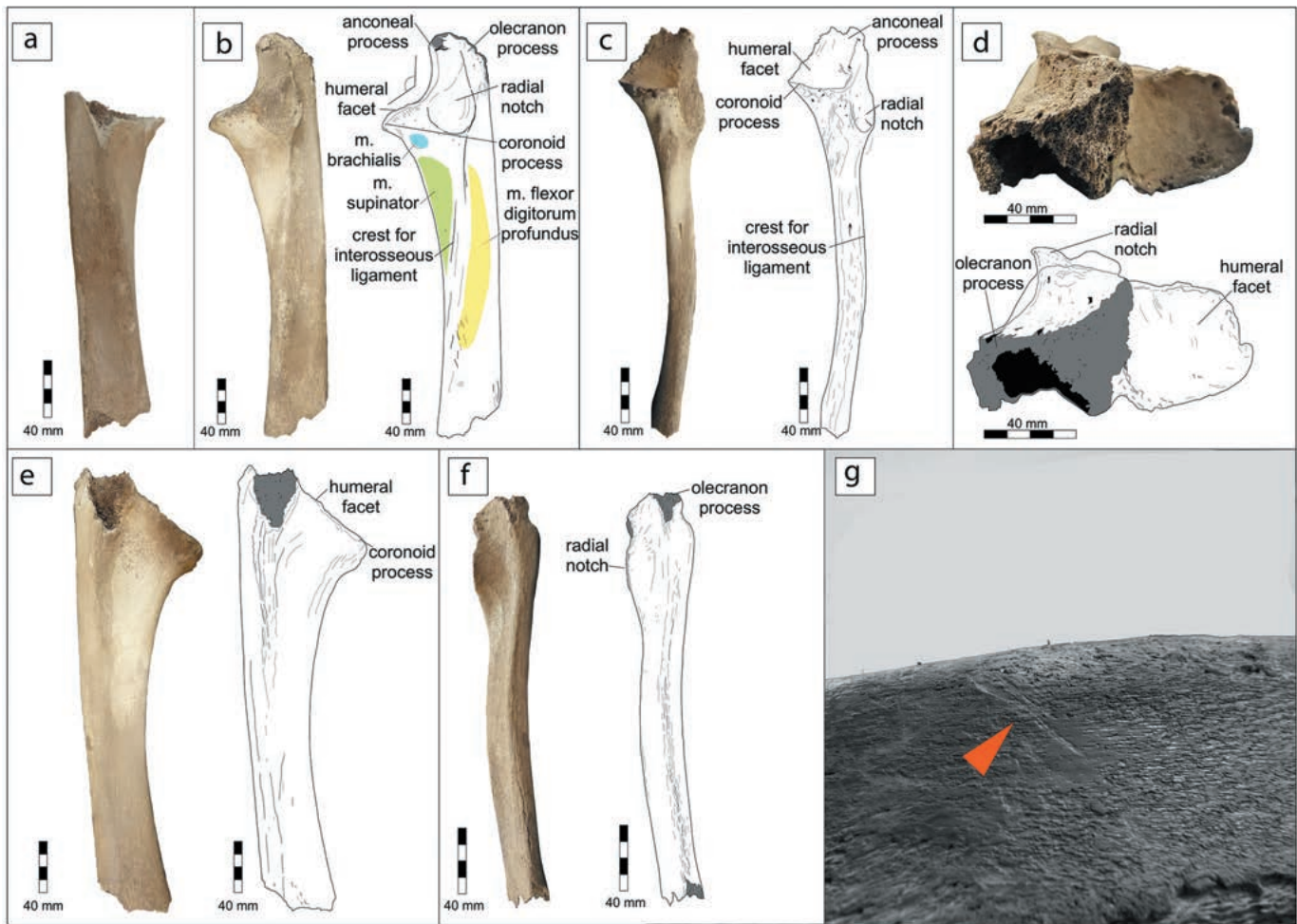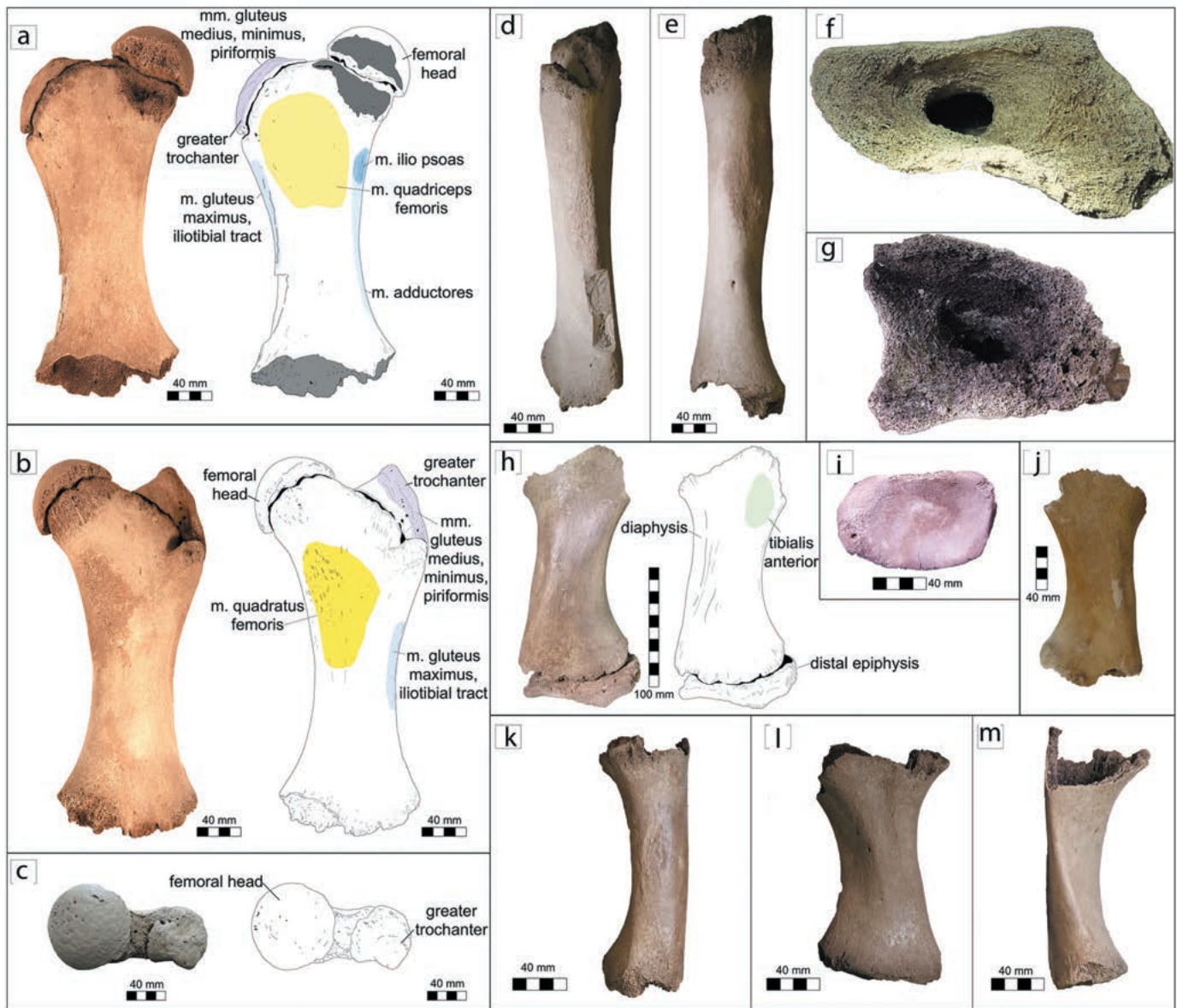
Figure 6. Photograph and interpretative line drawings of the ulnae of *Xibalbaonyx oviceps* from the El Zapote cenote. Photograph of the fragmented right ulna in lateral view (a). Photographs of the left ulna and interpretative line drawing in lateral (b), anterior (c), proximal (d), posterior (e) and posterior view (f). Close-up of the possible cut marks on the left ulna (g).

mid-shaft. Towards the distal end of the diaphysis the diameter increases by about 15%. Thus, the femur is elongate hourglass-shaped. The diaphysis is only slightly curved, concave anterior and convex posterior. In dorsal and medial views (Figure 8(c,d)) the femoral head is inclined anteriorly at an angle of 25° against the long axis of the bone and located anterior to the greater trochanter and femoral shaft. This orientation results in a short neck in posterior view reaching to a maximum length of about 15% of the femur, as preserved. In anterior view, the neck is barely visible and the head is the proximal-most extension of the femur. In posterior view, head and greater trochanter reach almost the same height, due to the anterior inclination of the femoral head. The femoral head is rounded and anteroposteriorly only 10% narrower than mediolaterally broad. The anterior face of the greater trochanter is flat. In dorsal view the greater trochanter reaches almost the same longitudinal diameter as the diaphysis. In dorsal and posterior view, the greater trochanter has the shape of a posteriorly pointing triangular cusp. In posterior view, the greater trochanter is triangular-shaped and laterally strongly convex. This convexity expands proximally to the tip and merges with the trochanteric fossa, which is laterally deep, gradually becoming shallower medially.

The lesser trochanter is only represented as a rugose area along the medioposterior surface of the diaphysis. The third trochanter is a rugose area on the lateral face of the femur. The compacta of the anterior and posterior surface as well as that of the remaining areas

are smooth, while the femoral head and the diaphysis are pierced by large foramina of about 1 mm diameter.

Tibia

The diaphyses of both tibiae (Figure 8(g-m)) are preserved. The distal epiphyses are disconnected in both tibiae (Figure 8(h)), but were found in the cenote at close distance to the tibial diaphyses. The articular facets for the astralagi are slightly visible; nevertheless, the distal surfaces of both tibae are strongly concave (Figure 8(i)). As observed for other long bones, both tibiae were hollowed (Figure 8(g)) and their proximal epiphyses are missing. Both are 165 mm long. The bone is hourglass shaped, with a proximal diameter of 106 mm and a distal one of 94 mm, while the minimum diameter in the middle of the bone measures 62 mm. The shaft is curved along its long axis, with the anteriomedial face being convex and the posteriolateral one concave. The surface of the diaphysis is smooth.

Pes

Both astragali (Figure 9(a-f)) and calcanei (Figure 9(g-j)) were recovered. All other bones of the pes are still in the sinkhole.

The astragalus is oval in dorsal view. The medial and lateral trochlea are convex and reniform. In distal view, the lateral trochlea forms a 160° angle against the medial trochlea (Figure 9(d)). Both are therefore almost at the same height and exhibit a faintly convex and smooth surface. This area is divided by a deep concave furrow
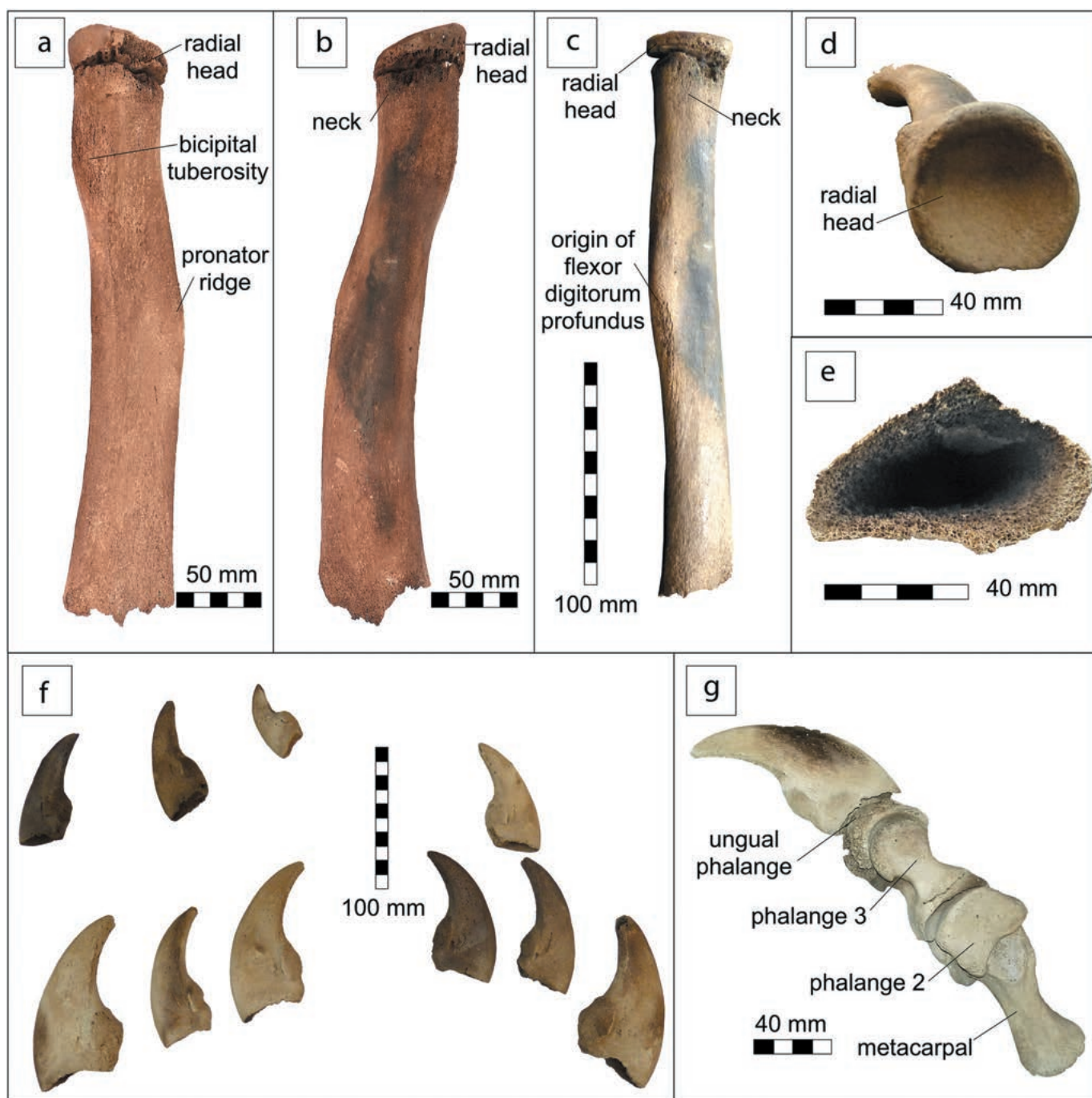
Figure 7. Photographs of radius and ungual phalanges of *Xibalbaonyx oviceps* from El Zapote cenote. Radius in medial (a), lateral (b), posterior (c) and dorsal view (d). Ventral view of the radius; note the removal of the bone marrow (e). Photographs of the ungual phalanges (f), and a single digit of the manus (g).

with the shape of an inverted isosceles triangle. The navicular process is rounded with a bulge-shaped, convex border. In anterior view, the navicular facet is oval in outline. In plantar view, the two convex articular faces with the calcaneus are visible. They are separated from each other by a mediolaterally running, concave interosseal sulcus.

The calcaneus is one half longer than wide as preserved. The attachment area to the astragalus exhibits a convex canal, the sinus tarsi. The proximal margins of both calcanei are broken, their proximodistal hour-glass-shape suggests the presence of posterior 'wing-like' expansions of the tuber calcis, as typically known in Megalonychidae.

Discussion

The original description of *Xibalbaonyx oviceps* was based on a skull and mandible (Stinnesbeck et al. 2017a) that were discovered in the El Zapote cenote, anatomically articulated between two limestone boulders (Figure 1). The postcranial skeletal elements here referred to the holotype were collected as scattered elements downslope the debris mount in a 2 m range from the skull, between 47 and 56 m water depth (Figure 1). Several postcranial remains, such as some vertebrae and ribs, are still in the cenote and not available to us. A complete description of the postcranial skeleton is therefore impossible, until the material is completely secured. For instance,

Figure 8. Photographs and interpretative line drawings of femur and tibia of *Xibalbaonyx oviceps* from El Zapote cenote. Photographs and interpretative line drawings of the right femur in anterior (a), posterior (b), proximal (c), lateral (d) and medial view (e). Distal view of the femur (f) and proximal view of the tibia (g); note the removal of the bone marrow. Photographs of the right tibia in anterior (h) and distal view (i). Photograph of the left tibia (j). Right tibia in lateral (k), posterior (l) and medial view (m).

vertebrae, manual and pedal elements can here only be reported without an unequivocal anatomical assignation.

Ontogenetic stage and comparative osteology

Based on the open cranial sutures *Xibalbaonyx oviceps* was a juvenile to subadult individual (Stinnesbeck et al. 2017a). The new postcranial material confirms this interpretation, because the epiphyseal sutures of all long bones are open and the coracoid was not yet fused to the scapula. Ontogenetic stages have been documented for other ground sloths, such as *Eremotherium* (Cartelle and De Iuliis 2006), *Paramylodon* (Grass 2014; Long et al. 2018) and *Megalonyx* (McDonald 1977; Holte 2012; Grass 2019). The authors reported on allometric growth of bones and, in some cases, even significant osteological changes during lifetime (Holte 2012; Grass 2019). This strongly suggests changes in the life style of ground sloths during the ontogeny of these animals (Grass 2019).

In *Xibalbaonyx oviceps* the scapula is only about 10% higher than long, giving the bone an almost circular outline (Figure 4). The scapula in adult *Paramylodon, Nothrotheriops, Thalassocnus* and *Choloepus* is rounded triangular in outline. Rounded scapulae are characteristic for juvenile sloths (Grass 2014, 2019), which is also evident in juvenile to subadult *Megalonyx jeffersonii* RMM-6353. In *Megalonyx*, the scapula increases in size by about 60% from juvenile to adult specimens (Holte 2012; Grass 2019), while the morphology of the bone remains similar. However, the scapula is approximately 5% higher than long in subadult *Megalonyx* (RMM-6353), which means that it is more rounded than in *Xibalbaonyx*. In *Xibalbaonyx* the coracoidal process was unfused as was a tubercle or posterior process on the spine, as seen in other subadult or juvenile ground sloth individuals (Grass 2019). In juvenile *Megalonyx*, both the glenoid fossa and the coracoacromial arch are unfused and missing in the Alabama individual RMM-6353 (Holte 2012). In the *Xibalbaonyx* material described here the coracoacromial arch was

Figure 9. Photographs of calcanae and astragali of *Xibalbaonyx oviceps* from El Zapote cenote. Both astragali in proximal (a) and distal view (b). Proximal (c), distal (d), medial (e) and lateral (f) view of the astragalus. Distal view of the calcaneum (g). Photographs of both calcanae in dorsal view (h). Calcaneum in medial (i) and lateral view (j).

already present, but broken off, while the coracoid process was unfused; it is missing in the material documented here. This suggests that the scapula comes from a subadult rather than a juvenile individual. This anatomical feature coincides with the same structure in the ontogenetic stages of *Megalonyx* (Holte 2012; Grass 2019).

Most of the long bones presented here are only preserved by their diaphyses. Apparently the symphyseal gap was still open and allowed the epiphyses to fall off. However, the humeral diaphysis is approximately 15% longer in *X. oviceps* than in the juvenile or subadult *X. exinferis* (Stinnesbeck et al., 2020), or subadult *Megalonyx* (Holte 2012). Similar length differences are visible in the hind limbs, in which the femoral diaphysis is about 15 to 18% longer in *X. oviceps* than in subadult *Megalonyx* (RMM-6389), also suggesting that the extremities of juvenile to subadult *X. oviceps* were longer than in *Megalonyx*. In *Megalonyx*, the humerus and femur increase by about 45% from subadult to adult size, whereas growth increase of the radius and ulna is only about 12%. These latter bones thus have about the same length in adult and immature stages (Holte 2012). This decoupled allometry is interesting, because both radius and ulna are about 20% shorter in *Xibalbaonyx oviceps* than in *Megalonyx* (RMM-6389).

Pathological indications

Rugosities and grooves were not identified in the gracile skull and mandible of *Xibalbaonyx oviceps* (Stinnesbeck et al. 2017a) and are absent in the atlas and axis. Rugosities and grooves on the surface of bones reflect muscle or ligament attachments. In *X. oviceps* these attachment areas show a pronounced relief, but not as pronounced as in other ground sloths. This could either be related to the subadult stage of the individual, or a little developed or even degenerated musculature. The atlas of *X. oviceps* is twice the size of that in *Megalonyx jeffersonii* with respect to the body size. It thus offered abundant space for a strong basicranial musculature, especially for the m. rectus capitis group. Therefore, it must have been well suited to support and operate the large skull and massive mandible. In direct comparison to the atlas of a specimen from cenote Tortugas, tentatively assigned to the recently established taxon *Xibalbaonyx exinferis* (Stinnesbeck et al. 2020a), the postcranial skeleton of *X. oviceps* was notably more gracile, even though the Tortugas individual was also a juvenile or subadult. The atlas of *X. exinferis*, however, exhibits prominent reliefs for muscle attachment, which are absent in *X. oviceps*.

Besides the absence of rugosities, the atlas of *Xibalbaonyx oviceps* from El Zapote cenote is also asymmetrical, with its left wing differing markedly from the right one. In caudal view, the different inclination of the wings is evident, as also the uneven vertebral canal. This asymmetry might have provoked irritation of transverse nerves and the vertical cord. Other vertebrae may also have been affected by this asymmetry, but this cannot be unequivocally decided due to their fragmentation.

Joint diseases, especially bone erosion, e.g. arthrosis and arthritis, have been reported for ground sloths (de Souza Barbosa et al.

2014; de Souza Barbosa et al. 2016; Tambusso et al. 2018; Andrade et al. 2019). However, left or right asymmetries are often documented as a case of degenerative enlargement or bone spur, e.g. osteophytes, but the pathology is also known as a born defect. In the El Zapote sloth, an erosive disease as part of an ageing process can be excluded, due to the subadult nature of the animal. In addition, the preservation of the vertebrae is excellent, which is not the case in bone diseases coupled with ageing, trauma, or other degenerative aspects. *Xibalbaonyx oviceps* rather seems to present a congenital anomaly of the cervical vertebrae. These anomalies are frequently caused either by genetics or environmental factors, such as stress, malnutrition, inbreeding, etc. In addition to the holotype of *X oviceps*, a left/right asymmetry of the atlas has also been documented in *X. exinferis* from cenote Tortugas (Stinnesbeck et al. 2020a). Slight asymmetric deviations of the atlas and other vertebrae are also documented in extant tree sloths (Buchholtz and Stepien 2009; Böhmer et al. 2018) and have been interpreted to result from a common mutation (hox gene) within sloths and other xenarthra, as well as other animals with a reduced number of vertebrae, such as manatees and dugongs (Varela-Lasheras et al. 2011; Böhmer et al. 2018). Whatever the cause for the pathology was, the cerebrospinal fluid probably impeded that *X. oviceps* suffered from strong neurological disorders. However, it is striking that this is already the second ground sloth discovered by us in the area in which pathological indications are visible.

Functional morphology and the locomotion of X. oviceps

The postcranial material documented here exhibits morphological and morphometric features that provide a surprising ecological distinction of *Xibalbaonyx oviceps* from all other ground sloths known to date.

Xibalbaonyx oviceps is based on a subadult individual, as already suggested by Stinnesbeck et al. (2017a) based on the skull. The scapula is rounded (Figure 4). Supraspinatus and infraspinatus fossae are of similar size in *Xibalbaonyx oviceps*, while the latter fossa is often smaller in large terrestrial ground sloths, such as in megatheria. The supraspinatus muscle performs the abduction of the arm and pulls the head of the humerus towards the glenoid cavity. In *X. oviceps*, the infraspinatus fossa reaches two-thirds of the height of the scapula. This muscle, in combination with the teres minor muscle, supports the lateral rotation of the shoulder. The secondary spine is of uniform width and marks the ventral border of the scapula; it also borders the origin of the teres major muscle. The teres major fossa reaches to 8–10% of the length of the scapula. The corresponding muscle conceives the pull-down of the scapula and rotates it laterally. It thus supports a down- and backward extension of the humerus. This movement is especially powerful in climbers and diggers (Argot 2001; Grass 2019).

In addition, the glenoid fossa of the scapula is shallow in *X. oviceps*, which would increase the range of humeral mobility and would favour some forms of climbing rather than digging, because digging would put too much strain on that joint (Grass 2019). On the other hand, a shallow glenoid fossa reduces the stability of the shoulder joint (Grass 2014). However, the supraspinous border of the scapula is convex, maximising the attachment area for the m. levator scapulae and mm. rhomboidei of the scapula (Toledo et al. 2013). The former elevates and rotates the scapula and provides additional stabilisation. The latter abducts the dorsal margin of the scapula towards the spinal processes and rotates the bone. Furthermore, the scapula of *Xibalbaonyx oviceps* also presents an unfused area at mid-length of the primary spine, which might represent a protuberance or even posterior process (Figure 4(b)).

A posterior process of the scapular spine has been described for *Thalassocnus, Planops* and myrmecophagids (Amson et al. 2015), but not for *Megatherium, Nothrotheriops* (Amson et al. 2015) or *Megalonyx* (McDonald 1977; Holte 2012). The scapular spine is the attachment area of the m. deltoideus, an additional adductor of the humerus. It also supports the body weight on the shoulders during brachiation. A posterior protuberance has also been described for knuckle walking apes (Potau et al. 2009). The posterior protuberance identified in the scapula of *Xibalbaonyx oviceps* likely supported stabilisation of the rotator cuff by the deltoid muscle. In *X. oviceps*, the morphology of the scapula suggests a massive and stable shoulder musculature. The scapulae of bipeds and arboreal animals are generally shorter and wider, allowing for slow but powerful movements.

Grass (2019) already compared juvenile ground sloths with bears and discussed their possibilities of climbing to escape from predators. According to the scapular anatomy, *X. oviceps* may therefore have been able to climb, too.

The humerus in *X. oviceps* is at least 10% longer than the humerus CPC-2776 assigned to *X. exinferis* from cenote Tortugas, 2 km north-west from El Zapote cenote (Figure 5(a, f)). Both humeri belong to juvenile or subadult individuals. However, *X. exinferis* was smaller and, according to the humerus, stouter than *X. oviceps*. Especially, the deltoid crest of the humerus is more prominent in *X. exinferis* than in *X. oviceps*, based on the length of the this bone, as preserved. Additionally, the pectoral tuberosity, in the latter taxon, almost lines up with the medial margin of the humeral shaft, while in *X. exinferis* the pectoral crest follows the long axis of the shaft and does not run medially. Nevertheless, compared with subadult *Megalonyx jeffersonii* (e.g. RMM 6389), both sloths from the Yucatán Peninsula are markedly more gracile. The subadult *Megalonyx* (RMM-6389) individual from Alabama (Holte 2012) already exhibits a deltoid crest during subadult age, which is 5% more pronounced than in both *Xibalbaonyx oviceps* and *X. exinferis*, based on the respective humeral lengths. However, although the humerus in *Megalonyx* is more massive, the long bones are more than 10% longer in *X. oviceps* than in subadult *Megalonyx* (RMM-6389).

Although both humeri of *X. oviceps* are highly fragmented and difficult to discuss, due to the subadult ontogenetic stage, the deltoid and pectoral areas are prominent, suggesting further development of these structures into adolescence. The deltopectoral shelf reaches almost 80% of the width of the shaft, while in subadult *Megalonyx* this area is ≥5% narrower. Furthermore, the deltopectoral shelf extends distally in *Xibalbaonyx oviceps*, suggesting a broad area for the development of the deltoid and pectoral muscles. The two muscles are responsible for adduction and flexion of the humerus. Also, the m. deltoideus originates at the unossified sesamoid process along the scapular spine, indicating a higher shoulder girdle mobility and stability compared to most other ground sloths, in which this posterior tuberosity is absent.

The proximal and medial surfaces of the humeral shaft exhibit several scars, probably representing the attachment sites of the mm. teres major and pectoralis major et latissimus dorsi. The pronounced tuberosity along the long axis of the metaphysis of the *Xibalbaonyx oviceps* humerus, represents a large attachment area for the m. brachialis. This area is smoother in *X. exinferis*, and even subadult *Megalonyx*. This indicates that the brachialis muscle, which flexes the forearm, may have been extraordinarily strong in *Xibalbaonyx oviceps* when compared to other ground sloths.

Both *X. oviceps* and *X. exinferis* share similar morphological features, such as well-developed pectoral and deltoid tuberosities or ridges suggesting a powerful and highly mobile shoulder girdle.

However, *X. oviceps* was furthermore characterised by a large attachment area for the m. brachialis, an area which is less pronounced in *X. exinferis*. For *X. exinferis* an ability for grasping was reconstructed (Stinnesbeck et al. 2020a). This interpretation is based on the well-developed attachment areas for the forearm flexors. As the distal third of the humerus is not preserved in *X. oviceps*, it is not known whether *X. oviceps* exhibits the morphology identified in *X. exinferis*. At least, the fragmentary lateral epicondyle suggests that *X. oviceps* had a broad m. brachioradialis, comparable to that of *X. exinferis*, a feature also suggested by the well-pronounced ulnar tuberosity for the m. brachialis. The option for a strong flexion of the forearm thus provides further evidence for a grasping to even a climbing ability of *X. oviceps*. The taxon is also characterised by longer humeri than *X. exinferis* or subadult *Megalonyx*. Arboreal to semi-arboreal species are characterised by long and gracile forearm bones, while terrestrial, semi-fossorial and aquatic species are characterised by short and robust long bones (Fabre et al. 2015).

The ulna and radius of *Xibalbaonyx oviceps* are of almost the same lengths as the diaphysis of the humerus (Table 1), thereby suggesting that the latter bone was approximately 10% longer than the forearms. The ulna is wide, giving the bone a robust appearance, comparable to *Eucholeops* or *Megalonyx*, rather than *Nothrotheriops*. Because the olecranon is incomplete; however, the precise length of the bone remains unknown.

The anterior border of the ulnar shaft is concave, comparable to the anteroposterior curvature in *Hapalops* (Toledo et al. 2013), and to a lesser degree in *Megalonyx* (McDonald 1977). As in *Megalonyx*, the shaft of the ulna is laterally curved, which is well seen in anterior and posterior view (Figure 6(b,f)). This curvature is combined with the crest for the interosseous ligament, as also by deep lateral and medial fossae for the m. flexor digitorum profundus and anconeus. These features result in a high forearm stability coupled with forearm strength, and are documented for arboreal or semi-arboreal rather than terrestrial species (Argot 2001; Fabre et al. 2015; Henderson et al. 2017). A strong posterior convexity in the ulnar diaphysis has been documented for *Diabolotherium* and *Hapalops*, and has there been interpreted as evidence for the ability of these sloths to climb (Pujos et al. 2007).

The anteroproximally facing trochlear notch reaches a 120° angle in *X. oviceps*, measured against the sigmoid cavity, while the notch is smaller than 90° in *Megalonyx* and slightly more anteriorly oriented, as in *Nothrotheriops*. This angle is even wider than in the climbing sloth *Diabolotherium* (Pujos et al. 2007). This wide angle and its orientation increases the range of pronation-supination movements (Argot 2001). The index of dorsal olecranon projection, corresponding to the ratio between the anteroposterior diameter of the proximal epiphysis and the proximodistal diameter of the trochlear notch is 0.8 in *X. oviceps* and thus is about equal to that of *Diabolotherium* in which the ratio is 0.78 (White 1993; Pujos et al. 2007).

The coronoid process is prominent, suggesting a strong attachment for the annular ligament and well-developed mm. abductor pollicis longus and flexor digitorum profundus. In contrast, the anconeal process is almost non-existent, a situation described for immature *Megalonyx* specimens (McDonald 1977). The circular radial notch is also prominent. It is twice as big as the same element in adult *Megalonyx* and is laterally oriented, instead of anteriorly.

Overall, the radius is slender (Figure 7(a)). The bicipital tuberosity, interosseous ligament and pronator ridge, is identified as rugose areas, rather than a crest, scars, or more pronounced tuberosities. A circular radial head is often associated with greater ranges of forearm mobility and increased capacity for supination (Fabre

et al. 2015). It is therefore often found in arboreal and semi-arboreal species.

The morphometric features identified in the forelimb of *Xibalbaonyx oviceps* indicate that the animal was capable of abduction and adduction, and thus of an extensive range of shoulder girdle mobility and strength, as well as forearm motion. According to the pectoralis and brachialis musculature areas of the humerus, ulna and radius, *X. oviceps* must have had a powerful arm musculature.

Unfortunately, except for a single digit the manus is not preserved. Based on this digit, however, two possible scenarios exist: (1) *X. oviceps* had its entire palm of the hand on the floor, similar to the reconstruction of locomotion in other megalonychids. This possibility would allow for a high mobility of the single digits, which coincides with the muscle attachment indications of radius and ulna. (2) Hands were flexed during gait. Then the ground sloth would have done a kind of 'knuckle-walking' in the style of a giant anteater (Orr 2005; de Faria et al. 2015) with the manus in a slightly but clearly supinated position.

The femur of *X. oviceps* is at least 40% shorter than that of adult *Megalonyx jeffersonii*, but already 15 to 20% longer than in subadult specimens of this taxon (Holte 2012). It is 15 to 20% shorter than that of *Australonyx aquae* and *Ahytherium aureum* (Cartelle et al. 2008). The femur of *X. oviceps* is thus not only shorter but also more gracile than that of other adult Megalonychidae. The femoral head lacks a fovea capitis, suggesting that the teres femoris ligament was feeble. The ligament of the femur head is believed to tense during combined flexion, adduction and external rotation of the hip joint; it is also reported to provide some mechanical stability to the hip joint (Crelin 1988). A weak teres femoris ligament, which is expressed by a small, shallow pit on the head of the femur, leads to a greater range in lateral femur motion. This morphological phenomenon has also been documented for orangutans (Muchlinski et al. 2018) and Asian Elephants (Crelin 1988). Owen (1842) already postulated that this feature could be an advantage in climbing sloths. The morphology of the femur in *X. oviceps* leads to a wide attachment area for the gluteal muscles along the greater trochanter, the deep trochanteric fossa and lateral diaphyseal margin, indicating that the hip musculature took over the stabilisation and mobility. The gluteal muscles are responsible for the extension, abduction, retraction, and both external and internal rotation of the hip joint. Compared to *Megalonyx*, the femur in *X. oviceps* is proximodistally and mediolaterally slender and consequently, the quadriceps muscle attachments are not as developed as in *Megalonyx jeffersonii*. The femoral strength coming from the vastus muscles (e.g. m. quadriceps) therefore plays a minor role in *X. oviceps*, as usually documented for ground sloths. The development of the m. quadriceps in *Megalonyx* supports a low gravity centre coupled with a femur showing anterolaterally, which gives the animal a wide stance. This morphological difference in the femur suggests that the centre of gravity was higher in *X. oviceps*.

In the material of *X. oviceps* revised here the tibias are only represented by their diaphyses. The fibulae are not available. The tibia is extraordinarily short, only reaching half the length of the femur, while in most other ground sloths this bone reaches three-fourths of the femur length. Although the distal end of the femur is not preserved, nor is the proximal articular area of the tibia, the compact and broad diaphysis of the tibia and the posterior convexity offer insertion surfaces for the m. tibialis posterior and for mm. flexor digitorium lateralis et medialis. These muscles are vital for flexion of the knee joint and plantar flexion of the pes. The femur shaft has the shape of a hyperboloid, suggesting a powerful knee musculature, which is supported by the compact tibia. The

animal had well-developed and highly flexible hip and crus muscles, which would be useful for climbing. The morphology of the astragalus and calcaneus suggest a proximal and proximolateral contact with the ground. This interpretation is also supported, by the morphology of the ungual phalanges in which the tips never pass the ventral base of the claw supporting an unrolling along the phalanges. *Xibalbaonyx* walked plantigrade, similar to *Megalonyx, Pliometanastes, Diabolotherium* and other Megalonychidae, but different from the pedolateral rotation often documented for Mylodontidae, Nothrotheriidae, and Megatheriidae (McDonald 2012).

Based on the postcranial material of the holotype of *Xibalbaonyx oviceps* documented here, we suggest that *X. oviceps* reached about 2 m length. Forelimbs were slightly longer than the hind limbs leading to a caudally sloping position of the back, thus supporting quadrupedalism rather than bipedalism. As repeatedly described for browsing ground sloths, *X. oviceps* likely had the ability to pull down branches to get in reach of leaves, fruits and inflorescences. The bone reliefs and the reconstruction of muscle origin and insertion areas, suggest that *X. oviceps* was able to climb. *X. oviceps* should not be compared to fully arboreal to semi-arboreal taxa, including extant tree sloths, but forearm musculature and hip joint indicate significantly higher degrees of liberty than usually seen in large terrestrial ground sloths. *X. oviceps* was able to overcome steep slopes, and perhaps even climb the rocky walls of cenotes. Femur and tibia length, suggest that *X. oviceps* was only able to take small steps, and probably did not cover long distances.

This ability has also been discussed for *X. exinferis* (Stinnesbeck et al. 2020a) from the same area, and for juvenile *Megalonyx* (Holte 2012; Grass 2019).

Grass (2019) discusses the possibility that young ground sloths grasped on their mother´s abdomen or back, as is seen in juveniles of extant sloths and other Xenarthra. This scenario may also have been possible for infant *X. oviceps*, as suggested by the configuration of the shoulder musculature. The subadult individual from El Zapote, however, weighted approximately 200 kg and was therefore too large and heavy for a clinging on the mother´s abdomen or back.

We therefore propose that the locomotion of *X. oviceps* was comparable to that of extant gorillas and bears, animals which are capable of brachiation and vertical climbing. Gorillas manage to climb, even as adults, although they do not use this ability frequently because of their weight. Nevertheless, different to the tropical jungle with high trees, the solid limestone wall of a cenote offers sufficient stability to even large-sized, heavy animals.

The northeastern Yucatán Peninsula is characterised by a flat topography, a feature resulting from an almost horizontal limestone bedrock on a tectonically inactive carbonate platform (Ward et al. 1985; Weidie 1985). The only vertical structures to climb in this karst-dominated region are the steep to vertical walls of sinkholes. Trees were no option, because during the Late Pleistocene forests were absent in the area, which was then covered by shrub savanna (Stinnesbeck et al. 2018b), analogous to the modern Irish Burren landscape (Feehan 2001). Following this argument, cenotes were the only places to access water. Even today, with water levels tens of metres higher than during Pleistocene stadial periods, there is no surface water in this karst region. Water could only be accessed by descending sinkholes and entering deep and completely dark parts of the cave system.

We suggest that *X. oviceps* was comparable in size and weight to a mature male gorilla, and that the animal was capable to overcome steep slopes. *X. oviceps* inhabited an area of steep to vertical cave entrances, and vegetation with deep branched roots anchored in brittle limestone. Under these circumstances the ability of clinging

and rock climbing would be highly useful even for an animal with the given body mass. Its locomotion included the ability of climbing. We are nevertheless aware that this interpretation is based on a juvenile to subadult individual and that this ability could have been lost during adolescence, as previously documented for the terrestrial ground sloth *Megalonyx* (Holte 2012; Grass 2019).

Taphonomy and potential human-environment interactions at the El Zapote cenote

The postcranial material of *Xibalbaonyx oviceps* was discovered scattered on the slope of the debris mount of El Zapote cenote, in water depths of 47 to 57 m depth. This situation suggests that an originally complete corpse decayed on the slope of this mount. During, or after skeletonisation, single bones or decayed portions of the corpse, were gravity-transported for a few metres downhill. Finally, flooding of the sinkhole during the Early Holocene covered all bones with fresh and finally salt water.

While most of the skeletal elements are complete and well preserved, the pelvis was severely fragmented. Fragmentation of such a massive bone may suggest that the animal fell into the sinkhole and that the pelvis was shattered when the animal hit the ground. As during the end of the Pleistocene the bottom of the deep El Zapote cenote was already water-filled (Ritter et al. 2019), the animal could then even have survived the fall cushioned by a water layer. Nevertheless, there was no way for it to climb out of the cenote, due to its bottleneck shape.

The bones present evidence for dissolution, mostly along the sutures, as already reported for the skull (Stinnesbeck et al. 2017a). However, while vertebrae or ribs are mostly intact, all long bones lack their proximal or/and distal epiphyses, suggesting that the joints were intentionally broken. In these bones (e.g. humeri, femora, ulnae, radii and tibiae) the medulla of the diaphyses, which is rich in adipose tissue is missing. Several of these bones were hollowed and appear to be scooped-out on purpose to retrieve the bone marrow (Figure 8(f,g)). The compacta is present only near the fragmented open ends of the diaphyses; in these parts of the bones the compacta is extremely thin and the spongiosa is completely missing. The further away from the breakage the more spongiosa is preserved. In occasions, the spongiosa in the centre of the bone is untouched, thus suggesting that tools may have been used to hollow the bones, which only reached to a certain depth. Dissolution cannot explain the phenomenon of hollowed diaphyses, as this process would then also have produced a decay of the bone compacta of the long bones, as well as in other bones such as ribs, atlas, axis, etc. Also, bones are hollowed and spongiosa excavated to a depth of 200 mm; this also rather suggests a tool. The epiphyses are also intact, such as the femoral head and greater trochanter, and their compacta and medulla are still present. However, in the long bones, in which either the proximal or distal epiphysis is broken off as well as the corresponding end of the diaphysis, only the medulla is missing. In these bones the compacta is generally present and shows an excellent preservation. This scenario is also supported by the identification of several small scratch or cut marks. Marks are identified on the few ribs, the fragmented pelvis and on the ulna (Figure 3(d-e); 6(g)). They only reach a length of about 20 mm, but they are well visible, deep, and with V-shaped cross-sections.

In 2014, the El Zapote skeleton was dated to 9.305 ± 35 14C BP (10.647–10.305 cal BP) by the LEMA lab at the UNAM (Stinnesbeck et al. 2017a). This unusually young age of the skeleton,

dating to the earliest Holocene, would make a co-existence of *Xibalbaonyx oviceps* with humans in the area very likely (González González et al. 2013; Stinnesbeck et al. 2017a, 2018c, 2020b; Hering et al. 2018). It is also known that some Caribbean ground sloths not only survived the end-Pleistocene mass extinction of American megafauna, but coexisted with humans even into the middle Holocene, e.g. *Neocnus* to about 4.391 ± 42 ky BP in Cuba (Steadman et al. 2005).

Further ground sloth material has been found in El Zapote with clear carnivore traces, among them two tibae of adult and a femur of an infant. Nevertheless, in these single bones the spongiosa is still present and the bones are not hollowed. The gnawing areal is circumscribed and differs from the postcranial traces described in *X. oviceps*. However, carnivorous gnawing cannot be excluded in the postcranial of *X. oviceps* and may even be more likely than human butchering.

Conclusions

Xibalbaonyx oviceps was a medium-sized ground sloth of approximately 2 m length and 200 kg weight. The forelimbs had twice the length of hind limbs, due to the shortness of the tibia. The anatomical proportions suggest a quadrupedal locomotion with facultative bipedalism. The forelimbs exhibited a great degree of liberty; this is typical for semi-arboreal to arboreal lever climbing animals, suggesting that *Xibalbaonyx* was capable for overcoming steep slopes and even climbing. A climbing ability, as seen in bears, is therefore discussed for *Xibalbaonyx*. Clinging to their mother´s abdomen or back, as well as climbing, is well documented for extant Xenarthrans and has also been discussed for fossil ground sloths. The postcranial skeleton of *Xibalbaonyx oviceps* described here represents a subadult ground sloth. The ability of climbing may have been lost in adults, as reported for *Megalonyx*.

The phenomenon of incomplete bone endings is seen in all long bones of the individual documented here. All diaphyses of these bones are hollowed intentionally and a few bones show small scratch or cut marks suggesting active damaging and scooping out by humans or carnivore gnawing.

Disclosure statement

No potential conflict of interest was reported by the authors.

References

Adam PJ, 1999. *Choloepus didactylus*. Mamm. Species 1–8.

Amson E, Argot C, McDonald HG, de Muizon C. 2015. Osteology and functional morphology of the forelimb of the marine sloth *Thalassocnus* (Mammalia, Tardigrada). J Mamm Evol. 22:169–242. doi:10.1007/s10914-014-9268-3

Andrade LC, Barbosa FHDS, Melki LB, Oliveira EV, de Araújo-júnior HI, Maniesi V. 2019. Revealing bone diseases in the Quaternary ground sloth Eremotherium laurillardi (Mammalia, Xenarthra). Hist Biol. 1–9. doi:10.1080/08912963.2019.1700977

Argot C. 2001. Functional-adaptive anatomy of the forelimb in the didelphidae, and the paleobiology of the paleocene Marsupials *Mayulestes ferox* and *Pucadelphys andinus*. J Morphol. 247:51–79. doi:10.1002/1097-4687-(200101)247:1<51::aid-jmor1003>3.0.co;2-%23

Bargo MS, Vizcaíno SF, Archuby FM, Blanco RE. 2000. Limb bone proportions, strength and digging in some lujanian (Late Pleistocene-Early Holocene) mylodontid ground sloths (Mammalia, Xenarthra). J Vertebr Paleontol. 20:601–610. doi:10.1671/0272-4634(2000)020[0601:LBPSAD]2.0.CO;2.

Blanchon P, Shaw J. 1995. Reef drowning during the last deglaciation: evidence for catastrophic sea-level rise and ice-sheet collapse. Geology. 23:4–8. doi:10.1130/0091-7613(1995)023<0004:RDDTLD>2.3.CO;2.

Böhmer C, Amson E, Arnold P, Van Heteren AH, Nyakatura JA. 2018. Homeotic transformations reflect departure from the mammalian "rule of seven" cervical vertebrae in sloths: inferences on the Hox code and morphological modularity of the mammalian neck. BMC Evol Biol. 18:1–11. doi:10.1186/s12862-018-1202-5

Buchholtz EA, Stepien CC. 2009. Anatomical transformation in mammals: developmental origin of aberrant cervical anatomy in tree sloths. Evol Dev. 11:69–79. doi:10.1111/j.1525-142X.2008.00303.x

Cartelle C, De Iuliis G. 2006. *Eremotherium laurillardi* (Lund) (Xenarthra, Megatheriidae), the Panamerican giant ground sloth: taxonomic aspects of the ontogeny of skull and dentition. J Syst Palaeontol. 4:199–209. doi:10.1017/S1477201905001781

Cartelle C, De Iuliis G, Pujos F. 2008. A new species of Megalonychidae (Mammalia, Xenarthra) from the Quaternary of Poço Azul (Bahia, Brazil). Comptes Rendus - Palevol. 8(7):335–346. doi:10.1016/j.crpv.2008.05.006.

Crelin ES. 1988. Ligament of the head of the femur in the orangutan and Indian elephant. Yale J Biol Med. 61:383–388.

de Faria LG, Rahal SC, Mesquita LDR, Agostinho FS, Kano WT, Teixeira CR, Monteiro FOB. 2015. Gait analysis in giant anteater (Myrmecophaga Tridactyla) with the use of a pressure-sensitive walkway. J Zoo Wildl Med. 46:286–290. doi:10.1638/2014-0057r1.1

De Iuliis G, Pujos F, Cartelle C. 2009. A new ground sloth (Mammalia: Xenarthra) from the quaternary of Brazil. Comptes Rendus - Palevol. 8 (8):705–715. doi:10.1016/j.crpv.2009.07.003.

de Muizon C, McDonald HG. 1995. An aquatic sloth from the Pliocene of Peru. Nature. 375:224–227. doi:10.1038/375224a0

de Souza Barbosa FH, Araújo-Júnior HI, De, Oliveira EV. 2014. Neck osteoarthritis in *Eremotherium laurillardi* (Lund, 1842; Mammalia, Xenarthra) from the Late Pleistocene of Brazil. Int J Paleopathol. 6:60–63. doi:10.1016/j.ijpp.2014.01.001

de Souza Barbosa FH, Porpino KO, Bergqvist LP, Rothschild BM. 2016. Elucidating bone diseases in brazilian pleistocene sloths nothrotheriidae and megalonychidae families. Ameghiniana. 54:331–340. doi:10.5710/AMGH.30.11.2016.3032.

Fabre AC, Cornette R, Goswami A, Peigné S. 2015. Do constraints associated with the locomotor habitat drive the evolution of forelimb shape? A case study in musteloid carnivorans. J Anat. 226:596–610. doi:10.1111/joa.12315

Feehan J. 2001. The rocks and landforms of the burren. In: O'Connell JW, Korff A, editors. The book of the burren. Dublin: Tir Eolas; p. 14–23.

González González AH, Terrazas Mata A, Stinnesbeck W, Benavente ME, Avilés Olguín J, Rojas Sandoval C, Padilla JM, Velázquez Morlet A, Acevez Nuñez E, Frey E. 2013. The first human settlers on the Yucatan Peninsula: evidence from drowned caves in the State of Quintana Roo (South Mexico). In: Graf KE, Ketron CV, Waters M, editors. Paleoamerican Odyssey. Santa Fe, New Mexico: Texas A&M University; p. 323–337.

González González AH, Rojas Sandoval C, Terrazas Mata A, Benavente Sanvicente M, Stinnesbeck W, Aviles Olguín J, De Los Ríos M, Acevez

Nuñez E, Aviles O, De Los J, et al. 2008. The arrival of humans on the Yucatan peninsula: evidence from submerged caves in the State of Quintana Roo, Mexico. Curr Res Pleistocene. 25:1–24.

Grass AD. 2014. Inferring lifestyle and locomotor habits of extinct sloths through scapula morphology and implications for convergent evolution in extant sloths. Iowa City, Iowa: University of Iowa.

Grass AD. 2019. Inferring differential behavior between giant ground sloth adults and juveniles through scapula morphology. J Vertebr Paleontol. 39:1–15. doi:10.1080/02724634.2019.1569018

Henderson K, Pantinople J, McCabe K, Richards HL, Milne N. 2017. Forelimb bone curvature in terrestrial and arboreal mammals. PeerJ 2017. doi:10.7717/peerj.3229

Hering F, Stinnesbeck W, Folmeister J, Frey E, Stinnesbeck SR, Avilés J, Acevez Nuñez E, González AH, Terrazas Mata A, Benavente Sanvicente ME, et al. 2018. The Chan Hol cave near Tulum (Quintana Roo, Mexico): evidence for long-lasting human presence during the early to middle Holocene. J Quat Sci. 33:444–454. doi:10.1002/jqs.3025

Hildebrand M. 1985. Digging of quadrupeds. In: Hildebrand M (ed) Functional Vertebrate Morphology. Cambridge: Cambridge University Press, pp 89–109.

Hirschfeld SE, Webb SD. 1968. Plio-Pleistocene megalonychid sloths of North America. Bull Florida State Museum Biol Sci. 12:213–296.

Holte SE, 2012. Description of Jefferson's ground sloth (Megalonyx jeffersonii) from ACb-3 cave, colbert county, alabama, with comments on ontogeny, taphonomy, pathology, and paleoecology. Electron. Theses Diss. East Tennessee State University.

Laurin M, Argot C, Amson E, de Buffrenil V, de Muizon C. 2014. Gradual adaptation of bone structure to aquatic lifestyle in extinct sloths from Peru. Proc R Soc B Biol Sci. 281:20140192. doi:10.1098/rspb.2014.0192

Leidy J. 1855. A memoir on the extinct sloth tribe of North America. Philadelphia: Smithsonian institution.

Long KM, Prothero DR, Madan M, Syverson VJP. 2018. Allometric shape changes during ontogeny of the Rancho La Brea ground sloth Paramylodon harlani. In: Lucas SG, Sullivan RM, editors. Fossil Record. Albuquerque: New Mexico Museum of Natural History and Science; p. 481.

McDonald HG. 1977. Description of the osteology of the exctinct gravigrade edentate Megalonyx with observations on its ontogeny, phylogeny and functional anatomy. Gainesville, Florida: University of Florida.

McDonald HG. 2005. Paleoecology of extinct xenarthrans and the Great American biotic interchange. Bull Florida Museum Nat Hist. 45:313–333.

McDonald HG. 2007. Biomechanical inferences of locomotion in ground sloths: integrating morphological and track data. Cenozoic Vertebrate Tracks and Traces. Bulletin 42(42):201–208.

McDonald HG. 2012. Evolution of the pedolateral foot in ground sloths: patterns of change in the astragalus. J Mamm Evol. 19:209–215. doi:10.1007/s10914-011-9182-x

McDonald HG, Carranza-Castañeda O. 2017. Increased xenarthran diversity of the Great American biotic interchange: a new genus and species of ground sloth (Mammalia, Xenarthra, Megalonychidae) from the Hemphillian (late Miocene) of Jalisco, Mexico. J Paleontol. 91:1069–1082. doi:10.1017/jpa.2017.45

McDonald HG, Harington CR, De Iuliis G. 2000. The ground sloth Megalonyx from pleistocene deposits of the old crow Basin, Yukon, Canada. Arctic. 53:213–220. doi:10.14430/arctic852.

Moseley GE, Richards DA, Smart PL, Standish CD, Hoffmann DL, Hove HT, Vinn O. 2015. Early–middle Holocene relative sea-level oscillation events recorded in a submerged speleothem from the Yucatán Peninsula, Mexico. The Holocene. 25:1511–1521. doi:10.1177/0959683615585832.

Muchlinski MN, Hammond AS, Deane AS, Purcell M, Hemingway HW, Hantke G, Pastor F, Garrosa M, Hartstone-Rose A. 2018. The ligamentum teres femoris in orangutans. Am J Phys Anthropol. 167(3):684–690. doi:10.1002/ajpa.23644.

Nyakatura, J. (2010). On the functional morphology and locomotion of the two-toed sloth (Choloepus didactylus, Xenarthra). Doctoral dissertation, Friedrich-Schiller-University, Jena

Nyakatura JA. 2012. The Convergent Evolution of Suspensory Posture and Locomotion in Tree Sloths. J Mamm Evol. 19(3):225–234. doi:10.1007/s10914-011-9174-x.

Orr CM. 2005. Knuckle-walking anteater: A convergence test of adaptation for purported knuckle-walking features of African hominidae. Am J Phys Anthropol. 128(3):639–658. doi:10.1002/ajpa.20192.

Owen R. 1842. Description of the skeleton of an extinct gigantic sloth, Mylodon robustus Owen, with observations on the osteology, natural affinities and probable habits of the megatherioid quadrupeds in general. London: Royal College of Surgeons.

Potau JM, Bardina X, Ciurana N, Camprubí D, Pastor JF, de Paz F, Barbosa M. 2009. Quantitative analysis of the deltoid and rotator cuff

muscles in humans and great Apes. Int J Primatol. 30(5):697–708. doi:10.1007/s10764-009-9368-8.

Presslee S, Slater GJ, Pujos F, Forasiepi AM, Fischer R, Molloy K, Mackie M, Olsen JV, Kramarz A, Taglioretti M, et al. 2019. Palaeoproteomics resolves sloth relationships. Nat Ecol Evol. 3(7):1121–1130. doi:10.1038/s41559-019-0909-z.

Pujos F, De Iuliis G, Argot C, Werdelin L. 2007. A peculiar climbing Megalonychidae from the Pleistocene of Peru and its implication for sloth history. Zool J Linn Soc. 149(2):179–235. doi:10.1111/j.1096-3642.2007.00240.x.

Pujos F, De Iuliis G, Cartelle C. 2016. A paleogeographic overview of tropical fossil sloths: towards an understanding of the origin of extant suspensory sloths? J Mamm Evol. 1–20. doi:10.1007/s10914-016-9330-4

Ritter SM, Isenbeck-Schröter M, Scholz C, Keppler F, Gescher J, Klose L, Schorndorf N, Avilés Olguín J, González-González A, Stinnesbeck W. 2019. Subaqueous speleothems (Hells Bells) formed by the interplay of pelagic redoxcline biogeochemistry and specific hydraulic conditions in the El Zapote sinkhole, Yucatán Peninsula, Mexico. Biogeosciences Discuss. 1–35. doi:10.5194/bg-2018-520

Rose KD, Emry RJ. 1993. Relationships of Xenarthra, Pholidota, and fossil "edentates": the morphological evidence. In: Szalay FS, Novacek MJ, McKenna MC (eds) Mammal Phylogeny: Placentals. New York: Springer-Verlag, pp 81–102

Steadman DW, Martin PS, MacPhee RDE, Jull AJT, McDonald HG, Woods CA, Iturralde-Vinent M, Hodgins GWL. 2005. Asynchronous extinction of late Quaternary sloths on continents and islands. Proc Natl Acad Sci U S A. 102 (33):11763–11768. doi:10.1016/j.quaint.2012.04.036.

Stinnesbeck SR, Frey E, Olguín JA, Stinnesbeck W, Zell P, Mallison H, González González A, Aceves Núñez E, Velázquez Morlet A, Terrazas Mata A, et al. 2017a. Xibalbaonyx oviceps, a new megalonychid ground sloth (Folivora, Xenarthra) from the Late Pleistocene of the Yucatán Peninsula, Mexico, and its paleobiogeographic significance. Palaontologische Zeitschrift. 91 (2):245–271. doi:10.1007/s12542-017-0349-5.

Stinnesbeck SR, Frey E, Stinnesbeck W. 2018a. New insights on the paleogeographic distribution of the Late Pleistocene ground sloth genus Xibalbaonyx along the Mesoamerican Corridor. J South Am Earth Sci. 85:108–120. doi:org/10.1016/j.jsames.2018.05.004

Stinnesbeck SR, Frey E, Stinnesbeck W, Avíles Olguín J, Zell P, Terrazas Mata A, Benavente Sanvicente M, González González A, Rojas Sandoval C, Acevez Nuñez E. 2017b. A new fossil peccary from the Pleistocene-Holocene boundary of the eastern Yucatán Peninsula, Mexico. J South Am Earth Sci. 77:341–349. doi:10.1016/j.jsames.2016.11.003

Stinnesbeck SR, Stinnesbeck W, Frey E, Avilés Olguín J, González González A. 2020a. Xibalbaonyx exinferis n. sp. (Megalonychidae), a new Pleistocene ground sloth from the Yucatán Peninsula, Mexico. Hist Biol. 1–12. doi:10.1080/08912963.2020.1754817

Stinnesbeck SR, Stinnesbeck W, Frey E, Avilés Olguín J, Rojas Sandoval C, Velázquez Morlet A, González H. 2018b. Panthera balamoides and other Pleistocene felids from the submerged caves of Tulum, Quintana Roo, Mexico. Hist Biol. 1–10. doi:10.1080/08912963.2018.1556649

Stinnesbeck SR, Stinnesbeck W, Terrazas Mata A, Avilés Olguín J, Benavente Sanvicente M, Zell P, Frey E, Lindauer S, Rojas Sandoval C, Velázquez Morlet A, et al. 2018c. The Muknal cave near Tulum, Mexico: an early-Holocene funeral site on the Yucatán peninsula. The Holocene. 1–14. doi:10.1177/0959683618798124

Stinnesbeck W, Becker J, Hering F, Frey E, González González AH, Fohlmeister J, Stinnesbeck SR, Frank N, Terrazas Mata A, Benavente Sanvicente ME, et al. 2017a. The earliest settlers of Mesoamerica date back to the late Pleistocene. PLoS One. 12(8):16–18. doi:org/10.1371/journal.pone.0183345.

Stinnesbeck W, Rennie SR, Stinnesbeck SR, Avilés Olguín J, Gonzalez S, Frank N, Warken S, Schorndorf N, Krengel T, Velázquez Morlet A, et al. 2020b. New evidence for an early settlement of the Yucatan Peninsula, Mexico: the Chan Hol 3 woman and her meaning for the Peopling of the Americas. PLoS One. 15(2):e0227984. doi:10.1371/journal.pone.0227984.

Tambusso PS, Varela L, McDonald HG. 2018. Fusion of anterior thoracic vertebrae in Pleistocene ground sloths. Hist Biol. 32:1–8. doi:10.1080/08912963.2018.1487419

Toledo N, Bargo MS, Vizcaíno SF. 2013. Muscular reconstruction and functional morphology of the forelimb of early miocene sloths (Xenarthra, Folivora) of patagonia. Anat Rec. 296(2):305–325. doi:10.1002/ar.22627.

Varela-Lasheras I, Bakker AJ, van der Mije SD, Metz JAJ, van Alphen J, Galis F. 2011. Breaking evolutionary and pleiotropic constraints in mammals: on sloths, manatees and homeotic mutations. Evodevo. 2(1):1–27. doi:10.1186/2041-9139-2-11.

Ward WC, Weidie AE, Back W. 1985. Geology and hydrogeology of the Yucatan and Quaternary geology of northeastern Yucatan Peninsula. New Orleans: Geological Society.

Weidie AE. 1985. Part I: geology of Yucatan Platform. In: Ward WC, Weidie AE, Back W, editors. Geology and hydrogeology of the yucatan and quaternary geology of Northeastern Yucatan Peninsula. New Orleans: Geological Society; p. 1–19.

White JL. 1993. Indicators of locomotor habits in xenarthrans: evidence for locomotor heterogeneity among fossil sloths. J Vertebr Paleontol. 13(2):230–242. doi:10.1080/02724634.1993.10011502.

White JL, MacPhee RDE. 2001. The sloths of the West Indies: a systematic and phylogenetic review. In: Woods, Charles A., and Florence E. Sergile, (eds) Biogeography of the West Indies: patterns and Perspectives. New York: CRC Press; p. 201–235.

New insights on the paleogeographic distribution of the Late Pleistocene ground sloth genus *Xibalbaonyx* along the Mesoamerican Corridor

Sarah R. Stinnesbeck[a,b,*], Eberhard Frey[a], Wolfgang Stinnesbeck[c]

[a] *Abteilung Geowissenschaften, Staatliches Museum für Naturkunde Karlsruhe (SMNK), Erbprinzenstraße 13, D-76133 Karlsruhe, Germany*
[b] *Institut für Geographie und Geoökologie, Karlsruher Institut für Technologie (KIT), Reinhard-Baumeister-Platz 1, 76131 Karlsruhe, Germany*
[c] *Institut für Geowissenschaften, Ruprecht-Karls-Universität Heidelberg, Im Neuenheimer Feld 234, 69120 Heidelberg, Germany*

A B S T R A C T

Here we describe the skull of a new species of Megaloychidae (Xenarthra) *Xibalbaonyx microcaninus* from the federal state of Jalisco in west-central Mexico based on a complete skull exhibited in the Museo Regional de Guadalajara (MRG). The specimen was originally collected in the Upper Pleistocene sediment of the Zacoalco paleolake (Jalisco) and is here assigned to the recently established genus *Xibalbaonyx* from the Late Pleistocene of Quintana Roo in south-eastern Mexico. The genus *Xibalbaonyx* thus had a wider geographic distribution than previously considered and ranges from central to southern Mexico.

1. Introduction

Ground sloths were exceedingly diverse and abundant Neogene members of the American megafauna and had a wide geographical distribution covering North- and South America and the Great Antilles. Nevertheless, only a few and mostly fragmentary remains are reported from Central America and Mexico (McDonald, 2002; Pujos et al., 2016), contrasting with the extensive fossil record of the group from North America and South America. This scarce fossil record from the Mesoamerican Corridor, i.e. the region extending from central Mexico to southern Mexico and Central America, presently restricts a detailed evaluation of the paleobiogeographical and paleoecological relationships between North- and South American ground sloths (Pujos et al., 2016; McDonald and Carranza-Castañeda, 2017).

New paleontological investigations from the Yucatán Peninsula (McDonald et al., 2017; Stinnesbeck et al., 2017a) and the Mexican basin (McDonald and Carranza-Castañeda, 2017) have markedly expanded the knowledge on the Mexican ground sloth fossil record. Here, we add a new input to this knowledge by describing a new ground sloth taxon from the central-western Mexican federal state of Jalisco, of which the skull is housed and exhibited in the Museo Regional de Guadalajara (MRG).

More than one dozen Miocene to Pleistocene vertebrate fossil localities are presently known from Jalisco. Most of this material is not stratified, because it was collected by locals and delivered to Ing. Federico Solórzano Barreto, a local layman collector. Often, not even the precise locality is known (Schreiber, 2004). Some of the most

complete specimens are exhibited in the Museo Regional de Guadalajara (MRG), but the main Solórzano collection is today housed in the Museo de Paleontología de Guadalajara (MPG). Although fossil preservation is excellent, none of the localities has ever been scientifically investigated or mapped geologically (Schreiber, 2004; Lucas, 2008a; b). To date, only a few and isolated paleontological reviews exist from the Jalisco area and these are restricted to fossil reptiles, birds, or mammals (Rufolo, 1998; Lucas, 2008a; b; Alberdi et al., 2009; Lucas et al., 2011; McDonald and Carranza-Castañeda, 2017).

Two ground sloth skulls are presently exhibited in the Museo Regional de Guadalajara (MRG). One specimen has been assigned to the giant ground sloth *Megatherium* and the second to Mylondontidae. The specimen assigned to as *Megatherium* was identified as the giant Megatheriinae *Eremotherium* (Polaco Ramos, 1981), which had a wide Pleistocene paleogeographic distribution across the Mesoamerican Corridor and is known from Mexico, Panama, Nicaragua, and El Salvador (Cartelle and De Iuliis, 2006; Pujos et al., 2016). Assignment of the second specimen to Mylodontidae turned out to be incorrect as it exhibits diagnostic features of Megalonychidae. It has therefore been subsequently assigned to *Megalonyx jeffersonii* by Lucas (2008a). Here we describe the skull and mandible of this specimen and assign the material to the recently established genus *Xibalbaonyx* (Stinnesbeck et al., 2017a), of which the holotype was found in the El Zapote cenote in the federal state of Quintana Roo in south-eastern Mexico. The new species of *Xibalbaonyx* expands the occurrence of the genus to central-western Mexico.

---

* Corresponding author. Abteilung Geowissenschaften, Staatliches Museum für Naturkunde Karlsruhe (SMNK), Erbprinzenstraße 13, D-76133 Karlsruhe, Germany.
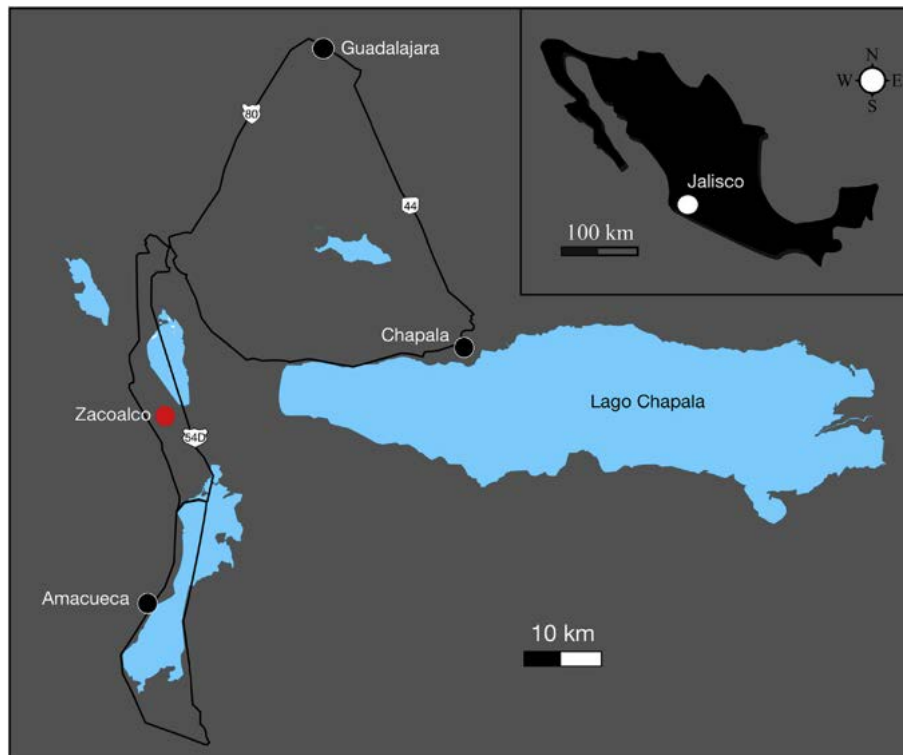 *E-mail address:* sarah.stinnesbeck@kit.edu (S.R. Stinnesbeck).

Fig. 1. Location of the finding locality Zacoalco of INAH MRG-10-294922 and INAH MRG-10-294923 in the federal state of Jalisco, central-western Mexico.

1.1. Geological setting

Lake Chapala (Spanish: Lago de Chapala) reaches a maximum east-western length of 70 km and a maximum depth of 10 m (Fig. 1). It is the largest natural freshwater lake in Mexico (Lucas, 2008a). Nevertheless, the lake is only a remnant of a much larger Plio-Pleistocene lake referred to as Lake Jalisco (Lucas, 2008b). This paleolake was formed in a Neogene tectonic *graben system* interpreted to be a rift structure (Ferrari et al., 1994; Ferrari, 1995; Ferrari and Rosas-Elguera, 2000). It is located in the intersection between Paleogene volcanic rocks of the Sierra Madre Occidental (SMO) to the north, Mesozoic volcanic rocks of the Jalisco Block (JB) to the south, and Plio-Pleistocene volcanic rocks of the western Mexican Volcanic Belt (MVB) between them (Ferrari, 1995; Ferrari and Rosas-Elguera, 2000). The basin is filled with Plio-Pleistocene alluvial, fluvial and lacustrine deposits (Michaud et al., 2000).

The ground sloth skull described here is from the Zacoalco area (Fig. 1), located in the Tepic-Zacoalco graben to the northwest of the Lake Chapala rift system (Lucas, 2008a; b). At Zacoalco, paleolake sediments contain a wide variety of vertebrate fossils, among them teleosts, reptilians, birds and mammals of Pleistocene age (Rufolo, 1998; Schreiber, 2004; Lucas, 2008a; b).

2. Material and methods

Institutional abbreviations:

INAH - Instituto Nacional de Antropología e Historia,

MRG - Museo Regional de Guadalajara - Jalisco, Mexico

MPG - Museo de Paleontología de Guadalajara - Jalisco, Mexico

The specimen comprises a complete skull and mandible (Figs. 2–6). It is housed and accessible in the paleontological section of the MRG in Guadalajara, central-western Mexico, under the INAH collection numbers MRG-10-294922 (skull) and MRG-10-294923 (mandible). The photographic documentation was executed with a Canon EOS Rebel T4i with 10–22 mm zoom lens set at 22 mm; f 4.5, 1/80 – f 8, 1/20 on a tripod. In all images, the background was manually masked.

2.1. Anatomical and phylogenetic terminology

The terminology used for the description of anatomical features of INAH-MRG 10–294922 (skull) and INAH-MRG 10–294923 (mandible) is based on sloth and ground sloth phylogenetic characteristics (Gaudin, 1995, 2004; Adam, 1999; White and MacPhee, 2001; Pujos et al., 2007; Hayssen, 2011; McDonald et al., 2013).

The term "nasion" refers to the point where the nasofrontal and internasal sutures meet (Groves, 2003), but it is also the deepest depression on the nasal bridge (Martin, 1914). We here use the term nasional impression (Stinnesbeck et al., 2017a), as this feature is characteristic and diagnostic in *Xibalbaonyx*, including the new species of this genus described here.

The basonasal length (BNL) is considered and measured from the rostral edge, or rhinion, of the nasals, to the caudal edge of the occipital condyles (Gaudin, 2004). The maximum mandibular length (MML) is measured from the rostral tip of the mandibular symphysis to the caudal-most edge of the condyloid process, or angular process, respectively (Gaudin, 2004).

List of specimens consulted and included in the comparison:

Nohochichak xibalbahkah (McDonald and Carranza-Castañeda, 2017; INAH DP5832; for skull and mandible), accessible at the INAH, Mexico City, Mexico.

Xibalbaonyx microcaninus: INAH-MRG-10-294922 (skull) and INAH-MRG-10-294923 (mandible), accessible at the MRG, Jalisco, Mexico.

Xibalbaonyx oviceps (Stinnesbeck et al., 2017a; INAH-Za2014-
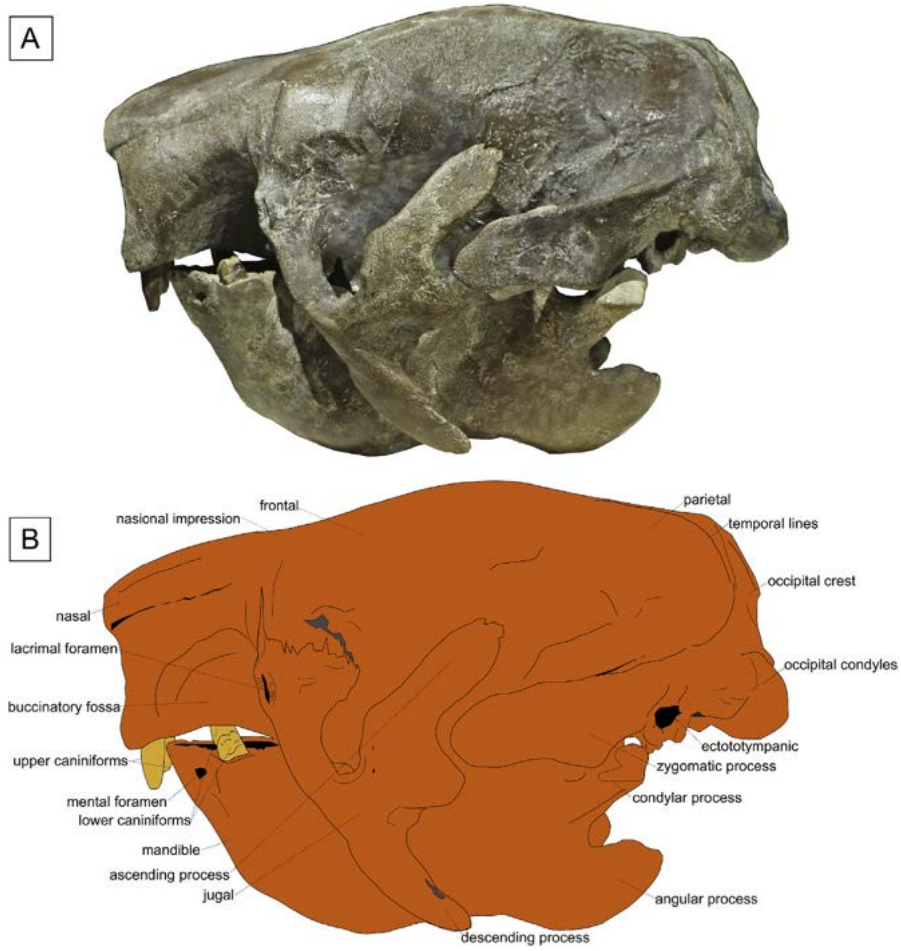
Fig. 2. *Xibalbaonyx microcaninus* (INAH MRG-10-294922 and INAH MRG-10-294923) in lateral view. A) Photograph and B) Interpretive line drawing.
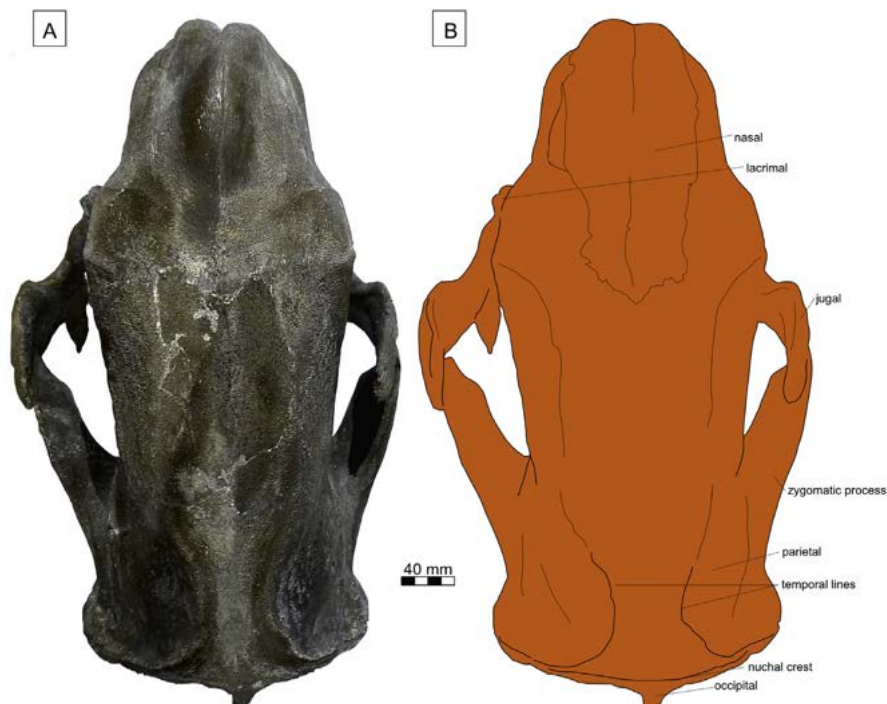

Fig. 3. *Xibalbaonyx microcaninus* (INAH MRG 10–294922) in dorsal view. A) Photograph and B) Interpretive line drawing.

01(skull) and INAH Za2014-02 (mandible)), accessible at the INAH Tulúm, Quintana Roo, Mexico.

The descriptive comparisons with North- Central- and South American Megalonychidae are based on the original descriptions:

Ahytherium aureum (Cartelle et al., 2008; De Iuliis, Pujos & Cartelle, 2009)

Australonyx aquae (De Iuliis, Pujos & Cartelle, 2009)

Megalonyx jeffersonii (Leidy, 1855; Hirschfeld and Webb, 1968; McDonald, 1977)

Megistonyx oreobios (McDonald et al., 2013)

Pliometanastes sp. (Hirschfeld and Webb, 1968)

Meizonyx salvadorensis (Webb and Perrigo, 1985; Florida Museum of Natural History, Gainsville, UF 27513)

Zacatzontli tecolotlanensis (McDonald and Carranza-Castañeda, 2017; MPG 1312G)

2.2. Phylogenetic analysis

A phylogenetic analysis was performed to interpret the relationships of *Xibalbaonyx microcaninus* nov. spec. within Megalonychidae. The skull (INAH Za2014-01) and mandible (INAH Za2014-02) of *Xibalbaonyx oviceps* from the El Zapote cenote in the federal state of Quintana Roo, Mexico (Stinnesbeck et al., 2017a) were used for comparison and are included in the analysis. The analysis was carried out using PAUP (version 4.0a 150 for Macintosh; Swofford, 2002). The methodology has been described in detail by several authors (Gaudin, 1995, 2004; Wible and Gaudin, 2004; McDonald et al., 2013; McDonald et al., 2017). The present analysis is based on 80 cranial and mandibular features as published in McDonald et al. (2017). '?' represents missing data or characters that are inapplicable to a given taxon. The following symbols are used to represent character states in polymorphic taxa: a = {0, 1}; b = {1, 2}; c = {2, 3}; d = {0, 2}; e = {0, 1, 2}.

The data matrix for all 18 megalonychids discussed in McDonald et al. (2013) and McDonald et al. (2017) has been used here, including the recently established *Nohochichak xibalbahkah* (INAH DP5832) from Quintana Roo, Mexico, as well as *Meizonyx salvadorensis* from El Salvador (McDonald et al., 2017). *Zacatzontli tecolotlanensis* McDonald and Carranza-Castañeda, 2017 from the federal state of Jalisco in Mexico was also included in the present analysis.

3. Results: Systematic paleontology

Order Xenarthra Cope, 1889
Suborder Pilosa Flower, 1883
Family Megalonychidae Gervais, 1855
Diagnosis of the family

Skull INAH-MRG 10–294922 and mandible INAH-MRG 10–294923 have been assigned to Megalonychidae based on cranial and mandibular features (Patterson et al., 1992; Gaudin, 1995, 2004; McDonald et al., 2013). Megalonychidae characters include, among others, a pair of caniniforms (C1/c1) separated from the molariform tooth-rows (M1-4 and m1-3) by a diastema, a dorsal contour of the skull that is evenly convex in lateral view, and a mediolaterally expanded glenoid fossa with a smooth posterior surface.

Genus *Xibalbaonyx* Stinnesbeck et al., 2017a
Diagnostic features of the genus *Xibalbaonyx*:

- Nearly horizontal rostral half of the nasals (rostrum).
- Nasional impression in the middle of the nasals, level with the lacrimal and jugal constriction.
- Smooth skull roof between nasal and occipital; no sagittal crest.
- Frontals and parietal of the skull roof convex with only the occipital crest and the nuchal line being visible in dorsal view; occipital vertical, almost not visible in dorsal view.
- Gracile jugal with ascending and middle processes proceeding dorsocaudally.
- Narrow and elongated ascending process being twice the length of the middle process.
- Strong constriction between horizontal and ascending ramus of the mandible. The shape of this constriction resembles a horizontally lying hourglass, of which the ventral base of the mandibular body is concave from the height of m2 to the coronoid process.

Xibalbaonyx microcaninus sp. nov.

Material studied. Skull and mandible are housed in the MRG under the collection numbers INAH-MRG-10-294922 (skull) and INAH-MRG-10-294923 (mandible). No postcranial material is known to us.

Etymology. *X. microcaninus* for the species: μικρός *(micro)* Greek for "small", and Latin *caninus* for eye tooth referring to the small upper and lower caniniforms.

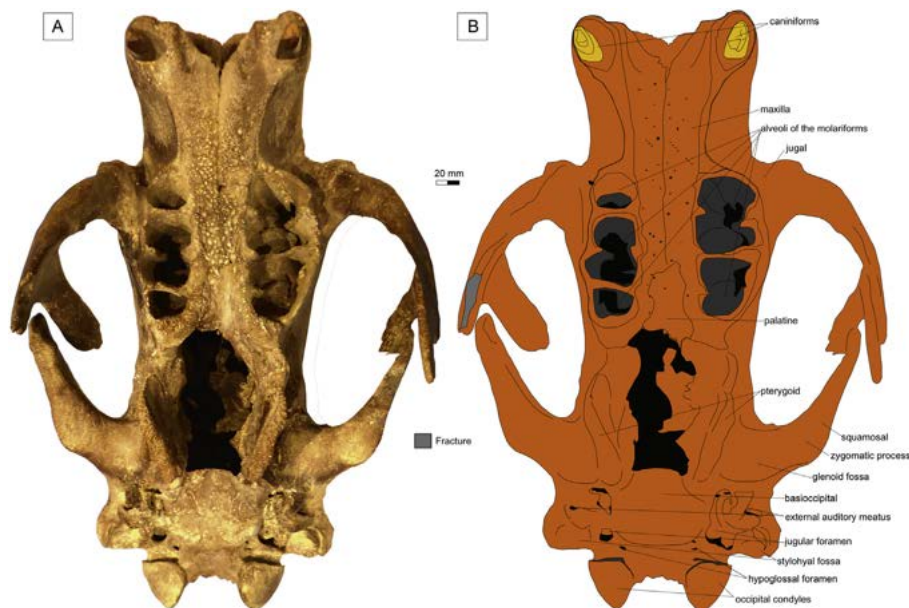*Type locality.* Zacoalco paleo-lake in the federal state of Jalisco,

Fig. 4. *Xibalbaonyx microcaninus* (INAH MRG 10–294922) in ventral view. A) Photograph and B) Interpretive line drawing.
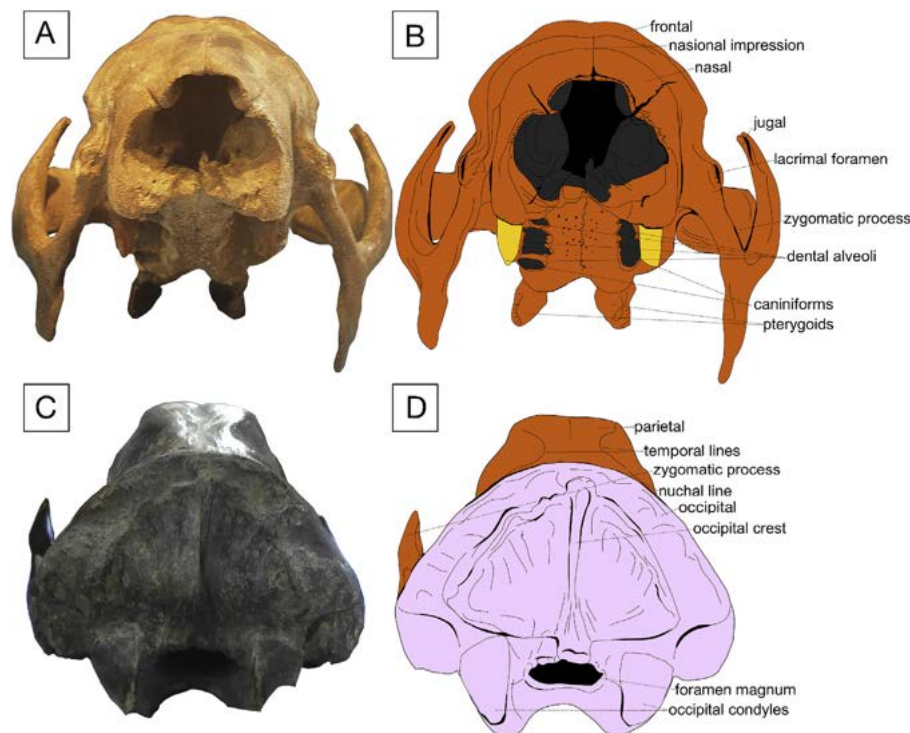
Fig. 5. *Xibalbaonyx microcaninus* INAH MRG-10-294922 in rostral (A and B) and caudal view (C and D). A) Rostral and C) caudal photographs and B) rostral and D) caudal interpretive line drawing.

Mexico (Fig. 1). The precise finding locality and circumstances are unknown.

Age. Biostratigraphical ranges of the associated megafaunal assemblage at Zacoalco (Lucas, 2008b) suggest a Late Pleistocene age for *Xibalbaonyx microcaninus*.

Diagnostic features of the species *X. microcaninus,* as seen in INAH-MRG-10-294922 and INAH-MRG-10-294923:

- Medium-sized ground sloth, similar in size as *Pliometanastes* Hirschfeld and Webb (1968).
- Pronounced temporal lines, which curve dorsocaudally without meeting each-other.
- Straight and conical small upper and lower caniniforms with vertical, oval occlusal surfaces.
- Lower caniniform is the smallest tooth of the mandible, while m1 is the largest one.
- Mandible narrow (MRG 10–294923), diverging caudally, with an isosceles triangular outline in dorsal view.
- Mandibular spout triangular in dorsal view, reaching < 20% of the MML.
- Mandibular spout and diastema between c1 and m1 of equal length.
- The dorsal tip of the coronoid process of the mandible is caudally sharp, pointed and hooked-shaped.

Description

The skull sutures are majorly fused, indicating an adult individual. Identification of all individual skull bones is therefore impossible. However, the rostrolateral and frontoparietal margins of the nasal bone are visible. The nasal and frontal sutures are faintly visible. The dark-grey to black color of the skull is due to impregnation of the bones by colloidal minerals, likely manganese hydroxids (Downs, 1958; Lucas, 2008b).

The skull of INAH-MRG 10–294922 has a maximum length of 290 mm, of which the rostrum refers to one-third and the rest to the cranium (see Table 1).

In dorsal view, the nasal shows parallel margins rostral to the orbits and is evenly transversally vaulted. The rostral nasal margin is evenly sinusoid in dorsal view, with two slight rostrolateral elevations and a depression between them. The nasal reaches one half of the entire skull length. The rostral two-thirds of the lateral margins of the nasal bones are barely visible and run parallel to each other, while the caudal third converges caudally to a rostrally open right angle (Fig. 3). The lateral surface of the cranium, between the postorbital and squamosal, is slightly concave in dorsal aspect. In lateral view, the dorsal surface of

Table 1

Xibalbaonyx microcaninus; measurements.

Skull (INAH-MRG 10–294922)	Millimeter (mm)
Alveolar length of toothrow (C1-M4)	140
Bicanine width (maximum width of muzzle across caniniform alveoli)	100
Maximum cranial width (in dorsal view; maximum horizontal distance of the postorbital constrictions, without jugals)	120
Condylobasal length (Alveolus of C1 to condyles)	290
Foramen magnum width	36
Maximum skull height	157
Alveolar length of toothrow (C1-M4)	140
C1: Mesiodistal diameter	12
C1: Crown height (right/left side)	20/21
Molariform toothrow	75
M1 mesiodistal width (lingual/right side)	27
M2 mesiodistal width (lingual/right side)	29
M3 mesiodistal width (lingual/right side)	30
M4 mesiodistal width (lingual/right side)	25
Mandible (INAH-MRG 10–294923)	
c1: crown height	11
c1: mesiodistal diameter	9
Mandibular spout (measured from rostral tip to rostral of c1)	31
Alveolar length of toothrow (m1 to m3)	65
Diastema length	28
Mandibular length	210
Maximum mandibular width (lateral tip of condylar process)	157
Maximum mandibular height; measured from the dorsal tip of the coronoid process to the ventral edge of the mandibular body	107

the cranium is convex, slightly domed, reaching its maximum height at the frontals. In dorsal aspect, the cranium is 120 mm wide between the orbits (Lucas, 2008a). The skull reaches its maximum width at the squamosal, and is there one-eighth wider than at the orbital area.

The strongly serrated frontoparietal suture is faintly visible. In dorsal view, the temporal lines arise caudal of the orbita and converge caudally, thereby running from the frontal onto the parietal, but without merging. The temporal lines become gradually prominent at their caudal fourth and begin to diverge at level with the mastoid process until they fuse with the prominent nuchal crest of the occipital (Fig. 3).

In lateral view, the dorsal surface of the rostrum is slightly convex, while its rostral and ventral walls are concave. The buccinatory fossa is located on the lateral wall of the maxilla. It is concave and bears a small ridge that begins dorsocaudally at the lateral alveolar wall of the caniniforms and terminates on the lacrimal.

The lacrimal foramen is high oval with convex and prominent rims that are convex and prominent (Fig. 2; 5). The lacrimal foramen opens rostrolaterally in a 45° angle with the maxillary wall. The jugal extends to almost one half of the skull length. The jugal has three processes. The ascending and the middle process run parallel to each other and include a 45° angle with the descending process. The ascending and descending processes are of equal length, while the middle process is only half the length of the other two. The ascending and middle processes form part of the lateral margin of the orbit. The dorsocaudally facing terminus of the ascending process end is blunt. The middle process is one third thicker than the ascending process and its end is straight and faces caudally. The descending process is as wide as the middle process. Its rostral surface is convex, while the caudal one is straight. The end of the process is pointed and faces caudoventrally.

The zygomatic process of the squamosal is twice as wide as the ascending process of the jugal. The blunt rostral end of the zygomatic process points rostrolaterally, forming an angle of 60° with the lateral wall of the squamosal. The dorsal margin of the zygomatic process runs horizontally. Its ventral margin diverges from the dorsal one caudally.

In caudal view, the nuchal crest is semi-circular and ventrally merges with the mastoid process. At its midpoint, there is a small projecting occipital protuberance of the shape of an inverted acute triangle (Fig. 5); it fuses ventrally with a superior nuchal line of the shape of an isosceles triangle. The occipital crest emerges ventral of the external occipital protuberance at the superior nuchal line; it runs vertically, terminating dorsally at the foramen magnum. In caudal view, the occipital crest is half the maximum height of the occipital and caudally pronounced. The articular facets of the occipital condyles have a rounded triangular outline in caudal view. They are strongly convex in all directions. Two small foramina are located dorsal of the foramen magnum.

In ventral view (Fig. 4), the maxilla is half the length of the skull. The rostral margins of the maxilla form a rostrally open 45° angle. At the lateral wall of the alveoli of the caniniforms, the rostrolateral walls of the maxilla are laterally bulging. The caniniforms are conical and of triangular cross-section. They are vertical and present an oval occlusal surface, of which the tip is broken. The caniniforms are short, only measuring 11 mm in length.

A diastema is present between canini- and molariforms; it reaches one third of the maxillary length and less than one fourth of the skull length. In ventral view, the distance between the lateral margins of the maxilla, level with the diastema, is half the orbital skull width and is thus the narrowest part of the skull. In this area, the lateral wall of the maxilla is concave. The caniniforms are slightly laterally set off from the row of molariforms. Their length is half the length of the maxilla and one fourth of the skull length. On the left side, all three molariform alveoli are confluent. On the right side, interdental septa and alveolar

margins of the molariforms are fragmentarily preserved (Fig. 4). Here, the apertures of all molar alveoli are oval and of approximately equal size. The alveoli of M3 and M4 are slightly larger on the buccal side than lingually. The surface of the maxilla is pierced with small foramina. Two small palatal foramina are located caudomedial to the M3.

In ventral view, the caudal half of the skull is only fragmentarily preserved. The pterygoids are narrow, ventrally enlarged. The rostral margin of the basisphenoid is convex, with an almost semi-circular outline. The suture between basisphenoid and basioccipital runs almost horizontally. The auditory region is laterally compressed at the caudalmost fourth of the skull, adjacent to the caudoventral margin of the zygomatic process of the squamosal. Most of the foramina adjacent to the tympanic are insufficiently preserved for a detailed description. In ventral view, the ectotympanic is medially convex. The rostral half of the ectotympanic ring is bulge-like and prominent, located caudally adjacent to the glenoid plane. The aperture of the external auditory meatus opens ventrolaterally. The ectotympanic reaches almost one eighth of the skull length, as the stylohyal fossa and the jugular foramen. The rostral eighth of the stylohyal fossa is hidden by the caudal half of the ectotympanic bulge. The stylohyal fossa is circular and its caudolateral margin is slightly elevated. The jugular foramen is rounded and of similar size and outline as the stylohyal fossa.

In ventral view, the mastoid process is convex and marks the widest part of the skull.

Mandible (Fig. 6)

The mandible INAH-MRG 10–294923 has a maximum length of 225 mm and a maximum height at the coronoid process of 115 mm.

The symphyseal spout, which is located rostral to the caniniforms, reaches a length of less than one eighth of the entire mandible length. In dorsal view, the lateral margins of the symphyseal spout form a caudally open 45° angle. The symphyseal spout is rostrally pointed in both dorsal and lateral views (Fig. 6). In lateral view, the dorsal margin of the mandibular spout runs horizontally, forming a caudally open 45° angle with its rostroventral margin. The rostroventral margin of the spout is straight and runs diagonal. A circular mental foramen is located on each lateral side of the mandible between the alveolar bulge of the caniniforms and the ventral wall of the symphyseal spout.

The lower caniniforms are conical, triangular in cross-section, and almost completely abraded, with a height of only 10 mm. Their occlusal surface is oval to triangular and distally pointed. The tip of the caniniforms are broken and their occlusal surface has small knobs resulting from breakage. The lower caniniforms are slightly smaller than m3 and are therefore the smallest teeth of mandible.

The length of the diastema, between canini- and molariforms, is similar to that of the symphyseal spout, reaching one-eighth of the entire mandible length. In dorsal view, the lateral wall of the mandible is concave at the diastema and its dorsal surface is pierced with eight small foramina on each side. In lateral view, the dorsal surface of the diastema is convex.

In dorsal view, the alveoli of the molariform toothrows are confluent, and interdental septa are partially missing. The alveolus of m1 is the biggest in the lower jaw toothrow, twice as large as alveoli of the caniniforms and the alveolus of m3. In dorsal view, the alveolus of m1 is oval, buccolingually as wide as mediodistally. The alveolus of m1 is lingually slightly convex, while its mesiobuccal margin is straight. The alveolus of m2 adjoins m1 and is one eighth smaller than the one of m1. In dorsal view, the alveolus of m2 is quadrangular and shows a rounded margin. The alveolus of m3 is the smallest of the lower toothrow alveoli. In dorsal view, it is elliptical in shape and buccolingually one third narrower than mesiodistally.

The posterior external opening of the mandibular canal opens dorsolaterally. It is located ventrolateral to m3 and its length equals that of
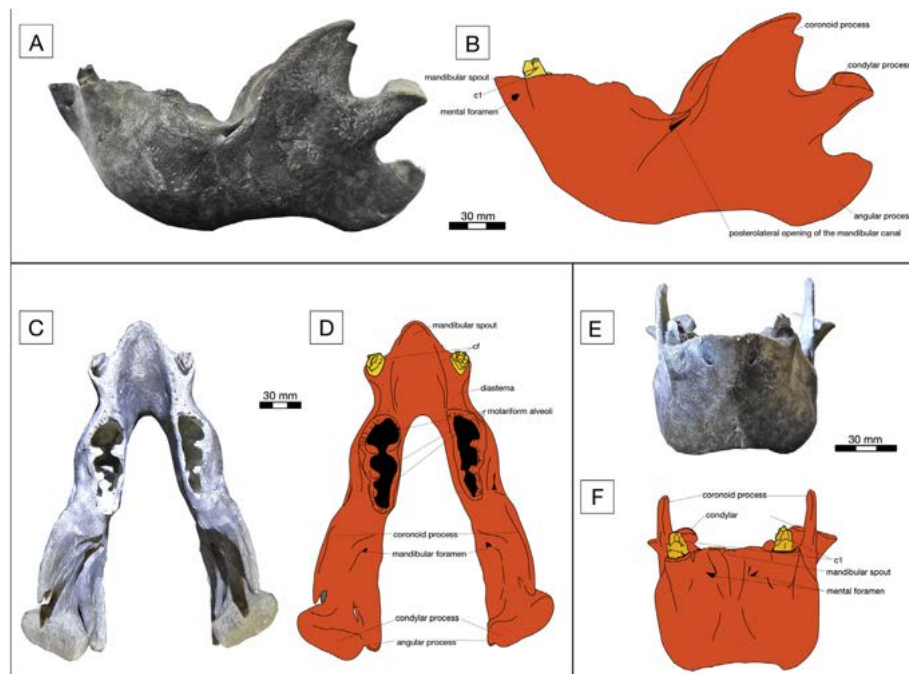
Fig. 6. *Xibalbaonyx microcaninus* (INAH MRG 10–294923) in lateral (A and B), dorsal (C and D) and rostral view (E and F). A, C, E) Photographs and B, D, F) Interpretive line drawings.

the alveoli of m3. In lateral view, the posterior external opening of the mandibular canal is located at the base of the ascending ramus of the coronoid process (Fig. 6). The rostral surface of the ascending ramus of the coronoid process is semi-circular in outline. The coronoid process curves caudally and tapers to a tip, which points caudally. The caudal margin of the process runs vertically. The adjacent condylar process is located at level with the caniniforms. In dorsal view, the condylar processes are hourglass-shaped, while in lateral view the end of each process is blunt and its lateral margins run longitudinally subparallel to each other. The caudal margin of the condylar process forms a caudally open 45° angle with the dorsal margin of the angular process of the mandible. The dorsal surface of the angular process is slightly concave, while its caudal and ventral surfaces are convex. The caudal end of the mandibular angle is blunt, almost flat, and points dorsocaudally.

3.1. Comparative osteology

3.1.1. Assignment to the genus Xibalbaonyx

The Guadalajara ground sloth (MRG 10–294922 and MRG 10–294923) strongly resembles *Xibalbaonyx oviceps* (Fig. 7) from the El Zapote cenote in the federal state of Quintana Roo in the following cranial aspects.

Xibalbaonyx microcaninus is characterized by a nasional impression in the middle of the nasals, at the height of the lacrimal and jugal constriction, leading to a rostrodorsally open angle between rostrum and postorbital cranium (Stinnesbeck et al., 2017a). However, this angle is approximately 20° wider in the Guadalajara individual than in *X. oviceps*, due to the more flattened dorsal skull surface. The genus *Xibalbaonyx* is further defined by regularly convex frontals and parietals, of which the parietals are caudally elongated resulting, in a coverage of the almost vertically running occipital in dorsal view. The skull is smooth without a sagittal crest (Stinnesbeck et al., 2017a), all features shared by the Guadalajara specimen INAH MRG 10–294922 and *Xibalbaonyx oviceps*. In dorsal view, the temporal lines converge on the skull roof but do not contact each other, another characteristic feature of the genus *Xibalbaonyx* (Fig. 7). In the Guadalajara specimen, the jugal is gracile and separated from the zygomatic process of the

squamosal, exhibiting a narrow, dorsocaudally inclined ascending process, comparable to *Xibalbaonyx oviceps*. Similar to this latter species, the mandible of the Guadalajara specimen (MRG 10–294923) has a strong constriction of both the horizontal and ascending ramus of the mandible. The mandibular spout is short, in both taxa reaching less than 20% of the maximum mandibular length (MML), but reaches at least the same length as the diastema between canini- and molariforms. Furthermore, the mandibles are extremely deep in both taxa, exhibiting > 27% of the MML. These characters are diagnostic and allow us to assign the Guadalajara specimen INAH MRG 10–294922 to the genus *Xibalbaonyx*.

3.1.2. Xibalbaonyx microcaninus versus X. oviceps

Xibalbaonyx microcaninus (INAH MRG 10–294922 and 10–294923) differs from *Xibalbaonyx oviceps* (INAH Za2014-01/CPC-1875, INAH Za2014-05/CPC-1879; Fig. 7) in the small, conical caniniforms. The temporal lines and nuchal crest are more pronounced in *Xibalbaonyx microcaninus* than in the Yucatán specimen, although this difference could be due to the immaturity of the latter (Stinnesbeck et al., 2017a). However, in *X. microcaninus* the temporal lines converge caudally but fuse with the nuchal crest, while they join with the dorsal margin of the zygomatic process of the squamosal in *X. oviceps* running parallel to the nuchal crest.

In ventral view, the stylohyal fossa is circular in *X. microcaninus* but oval in *X. oviceps*. Also, the glenoid fossa of the squamosal is located ventral to the external auditory meatus in *X. microcaninus*, in contrast to *X. oviceps* where they are at the same level.

The pterygoid flanges are semicircular in outline, ventrocaudally elongated and thin in *X. microcaninus*, while the ones in *X. oviceps* are inflated at their base (Fig. 7; Stinnesbeck et al., 2017a).

These cranial and mandibular features thus suggest that the Guadalajara individual (INAH MRG-10-294922 and MRG-10-294923) belongs to a species different from *X. oviceps*. It was a medium-sized ground sloth which only reached two-thirds to half the size of *X. oviceps* (Fig. 7).
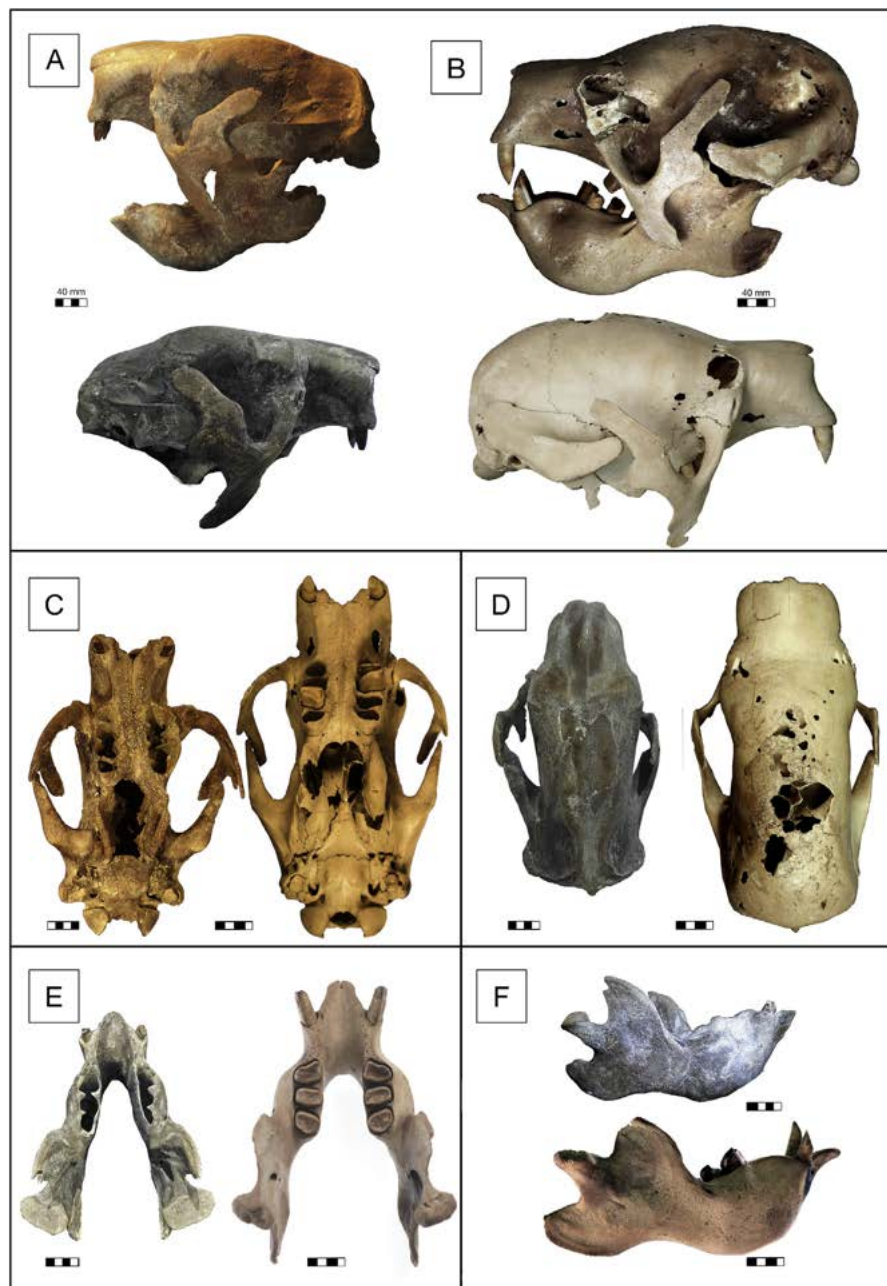
Fig. 7. Photographs of *Xibalbaonyx microcaninus* (INAH MRG 10–294922 and MRG 10–294923) and *Xibalbaonyx oviceps*. A) *X. microcaninus* and B) *X. oviceps* in lateral view. C) Skulls in ventral and D) dorsal view. *X. microcaninus* and *X. oviceps* mandibles in E) dorsal and F) lateral view.

3.1.3. Comparison with North-, Central- and South American Megalonychidae

Skull: The general morphologies of *Xibalbaonyx microcaninus* and *X. oviceps* are similar to the Late Pleistocene *Nohochichak xibalbahkah* McDonald et al. (2017; INAH DP5832) from the Hoyo Negro sinkhole near Tulúm on the Yucatán Peninsula of Mexico. The fragmentary remains from the Hoyo Negro sinkhole come from a large ground sloth, similar in size to *X. oviceps* from the El Zapote cenote and therefore one-third to half the size larger than *X. microcaninus*. According to McDonald et al. (2017), there is a strong postorbital process of the frontal in *N. xibalbahkah*, which is absent in *X. oviceps* and rudimentary in *X. microcaninus*. This could be due to immaturity of the *X. oviceps* individual, which then, however would have grown significantly larger than *N. xibalbahkah* (Stinnesbeck et al., 2017a). In dorsal view, the rostrolateral margin of the nasal is straight, but concave at the midline

in *Nohochichak xibalbahkah* and in *X. microcaninus*; the rostral margin of the nasals is convex at midline in *X. oviceps*, a feature there described as rhinium (Stinnesbeck et al., 2017a). The infraorbital foramen is located at the narrow, slotted column between maxilla and lacrimal, at the height of the ventral margin of the lacrimal foramen in *X. microcaninus*, but ventral to the lacrimal, at the height of the dorsal margin of the jugal to the maxilla in *X. oviceps* and *Nohochichak xibalbahkah*. The lacrimal foramen in *X. microcaninus* opens rostrolaterally. The angle between the lacrimal foramen and the maxilla is therefore between the particularly rostral orientation of the aperture in *X. oviceps*, and in lateral alignment in *Nohochichak xibalbahkah*. The jugal is of similar shape in all three individuals: The ascending process of the jugal is elongated and caudally inclined, a characteristic feature in *X. microcaninus*, but it is also present in the El Zapote and Hoyo Negro individuals. However, the ascending process of the jugal is twice the

length of the descending process in *X. oviceps*, but is only one-fourth longer in *Nohochichak xibalbahkah* and of equal length in *X. microcaninus*. The ventral margin of the descending process is rounded in *Nohochichak xibalbahkah* (McDonald et al., 2017), and thus differs from the tapering end of the process in both *X. microcaninus* and *X. oviceps*. In *X. oviceps* the maxillary foramen is located ventral, in the gap between the jugal and the maxilla, dorsal to m2 and therefore overhung by the jugal. In *Nohochichak xibalbahkah* this aperture is situated caudal, directly adjacent to the jugal, dorsal to the molariforms, but between m1 and m2 and thus visible in lateral view. In *X. microcaninus*, the position of the maxillary foramen is also caudal to the jugal and dorsal to the molariforms, as in *N. xibalbahkah*, but level with m2 and m3. McDonald, Chatters & Gaudin (2017) describe the rostrum of *Nohochichak* as narrower than the braincase, with a pronounced angle between nasals and frontals, a feature described as a nasional impression for *X. oviceps* (Stinnesbeck et al., 2017a). Which is also present in *X. microcaninus*. The impression, in *X. oviceps* and *Nohochichak* (McDonald et al., 2017) from the Yucatán Peninsula, is reminiscent to the South American *Megistonyx oreobios* (McDonald et al., 2013). Nevertheless, the depth of the nasional impression is variable. It is more pronounced in *X. oviceps* than in *N. xibalbahkah* and *X. microcaninus*. However, in *Australonyx aquae* (De Iuliis, Pujos & Cartelle, 2009) from Brazil, the rostrum, slopes rostrally (De Iuliis, Cartelle & Pujos, 2016) in lateral view. In the latter, the rostral slope is therefore convex and not concave as in *Xibalbaonyx*. It is further located between nasals and frontals and not a midline of the nasal bones itself as in *Xibalbaonyx* or *Nohochichak*. A nasional impression is absent in *M. jeffersonii* (McDonald, 1977), although some individuals show a shallow impression. In *Xibalbaonyx,* the nasional impression is at the height of the lacrimal and jugal constriction and therefore more rostral than in *M. jeffersonii* and *M. oreobios* (McDonald et al., 2013), and more caudal than in *Ahytherium aureum* (Cartelle et al., 2008) from Brazil.

In *Xibalbaonyx*, the rostrum is parallel-sided in dorsal view, and not laterally widened as in *Megalonyx jeffersonii* or *Ahytherium aureum* (McDonald, 1977; Cartelle et al., 2008; De Iuliis, Pujos & Cartelle, 2009). *M. jeffersonii* is characterized by a broad and deep skull, with a closed zygomatic arch (McDonald, 1977). In the Guadalajara specimen, the skull is elongate and slender and the zygomatic arch is open. In dorsal view, the skull of *M. jeffersonii* is cylindrical (McDonald, 1977) including rostrum and braincase, while in *X. microcaninus* the braincase laterally one eighth wider than the rostrum. In lateral view, the skull roof is nearly horizontal in *M. jeffersonii*, while it is domed in *X. microcaninus*. The presence of a sagittal crest is a common character in many Megalonychidae, such as *M. jeffersonii* (Hirschfeld and Webb, 1968; McDonald, 1977), *M. oreobios* (McDonald et al., 2013), *A. aquae* and *A. aureum* (Cartelle et al., 2008; De Iuliis, Pujos & Cartelle, 2009), but is absent in *Xibalbaonyx*, including *X. microcaninus*. In *M. jeffersonii* the temporal lines converge caudally and merge to a low sagittal crest along the midline of the skull (Leidy, 1855), whereas in *X. microcaninus*, the temporal lines, although converging caudally, remain separated and only merge with the nuchal crest. The temporal lines of *Pliometanastes* also curve caudally, without meeting each other as in *Xibalbaonyx microcaninus*; they merge with the nuchal crest, but the temporal lines in *Xibalbaonyx microcaninus* are twice as far apart from each other (Fig. 3). Furthermore, the surface of the occipital bone lateral to the occipital crest is concave in *Pliometanastes* (Hirschfeld and Webb, 1968) but convex in *Xibalbaonyx microcaninus*.

Dentition: The caniniforms are diagnostic in *X. microcaninus*. They differ from those of all other megalonychids, including *X. oviceps*, the sloths from the West Indies, *Australonyx aquae, Ahytherium aureum, Pliometanastes* and especially *Megalonyx jeffersonii* (Hirschfeld and Webb, 1968; White and MacPhee, 2001; Cartelle et al., 2008; De Iuliis, Pujos & Cartelle, 2009). Although no upper and lower caniniforms are preserved in *Nohochichak xibalbahkah*, McDonald et al. (2017) assume that these teeth must have been triangular in cross-section with rounded margins. If so, they would have been similar to *X. oviceps* and

thus of equal size as the molariforms. However, the caniniforms of *X. microcaninus* are conical, with a vertical occlusal surface and small. The lower caniniforms are the smallest teeth of the mandible.

Mandible: The mandible in *X. microcaninus* is compact and massive, with a short mandibular spout, a strong constriction between the horizontal and ascending ramus. Such a morphology is also known from other Megalonychidae, such as *X. oviceps, N. xibalbahkah, Megalonyx jeffersonii,* and *Meizonyx* from El Salvador (Hirschfeld and Webb, 1968; Webb and Perrigo, 1985). However, the length of the mandibular spout in *X. microcaninus* equals that of the diastema between canini- and molariforms, while in *M. jeffersonii and Meizonyx,* the mandibular spout is shorter. In *Pliometanastes* (Hirschfeld and Webb, 1968) the mandibular spout is twice the length as in *Xibalbaonyx microcaninus.* The lateral margins of the mandibular spout run parallel to each other in *Pliometanastes* and its rostral terminus is rounded (Hirschfeld and Webb, 1968), while that in *X. microcaninus* is shorter, pointed, with margins that are converging rostrally. The mandibular spout is triangular in dorsal view and short in *Xibalbaonyx* and *Nohochichak*, but pointed in *N. xibalbahkah* (McDonald et al., 2017) and *X. microcaninus,* while rounded in *X. oviceps* (Stinnesbeck et al., 2017a). In *X. oviceps*, a rostral notch is present at the mandibular symphysis (Stinnesbeck et al., 2017a), while this notch, or keel, is absent in both *Nohochichak xibalbahkah* (McDonald et al., 2017) and *X. microcaninus*. In dorsal view, the dorsal surface of the mandibular spout is concave or trough-shaped in *X. microcaninus* and *Nohochichak xibalbahkah* (McDonald et al., 2017). In lateral view, the dorsal and ventral surfaces of the mandibular spout are flat in *X. microcaninus* and *Nohochichak xibalbahkah*, but the dorsal surface is convex, while the ventral surface of the mandibular spout is concave in *X. oviceps*. The latter exhibits two mental foramina on both sides of the mandibular spout (Stinnesbeck et al., 2017a), as well as two mandibular foramina on the medial side of the mandible. The presence of these foramina suggests a branching of the mandibular nerves in *X. oviceps*. There is only one mental and mandibular foramen in *X. microcaninus,* as in *Nohochichak* (McDonald et al., 2017). In dorsal view, the caudal margin of the mandibular symphysis lies level with the rostral margin of the m1 in *N. xibalbahkah* (McDonald et al., 2017) and in *X. microcaninus*, whereas in *X. oviceps* the caudal margin of the mandibular symphysis terminates between m1 and m2.

In the three taxa, the shape of the mandible differs in dorsal view. While the mandibular rami diverge gradually from the symphysis to the angular process in *X. microcaninus* and in *N. xibalbahkah* at an angle of 45°, the mandibular rami in *X. oviceps* run parallel to each other. In lateral view, the rostrodorsal surface of the ascending ramus of the coronoid process is flat in *N. xibalbahkah,* running oblique to the mandibular body. This feature differs from the convex surface of the ascending ramus in *X. microcaninus* and *X. oviceps*. The dorsal margin of the coronoid process of the mandible is evenly rounded in *N. xibalbahkah* and *X. oviceps*, whereas it is hooked-shaped with a deep caudal recess in *X. microcaninus*. In *N. xibalbahkah*, the posterior aperture of the mandibular canal is located on the lingual side of the mandibular rami at the base of the coronoid process (McDonald et al., 2017). In *X. microcaninus* and *X. oviceps,* the posterior external opening of the mandibular canal opens dorsolaterally at the base of the ascending ramus of the mandibular rami. It is visible in lateral view.

In lateral view, the articular surface of the head of the condylar process is flat and almost horizontal in *N. xibalbahkah*, but convex and dorsocaudally inclined in *X. oviceps* and *X. microcaninus*. The subcondylar area of the condylar process is concave in lateral view in *X. oviceps* and straight in both *X. microcaninus* and *N. xibalbahkah*. The angular process of the mandible has a similar overall shape in all three taxa, but is twice as long in *N. xibalbahkah* as in *X. microcaninus* and *X. oviceps*.

According to these similarities and differences in diagnostic features that are not aligned with ontogenetic changes, we here favor the existence of two coeval Late Pleistocene megalonychid taxa on the Yucatán Peninsula, which belong to a single genus.

Meizonyx salvadorensis from El Salvador is based on a fragmented mandibular ramus (Webb and Perrigo, 1985) of a large ground sloth, similar in size, or even larger than *Megalonyx*, and therefore one third to twice as large as *X. microcaninus*. Although the symphysis is fragmented in *Meizonyx*, Webb & Perrigo (1985) describe the mandibular spout as rudimentary, therefore shorter than in *Megalonyx*, or even completely absent (Webb and Perrigo, 1985). It is thus even shorter than the mandibular spout of *X. microcaninus*. In the latter, the caudal margin of the symphysis terminates rostral to m1 (Webb and Perrigo, 1985), similar to *X. microcaninus* and *N. xibalbahkah* (McDonald et al., 2017), but different from *X. oviceps* (Stinnesbeck et al., 2017a). In *Meizonyx*, the caniniforms are in line with the molariform tooth row (Webb and Perrigo, 1985), a feature shared with the sloths from the Yucatán Peninsula, but the caniniforms are slightly laterally exposed in *X. microcaninus*. In *Meizonyx* the caniniforms are triangular in cross-section, straight and pointed (Webb and Perrigo, 1985), and thus similar to *Pliometanastes* and *Xibalbaonyx*, but in *X. microcaninus* the lower caniniforms are conical and the smallest teeth of the row, different to *Meizonyx* (Webb and Perrigo, 1985). In lateral view, the coronoid and condylar processes are at nearly the same level in *Meizonyx* (Webb and Perrigo, 1985), different to *Xibalbaonyx* species where the coronoid process is higher than the condylar process. Therefore, the angle between coronoid and condylar process is narrower in *Meizonyx*. The condylar process reaches < 10% of the MML in *Meizonyx*, while this process is longer in all *Xibalbaonyx* species. Also, the head of the condyle is medially convex, while laterally concave in *X. microcaninus* and *X. oviceps*. This differs from *Meizonyx*, in which the head of the process forms a confluent surface. In lateral view, the temporal fossa of *Meizonyx* is deep (Webb and Perrigo, 1985), but shallow in *X. microcaninus* and *X. oviceps*. According to Webb and Perrigo (1985) the concavity of the ventral surface of the mandible is shallower in *Meizonyx* than in *Megalonyx*, and therefore also shallower than in *X. microcaninus* and *X. oviceps*. The constriction between the horizontal and ascending ramus of the mandible is therefore different in the two genera, consisting in a horizontally lying hourglass-shape in *Xibalbaonyx*. In *Meizonyx* the dorsal surface of the horizontal ramus of the mandible is at the same level as the dorsal surface of the condylar process, while in *Xibalbaonyx* the condylar process is higher than the dorsal surface of the horizontal ramus of the mandible. The angular process of the mandible is medially inclined and shorter than the condylar process in *Meizonyx* (Webb and Perrigo, 1985), which is not the case in *Xibalbaonyx*, in which the angular process points caudally and its caudal terminus reaches the maximum mandibular length. Although, the only preserved specimen of *Meizonyx* is based on a fragmentary mandibular ramus, the osteological differences support a generic differentiation.

Zacatzontli tecolotlanensis (McDonald and Carranza-Castañeda, 2017) was collected from the Jal-Teco 8 Santa Maria locality in the federal state of Jalisco, and is known by a partial mandible (MPGJ 3534) with a complete left ramus including the caniniforms. The stratigraphic unit of the mandible was $^{40}Ar/^{39}Ar$ dated to 4.95 ± 0.02 Ma (McDonald and Carranza-Castañeda, 2017). The *Zacatzontli* mandible (MPGJ 3534) is thus early Pliocene in age, or possibly even late Miocene as suggested by the authors (McDonald and Carranza-Castañeda, 2017). However, *Xibalbaonyx microcaninus* dates to the Late Pleistocene (Lucas, 2008a). According to the maximum length of the mandible of 120 mm, *Z. tecolotlanensis* was a small ground sloth (McDonald and Carranza-Castañeda, 2017) that only reached half the size of *X. microcaninus*. The mandibular spout is short, reaching approximately 21% of the maximum mandibular length. In *X. microcaninus*, the spout is even shorter, only reaching 15% of the maximum mandibular length. It is triangular and rostrally pointed in dorsal view (McDonald and Carranza-Castañeda, 2017), similar to that of *Megalonyx* and *X. microcaninus*. The caudal margin of the symphysis ends at about midpoint of the diastema and rostral to the m1, which is also similar to *X. microcaninus*. Different from the latter, there is a middle keel on the rostral half of the spout (McDonald and Carranza-Castañeda, 2017). In *Z.*

tecolotlanensis, there is a shallow concavity on either side of the keel, in which the single mental foramen is located. In *X. microcaninus* this foramen is located on the rostral surface of the spout, closer to median plane. The lower caniniforms are triangular in cross-section, with a prominent carina on the distal margin of the tooth, while the lower caniniforms are conical in *X. microcaninus* with rounded occlusal surfaces. The caniniform of *Zacatzontli* is slightly displaced laterally, so that its lingual margin lies in the same plane as the midline of the molarifom series (McDonald and Carranza-Castañeda, 2017), similar to *X. microcaninus*. In *Zacatzontli,* the diastema reaches 29% of the length of the molariform tooth-row (McDonald and Carranza-Castañeda, 2017) and is thus similarly long as in *X. microcaninus* (30%).

In *Zacatzontli,* all lower molariforms are similar in size and only slightly larger than the caniniform (McDonald and Carranza-Castañeda, 2017), whereas in *X. microcaninus* m1 is the largest and the lower caniniforms the smallest of all lower teeth. In lateral view, the dorsal surface of the horizontal ramus of the mandible is straight in *Zacatzontli*, while its surface is convex in *X. microcaninus*. The outline of the molariform alveoli of *X. microcaninus* are not as well preserved as in *Zacatzontli,* but the alveoli in *Zacatzontli* are oval (McDonald and Carranza-Castañeda, 2017), while those in *X. microcaninus* are trapezoidal (m2) to elliptical (m3) in outline. In lateral view, the base of the ascending ramus in *Zacatzontli* is at the midpoint of m3. In consequence, the caudal half of the tooth is not visible in lateral view (McDonald and Carranza-Castañeda, 2017), similar as in *X. microcaninus*. Furthermore, as in *X. microcaninus,* the posterior external opening of the mandibular canal opens on the lateral face on the base of the horizontal ramus of the mandible. In dorsal view, the lower molariform tooth-rows and the caudal halves of the mandibular rami run parallel to each other in *Zacatzontli*, while tooth rows and rami diverge caudally in *X. microcaninus*, giving the mandible a triangular outline.

X. microcaninus and *Z. tecolotlanensis* are thus clearly distinguished based on mandibular characters, but there are also numerous similar features indicating a close relationship. However, the stratigraphic gap of 4.9 million years supports the presence of two distinct genera.

4. Discussion

Xibalbaonyx microcaninus exhibits a masticatory apparatus that differs from that of *X. oviceps,* suggesting a functional and structural differentiation likely related to diet.

In *X. microcaninus* the temporal lines merge with the nuchal crest, and the temporal lines are more prominent than those of *X. oviceps* and the coronoid process of the mandible is hook-shaped. This suggests a more powerful m. temporalis compared with that of *X. oviceps,* and a likely retraction movement of the mandible at the end of the occlusion phase. Even though, thickness and length of the m. temporalis along the temporal lines must have been similarly in both *Xibalbaonyx* taxa and thus weak when compared to megalonychids that poses a sagittal crest, e.g. *Megalonyx jeffersonii* (Hirschfeld and Webb, 1968; McDonald, 1977), *Ahytherium aureum* (Cartelle et al., 2008), *Australonyx aquae* (De Iuliis, Pujos & Cartelle, 2009), *Megistonyx oreobios* (McDonald et al., 2013), and markedly, all sloths of the West Indies (White and MacPhee, 2001). The presence of a sagittal crest provides evidence for a powerful m. temporalis, which would have enabled the animals to chew tough food. The presence of a masticatory apparatus suitable for soft vegetation strongly suggests a generic differentiation between *Xibalbaonyx* and other Megalonychidae.

The pterygoids are ventrally elongated in both, *X. microcaninus* and *X. oviceps*, but inflated only in the latter one. The elongation serves to connect the m. pterygoideus medialis and m. pterygoideus lateralis with the condylar and angular processes of the mandible. It thus allows for the m. masseter to expand through the wide buccinatory fossa to the jugal. These muscles allow for the closure as well as lateral and longitudinal movements of the jaw and thus ensure the crushing of food. Such chewing movements are reflected, in *X. oviceps,* in the occlusal

surface of the molariforms. In both *X oviceps* and *X. microcaninus*, the m. masseter plays the bigger role in mastication than the m. temporalis. Therefore, both taxa applied a mediolateral grinding strategy for soft vegetation with a small bite force. The caniniforms are relatively small in both taxa, when compared with their molariforms and with caniniforms of other megalonychids, and presented a small interlock. Therefore, their role in the masticatory apparatus was minor. The morphological and functional differences of the caniniforms as well as the different spout size relative to the mandibular length suggest that *X. microcaninus* and *X. oviceps* differed from other megalonychids in the style of occlusion and thus food sources.

As feeding strategies are correlated with the environment and the resources, the morphological differences of the masticatory apparatus between *X. microcaninus* and *X. oviceps* must be species-specific, because of their allopatry and the inhabitance of different habitats with respect to vegetation. Even though Megalonychidae are considered as browsers (McDonald et al., 2017), the paleoenviromental conditions in the Guadalajara area must have been markedly different from those on the Yucatán Peninsula. The Guadalajara basin, which is surrounded by huge volcanic mountain chains, exhibited gallery forests with lakes and wide river systems. Evidence comes from the paleolakes of the area, among them Lake Chapala, which was twice the size than today and was connected to other lakes in Jalisco. The abundant and diverse fossil assemblage from the area includes elephants (*Mammuthus* sp., *Cuvieronius* sp., *Stegomastodon* sp.), capybaras (*Neochoerus* sp.), glyptodontids (*Glyptotherium* sp.), deers (*Odocoileus* sp., *Cervus* sp.), horses (*Equus* sp.), tapirs (*Tapirus* sp.), camels (*Hemiauchenia* sp., *Camelops* sp.) and several members of North American ground sloths (*Eremotherium* sp., *Megalonyx* sp., *Paramylodon* sp., *Nothrotheriops* sp.). The abundance of *Eremotherium laurillardi* (Schreiber, 2004; Lucas, 2008a; b; Lucas et al., 2011) in the faunal assemblage suggests a rich arboreal vegetation.

On the other side, the low latest Pleistocene sea level, combined with increased limestone karstification, led to dry surface and edaphic desert conditions on the Yucatán Peninsula, with xeric shrub vegetation and reduced surface water availability. Fossil evidence for these environmental conditions comes from the wide-spread cave system of Quintana Roo and Yucatán, and includes numerous remains of horses (*Equus* sp.), elephants (*Cuvieronius* sp.), lamas (*Hemiauchenia* sp.), tapirs (*Tapirus* sp.), peccaries (*Muknalia minima*) and ground sloths (*Nothrotheriops shastensis*, *Xibalbaonyx oviceps*; González et al., 2008, 2013, Stinnesbeck et al., 2017a,b). The masticatory apparatus identified in *X. oviceps* suggests the presence of a strong m. masseter for the mediolateral and longitudinal movements of the masticating mandible, as in *X. microcaninus*. Different from this latter taxon, however, a highly flexible tongue is suggested based on the shape of the mandibular spout. *X. oviceps* must therefore have been a more selective feeder, which probably used the tongue to pick up fruits or leaves from xeric plants. A higher blood circulation rate in the rostral part of the mandible of *X. oviceps* is also supported by the two mental and mandibular foramina.

In both taxa, the nuchal and occipital crests are prominent, suggesting well-developed m. rectus capitis, m. trapezius and m. semispinalis capitis.

The anatomical differences strongly support an allopatric specification of the genus *Xibalbaonyx* with respect to the vegetation, which differed between the Yucatán Peninsula and the Guadalajara basin. Even though, the Guadalajara individual shares a mixture of anatomical features of both megalonychid ground sloths from the Yucatán Peninsula. The morphological differences among the two *Xibalbaonyx* taxa from Guadalajara and El Zapote, Quintana Roo, and the Hoyo Negro ground sloth, could eventually be explained by the assumption of an extraordinary intraspecific variability within a single species and an evolutionary speeding, as all three are Late Pleistocene and approximately coeval species. *N. xibalbahkah* and *X. oviceps* even shared the same habitat on the Yucatán Peninsula. Morphological variation within this extinct population of Mexican ground sloths could then result from

diagenetic deformation, pathology, ontogenetic variation, or sexual dimorphism (McDonald et al., 2004; Prothero and Raymond, 2008). While the cranial and mandibular biometry suggests that both Quintana Roo species (Hoyo Negro and El Zapote) were of similar size, the Guadalajara individual was about one third smaller, which is here interpreted as species differentiation. Also, the absence of a sagittal crest is interpreted as generic feature of the genus *Xibalbaonyx*, and not as sexual dimorphism as in Scelidotheriinae (Miño-Boilini and Zurita, 2015). However, the differences in overall robustness in *X. oviceps* and *Nohochichak* could also result from different ontogenetic stages, especially because *X. oviceps* was referred to a subadult specimen (Stinnesbeck et al., 2017a), and/or sexual dimorphism. For instance, the postorbital process, which is absent in *X. oviceps*, but present in *X. microcaninus* and *Nohochichak*, marks the rostral extension of the m. temporalis, which must have been weak in *Xibalbaonyx oviceps*, but could evolve during adult stadium. The Hoyo Negro individual, on the other side, represents an adult individual, which explains why the postorbital process is more pronounced, as also cranial and mandibular features (McDonald et al., 2017).

Although rare among ground sloths, sexual dimorphism has been reported for *Scelidotheriinae* (Miño-Boilini and Zurita, 2015), *Eremotherium laurillardi* (Cartelle and Bohorquez, 1982; Cartelle and De Iuliis, 1995, 2006; Prothero and Raymond, 2008) and *Paramylodon harlani* (McDonald et al., 2004). In the latter, differences in the size and shape of the caniniforms have been interpreted by McDonald et al. (2004) as related to sexual dimorphism. In other sloths, however, and even in ground sloth species with an excellent and abundant fossil record such as *Nothrotheriops shastensis*, and the extant *Choloepus*, no sexual dimorphism has yet been identified (McDonald et al., 2004; Prothero and Raymond, 2008). Clearly, the question of sexual dimorphism of the two ground sloths from Quintana Roo, the Hoyo Negro and the El Zapote individuals, can only be resolved by a future larger sample size. To date, only the two holotype individuals are known, which even represent different ontogenetic stages.

The shape of the rostrodorsal margin of the ascending ramus is significantly more gracile in *Xibalbaonyx*. The position of the mandibular canal is, however, identical, contrary to the interpretation of McDonald et al. (2017). These authors suggested the median location of the mandibular canal to be a diagnostic phylogenetic character and major difference to *Xibalbaonyx oviceps* (Fig. 8; see below). Here we suggest the location of the foramen to be identical in both *Xibalbaonyx* and *Nohochichak* and thus not to be a diagnostic character. Rather, differences in the thickening of the rostrodorsal margin of the ascending ramus could reflect two different species within the same genus, or intraspecific range, e.g. sexual dimorphism or even a pathological feature, but this cannot be decided here.

Even though the skull and mandible of the Guadalajara *X. microcaninus* present more similarities with the Hoyo Negro individual than the one from El Zapote, the phylogenetic analysis (see below) suggests a closer relationship with *X. oviceps*, although the latter may result from the fragmented nature of the *Nohochichak* cranium. We here favor the existence of two coeval Late Pleistocene megalonychid taxa from the Yucatán Peninsula conforming a single genus. In this case, the Hoyo Negro specimen would have to be assigned to the genus *Xibalbaonyx* (junior synonym *Nohochichak*). Nevertheless, we are aware that a larger and statistically valid sample size is needed to evaluate the question of inter- or intraspecific differentiation, which is not available to date. We therefore maintain the generic assignation of the Hoyo Negro to *Nohochichak* until a larger reference collection is available.

4.1. Phylogenetic analysis

The preliminary phylogenetic analysis presented here is based on 80 cranial and mandibular character states (Fig. 8) of 18 taxa of North-, Central- and South American megalonychid ground sloths. The analysis yields two parsimony trees (tree length (TL) = 282, consistency index
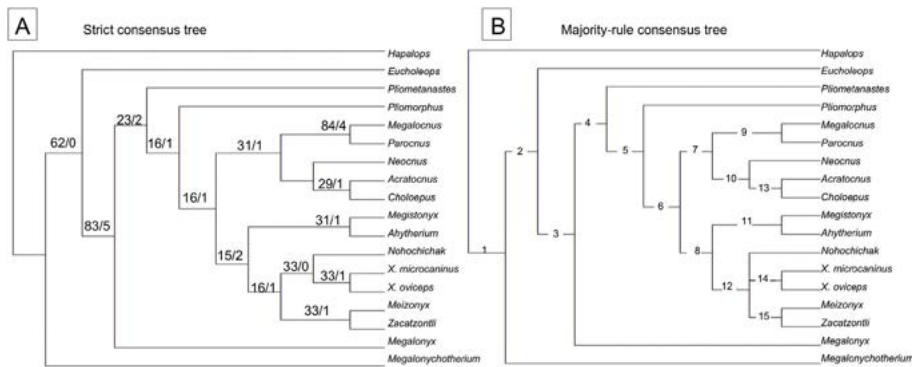
Fig. 8. A) Strict consensus tree and B) a majority-rule consensus tree of the ground sloth family Megalonychidae, to assess the positions of *Xibalbaonyx microcaninus* nov. spec. (INAH MRG 10–294922 and MRG 10–294923) and the recently described *Xibalbaonyx oviceps* (Stinnesbeck et al., 2017a). The tree is based on 80 cranial and mandibular features. For the analysis, the genus *Xibalbaonyx* was included in the database published in Gaudin (2004), McDonald et al. (2013) and McDonald et al. (2017).

(CI) = 0.3865, retention index (RI) = 0.4820).

Megalonychotherium is here regarded to be a sister taxon to all other Megalonychidae, merging with *Eucholeops* in the node. The bootstrap value is extremely low, with a bootstrap value of 62, uniting all non-Santacrucian Megalonychidae. All non-Santacrucian Megalonychidae fall within a bootstramp value of 83 and a Bremer value of 5.

Megalonyx is a more basal taxon, uniting the Miocene *Pliometanastes* and *Pliomorphus* with all Mexican, especially Pleistocene to recent sloths. However, the clade is only weakly supported by a bootstrap value of 23 and a Bremer value of 2. The node uniting all sloths from the West Indies, the Mexican ground sloths, including *Zacatzontli,* and the Pleistocene sloths from Central- and South American is even weaker with a bootstrap value of only 16 and a Bremer support of 1.

The Megalocninae *Megalocnus* and *Parocnus* (White and MacPhee, 2001) have the strongest node on the tree with a bootstrap value of 84. *Megalocnus* and *Parocnus* are a sister-group to *Neocnus* and the subclade of *Acratocnus* and *Choloepus*. The present analysis thereby confirms the close relationship of these megalonychids from the West Indies with the extant tree sloth *Choloepus* (White and MacPhee, 2001; Gaudin, 2004).

The strict consensus tree (Fig. 8) also reveals the positions of the South American *Ahytherium* and *Megistonyx* conforming a sister-group to the Mesoamerican ground sloths, including the genus *Xibalbaonyx, Nohochichak, Meizonyx* and *Zacatzontli* within the North American and Caribbean ground sloths, suggesting an independent Pleistocene megalonychid group in South America.

The genus *Xibalbaonyx* is allied with the Mexican *Nohochichak* and *Zacatzontli*, but also with the Central American ground sloth *Meizonyx*, into a clade in the strict and majorly rule consensus tree (Fig. 8). The node uniting *Nohochichak* from Quintana Roo with *X. microcaninus* and *X. oviceps* has only weak bootstrap and Bremer support values. However, this node is biogeographically logical and supports our anatomical interpretation that *Nohochichak* is closely related to *Xibalbaonyx*. The *Xibalbaonyx* and *Nohochichak* clade is supported by 5 ambiguous and one unambiguous features. The strongest differentiation between *Nohochichak* and the rest of the Mexican an Central American group is the medial location of the posterior opening of the mandibular canal at the base of the coronoid process, while this opening is located laterally at the base of the coronoid process in *Xibalbaonyx*. The analysis presents a strong phylogenetic signal for this subclade, although other reasons (e.g. pathological issues, sexual dimorphism, intraspecific variation) cannot be excluded at this point.

Both *X. microcaninus* and *Zacatzontli tecolotlanensis* inhabited the Mexican basin, the latter one during the early Pliocene and *X. microcaninus* during the Late Pleistocene. The analysis places *Zacatzontli tecolotlanensis* (McDonald and Carranza-Castañeda, 2017) in a group with the middle Pleistocene *Meizonyx* from El Salvador (Webb and Perrigo, 1985). The bootstrap values for *Meizonyx* and *Zacatzontli* are identical (33) with the Mexican ground sloths, therefore the analysis reveals a second tree in which the genus *Xibalbaonyx* forms a sister-taxa to the subclade of *Nohochichak, Meizonyx* and *Zacatzontli*. This Mesoamerican

group of Mexican and Central American ground sloths, is supported only by one ambiguous feature, revealing that their phylogenetic relationship remains unresolved, probably due to the fragmentary type material and the reduced number of comparable mandible characters. Although weakly established to date, the Pliocene *Zacatzontli* may form a link between North- and South American ground sloth taxa.

The phylogenetic analysis of the Mesoamerican ground sloth record presented here must be interpreted with caution and regarded as a support for what is concluded from the osteological data. As already pointed out, the fossil material from Mexico and Central America is sparse to date and many type fossils are only fragmentarily preserved (e.g. *Nohochichak* by McDonald et al. (2017), *Zacatzontli tecolotlanensis* McDonald and Carranza-Castañeda (2017), *Meizonyx salvadorensis* Webb and Perrigo, 1985). More realistic phylogenetic relationships between the Mexican and Central American megalonychid ground sloths *Xibalbaonyx microcaninus, X. oviceps*, *Nohochichak*, *Meizonyx salvadorensis* and *Zacatzontli tecolotlanensis* can only be established with a more and better preserved material. It is nevertheless evident that the Mesoamerican Corridor did indeed play a crucial role for the paleogeographic dispersal and diversification of ground sloths within the Americas, not only during the Great American Biotic Interchange, GABI (Pujos et al., 2016; McDonald and Carranza-Castañeda, 2017).

5. Conclusions

MRG 10–294922 (skull) and MRG 10–294923 (mandible), housed in the Museo Regional de Guadalajara and originally found at Zacoalco, Jalisco, central-west Mexico, is assigned by us to the recently established genus *Xibalbaonyx* Stinnesbeck et al. (2017a), based on a nasional impression level with the lacrimal and jugal constriction of the skull, the evenly convex dorsal skull surface of the skull roof, and the absence of a sagittal crest. Osteological differences, such as the temporal lines which merge with the nuchal crest, dentition, size and shape of the mandibular spout, are here interpreted to represent species-specific variations within the genus *Xibalbaonyx*. *Xibalbaonyx microcaninus* is taxonomically separated from the coeval ground sloths from the Yucatán Peninsula, *X. oviceps* and *Nohochichak xibalbahkah* from Quintana Roo in southern Mexico. The latter is closely related to *Xibalbaonyx* and perhaps congeneric. A statistically relevant sample size and detailed osteological comparison are needed to clarify and understand the genetic and species-specific ground sloth diversity on the Yucatán Peninsula. According to the phylogenetic analysis, *Xibalbaonyx microcaninus* nov. spec. had a North American ancestor that migrated south along the Mesoamerican Corridor and evolved into the three Pleistocene Mexican species. *Xibalbaonyx microcaninus* adds a new late Pleistocene constituent to a yet small list of Mexican ground sloths. Future fossil findings will allow for a more precise phylogenetic evaluation of ground sloth taxa from this region.

Acknowledgements

Appendix A. Supplementary data

Supplementary data related to this article can be found at http://dx.doi.org/10.1016/j.jsames.2018.05.004.

References

Adam, P.J., 1999. Choloepus didactylus. Mamm. Species 1–8.

Alberdi, M.T., Juárez-Woo, J., Polaco, O.J., Arroyo-Cabrales, J., 2009. Description of the most complete skeleton of *Stegomastodon*; (Mammalia, Gomphotheriidae) recorded for the Mexican late pleistocene. Neues Jahrbuch Geol. Palaontol. Abhand. 251, 239–255.

Cartelle, C., Bohorquez, G.A., 1982. *Eremotherium laurillardi* Lund, 1842. Parte I: determinaçaõ especifica e dimorfismo sexual. Iheringa 7, 45–63.

Cartelle, C., De Iuliis, G., 1995. *Eremotherium laurillardi*: the Panamerican late Pleistocene megatheriid sloth. J. Vertebr. Paleontol. 15, 830–841.

Cartelle, C., De Iuliis, G., 2006. *Eremotherium laurillardi* (Lund)(Xenarthra, Megatheriidae), the Panamerican giant ground sloth: taxonomic aspects of the ontogeny of skull and dentition. J. Syst. Palaeontol. 4, 199–209.

Cartelle, C., De Iuliis, G., Pujos, F., 2008. A new species of Megalonychidae (Mammalia, Xenarthra) from the quaternary of poço Azul (Bahia, Brazil). Comptes Rendus Palevol 8 (7), 335–346.

Cope, E., 1889. The edentata of North America. Am. Nat. 23, 657–664.

Downs, T., 1958. Fossil vertebrates from Lago de Chapala, Jalisco, Mexico. In: 20th International Geological Congress. Universidad Nacional Autónoma de México, Mexico City, pp. 75–77.

Ferrari, L., 1995. Miocene shearing along the northern boundary of the Jalisco block and the opening of the southern Gulf of California. Geology 23, 751–754.

Ferrari, L., Pasquare, G., Venegas, S., Castillo, D., Romero, F., 1994. Regional tectonics of western Mexico and its implications for the northern boundary of the Jalisco block. Geofisc. Int. 33, 139–151.

Ferrari, L., Rosas-Elguera, J., 2000. Late Miocene to Quaternary extension at the northern boundary of the Jalisco block, western Mexico: the Tepic-Zacoalco rift revised. Geol. Soc. Am. Spec. Pap. 334, 41–64.

Flower, W.H., 1883. An Introduction to the Osteology of the Mammalia. London. .

Gaudin, T.J., 1995. The ear region of edentates and the phylogeny of the Tardigrada (Mammalia, Xenarthra). J. Vertebr. Paleontol. 15, 672–705.

Gaudin, T.J., 2004. Phylogenetic relationships among sloths (Mammalia, Xenarthra, Tardigrada): the craniodental evidence. Zool. J. Linn. Soc. 140, 255–305.

Gervais, P., 1855. Recherches sur les mammifères fossils de l'Amérique méridionale. Annales des Sciences Naturelles, Zoologie 3, 330–338.

González González, A.H., Rojas, C., Terrazas, A., Benavente Sanvicente, M., Stinnesbeck, W., Aviles, J., De los Ríos, M., Acevez, E., 2008. The arrival of humans on the yucatan peninsula: evidence from submerged caves in the state of Quintana Roo, Mexico. Curr. Res. Pleistocene 25, 1–24.

González González, A.H., Terrazas, A., Stinnesbeck, W., Benavente, M.E., Avíles, J., Padilla, J.M., Velásquez, A., Aceves, E., Frey, E., 2013. The first human settlers on the Yucatan peninsula: evidence from drowned caves in the state of Quintana Roo (south

Mexico). In: Graf, K.E., Ketron C, V., Waters, M. (Eds.), Paleoamerican Odissey, Center for the Study of the First Americans. Texas A&M University, pp. 323–338.

Groves, C.P., 2003. Morphology, morhometrics and taxonomy. In: Curtis, D., Setchell, J. (Eds.), Field and Laboratory Methods in Primatology. Cambridge University Press, Cambridge, pp. 140–157.

Hayssen, V., 2011. *Choloepus hoffmanni* (Pilosa: Megalonychidae). Mamm. Species 43, 37–55.

Hirschfeld, S.E., Webb, S.D., 1968. Plio-Pleistocene megalonychid sloths of North America. Bull. Fla. State Mus. Biol. Sci. 12, 213–296.

De Iuliis, G., Cartelle, C., Pujos, F., 2016. New Pleistocene remains of megalonychid ground sloths (Xenarthra: Pilosa) from the intertropical Brazilian region. J. Paleontol. 90, 578–587.

De Iuliis, G., Pujos, F., Cartelle, C., 2009. A new ground sloth (Mammalia: Xenarthra) from the Quaternary of Brazil. Comptes Rendus Palevol 8 (8), 705–715.

Leidy, J., 1855. A Memoir on the Extinct Sloth Tribe of North America. Smithsonian institution.

Lucas, S.G., 2008a. Late Cenozoic Fossil Mammals from the Chapala Rift Basin, Jalisco, Mexico. Neogene mammals, New Mexico, USA, pp. 39–49.

Lucas, S.G., 2008b. Late cenozoicvertebrate fossilassemblages fromjalisco, Mexico. Neogene mammals: Bulletin 44, 51.

Lucas, S.G., Aguilar, R.H., Spielmann, J.A., 2011. Stegomastodon (Mammalia, proboscidea) from the Pliocene of Jalisco, Mexico and the species-level taxonomy of Stegomastodon. Fossil Record 3, 517–553.

Martin, R., 1914. Lehrbuch der Anthropologie in systematischer Darstellung mit besonderer Berücksichtigung der anthropologischen Methoden. Gustav Fischer Verlag, Jena.

McDonald, H.G., 1977. Description of the Osteology of the Extinct Gravigrade Edentate Megalonyx with Observations on its Ontogeny, Phylogeny and Functional Anatomy. University of Florida.

McDonald, H.G., 2002. Fossil Xenarthra of Mexico: a review. In: Avances en los estudios paleomastozoológicos: México. DF: Instituto Nacional de Antropología e Historia, pp. 227–248.

McDonald, H.G., Agenbroad, L.D., Manganaro Haden, C., 2004. Late pleistocene mylodont sloth *paramylodon harlani* (mammalia: XENARTHRA) from Arizona. SW. Nat. 49, 229–238.

McDonald, H.G., Carranza-Castañeda, O., 2017. Increased xenarthran diversity of the great American biotic Interchange: a new genus and species of ground sloth (Mammalia, Xenarthra, Megalonychidae) from the hemphillian (late Miocene) of Jalisco, Mexico. J. Paleontol. 91, 1069–1082.

McDonald, H.G., Chatters, J.C., Gaudin, T.J., 2017. A new genus of megalonychid ground sloth (Mammalia, Xenarthra) from the late Pleistocene of Quintana Roo, Mexico. J. Vertebr. Paleontol. 37. http://dx.doi.org/10.1080/02724634.2017.1307206.

McDonald, H.G., Rincón, A.D., Gaudin, T.J., 2013. A new genus of megalonychid sloth (Mammalia, Xenarthra) from the late Pleistocene (Lujanian) of Sierra de Perija, Zulia State, Venezuela. J. Vertebr. Paleontol. 33, 1226–1238.

Michaud, F., Gasse, F., Bourgois, J., Quintero, O., 2000. Tectonic controls on lake distribution in the Jalisco block area (western Mexico) from Pliocene to present. Geol. Soc. Am. Spec. Pap. 334, 99–110.

Miño-Boilini, Á.R., Zurita, A.E., 2015. Dimorphism in quaternary Scelidotheriinae. Palaeontol. Electron. 18, 1–16.

Patterson, B., Segall, W., Turnbull, W.D., Gaudin, T.J., 1992. The ear region in xenarthrans (=Edentata, Mammalia): Part II. Pilosa (sloths, anteaters), palaeanodonts, and a miscellany. Geology 24, 1–79.

Polaco Ramos, O., 1981. Restos fósiles de Glossotherium y Eremotherium (Edentata) en México. In: Anais II Congresso Latino-americano Paleontología, pp. 819–833.

Prothero, D.R., Raymond, K.R., 2008. Variation and sexual size dimorphismin pleistocene groundsloths (Xenarthra). New Mexico: New Mexico Museum of Natural History and Science 44.

Pujos, F., De Iuliis, G., Argot, C., Werdelin, L., 2007. A peculiar climbing Megalonychidae from the Pleistocene of Peru and its implication for sloth history. Zool. J. Linn. Soc. 149, 179–235.

Pujos, F., De Iuliis, G., Cartelle, C., 2016. A paleogeographic overview of tropical fossil sloths: towards an understanding of the origin of extant suspensory sloths? J. Mamm. Evol. 1–20.

Rufolo, S., 1998. Taxonomy and Significance of the Fossil Mammals of Lake Chapala, Jalisco. Brigham Young University, Mexico.

Schreiber, H.D., 2004. Faunal characterisation of Neogene and pleistocene localities of the state Jalisco, Mexico. Carolinea 62, 63–68.

Stinnesbeck, S.R., Frey, E., Olguín, J.A., Stinnesbeck, W., Zell, P., Mallison, H., González González, A., Aceves Núñez, E., Velázquez Morlet, A., Terrazas Mata, A., Benavente Sanvicente, M., Hering, F., Rojas Sandoval, C., 2017a. *Xibalbaonyx oviceps*, a new megalonychid ground sloth (Folivora, Xenarthra) from the Late Pleistocene of the Yucatán Peninsula, Mexico, and its paleobiogeographic significance. Paläontol. Z. 91, 245–271.

Stinnesbeck, S.R., Frey, E., Stinnesbeck, W., Avíles Olguín, J., Zell, P., Terrazas Mata, A., Benavente Sanvicente, M., González González, A., Rojas Sandoval, C., Acevez Nuñez, E., 2017b. A new fossil peccary from the Pleistocene-Holocene boundary of the eastern Yucatán Peninsula, Mexico. J. S. Am. Earth Sci. 77, 341–349.

Swofford, D.L., 2002. PAUP: Phylogenetic Analysis Using Parsimony, Version 4.0b10. Sinauer Associates, Sunderland, Massachusetts.

Webb, S.D., Perrigo, S., 1985. New megalonychid sloths from El Salvador. In: Montgomery (Ed.), The Evolution and Ecology of Armadillos, Sloths, and Vermilinguas. Smithsonian Institution Press, Washington & London, pp. 113–120.

White, J.L., MacPhee, R.D.E., 2001. The sloths of the West Indies: a systematic and phylogenetic review. In: Biogeography of the West Indies: Patterns and Perspectives. CRC Press, New York, pp. 201–235.

Wible, J.R., Gaudin, T.J., 2004. On the cranial osteology of the yellow armadillo Euphractus sexcintus (Dasypodidae, Xenarthra, Placentalia). Annalscarnegie Museum Pittsburgh 73, 111–117.

Taylor & Francis
Taylor & Francis Group

ARTICLE

Check for updates

Xibalbaonyx exinferis n. sp. (Megalonychidae), a new Pleistocene ground sloth from the Yucatán Peninsula, Mexico

Sarah R. Stinnesbeck[a], Wolfgang Stinnesbeck[b], Eberhard Frey[a], Jerónimo Avilés Olguín[c] and Arturo González González[c]

[a]Abteilung Geowissenschaften, Staatliches Museum Für Naturkunde Karlsruhe, Karlsruhe, Germany; [b]Institut Für Geowissenschaften, Ruprecht-Karls-Universität Heidelberg, Heidelberg, Germany; [c]Instituto de la Prehistoria de América, Museo Del Desierto, Saltillo, Mexico

ABSTRACT

Recent palaeontological research in submerged caves of the north-eastern Yucatán Peninsula (YP) in Mexico has resulted in the identification of a diverse megafaunal assemblage in the area, among them Late Pleistocene ground sloths assigned to the family Megalonychidae (Xenarthra). Here we report on a new species of Megalonychidae, *Xibalpanyx exinferis* n. sp., from a new fossil locality named cenote Tortugas, located west of Puerto Morelos in the federal state of Quintana Roo. The taxon is based on a fragmentary left mandibular ramus, an atlas, and a left humerus. The new taxon is diagnosed by the presence of two mental foramina on the short symphyseal spout, a caniniform being the smallest mandibular tooth, and the anterolaterally directed aperture of the mandibular foramen on the lateral surface of the mandible. *Xibalbaonyx exinferis* is the third endemic megalonychid documented for the north-eastern Yucatán Peninsula and thus provides increasing evidence for an ecological isolation of the area from the rest of Mexico during the Pleistocene.

Introduction

Recent research on megafaunal assemblages of the north-eastern Yucatán Peninsula (YP) in Mexico has revealed a steadily increasing number of taxa, including gomphotheres (*Cuvieronius* sp.), tayas-suids (*Muknalia minima*), felids (*Panthera balamoides, Smilodon* sp.), camelids (*Hemiauchenia* sp.), equids (*Equus* sp.), ursids (*Arctotherium* sp.), canids (*Protocyon troglodytes*), and xenarthrans (*Glyptotherium* sp., *Nothrotheriops shastensis, Xibalbaonyx oviceps, Nohochichak xibalbakah*; González González et al. 2008, 2013; McDonald et al. 2017; Stinnesbeck et al. 2017a, 2017b, 2018b; Schubert et al. 2019). The faunal assemblage is of Late Pleistocene age and was discovered in submerged karst caves and sinkholes (cenotes) in the Mexican state of Quintana Roo (Figure 1).

Ground sloths remains assigned to Megalonychidae are remarkably abundant in the area, and more diverse than elsewhere in Central America. Here we introduce the new locality named Tortugas, locally also known as Cementerio de Xenartros (Xenarthran Graveyard), located west of Puerto Morelos, and we present a new species of Megalonychidae from this site, *Xibalbaonyx exinferis*. This is already the third species of Pleistocene Megalonychidae reported from the area, alongside *Xibalbaonyx oviceps* (Stinnesbeck et al. 2017a) and *Nohochichak xibalbakah* (McDonald et al. 2017), which emphasises the importance of the north-eastern YP as an area of an unusual ground sloth biodiversity.

Geological background

The north-eastern YP consists of horizontally layered shallow-water carbonate rocks of Miocene, Pliocene and Pleistocene ages (Weidie 1985; Lefticariu et al. 2006; Bauer-Gottwein et al. 2011) and hosts one of the most extensive active karst cave systems worldwide. The Mexican state of Quintana Roo is particularly well known for its

extended labyrinth of underwater caves, with a total estimated length of >7,000 km and a confirmed total length of ~1,500 km (QRSS 2018). Water-filled sinkholes, locally termed *cenotes*, form the entrances to this cave labyrinth and were formed by dissolution and collapse of the carbonate rock (Schmitter-Soto et al. 2002; Beddows 2004). The aquifer in this porous karst system consists of a meteoric freshwater lens above a saline water mass intruding from the Caribbean Sea (Kovacs et al. 2017; Stinnesbeck et al. 2017b; Ritter et al. 2019). The two water bodies are separated by a strong vertical salinity gradient, the halocline, which is usually characterised by under-saturation with respect to $CaCO_3$, leading to cave formation and conduit enlargement. Karstification was most intensive during glacial stages of the Pleistocene, when large parts of the cave system were exposed and drained (Weidie 1985; Moseley et al. 2013). During these periods, sea-level was more than 100 m below the present day sea-level, and large parts of the cave system were dry and accessible for animals and humans. The rise in sea-level during interglacial stages of the Pleistocene, and again during the early-middle Holocene, between ~12,000 and 7,600 years (yr) BP, caused flooding of the cave system (Smart et al. 2006; Collins et al. 2015; Hering et al. 2018). Modern water levels were reached at ~4,500 yr BP (van Hengstum et al. 2010; Grant et al. 2012), although oscillations of up to a few metres are known to have occurred during Maya times (Curtis et al. 1996; Kennett et al. 2012; Moseley et al. 2015; Medina-Elizalde et al. 2016).

The Tortugas sinkhole and other cenotes west of Puerto Morelos

A small cluster of submerged sinkholes is located about 36 km south of Cancun in the region 15 to 26 km west of Puerto Morelos (e.g. El Zapote, Tortugas, Maravilla, Siete Bocas) along
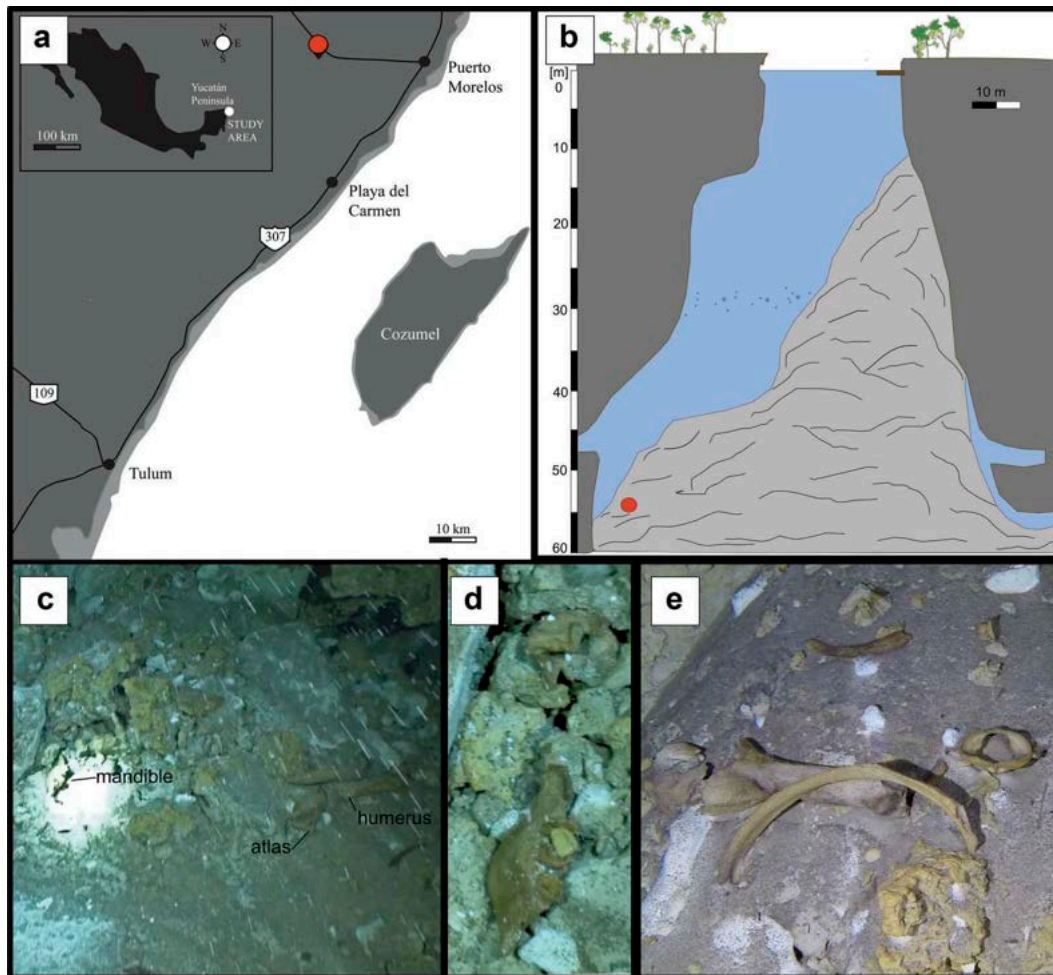
Figure 1. (a) The YP in southeastern Mexico and location of the cenote Tortugas (red dot) west of Puerto Morelos. (b) Cross-section of the cenote Tortugas (modified after Klose 2018) and red dot marking the finding locality of *Xibalbaonyx exinferis*. c, d and e) Photographs of the finding situation of the ground sloth material.

the *Ruta de los Cenotes* (Figure 1(a)); they are characterised by bottle-shaped cross sections with narrow cenote entrances widening to extended deep cavities which reach to >50 m water depth, and high debris mounts located below the surface opening. The water body of these deep sinkholes is density stratified and characterised by stagnant conditions within the halocline, the latter being substantially more extended vertically than in cenotes in other regions of Quintana Roo (e.g. in the Tulum area). A redoxcline and turbid layer is situated on top of the halocline and divides the sub-oxic freshwater body from the anoxic halocline. Within the latter, anaerobic degradation of organic matter from the debris mount on the cenote floor leads to the release of reduced sulphur (Stinnesbeck et al. 2017b; Ritter et al. 2019).

The group of cenotes west of Puerto Morelos has recently received considerable attention in the scientific community due to the presence of hanging bell-shaped speleothems. Termed by the local diving community as *Hells Bells*, these speleothems reaching to a length of 2 m (at El Zapote) were precipitated underwater. In addition, a new genus and species of a giant ground sloth, *Xibalbaonyx oviceps* (Stinnesbeck et al. 2017a), has previously been described from the El Zapote cenote.

The remains of a new ground sloth species from cenote Tortugas are documented here. This sinkhole is located at only 2 km southwest of El Zapote on the east-west-directed *Ruta de Cenotes* connecting Puerto Morelos with national road 180 to Valladolid. The surface opening of the cenote Tortugas is circular, about 25 m in

diameter (Figure 1(b)). Water surface is approximately 5 m below terrain surface. The vertical cross-section of the cenote is asymmetrical (Figure 1), with one wall vertical and the other strongly inclined inversely, leading to an enlargement of cavity space with increasing depth. Cenote Tortugas is characterised by a laterally located debris mount, of which the top is reached at 29 m water depth adjacent to the vertical cave wall. From there, it gradually slopes to about 55 m water depth towards the opposite cave wall, which is also the deepest point of the cenote known to date. The water body of the Tortugas cenote is stratified into a fresh water unit reaching to 32 m depth, and a 23 m thick transition zone with increasing salinity reaching from 32 m to the maximum cave depth at 55 m (Klose 2018; Ritter 2020). The halocline is thus extraordinarily extended. No passages or conduits are known to connect cenote Tortugas to a cave system, or to other cenotes (e.g. El Zapote).

Materials and methods

Institutional abreviations: CPC – Colección Paleontológica de Coahuila; INAH – Instituto Nacional de Antropología e Historia, Mexico City, Mexico; IPA – Instituto de la Prehistoria de América, Solidaridad, Quintana Roo, Mexico; MUDE – Museo del Desierto, Saltillo, Coahuila, Mexico; MRG – Museo Regional de Guadalajara, Jalisco, Mexico.

The ground sloth material presented here was discovered in 2019 by the cave explorers Vicente Fito and Dirk Penzel, and

reported to one of us. The three bones (mandible fragment, atlas, left humerus) were found clustered on the debris mount at about 54 metres water depth (Figure 1(b, c)). A rib associated with the three undetermined bones remained on site.

The material was transported to the IPA, a facility of the MUDE. Therefore, the fossils are here registered with the CPC (MUDE) collection numbers. The osteological remains were treated for several months with distilled water, later dried gradually, and treated with a solution of adhesive and distilled water (30/70), because the bones were extremely thin and fragile.

The material was photographed with a Panasonic Lumix G9 and a Canon EOS Rebel T4i with 10–22 mm zoom lens set at 22 mm; f 4.5, 1/80 – f 8, 1/20, using a tripod. The background of the photographs has been masked manually.

Anatomical terminology is based on phylogenetic characters of tree and ground sloths. Furthermore, descriptive comparison with North-, Central-, and South American Megalonychidae is based on the original descriptions and fossil material of *Ahytherium aureum* (Cartelle et al. 2008; De Iuliis et al. 2009), *Australonyx aquae* (Cartelle et al. 2008; De Iuliis et al. 2009), *Megalonyx jeffersonii* (Leidy 1855; Hirschfeld and Webb 1968; McDonald 1977), *Pliometanastes* sp. (Hirschfeld and Webb 1968) and *Diabolotherium* sp. (Pujos et al. 2007; Shockey et al. 2009).

The following specimens were included in the comparison:

Nohochichak xibalbahkah (McDonald et al. 2017); INAH-DP5832 (for skull and mandible), accessible at the INAH, Mexico City, Mexico.

Xibalbaonyx microcaninus (Stinnesbeck et al. 2018a); INAH-MRG-10-294923 (mandible), accessible at the MRG, Guadalajara, Mexico.

Xibalbaonyx oviceps (Stinnesbeck et al. 2017a); INAH Za2014-131-02 (mandible), housed at the Museo Maya de Cancún y Zona Arqueológica de San Miguelito in Cancun, Quintana Roo, Mexico.

Phylogenetic analysis

A phylogenetic analysis was performed to establish the phylogenetic position of *Xibalbaonyx exinferis* from cenote Tortugas within Megalonychidae (Appendices 1, 2 and 3). The analysis was carried out using PAUP (version 4.0a 150 for Macintosh; Swofford 2002). The methodology has been described in detail by Gaudin (1995, 2004)) and is based on a data matrix of 80 cranial and mandibular features (McDonald et al. 2017) compared within 19 Megalonychidae (Patterson et al. 1992; Gaudin 1995, 2004; Wible and Gaudin 2004; McDonald et al. 2013), including the new species *Xibalbaonyx exinferis*. Here we only apply the mandibular features. '?' indicates missing data or characters that are inapplicable to a given taxon. The following symbols are used to mark character states in polymorphic taxa: a = {0, 1}; b = {1, 2}; c = {2, 3}; d = {0, 2}; e = {0, 1, 2}. The data matrix used and a list of apomorphies for each of the numbered nodes of one of three most parsimonious trees are provided in appendix 1. The list of characters and character states from McDonald et al. (2017) has been used in the phylogenetic analysis applied here (appendix 3).

Systematic palaeontology
XENARTHRA Cope, 1889
PILOSA Flower, 1883
MEGATHERIOIDEA Gray, 1821
MEGALONYCHIDAE Gervais, 1855
Xibalbaonyx Stinnesbeck et al., 2017
Xibalbaonyx exinferis sp. nov.
(Figs 2–7, Table 1 and 2)

Holotype.
CPC-2774 mandible (Table 1).
Referred specimens.
CPC-2775 atlas and CPC-2776 humerus (Table 2).

Etymology. For the species: *exinferis – ex inferis* Latin for 'from the underworld'. The species is dedicated to the cave explorers, who dive into the 'Maya underworld', the cenotes of the Yucatán Peninsula. Without their courage and commitment to extreme diving, the Pleistocene history of the area would be unknown.
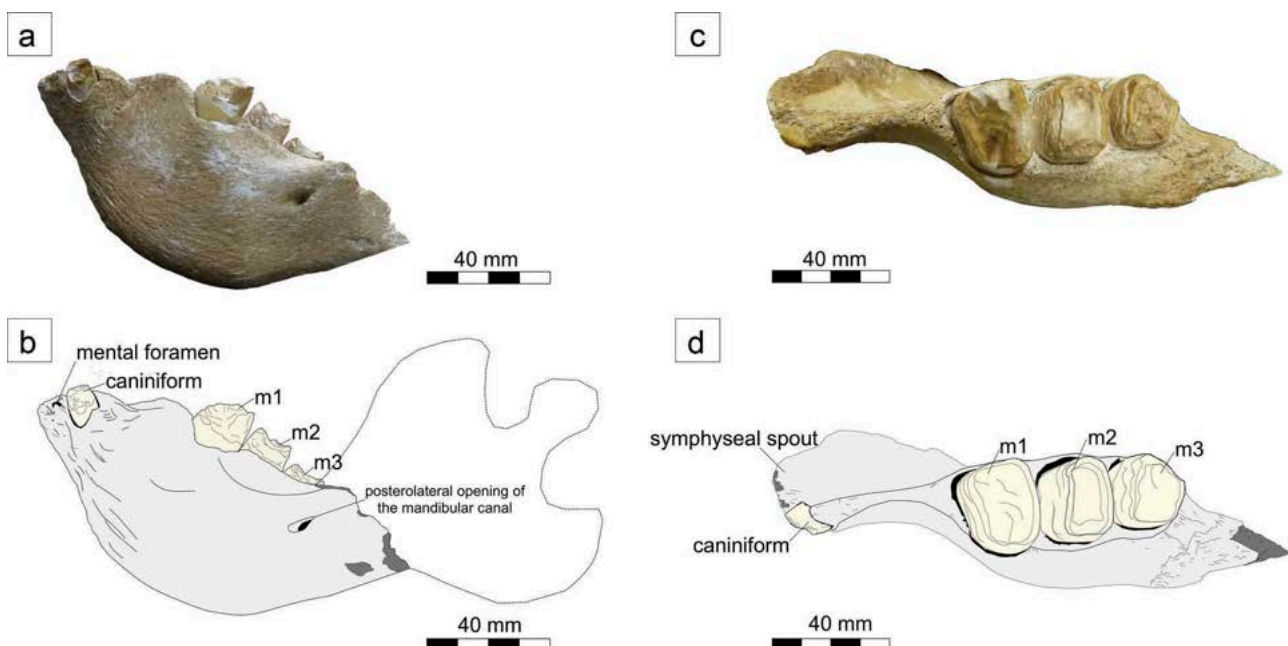
Figure 2. *Xibalbaonyx exinferis* mandible fragment CPC-2774 from cenote Tortugas. (a and b) Mandibular ramus in lateral view, c and d) in dorsal view. a and c) Photographs and (b and d) interpretative line drawings.

Table 1. *Xibalbaonyx exinferis* CPC-2774 mandibular and dental measurements in millimetres (mm).

Description	mm
Mandible CPC-2774	
Maximum rostrocaudal length	168
Maximum mandibular height measured at diastema	75
Lowest mandibular height measured posterior to m3	50
Mandibular canal diameter in lateral view	12
Length of symphyseal spout as preserved	10
Distance between anterior margin of the symphyseal spout and posterior margin of m3	123
Length of diastema between c1 and m1	40
Length of tooth-row from the anterior margin of c1 to the posterior margin of m3	113
Length of molariform-row from the anterior margin of m1 to the posterior margin of m3	64
Left mandibular caniniform (c1):	
Mesiodistal length	10
Buccolingual width	8
Left m1:	
Mesiodistal length lingually	17
Mesiodistal length buccally	14
Maximum buccolingual diameter	25
Left m2:	
Mesiodistal length lingually	12
Mesiodistal length buccally	15
Maximum buccolingual diameter	24
Left m3:	
Mesiodistal length lingually	15
Mesiodistal length buccally	14
Maximum buccolingual diameter	22

Table 2. Atlas and humerus from cenote Tortugas referred to *Xibalbaonyx exinferis*. All measurements in millimetres (mm).

Description	mm
Atlas CPC-2775	
Maximum anteroposterior length of body	68
Mediolateral width across the cranial articular facets	83
Dorsal anteroposterior length at midline	36
Ventral anteroposterior length at midline	24
Maximum dorsoventral height	58
Maximum width across transverse processes	130
Dorsoventral height of the vertebral foramen in anterior view	36
Mediolateral width of the vertebral foramen in anterior view	42
Dorsoventral height of the vertebral foramen in posterior view	45
Mediolateral width of the vertebral foramen in posterior view	40
Width across posterior condyles	72
Maximum dorsoventral height of the posterior condyles	26
Humerus CPC-2776	
Humerus maximum length as preserved	320
Proximodistal diameter of entepicondylar foramen	32
Distal width across medial to lateral metaphysis	141
Mid-shaft anteroposterior diameter	35
Minimum mediolateral width at mid-shaft	46
Mediolateral width at deltoid crest	50

Type locality. Cenote Tortugas, also known as Cementerio de Xenartros (span. for *Xenarthra cemetery*), along the Ruta de los Cenotes, Puerto Morelos, Quintana Roo, Mexico.

Stratigraphic distribution. The material has not been ^{14}C dated because of the ubiquitous dissolution of collagen in prehistoric bones found in the water-filled caves of Quintana Roo (Stinnesbeck et al. 2017a). Even though the present material is thus undated, most of the megafaunal assemblage found in the cenotes of Quintana Roo is Late Pleistocene in age.

Diagnosis. Medium-sized ground sloth; similar in size to that of the ground sloth *Xibalbaonyx microcaninus* from Jalisco, west-

central Mexico. Mandibular ramus with a small lower caniniform with a triangular occlusal face, mesiobuccally oriented. Short symphyseal spout reaching to less than 15% of the spout to molariform length (Table 1) as preserved. Two mental foramina on the symphyseal spout, one of which is located on the rostrolateral border of the spout, and the second one on the rostrodorsal surface (Figure 2). Diastema reaching to 35% of the tooth row length, including the caniniform. Lateral opening of the mandibular canal is located ventral to m3 and rostroventral to the mandibular ascending ramus, perforating the lateral surface of the horizontal mandibular ramus.

Description

The rostral half of a left mandibular ramus is preserved (Figure 2). The left mandible fragment is stout and exhibits the caniniform, the post-caniniform diastema and all three molariforms. It also includes the symphyseal spout and the horizontal mandibular body. The rostrodorsal border of the symphyseal spout is missing, as are the left condylar and coronoid processes and the entire right ramus. In lateral view, the dorsal and ventral borders of the mandibular body converge caudally from the diastema between caniniform and molariforms, where the mandibular ramus reaches its greatest height. The horizontal body is caudally one-half lower than the rest of the mandible fragment. The surface of the mandibular body is rough. The outermost layer of the cortical bone around the symphysis is split off. The horizontal ramus is laterally convex and medially flat. The mandibular foramen is located ventral to m3, at the middle half of the lateral surface of the horizontal ramus. Its rounded opening is rostrolaterally oriented (Figure 2).

The symphyseal spout is incomplete. Nevertheless, the oblique rostral surface of the mandible in lateral view suggests that the spout was short and funnel-shaped with a triangular outline in dorsal view, and that it had horizontal rostrodorsal margins. Two mental foramina are visible in rostral view. One is located almost at midline on the rostral surface immediately ventral to the dorsal margin of the spout. The second foramen is located at the dorsolateral margin of the spout in about the middle between the anterior terminus of the spout as preserved and the caniniform.

The caniniform of *Xibalbaonyx exinferis* has about one fourth of the size of m1 and exhibits a triangular occlusal face. Its wear facet is oblique and mesiodistally oriented. Therefore, the apex of the occlusal surface of the caniniform is lingually inclined and reaches its highest point distally. The caniniform length is half the smallest molariform (m3) and exhibits a deep sulcus on the distobuccal face. Such a sulcus is absent in all molariforms. The diastema between c1 and m1 equals the length of m1 plus m2. Despite being slightly fragmented the anteroposterior convexity of the dorsal face of the diastema is evident. M1 is the largest tooth of the mandible. It is trapezoid in occlusal view with a convex buccal margin. Its lingual margin is straight with mesial and distal rounded borders. The mesial face of m1 is vertically concave, while the distal one is vertically convex. The m1 resembles m2 in general shape and outline. The lingual face of m2 is mesiodistally by about one fourth shorter than the buccal face. In occlusal view, m2 has a rounded rectangular outline. The m3 is one third narrower than m1 and of rounded triangular outline. Transversally, m3 is one third wider than mesiodistally short. All molariforms exhibit a pronounced mesiobuccal wear facet. This is the most pronounced in m1, while in m2 and m3 the wear facet is slightly flatter and more buccally oriented as compared to m1.
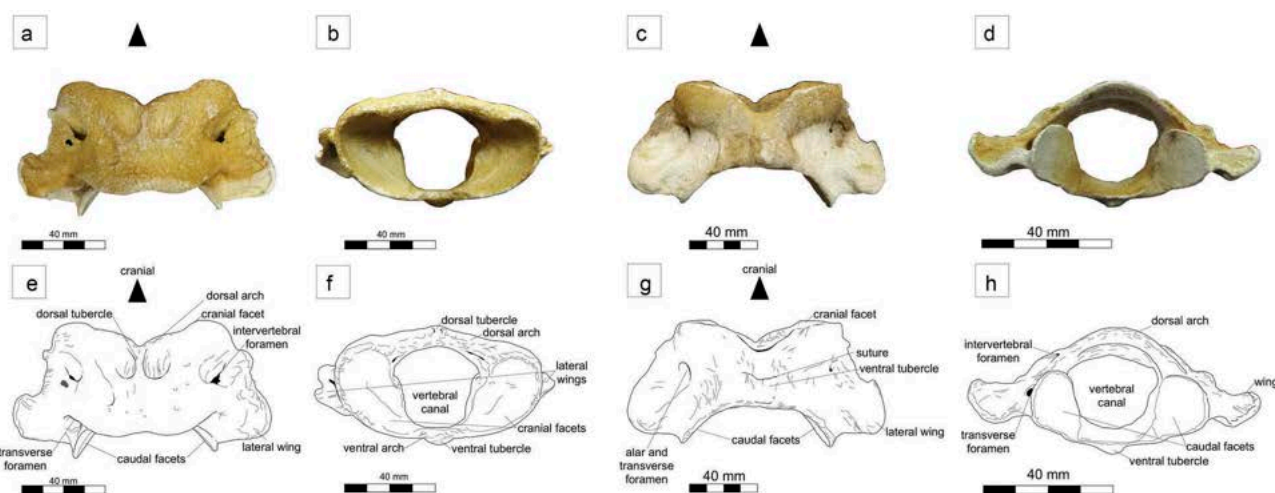
Figure 3. Atlas CPC-2775 from cenote Tortugas referred to *Xibalbaonyx exinferis* in (a) dorsal, (b) cranial, (c) ventral and (d) caudal view. (e, f, g and h) respective interpretative line drawings.

Atlas

The atlas (CPC-2775; Table 2; Figure 3) is anteroposteriorly compressed and of rhomboidal outline. The aperture of the vertebral canal has the outline of an inverted trapezoid with blunt margins. The dorsal arch is twice as thick as the ventral one. The surface of the bone is rough and pierced by numerous small foramina. In dorsal view, the atlas is trapezoidal in outline. The anterodorsal surface bears a bulgy dorsal tubercle. On each lateral face, an elongated intervertebral foramen is visible, with a drop-shaped outline. In dorsal view, the anterolateral two-thirds of the lateral margins of the atlas are straight, with a small lateral bulge level with the transverse foramina. The caudal third is convex. In anterior view, the posterior half of the wings is dorsally oriented. Adjacent to the intervertebral foramina, the evenly rounded transverse foramina are located on the lateral wings of the bone, almost covered by the articular surfaces of the occipital condyles. The articular surfaces for the occipital condyles are one-third dorsoventrally longer than wide. Their shape resembles an inverted scalene rounded triangle with a smooth surface. In ventral view, the ventral arch is narrowest at midline and diverges laterally to twice its central width. Its surface is rough, and the ventral tubercle is bulgy and twice as pronounced as the dorsal one. In ventral view, a short and thin suture runs along the ventral tubercle. In posterior view, the atlas has a semi-circular outline, in which the dorsal arch of the atlas runs horizontally. The articular caudal surfaces are smooth, concave and of reniform-shape.

Left humerus

The bone lacks both epiphyses. These were thus unfused, strongly suggesting an immature age of the animal (Figure 4; Table 2).

The greater tuberosity is not preserved, but the proximal fourth of the diaphysis is partially preserved and laterally expanded. The humeral diaphysis has a rough surface and is only one-third longer than the metaphysis, which gives the bone a short and compact appearance. The deltopectoral shelf is flat and merges proximally with the deltoid crest at mid-half of the diaphysis.

The pectoral tuberosity is only visible on the distal two-thirds of the diaphysis and becomes more rugose distally, while merging with the deltoid crest at the anterior surface of the metaphysis. This junction forms a flat deltopectoral plate. In lateral view, the deltoid

crest is convex and laterally most expanded and pronounced at the middle third of the diaphysis.

The diaphysis reaches its narrowest diameter at about half the bone´s length and becomes distally wider and flatter transversely, while merging with the metaphysis (Figure 4).

The distal medial and lateral margins of the humerus are straight, giving the metaphysis a symmetrical appearance. The metaphysis is triangular in outline and flat, both anteriorly and posteriorly. The epicondylar ridge is also flat. The entepicondylar foramen is elliptical and reaches approximately 16% of the humeral maximum height (Table 2).

The entepicondylar foramen is large, reaching to one-third of the metaphysis. In anterior view, the aperture of the foramen is laterodistally oriented. In medial view, the aperture of the foramen is narrow, reaching less than one-third of the bone's width and is elliptical in outline. In anterior view, the entepicondylar bar is broad and covers the foramen´s aperture. The lateral margins of the entepicondylar bar diverge distally and merge with the medial epicondyle. The latter is located at the distal-most end of the humerus; it is convex and medially expanded.

The distal end of the humerus is transversally expanded and fan-shaped. The lateral epicondyle is fragmentarily preserved, as only the laterally expanded epicondylar ridge is proximally present. The anterior distal surface of the metaphysis is continuously flat, but becomes slightly concave in its distal-most fourth. In posterior view, the metaphysis is flat, while the olecranon fossa is slightly concave along the long axis at the distal-most fourth of the metaphysis.

Comparisons

Based on the mandibular fragment CPC-2774, the mandible of *Xibalbaonyx exinferis* was about 50% smaller than that of *Megalonyx jeffersonii* (McDonald 1977) and *Xibalbaonyx oviceps* (Stinnesbeck et al. 2017a), while *X. microcaninus* (Stinnesbeck et al. 2018a) (INAH-MRG-10-294923) from Guadalajara was similar in size (Figures 5 and 6).

In dorsal view, the preserved portion of the mandibular spout of *Xibalbaonyx exinferis* is short and triangular. Its lingual symphyseal area is trough-shaped, rising medially level with the anterior margin of the molariform m1. These features are shared with *Nohochichak xibalbakah* (McDonald et al. 2017), *Xibalbaonyx microcaninus* and
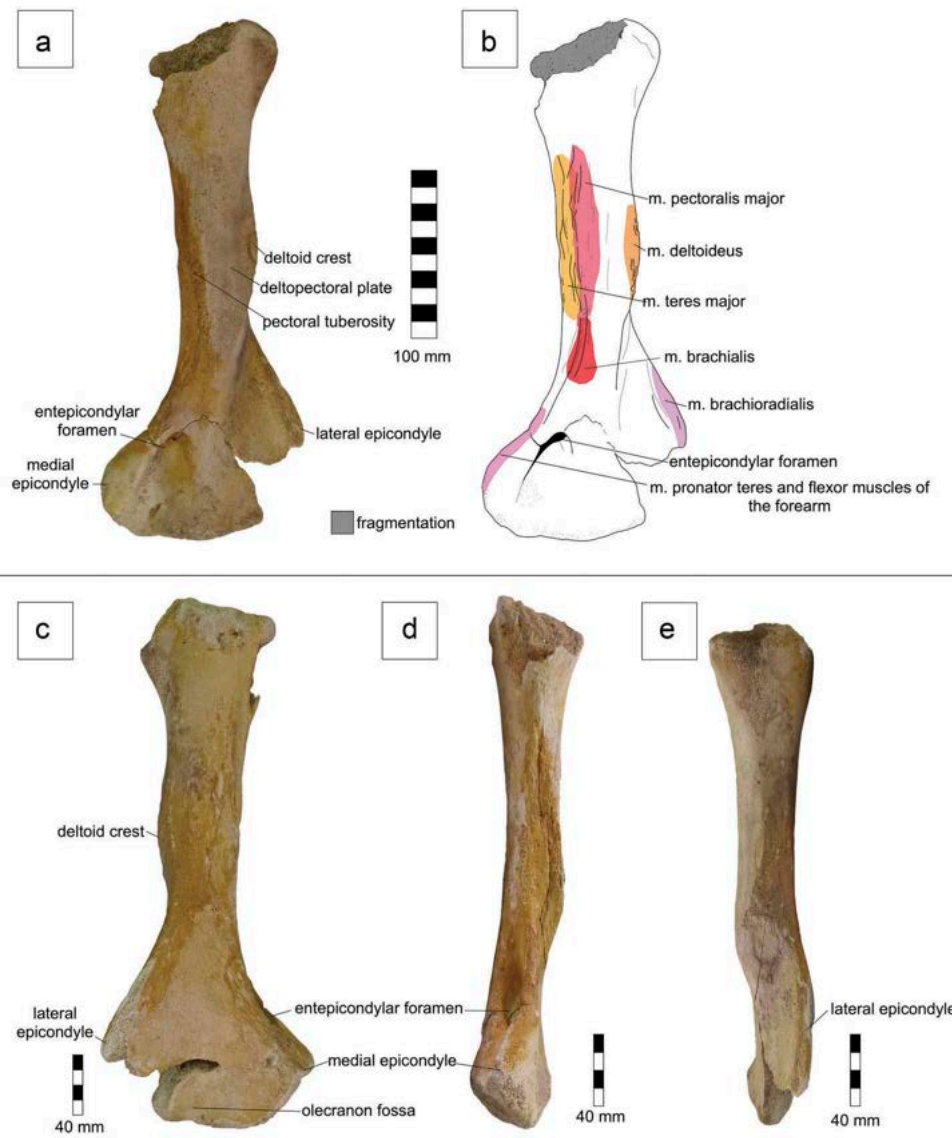
Figure 4. *Xibalbaonyx exinferis*. Left humerus CPC-2776 in (a and b) anterior, (c) posterior, (d medial and e) lateral view. (b) Interpretative line drawing of the humerus in anterior view.

Figure 5. Comparison of the mandibles of (a) *Xibalbaonyx exinferis* CPC-2774 from cenote Tortugas, (b) *Xibalbaonyx oviceps* from El Zapote cenote INAH Za2014-131-02 in Quintana Roo and (c) *X. microcaninus* INAH-MRG-10-294923 from Jalisco, all in lateral view.

Megalonyx jeffersonii. The length of the mandibular spout in *Xibalbaonyx exinferis* is one-third of the diastema length as preserved, which resembles the configuration in *Megalonyx jeffersonii, Nohochichak xibalbakah* and *Meizonyx salvadorensis* (Webb and Perrigo 1985), but differs from *X. oviceps* and *X. microcaninus*, in which the symphyseal spout is as long as the diastema (Figures 5 and 6). In lateral view, the anterior surface of the mandibular spout in *Xibalbaonyx exinferis* is flat and straight, thus resembling that of *X. microcaninus* and *Nohochichak*, but differing from the convex anterior surface in *X. oviceps*. In *Xibalbaonyx exinferis* the diastema
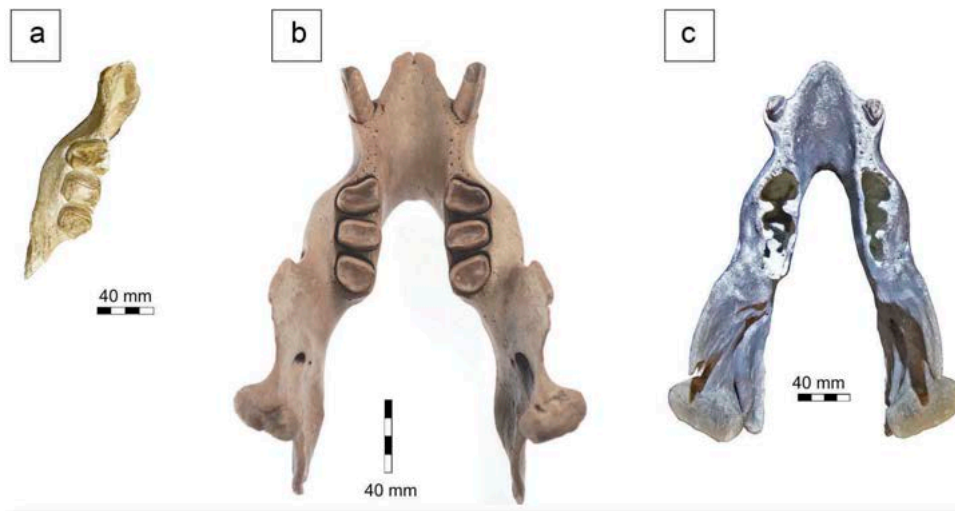
Figure 6. Comparison of the mandibles of (a) *Xibalbaonyx exinferis* CPC-2774, (b) *X. oviceps* from El Zapote cenote INAH Za2014-131-02 in Quintana Roo and (c) *X. microcaninus* from Jalisco INAH-MRG-10-294923, all in dorsal view.
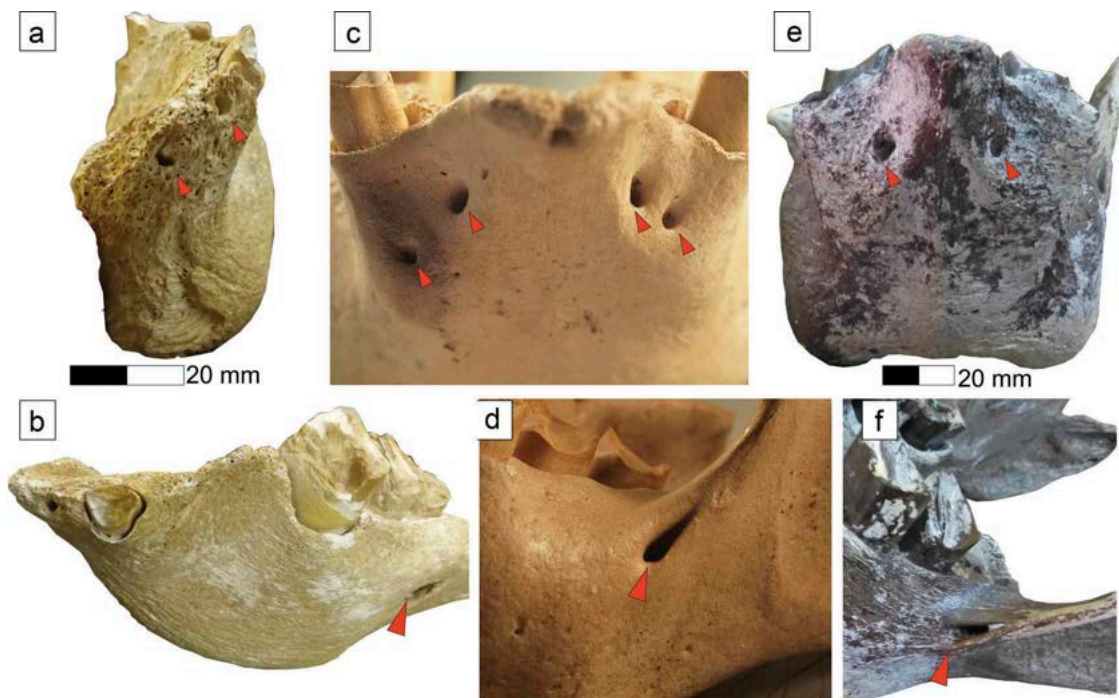
Figure 7. Photographs showing the location of the mental and mandibular foramina, marked by red arrows, in fossil ground sloth taxa from Quintana Roo on the Mexican Yucatán Peninsula: (a and b) *Xibalbaonyx exinferis* from cenote Tortugas CPC-2774, c and d) *Xibalbaonyx oviceps* from El Zapote cenote INAH Za2014-131-02, and e and f) *Nohochichak xibalbakah* from Hoyo Negro INAH-DP5832.

between the caniniform and molariforms reaches 35% of the tooth-row length; it is thus 10% longer than that of *Nohochichak, Meizonyx*, and some *Megalonyx* individuals (McDonald 1977; Webb and Perrigo 1985; McDonald et al. 2017). *Megalonyx* closely resembles the new species in having a similar posterolateral mandibular foramen piercing the lateral surface of the horizontal ramus. This anatomical feature, which is shared by *Xibalbaonyx exinferis* and *Megalonyx jeffersonii*, differs from the position of the mandibular foramen at the base of the coronoid process in *X. oviceps* and *X. microcaninus*, and its medial position in *Nohochichak* (Figure 7).

Xibalbaonyx exinferis has two mental foramina, a feature otherwise only seen in *X. oviceps* (Figure 7), but absent in *X. microcaninus, Nohochichak* and *Megalonyx*. In *Xibalbaonyx exinferis*, the first,

medially located mental foramen is present on the rostral surface of the symphyseal spout, which is also the case in *X. oviceps* and *Nohochichak*. The second mental foramen is located on the lateral face of the symphyseal spout anterior to the caniniform, immediately adjacent to the dorsal margin of the spout. This is a unique feature of *Xibalbaonyx exinferis* within Megalonychidae, including *X. oviceps*, in which the second foramen is located ventrolaterally to the first one.

In *Xibalbaonyx exinferis* (CPC-2774), the cross-section of the lower caniniform is triangular with rounded corners, as in the other Megalonychidae from the north-eastern YP, *X. oviceps* and *Nohochichak*. This feature is not seen in other megalonychids, such as *Meizonyx salvadorensis* from El Salvador. In occlusal view, the alveoli and caniniform in *Xibalbaonyx exinferis* are also

triangular, as in *X. microcaninus*, but they are rounded in *X. oviceps*. However, the buccodistal sulcus of the caniniform is as pronounced in *Xibalbaonyx exinferis* as in *Meizonyx salvadorensis* from El Salvador, and in *Nohochichak xibalbakah* from Hoyo Negro and *X. oviceps* from El Zapote cenote, both from Quintana Roo. In *X. microcaninus* the caniniforms are conical to peg-shaped, without a distal sulcus. *Xibalbaonyx exinferis* and *X. microcaninus* do not exhibit a mesiobuccal sulcus on the caniniform. This sulcus is deep in *Meizonyx salvadorensis* and *X. oviceps*, and is also expressed by the alveolus in *N. xibalbakah*.

In anterior and occlusal views, the mesiobuccal inclination of the caniniform of *Xibalbaonyx exinferis* differs from the mesio-occlusal orientation of this tooth in *X. microcaninus, X. oviceps, N. xibalbakah* and *Meizonyx salvadorensis*. In *Xibalbaonyx exinferis*, the caniniform is the smallest tooth of the mandible, as in *X. microcaninus*, which is not the case in any other Mexican and Central American Megalonychidae. In contrast, the shape of the occlusal faces of the molariforms of *Xibalbaonyx exinferis* resembles those of *X. oviceps* and *Nohochichak*, but differs from that of *X. microcaninus, Meizonyx* and *Megalonyx obtusidens*. All molariforms in *Megalonyx obtusidens* (UF-27512; Webb and Perrigo 1985) from the Barraca del Sisimico exhibit a rounded occlusal molariform shape, strongly different to *Meizonyx* and the ground sloths from the YP. In the Megalonychidae (*Xibalbaonyx* and *Nohochichak*) from the YP, the mesial margin of m1 and m2 is slightly concave, which is only seen in the m1 of *Meizonyx*. In *Xibalbaonyx exinferis* the m1 is the largest tooth of the mandible. It is rounded rectangular in occlusal view with a straight lingual margin, which is also the case in *X. oviceps*, while it is slightly concave in *N. xibalbakah* and *M. salvadorensis*. M2 also exhibits a rectangular occlusal outline in all Quintana Roo Megalonychidae. In *Xibalbaonyx exinferis* the m3 is buccolingually one third wider than mesiodistally short, which is also the case in *X. oviceps, Nohochichak xibalbakah* and *Meizonyx salvadorensis*.

The humerus of *Xibalbaonyx exinferis* differs from that of most Megalonychidae in being short and compact. In the semi-arboreal sloths from the West Indies (*Acratocnus, Neocnus*; White 1993), as well as in the larger ground sloths from the continent (e.g. *Eucholeops, Diabolotherium, Pliometanastes*), the diameter of the distal metaphyseal humerus end reaches ≤40% of the diaphyseal humeral length. The corresponding area, as preserved in *Xibalbaonyx exinferis*, extends to slightly >40%, as in *Megalonyx*.

The proximal and distal epiphyses are missing in *X. exinferis*, because they apparently were unfused with the diaphysis, suggesting that the animal was a juvenile at the time of death. The distal fanning of the metaphysis strikingly resembles that of the humeri of juveniles of *Megalonyx jeffersonii*, which would be consistent with the ontogenetic stage of *X. exinferis* as proposed. However, the deltopectoral area is pronounced in juvenile *M. jeffersonii* and runs vertically along the long axis of the humeral shaft. This area is flat in *X. exinferis* and lacks any tuberosity, suggesting a mediolaterally broader deltopectoral plate and more medially located pectoral tuberosity in adult stage, than that seen in *Megalonyx*. Also, in juvenile *Megalonyx* the entepicondylar foramen is located at the mediodistal-most margin of the metaphysis, while it is more proximally located in *X. exinferis*.

Discussion

Xibalbaonyx exinferis from cenote Tortugas is based on a fragmentary left mandibular ramus. We also referred an atlas and a left humerus to this specimen. These were found at approximately 0.3 m distance between each other on a debris mount of the cenote, while the mandibular fragment was discovered isolated next to a rock about 0.90 to 1.2 m aside from the postcranial material. At only a few meters distance of the *Xibalbaonyx exinferis* bones, a skull and associated partially articulated postcranial material of a nothrotheriid sloth were also discovered. Both humeri with the corresponding epiphyses of the nothrotheriid are present. Even though, we cannot completely exclude that the atlas and humerus here referred to the holotype of *Xibalbaonyx exinferis* belong to another individual. However, atlas, humerus and mandible were clustered together, while the nothrotheriid was partially articulated, suggesting that the animal died in situ.

Implications for locomotion and life style

The postcranium of *Xibalbaonyx exinferis* is only represented by an atlas and a fragmented humerus, as suggested by the taphonomical circumstances. We can exclude the possibility that the humerus belongs to the articulated nothrothere, since both humeri of this latter ground sloth are present. However, the atlas could belong to the nothrothere or another megalonychid and does not necessarily belong to *X. exinferis*. Therefore we will only discuss the diaphyseal humerus as part of the postcranium of *X. exinferis*. This highly fragmentary material still allows for a discussion of the locomotor options of *X. exinferis*. The metaphysis reaches 40% of the humerus as preserved (Figure 4) and is 60% mediolaterally broader than the humeral shaft, suggesting that the medial and lateral epicondyles played an important role in the locomotion of this animal. In *Megalonyx*, the medial epicondyle is also medially enlarged in adults, but this area is reduced in juveniles. In *X. exinferis*, which is a juvenile, the medial epicondyle already reaches one-third of the distal humeral width, suggesting an even larger or more massive and medially expanded epicondyle in adult individuals, provided the growth of this structure is allometric as in *Megalonyx*. The humeral epicondyles are the areas in which the elbow flexors and the long extensors of metacarpus and digits originate. M. pronator teres, which pronates and flexes the forearm, originates from the medial epicondyle, while m. brachioradialis, originating from the lateral epicondyle, contributes to the flexion, pronation and supination of the forearm. M. extensor carpi radialis, also originating on the lateral epicondyle, flexes the forearm, extends the manus in the wrist and abducts the manus in the direction of the radius. The dimensions of the epicondyles of *Xibalbaonyx exinferis*, suggest an unusually large diameter of these muscles that operate forearm and manus. These muscle movements were thus aligned with force.

The shortness and morphology of the humerus and the position of the origins of the forearm and manus flexors, suggest that the forearm of *Xibalbaonyx exinferis* corresponds to a long power arm compared with that of other ground sloths and powerful muscles for flexing forearm and manus. Such a configuration is a prerequisite not only for arm-pull dominated terrestrial locomotion, but also for paddle swimming and climbing. Extant tree sloths are surprisingly good swimmers, an ability which has also been discussed for ground sloths (Amson et al. 2015a, 2015b; de Muizon and McDonald 1995; Amson et al. 2014). Nevertheless, a potential reconstruction of an obligatory swimming locomotion for *Xibalbaonyx exinferis* to the degree of *Thalassocnus* (Amson et al., 2014) would be speculative because of the sparse remains.

The short humerus with powerful flexors for forearm and manus would also have allowed for a 'hook-and-pull' operation (Hildebrand 1985; Amson et al. 2017; Gaudin et al. 2018), which is used by extant xenarthrans such as armadillos and anteaters. The morphology of the humerus suggests that *Xibalbaonyx exinferis* was capable of digging out tubers or succulent roots as a source of water and starch, e.g. *Yucca, Manihot* etc.

The hook-and-pull technique would also have allowed for climbing. Climbing abilities would have been essential, in case *Xibalbaonyx exinferis* wanted to surmount the steep limestone walls that border the Tortugas and other cenotes in the area to reach the bottom of these sinkholes to hide away from predators or access ground water.

The pronounced muscle attachment areas on the humerus and atlas suggest that *X. exinferis* was a small animal of approximately 200 kg mass, equipped with a massive musculature already as a juvenile. The powerful forearms of *Xibalbaonyx exinferis* and the ability of the animal for grasping, or hooking and pulling, are unusual and are here interpreted to have evolved in the context of a life in a dry area of the northeastern YP. The area was only pierced by sinkholes in which water was present only at the bottom.

Phylogenetic analysis and Mesoamerican radiation of ground sloths

The phylogenetic analysis (Figure 8) supports our interpretation of *Xibalbaonyx exinferis* as a new species, instead of an assignation of the Tortugas individual to an already established species, *Xibalbaonyx oviceps* or *Nohochichak xibalbakah*. Our analysis yields three parsimony trees (tree length 340, consistency index (CI) = 0.4971, retention index (RI) = 0.4926). As already reported by others (McDonald et al. 2013, 2017) *Megalonychotherium* is positioned as the sister taxon to all other Megalonychidae, merging with *Eucholeops* in the node. The North American *Megalonyx* is presented here as a basal taxon uniting all other Megalonychidae. *Xibalbaonyx exinferis* is therefore not more closely related to *Megalonyx* than to other members of the family, although both share a similar location of the mandibular foramen and both present a similar short mandibular spout. On the contrary, *Megalonyx* and *Pliometanastes* are here presented as more basal taxa. The position of *Pliomorphus* as the sister taxon to all Antillean sloths, the extant *Choloepus*, and Central and South American ground sloths, is only weakly supported as already discussed in McDonald et al. (2017).

Megalocnus and *Parocnus* have the strongest node on the tree, with a bootstrap value of 87. Other than these, the relationship within the sloths from the West Indies (MacPhee et al. 2000) is unresolved.

The strict consensus tree also confirms the position of the South American *Ahytherium* and *Megistonyx* as a sister-group of all Mexican and Central American sloths, whereas the relationship between *Xibalbaonyx oviceps* and *Nohochichak xibalbakah*, both from the YP, remains unresolved (Figure 8). In one tree, *Xibalbaonyx oviceps* is here allied to all Mexican and Central American sloths, including *X. microcaninus* from Jalisco and the new species *X. exinferis*. In the second (Figure 8), *Xibalbaonyx oviceps* is the sister taxon of *X. microcaninus* and *X. exinferis*, while *Nohochichak* unites *Meizonyx* and *Zacatzontli*. The first tree, however, presents *Meizonyx* and *Zacatzontli* as a sister-group to the rest of the Mexican sloths and includes *Nohochichak* as a basal taxon to the genus *Xibalbaonyx*.

Xibalbaonyx exinferis and *X. microcaninus* form a subclade to *X. oviceps*, suggesting a special status of *Xibalbaonyx oviceps* within this group, which might indicate that latter taxon diverged earlier or possibly even shows a generic differentiation to *X. microcaninus* and *X. exinferis*. Also, the Late Pleistocene *Nohochichak* from Hoyo Negro is here presented as more basal than *Meizonyx* from El Salvador and the west-central Mexican *Zacatzontli*, although *Meizonyx* and *Zacatzontli* are of Plio- to early Pleistocene age.

The analysis therefore supports the specific, and even generic differentiation of all three Quintana Roo taxa: In *Nohochichak*, the medial location of the mandibular foramen is a unique feature (Figure 7), supporting a different origin, as also the lateral location of the equivalent foramen on the horizontal ramus in *Xibalbaonyx exinferis* and on the base of the ascending ramus in *X. oviceps* (Figures 5 and 7).

Mesoamerican sloths form a common clade, uniting not only the sloths from the YP but also *Meizonyx* and *Zacatzontli*. The phylogenetic analysis supports a Mexican-Central American radiation of ground sloths. However, our phylogenetic analysis only provides an additional support in interpretation, especially since latest DNA research has shown that the relationship between fossil and extant sloths (e.g. *Choloepus*) may differ significantly from previous interpretations (Presslee et al. 2019).

Paleobiogeographical implications

A South American origin of Mesoamerican ground sloths, including *Xibalbaonyx exinferis* and the other megalonychid sloths from
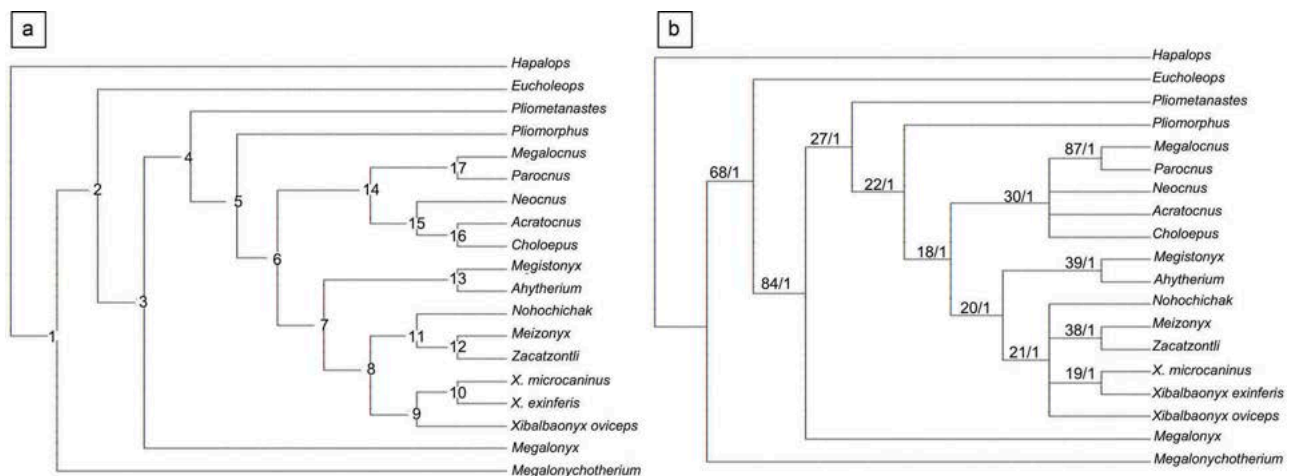

Figure 8. Results from a phylogenetic analysis of the sloth family Megalonychidae and *Choloepus* based on PAUP analysis of 80 cranial features from McDonald et al. (2013) and Gaudin (2004), to assess the position of the new taxon *Xibalbaonyx exinferis*. (a) One of three most parsimonious majority rule consensus trees (Tree length = 340; CI = 0.4971; HI = 0.6588; RI = 0.4926) and 50% majority rule consensus tree. A list of apomorphies for each of the numbered nodes is provided in Appendix 1. (b) Strict consensus tree of the three MPTs produced by the phylogenetic analysis. The first number associated with each node represents a bootstrap value, the second a Bremer support value.

the YP, is supported by the phylogenetic analysis, which shows a close relationship between the South American *Megistonyx* and *Ahytherium* and Mesoamerican ground sloths (e.g. *Xibalbaonyx* and *Nohochichak*). This phylogenetic relationship is closer than that with sloths from the West Indies, even though these are geographically closer. Varela et al. (2019) suggested a Plio- or Pleistocene dispersal of a South American clade of ground sloths into tropical Central America, giving rise to the Late Pleistocene sloths known from this region. The close phylogenetic relationship between *Xibalbaonyx exinferis* and the late Miocene-early Pliocene *Zacatzontli* from Jalisco and early Pleistocene *Meizonyx* from El Salvador supports a hypothetical Central American origin and radiation of sloths. This hypothesis is further supported by the presence of *Xibalbaonyx* in the state of Jalisco (Stinnesbeck et al. 2018a).

Xibalbaonyx exinferis is already the third Pleistocene Megalonychidae reported from the Quintana Roo cave system, alongside *Xibalbaonyx oviceps* (Stinnesbeck et al. 2017a) and *Nohochichak* (McDonald et al. 2017). All three taxa represent new species. Endemism is also documented for other Late Pleistocene faunal elements from Quintana Roo, including the peccary *Muknalia minima* (Stinnesbeck et al. 2017b) and the felid *Panthera balamoides* (Stinnesbeck et al. 2018b). Furthermore, *Protocyon* and *Arctotherium* of South American origin have been reported (Schubert et al. 2019), confirming the importance of Central America as a biogeographical corridor (Stinnesbeck et al. 2018b). Because these endemic taxa are to date the only Late Pleistocene vertebrates described in detail from the submerged cave system of Quintana Roo to date, further investigations will likely yield more and better preserved endemic taxa.

The increasing number of endemic vertebrates in Quintana Roo is remarkable and can only be explained by an intermittent isolation of the area, either geographically or ecologically. Stinnesbeck et al. (2018b) already suggested that periods of habitat diversification may have altered during the Pleistocene with intervals of ecological isolation of the north-eastern YP. Faunal exchange between south-central Mexico and the YP was likely restricted to humid periods. During dry periods, the habitat became patchy. During these intervals, small populations of herbivores depending on specific food sources became isolated. These ecological isolations boosted local diversification. We further suggest that this ecological situation may not only have caused endemisms, but evidently has created a biodiversity hotspot concerning ground sloth diversity on the Late Pleistocene Mexican Corridor. Biodiversity hotspots are defined as geographical areas harbouring a major portion of species genetic diversity. They are frequently triggered by climate-driven cycles of allopatric differentiation within sub-refugia with respect to vegetation (Canestrelli et al. 2014). Both processes, the repeated changes of Pleistocene climate followed by changes of vegetation on the YP, along with a geographic isolation of the northeastern portion of the peninsula, likely formed an ecological barrier to the previously connected open habitat. The loss of migratory pathways to west-central Mexico and the resulting isolation of habitats during dry periods resulted in anatomical and genetic changes among the isolated ground sloths populating the peninsula.

Conclusions

Xibalbaonyx exinferis sp. nov. from the Tortugas cenote west of Puerto Morelos in the Mexican state of Quintana Roo, was a medium sized ground sloth similar in size to *X. microcaninus* from Jalisco, west-central Mexico, and half the size of the North American *Megalonyx*, the Central American *Meizonyx* (Webb and Perrigo 1985) and the South American *Ahytherium* (Cartelle et al.

2008), but also smaller than *Nohochichak* (McDonald et al. 2017) and *Xibalbaonyx oviceps* (Stinnesbeck et al. 2017a) from the YP.

Xibalbaonyx exinferis differs from other megalonychid ground sloths by a mesiobuccally oriented lower caniniform of triangular occlusal shape and cross section, which is about one fourth the size of m1 and the smallest mandibular teeth. The symphyseal spout is short, reaching to <15% of the spout to molariform length. Two mental foramina are present on the rostral and lateral face of the symphyseal spout, one of which is located medially on the rostral surface of the spout; it is thus only visible in rostral view. The second foramen is located on the dorsolateral margin of the spout adjacent to the caniniform. The diastema reaches to 35% of the entire tooth-row length, including the caniniform. A mandibular foramen pierces the dorsolateral third of the mandibular ramus.

The strong forearm adductors and flexors, combined with a short humerus, suggest powerful hook-and-pull movements that could have been used for unearthing roots and even climbing vertical rock walls, similar to small bears (Grass, 2019). The phylogenetic analysis indicates that *Xibalbaonyx exinferis* was closer related to *Meizonyx* from El Salvador and *Zacatzontli* from Jalisco, rather than to other megalonychids, e.g. from the West Indies or North America. *Xibalbaonyx exinferis* is the third new endemic species of megalonychid ground sloth from the Late Pleistocene of Quintana Roo, suggesting isolation of the study area during dry periods, followed by habitat splitting.

References

Amson E, Argot C, McDonald HG, de Muizon C. 2015a. Osteology and functional morphology of the forelimb of the marine sloth *Thalassocnus* (Mammalia, Tardigrada). J Mamm Evol. 22(2):169–242. doi:10.1007/s10914-014-9268-3.

Amson E, Argot C, McDonald HG, de Muizon C. 2015b. Osteology and functional morphology of the axial postcranium of the marine sloth *Thalassocnus* (Mammalia, Tardigrada) with Paleobiological Implications. J Mamm Evol. doi:10.1007/s10914-014-9280-7

Amson E, Arnold P, van Heteren AH, Canoville A, Nyakatura JA. 2017. Trabecular architecture in the forelimb epiphyses of extant xenarthrans (Mammalia). Front Zool. 14(1):52. doi:10.1186/s12983-017-0241-x.

Amson E, de Buffrenil V, Laurin M, de Buffrenil V, de Muizon C. 2014. Gradual adaptation of bone structure to aquatic lifestyle in extinct sloths from Peru. Proc R Soc B Biol Sci. 281(1782):20140192–20140192. doi:10.1098/rspb.2014.0192.

Bauer-Gottwein P, Gondwe BRN, Charvet G, Marín LE, Rebolledo-Vieyra M, Merediz-Alonso G. 2011. Review: the Yucatán Peninsula karst aquifer, Mexico. Hydrogeol J. 19(3):507–524. doi:10.1007/s10040-010-0699-5.

Beddows PA. 2004. Groundwater hydrology of a coastal Conduit carbonate aquifer: caribbean Coast of the Yucatán Peninsula. México (UK): University of Bristol.

Canestrelli D, Bisconti R, Sacco F, Nascetti G. 2014. What triggers the rising of an intraspecific biodiversity hotspot? Hintsfrom the agile frog. Sci Rep. 4:1–9. doi:10.1038/srep05042

Cartelle C, De Iuliis G, Pujos F. 2008. A new species of Megalonychidae (Mammalia, Xenarthra) from the Quaternary of Poço Azul (Bahia, Brazil). Comptes Rendus Palevol. 8(7):335–346. doi:10.1016/j.crpv.2008.05.006.

Collins SV, Reinhardt EG, Werner CL, Le Maillot C, Devos F, Rissolo D. 2015. Late Holocene mangrove development and onset of sedimentation in the Yax Chen cave system (Ox Bel Ha) Yucatan, Mexico: implications for using cave sediments as a sea-level indicator. Palaeogeogr Palaeoclimatol Palaeoecol. 438:124–134. doi:10.1016/j.palaeo.2015.07.042

Curtis JH, Hodell DA, Brenner M, Hodelle DA, Brenner M. 1996. Climate Variability on the Yucatan Peninsula (Mexico) during the Past 3500 Years, and Implications for Maya Cultural Evolution. Quat Res. 46(1):37–47. doi:10.1006/qres.1996.0042.

De Iuliis G, Pujos F, Cartelle C. 2009. A new ground sloth (Mammalia: xenarthra) from the Quaternary of Brazil. Comptes Rendus Palevol. 8(8):705–715. doi:10.1016/j.crpv.2009.07.003.

de Muizon C, McDonald HG. 1995. An aquatic sloth from the Pliocene of Peru. Nature. 375(6528):224–227. doi:10.1038/375224a0.

Gaudin TJ. 1995. The ear region of edentates and the phylogeny of the Tardigrada (Mammalia, Xenarthra). J Vertebr Paleontol. 15(3):672–705. doi:10.1080/02724634.1995.10011255.

Gaudin TJ. 2004. Phylogenetic relationships among sloths (Mammalia, Xenarthra, Tardigrada): the craniodental evidence. Zool J Linn Soc. 140 (2):255–305. doi:10.1111/j.1096-3642.2003.00100.x.

Gaudin TJ, Hicks P, Di Blanco Y. 2018. Myrmecophaga tridactyla (Pilosa: myrmecophagidae). Mamm Species. 50(956):1–13. doi:10.1093/mspecies/sey001.

González González AH, Terrazas Mata A, Stinnesbeck W, Benavente M, Avilés Olguín J, Rojas Sandoval C, Padilla JM, Velázquez Morlet A, Acevez Nuñez E, Frey E, et al. 2013. The first human settlers on the Yucatan Peninsula: evidence from drowned caves in the state of Quintana Roo (South Mexico). In: Graf KE, Ketron CV, Waters M, editors. Paleoamerican Odyssey. Texas A&M University; p. 323–337.

González González AH, Rojas Sandoval C, Terrazas Mata A, Benavente Sanvicente M, Stinnesbeck W, Aviles Olguín J, De Los Ríos M, Acevez Nuñez E, Aviles OJ, De Los Ríos M, et al. 2008. The arrival of humans on the yucatan peninsula: evidence from submerged caves in the state of Quintana Roo, Mexico. Curr Res Pleistocene. 25:1–24.

Grant KM, Rohling EJ, Bar-Matthews M, Ayalon A, Medina-Elizalde M, Bronk Ramsey C, Satow C, Roberts AP. 2012. Rapid coupling between ice volume and polar temperature over the past 150,000 years. Nature. 491 (7426):744–747. doi:10.1038/nature11593.

Grass AD. 2019. Inferring differential behavior between giant ground sloth adults and juveniles through scapula morphology. J Vertebr Paleontol. 39 (1):1–15. doi:10.1080/02724634.2019.1569018.

Hering F, Stinnesbeck W, Folmeister J, Frey E, Stinnesbeck SR, Avilés J, Acevez Nuñez E, González AH, Terrazas Mata A, Benavente Sanvicente ME, et al. 2018. The Chan Hol cave near Tulum (Quintana Roo, Mexico): evidence for long-lasting human presence during the early to middle Holocene. J Quat Sci. 1–12. doi:10.1002/jqs.3025

Hildebrand M. 1985. Digging of quadrupeds. In: Hildebrand M, editor. Functional Vertebrate Morphology. Cambridge (UK): Cambridge University Press; p. 89–109.

Hirschfeld SE, Webb SD. 1968. Plio-Pleistocene megalonychid sloths of North America. Bull Florida State Museum Biol Sci. 12:213–296.

Kennett DJ, Breitenbach SFM, Aquino VV, Asmerom Y, Awe J, Baldini JUL, Bartlein P, Culleton BJ, Ebert C, Jazwa C, et al. 2012. Development and disintegration of maya political systems in response to climate change. Science (80-). 338(6108):788–791. doi:10.1126/science.1226299.

Klose L. 2018. Hydrogeologischer und hydrogeochemischer Vergleich unterschiedlicher Cenoten auf der Yucatán Halbinsel, Mexiko. Germany: Ruprecht-Karls University Heidelberg.

Kovacs SE, Reinhardt EG, Chatters JC, Rissolo D, Schwarcz HP, Collins SV, Kim S-T, Nava Blank A, Erreguerena PL, Luna Erreguerena P. 2017. Calcite raft geochemistry as a hydrological proxy for Holocene aquifer conditions in Hoyo Negro and Ich Balam (Sac Actun Cave System), Quintana Roo, Mexico. Quat Sci Rev. 175:1–15. doi:10.1016/j.quascirev.2017.09.006

Lefticariu M, Perry EC, Ward WC, Lefticariu L. 2006. Post-Chicxulub depositional and diagenetic history of the northwestern Yucatan Peninsula, Mexico. Sediment Geol. 183(1–2):51–69. doi:10.1016/j.sedgeo.2005.09.008.

Leidy J. 1855. A memoir on the extinct sloth tribe of North America. Smithsonian institution, Philadelphia.

MacPhee RDE, White JL, Woods CA. 2000. New Megalonychid Sloths (Phyllophaga, Xenarthra) from the Quaternary of Hispaniola. Am Museum Novit. 3303:1–32. doi:10.1206/0003-0082(2000)3303<0001:NMSPXF>2.0.CO;2

McDonald HG. 1977. Description of the osteology of the exctinct gravigrade edentate Megalonyx with observations on its ontogeny, phylogeny and functional anatomy. University of Florida, Florida.

McDonald HG, Chatters JC, Gaudin TJ. 2017. A new genus of megalonychid ground sloth (Mammalia, Xenarthra) from the late Pleistocene of Quintana Roo, Mexico. J Vertebr Paleontol. 37(3):e1307206. doi:10.1080/02724634.2017.1307206.

McDonald HG, Rincón AD, Gaudin TJ. 2013. A new genus of megalonychid sloth (Mammalia, Xenarthra) from the late Pleistocene (Lujanian) of Sierra de Perija, Zulia State, Venezuela. J Vertebr Paleontol. 33(5):1226–1238. doi:10.1080/02724634.2013.764883.

Medina-Elizalde M, Burns SJ, Polanco-Martinez J, Beach T, Lases-Hernández F, Shen CC, Wang HC. 2016. High-resolution speleothem record of precipitation from the Yucatan Peninsula spanning the Maya Preclassic Period. Glob Planet Change. 138:93–102. doi:10.1016/j.gloplacha.2015.10.003.

Moseley GE, Richards DA, Smart PL, Standish CD, Hoffmann DL, Ten Hove H, Vinn O. 2015. Early–middle Holocene relative sea-level oscillation events recorded in a submerged speleothem from the Yucatán Peninsula, Mexico. Holocene. 25(9):1511–1521. doi:10.1177/0959683615585832.

Moseley GE, Smart PL, Richards DA, Hoffmann DL. 2013. Speleothem constraints on marine isotope stage (MIS) 5 relative sea levels, Yucatan Peninsula, Mexico. J Quat Sci. 28(3):293–300. doi:10.1002/jqs.2613.

Patterson B, Segall W, Turnbull WD, Gaudin TJ. 1992. The ear region in xenarthrans (=Edentata, Mammalia): part II. Pilosa (sloths, anteaters), palaeanodonts, and a miscellany. Geology. 24:1–79.

Presslee S, Slater GJ, Pujos F, Forasiepi AM, Fischer R, Molloy K, Mackie M, Olsen JV, Kramarz A, Taglioretti M, et al. 2019. Palaeoproteomics resolves sloth relationships. Nat Ecol Evol. 3(7):1121–1130. doi:10.1038/s41559-019-0909-z.

Pujos F, De Iuliis G, Argot C, Werdelin L. 2007. A peculiar climbing Megalonychidae from the Pleistocene of Peru and its implication for sloth history. Zool J Linn Soc. 149(2):179–235. doi:10.1111/j.1096-3642.2007.00240.x.

QRSS. 2018. Survey and cartography of the underwater caves of quintana Roo Mexico [WWW Document]. Quintana Roo Speleol Surv.

Ritter SM. 2020. Unravelling the formation of Hells Bells: underwater speleothems from the Yucatán Peninsula in Mexico. Germany: Ruprecht-Karls University Heidelberg.

Ritter SM, Isenbeck-Schröter M, Scholz C, Keppler F, Gescher J, Klose L, Schorndorf N, Avilés Olguín J, González-González A, Stinnesbeck W. 2019. Subaqueous speleothems (Hells Bells) formed by the interplay of pelagic redoxcline biogeochemistry and specific hydraulic conditions in the El Zapote sinkhole, Yucatán Peninsula, Mexico. Biogeosci Discuss. 1–35. doi:10.5194/bg-2018-520

Schmitter-Soto JJ, Comín FA, Escobar-Briones E, Herrera-Silveira J, Alcocer J, Suárez-Morales E, Elías-Gutiérrez M, Díaz-Arce V, Marín LE, Steinich B. 2002. Hydrogeochemical and biological characteristics of cenotes in the Yucatan Peninsula (SE Mexico). Hydrobiologia. 467(1/3):215–228. doi:10.1023/A:1014923217206.

Schubert BW, Chatters JC, Arroyo-Cabrales J, Samuels JX, Soibelzon LH, Prevosti FJ, Widga C, Nava A, Rissolo D, Erreguerena PL. 2019. Yucatán carnivorans shed light on the great American biotic interchange. Biol Lett. 15 (5):13–15. doi:10.1098/rsbl.2019.0148.

Sesoko NF, Rahal SC, Bortolini Z, de Souza LP, Vulcano LC, Monteiro FOB, Teixeira CR. 2015. Skeletal Morphology of the Forelimb of Myrmecophaga tridactyla. J Zoo Wildl Med. 46(4):713–722. doi:10.1638/2013-0102.1.

Shockey BJ, Salas-Gismondi R, Baby P, Guyot J-L, Baltazar MC, Huaman L, Clack A, Stucchi M, Pujos F, Emerson JM, et al. 2009. New Pleistocene cave faunas of the Andes of central Peru: radiocarbon ages and the survival of low latitude, Pleistocene DNA. Palaeontol Electron. 12:15p.

Smart PL, Beddows P, Coke J, Doerr S, Whitaker FF. 2006. Cave development on the caribbean coast of the Peninsula, Yucatan Roo, Quintana. Geol Soc Am Spec Pap. 404:105–128. doi:10.1130/2006.2404(10)

Stinnesbeck SR, Frey E, Olguín JA, Stinnesbeck W, Zell P, Mallison H, González González A, Aceves Núñez E, Velázquez Morlet A, Terrazas Mata A, et al. 2017a. *Xibalbaonyx oviceps*, a new megalonychid ground sloth (Folivora, Xenarthra) from the Late Pleistocene of the Yucatán Peninsula, Mexico, and its paleobiogeographic significance. Palaontologische Zeitschrift. 91 (2):245–271. doi:10.1007/s12542-017-0349-5.

Stinnesbeck, Sarah R., et al. "A new fossil peccary from the Pleistocene-Holocene boundary of the eastern Yucatán Peninsula, Mexico." *Journal of South American Earth Sciences*. 77 (2017b):341–349.

Stinnesbeck SR, Frey E, Stinnesbeck W. 2018a. New insights on the paleogeographic distribution of the Late Pleistocene ground sloth genus *Xibalbaonyx* along the Mesoamerican Corridor. J South Am Earth Sci. 85:108–120. doi:10.1016/j.jsames.2018.05.004

Stinnesbeck SR, Stinnesbeck W, Frey E, Avilés Olguín J, Rojas Sandoval C, Velázquez Morlet A, González AH. 2018b. *Panthera balamoides* and other Pleistocene felids from the submerged caves of Tulum, Quintana Roo, Mexico. Hist Biol. 00:1–10. doi:10.1080/08912963.2018.1556649

Stinnesbeck W, Becker J, Hering F, Frey E, González González AH, Fohlmeister J, Stinnesbeck SR, Frank N, Terrazas Mata A, Benavente Sanvicente ME, et al. 2017a. The earliest settlers of Mesoamerica date back to the late Pleistocene. PLoS One. 12(8):16–18. doi:10.1371/journal.pone.0183345.

Stinnesbeck W, Frey E, Zell P, Avilés J, Hering F, Frank N, Arps J, Geenen A, Gescher J, Isenbeck-Schröter M, et al. 2017b. Hells Bells – unique speleothems from the Yucatán Peninsula, Mexico, generated under highly specific subaquatic conditions. Palaeogeography, palaeoclimatology, palaeoecology. 489:209–229. DOI:10.1016/.

Swofford DL. 2002. PAUP: phylogenetic Analysis Using Parsimony, version 4.0b10. Sunderland (Massachusetts): Sinauer Associates.

van Hengstum PJ, Reinhardt EG, Beddows PA, Gabriel JJ. 2010. Linkages between Holocene paleoclimate and paleohydrogeology preserved in a Yucatan underwater cave. Quat Sci Rev. 29(19–20):2788–2798. doi:10.1016/j.quascirev.2010.06.034.

Varela L, Tambusso PS, McDonald HG, Fariña RA. 2019. Phylogeny, macroevolutionary trends and historical biogeography of sloths: insights from a bayesian morphological clock analysis. Syst Biol. 68(2):204–218. doi:10.1093/sysbio/syy058.

Webb SD, Perrigo S. 1985. New megalonychid sloths from El Salvador. In: Montgomery, editor. The evolution and ecology of armadillos, sloths, and vermilinguas. Washington & London: Smithsonian Institution Press; p. 113–120.

Weidie AE. 1985. Part I: geology of Yucatan Platform. In: Ward WC, Weidie AE, Back W, editors. Geology and hydrogeology of the Yucatan and Quaternary Geology of Northeastern Yucatan Peninsula. New Orleans: Geological Society; p. 1–19.

White JL. 1993. Indicators of locomotor habits in xenarthrans: evidence for locomotor heterogeneity among fossil sloths. Journal of Vertebrate Paleontology. 13(2):230–242. doi:10.1080/02724634.1993.10011502.

Wible JR, Gaudin TJ. 2004. On the cranial osteology of the yellow armadillo *Euphractus sexcintus* (Dasypodidae, Xenarthra, Placentalia). Ann MUSEUM PITTSBURGH. 73:111–117.

A new fossil peccary from the Pleistocene-Holocene boundary of the eastern Yucatán Peninsula, Mexico

Sarah R. Stinnesbeck [a, *], Eberhard Frey [a], Wolfgang Stinnesbeck [b],
Jeronimo Avíles Olguín [c], Patrick Zell [d], Alejandro Terrazas Mata [e],
Martha Benavente Sanvicente [e], Arturo González González [f], Carmen Rojas Sandoval [g],
Eugenio Acevez Nuñez [c]

[a] Abteilung für Paläontologie und Evolutionsforschung, Staatliches Museum für Naturkunde Karlsruhe, Erbprinzenstr. 13, 76133 Karlsruhe, Germany
[b] Institut für Geowissenschaften, Heidelberg University, Im Neuenheimer Feld 234, 69120 Heidelberg, Germany
[c] Instituto de la Prehistoria de las Américas, Carretera Federal 307, Km 282, 77711 Solidaridad, Quintana Roo, Mexico
[d] Hessisches Landesmuseum Darmstadt, Friedensplatz 1, 64283 Darmstadt, Germany
[e] Área de Prehistoria y Evolución del Instituto de Investigaciones Antropológicas de la Universidad Nacional Autónoma de México (UNAM), Investigación
Científica, 04510 Coyacán, D.F., Mexico
[f] Museo del Desierto, Carlos Abedrop Dávila 3745, Nuevo Centro Metropolitano de Saltillo, 25022 Saltillo, Coahuila, Mexico
[g] Instituto Nacional de Antropología e Historia, carretera federal 307, km 128, 77710 Tulúm, Quintana Roo, Mexico

ARTICLE INFO

ABSTRACT

Here we describe the left mandibular ramus of a fossil peccary from the submerged karst cave system in the southeastern Mexican state of Quintana Roo. The specimen, which was discovered in the Muknal cave northwest of Tulúm, is a new genus and species of peccary termed *Muknalia minima*. The taxon likely dates from the latest Pleistocene and differs significantly from all extant peccaries and their Pleistocene relatives by a concave notch at the caudal edge of the mandibular ramus and prominent ventrally directed angular process. These diagnostic osteological differences suggest that the masticatory apparatus differed from all other peccaries, which may hint to an ecological isolation on the late Pleistocene Yucatán Peninsula.

© 2016 Elsevier Ltd. All rights reserved.

1. Introduction

The New World Pigs, Tayassuidae (Palmer, 1897), evolved in North America (Prothero, 2009; Woodburne, 1969, 2010) during the late Eocene (Li-Ping, 2000; Meng and McKenna, 1998; Ducrocq et al., 1998; Ducrocq, 1994) and invaded South America in the Pliocene during the Great American Biotic Interchange (GABI; Harris and Liu, 2007; Woodburne, 2010). Five Pleistocene/Holocene tayassuid genera are presently known from the Americas: The extinct *Platygonus* (Le Conte, 1848) and *Mylohyus* (Leidy, 1868) as well as the extant genera *Pecari* (Reichenbach, 1835), *Tayassu* (Fischer [von Waldheim], 1814) and *Catagonus* (Ameghino, 1904; Woodburne, 1969; Wright, 1998).

The Mexican fossil record includes the extant *Pecari tajacu* from the Loltún and Actún Spukil caves in Yucatán (Ferrusquía-Villafranca et al., 2010) and three Late Blancan to Rancholabrean species of the genus *Platygonus*, *Platygonus "alemanii"*, *Platygonus compressus* and *Platygonus ticuli*, from Moroleón in Guanajuato, El Cedazo in Aguascalientes, Tequixquiac in the state of Mexico and Valsequillo in Puebla (Ferrusquía-Villafranca et al., 2010). An Oligocene mandible fragment of *Perchoerus probus* from Oaxaca. And non Tayassuidae fossils include a mandibular fragment of *Leptochoerus* sp. from Oaxaca and a fragment of *Simojovelhyus pocitosense* from Chiapas of Late Oligocene age (Carranza-Castañeda, 2006; Ferrusquía-Villafranca, 2006; Ferrusquía-Villafranca et al., 2010; Jiménez-Hidalgo et al., 2015).

Representatives of the families Suidae and Tayassuidae, both members of Suina (Gray, 1868), inhabit a large variety of wood- and shrubland habitats (Simpson, 1944). Both groups are omnivorous with bunodont and occasionally zygodont or zygolophodont molars and premolars (Wright, 1998). Tayassuidae differ from Suidae by the following features: The pes of peccaries is either tridactyl

---

(*Pecari*, *Tayassu*), or bidactyl (*Catagonus*), whereas the pes of Suidae is tetradactyl. The tail of Tayassuidae has six to nine caudal vertebrae, compared to 20 and more in Suidae. The total tooth count is 38 in Tayassuidae, that of Suidae is 44. Tayassuidae possess an angular process, which is absent in Suidae (Li-Ping, 2003). In contrast to Suidae, Tayassuidae have paired scent glands ventral to the eye and an impair one on the back (Harris and Liu, 2007; Wright, 1998).

1.1. Geological setting and faunal context

The mandibular ramus described here was discovered in 2012 by two of us, JAO and EAN, in the submerged Muknal cave near Tulúm in the Mexican state of Quintana Roo (Fig. 1). This cave is part of the limestone karst system of the northern Yucatán Peninsula. During the Wisconsin Glacial when sea level was 120 m lower than today, large parts of the cave system were exposed and accessible, namely from the coast. Sea level rise during the Pleistocene-Holocene transition resulted in a gradual flooding of the caves and the preservation of paleontological and archaeological archives inside (Collins et al., 2015; Chatters et al., 2014; González González et al., 2013; Smart et al., 2006). In the Muknal cave, for instance, two human skeletons of late Pleistocene or early Holocene age have been discovered: the Muknal Man and the Las Palmas Woman (Gonzaléz Gonzaléz et al., 2013; 2008a; 2008b). Our ongoing investigations in the area revealed an abundant and diverse, hence predominantly fragmented fossil assemblage of late Pleistocene age, consisting of camelids, equids, glyptodonts, gomphotheriids and ground sloths. Peccaries also belong to this assemblage but remain undocumented to date (Chatters et al., 2014; González González et al., 2013).

The Muknal cave forms part of the Ox Bel Ha system, which is one of the largest cave systems on the Yucatán Peninsula. Access to the Muknal archaeological site is via the Jailhouse Cenote (sinkhole), also known as Las Palmas (Fig. 1). The Muknal cave is an east-west directed tunnel with an average diameter of approximately 2–3 m and a length of >300 m, with several intermittent chambers decorated with speleothems. At about 150 west of the Jailhouse Cenote, an internal sinkhole at 25 m water depth leads into a north-south orientated tunnel that descends to 34 m water depth. At its blind end, a small speleothem-decorated chamber contains abundant charcoal dated to 9139-8840 cal BC, and a partial human skeleton, the Muknal Grandfather (González González et al., 2013, 2008a, 2008b). The mandibular ramus was found in the descending tunnel at a distance of about <13 m south of the Muknal Grandfather in a water depth of 30 m. The mandible was found standing on its caudal margin, which was inserted into an accumulation of charcoal and cave sediment in the vicinity of four small stalagmites (Fig. 1.2).
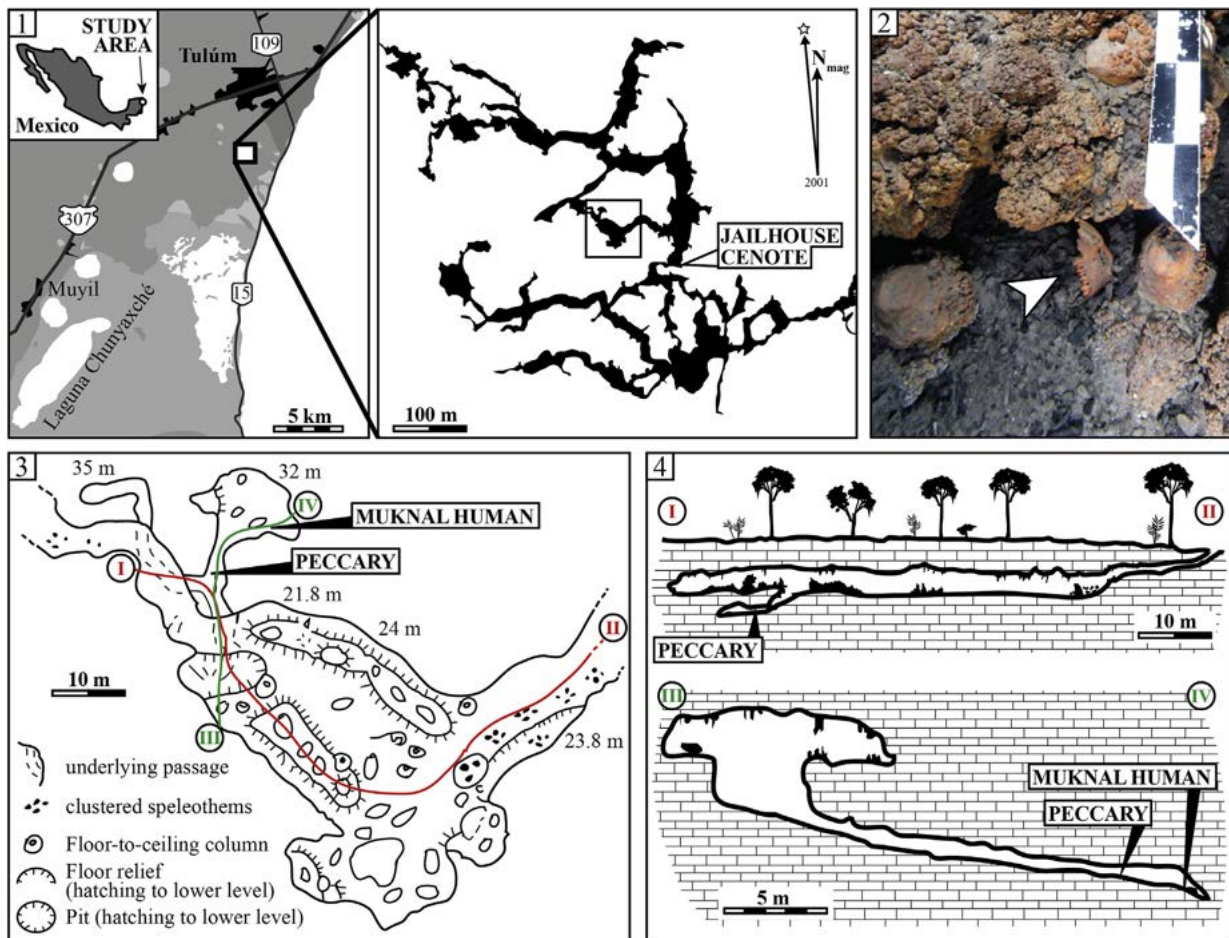
Fig. 1. Map of the Ox Bel Ha system (1.1) near Tulúm on the Yucatán Peninsula of southeast Mexico (1.1) and location of the Muknal cave within the cave system. The box in the upper middle figure is detailed in Figure and illustrates the cave near the Las Palmas and Muknal archaeological sites. Access is via cenote Jailhouse (to the right). Fig. 1.2 location of PQR2011-PALMAS-V-1 in the Muknal cave. Fig. 1.4. Illustrates cross sections through the Muknal cave. For position of sections I-II and III-IV see Fig. 1.3. The peccary mandible PQR2011-PALMAS-V-1 was found at 30 m water depth at a distance of <13 m from the Muknal human site.

1.2. Material and methods

The fragmentary left mandibular ramus of peccary described here under the collection number PQR2011-PALMAS-V-1, was found in 2012 by two of us (JAO, EAN) and was recovered within the same year.

The specimen was collected from the saltwater unit of the submerged Muknal cave. In the lab it was treated for eight months with distilled water and one month with a combination of distilled water and polyvinyl acetate. Subsequently the specimen was slowly dried.

Photographs were made with an Olympus E 620 SLR camera with a Zuiko digital lense (14–42 mm, 1:3.5–5.8).

Following institutional abbreviations are used in the text: IPA - Instituto de la Prehistoria de las Américas, Quintana Roo, Mexico; MICADAS - Klaus-Tschira-Archäometrie-Zentrum Mini radiocarbon Dating System, Mannheim, Germany; UNAM - Universidad Nacional Autónoma de México, Mexico; SMNK — Staatliches Museum für Naturkunde Karlsruhe.

Premolar 4 from PQR2011-PALMAS-V-1 was removed for radiocarbon dating at the Klaus-Tschira-Archäometrie-Zentrum (MICADAS) at Mannheim, Germany, but without giving a result.

Anyway, ^{14}C dating of fossils from submerged caves of the Yucatán Peninsula must be treated with considerable caution as collagen levels of these underwater fossils are extremely low (Burr et al., 2009; Taylor, 2009).

The rostral three-thirds of the mandible and the mandibular body are red-colored, whereas the caudal fourth, including coronoid and condylar process, ramus and angular process of the mandible are brown colored (Fig. 2; 3). The rostral margin of the mandible is broken off at the level of the rostral wall of the canine alveolus in a way that the lateral wall of the alveolus of the canine is visible. The dorsal margin of the canine alveolus is also broken. All incisors, the canine and premolars two and three are missing. The fourth premolar was removed by us for laboratory analysis, including strontium isotopy and radiocarbon dating.

The Yucatán peccary mandible was compared with mandibles from extant Tayassuidae housed in the zoological collection of the State Museum of Natural History Karlsruhe, Germany (SMNK; SMNK-12010 and SMNK-1539 for *Pecari tajacu*, SMNK-412 and SMNK-1645 for *Tayassu pecari*). A phylogenetic analysis has not been executed, due to the fragmentary material that only consists of a single mandibular ramus.
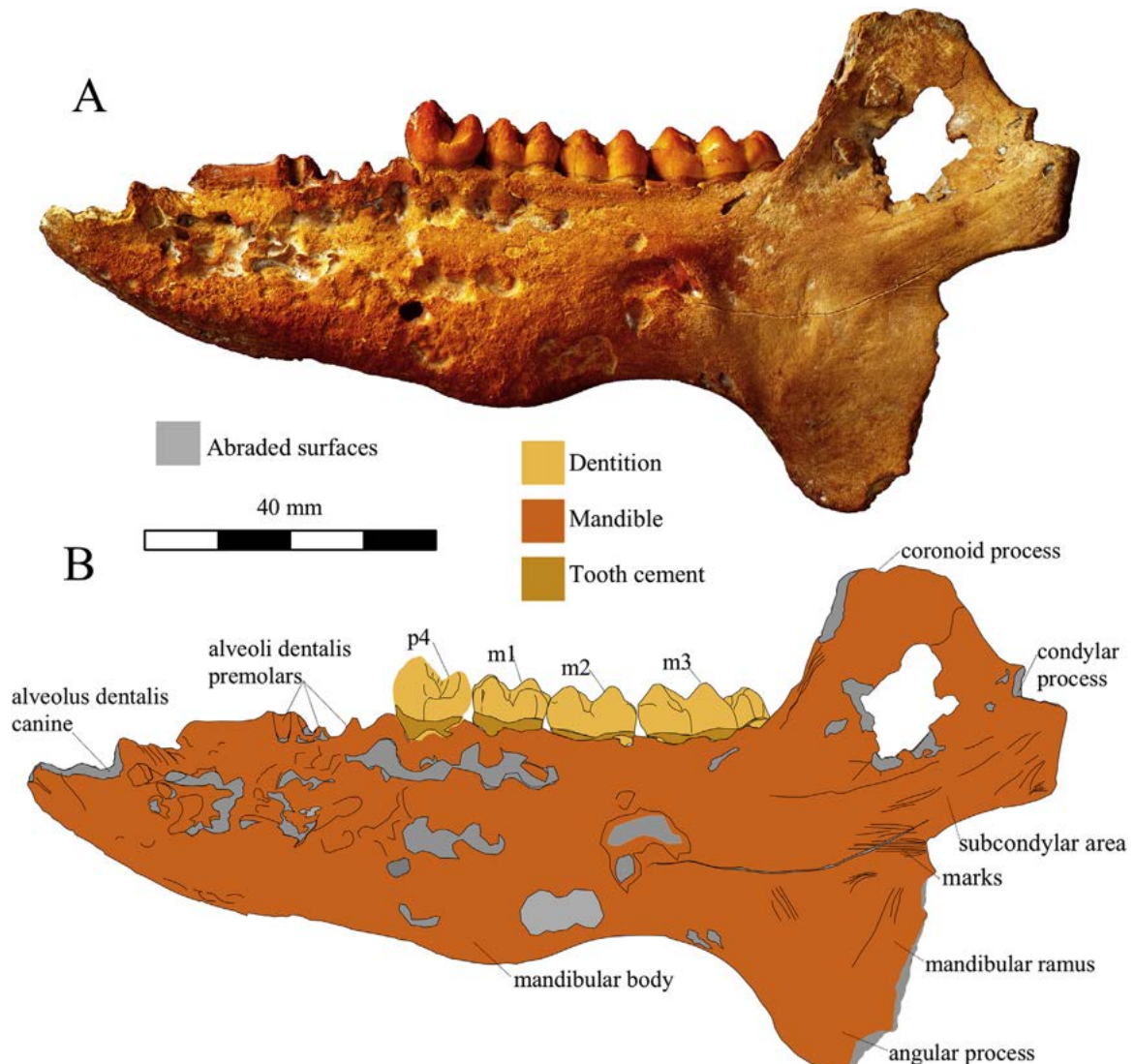
Fig. 2. *Muknalia minima* PQR2011-PALMAS-V-1, left mandibular ramus. A) Photograph of the buccal face, B) interpretative line drawing.

2. Systematic paleontology

Class MAMMALIA Linnaeus, 1758.
Order ARTIODACTYLA Owen, 1848.
Suborder SUINA Gray, 1868.
Family TAYASSUIDAE Palmer, 1897.
Genus ***Muknalia*** gen. nov.
Type species ***Muknalia minima*** spec. nov.

Diagnosis: As for the single included species described below.

Etymology: For the genus: *Muknalia* refers to the name of the finding locality Muknal = Maya for "underworld"-

Muknalia minima gen. et sp. nov.

Holotype: A left mandibular ramus, PQR2011-PALMAS-V-1, from the Muknal cave. The holotype is housed and accessible in the Instituto de Investigaciones Antropológicas of the UNAM under collection number PQR2011-PALMAS-V-1.

Etymology for the species: *minima* = Latin for smallest.

Locality: The Muknal cave tunnel system, which forms part of the Ox Bel Ha cave system, northwest of Tulúm, in the federal state of Quintana Roo, Mexico.

Diagnosis:

1) Deep concavity formed by the caudoventral edge of the condylar process and the caudal edge of the mandibular ramus, with an aperture angle of 110°. Such a concavity is absent in all other Tayassuidae, no matter whether extinct or extant.

2) Ventrally pronounced angular process, reaching almost one third of the maximum mandibular height. In all other extant and fossil Tayassuidae the angular process reaches no more than one fourth of the maximum mandibular height.

3) Angular process is laterally and ventrally convex, while the medial surface of the mandible is concave. In all other Tayassuidae the lateral and medial surface of the angular process is flat.

4) Condylar process forms the caudal-most extremity of the mandible. In other Pleistocene and extant Tayassuidae the caudal margin of the angular region reaches further caudally than the condylar process.

5) Outline of the coronoid process is trapezoidal in lateral view, with a horizontal dorsal margin. In all other Tayassuidae the dorsal margin of the coronoid process is convex.

6) Diastema between canine and p2 having approximately one eighth of the mandibular length. In all other Tayassuidae this diastema is one third to one half shorter.

7) Small body size (approximately 17–24 kg body mass); mandible at least one fourth to one half smaller than mandibles of adult Pleistocene (*Mylohyus* and *Platygonus*) and extant Tayassuidae.

Age: Latest Pleistocene or earliest Holocene (see below).

Description: PQR2011-PALMAS-V-1 measures 138.5 mm from the rostral edge of the c1 alveolus to the caudal extremity of the condylar process (Fig. 2; 3). The reconstructed length is about 145 mm. The specimen has a maximum height of 75 mm measured from the dorsal tip of the condylar process to the ventral margin of the angular process. The caudolateral surface of the mandible is convex, while the medial one is concave (Fig. 4). In lateral aspect the ventral margin of the mandible is convex and the mandibular body is like a reverse triangle in outline, reaching its maximum height level with m1. The dorsal and ventral margins of the mandible taper rostrally at an angle of 20° from the alveolus of the canine to m1. Caudal to m1 these margins converge towards the mandibular ramus. The mesiodistal diameter of the aperture of the canine alveolus is twice as long as that of p4. There is a diastema, which has one eighth the length of the mandible, between the canine and p2. The tooth-bearing part of the mandible is twice as long as the ramus mandibulae. The maximum width of the mandible reaches 8 mm at the height of the alveolus of the canine and declines caudally to 2 mm at the mandibular ramus. In lateral aspect, the coronoid process is trapezoidal in outline. At its base it has a length of 34 mm and is 25 mm high. Its horizontally running dorsal margin measures 15 mm. The rostral and caudal margins of the coronoid process diverge at an angle of 30° in ventral direction. The masseteric fossa is concave and of a rounded triangular outline. It is bordered by the caudally diverging coronoid roots and the condylar crest. Its rostral and ventral margins are each 40 mm long. The condylar process is broken off but its neck and ventral margin suggest that it had a height of 20 mm. The condylar process forms the caudolateral-most extremity of the mandible. The caudoventral margin of the condylar process on the subcondylar area runs rostrally for 18 mm with a near horizontal orientation. The caudoventral edge of the condylar process includes a 110° angle with the caudal edge of the mandibular ramus. Caudal to this angle, the mandibular ramus is almost vertical and 34 mm long. Its caudal margin is majorly preserved and only little material has flaked off. The angular process reaches almost one third of the maximum mandibular height. It is ventrally pronounced and has a rostrocaudal diameter of 40 mm.

The lateral surface of the mandible, between the alveolus of the canine and the first molar, is densely covered with circular to oval erosional pits. The diameter of these pits ranges from 0.2 mm to 15 mm. Confluent erosion holes with polymorph outlines with a depth up to 5 mm and a diameter of up to 30 mm perforate the lateral face of the mandible between the levels of p2 and m2. A hole with a diameter of 20 mm on the masseteric fossa of the mandible may also result from saltwater dissolution. Further dissolution traces are seen along the dorsal edge of the coronoid process and

Table 1
Measurements in Millimeter (mm) of *Muknalia minima* PQR2011-PALMAS-V-1, left mandibular ramus.

Total length of lower jaw, from rostral edge of alveolus of the canine to caudal edge of condylar process		138.5
Maximum mandibular height, from dorsal tip of the coronoid process to ventral edge of mandibular angle		70
Depth of lower jaw at m1		33
Total length of lower dental series (c1-m3), from rostral edge of alveolus of c1 to caudal edge of m3		105
Length of diastema		21
Length of premolar/molar toothrow; p2 to m3		69

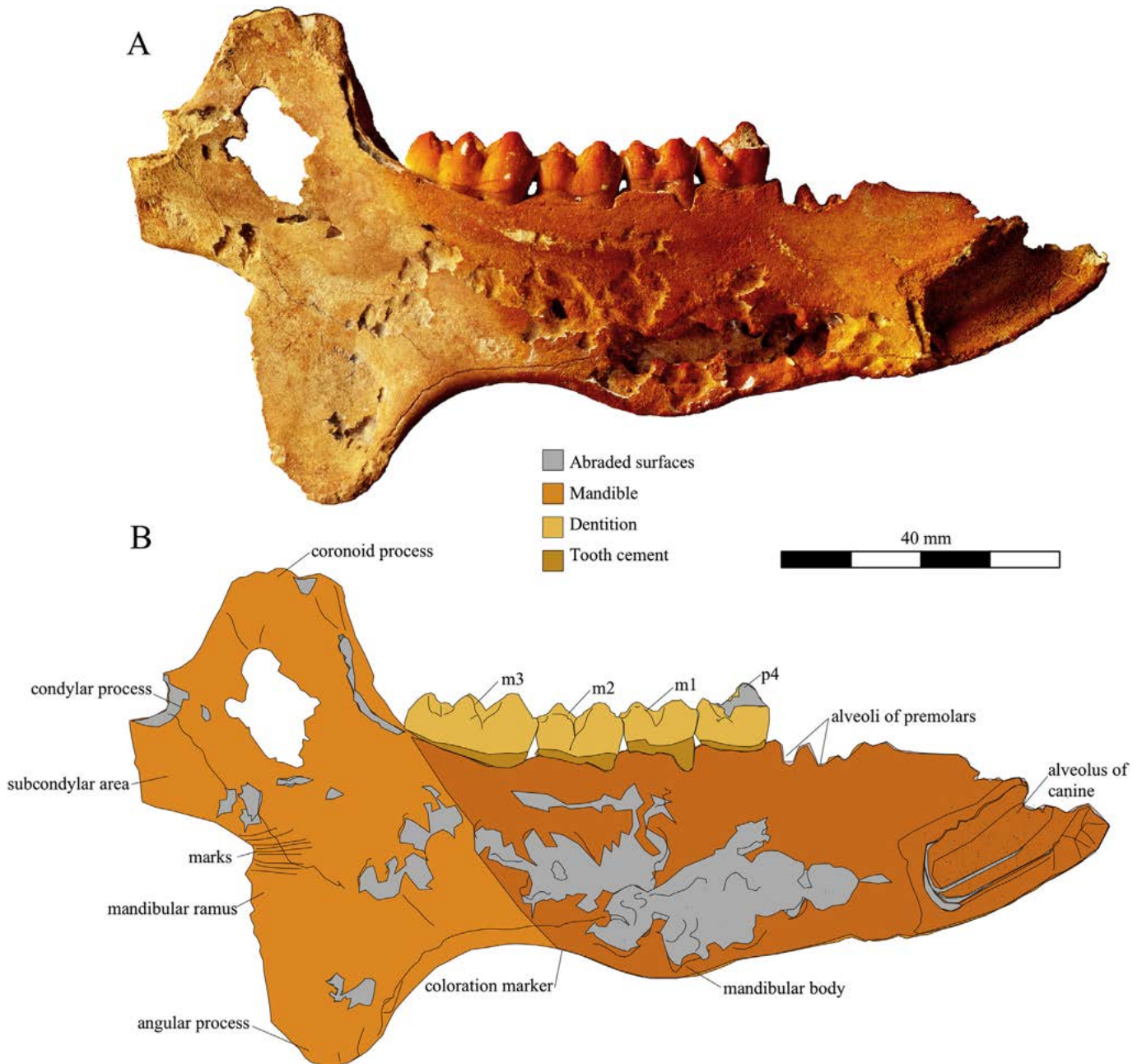| Dentition	Buccolingual	Mesiodistal
Alveolus of c1	Approx. >10.3	10.2
Alveolus of p2 (buccolingual measurement from caudal to rostral)	3 to 4	6.2
Alveolus of p3 (buccolingual measurement from caudal to rostral)	5 to 6.2	8
p4	8.5	10.1
m1	8.1	10.15
m2	9	12
m3 (buccolingual measurement from caudal to rostral)	6.5 to 9.75	18.3

Fig. 3. *Muknalia minima* PQR2011-PALMAS-V-1, left mandibular ramus. A) photograph of the lingual face, B) interpretative line drawing.

the caudal margin of the mandibular ramus. The condylar process is broken off. The margins of the condylar neck in lateral aspect form an angle of about 100°. Dissolution is strongest on the lateral and medial surfaces of the rostral half of the mandibular ramus, which was exposed to saltwater.

The dentition (Fig. 5; Table 1) of PQR2011-PALMAS-V-1 preserves p4 and m1 - m3. Seen from medially the lateral wall of the caninae alveolus is visible (Fig. 3). As preserved it is 30 mm deep and has a mesodistal length of 10 mm. In dorsal view, the alveoli of p2 and p3 are separated by a transversely running interradicular septum. The rostral subalveolus of p3 is buccolingually oval and similar in outline to those of p2. The caudal subalveolus of p3 is kidney-shaped and has a buccolingual diameter, which is twice as wide as the mesiodistal one. The p4 and m1 - m3 are brachy-

bunodont. They bear four prominent cuspids comprising the proto-, meta-, ento-, and hypoconid. The occlusal surface of p4 is rounded quadrangular in outline. The four cusps are conical. The occlusal surface of m1 is quadrangular in outline and buccolingually slightly wider than p4. This is due to the protoconid of m1, which is buccolingually one eighth wider than that of p4. The tips of all four cusps are worn. The m2 is mesiodistally one third longer than m1 (Table 1). The tips of proto-, ento-, and hypoconid are worn, while the metaconid does not show any abrasion. The m3 is half as wide as it is long (Fig. 5; Table 1). It is rounded triangular in outline and one third longer than m2. It bears a fifth cusp, the pentaconid. None of the cusps of m3 show any traces of abrasion. All valleys between the main cuspids of molars and p4 have accessory cuspids.
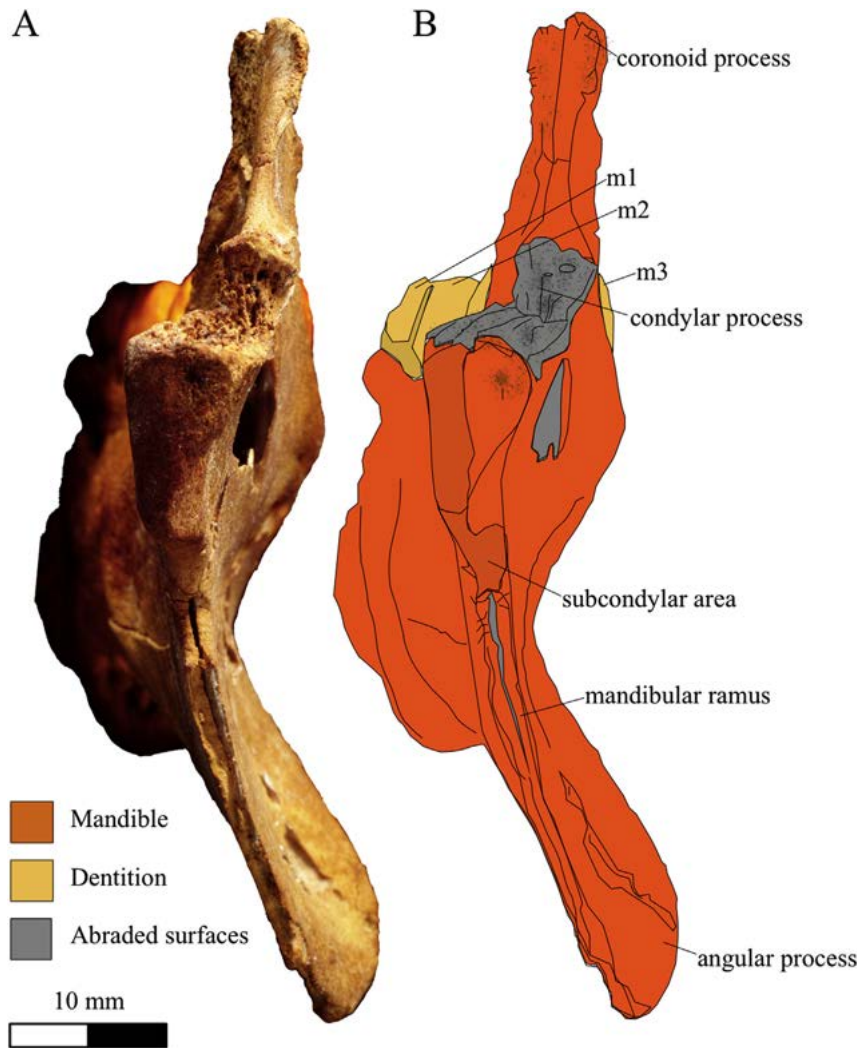
Fig. 4. *Muknalia minima* PQR2011-PALMAS-V-1: Photograph of the mandible A) in caudal view B) interpretative line drawing.

3. Discussion

Muknalia minima belongs to the family Tayassuidae because of the presence of the angular process of the mandible, which is absent in Suidae (Li-Ping, 2003). The molars of Suidae are characterized by the presence of three furrows on each of the four main cusps of molars (Cucchi et al., 2009; Pickford, 1986; Hünermann, 1968), which are absent in *M. minima*.

The preserved teeth and tooth positions of *M. minima* (alveolus of c1; alveoli of p2 − p3, p4, m1-3) correspond to the mandibular dental formula of Tayassuidae 2/3 1 3 3 (Redford and Eisenberg, 1992; Herring, 1985, 1974; Kirkpatrick and Sowls, 1962). All three molars of PQR2011-PALMAS-V-1 are fully erupted suggesting an adolescent or adult individual (Kirkpatrick and Sowls, 1962). The number of incisors of PQR2011-PALMAS-V-1 cannot be identified because of the lack of the rostral part of the mandible. Despite the rim of the aperture of the canine alveolus is missing, the curvature of the alveolus strongly suggests an almost horizontal aperture, which is diagnostic for Tayassuidae (Sowls, 1984).

4. Comparative anatomy

North American Tayassuidae of Miocene to Pliocene age are not discussed here because of the large chronological gap between

Muknalia minima and these species. Additionally *Muknalia minima* is also significantly smaller than these early species (Prothero, 2009; Harris and Liu, 2007; Wright, 1998; Slaughter, 1966; Hoare et al., 1964). Therefore, we only provide osteological comparisons with Pleistocene and Holocene Tayassuidae from the Americas.

Muknalia minima cannot be referred to any extant species of Tayassuidae (*Pecari tajacu*, *P. maximus*, *Tayassu pecari* and *Cataconus wagneri*) because of the horizontal dorsal margin of the coronoid process and the deep subcondylar concavity. All extant Tayassuidae have a dorsally convex margin of the coronoid process and the ventral root of the condylar process continues vertically into the caudal margin of the ramus mandibulae, without the trace of any subcondylar concavity (Harris and Liu, 2007). Furthermore, in *M. minima* the diastema between canine and p2 is significantly shorter, by at least one fourth, with respect to the preserved mandibular length equivalent in all extant Tayassuidae (Harris and Liu, 2007; Mayer and Wetzel, 1987, 1986).

The Collared Peccary *Pecari tajacu* (Linnaeus, 1758) is the smallest of the extant peccaries (Sowls, 1984) and has the widest geographical distribution (Mayer and Wetzel, 1987; Mayer and Brandt, 1982), ranging from the southern US as far south as Peru, Argentina and Brazil (Gongora et al., 2011; Mayer and Brandt, 1982; van Roosmalen et al., 2007). Remains of *P. tajacu* are also found in the cenotes (pers. obs. of JA). The mandibular fragment of *Muknalia*
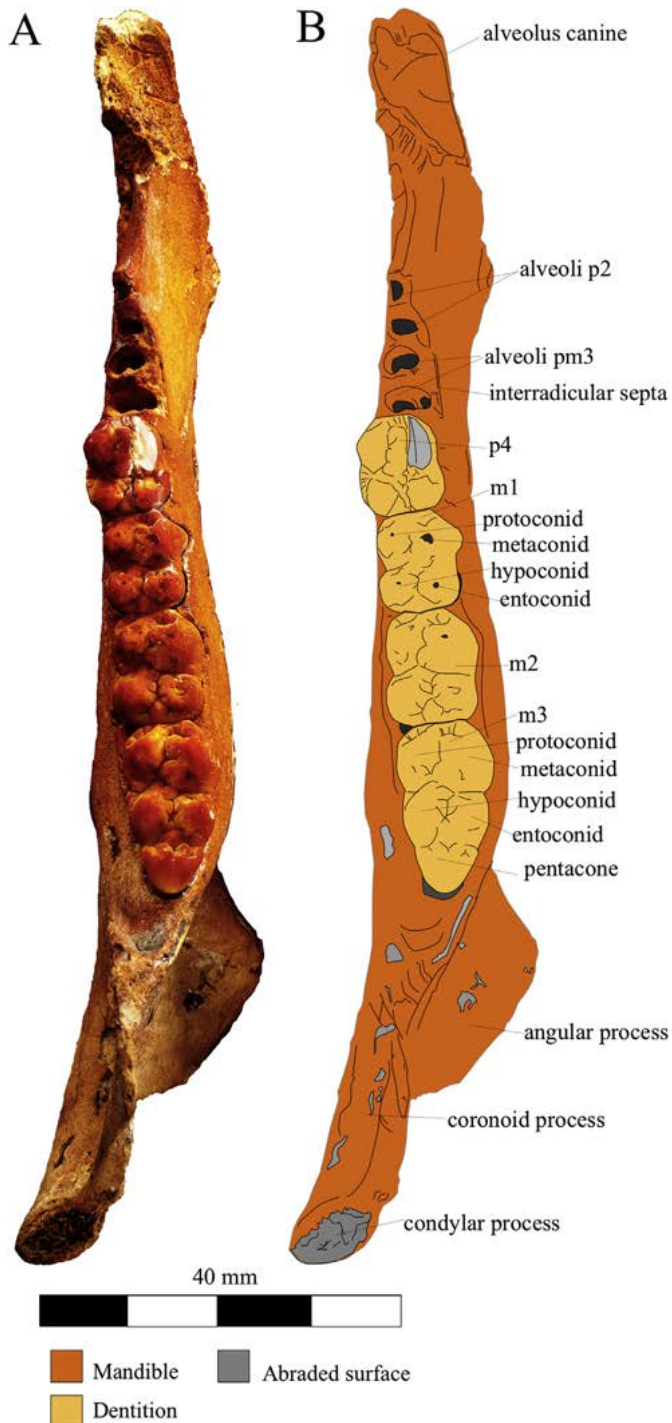
Fig. 5. A) Photograph of the mandible PQR2011-PALMAS-V-1 from Muknal in occlusal view B) interpretative line drawing.

minima measures 138.5 mm from alveolus of the canine to the caudal edge of the condylar process (Fig. 2; 3); it is therefore slightly smaller than SMNK-1539 with an equivalent length of 145 mm. It is concluded from the preserved part of PQR2011-PALMAS-V-1 that *M. minima* would have had a mass of between 17 and 24 kg, slightly less than the mass of *Pecari tajacu*, which has a body mass of 23–30 kg (Gongora et al., 2011; Sowls, 1984).

Specific osteological differences: In *Pecari* the dorsal and ventral margins of the mandibular body taper rostrally from the caudal end of the tooth row to the canine, and its ventral margin is slightly

vaulted. Therefore, the maximum mandibular body height of 47 mm is level with p2. In contrast, the dorsal and ventral mandibular margins of the mandibular body in *M. minima* taper cranially and caudally from m1. The maximum mandibular body height of 33 mm in *M. minima* is level with m1. The angular process of the *M. minima* mandible is pronounced and reaches one third of the maximum mandibular height, from the dorsal tip of the coronoid to the ventral edge of the angular process. In *Pecari* the angular process of the mandible reaches one eighth of the maximum mandibular height. The lateral surface of the mandibular ramus is convex in *M. minima*, but flat in *Pecari tajacu* (Kiltie, 1982; Reichenbach, 1835).

The White-lipped Peccary, *Tayassu pecari* (Link, 1795), ranges from Mexico (Veracruz, Oaxaca) to South America (Ecuador, Argentina) and thus lives in the area where *M. minima* occurred (Mayer and Wetzel, 1987). Reaching a body mass of 28–36 kg (Mayer and Wetzel, 1987) the species significantly exceeds the mass of *M. minima*.

In *T. pecari*, the dorsal edge of the mandibular body is slightly concave and not flat as in *M. minima*. The dorsal and ventral margins of the mandible taper rostrally from m3 to the canine in *Tayassu*, while the same margins in *M. minima* taper rostrally and caudally from m1.

The Chaco Peccary, *Catagonus wagneri* (Rusconi, 1930), is only known from the Gran Chaco region of northern Argentina, southeastern Bolivia and western Paraguay (Mayer and Wetzel, 1986). The Pleistocene fossil record of this species is restricted to South America, and more specifically to Argentina (Mayer and Wetzel, 1986). (Mayer and Wetzel, 1986). *Muknalia minima* was one fourth smaller than an adult *Catagonus wagneri* (Mayer and Wetzel, 1986).

The dorsal and ventral margins of the mandible corpus run parallel to each other between c and m3, whereas in *Muknalia* these margins converge rostrally at an angle of 20°, beginning level with m1. The condylar process of *M. minima* is located four times further caudal to the coronoid process than that of *Catagonus*, where the condylar and coronoid processes are exceedingly close to each other (Mayer and Wetzel, 1986). *Catagonus* shows a deep masseteric fossa, the ventral margin of which ends dorsal to the condylar process. In *M. minima,* the masseteric fossa is shallow and its ventral margin ends ventral to the condylar process. Furthermore, the surface of the ramus mandibulae of *Muknalia* is laterally convex, but flat in *Catagonus* (Mayer and Wetzel, 1986). The angular process of the mandibular ramus of *Muknalia* reaches almost one third the maximum height of the mandible, which is not the case in *Catagonus*, where it reaches one eighth only (Mayer and Wetzel, 1986). The Chaco Peccary has hypsodont or lophodont teeth (Herring, 1985; Mayer and Wetzel, 1986), which are one eighth to one fourth larger than those of *M. minima*. P4 of *Catagonus* and molars have four major cuspids (proto-, meta-, hypo- and entoconid) and numerous small accessory cuspids (Mayer and Wetzel, 1986), which is similar to *M. minima*. However, m3 in *M. minima* has five major cuspids, including the pentaconid, and therefore a fifth cuspid, which is absent in the m3 in *Catagonus* (Mayer and Wetzel, 1986).

4.1. Coeval tayassuids

The late Pliocene to early Pleistocene *Platygonus* was common across North America and migrated to South America during GABI (Gasparini and Ubilla, 2011; Woodburne, 2010). *Platygonus* was twice as big as *M. minima*, based on mandible length, but also differed by a number of other features: The diastema in *Patygonus* reached almost one fourth of the entire mandibular length (Hoare et al., 1964), while it is only one eighth in *M. minima*. The

coronoid process is dorsally convex, and not straight as in *M. minima*. Similar to all recent species of peccaries, *Platygonus* had a straight vertically running caudal margin of the ramus mandibulae without any subcondylar concavity. The masseteric fossa extends dorsal to the condylar process and does not terminate ventral to it as in *M. minima*. *Platygonus* has high-crowned, lophodont teeth and shows an increase of the occlusal area (Herring, 1985; Wetzel, 1977), which is not the case in *M. minima*. The p4 of *Platygonus* is characterized by only two major cuspids, the proto- and metaconid (Mayer and Wetzel, 1986). In *M. minima* all preserved molariforms (p4 and m1 - 2) have four major cuspids, with the exception of m3 with five cuspids.

The long-nosed peccary *Mylohyus* (Leidy, 1868), a North American genus of Pliocene to late Pleistocene age, is characterized by a long and slender skull and mandible (Lundelius, 1960), whereby the corresponding length of the mandible was twice as long as that of *M. minima* and the length of the diastema about one third of the mandibular length (Lundelius, 1960). In *M. minima* it measures one eighth. The rostrodorsal margin of the coronoid process is rounded in *Mylohyus* and its dorsocaudal end caudally pointed (Lundelius, 1960), whereas in *M. minima* the dorsal margin of the coronoid process runs horizontally. The masseteric fossa is deep in *Mylohyus* and its ventral margin extends rostrally until level with the tooth row, and dorsally to the coronoid process, which is not the case in *M. minima* where the masseteric fossa extends ventral to both the tooth row and the condylar process. A subcondylar angle is also missing in *Mylohyus* and the prominent angular process reaches almost one third of the maximum mandibular height. The ventral margin of the mandibular body of *Mylohyus* is straight in lateral view (Lundelius, 1960), while that of *M. minima* is convex. *Mylohyus* has brachy-bunodont teeth (Wetzel, 1977), similar to *M. minima*, but it differs from the latter by a variation of one to two large (proto- and metaconid) and two to three small cusps in m3 (Lundelius, 1960).

5. Individual age

The three fully erupted molars of *M. minima* provide evidence that the animal was mature, presumably representing an adolescent, because the teeth are barely or not abraded (Sowls, 1984). Compared with tooth conditions of extant peccaries the Muknal individual was approximately 1.5−2 years old at the time of death (Sowls, 1984; Kirkpatrick and Sowls, 1962). Given the fact that *M. minima* has almost achieved the final body size, it represents the smallest species of Tayassuidae from the Pleistocene and early Holocene known to date.

6. Stratigraphic age

Tayassuidae were abundant in North America during the latest Pleistocene, but a significant decrease in diversity is reported around the Pleistocene−Holocene transition (Dutra et al., 2016; Gasparini and Ubilla, 2011). Most Pleistocene Tayassuidae were radiocarbon dated to the end of this period, e.g. *Platygonus* to 11.900 ± 750 BP and *Mylohyus* to 10.790 ± 150 BP (Haynes, 2016, 2013; Sowls, 1984; Wetzel, 1977). The *M. minima* specimen described here from the submerged Muknal cave near Tulúm in the Mexican state of Quintana Roo could not be radiocarbon dated, but the fact that this species is now extinct and that the 33 m level of the cave were flooded during the early Holocene, at about 9.600 BP (Grant et al., 2012; Beddows, 2004; Moore et al., 1992; Marín, 1990; Back and Hanshaw, 1970), suggests a late Pleistocene age, *Muknalia minima* thus increases the late Pleistocene diversity of Tayassuidae.

7. Conclusions

The mandible fragment of *M. minima* is characterized by a deep concavity formed by the caudoventral edge of the condylar process and the caudal edge of the mandibular ramus, with an aperture angle of 110°. The ventrally pronounced angular process, reaches almost one third of the maximum mandibular height. These features thus differ significantly from all extant Tayassuidae and their Pleistocene relatives *Platygonus* and *Mylohyus*. The most striking feature of the animal is its small body mass of between 17 and 24 kg compared to *Mylohyus* and *Platygonus*. We assume that the *M. minima* belonged to a late Pleistocene population of Tayassuidae that may well have been endemic to the Yucatán Peninsula.

The particular shape of the mandible of *M. minima* suggests a masticatory apparatus that differed from all other coeval or extant Tayassuidae (Kiltie, 1982, 1981). However, more fossils from Central America, especially complete skulls, are needed for further substantial conclusions.

References

Ameghino, F., 1904. Neuvas especies de mamíferos cretáceos y terciarios de la República Argentina (continuación). Ann. Soc. Cient. Argent. 58, 182−192.

Back, W., Hanshaw, B.B., 1970. Comparison of chemical hydrogeology of the carbonate peninsulas of Florida and Yucatan. J. Hydrol. 10, 330−368.

Beddows, P.A., 2004. Groundwater Hydrology of a Coastal Conduit Carbonate Aquifer: Caribbean Coast of the Yucatan Peninsula, Mexico. University of Bristol, UK.

Burr, G.S., Beck, J.W., Correge, T., Cabioch, G., Taylor, F.W., Donahue, D.J., 2009. Modern and Pleistocene reservoir ages inferred from south. Radiocarbon 51, 319−335.

Carranza-Castañeda, Ó., 2006. Late Tertiary fossil localities in central Mexico, between 19°−23°N. In: Carranza-Castañeda, Ó., Lindsay, E. (Eds.), Advances in Late Tertiary Vertebrate Paleontology in Mexico and the Great American Biotic Interchange. Universidad Nacional Autónoma de México, Instituto de Geología and Centro de Geociencias, Mexico City, pp. 45−60.

Chatters, J.C., Kennett, D.J., Asmerom, Y., Kemp, B.M., Polyak, V., Blank, A.N., Beddows, P. a, Reinhardt, E., Arroyo-Cabrales, J., Bolnick, D. a, Malhi, R.S., Culleton, B.J., Erreguerena, P.L., Rissolo, D., Morell-Hart, S., Stafford, T.W., 2014. Late Pleistocene human skeleton and mtDNA link Paleoamericans and modern Native Americans. Science 344, 750−754.

Collins, S.V., Reinhardt, E.G., Rissolo, D., Chatters, J.C., Nava Blank, A., Luna Erreguerena, P., 2015. Reconstructing water level in Hoyo Negro, Quintana Roo, Mexico, implications for early Paleoamerican and faunal access. Quat. Sci. Rev. 124, 68−83.

Le Conte, J.L., 1848. On *Platygonus compressus*: a new fossil pachyderm. Am. Acad. Arts Sci. 3, 257−274.

Cucchi, T., Fujita, M., Dobney, K., 2009. New insights into pig taxonomy, domestication and human dispersal in island South East Asia: molar shape analysis of Sus remains from Niah Caves, Sarawak. Int. J. Osteoarchaeol. 19, 508−530.

Ducrocq, S., 1994. An Eocene peccary from Thailand and the biogeographical origins of the Artiodactyl family Tayassuidae. Palaeontology 37, 765−780.

Ducrocq, S., Chaimanee, Y., Suteethorn, V., Jaeger, J.J., 1998. The earliest known pig from the upper Eocene of Thailand. Palaeontology 41, 147−156.

Dutra, P.R., Missagia, R.V., Perini, F.A., Cozzuol, M.A., Gasparini, G.M., Guedes, P.G., Salles, L.D.O., 2016. Fossil peccaries of the Late Pleistocene/Holocene

(Cetartiodactyla, Tayassuidae) from underwater caves of Serra da Bodoquena (Mato Grosso do Sul State, Brazil). Hist. Biol. 1–8.

Ferrusquía-Villafranca, I., 2006. The first Paleogene mammal record of Middle America: *Simojovelhyus pocitosense* (Helohyidae, Artiodactyla). J. Vertebrate Paleontol. 26, 989–1001.

Ferrusquía-Villafranca, I., Arroyo-Cabrales, J., Martínez-Hernández, E., Gama-Castro, J., Ruiz-González, J., Polaco, O.J., Johnson, E., 2010. Pleistocene mammals of Mexico: a critical review of regional chronofaunas, climate change response and biogeographic provinciality. Quat. Int. 217, 53–104.

Fischer [von Waldheim], J.G., 1814. Tayassu. Zoognosia 284.

Gasparini, G.M., Ubilla, M., 2011. *Platygonus* sp. (Mammalia:Tayassuidae) in Uruguay (Raigón? Formation; Pliocene-early Pleistocene), comments about its distribution and palaeoenvironmental significance in South America. J. Nat. Hist. 45, 2855–2870.

Gongora, J., Biondo, C., Cooper, J.D., Taber, A., Keuroghlian, A., Altrichter, M., Nascimento, F.F., Chong, A.Y., Miyaki, C.Y., Bodmer, R., Mayor, P., González, S., 2011. Revisiting the species status of *Pecari maximus* van Roosmalen et al., 2007 (Mammalia) from the Brazilian Amazon. Bonn. Zool. Bull. 60, 95–101.

González González, A.H., Rojas, C., Terrazas, A., Benavente Sanvicente, M., Stinnesbeck, W., Aviles, J., De los Ríos, M., Acevez, E., 2008a. The arrival of humans on the yucatan peninsula: evidence from submerged caves in the State of Quintana Roo, Mexico. Curr. Res. Pleistocene 25, 1–24.

González González, A.H., Rojas Sandoval, C., Acevez Nuñez, E., Avilés Olguín, J., Analco Ramírez, S., Del Rio Lara, O., Luna Erreguerena, P., Velazquez Morlet, A., Stinnesbeck, W., Terrazas Mata, A., Benavente Sanvicente, M., 2008b. Evidence of early inhabitants in submerged caves in Yucatan, Mexico. In: Leshikar-Denton, M.E., Erreguerena, P.L. (Eds.), Underwater and Maritime Archaeology in Latin America and the Caribbean. Left Coast Press, Walnut Creek, CA, pp. 127–142.

González González, A.H., Terrazas, A., Stinnesbeck, W., Benavente, M.E., Avíles, J., Padilla, J.M., Velásquez, A., Aceves, E., Frey, E., 2013. The first human settlers on the Yucatan peninsula: evidence from drowned caves in the state of Quintana Roo (south Mexico). In: Graf, K.E., Ketron, C.V., Waters, M. (Eds.), Paleoamerican Odissey, Center for the Study of the First Americans. Texas A&M University, pp. 323–338.

Grant, K.M., Rohling, E.J., Bar-Matthews, M., Ayalon, A., Medina-Elizalde, M., Bronk Ramsey, C., Satow, C., Roberts, A.P., 2012. Rapid coupling between ice volume and polar temperature over the past 150,000 years. Nature 491, 744–747.

Gray, J.E., 1868. Synopsis of the species of pigs (Suidae) in the British Museum. Proc. Zool. Soc. Lond. 17–49.

Harris, J.M., Liu, L.-P., 2007. Superfamily Suoidea. In: Prothero, D.R., Foss, S.E. (Eds.), The Evolution of Artiodactyls. The Johns Hopkins University Press, Baltimore, pp. 130–150.

Haynes, G., 2013. Extinctions in North America's Late Glacial landscapes. Quat. Int. 285, 89–98.

Haynes, G., 2016. North American Megafauna Extinction: Climate or Overhunting? Encyclopedia of Global Archaeology, pp. 5382–5390.

Herring, S.W., 1974. A biometric study of suture fusion and skull growth in peccaries. Anat. Embryol. 146, 167–180.

Herring, S.W., 1985. Morphological correlates of masticatory patterns in peccaries and pigs. J. Mammal. 66, 603–617.

Hoare, R.D., Coash, J.R., Innis, C., Hole, T., 1964. Pleistocene peccary *Platygonus compressus* LeConte from Sandusky County, Ohio. Ohio J. Sci. 64, 207–214.

Hünermann, K.A., 1968. Die Suidae (Mammalia, Artiodactyla) aus den Dinotheriensanden (Unterpliozän: Pont) Rheinhessens (Südwestdeutschlands). Schweiz. Paläontol. Abh. 86, 1–96.

Jiménez-Hidalgo, E., Smith, K.T., Guerrero-Arenas, R., Alvarado-Ortega, J., 2015. The first Late Eocene continental faunal assemblage from tropical North America. J. S. Am. Earth Sci. 57, 39–48.

Kiltie, R.A., 1981. The function of interlocking canines in rain forest peccaries (Tayassuidae). J. Mammal. 62, 459–469.

Kiltie, R.A., 1982. Bite force as a basis for niche differentiation between rain forest peccaries (*Tayassu tajacu* and *T. pecari*). Biotropica 14, 188–195.

Kirkpatrick, R.D., Sowls, L.K., 1962. Age determination of the collared peccary by the tooth-replacement pattern. J. Wildl. Manag. 26, 214–217.

Leidy, J., 1868. Notice of some remains of extinct pachyderms. Proc. Acad. Nat. Sci. Phila. 20, 230–233.

Li-Ping, L., 2000. Eocene suoids (Artiodactyla, mammalia) from Bose and Yongle basin, China, and the classification and evolution of the Paleogene suoids. Vertebr. Pal Asiat. 39, 115–128.

Li-Ping, L., 2003. Chinese Fossil Suoidea - Systematics, Evolution, and Paleoecology. University of Helsinki.

Link, H.F., 1795. Beiträge zur Naturgeschichte, 2nded. Rostock and Leipzig.

Linnaeus, C., 1758. Systema Naturæ. Lars Salvius, Stockholm.

Lundelius, E.L., 1960. *Mylohyus nasatus*. long-nosed peccary of the Texas Pleistocene. Bull. Tex. Meml. Mus. 1–41.

Marín, L.E., 1990. Field Investigations and Numerical Simulation of Groundwater Flow in the Karstic Aquifer of Northwestern Yucatan. Northern Illinois University, Mexico.

Mayer, J.J., Brandt, P.N., 1982. Identity, distribution and natural history of the peccaries, Tayassuidae. Mammalian Biol. S. Am. 6, 85–93.

Mayer, J.J., Wetzel, R.M., 1986. Catagonus Wagneri. Mammalian Species, pp. 1–5.

Mayer, J.J., Wetzel, R.M., 1987. Tayassu pecari. Mammalian Species, pp. 1–7.

Meng, J., McKenna, M.C., 1998. Faunal turnover of Palaeogene mammals from the Mongolian Plateau. Nature 394, 364–367.

Moore, Y.H., Stoessel, R.K., Easley, D.H., 1992. Fresh-water sea-water relationship within a groundwater-flow system, northeastern coast of the Yucatan Peninsula: ground water. Ground water 30, 343–350.

Owen, R., 1848. Description of teeth and portions of jaws of two extinct anthracotheroid quadrupeds (*Hyopotamus vectianus* and *Hyop. bovinus*) discovered by the Marchioness of Hastings in the Eocene deposits on the N. W. coast of the Isle of Wight: with an attempt to devel. Quaterly J. Geol. Soc. Lond. 4, 103–141.

Palmer, T.S., 1897. Notes on the nomenclature of four genera of tropical American mammals. Proc. Biol. Soc. Wash. 11, 173–174.

Pickford, M., 1986. A revision of the Miocene Suidae and Tayassuidae, (Artiodactyla, mammalia) of Africa. Tert. Res. 82.

Prothero, D.R., 2009. The early evolution of the North American peccaries (Artiodactyla: Tayassuidae). Mus. North. Ariz. Bull. 65, 509–541.

Redford, K.H., Eisenberg, J.F., 1992. Mammals of the Neotropics. The Southern Cone, vol. 2. The University of Chicago Press, Chicago and London.

Reichenbach, L., 1835. Pecari. Bildergalerie Der Thierwelt, p. 1.

van Roosmalen, M.G.M., Frenz, L., Van Hooft, P., De Iongh, H.H., Leirs, H., 2007. A new species of living peccary (Mammalia: Tayassuidae) from the Brazilian Amazon. Bonn. Zool. Beiträge 55, 105–112.

Rusconi, C., 1930. Las especies fósiles argentinas de pecaríes (Tayassuidae) y sus relaciones con las de Brasil y Norte America. An. del Mus. Nac. Hist. Nat. Buenos Aires 36, 121–241.

Simpson, G.G., 1944. Tempo and mode in evolution. Columbia Biol. Ser. 18, 1–237.

Slaughter, B.H., 1966. *Platygonus compressus* and associated fauna from the Laubach Cave of Texas. Am. Midl. Nat. 475–494.

Smart, P.L., Beddows, P., Coke, J., Doerr, S., Whitaker, F.F., 2006. Cave development on the Caribbean coast of the Peninsula, Yucatan Roo, Quintana. Geol. Soc. Am. Special Pap. 404, 105–128.

Sowls, L.K., 1984. The Peccaries. The University of Arizona Press, Tucson, Arizona.

Taylor, R.E., 2009. Six decades of radiocarbon dating in new world archaeology. Radiocarbon 51, 173–212.

Wetzel, R.M., 1977. The extinction of peccaries and a new case of survival. Ann. N. Y. Acad. Sci. 288, 538–544.

Woodburne, M.O., 1969. Systematics, Biogeography, and Evolution of Cynorca and Dyseohyus (Tayassuidae). American Museum of Natural History.

Woodburne, M.O., 2010. The Great American Biotic Interchange: dispersals, tectonics, climate, sea level and holding pens. J. Mammalian Evol. 17, 245–264.

Wright, D.B., 1998. Tayassuidae. In: Janis, C.M., Scott, K.M., Jacobs, L.L. (Eds.), Evolution of Tertiary Mammals of North America. Cambridge University Press, Cambridge, pp. 389–401.

Taylor & Francis
Taylor & Francis Group

ARTICLE

Check for updates

Panthera balamoides and other Pleistocene felids from the submerged caves of Tulum, Quintana Roo, Mexico

Sarah R. Stinnesbeck[a,b], Wolfgang Stinnesbeck[c], Eberhard Frey[a,b,d], Jerónimo Avilés Olguín[e], Carmen Rojas Sandoval[f], Adriana Velázquez Morlet[f] and Arturo H. González[e]

[a]Department of Earth Sciences, Staatliches Museum für Naturkunde Karlsruhe, Karlsruhe, Germany; [b]Institute for Geography and Geoecology, Karlsruhe Institut of Technology (KIT), Karlsruhe, Germany; [c]Institute for Earth Sciences, Heidelberg University, Heidelberg, Germany; [d]Institute for Zoology, Karlsruhe Institute of Technology (KIT), Karlsruhe, Germany; [e]Museo del Desierto, Carlos Abedrop Dávila, Saltillo, Mexico; [f]Instituto Nacional de Antropología e Historia, Tulúm, Mexico

ABSTRACT

Here we describe a new species of a Pleistocene felid based on the distal third of a right humerus from the submerged El Pit cenote (sinkhole) near Tulum in Quintana Roo, Mexico. The new taxon, *Panthera balamoides* sp. nov., is characterized by a large entepicondylar foramen, a gracile and straight humeral shaft with a prominent supracondylar ridge with a small depression on the lateral epicondyle and a distal articular surface located medially with respect to the long axis of the shaft.

Two felid clavicles from the same locality have been assigned to *Panthera atrox*, while a humerus fragment from the Kim Ha cave near Tulum likely corresponds to *Smilodon gracilis*. *Panthera balamoides* lines up with other likely endemic mammals in the region, which suggest that at least northern Quintana Roo, if not the entire Yucatán peninsula, may have been ecologically isolated during the Pleistocene, due to the repeated expansion of grassland.

Introduction

The Pleistocene felid fossil record in the Americas includes the genera *Panthera*, *Puma*, *Felis*, *Lynx*, *Leopardus*, *Miracinonyx* and the machairodontids *Smilodon*, *Xenosmilus* and *Homotherium* (Antón et al. 2014; Bravo-Cuevas et al. 2016). With the exception of *Xenosmilus*, which is only known from Florida, all other genera are reported from Mexico (Bravo-Cuevas et al. 2016). While the American cheetah *Miracinonyx inexpectatus* and the American lion *Panthera atrox* have only been documented from a few Mexican localities, remains of machairodontid cats are significantly more abundant (Ferrusquía-Villafranca et al. 2010; Bravo-Cuevas et al. 2016). Among Machairodontinae, *Homotherium* became extinct in Africa and Eurasia during the middle Pleistocene (Pre-Late Glacial Maximum, PLGM; Antón et al. 2014; Serangeli et al. 2015), but survived in America until the late Pleistocene (Rincón et al. 2011; Antón et al. 2014). Three recognized *Smilodon* species are known from the American continent: *S. gracilis*, *S. fatalis* and *S. populator*. All three have been reported from South America (Lewis 2018; Manzuetti et al. 2018), but only *S. gracilis* and *S. fatalis* are to date restricted to North America (Berta 1985; Björn and Werdelin 1990; Rincón et al. 2011). The latest appearance of *Smilodon gracilis* dates back to the middle Pleistocene in North and South America (Rincón et al. 2011), while *S. fatalis* is known from the late Pleistocene of both subcontinents (Björn and Werdelin 1990; Prevosti and Martin 2013).

The extant *Panthera yagouaroundi*, *Leopardus pardalis* and *Puma concolor* have been reported from the late Pleistocene

of the Yucatán peninsula (Alvarez and Polaco 1982; Bravo-Cuevas et al. 2016). The presence of the early to middle Pleistocene *Smilodon gracilis* on the Yucatán peninsula (YP) has been discussed, but not demonstrated conclusively (Alvarez and Polaco 1982; Bravo-Cuevas et al. 2016).

Here we present a fragmentary felid humerus from the El Pit cenote (sinkhole) near Tulum on the YP. El Pit cenote is recognized as an anthropological site, because it yielded skeletal remains of two human individuals dated to about 13 ky (thousand years) BP (before present; González et al. 2008b; González et al. 2013). The felid humerus fragment described here exhibits anatomical features that combine characters of *S. gracilis* and *Panthera*. It is described as a new species of *Panthera*. Two clavicles found on the debris mount of the El Pit cenote agree with *Panthera atrox*, whereas a humerus fragment collected in the submerged Kim Ha cave a few km to the South of El Pit is here assigned to *Smilodon gracilis*.

The El Pit locality

The distal end of a right felid humerus has been discovered on the debris mount of El Pit cenote (Figure 1). El Pit cenote is part of the private diving and snorkel park Dos Ojos, which is located 15 km north of Tulum in the Mexican federal state of Quintana Roo. El Pit cenote is a bottle-shaped sinkhole that formed in horizontally layered shallow-water limestone of Miocene-Pliocene age. The surface aperture of the cenote measures 6 by 6 meters, but gradually widens to 52 m at a depth of about 20 m and reaches a maximum depth of about 60 m below present day
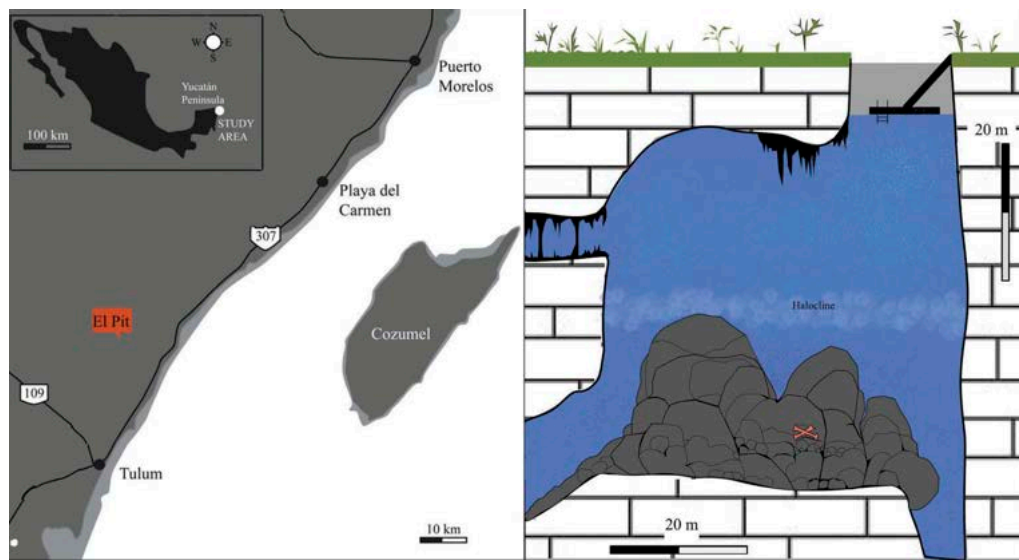

Published online 18 Dec 2018

Figure 1. (a) Location of the El Pit cenote in the federal state of Quintana Roo, Mexico. (b) Vertical section of the El Pit cenote and the finding location of *Panthera balamoides* (CPC-2205).

water level (Figure 1). Below the center of the cenote, an enormous debris mount reaches to about 30 m height. The halocline is located at about 15 m water depth. El Pit cenote forms part of the Dos Ojos subsystem and the latter is part of the Sac Actun system of underwater caves (Figure 1). To date, the Sac Actun system has a total registered length of 353 km and maximum known depth of 119 m (QRSS 2018). Sac Actun is thus the most extended cave system in Mexico (Kambesis and Coke 2013, 2016; QRSS 2018). The recently discovered connection of Sac Actun with the Ox Bel Ha system makes this combined submerged cave system the longest worldwide (Kambesis and Coke 2016; QRSS 2018).

Material and methods

The distal third of the right humerus described here and assigned to *Panthera balamoides* (collection number CPC-2205), was discovered in 2012 by JAO and was collected within the same year. The approximate finding position is depicted in Figure 1, in 44 m water depth on the SW quadrant of the El Pit debris mount. The specimen was thus discovered in the saltwater unit of El Pit cenote. In the lab, the bone was treated for four months with distilled water. Then the specimen was gradually dried. A similar procedure was used for the other felid bones documented here. A sample of CPC-2205 was removed for radiocarbon dating at the Klaus-Tschira-Archäometrie-Zentrum (MICADAS) at Mannheim, Germany, but without yielding a result.

Photographs were made with an Olympus E 620 SLR camera with a Zuiko digital lense (14e42 mm, 1:3.5e5.8).

The following institutional abbreviations are used in the text: AMNH – American Museum of Natural History, New York City, USA; CPC – Colección Paleontológica de Coahuila, Museo del Desierto, Saltillo, Coahuila; GPIT – Geologisch-Paläontologisches Institut

der Universität Tübingen, Germany; INAH – Instituto Nacional de Antropología e Historia, Mexico; NMB – Naturhistorische Museum Basel, Switzerland; MICADAS – Mini Radiocarbon Dating System, Klaus-Tschira-Archäometrie-Zentrum, Mannheim, Germany; MUDE – Museo del Desierto, Saltillo, Coahuila; UNAM – Universidad Nacional Autónoma de México, Mexico; SMNK – Staatliches Museum für Naturkunde Karlsruhe, Germany.

Comparisons were made with specimens of extinct and extant taxa, including *Puma concolor, Panthera onca*, both housed in the zoological collection of the MUDE without collection number, a female *Panthera leo* SMNK-MAM 13592, a male *Panthera pardus melas* SMNK-MAM 11763, a male *Panthera tigris* SMNK-MAM 223, a female *Puma concolor* SMNK-MAM 11998, all housed in the zoological collection of the SMNK, a cast of *Smilodon populator* (NMB S.A.1536) from the collection of the Natural History Museum Basel, Switzerland, *Smilodon gracilis* (AMNH 69227) from McLeod Pocket, and two humeri of *Smilodon* sp. (AMNH 23456) from Allen Cave, both from Florida and housed at the American Museum of Natural History in New York City, and a *Smilodon fatalis* (GPIT-MA-10023) skeleton from La Brea housed at the University of Tübingen, Germany. Photographs and published descriptions of the following taxa have been compared with the humerus from El Pit: *Xenosmilus hodsonae* from Alachua County, Florida, USA, *Miracinonyx inexpectatus* (UF-95766) from the early Pleistocene of Florida, USA, the Pleistocene *Panthera onca, Panthera atrox* and European and American *Homotherium* species. A phylogenetic analysis of the new species documented here (*Panthera balamoides*) has not been executed, because the material only consists of a single fragmentary right humerus.

Systematic palaeontology

CARNIVORA Bowdich 1821
FELIDAE Fischer de Waldheim 1817
PANTHERINAE Pocock, 1917
Panthera Oken, 1816
Panthera balamoides sp. nov.

Etymology

P. balamoides sp. nov. 'Jaguar-like'; balam = Maya word for jaguar, εἶδος (eidos) Greek for 'similarity'.

Holotype

Distal third of a right humerus, CPC-2205 from El Pit cenote in Quintana Roo, Mexico (Table 1; Figure 2). The holotype is housed and accessible at the Instituto Nacional de Antropología y Historia (INAH) at Tulúm.

Locality

El Pit cenote, Quintana Roo, Mexico.

Diagnosis

Panthera balamoides is based on a large entepicondylar foramen, a gracile and straight humeral shaft with a prominent supracondylar ridge with a small depression on the lateral epicondyle and a distal articular surface, which is significantly set off medially against the long axis of the humeral shaft.

Table 1. *Panthera balamoides* measurements in millimeters.

Greatest length of humerus	136
Greatest width of the distal end of the humerus	81
Greatest proximal width of the shaft	28
Mediolateral width of the trochlea and capitulum	61
Maximum diameter of the entepicondylar foramen	24
Greatest width of the olecranon fossa	33
Greatest height of the olecranon fossa	30

Description

The specimen consists of the distal third of a right humerus. The fragment has a maximum distal width of 81 mm and a maximum length of 136 mm. The proximal two-thirds of the bone are missing. The medial epicondyle, the lateral surface of the trochlea and the distal surface of the capitulum are also not preserved.

The medial and lateral margins of the shaft parallel each other before significantly diverging distally level with the metaphysis at an angle of 60° to the long axis of the shaft (Figure 2). The posterior face of the shaft is slightly concave. This concavity extends from the proximal margin of the metaphysis to the proximal margin of the olecranon fossa (Figure 2).

The lateral supracondylar ridge of the humerus is prominent and becomes distally thickened (Figure 2). The laterally convex supracondylar ridge emerges from the distal half of the preserved shaft. The lateral margin of this ridge bears a crescent-shaped concave depression proximal to the articular surface. This depression results in a medial torsion of the supracondylar ridge (Figure 2).

Level with the supracondylar ridge, a bony entepicondylar bridge encloses the entepicondylar foramen. In both anterior and posterior view, the entepicondylar bridge is strongly convex medially and is set off by 8 mm medially to the medial face of the humeral shaft (Figure 2). The entepicondylar foramen is prominent and visible in both anterior and posterior view. It is proximodistally elongated elliptical in outline with a maximum length of 24 mm and maximum width of 12 mm. The long axis of the foramen runs diagonally to the long axis of the shaft at an angle of 40°. In anterior view, the entepicondylar foramen is located directly medially to the medial margin of the shaft. The entepicondylar foramen must have been confluent with the distally located medial epicondyle, which is not preserved.

In anterior view, the surface of the foramen edge is smooth. Its medial margin is straight and adjacent to the
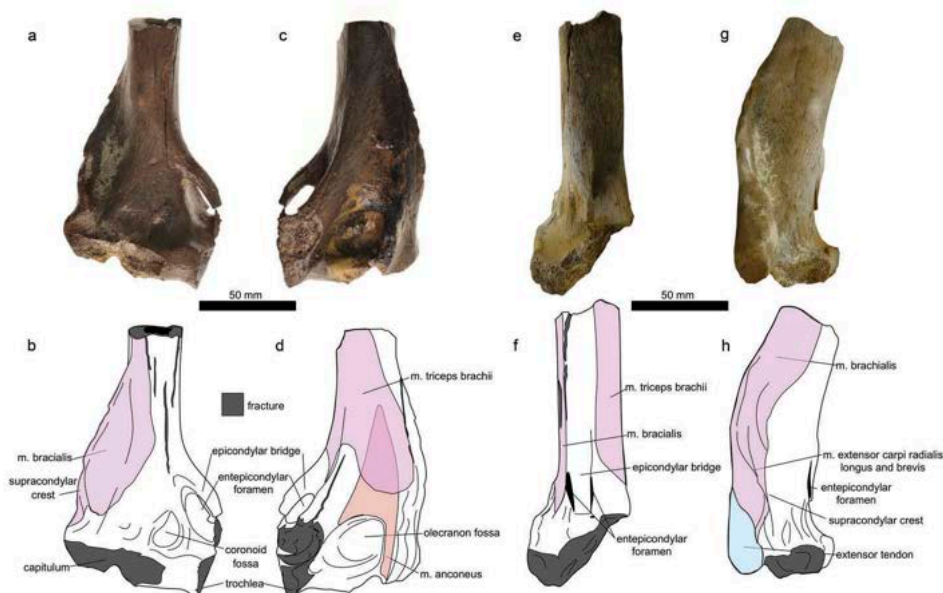
Figure 2. *Panthera balamoides* in anterior (a, b), posterior (c, d), medial (e, f) and lateral view (g, h). Photos (a, c, e, g) and interpretative line drawings (b, d, f, h).

entepicondylar foramen. The coronoid fossa is shallow and is located on the anterior face of the epiphysis adjacent to the distal articular surface. Capitulum and trochlea are abraded, but it is evident that the proximal margin of the capitulum diverges laterally against the medioproximal edge of the trochlea at an angle of 20°. The connection between capitulum and trochlea is located level with the medial edge of the shaft (Figure 2(a,b)).

The olecranon fossa is located proximal to the distal articular surface (Figure 2(c,d)). Its maximum height of 33 mm and width of 30 mm are almost identical. Its shape is that of an obtuse, scalene triangle, in which the tip is proximolaterally pointed, and its lateral margin forms a right angle with the distal margin. The lateral margin of the fossa lies level with the lateral margin of the shaft. The posterior surface of the epiphysis surrounding the olecranon fossa is convex laterally and forms a prominent proximodistal ridge.

<div align="center">

CARNIVORA Bowdich 1821
FELIDAE Fischer de Waldheim 1817
PANTHERINAE Pocock, 1917
Panthera Oken 1816
Panthera atrox Leidy 1853

</div>

Material

CPC-2236 is a brown-colored clavicle, 105 × 12 mm wide. CPC-2237 is a buff colored clavicle, 105 × 95 mm (Figure 3). Both clavicles are from El Pit cenote in Quintana Roo, Mexico.

Description

Large and curved clavicles, becoming thicker at the acromial end.

<div align="center">

CARNIVORA Bowdich 1821
FELIDAE Fischer de Waldheim 1817
MACHAIRODONTINAE Gill, 1872
Smilodon Lund 1842
Smilodon gracilis Cope 1880

</div>

Material

CPC-2238, the distal third of a right humerus from Kim Ha cave in Quintana Roo, Mexico (Figure 4 (u, v)).

Description

The felid humerus from Kim Ha is only fragmentarily preserved, reaching maximum measurements of 93 × 64 mm, suggesting a medium-sized animal. The pectoral ridge is straight. The small entepicondylar foramen is enclosed by a straight bridge of bone. The entepicondylar foramen reaches a length of 14 mm. The olecranon fossa is with 32 × 24 mm slightly higher than wider.

Discussion

Comparative anatomy of Panthera balamoides

Felids, canids and ursids are large predators that have been reported from the Pleistocene of the Yucatán Peninsula (González et al. 2008a). The humerus fragment from El Pit cannot come from a canid, as canids have no entepicondylar foramen, but instead a supratrochlear foramen. An entepicondylar foramen is also absent in the humeri of ursids, with exception of the subfamily Tremarctinae. *Tremarctos floridanus* has been documented from North- and Central America, including Mexico and Belize (Arroyo-Cabrales et al. 2016; Czaplewski et al. 2003). *Tremarctos* has also been reported from cenotes in the Tulum region, including Hoyo Negro (Arroyo-Cabrales et al. 2016; Chatters et al. 2014), but generic and specific assignation needs to be verified taxonomically. An assignation of the El Pit humerus (CPC-2205) to *Tremarctos floridanus* is excluded here, since the humerus of this latter species is characterized by a concavity along the

Figure 3. *Panthera atrox* clavicles (CPC-2236 and 2237) from the El Pit cenote.
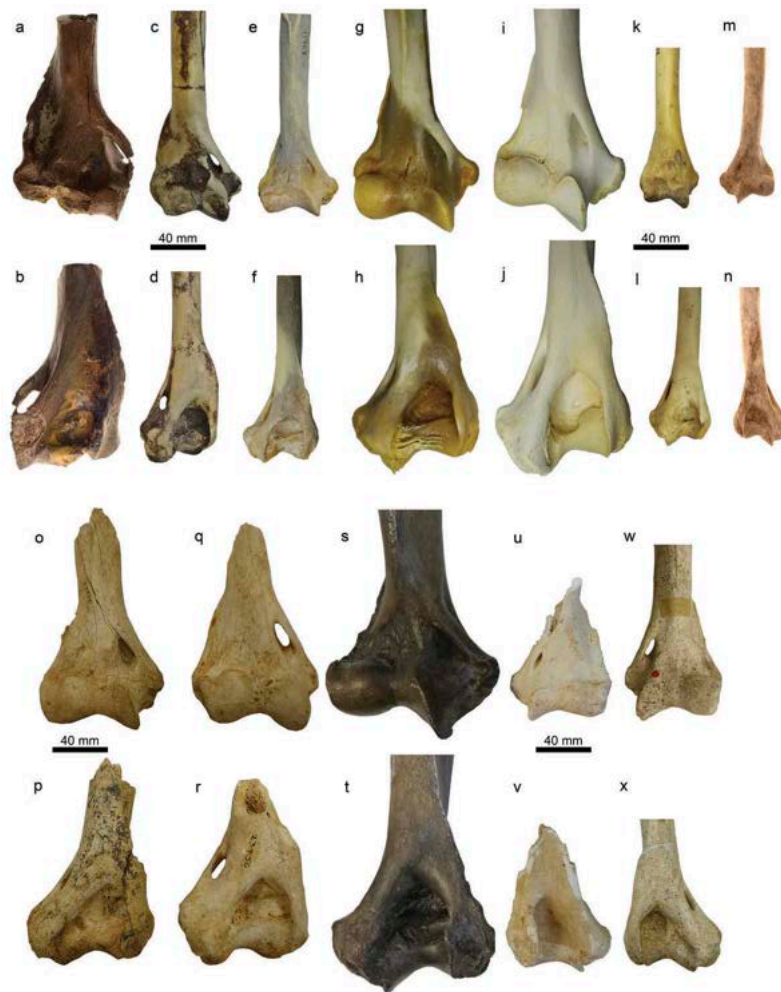
Figure 4. Comparative photos of felid humeri: a, b) *Panthera balamoides* CPC-2205 from El Pit cenote, c, d) *Panthera onca* (extant from Quintana Roo, Mexico), e, f) *Panthera pardus melas* SMNK-MAM 11763 (extant), g, h) *Panthera leo* SMNK-MAM 13592 (extant), i, j) *Panthera tigris* SMNK-MAM 223 (extant), k, l) *Puma concolor* SMNK-MAM 11998 (extant), m, n) *Puma concolor* (extant from Quintana Roo, Mexico), o, p) *Smilodon* sp. AMNH-23456, q, r) *Smilodon* sp. AMNH-23456, s, t) *Smilodon fatalis* GPIT-MA-10023, u, v) *Smilodon gracilis* CPC-2238 from Kim Ha, w, x) *Smilodon gracilis* AMNH-69227.

medial edge of the humerus, which is absent in the El Pit specimen. Rather, the medial margin of the El Pit humerus is convex, including a bony bridge of the entepicondylar foramen. The size and outline of the entepicondylar foramen of the El Pit humerus also corresponds to that seen in felids and differs from the one documented for *Tremarctos floridanus*.

The genera *Panthera, Puma, Felis, Lynx, Leopardus, Miracinonyx* and the machairodontids *Smilodon* and *Homotherium* have been reported from Mexico (Bravo-Cuevas et al. 2016). Body size of extant and fossil genera of *Felis, Leopardus* and *Lynx* exclude a close relationship with the felid humerus fragment from El Pit. Compared to the humeri of these extant species, the El Pit humerus is twice as large. The El Pit humerus comes from a mature individual, because the articulation is completely ossified and the muscle attachment areas show bone mineralization that grew into the muscle insertions and tendons. Besides the body size, the El Pit humerus fragment preserves sufficient diagnostic features to separate the specimen from the subfamily Felinae:

In leopard, lynx and puma the entepicondylar foramen is located at the anterior surface of the shaft (Madurell-Malapeira et al. 2010), not medial on the shaft as in *Panthera* and the El Pit humerus. Furthermore, the bridge of the foramen begins at the flexor origins and ends proximally at the anterior surface of the shaft, different to the El Pit humerus. The coronoid fossa is oval and deep in *Puma* and *Lynx* (Madurell-Malapeira et al. 2010), and not triangular as in the El Pit specimen. Anatomical and genetic analysis suggest a close relationship of *Puma* and the North American cheetah *Miracinonyx* (Hemmer et al. 2011). *Miracinonyx*, as also the extant cheetah *Acinonyx*, exhibited slim and elongated limb bones. The humerus in *Miracinonyx* was 20 to 25% longer than that of extant puma and cheetah (Van Valkenburgh et al. 1990). The El Pit specimen rather exhibited short and robust forelimbs. Similar to puma and lynx, *Miracinonyx* presents a weak supracondylar crest and medial epicondyle (Van Valkenburgh et al. 1990, Hemmer et al. 2011), which differs from the pronounced distal morphology seen in the El Pit humerus. The anteromedial border of the trochlea is oriented in line with the humeral shaft in *Miracinonyx inexpectatus* (Van Valkenburgh et al. 1990) and not medial to the long axis of the shaft as in the El Pit specimen.

The humerus of *Smilodon* differs from other felids in the morphology of its proximal articular head shown by a nearly orthogonal greater tuberosity to the anterior surface of the shaft (Berta 1985). In true cats (e.g. *Panthera*) these surfaces form arcuate connections. However, this feature is not preserved in the specimen from El Pit.

In medial view (Figures 2 and 4), the preserved distal part of the shaft of the El Pit specimen is straight (Figures 2 and 4) like in homotherian felids (Antón et al. 2014; Serangeli et al. 2015). It differs from *Panthera* (Figure 4(c–j)), in which the distal half of the humeral shaft is cranially curved. The straight shaft in the El Pit felid results from the absence of a distal expansion of both the deltoid crest and the supracondylar ridge, which contrasts the distal humeral anatomy of *Panthera, Homotherium,* and *Smilodon*. The thickness of the cortical bone is an indicator for the robustness of the forelimbs. In smilodontids the cortex is massive compared to the medulla. This results from its supposed hunting strategy to wrestle down prey, fix it with the front paws and kill it (Meachen-Samuels and Van Valkenburgh 2010). The relative cortical bone thickness ratio is defined by the medullar diameter of the shaft divided by the external cortical diameter. In the El Pit felid this ratio is 0,43, which is close to the ratio of 0,49 for Smilodontini (Meachen-Samuels and Van Valkenburgh 2010). In true cats including *Panthera*, this ratio ranges between 0,52 and 0,58 (Meachen-Samuels and Van Valkenburgh 2010). This suggests that *Panthera balamoides* had powerful front limbs, thus resembling smilodontids rather than modern felids. In *Smilodon* the supracondylar ridge is concave or straight (Chimento and Agnolin 2017; Chimento and Dondas 2017), rather than convex as in *P. balamoides*. The size and shape of this ridge is sometimes considered as sexual dimorphism (Serangeli et al. 2015). According to the dimensions of the preserved remnant of the shaft, the El Pit humerus must have been significantly more slender than the humeri of all large Pleistocene Pantherinae and Machairodontinae known to date (Figure 4). However, the measurements of the El Pit humerus are comparable to the wide range documented from the short and massive forelimbs of fossil specimens of *P. onca* (Kurtén 1973).

The genus *Panthera* contains the extant lion *Panthera leo*, leopard *Panthera pardus*, snow leopard *Panthera uncia*, tiger *Panthera tigris* and jaguar *Panthera onca*, and the fossil American lion *Panthera atrox*, European jaguar *Panthera gombaszoegensis*, often referred to as a subspecies of *Panthera onca*, and the American jaguar *Panthera onca augusta*.

The Pleistocene *P. onca* was 15 to 20% larger than the largest extant individuals of the species (Seymour 1983). The prominent lateral supracondylar ridge combined with a gracile humeral shaft of the El Pit humerus resemble the genus *Panthera* (Harington 1969; Van Logchem and Mol 2008). However, the deep lateral depression in the supracondylar ridge proximal to the lateral epicondyle in the El Pit felid is absent in most other felids, including *Smilodon*, and very shallow in large *Panthera* species (Figure 4; Chimento and Agnolin 2017).

Similar to the El Pit specimen, jaguars exhibit a large entepicondylar foramen with a robust epicondylar bridge and a pronounced supracondylar crest, with a convex medial edge (Chimento and Agnolin 2017). Even though, the shape of the epicondylar bridge and the size of the foramen itself are extremely variable features. The entepicondylar foramen has twice the length in the El Pit felid than in all other felids of similar size (Figures 2 and 4). The dimensions of the entepicondylar foramen and its oval outline are similar to Smilodontini, but the foramen in the El Pit specimen, relative to the size of the humeral fragment, is twice as big as in *Smilodon* and homotheres (Serangeli et al. 2015). The entepicondylar foramen is known to be a highly variable intraspecific feature in felids (Figure 4) especially within the genus *Smilodon* (Merriam and Stock 1932; Landry 1958). However, the extreme size of the entepicondylar foramen in the El Pit specimen is beyond any known variability. An entepicondylar foramen is absent in *S. populator* (Gervais and Ameghino 1880; Merriam and Stock 1932). The absence of the foramen and the large body size of *S. populator* (Berta 1985; Kurtén and Werdelin 1990; Rincón et al. 2011) exclude a close relationship with the El Pit felid. In both, *Panthera* and *Smilodon*, the entepicondylar bridge is straight, compared to the medially convex entepicondylar bridge in the El Pit specimen. Although, the shape of the bridge is variable in the genus *Panthera*, the convexity of the entepicondylar bridge is strongly pronounced and therefore a unique feature of the El Pit felid, seen neither in *Panthera* nor *Smilodon*. In addition, the medial position with respect to the humeral shaft of the entepicondylar foramen of the El Pit felid rather resembles *Panthera* than machairodontids. In the latter, the foramen is located medially against the long axis of the shaft, with a distal orientation of its anterior aperture (Serangeli et al. 2015). In the El Pit felid, the entepicondylar area is located at the extreme edge, medially to the medial face of the humeral shaft, and the opening of the entepicondylar foramen is cranially oriented.

In posterior view, the outline of the olecranon fossa tapers laterally, like in *Panthera* (Figure 4). In *Smilodon* the outline of the olecranon fossa tapers medially at midline with the long axis of the shaft. A ridge, arising from the lateral margin of the olecranon fossa, is seen in *P. balamoides* and large and robust *Panthera* species, but also in *Smilodon populator* and *S. fatalis* (Chimento and Agnolin 2017). The anterior surface of the coronoid fossa is shallow in *P. balamoides*, while more pronounced in *Xenosmilus* (Martin et al. 2000, 2011).

In both anterior and posterior view of the El Pit humeral fragment the connection between trochlea and capitulum is located medially to the long axis of the shaft and lies level with the entepicondylar foramen (Figures 2 and 4), and not along the longitudinal axis of the shaft as in *S. fatalis* (Wallace and Hulbert 2013). In anterior view, the transition between trochlea and capitulum forms a distally open angle of 145°, suggesting a mediolaterally broader distal articular surface compared to the more acute angle of 130° in *Panthera* and *Smilodon*.

Panthera balamoides thus presents a unique combination of features seen in Pantherinae, especially *Panthera onca*, and Machairodontinae (e.g. *Smilodon*). We here prefer to include the new taxon in the genus *Panthera* due to the limited information provided by a single humerus fragment. However, more complete osteological material of *Panthera balamoides* may well allow for the future erection of a new genus of endemic Quintana Roo felids.

Other Felidae from the submerged caves in the Tulum area

Two clavicles have been collected from the same debris mount at El Pit on which *P. balamoides* has been found (Figure 4). The brownish clavicle (CPC-2236) illustrated in Figure 4 is the larger one. It is 105 mm long and reaches a maximum width of 12 mm. The buff coloured clavicle (CPC-2237) reaches the same width as the brownish one, but is only 95 mm long. The length of both clavicles suggests a large felid predator. This is also supported by a thicker acromial end for the manubrium and scapula muscle attachments. Both clavicles resemble those of *Panthera atrox* from Rancho La Brea in California (Hartstone-Rose et al. 2012) and are therefore tentatively assigned to this species.

The distal fragment of a left felid humerus has been discovered by us in the submerged Kim Ha (CPC-2238) cave near Tulum (Figure 4(u,v)). The fragment consists of the distal articular region that strongly resembles that of *Smilodon* and is thus referred here to this genus (Figure 4(u,v)). The entepicondylar foramen is one-fourth smaller than that of *P. balamoides*. The olecranon fossa of the Kim Ha felid (Figure 4(u,v)) is deep and not shallow as in *P. balamoides*. Furthermore, the proximal margin of the olecranon fossa is at midline of the long axis of the humeral shaft (Figure 4(u,v)) and differs strongly from the laterally pointed proximal margin of the fossa in *P. balamoides*. The medial projection of the epicondylar area and the straight pectoral ridge of the felid humerus from Kim Ha suggest a closer relationship to smilodontids rather than to *Panthera*, and differ from the sharp distal curvature of the lateral epicondylar crest seen in *P. balamoides*. However, despite the small size of the felid humerus from Kim Ha, the epiphyseal gap is completely closed suggesting an adult individual. This suggests that the humerus fragment comes from a felid about one third smaller and more gracile than *S. fatalis*. The size and the anatomy of the condylar relief of the humerus fragment from the Kim Ha felid is identical to the North American middle Pleistocene *Smilodon gracilis* (Figure 4(u,v)). In Quintana Roo, this species may thus have survived until the late Pleistocene.

Locomotion and habitat reconstruction

In mammals, the humerus forms part of the forelimb intercepting system. Its morphology is therefore considered an essential proxy for the reconstruction of locomotor options and thus habitat preferences (Kümmell and Frey 2012). In some cases, including felids, the humeral morphology helps to tell cursorial from non-cursorial mammals (Meachen-Samuels and Van Valkenburgh 2010; Meloro 2011; Meloro et al. 2013). Most felids, like many other mammals, have an entepicondylar foramen, through which the medial nerve and brachial artery pass (Landry 1958). Its absence in *S. populator* has been interpreted as indicative for a reduction of the amount of humeral abduction and lateral rotation and thus a more cursorial lifestyle with a more parasagittal locomotor mode (Landry 1958). Then there would have been no need to keep the median nerve in place when the elbow was flexed. The presence of a large entepicondylar foramen in the El Pit felid suggests that the median nerve and the brachial artery did pass through this aperture and were thus kept in place by this aperture during abduction, lateral rotation and flexion. This would have allowed for a higher freedom of movement of the front limb, which was necessarily combined with enhanced muscular control. This freedom of movement allowed for short distance acceleration, jumping, holding and wresting down prey as well as climbing. This contrasts with the lifestyle assumed for some big cursorial Pleistocene felids such as *Smilodon populator* and *Panthera atrox*.

Felids, in contrast to canids, seize their prey with the strong clawed front paws, mainly with an outreaching lateral abduction and rotation movement under powerful muscular control (Leyhausen and Tonkin 1979). The more powerful the prey stroke, the more prominent are the muscle attachment areas on the humerus. In the El Pit humerus fragment the prominent lateral supracondylar ridge provides a large attachment area for m. brachialis et anconeus (Figure 2). Both muscles contribute to elbow extension and carpal flexion. The olecranon fossa is small in *P. balamoides* compared to other felids (Figure 3). This indicates that the olecranon process must have been short, relative to the length of the ulna. A shallow and short olecranon fossa, as is seen in the humerus from the El Pit felid, suggests a greater range of extension movement of the elbow, probably resulting in the option to overextend the forearm, an ability which is typically seen in arboreal or scansorial species (Antón et al. 2014). In addition to the large size of the entepicondylar foramen, the medial location of the trochlear sulcus on the humeral shaft and the wide distal angle between capitulum and trochlea also suggest an increased mobility of the front limb and thus possible scansorial abilities. It is therefore highly likely that *P. balamoides* was an accelerator rather than a cursor and had the ability to jump and climb steep rocks. Despite its size with a supposed body mass of >100 kg, the locomotor options reconstructed for the El Pit felid resemble those of medium and smaller sized felines like jaguar (*Panthera onca*), ocelot (*Leopardus pardalis*), or even the short-legged jaguarundi (*Puma yagouaroundi*). These species are short distance acceleration hunters in trees and on the ground. They are reasonable swimmers, good climbers and jumpers, and thus are able to cope with a variety of habitats, but they are no cursors (Gittleman 1985; Kitchener 1991; Kitchener et al. 2010; Meloro et al. 2013). Therefore, *P. balamoides* likely avoided open steppe habitats, where ambush hunting is difficult. These ecosystems were inhabited by cursorial Pleistocene felids, e.g. *Homotherium* sp., *Smilodon populator* and *Panthera atrox*.

P. balamoides is presently too rare to suggest that this felid used the Tulum caves for feeding and breeding. Such a behavior has been postulated for *Homotherium* and is well documented for the modern jaguar (*Panthera onca*) and the leopard (*P. pardus*; Chimento and Agnolin 2017). During the late Pleistocene the Yucatán peninsula was covered by a shrub savannah with patchy small forests (González et al. 2013). Surface water was exceedingly rare due to intensive karst conditions (Stinnesbeck et al. 2018). For hunting, acceleration, jumping and climbing abilities may have been essential for *P. balamoides*, because of the otherwise open landscape. The absence of surface water probably forced the cat to deeply climb into the caves to drink.

The two other felids, the remains of which have been found in the cenotes at Tulum, refer to cursorial species. This implicates that large areas of open steppe existed between the shrub savannah patches on the Yucatán Peninsula. One of these felids is *Panthera atrox* (Wheeler and Jefferson 2009), which is evidenced by two isolated clavicles from El Pit (Figure 4). The humerus fragment from Kim Ha is referred to *Smilodon gracilis*, another large predominantly cursorial felid (Lewis 2018). The species is considered to have become extinct at the end of the middle Pleistocene (Alvarez and Polaco 1982; Bravo-Cuevas et al. 2016). However, the entire faunal assemblage found so far in the cenotes is of late Pleistocene to early Holocene age (González et al. 2008b; Stinnesbeck et al. 2017a, 2017b). It might therefore well be that *Smilodon gracilis* survived on the Yucatán Peninsula because of the extremely diverse habitat structure in this region.

Palaeogeographic significance

The new felid *P. balamoides* from El Pit is another faunal element identified as endemic to the northern Yucatán Peninsula (YP). It thus lines up with other recently described hitherto unique and thus probably endemic late Pleistocene mammals from the region, i.e. the peccary *Muknalia minima* (Stinnesbeck et al. 2017b) and the ground sloths *Xibalbaonyx oviceps* (Stinnesbeck et al. 2017a) and *Nohochichak xibalbakah* (McDonald et al. 2017). The new felid provides further evidence for the hypothesis that the region must have passed periods of ecological isolation, which lasted long enough to allow for a hitherto unexpected diversification of mammals in the area. The precise intervals of isolation are unknown to date because there is no stratigraphical information. No stratifiable sediments have been reported from the submerged caves and ^{14}C dating methods cannot be applied to this underwater material because of the dissolution of bone collagen (Stinnesbeck et al. 2017).

During the middle to late Pleistocene stadial periods, dry, semi-desertic or even desertic conditions existed on the northeastern YP. They were a consequence of the almost horizontally-lying thick-bedded limestone base rock platform in this region and the enormous karstification due to a sea-level of about 120 m lower than today (Bauer-Gottwein et al. 2011). Under these conditions, no soil developed on the carbonate platform and rain water seeped away almost instantaneously. Because phreatic levels only existed tens of meters below surface beyond the reach of roots, no surface water existed and even the presence of extended grassland areas in the region therefore appears unlikely. Xeric shrub-land could only exist in depressions, especially around the hundreds of sinkholes in the Tulum area. It thus appears likely to us that periods of habitat diversification alternating with intervals of ecological isolation triggered a short term burst of biodiversity on the YP. The intermittent expansion of grass- and shrubland may have triggered the isolation of the region and formation of an ecological barrier for non-cursors, such as *P. balamoides*, between the northeastern YP and south-central Mexico. We further hypothesize that faunal exchange between south-central Mexico and the YP was restricted to humid periods, while during dry periods small faunal populations were isolated on the YP and rapidly diversified locally.

Conclusions

A new genus and species of a late Pleistocene felid from the northeastern Yucatán Peninsula is here described based on the distal third of a right humerus from the El Pit cenote near Tulum. *Panthera balamoides* sp. nov. combines characters of smilodontids and *Panthera*, with more similarities to *Panthera onca*. Diagnostic features of *Panthera balamoides* are a gracile and straight humeral shaft, a prominent condylar relief, such as a pronounced supracondylar crest with a semicircular depression on the lateral epicondylar ridge, a large entepicondylar foramen and a medially distal articular surface located 15 mm medially against the middle axis of the shaft. Further late Pleistocene felids are evidenced by a distal fragment of a humerus from the Kim Ha cave assigned to *Smilodon gracilis* and two clavicles strongly resembling those of *Panthera atrox* in both morphology and size. The new felid from El Pit may have been endemic to the northern Yucatán Peninsula; along with other likely endemic mammals the new felid provides new evidence for an ecological isolation of this region from the rest of Mexico, likely during the dry (stadial) phases of the late Pleistocene.

References

Alvarez T, Polaco OJ. 1982. Restos de moluscos y mamíferos cuaternarios procedentes de Loltún, Yucatán. unpublished INAH report. Mexico.

Antón M, Salesa MJ, Galobart A, Tseng ZJ. 2014. The Plio-Pleistocene scimitar-toothed felid genus *Homotherium* Fabrini, 1890 (Machairodontinae, Homotherini): diversity, palaeogeography and taxonomic implications. Quat Sci Rev. 96:259–268.

Arroyo-Cabrales J, Johnson E, Graham RW, Pérez-Crespo VA. 2016. North American ursid (Mammalian: Ursidae) defaunation from Pleistocene to recent. Cranium 33:51–56.

Bauer-Gottwein P, Gondwe BRN, Charvet G, Marín LE, Rebolledo-Vieyra M, Merediz-Alonso G. 2011. Review: the Yucatán Peninsula karst aquifer, Mexico. Hydrogeol J. 19:507–524.

Berta A. 1985. The status of *Smilodon* in North and South America. Contributions in sciences, Natural History Museum of Los Angeles County. p. 1–15.

Björn K, Werdelin L. 1990. Relationships between North and South American *Smilodon*. J Vert Paleontol. 10:158–169.

Bravo-Cuevas VM, Priego-Vargas J, Cabral-Perdomo MA, Maldonado MAP. 2016. First occurrence of *Panthera atrox* (Felidae, Pantherinae) in the Mexican state of Hidalgo and a review of the record of felids from the Pleistocene of Mexico. Foss Rec. 19:131–141.

Chatters JC, Kennett DJ, Asmerom Y, Kemp BM, Polyak V, Blank AN, Beddows P, Reinhardt E, Arroyo-Cabrales J, Bolnick D, et al. 2014. Late Pleistocene human skeleton and mtDNA link Paleoamericans and modern native Americans. Science. 344:750–754.

Chimento NR, Agnolin FL. 2017. The fossil American lion (*Panthera atrox*) in South America: palaeobiogeographical implications. Comptes Rendus - Palevol. 16:850–864.

Chimento NR, Dondas A. 2017. First record of *Puma concolor* (Mammalia, Felidae) in the early-middle Pleistocene of South America. J Mamm Evol. 470:1–9.

Czaplewski NJ, Krejca J, Miller TE. 2003. Late quaternary bats from Cebada Cave, Chiquibul cave system, Belize. Caribb J Sci. 39:23–33.

Ferrusquía-Villafranca I, Arroyo-Cabrales J, Martínez-Hernández E, Gama-Castro J, Ruiz-González J, Polaco OJ, Johnson E. 2010. Pleistocene mammals of Mexico: a critical review of regional chronofaunas, climate change response and biogeographic provinciality. Quat Int. 217:53–104.

Gervais H, Ameghino A. 1880. Les mammifères fossiles de l'Amérique du Sud. In: Torcelli AJ, editor. Obras Completas y Correspondencia Científica. Vol. 2. Buenos Aires: Taller de Impresiones Oficiales; p. 512–645.

Gittleman JL. 1985. Carnivore body size: ecological and taxonomic correlates. Oecologia. 67:540–554.

González AH, Rojas Sandoval C, Acevez Nuñez E, Avilés Olguín J, Analco Ramírez S, Del Rio Lara O, Luna Erreguerena P, Velazquez Morlet A, Stinnesbeck W, Terrazas Mata A. 2008a. Evidence of early inhabitants in submerged caves in Yucatan, Mexico. In: Leshikar-Denton ME, Luna Erreguerena P, editors. Underwater and maritime archaeology in Latin America and the Caribbean. 56th ed. Walnut Creek (CA): Left Coast Press; p. 127–142.

González AH, Terrazas Mata A, Stinnesbeck W, Benavente M, Avilés Olguín J, Rojas Sandoval C, Padilla JM, Velázquez Morlet A, Acevez Nuñez E, Frey E. 2013. The first human settlers on the Yucatan Peninsula: Evidence from drowned caves in the State of Quintana Roo (South Mexico). In: Graf KE, Ketron CV, Waters M, editors. Paleoamerican Odyssey. Texas A&M University Press; p. 323–337.

González AH, Rojas Sandoval C, Terrazas Mata A, Benavente Sanvicente M, Stinnesbeck W, Aviles Olguín J, De Los Ríos M, Acevez NE. 2008b. The arrival of humans on the Yucatan Peninsula: evidence from submerged caves in the State of Quintana Roo, Mexico. Cur Res Pleistocene. 25:1–24.

Harington CR. 1969. Pleistocene remains of the lion-like cat (*Panthera atrox*) from the Yukon territory and northern Alaska. Can J Earth Sci. 6:1277–1288.

Hartstone-Rose A, Long RC, Farrell AB, Shaw CA. 2012. The clavicles of *Smilodon fatalis* and *Panthera atrox* (mammalia: Felidae) from Rancho La Brea, Los Angeles, California. J Morphol. 273:981–991.

Hemmer H, Kahlke RD, Vekua AK. 2011. The cheetah Acinonyx pardinensis (Croizet et Jobert, 1828) s.l. at the hominin site of Dmanisi (Georgia) - A potential prime meat supplier in Early Pleistocene ecosystems. Quaternary science Reviews 30(19-20):2703–2714.

Kambesis PN, Coke JG. 2013. Overview of the controls on eogenetic cave and karst development in Quintana Roo, Mexico. In: Lace M, Mylroie J, Landforms CK, editors. Coastal research library. Vol. 5. Dordrecht: Springer; p. 347–373.

Kambesis PN, Coke JG. 2016. The Sac Actun system, Quintana Roo, Mexico. Boletín Geológico y Minero. 127:177–192.

Kitchener AC. 1991. The natural history of the wild cats. Comstock Publishing Associates, Cornell University.

Kitchener AC, Van Valkenburgh B, Yamaguchi N. 2010. Felid form and function. In: Macdonald DW, Loveridge AJ, editors. Biology and Conservation of Wild Felids. Oxford University Press; p. 83–106.

Kümmell SB, Frey E. 2012. Digital arcade in the autopodia of synapsida: standard position of the digits and dorsoventral excursion angle of digital joints in the rays II-V. Paleobiodivers Paleoenviron. 92:171–196.

Kurtén B. 1973. Pleistocene jaguars in North America. Commentationes Biol. 62:1–23.

Kurtén B, Werdelin L. 1990. Relationships between North and South American *Smilodon*. J Vert Paleontol. 10:158–169.

Landry SO. 1958. The function of the entepicondylar foramen in mammals. Am Midl Nat. 60:100–112.

Lewis ME. 2018. The postcranial morphology of *Smilodon*. In: Werdelin L, McDonald HG, Shaw CA, editors. *Smilodon*: the iconic sabertooth. Baltimore: John Hopkins University Press; p. 171–196.

Leyhausen P, Tonkin BA. 1979. Cat Behaviour: The predatory and social behaviour of domestic and wild cats. Garland: STPM Press, New York.

Madurell-Malapeira J, Alba DM, Moyà-Solà S, Aurell-Garrido J. 2010. The Iberian record of the puma-like cat *Puma pardoides* (Owen, 1846) (Carnivora, Felidae). Comptes Rendus - Palevol. 9:55–62.

Manzuetti A, Perea D, Ubillaa M, Rinderknecht A. 2018. First record of *Smilodon fatalis* Leidy, 1868 (Felidae, Machairodontinae) in the extra-Andean region of South America (late Pleistocene, Sopas Formation), Uruguay: taxonomic and paleobiogeographic implications. Quat Sci Rev. 180:57–62.

Martin LD, Babiarz JP, Naples VL. 2011. The osteology of a cookie-cutter cat, *Xenosmilus hodsonae*. In: Naples VL, Martin DL, Babiarz JP, editors. The other saber-tooths: scimitar-tooth cats of the Western hemisphere. Baltimore (MD): Johns Hopkins University Press; p. 43–97.

Martin LD, Babiarz JP, Naples VL, Hearst J. 2000. Three ways to be a saber-toothed cat. Naturwissenschaften. 87:41–44.

McDonald HG, Chatters JC, Gaudin TJ. 2017. A new genus of megalonychid ground sloth (Mammalia, Xenarthra) from the late Pleistocene of Quintana Roo, Mexico. J Vert Paleontol. 37: e1307206.

Meachen-Samuels J, Van Valkenburgh B. 2010. Radiographs reveal exceptional forelimb strength in the sabertooth cat, *Smilodon fatalis*. PLoS One. 5:e11412.

Meloro C. 2011. Locomotor adaptations in Plio-Pleistocene large carnivores from the Italian Peninsula: palaeoecological implications. Current Zool. 57:69–283.

Meloro C, Elton S, Louys J, Bishop LC, Ditchfield P. 2013. Cats in the forest: predicting habitat adaptations from humerus morphometry in extant and fossil Felidae (Carnivora). Paleobiology. 39:323–344.

Merriam JC, Stock C. 1932. The Felidae of Rancho La Brea. 422nd ed. Carnegie Institution of Washington Publication, Washington.

[QRSS] Quintana Roo Speleological Society. 2018. Survey and cartography of the underwater caves of Quintana Roo Mexico. [accessed 2018 Oct 20]. http://caves.org/project/qrss/qrss.htm

Prevosti FJ, Martin FM. 2013. Paleoecology of the mammalian predator guild of Southern Patagonia during the latest Pleistocene: ecomorphology, stable isotopes, and taphonomy. Quat Int. 305:74–84.

Rincón AD, Prevosti FJ, Parra GE. 2011. New saber-toothed cat records (Felidae: Machairodontinae) for the Pleistocene of Venezuela, and the Great American biotic interchange. J Vert Paleontol. 31:468–478.

Serangeli J, Van Kolfschoten T, Starkovich BM, Verheijen I. 2015. The European saber-toothed cat (*Homotherium latidens*) found in the "Spear Horizon" at Schöningen (Germany). J Hum Evol. 89:172–180.

Seymour KL. 1983. The Felinae (Mammalia: Felidae) from the Late Pleistocene Tar Seeps at Talara, Peru, with a critical examination of the fossil, and recent Felines of North and South America. University of Toronto, Toronto.

Stinnesbeck SR, Frey E, Avilés Olguín J, Stinnesbeck W, Zell P, Mallison H, González González AH, Aceves Núñez E, Velázquez Morlet A, Terrazas Mata A, Benavente Sanvicente M, Hering F, Zell P, Rojas Sandoval C. 2017a. *Xibalbaonyx oviceps*, a new megalonychid ground sloth (Folivora, Xenarthra) from the Late Pleistocene of the Yucatán Peninsula, Mexico, and its paleobiogeographic significance. Paläontologische Zeitschrift. 91:245–271.

Stinnesbeck SR, Frey E, Stinnesbeck W, Avilés Olguín J, Zell P, Terrazas Mata A, Benavente Sanvicente M, González González AH, Rojas Sandoval C, Acevez Nuñez E. 2017b. A new fossil peccary from the Pleistocene-Holocene boundary of the eastern Yucatán Peninsula, Mexico. J S Am Earth Sci. 77:341–349.

Stinnesbeck SR, Stinnesbeck W, Terrazas Mata A, Avilés Olguín J, Benavente Sanvicente M, Zell P, Frey E, Lindauer S, Rojas Sandoval C, Velázquez Morlet A, et al. 2018. The Muknal cave near Tulum, Mexico: an early-Holocene funeral site on the Yucatán Peninsula. Holocene 28(12): 1–14.

Stinnesbeck W, Becker J, Hering F, Frey E, González González AH, Fohlmeister J, Stinnesbeck SR, Frank N, Terrazas Mata A, Benavente Sanvicente ME, et al. 2017. The earliest settlers of Mesoamerica date back to the late Pleistocene. PLoS One. 12:16–18.

Van Logchem W, Mol D. 2008. De vroeg-pleistocene sabeltandkat, *Homotherium crenatidens* (Weithofer, 1889), voor het eerst opgevist van de bodem van de Noordzee. Cranium. 25:3–16.

Van Valkenburgh B, Grady F, Kurten B. 1990. The Plio-Pleistocene cheetah-like cat *Miracinonyx inexpectatus* of North America. J Vert Paleontol. 10:434–454.

Wallace SC, Hulbert CR. 2013. A new machairodont from the Palmetto Fauna (Early Pliocene) of Florida, with comments on the origin of the Smilodontini (Mammalia, Carnivora, Felidae). PLoS One. 8:14–19.

Wheeler HT, Jefferson GT. 2009. *Panthera atrox*: body proportions, size, sexual dimorphism, and behavior of the cursorial lion of the North American plains. Mus North Arizona Bull. 65:423–444.

Guatemala's Late Pleistocene (Rancholabrean) fauna: Revision and interpretation

S. Lorena Dávila [a], Sarah R. Stinnesbeck [b, c, *], Silvia Gonzalez [d], Susanne Lindauer [e], Juan Escamilla [a], Wolfgang Stinnesbeck [f]

[a] Coleccion de Fosiles, Museo Historia Natural, Universidad de San Carlos de Guatemala, Calle Mariscal Cruz 1-56, Zona 10, Ciudad de Guatemala, Guatemala
[b] Abteilung Geowissenschaften, Staatliches Museum für Naturkunde Karlsruhe, Erbprinzenstraße 13, 76133 Karlsruhe, Germany
[c] Institut für Geographie und Geoökologie, Karlsruher Institut für Technologie (KIT), Reinhard-Baumeister-Platz 1, 76131 Karlsruhe, Germany
[d] School of Biological and Earth Sciences, Liverpool John Moores University, Liverpool L33AF, United Kingdom
[e] Curt-Engelhorn-Center Archaeometry, C4, 8, 68159 Mannheim, Germany
[f] Institut für Geowissenschaften, Ruprecht-Karls-Universität Heidelberg, Im Neuenheimer Feld 234, 69120 Heidelberg, Germany

ARTICLE INFO

ABSTRACT

We present a revision, dating and interpretation of the Late Pleistocene megafauna of Guatemala based on paleontological material located in collections in the country and other fossils housed in the American Museum of Natural History, New York. Assemblages are dominated by proboscideans (*Cuvieronius*) and xenarthrans (*Eremotherium*, *Glyptotherium*), while co-occurring *Equus* and *Mixotoxodon* are significantly less frequent, and *Holmesina*, *Palaeolama*, *Tapirus*, *Neocherus*, *Mammuthus* and other ground sloth taxa (*Paramylodon*; *Megalonyx*) are rare. Contrary to published records the faunal assemblage is dominated by North American faunal elements. The underrepresentation of typical South American fauna therefore suggests a more southernly located biogeographic juncture between the two subcontinents, at least for the Late Pleistocene. The biogeographical barrier was either formed by the high mountain chains, or alternating periods of low and high precipitation that triggered the intermittent expansion of either grass- or woodland, thus leading to an alternating filter for either grazers or browsers. The presence of an oak-dominated forest vegetation with *Mixotoxodon*, *Eremotherium* and *Cuvieronius* supports high precipitation rates during MIS 3 and 2, followed by drought during the Late Pleistocene deglaciation. The expansion of grassland during the Younger Dryas period favored the migration of *Mammuthus* along the Mesoamerican Corridor, which is otherwise absent in Guatemala. Our data also suggest a survival of *Cuvieronius* into the early Holocene in the southeastern lowlands of Guatemala along the Motagua river. Our review is important as Guatemala is key to understanding migrations along the Mesoamerican Corridor that acted as a bridge but also as a filter of faunal interchange between North- and South America.

© 2019 Elsevier Ltd. All rights reserved.

1. Introduction

Even though Central America is of prominent importance to the overall understanding of changing faunal communities in the Western Hemisphere, the region has received little attention compared with high latitude regions in the Americas (Lucas, 2008a; Morgan, 2008; Lucas and Alvarado, 2016). This is due to a scarcity of high resolution biostratigraphic data and limited conceptual understanding of the continental record of sediments, but the absence of solid data is also a result of unstable political circumstances in the area and difficulties of scientific access. Information on environmental changes is also highly scattered to date and varies enormously throughout the entire Central American region in terms of quantity, quality, chronologic positioning, geographic distribution, and statistical significance (Morgan, 2008).

The first reference of fossils from Guatemala comes from a chronicle written by D. Francisco Antonio de Fuentes and Guzmán in 1690, in which the authors mention huge vertebrate bones at

Chiquimula, attributed at that time to "biblical giants". In 1722, Fray Francisco Ximenes recorded the presence of fossil impressions on stones from Sacapulas, Quiché, which he attributed to the effect of ice. The first scientific paper on a Pleistocene fossil from Guatemala described *Serridentinus guatemalensis* from Chinautla (Osborn, 1923). Today, this fossil is referred to *Cuvieronius hyodon*.

During the 1940s, Barnum Brown collected abundant fossil material of tortoises, ground sloths and proboscideans from Río La Pasión, close to Santa Amelia and Sayaxché in the Petén region of Guatemala. During his field trips he also discovered the paleontological site of Estanzuela, in the southern department of Zacapa. The material collected by him is now housed in the American Museum of Natural History in New York (AMNH) and has never been scientifically revised (Ibarra, 1980).

In the mid 1950s, Lewis Gazín from the Smithsonian National Museum of Natural History in Washington, D.C., visited Guatemala and collected Pleistocene fossils in the departments of Salamá, Baja Verapaz and Jutiapa. Nevertheless, he only reported on the tibia of a megathere, probably *Eremotherium,* from Progreso, and a proboscid from Jutiapa (Ibarra, 1980).

The Late Miocene proboscidean *Rhynchotherium blicki* has also been identified in Carboneras in the department of Izabal by Byron Mota (Lucas and Alvarado, 1995).

During the late 1970s, two major Late Pleistocene sites were excavated and documented, at Los Tapiales in the Western Highlands, and at Chivacabé near Huehuetenango in the Altos Cuchumatanes region. At Los Tapiales no megafaunal remains have been found (Gruhn et al., 1977), while mastodontids, deers, horses, glyptodontids and ground sloths have been documented from Chivacabé (Mead et al., 2012, and discussion therein). In both sites, the co-existence of men and megafauna has been discussed by several authors based on cut marks and artifacts, but without a clear result (Cano and Schuster, 1993; Yelacic, 2010; Mead et al., 2012).

Published records on Pleistocene vertebrate species from the above and other sites in Guatemala are generally rare (Woodburne, 1969; García García and Ericastilla Gody, 1995; Mead et al., 2012) and the fossil record has never been described and interpreted in detail. Faunal listings (Woodburne, 1969; Morgan, 2008; Mead et al., 2012; Lucas, 2014a,b), internal reports (Lohse and Paiz, 2010) and photographs suggest that both North- and South American faunal elements were present. This listed material of Pleistocene mammals includes *Equus, Tayassu tajuco, Eremotherium, Felis, Dasypus, Pampatherium, Camel, Tapirus, Glyptodon, Megalonyx, Megatherium, Paramylodon, Mylodon, Mixotoxodon, Odocoileus, Cuvieronius, Mammuthus* and *Hydrochoerus* (Woodburne, 1969; Morgan, 2008; Mead et al., 2012; McDonald and Dávila, 2017), most of which are elements of South American origin. Only *Equus, Cuvieronius, Mammuthus,* Camelidae and *Odocoileus* are considered to represent typical North American faunal elements (Morgan, 2008; Woodburne, 2010). On the other hand, there are substantial doubts regarding the classification of some of these species. For instance, the ground sloths *Mylodon* and *Megatherium* listed above, are apparently not represented in the paleontological collections.

Here we present a detailed review of the principal Late Pleistocene localities of Guatemala and a systematic revision of the faunal content, based on the material housed in paleontological collections in the country and initial radiocarbon dating of the fossils. We also include an overview of the megafauna collected by Barnum Brown, housed in the collections of the AMNH, New York, which have not been presented before.

1.1. Paleontological localities in Guatemala containing Late Pleistocene fossils

In the department of Huehuetenango two fossil sites with Late Pleistocene megafauna, Chivacabé and Santa Cruz Barillas, are represented by material housed in collections in the country (Fig. 1). In 1972, the remains of a *Cuvieronius* were exposed during a flood of the Kam Balam River at Santa Cruz Barillas. The skeleton lacks the skull but was otherwise complete; it is now housed in the Casa de la Cultura of Santa Cruz Barillas.

Chivacabé, Huehuetenango (15°18′47.08 N, 91°32′49.100″ W)

In 1976, Octavio Alvarado Villatoro discovered a tusk fragment of *Cuvieronius* while digging a well for water. Throughout the 1970s several archaeologists and paleontologists including Dr. Herbert Alexander and Bryan Hayden of Simon Fraser University, British Columbia, Canada, and Oscar Polaco of the Archaeozoology Laboratory of the Instituto Nacional de Antropología y Historia (INAH), Mexico City, excavated the site. Sergio Ericastilla of the Instituto de Antropología e Historia de Guatemala (IDAEH) reported on the presence of *Glyptotherium* sp., *Eremotherium* sp., *Odocoileus* sp., *Equus* sp. and *Cuvieronius* sp. However, only *Glyptotherium* sp., *Odocoileus* sp., *Equus* sp. and *Cuvieronius* sp. have been verified by Mead et al. (2012) and are actually present in the IDAEH collection (Table 1). Our observations at the site indicate that the fossils were deposited as part of a lahar of reworked rhyolitic ash, associated with a fluvial terrace in an incised river channel. The fossils are fragmented and present evidence of short distance transport. The lahar has been radiocarbon dated to 13,065 ± 145 y BP for the top of the unit (Yelacic, 2010; Yelacic et al., 2018).

Santa Amelia, Río la Pasión in Petén (16.5314°N, 90.1892°W)

Fossils from the Río de la Pasión site, also known as Santa Amelia, were collected by Barnum Brown during repeated field campaigns between 1940 and 1945. The collection is housed at the American Museum of Natural History at New York (AMNH). Although the material is referred to a single locality, it has been collected from several sites along the La Pasión river near the villages of Sayaxché and Santa Amelia in the department of Petén. For the Río de la Pasión area we confirm the presence of *Canis* sp., *Cuvieronius* sp., *Eremotherium* sp., *Glyptotherium* sp., *Peccary* sp., *Palaeolama* sp., *Odocoileus* sp., *Pampatherium* sp., *Mammuthus* sp., *Mixotoxodon* sp., *Tapirus* sp., *Neocherus* sp., *Paramylodon* sp. and an undetermined Megalonychidae (Table 1), while other taxa reported by Barnum Brown (Woodburne, 1969; Mead et al., 2012) have not been confirmed by our recent review (June 2018) of the AMNH collection.

Barnum Brown found several lithic flint flakes (Fig. 3I) along the Río de la Pasión sites, which are present at the AMNH without a collection number. A co-existence of humans and megafauna is possible, but no further evidence has been documented.

La Estanzuela, Department of Zacapa (14.9989° N, 89.7078° W)

Megafaunal specimens from Estanzuela in the department of Zacapa are here named as one locality, termed Estanzuela, although the material clearly results from different approximately coeval sites along the Motágua river, which today are all located in the urban area of Estanzuela.

The Estanzuela locality was discovered by Barnum Brown in 1945; several taxa were collected by him during the 1940s and by other scientists and laymen in the 1970s, including *Equus, Glyptotherium* and *Cuvieronius* species. It should be noted that according to a recent field survey by us (March 2018) all fossil findings appear to be located in a single stratigraphic unit, several meters thick, of fluvially transported pumitic sand and silt of volcanic origin (lahar) with convolute deformation and water-escape structures, due to repeated earthquakes. These sediments form a fluvial terrace along
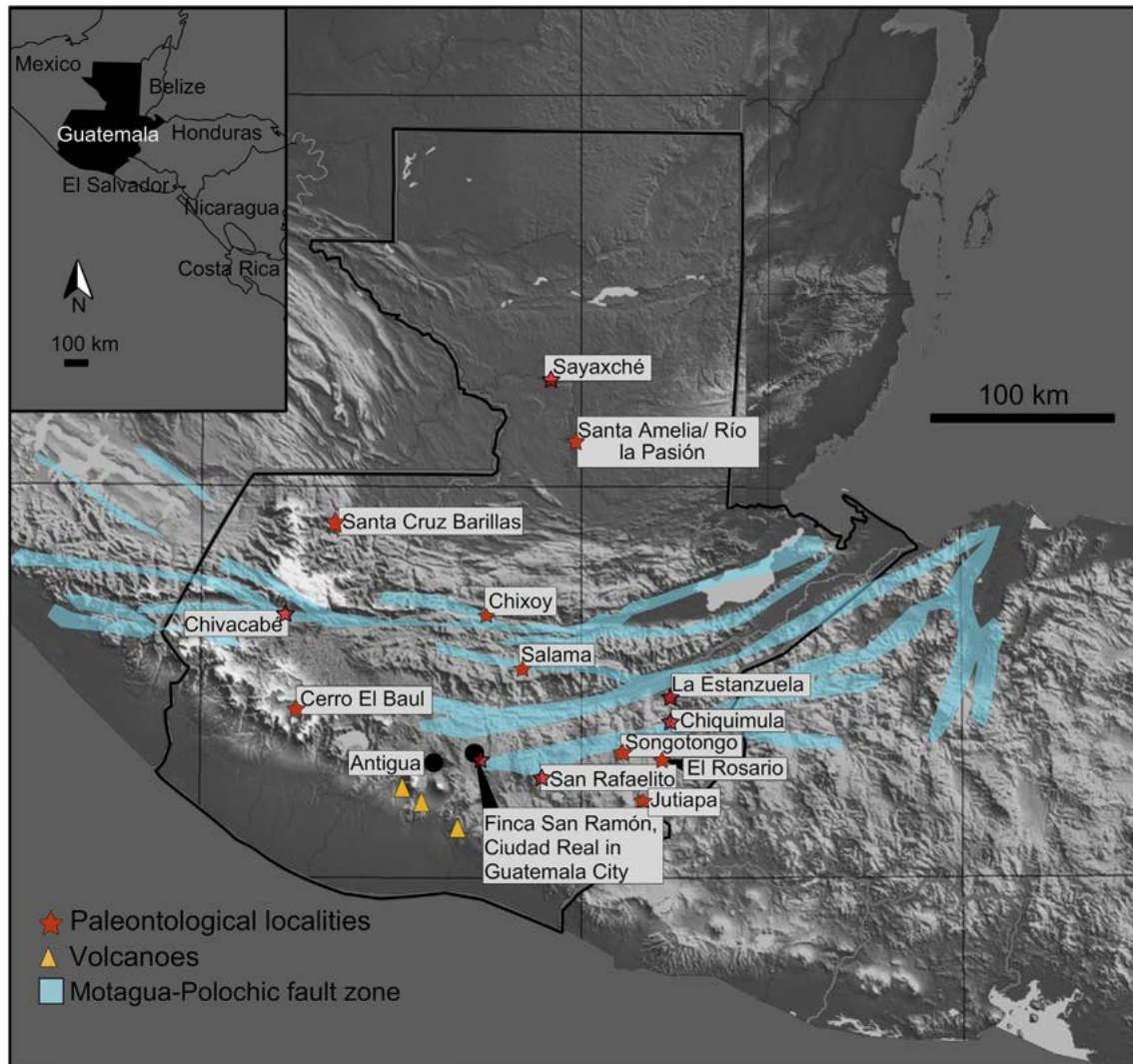
Fig 1. Late Pleistocene paleontological localities in Guatemala. Note that Guatemala mountain chains reach maximum altitudes of >3000 m. The sites of Chivacabé, Santa Cruz Barillas and Cerro El Baúl are situated at >1800 m altitude, while Santa Amelia and Sayaxché are lowland sites in Petén, with altitudes only reaching to 130 m. The sites Finca San Ramón, Ciudad Real, San Rafaelito, Jutiapa, El Rosario, Songotongo, Chiquimula, Salama, La Estanzuela and Chixoy are located along the east-west trending morphological depression following the Motagua-Polochic lineament zone and range between 1400 m and 180 m altitude.

the Móntagua river. The matrix consists of fine silty-clayey rhyolitic volcanic sediments with pumice clasts up to 0.2 m in diameter. A total of 148 fossils have been documented from the Estanzuela area, among them 52 fragments of *Cuvieronius hyodon*, 51 of *Glyptotherium* sp., eleven of *Equus* sp. and twelve of *Eremotherium laurillardi*. The collection also includes the fragmented skulls of *Neocherus* sp. and *Mixotoxodon laurensis* fragments. A *Mammuthus* molar in the collection represents an isolated find from a different stratigraphic unit due to its different colour and preservation.

The fossil material is housed at the Museo de Paleontología y Arqueología Ingeniero Roberto Woolfolk Saravia (ME) in the village of Estanzuela. The museum is well-known for the mounted skeletons of a *Cuvieronius* and an *Eremotherium*. The gompothere was collected at Estanzuela (Lucas and Alvarado, 2016), while the ground sloth originally comes from the Finca San Ramón site of Colonia Senahu, zona 6 of Guatemala City. A fossil identified as *Tapirus guatemalensis*, from Calle del Comercio at Estanzuela, Zacapa (PV-H-103), has later been identified as the mandible of a domestic cow (McDonald and Dávila, 2017).

In the wider vicinity of La Estanzuela, carapace fragments of *Glyptotherium* were discovered during excavations at Teculután and a *Mammuthus* molar near the Motagua river, also in the department of Zacapa (Table 1).

Ciudad Real, Zona 12, Guatemala City (90° 33′ 37.32″, 14° 33′ 22.122″)

The fossil site known as Ciudad Real is located within the urban area of Guatemala City and was excavated from 1970 to 1972 as a rescue campaign, directed by Lic. Mario Dary Rivera and staff of the Museo de Historia Natural of the University of San Carlos at Guatemala. J.T. Thurmond of the Birmingham-Southern College in Alabama, U.S.A. participated in the taxonomic determination of the specimens collected. He documented *Eremotherium* sp., *Cuvieronius* sp., *Mixotoxodon* sp. (previously identified as *Toxodon* sp.), *Odocoileus* sp. and *Equus* sp. (Thurmond, 1973; Mead et al., 2012). Most of the material from Zona 12, is today either exhibited or stored in the Museo de Historia Natural de la Universidad de San Carlos in Guatemala City (MUSHNAT). All fossils have catalogue numbers USC (Universidad de San Carlos). A large block of sediment with fossils still *in situ* is on display at the Museum, showing them to be fragmentary, chaotic and reworked in a fine sandy lahar matrix

Table 1
Radiocarbon dating of fossil bones and charcoal from Late Pleistocene paleontological localities in Guatemala. Note that Early Holocene ages are here presented for *Cuvieronius* sp. and *Glyptotherium* sp. from La Estanzuela and Xela. All samples have been dated at the CEZ in Mannheim, Germany, lab number MAMS. Calibrated ages are given as a weighted mean 1-sigma standard deviation.

Lab No. MAMS	Locality	Taxa	Description	^{14}C yr BP	δ13C AMS [‰]	Cal 1-sigma Cal BC
37495	Chinautla	*Mammuthus*	bone	12.340 ± 50	2,9	12.510—12.205
35558	Ciudad Real	*Cuvieronius*	bone	No data		
35559	Ciudad Real	*Eremotherium*	bone	No data		
37499	Ciudad Real	*Mixotoxodon*	bone	27.850 ± 120	−8,0	29.720—29.445
37500	Ciudad Real	*Cuvieronius*	bone	29.350 ± 130	−12,2	31.790—31.520
36385	La Estanzuela	*Cuvieronius*	tusk	9.539 ± 30	−4,0	9.117—8.793
36386	La Estanzuela	*Cuvieronius*	tusk	21.550 ± 70	−13,8	23.970—23.824
36387	La Estanzuela	*Cuvieronius*	molar	19.910 ± 70	−5,3	22.120—21.910
36388	La Estanzuela	*Cuvieronius*	molar	9.725 ± 30	−3,1	9.256—9.213
36389	La Estanzuela	*Cuvieronius*	tusk	12.450 ± 40	−10,0	12.800—12.439
36390	La Estanzuela	*Cuvieronius*	tusk	22.400 ± 90	−15,4	24.930—24.558
36391	La Estanzuela	*Cuvieronius*	molar	15.730 ± 50	−8,9	17.080—16.950
36383	La Estanzuela		charcoal in lahar	39.670 ± 290	−22,0	41.630—41.087
36384	La Estanzuela		charcoal in lahar	14.570 ± 60	−38,0	15.900—15.709
35562	San Rafaelito	*Cuvieronius*	molar	26.800 ± 150	−4,7	29.110—28.900
35563	San Rafaelito	*Eremotherium*	bone	27.100 ± 120	−11,2	29.240—29.067
36380	San Rafaelito	*Eremotherium*	molariform	25.590 ± 120	−9,9	27.940—27.542
36381	San Rafaelito	*Eremotherium*	bone	27.080 ± 120	−10,4	29.240—29.054
36378	Xela	*Glyptotherium*	osteoderm	9.941 ± 45	−10,7	9.448—9.306
36379	Xela	*Glyptotherium*	molariform	13.800 ± 110	−23,7	14.940—14.575
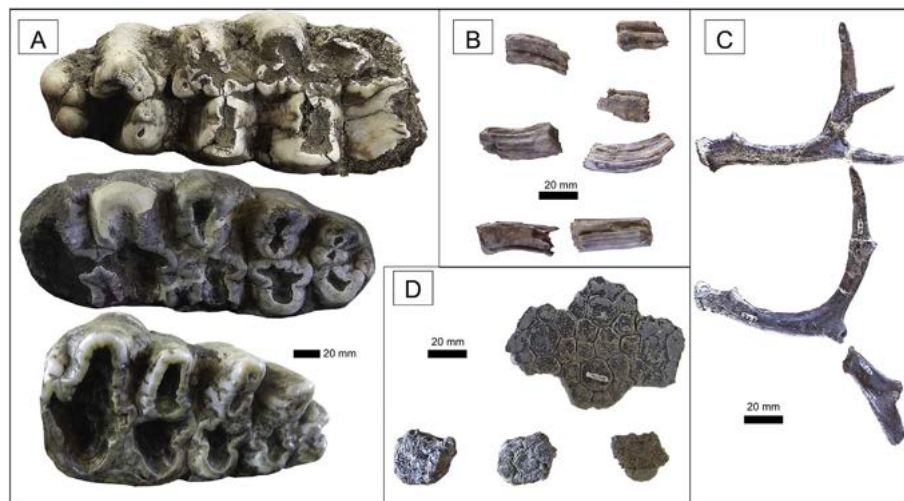
Fig. 2. Selected megafaunal evidence from Chivacabé housed in the paleontological museum of the IDAHE (without collection numbers). A) *Cuvieronius* sp. molars, all in occlusal view, B) *Equus* sp. molars, C) *Odocoileus* sp. antlers in lateral view and D) *Glyptotherium* sp. osteoderms.

(reworked volcanic sediments) of basaltic-andesitic composition (Fig. 4A).

Finca San Ramón, zona 6, Guatemala City

The locality Finca San Ramón is located in Zona 6, in the northwestern suburbs of the capital, while zona 12 (see above) is located in the southeastern quadrant. An almost complete skeleton of *Eremotherium laurillardi*, discovered at Finca San Ramón by Roberto Wolfook in Zona 6, is now exhibited in the Paleontological Museum at Estanzuela (ME), Zacapa. *Cuvieronius hyodon* and *Mixotoxodon laurensis* fragments have also been collected and are also housed at ME.

El Rosario, Ipala, Department of Chiquimula

In 1948 Salomé de María López Pérez discovered fossil bones on his ranch at El Rosario, which is located 6 km north of Ipala in the department of Chiquimula. After these first findings, the location was excavated and documented by García García and Ericastilla Gody (1995). The fauna includes *Eremotherium laurillardi*, *Cuvieronius hyodon*, *Mixotoxodon laurensis*, *Glyptotherium* sp. and a deer,

although the latter has been wrongly classified as a rodent by García García and Ericastilla Gody (1995). A total of 100 fossils have been documented from El Rosario, among them 23 fragments assigned to *Eremotherium laurillardi*, 13 to *Cuvieronius hyodon*, three to *Glyptotherium* sp., and two to *Mixotoxodon laurensis*, while 59 bone fragments remain unclassified.

Since 1994, most fossil remains collected at El Rosario, Chiquimula and Songotongo in San Luis Jilotepeque, Jalapa, are housed at the MUSHNAT, but still with the collection numbers of the IDAEH.

Other than the above, most findings of Pleistocene mammals in Guatemala are random and scattered discoveries without a proper stratigraphic context. For instance, most of these fossils were discovered while digging well shafts, roads, or during construction work.

Random findings of *Cuvieronius* molars, mandible and tusk fragments have been reported from Finca Roca Linda and Oratorio in Santa Rosa, Jutiapa, but also from Tívoli, Mixco and Km 31, close to Antigua in the department of Guatemala. A *Mammuthus* molar
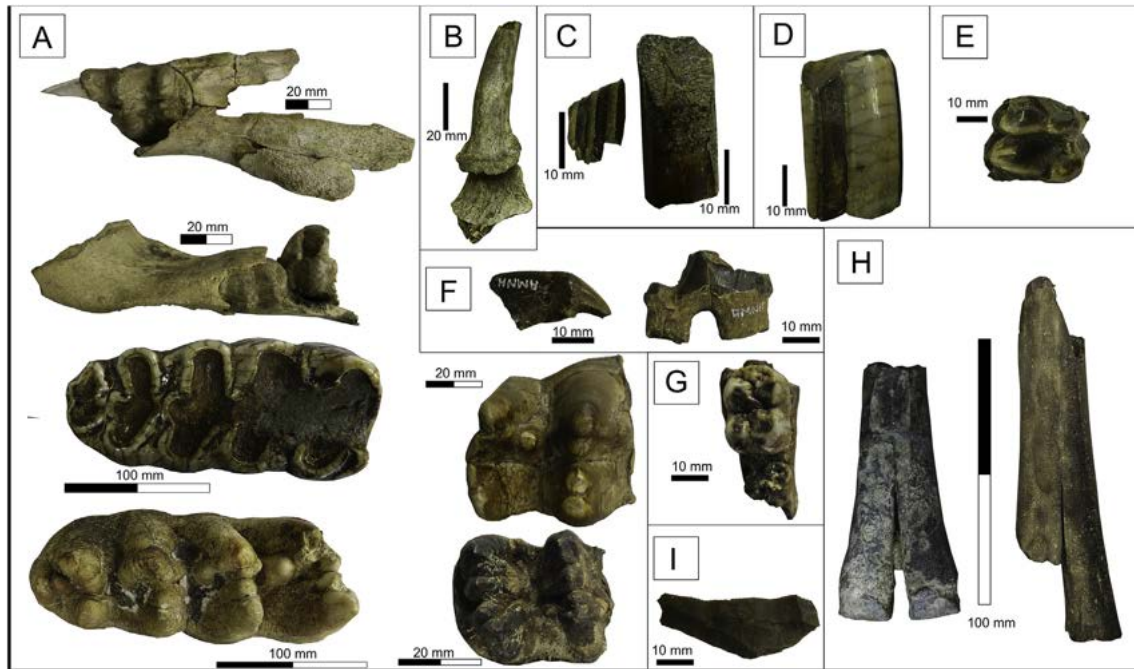
Fig. 3. Selected megafaunal evidence from Santa Amelia, also known as Río la Pasión. All specimens are housed in the AMNH in New York (without collection numbers). A) *Cuvieronius* sp. mandible fragments of juveniles and adult molars in occlusal view. B) *Odocoileus* sp. antler. C) *Neocherus* teeth fragments, D) *Mixotoxodon* teeth, E) *Tapirus* molar, F), *Canis* sp. canine and molar, G) *Pecari* sp. mandible fragment with molar, H) *Palaeolama* sp. fragmented metapodials, I) Example of flint flake from Santa Amelia included in the Barnum Brown collection.

was discovered near the Motagua river at Teculután, while other findings of proboscidean molars are from Zacapa and El Progreso. *Eremotherium* fragments have been documented from Salamá in the department of Baja Verapaz by Lewis Gazín of the Smithsonian Institute, Washington, while *Eremotherium* sp. and *Cuvieronius* sp. were reported from Songotongo, and a *Glyptotherium* carapace was found at Paso Calambrias in the department El Progreso. All this material has never been published.

In 1996, José Irineo Montoya discovered a skull fragment of the bovid *Euceratherium*, one *Equus* molar and two molars of a mammoth while digging the roots of a tree in his garden at Chinautla, in the department of Guatemala, (14.0700° N, 90.4994° W). These fossils were described by McDonald and Dávila (2017) and are now housed at Museo Nacional de Historia Natural de la Universidad de San Carlos.

In 2005 a *Cuvieronius* mandible and carapace fragments of *Glyptotherium* were discovered at Brisas del Chixoy in Alta Verapaz, approximately 150 km north of the capital. *Equus* sp. molars have been reported from Finca Roca Linda in the department Santa Rosa and Río Ostua. During the digging of a well near San Rafael Las Flores in Santa Rosa, *Cuvieronius* sp., *Eremotherium* sp., *Glyptotherium* sp., *Mixotoxodon* sp. and *Odocoileus* sp. were discovered. A second well, excavated 20 m south of the locality, exposed more fossils. The material is preliminarily housed at the Cooperativa de San Rafaelito (COCODE), in order to build a regional on-site museum.

Two *Glyptotherium* carapaces and cranial fragments were discovered in 2012 in a layer of volcanic ash at Quetzaltenango, during construction work of the City Hospital. The locality is known as Cerro el Baúl. Further armor fragments of *Glyptotherium* were found in Teculután in 1997, in the lower part of the Motagua River.

2. Material and methods

Institutional abbreviations

AMNH - American Museum of Natural History, New York City, USA

BX — Catalogue number of Santa Cruz Barillas, Casa de la Cultura, Huehuetenango

CCSC — Casa de la Cultura Santa Cruz Barillas, Huehuetenango

COCODE — Consejo Comunitario de San Rafaelito, San Rafael las Flores, Santa Rosa

IDAHE — Instituto de Antropología e Historia de Guatemala

MUSHNAT — Museo Nacional de Historia Natural de la Universidad de San Carlos, Guatemala City

USC — Catalogue number of the MUSHNAT

ME — Museo de Paleontología y Arqueología Roberto Woolfolk Saravia at Estanzuela, Zacapa

MNHN — Museo Nacional de Historia Natural Jorge Ibarra, Guatemala City

SR — San Rafaelito, San Rafael las Flores

UV — Universidad del Valle, Guatemala City

2.1. Anatomical terminology

For the present revision of Pleistocene megafossils of Guatemala we revised 719 fossil bones and fragments from 24 localities (Table 2). The material was assigned to 18 taxa. Most specimens are housed at the paleontological collections of the MUSHNAT and have USC catalogue numbers. A total of 1081 non-diagnostic fragments from Ciudad Real have not been assigned to taxon level, among them 23 cranial fragments, 63 long bone fragments such as humeri and femuri, 37 vertebral fragments, 167 rib fragments and 791 fragments without further determination.

A total of 280 fossil fragments have been documented and revised from the paleontological collection of ME in the

Fig. 4. Selected megafaunal evidence from Ciudad Real and Chinautla. A) Sediment block (volcanoclastic consolidated sand) with fragmented molars and bones of *Cuvieronius* sp. indicating water transport by a lahar from Ciudad Real. B) *Cuvieronius* sp. molars from Ciudad Real, upper row left (USC-443/71) in occlusal view, right (USC 546/72) in lateral view, lower row left (USC-152/71) and right (USC-222/71) in occlusal view, C) *Eremotherium* sp. (USC-349/72) humerus fragment from Ciudad Real, upper row claw (USC-345/72) and molariform (USC-441/72), lower row claw (USC-332/72) and molariform (USC-199/72), all in lateral view. D) *Euceratherium* sp. dorsal skull fragment (USC-1067) from Chinatula, associated with *Mammuthus*. E) *Odocoileus* sp. antler fragment (USC-163/72), F) *Mazama* sp. antler fragment (USC-264/72) both from Ciudad Real, G) *Mixotoxodon* sp. incisions from Ciudad Real (upper row USC-531/72, lower row USC-533/70).

Table 2
Megalonyx sp. measurements (mm) from Río la Pasión.

Locality	Specimen	Taxon	Description	Measurements
Santa Amelia,	AMNH 96344	*Megalonyx*	molariform	32 × 15/10
Río la Pasión	AMNH 96345	*Megalonyx*	molariform	22 × 12/6

department of Zacapa, whilst 567 fossil fragments have not been assigned to taxon level from the Estanzuela area and remaining localities.

A total of 175 fossil fragments from San Rafaelito in San Rafael las Flores have been documented, among them 80 non-diagnostic rib fragments, which have not been assigned to taxon level. All

measurements are in millimeters (mm).

The findings of *Mammuthus columbi* are listed (Table 2), but are not described here, since there is already a recent review provided by McDonald and Dávila (2017).

The fossil material from Chivacabé has been documented by Mead et al. (2012), and is therefore only listed here without further description.

2.2. Radiocarbon dating

A total of 17 fossil samples (Table 1) were radiocarbon dated at the Curt-Engelhorn-Center Archaeometry gGmbH (CEZA) at Mannheim, Germany, with a MICADAS (Mini Carbon Dating System) AMS system. Both charcoal samples were prepared using a

standard protocol including acid and base treatments to remove contaminants such as carbonate and humic acids (Lindauer et al., 2017). Radiocarbon ages were calibrated with OxCal version 4.2.4 (Bronk Ramsey, 2013) using the IntCal13 dataset (Reimer et al., 2013). Calibrated ages (Cal yr BC; Table 1) are given as a weighted mean and 1-sigma standard deviations.

Our analysis includes several specimens of the proboscidean *Cuvieronius* and of the ground sloth *Eremotherium*. Four samples are from Ciudad Real, seven from La Estanzuela, four from Chinautla, while single samples have been taken from a *Mammuthus* from Chinautla and a *Glyptotherium* from Xela. The bones did not preserve enough collagen for routine radiocarbon dating (Lindauer et al., 2017). Instead, a sample pretreatment (Koch et al., 1997) that is usually applied for stable isotopes on bone apatite was used to obtain at least a rough age estimation. In a test on samples from neighboring areas, it turned out that this pretreatment systematically leads to older ages, hence the radiocarbon data on bone apatite presented here provide maximum ages.

No ^{14}C age could be obtained from two of the fossil samples, but all other samples yielded plausible results based on bone apatite (Table 1).

3. Revision of the paleontological fossil material of Guatemala

PROBOSCIDEA Illiger, 1811
GOMPHOTHERIIDAE Hay, 1922
Cuvieronius Osborn, 1923
Cuvieronius hyodon Fischer, 1814
(Figs. 1–5, 7; Appendix 1)

Material. Cranial and postcranial material has been collected from Barranco de Ciudad Real, Zona 12, Guatemala City (USC), Department Guatemala, Finca San Ramón, Colonia Senahú, Zona 6, Guatemala City, department Guatemala (ME), Estanzuela area, Zacapa (ME), Barrio la Reforma, City of Zacapa (ME), Santa Amelia, Río la Pasión (AMNH), El Rosario, Ipala, department Chiquimula (IDAEH), San Rafaelito, San Rafael las Flores (SR), Santa Cruz Barillas, Huehuetenango (BX), Oratorio, Santa Rosa (IDAEH) and Jutiapa area (IDAEH). For detail listing of the material see Appendix 1.

Description and remarks.

Most of the material from Guatemala is highly fragmented; only a few specimens are mainly complete, such as the skeletons from Estanzuela and Santa Cruz Barillas. Most *Cuvieronius* molars are root fragments or isolated crowns (Fig. 2). The molars display a gomphotheriid pattern of enamel folding; they are bunolophodont, with an m3s presenting four to five angular lophs. Opposite pretrite
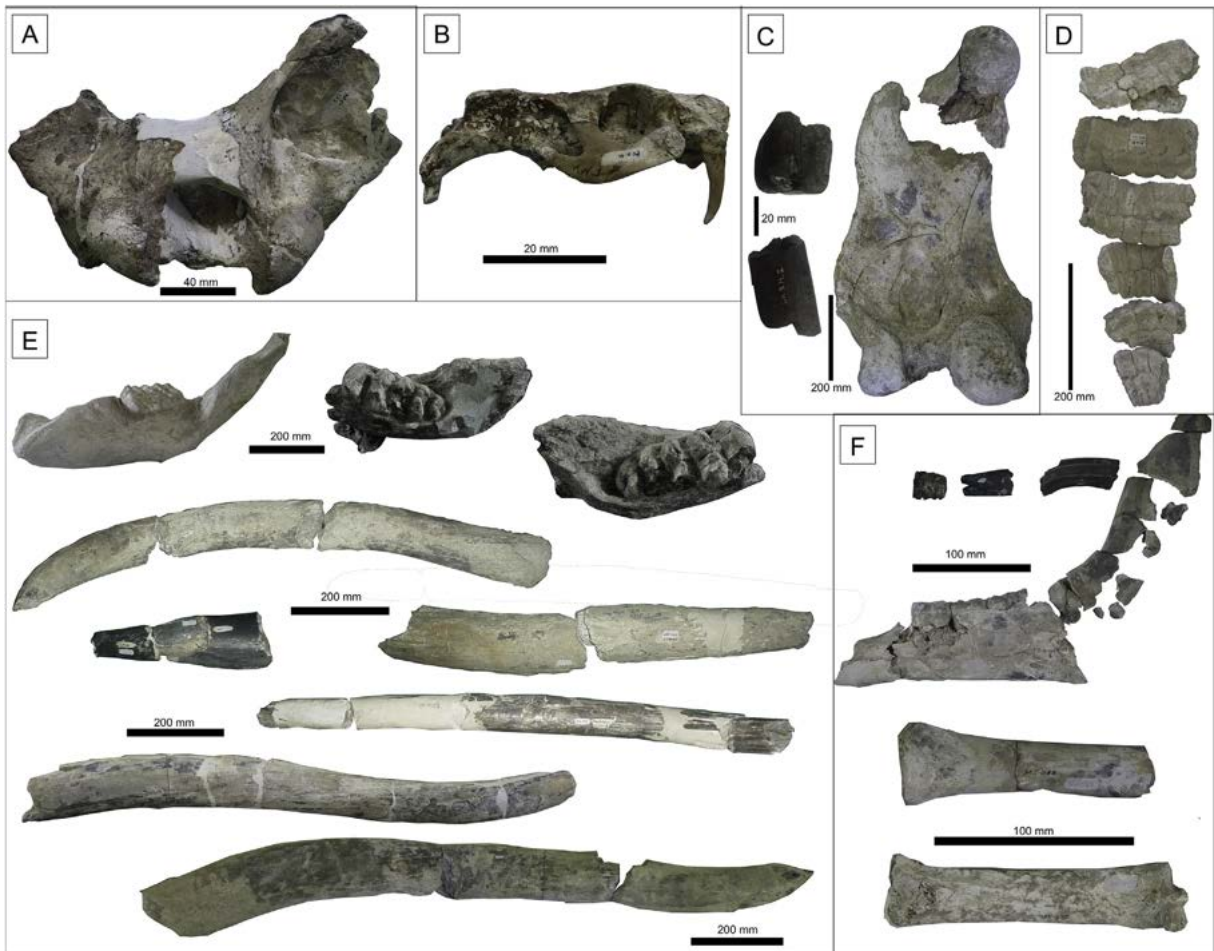
Fig. 5. Selected megafaunal evidence housed at the paleontological museum in La Estanzuela. A) *Mixotoxodon* sp. basicranium in caudal view (ME-122) from Finca San Ramón, B) *Neocherus* sp. (ME-165) skull in lateral view, C) *Eremotherium* sp. femur (ME-132) and molariform fragments, D) *Glyptotherium* sp. tail osteoderms (ME-143, 144, 145, 146, 147, 148), D) *Cuvieronius* sp. upper row mandible fragments with molar, lower rows tusk fragments (ME-72, 104), E) *Equus* sp. mandible (ME-27 and ME-38) and molar fragments (ME-40, ME-57, ME-58) in lateral view, metatarsals (ME-32, ME-35).
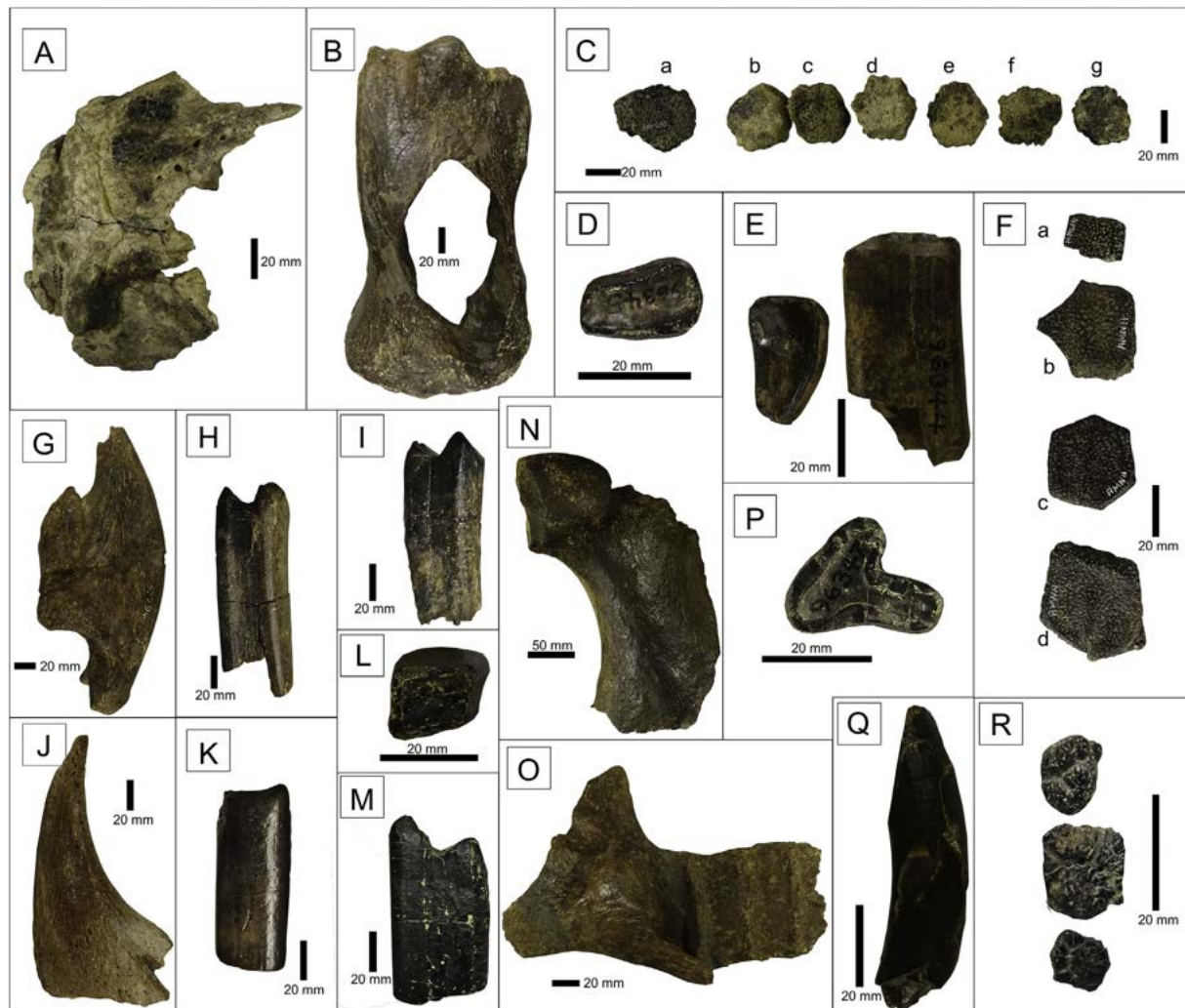
Fig. 6. Selected megafaunal evidence from Santa Amelia and Sayaxché along the Río la Pasión. A) *Glyptotherium* sp. skull in dorsal view, B) tibiofibula and C) osteoderms. *Megalonyx* sp. D) molariforms 96345 and E) 96344 in occlusal view. F) *Holmesina* sp. osteoderms. *Eremotherium* sp. G) claw, H) molariform I) molariform J) claw K) molariform L) molariform in occlusal view and M) molariform. *Paramylodon* sp. N) femur fragment, O) mandible fragment P) molariform in occlusal view and Q) caniniform in lateral view. R) *Dasypus* sp. osteoderms.

and postrite cusps alternate within the posterior lophs. Some molars are completely abraded, while other display trefoil wear facets.

The material from Estanzuela consists of a fragmented fibula, three tibiae, one ulna, the articular condyle of a femur, four femuri, a left humerus, one atlas, 12 isolated tusk fragments of approximately 400 mm length, one complete mandible, six mandibular rami including m3s, one mandibular ramus with m2 and m3, one scapula, dorsal vertebral spines, and a skull of a juvenile individual (Fig. 5). The mounted skeleton, collection number ME-66, is incomplete as podials, left femur, left tibula and fibula, left tusk and molars are missing and have been replicated. Also, many of the post-cranial bones, such as the ribs, have been mounted in an anatomically wrong position. The skeleton contains the original escapulae, sacrum, pelvis, ribs, right femur, right fibula and tibia, 28 vertebrae, skull and mandible. The skull from the Estanzuela *Cuvieronius* is low, depressed and elongated. The cranium is short-jawed with a pair of large and twisted upper tusks, which have a spiraled enamel band along their entire length and a short dentary symphysis, diagnostic characters of *Cuvieronius hyodon* (Prado et al., 2005).

The isolated tusk fragments from other localities also exhibit similarly twisted enamel bands, and are also assigned to *Cuvieronius hyodon* (Prado et al., 2005; Ferretti, 2008; Mothé et al., 2013; Mothé and Avilla, 2015). Tusk fragments of juvenile individuals are present in the fossil material of Ciudad Real and are particularly abundant at Chivacabé, where at least six neonate individuals are differentiated. Lower deciduous incisors are found in some juveniles, a feature which is absent at adult stages (Prado et al., 2005; Ferretti, 2008; Mothé et al., 2013).

ELEPHANTIDAE Gray, 1821
Mammuthus Brookes, 1828
Mammuthus columbi Falconer, 1857

Material. The *Mammuthus columbi* molars from the localities Río la Pasión, Teculután, Chinautla and Estanzuela have been described in detail by McDonald and Dávila (2017), and are therefore only listed by us (Table 1).

XENARTHRA Cope, 1889
PILOSA, Flower, 1883
MEGATHERIIDAE Gray, 1821
Eremotherium Spillmann, 1948
Eremotherium laurillardi Lund, 1842
(Figs. 4—6; Table 1; Appendix 1)
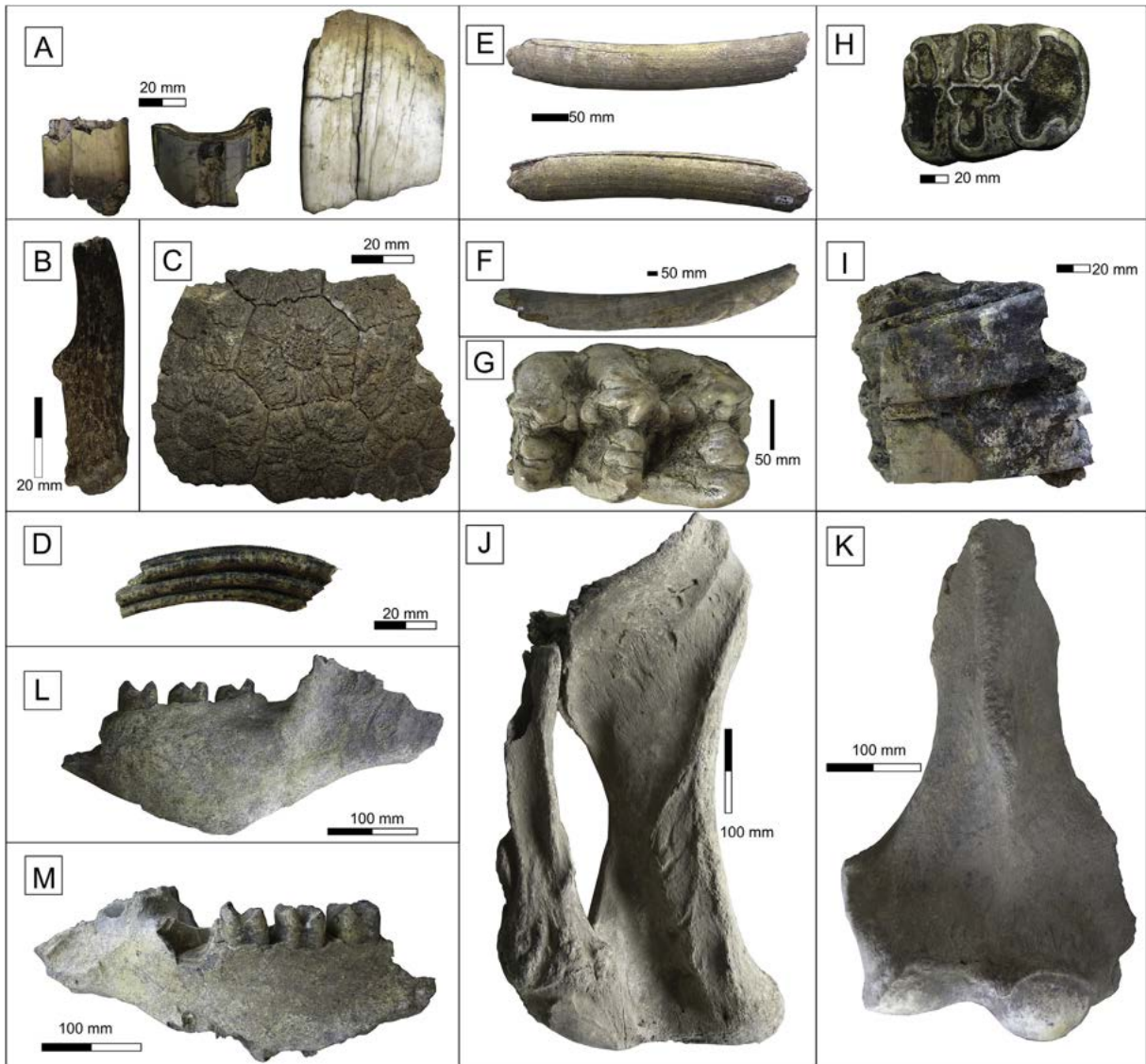
Fig. 7. Selected megafaunal evidence from San Rafaelito and Teculutlán: A) *Mixotoxodon* sp. incisives in rostral view from San Rafaelito (from left to right SR-171, 172, 170), B) *Odocoileus* sp. antler in lateral view (SR-173), C) *Glyptotherium* sp. osteoderms from Teculutlán and D) a molariform from San Rafaelito (SR-173). *Cuvieronius* sp. from San Rafaelito, E) tusk fragment (SR-44), F) tusk fragment (SR-42), G), molar in occlusal view (SR-19), H) molar in occlusal view (SR-17). *Eremotherium* sp. from San Rafaelito I) maxilla fragment with molariforms (SR-41), L) and M) mandible fragments with molariforms (SR-35, 36). *Cuvieronius* sp. San Rafaelito long bones J) tibiofibula (SR-37) and K) humerus fragment (SR-39).

Material. Eremotherium laurillardi is an abundant taxon in Guatemala and has been collected from the following localities: Barranco de Ciudad Real, Zona 12, Guatemala City, Department Guatemala, Finca San Ramón, Colonia Senahú, Zona 6, Guatemala City, department Guatemala, Estanzuela, Zacapa, Santa Amelia, Río de la Pasión, El Rosario, Ipala, department Chiquimula, Salamá, department Baja Verapaz, San Rafaelito, San Rafael las Flores, Jalapa. For the complete assignation of the revised material see Appendix 1.

Description and remarks.

A partially articulated adult individual was recovered from Ciudad Real and is comprised of a complete skull and mandible as well as abundant postcranial material (both humeri, calcaneum, astragalus etc.). Both femuri, hands, hind feet, tail, both scapulae, sternum and sternal ribs are lacking. This specimen is the most complete individual of *Eremotherium* in Guatemala and it is exhibited in the ME at La Estanzuela, Zacapa (ME-65). While this mounted individual was thus originally found at Finca San Ramón in Guatemala City, other material exhibited at Estanzuela originates from this locality; this latter material includes several ribs, three left femuri, one right femur, an articular condyle of a femur, vertebral fragments, a diaphysis from a humerus and one radius.

Several hypsodont molariforms from Ciudad Real, Estanzuela, San Rafaelito and Santa Amelia (also known as Río la Pasion), present the characteristic quadrangular shape of *Eremotherium*, with two transverse, sharp-edged ridges (De Iuliis and Cartelle, 1999). The molariforms from Río la Pasion are some of the largest ones, reaching 55 mm width and 130 mm height (Fig. 6). Also, the shallow tooth-bearing ramus is a characteristic feature of *Eremotherium laurillardi* (De Iuliis and Cartelle, 1999). The post-cranial material consists of fragmentary thoracic vertebrae and long-bones, such as humeri and femuri, mostly of smaller individuals.

MEGALONYCHIDAE Gervais, 1855

Megalonyx Harlan, 1825

(Fig. 6D, E, Table 2)

Material. Río la Pasión close to El Prado.

Description and remarks.

The two molariforms are subtriangular in occlusal view, with rounded, convex margins. The left upper molariform (AMNH 96344) has a maximum width of 32 mm and a maximum mesodistal length of 15 mm, while the buccal length is 10 mm and thus one third smaller. The second molariform (AMNH 96345) is slightly smaller with an occlusal width of 22 mm, a maximum mesodistal length of 12 mm and a minimum of 6 mm. The buccal margin of AMNH 96345 is almost flat, thus differing from AMNH 96344 in which the buccal margin is significantly more pointed. Furthermore, AMNH 96345 is straight, while AMNH 96344 exhibits a slight curvature in lateral view.

The Megalonychidae molariforms from Río la Pasión have been assigned to *Megalonyx* by Brown and other authors (Woodburne, 1969; Lucas et al., 1997; Morgan, 2008). Indeed, the overall morphology of the two molariforms resembles the one of an upper molariform (M2) of *Megalonyx curvidens or M. leptostomus* rather than *M. jeffersonii. M. obtusidens* can be precluded, since all occlusal surfaces are oval to rounded (Webb and Perrigo, 1984, 1985). Both the endemic *Meizonyx salvadorensis* from El Salvador (Webb and Perrigo, 1985) and *Xibalbaonyx oviceps* from Puerto Morelos, Mexico (Stinnesbeck et al., 2017), can also be excluded, since their occlusal molariforms are more rectangular than subtriangular. No upper molariforms have been found from *Nohochichak xibalbakah* (McDonald et al., 2017), but the overall cranial morphology and lower molariforms resemble that of *X. oviceps* (Stinnesbeck et al., 2018). However, AMNH 96344 strongly resembles 2SSAP30-518 from El Salvador (Cisneros, 2005). The individual from El Salvador was referred to *Megalonyx* but not determined to species level. The molariforms from Guatemala are undiagnostic (Woodburne, 1969; Cisneros, 2005), even though similarities with *Megalonyx leptostomus* are evident based on the smaller size, and subtriangular and convex margins of the occlusal surface. The two molariforms of Río la Pasión, may thus represent an endemic Central American Megalonychidae.

MYLODONTIDAE Gill, 1872
Paramylodon Owen, 1840
(Fig. 6N, O, P, Q, Appendix 1)

Material. Santa Amelia, Río la Pasión.

Description and remarks.

The proximal two-thirds of a left femur are preserved and the bone is transversely expanded. The attachment area of the vastus muscles originates next to the femoral head, a feature characteristic for *Paramylodon* (McAfee, 2007). The lateral margin of the femur is straigth, but its proximal and distal ends are missing; therefore, further characteristic features are not preserved. The femur is about a quarter smaller than comparable femuri from adult individuals (McAfee, 2007), even though, the anterior surface of the femoral shaft is smooth, which suggests a subadult individual. On the other hand, radii reach the minimum size of adult individuals (McAfee, 2007). The lateral margin of the radius AMNH-96348 is straight, without any lateral flange which is a characteristic of Mylodontinae (McAfee, 2007). The lateral surface of the radius shaft exhibits distally reaching muscle scarring, a feature documented from *Glossotherium* instead of *Paramylodon* (McAfee, 2007).

The isolated caniniforms from Santa Amelia exhibit a vertical occlusal surface to the axis of the tooth. Two, half as large and gracile caniniforms, with oblique occlusal surfaces to the tooth axis, have also been collected along Río la Pasión. Both caniniforms belonged to juvenile individuals. An upper molariform presents the characteristic triangular horizontal section of *Paramylodon* (McDonald, 2006; McAfee, 2007, 2009).

The genus *Paramylodon* is characterized by high anatomical diversity, e.g. of body size and cranial paramaters, including the retention or loss of caniniforms (McDonald, 2006; McAfee, 2007). The presence of several caniniforms and the body size of the individuals from Petén, suggest an Irvingtonian to early Rancholabrean age (McDonald, 2006).

GLYPTODONTIDAE Burmeister, 1879
Glyptotherium Osborn, 1903
(Figs. 2, 4–6, Appendix 1)

Material. The material from Guatemala consists mainly of armor fragments or individual osteoderms, which has been found in Estanzuela, Zacapa, Santa Amelia, Río la Pasión, Petén, El Rosario, Ipala, Chiquimula, Paso Calandrias, El Progreso and Cerro del Baul, Quetzaltenango, Teculutlán, Zacapa. For detailed registration see Appendix 1.

Description and remarks.

The material is extremely porous and light. Carapace osteoderms present hexagonal shape and reach approximately 30 mm thickness, although some have broken borders (Fig. 6C: a, b and f) and the dorsal surfaces have deteriorated, but some characteristics are still visible. The surface has a rugose and punctuated texture. The central figure is flat and delimited by an exceedingly faint central annular sulcus. Peripheral figures and sulci are not identified, presumably due to deterioration; only one (Fig. 6C: e) osteoderm shows extremely faint radial sulci that mark the boundary between possibly four peripheral figures located along its margin. Between two to four hair follicles are observed on each osteoderm. Due to the deterioration of the present osteoderm material a correct diagnosis of the species is not possible to date.

A single isolated and broken molariform (AMNH-96336) presents the typical trilobated and asymmetrical shape of Glyptodontidae. *Glyptotherium* tooth material is scarce, as osteoderms are by far the most common findings. The maximum anteroposterior diameter (25 mm), measured through the center of the molariform, is larger than that of most described molariforms, which range between 22 and 26 mm (Gillette and Ray, 1981; Carlini et al., 2008; Oliveira et al., 2010; Ramírez-Cruz and Montellano-Ballesteros, 2014; Gillette et al., 2016). The occlusal surface is flat. The alveolar portion curves slightly posteriorly. The maximum transverse diameter of the anterior lobe measures 15 mm. The anterior lobe presents a straight anterior border, whilst the labial side of the lobe is almost symmetrical against the lateral axis. The lingual side is more pronounced than the labial one. The minimum transverse diameter of the anterior constriction measures 5 mm. The maximum transverse diameter of the middle lobe is 17 mm. The middle lobe is oval-shaped and almost symmetrical on a lateral axis, with a more pronounced labial side. The minimum transverse diameter of the posterior constriction is 3 mm. The posterior lobe is broken from the lingual side; the posterior border and the posterolabial angle are rounded; the anterolabial angle of the lobe presents a small labial expansion at about 6 mm distance from the central anteroposterior axis.

The osteodentine core is clearly visible along the central anteroposterior axis, from the center of the anterior lobe to the center of the posterior lobe. This presents perpendicular lateral ramifications on the anterior and middle lobe reaching the lateral apices of the lobes; lateral ramifications on the posterior lobe are not visible. The poor and fragmentary skull material and ontogenetic variations noted by Gillette et al. (2016) do not allow us to establish diagnostic characters for species identification based on basicranium morphology.

The material from Salinas close to Río la Pasión consists of a tibiofibula, enclosed into a single and stout element, typical of glyptodonts (Gillette and Ray, 1981). Gillette and Ray (1981) provide morphoanatomical descriptions for several *G. texanum* specimens (adults then identified as *G. arizonae*), and two fragmentary

tibiofibulae of *G. floridanum*. The tibiofibula from Salinas has a proximodistal length of 265 mm, measured from the posterior margin of the proximal articular facet to the posterior malleolus, larger than in adult specimens described by Gillette and Ray (1981) ranging from 220 to 235 mm. Morphoanatomical descriptions correspond to those provided for *Glyptotherium*. Gillette and Ray (1981) differentiated *G. arizonae* (*G. texanum*) from *G. floridanum* based on the shape of the proximal tibial facet; in *G. floridanum* the facet is more elongated in the anteroposterior plane, rather than circular as in *G. arizonae*. The proximal tibial facet is oval shaped in the Salinas specimen and more compressed in the mediolateral axis than that of *G. arizonae*. However, no further differentiation is provided for *Glyptotherium* species and no specific assignation of the Guatemala material from Salinas is thus possible to date.

The basicranium of *Glyptotherium* is rarely preserved in the fossil record (Gillette et al., 2016). The basicranium from Río la Pasión is highly fragmented (Fig. 6A), consisting of the occipital, parietal, and squamosal bones. The morphology corresponds to descriptions of *Glyptotherium* by Gillette and Ray (1981). The sutures between parietal and squamosal are completely fused, suggesting a subadult to adult individual. This is also supported by the transverse diameter between paroccipital processes reaching 120 mm, slightly larger than in juvenile *G. texanum* specimens (Gillette and Ray, 1981), but significantly smaller than in adult *Glyptotherium* specimens reaching 132–160 mm (Gillette et al., 2016). In dorsal view, the transverse diameter of the occipital condyles is 95 mm. The proportions of the occipital condyles (35 mm × 22 mm) and foramen magnum (30 × 22 mm) are comparable to *G. floridanum* (Gillette and Ray, 1981).

PAMPATHERIIDAE Burmeister, 1879
Holmesina Simpson, 1903
(Fig. 6F, Table 3)

Material. Holmesina is only known from Santa Amelia, Río la Pasión, Petén. The material, housed at the AMNH, without a collection number (Table 3) and is composed of four osteoderms (three cephalic and one fixed non-marginal buckler osteoderm).

Description and *remarks.*

North American Pampatheriidae include the genera *Pampatherium* and *Holmesina* (Scillato-Yané et al., 2005). A third genus, *Plaina* (Carranza-Castañeda and Miller, 1995), has not been illustrated nor described in detail, so its taxonomy thus remains uncertain (Aguilar and Laurito, 2009). Distinction between *Pampatherium* and *Holmesina* is based on osteoderm morphology (Scillato-Yané et al., 2005; Aguilar and Laurito, 2009). Cephalic osteoderms from Rio La Pasión are smaller than fixed osteoderms (Fig. 6F: a and b are broken). Fig. 6F: c is of pentagonal shape. The marginal band is rugged. The foramina on the anterior margin are almost twice the size of those located along the lateral margins. The marginal elevation is slightly pronounced.

The fixed non-marginal osteoderm (Fig. 6C: d) presents a pentagonal shape. The anterior and lateral margins are wide and rugged. The submarginal band is reduced. The marginal elevation is a pronounced ridge. The central figure is narrow, as known for *Holmesina*, and differs from that of *Pampatherium mexicanum* (Aguilar and Laurito, 2009). The longitudinal depression is

horseshoe-shaped, deep and wide, as in *Holmesina* and thus differs from that seen in *Pampatherium mexicanum*. The lateral projection is a ridge located on the posterior half of the scute, with a rounded anterior and a narrow posterior border. Two species of *Holmesina* are presently known in North America, *H. septentrionalis* Leidy, 1889 and *H. floridanus* Robertson, 1976.

Holmesina septentrionalis is present in Pleistocene (Irvingtonian and Rancholabrean) strata of Florida, Kansas, South Carolina, Texas and Georgia in the US as well as in Mexico (Aguilar and Laurito, 2009). The only reported occurrence in Central America is from the Irvingtonian of Río Tomayate in El Salvador (Aguilar and Laurito, 2009). *H. floridanus* is only known from the Blancan (Late Pliocene – Early Peistocene) of Florida (Gaudin and Lyon, 2017).

DASYPODIIDAE Gray, 1821
Pachyarmatherium Downing and White, 1995
Pachyarmatherium leyisei Downing and White, 1995
(Fig. 6R, Table 4)

Material. Three small osteoderms from Santa Amelia, Río la Pasión, Petén are housed at the AMNH, without collection number, and here assigned to *Pachyarmatherium leyisei* Downing and White (1995), according to their sizes and morphology.

Description and remarks.

The material is conformed by three broken buckler osteoderms. The osteoderms are small reaching 15.71–24.55 mm at the major axis and 17.19–17.9 mm at the minor axis. The osteoderms are thick, different to Glyptodontidae and Pampatheriidae which are flat and large-sized (Downing and White, 1995; Valerio and Laurito, 2011). The nearly complete osteoderms (Fig. 6R) are hexagonal in outline. The central figure is slightly inflated and convex, with a hexagonal rounded border and a sleek surface, thus differing from *Dasypus bellus* (Simpson, 1929), another North American Dasypodidae member presenting a rugged dorsal surface and flatter central figure (Rincón et al., 2008). The central figure is located on the anterior border and is surrounded by 4–5 slightly smaller peripheral figures (about 90% the size), again differing from *D. bellus* in which the central figure is much larger than peripheral figures (Rincón et al., 2008). The central figure is isolated by a central annular sulcus which is deep and wide, containing 1 to 3 foramina. The peripheral figures are separated by deep and wide radial sulci and do not present any foramina.

The fossil material described here differs from *Pachyarmatherium tenebris* by having a smooth inflated central figure and wider sulci (Rincón and White, 2007; Valerio and Laurito, 2011). *Pachyarmatherium leyisei* is known from the southern United States and Costa Rica, whereas *P. tenebris* has been documented from Venezuela (Valerio and Laurito, 2011). *Dasypus bellus* is known from the US and Mexico (Rincón et al., 2008; Carbot-Chanona, 2010).

NOTOUNGULATA Roth, 1903
TOXODONTIDAE Owen, 1845
Mixotoxodon van Frank, 1957
Mixotoxodon larensis van Frank, 1957
(Figs. 3, 5, 7, Appendix 1)

Material. Mixotoxodon larensis is known from Barranco de Ciudad Real, Zona 12, Guatemala City, Department Guatemala, Estanzuela, Zacapa, Santa Amelia, Río la Pasión, Petén, El Rosario, Ipala, Department Chiquimula and San Rafaelito in San Rafael las Flores. A detailed listing is provided in Appendix 1.

Description and remarks.

The Guatemala material of the taxon is conformed by a basicranium (from Estanzuela, Fig. 5) and euhypsodont teeth (incisives and molars; Fig. 7A). All teeth exhibit enamel bands on their outer surface, which is typical for *Mixotoxodon* (Laurito, 1993; Rincón, 2011; Lundelius et al., 2013). The incisors are transverse in cross section, with the labial sides convex and lingual sides concave. The

Table 3
Holmesina sp. measurements (mm) from Río la Pasión.

Locality	Specimen	Taxon	Description	Measurements
Santa Amelia, Río la Pasión	AMNH without collection number	*Holmesina*	osteoderm	50 × 40
		Holmesina	osteoderm	37 × 33
		Holmesina	osteoderm	40 × 38
		Holmesina	osteoderm	24 × 15

Table 4
Pachyarmatherium sp. measurements (mm) from Río la Pasión.

Locality	Specimen	Taxon	Description	Measurements
Santa Amelia, Río la Pasión	AMNH without collection number	*Pachyarmatherium* *Pachyarmatherium* *Pachyarmatherium*	osteoderm osteoderm osteoderm	15.71 17.19 24.55

absence of enamel in the lingual margin of the premolars is a diagnostic character of *Mixotoxodon larensis* (van Frank, 1957). The upper third molar from San Rafaelito is vertically curved, with a characteristical concave occlusal surface and wavy ectoloph (Lundelius et al., 2013). The anterior and posterior molars end taper.

The basicranium from La Estanzuela (Fig. 5) is highly compressed and only fragmentarily preserved, which affected the morphology. The twisted deformation of the skull is due to preservation, which is well seen in posterior view. The basicranial sutures are all fused, suggesting an adult individual. The foramen magnum is oval, twice as wide as height. A pronounced nuchal crest rises adjacent to the foramen, which is only visible in dorsal view. The occipital condyles are triangular and outstanding.

PERISSODACTYLA Owen, 1848
EQUIDAE Gray, 1821
Equus Linnaeus, 1758
(Figs. 2 and 5, Appendix 1)

Material. Molars and postcranial material has been collected in Barranco de Ciudad Real, Zona 12, Guatemala City, Department Guatemala, Chinautla, Department Guatemala, Estanzuela, Zacapa, Calle del Comercio, City of Zacapa, Rio Ostúa, Jutiapa, Santa Rosa. A detailed listing of the fossils is provided in Appendix 1.

Description and remarks.

The material from Guatemala consists of isolated teeth and postcranial elements. The teeth are high crowned, with a complex enamel pattern typical for the genus *Equus*. The material of La Estanzuela, Zacapa consists of a left mandibular ramus with dm 2 to 4, one astragalus, four metacarpals and metatarsals and one metapodial.

The fragmentary nature of most Guatemala records, as well as the problematical nomenclatural state of *Equus* in North America (Kurten and Anderson, 1980; Morgan, 2015), has not allowed for a determination to species level of the present material.

TAPIRIDAE Gray, 1821
Tapirus Brisson, 1762
(Fig. 3E, Table 5)

Material. Santa Amelia, Río la Pasión.
Description and remarks.

The isolated bilophodont molars from Petén are characteristical for the genus *Tapirus*. The large size of the molar suggests a Pleistocene rather than an extant species, but size and proportion could also fall within the range variation of extant species (Perini et al., 2011). However, two single teeth are not enough for species assignation, since the identification of the exact tooth position is not possible here.

ARTIODACTYLA Owen, 1848
CERVIDAE Gray, 1821
Odocoileus Rafinesque, 1832
Odocoileus virginianus Zimmerman, 1780

Table 5
Tapirus sp. measurements (mm) from Río la Pasión.

Locality	Specimen	Taxon	Description	Measurements
Santa Amelia, Río la Pasión	AMNH without collection number	*Tapirus* *Tapirus*	molar premolar	32 × 25 12 × 9

(Figs. 2, 3, 7, Appendix 1)

Material. Barranco de Ciudad Real, Zona 12, Guatemala City, Department Guatemala and

Santa Amelia, Río la Pasión, Petén (AMNH).
Description and remarks.

The main structure of the antlers present a helix-shape, in which the beam and anterior branch form a continuous curvature. The tines rise vertically from the dorsal side of this basic structure (Pocock, 1933). *Odocoileus* is the only deer documented from the Pleistocene of Central America known to present branched antlers.

Mazama Rafinesque, 1817

Material. Barranco de Ciudad Real, Zona 12, Guatemala City, Department Guatemala (Table 6).

Description and remarks.

The genus *Mazama* is only present by one single antler with a conical or spike-like shape and a prominent burr (Table 6). In consequence, assignation has to be taken with caution, as the more frequent *Odocoileus* presents a wide range of antler morphologies (Webb, 2000).

TYLOPODA Illiger, 1811
CAMELIDAE Gray, 1821
Palaeolama Gervais, 1869
(Fig. 3, Appendix 1)

Material. Santa Amelia, Río la Pasión.
Description and *remarks.*

Two distal fragments of metapodials have been found at Santa Amelia. Both are small and slender. The smaller metapodial fragment (130 × 60 mm) presents the distal end of a metatarsal, while no diagnostic characters are preserved in the longer fragment (270 × 50 mm). However, a complete left metatarsal (280 × 50 mm) is also present. Characteristic of the genus *Palaeolama* are the short and robust proportions (Menegaz and Jaureguizar, 1995; Webb and Stehli, 1995). In contrast to the more gracil and larger metapodials in *Hemiauchenia* (Breyer, 1983). *Palaeolama* has already been reported from Central America (Cisneros, 2005).

BOVIDAE Gray, 1821
Euceratherium Furlong and Sinclair, 1904
(Fig. 4D, Appendix 1)

Material. Chinautla, department Guatemala.

Description and remarks. Several horn fragments have been collected from Chinautla and are now housed at the MUSHNAT. The horn cores arise from the posterior margin of the frontals, twist upward and backward, and curve upward to become rounded at their tips. No burr is present on the horn cores, and there is no inflation of the frontals or extension of the horns as in *Ovibos*. Rather, the shapes, sizes, and the longitudinal nutrient grooves of the horns, are typical for the genus *Euceratherium*. The shrubox *Euceratherium* is known from several Rancholabrean sites in North America, including Mexico (Morgan and Harris, 2015). *Euceratherium* has been interpreted as robust stoutly built grazing ruminant, inhabiting rough rocky terrain (Morgan and Harris, 2015). New analysis of dung pellets from Utah and New Mexico in the US, suggest that *Euceratherium* was a browser, rather than a grazer, and preferred a tree and shrub dominated diet, including *Quercus*, *Artemisia* and *Chrysothamnus* (Kropf et al., 2007).

Table 6
Mazama sp. measurements (mm) from Barranco de Ciudad Real.

Locality	Specimen	Taxon	Description	Measurements
Barranco de Ciudad Real, Zona 12, Guatemala City	USC 265/72	*Mazama*	antler fragment	106×13.5

SUINA Gray, 1868
TAYASSUIDAE Palmer, 1897
Pecari Reichenbach, 1835
Pecari tajacu Linnaeus, 1758
(Fig. 3, Appendix 1)
Material. Santa Amelia, Río la Pasión.
Description and remarks.

The mandible fragment is only 35×10 mm small and only exhibits m2. The latter is mesiodistally one quarter longer than buccolingually, bearing four prominent cuspids. The small mandible fragment exhibits the typical tayassuid brachybunodont dentition and is assigned to the Collared peccary (*Pecary tajacu*). The presence of *Pecary tajacu* in the faunal assemblage of Santa Amelia has already been described by Woodburne (1969) based on a right maxillary fragment (AMNH 48799) from the same locality.

RODENTIA Bowdich, 1821
HYDROCHAERIDAE Gray, 1825
Neochoerus Hulbert, 2001
(Figs. 3 and 5, Appendix 1)
Material. Estanzuela, Zacapa and Santa Amelia, Río la Pasión.
Description and remarks.

Isolated teeth from Río de la Pasión are only fragmentary preserved. However, they are euhypsodont and elasmodont, consisting of multiple transverse laminae separated by cementum, which is typical for Hydrochoeridae (Mones, 1984; Moreira et al., 2012; Guiomar Vucetich et al., 2015; Aeschbach et al., 2016). The incisors show a labiomedial groove. The skull from La Estanzuela is long, low and narrow. It is slightly deformed, but the dorsal surface of the frontal and parietal are flat and at the same height as the nasal. The left zygomatic arch has been restored. The cranial sutures are well visible, suggesting a juvenile to subadult individual.

CARNIVORA Bowdich, 1821
CANIDAE Fischer de Waldheim, 1817
Canis Linnaeus, 1758
(Fig. 3, Appendix 1)
Material. Santa Amelia, Río la Pasión.
Description and remarks.

The m1 is slightly fragmented, lacking the paracone cusps. The overall morphology of the incisor and the molar suggest a large *Canis* taxon, larger than *C. latrans* and *C. rufus*. The material is here tentatively assigned to *C. dirus*. However, two teeth are insufficient for a proper species assignment.

4. Discussion

The Pleistocene fossil assemblage of Guatemala consists of large herbivores in which proboscideans (*Cuvieronius*) and xenarthrans (*Eremotherium*, *Glyptotherium*) are the dominant elements, while co-occurring *Equus* and *Mixotoxodon* are significantly less frequent, and *Holmesina*, *Palaeolama*, *Tapirus*, *Neocherus, Mammuthus* and other ground sloth taxa (*Paramylodon*; *Megalonyx*) are rare. From the systematic point of view, the Guatemala megafaunal assemblage is thus approximately consistent with other associations documented along the Mesoamerican Corridor (e.g. Honduras, El Salvador, Nicaragua, Costa Rica, Panama) and northern South America (Venezuela, Colombia) (Stirton and Gealey, 1949; Webb and Perrigo, 1985, 2018; Lucas et al., 1997; Cisneros, 2005; Lucas, 2008a, 2014), which also include predominantly *Cuvieronius*,

Eremotherium, *Glyptotherium* and *Mammuthus*.

4.1. Dating

A total of 20 fossil bones and two charcoal samples in sediments (Table 1) were here radiocarbon dated to the Late Pleistocene or the Early Holocene. The Pleistocene ages correspond to the Rancholabrean stage in the North American classification, or Lujanian in the South American land-mammal biochronology.

Nine results, based on *Cuvieronius, Eremotherium* and *Mixotoxodon,* range between $29,350 \pm 130$ to $19,910$ uncal BP and provide a reasonable time range estimation of the faunal composition before and during the Last Glacial Maximum (LGM). Latest Pleistocene to even Early Holocene ages ($15,730 \pm 50$ to $9,539 \pm 30$ uncal BP) have been obtained for *Cuvieronius* specimens from La Estanzuela and a *Glyptotherium* from Xela, Quetzaltenango.

These extremely young ages from the Motagua river in south-central Guatemala suggest that a local population of *Cuvieronius* may have survived into the Early Holocene. The area, located in the Río Motagua valley at only 200 m altitude, today presents a tropical climate. *Cuvieronius* is known to have adapted to temperate and tropical temperatures and high humidity (Prado et al., 2005; Mothé and Avilla, 2015); a survival of these adaptive mix-feeders into the Early Holocene therefore appears plausible. We are aware, however, that all fossils reported here were dated based on apatite and not collagen due to preservation issues. Bioapatite is known to have a greater exchange with the environment, but it is an accepted technique (Cherkinsky, 2009; Dantas et al., 2013) and in this case the only material available to be dated.

A precise age assignment remains doubtful in the cases of isolated findings of molars, or bones, without a context with other fossils, as is the case for *Mammuthus*. A better stratigraphic context would provide additional credibility to the youngest ^{14}C data for *Mammuthus* (e.g. $12,340 \pm 50$ uncal BP; Table 1). Unfortunately, the stratigraphical and sedimentological context of these findings is unavailable, except for rare exceptions such as the sites of Chivacabé, San Rafaelito, and Estanzuela.

Two out of 17 of the ^{14}C fossil samples analysed here failed to provide ages (Table 1). This is a consequence of intensive hydrothermal alteration and mineralization of these bones. The volcanosedimentary character of the fossil-bearing sediment in most regions of Guatemala also precludes the application of luminescence methods. It is important to stress that in the case of the La Estanzuela, Chivacabé, Ciudad Real and San Rafaelito sites the fossils are embedded in sequences of fluvially reworked volcanic ashes (lahars). In the case of Ciudad Real (Fig. 4) and Chivacabé the fossils are deposited in lahars which infilled a steep gully. Therefore, the fossils are incomplete, sometimes with evidence of short transport (Fig. 4).

Indeed, most of the fossil material found *in situ* is embedded in volcanic sediments, emphazising the abundance of volcanic eruptions during the Middle to Late Pleistocene. For example, the rhyolitic eruption of Los Chocoyos, which caused the Atitlán caldera in the Guatemalan highlands, was dated to 84,000 BP (Bush et al., 2009), while the last eruption causing one of the calderas of Lago Ayarza in the department Santa Rosa, was dated to 23,000 uncal BP (Mayorga et al., 1979), with the fossils from the nearby San Rafaelito site with dates around 27,000 uncal BP (see Table 1). The strong

mineralization of the fossils is also a reason for the absence of bone collagen required for standard radiocarbon dating.

Glyptotherium sp., *Mixotoxodon* sp., *Equus* sp. and *Mazama* sp. are typical Pleistocene faunal elements (Gillette and Ray, 1981; Lucas et al., 1997; Webb, 2000) and are present throughout the stage. In consequence, some of the faunal elements described here may be older than Rancholabrean. The oldest record for *Mazama* is from the Early Pleistocene of El Salvador (Lucas et al., 1997), while the earliest evidence for *Cuvieronius* in El Salvador is from the Early Irvingtonian, although a late Blancan age has also been suggested based on findings from the US and Mexico (Lucas et al., 1999; Lucas and Alvarado, 2010). Megalonychidae molariforms from Río la Pasión resemble the upper molariform (M2) of either *Megalonyx curvidens* or *M. leptostomus*, both known to range from the Late Miocene to Early Pleistocene. *Palaeolama* may be another taxon ranging through stages older than Rancholabrean.

4.2. Paleobiogeographic distribution of the megafauna

Other than *Eremotherium* and *Mixotoxodon*, no other taxa of South American origin is documented here. This supports the interpretation of Simpson (1950) and Webb (2006), that North American taxa were more successful in South America during GABI (and post-GABI migrations) than South American invasive taxa in North America. Webb (2006) explains this asymmetry by a longer and wider-ranging original history of Northamerican taxa and repeated faunal exchange with Eurasia.

Cuvieronius, as other Gomphotheriidae, is characterized by a specialized dentition consisting of six pairs of upper and lower molars (Ferretti, 2008; Mothé et al., 2013). Although the taxonomic and phylogenetic status of *Cuvieronius* within the Gomphotheriidae is still under debate (Prado et al., 2003; Alberdi and Corona, 2005; Mothé and Avilla, 2015), the recognition of *C. hyodon* as a valid species has been accepted in recent publications (Prado et al., 2003, 2005; Mothé and Avilla, 2015). *Cuvieronius hyodon* had a wide geographic distribution ranging from Florida, U.S., through the Veracruz coastal region of the Mexican Gulf coast plain to the Mexican Yucatán Peninsula (González González et al., 2008; González González et al., 2013; Chatters et al., 2014), El Salvador, Nicaragua, Costa Rica and Panama in Central America (Woodburne, 1969; Lucas et al., 1999), to Ecuador, Bolivia and Peru in South America (Mothé and Avilla, 2015). *Cuvieronius* is reported in most paleontological sites (Table 1) in Guatemala and therefore presents the widest distribution of all Guatemalan taxa. The paleogeographic distribution of *Cuvieronius* as limited to lowlands has been discussed (Mothé et al., 2013), but topography was probably not a limiting factor (Mothé and Avilla, 2015) since *Cuvieronius* is here reported in both the high- and lowlands of Guatemala. Its wide distribution is probably due to its adaptation as a mixed feeder, inhabiting high grasslands of temperate to tropical regions with a higher humidity (Prado et al., 2005; Mothé and Avilla, 2015).

The Panamerican ground sloth *Eremotherium laurillardi* is also a dominant element which is present in one third of the faunal assemblages of Guatemala. *Eremotherium laurillardi* has been reported from Long Branch and Monmouth County in New Jersey, Florida, South Carolina and Georgia along the Gulf Coastal Plain, Texas (Webb and Perrigo, 1984, 1985; Morgan and Harris, 2015), west-central and southwestern Mexico (McDonald, 2002; Stinnesbeck et al., 2018) throughout Central America (e.g. Belize; Larmon et al., 2019), to Peru, Ecuador and Rio Grande do Sul (Brazil) in South America (Cartelle and De Iuliis, 1995; Pujos and Salas, 2004; Morgan, 2008). This giant ground sloth is largely restricted to the lowland areas of Guatemala along the river systems of Río la Pasión and Móntagua; only the findings at Ciudad Real and Finca

San Ramón in the capital are from locations >1400 m asl, but these are located at close distance to the Las Vacas river, which joins the Motagua river system about 50 km downstream to the north.

Other ground sloth taxa are only based on random findings along Río La Pasión in the northern lowlands of Guatemala (>130 m asl; Table 7). *Paramylodon* and *Megalonyx* fossils have been collected by Barnum Brown in the late 1940s close to the villages El Prado and Santa Amelia. The occurrence of *Paramylodon* in northern Guatemala is the southernmost evidence of this genus in North- and Central America (Morgan, 2008), while *Megalonyx* has been documented from El Salvador (Cisneros, 2005), El Bosque in Nicaragua (Page, 1978) and Río Humuya in Honduras (Webb and Perrigo, 1984). The presence of *Megatherium* and *Mylodon*, originally suggested by Brown (Woodburne, 1969), cannot be confirmed here.

Glyptotherium also had a wide geographic distribution across Guatemala and is here recorded in more than one third of Guatemalan localities (Table 7). Unfortunately, potentially diagnostic cranial elements of *Glyptotherium* have not yet been identified from Guatemala, but North American glyptodonts of Late Pleistocene age are mainly referred to *Glyptotherium cylindricum* or *G. floridanum* (Gillette and Ray, 1981). *Glyptotherium* has been documented from Honduras, El Salvador, and now Chicavabé, Chixoy, Ciudad Real, Cerro del Baul, El Rosario, Santa Amelia, San Rafaelito and Estanzuela in Guatemala. As already noted by McDonald (2002) *Glyptotherium* has been documented at higher topographic elevations in Mexico and is there frequently associated with *Eremotherium*, *Holmesina* and *Pampatherium*, which is also the case in Guatemala.

Other taxa are under-represented and most are isolated findings (Table 7). This is the case for *Equus* sp., which has only been found at Chivacabé, Ciudad Real and Estanzuela.

Mixotoxodon larensis also shows a wide geographic distribution in Central America, with occurrences from southern US (Lundelius et al., 2013), Mexico (Polaco et al., 2004), El Salvador (van Frank, 1957; Webb and Perrigo, 1984), Honduras (Webb and Perrigo, 1984), Nicaragua (Leidy, 1886), Panama (Gazin, 1956), Costa Rica (Laurito, 1993). In Guatemala however, the taxon has only been documented from Ciudad Real, Santa Amelia in Petén, San Rafaelito and Chiquimula. *Mammuthus* is rare and has only been reported from Río la Pasión, Estanzuela and Chinautla (McDonald and Dávila, 2017). *Odocoileus* has previously been identified in El Salvador (Cisneros, 2005), Honduras (Webb and Perrigo, 1984), Panama (Gazin, 1956) and Nicaragua (Page, 1978) and is present in four of the 24 localities revised here from Guatemala. *Palaeolama* has been documented in Santa Amelia, whereas *Neocherus* is present only at Estanzuela and Santa Amelia. *Euceratherium* is documented by a single finding from Ciudad Real. Most of the single findings, of *Canis*, *Holmesina*, *Paramylodon*, *Pecary* and *Tapirus*, are from the northern lowlands of Guatemala, along Río la Pasión in Petén. The presence of *Dasypus*, *Hydrochoerus, Hemiauchenia* and *Felis* in Guatemala, that have been listed in the past (Lucas, 2014a,b; Morgan, 2008; Woodburne, 2010, 1969), cannot be confirmed here.

Nothrotheriops shastensis has not been reported so far from Guatemala. This ground sloth was widely distributed throughout North America (McDonald, 2002) and even reached the Mexican Yucatán Peninsula (González González et al., 2008) and Belize (De Iuliis et al., 2015). Its absence in the Guatemala faunal assemblage suggests that *Nothrotheriops* may not have migrated further south, or even may have evaded the Guatemala region on its way to southern Central America. Also, some Holarctic taxa such as *Bison* were not able to cross Central America (Webb and Rancy, 1996; Webb, 2006; Woodburne, 2010).

The striking absence of large carnivores in Guatemala and their scarcity in the Central American faunal assemblages is puzzling. To

Table 7
List of Late Pleistocene to Early Holocene taxa according to the paleontological localities in Guatemala. For further information on the ^{14}C ages uncal BP see Table 1.

Department	Locality	Altitude [msl]	Taxa	Collection	Age/uncal yrs BP	Reference
Guatemala	Ciudad Real and Frutal, Zona 12, Guatemala City	1319–1377	*Cuvieronius hyodon* *Equus* sp.	MUSHNAT	29,350 ± 130	This paper
			Eremotherium laurillardi *Mazama* sp.	ME		
			Mixotoxodon larensis *Odocoileus*	MUSHNAT	27,850 ± 120	This paper
	Finca San Ramón, Colonia Senahú, Zona 6, Guatemala City	1366	*Cuvieronius hyodon* *Eremotherium laurillardi*	ME		
	Chinautla	1227	*Equus* sp. *Euceratherium* sp. *Mammuthus columbi*	MUSHNAT	12,340 ± 50	This paper
Zacapa	Teculután	189	*Glyptotherium* sp. *Mammuthus columbi*	MUSHNAT		
	Río Motagua Teculután	196		UV		
	La Estanzuela	189	*Cuvieronius hyodon* *Equus* sp. *Eremotherium laurillardi* *Glyptotherium* sp. *Mammuthus columbi* *Mixotoxodon larensis* *Neocherus* sp.	ME	22,400-9,539	This paper
	Calle del Comercio		*Equus* sp.	ME		
	Barrio la Reforma		*Cuvieronius hyodon*	ME		
Petén	Río la Pasión, Sayaxché	118	*Mammuthus columbi*	ME		Gordon Edmond (Royal Ontario Museum, Canada)
	Santa Amelia, Petén.	128	*Canis* sp. *Cuvieronius hyodon* *Dasypus* sp. *Eremotherium laurillardi* *Glyptotherium* sp. *Palaeolama* sp. *Holmesina* sp. *Odocoileus* sp. *Megalonyx* sp. *Mixotoxodon larensis* *Neocherus* sp. *Paramylodon* sp. Pecary *Tapirus* sp.	AMNH		
El Progreso	Paso Calandrias		*Glyptotherium* sp.	MUSHNAT		
Chiquimula	El Rosario, Ipala	1012	*Cuvieronius hyodon* *Eremotherium laurillardi* *Glyptotherium* sp. *Mixotoxodon larensis*	MUSHNAT		
Izabal	Carboneras	112	*Rhynchotherium*	Museum Carlos F. Novella	15,700–12,920	Lucas and Alvarado (1995).
Huehuetenango	Chivacabé	1899	*Cuvieronius hyodon* *Equus* sp. *Glyptotherium* sp. *Odocoileus virginianus*	IDAHE		This paper
Santa Rosa	Santa Cruz Barillas		*Cuvieronius hyodon*	CCSC	26,800 ± 150	This paper
	San Rafaelito		*Cuvieronius hyodon* *Eremotherium laurillardi*	COCODE	27,100–25.590	This paper

Table 7 (continued)

Department	Locality	Altitude [msl]	Taxa	Collection	Age/uncal yrs BP	Reference
			Glyptotherium sp.			
			Mixotoxodon larensis			
			Odocoileus virginianus			
Jutiapa	Oratorio	1038	Cuvieronius hyodon	MUSHNAT		
	Río Ostúa	1085	Equus sp.	MUSHNAT		
	Las Lajas, Ixtepeque, Asunción Mita		Cuvieronius hyodon	MUSHNAT		
	Los Timos, Río Ostúa		Cuvieronius hyodon	MUSHNAT		
Quiché	Hidroelectrica Chixoy	325—809	Glyptotherium sp.	MUSHNAT		
Baja Verapaz	Salamá	947	Eremotherium laurillardi	MNH		
Quetzaltenango	Cerro del Baul	2289	Glyptotherium sp.	MUSHNAT	13,800-9,941	This paper

date, this record is confined to the Pleistocene bear *Tremarctos* from Belize, the saber-tooth cat *Smilodon*, from El Salvador (Morgan, 2008), and now two *Canis* teeth from the Petén area in northern Guatemala.

The complete absence of small-sized faunal elements (e.g. rodents etc.), on the other hand, may be attributed to collection bias and preferred collection of large bones (Webb and Perrigo, 1984), which are easily identified in the field by laymen.

4.3. Climate and environmental conditions in Guatemala inferred from megafaunal evidence

In the Guatemala sites and elsewhere in the region, *Cuvieronius* is usually associated with the giant ground sloth *Eremotherium*, thus suggesting similar habitat preferences. *Cuvieronius* sp. has been interpreted as a mixed C_3—C_4 plant-feeder based on isotope analyses (Sánchez et al., 2004). Ecological interpretation for *Eremotherium* sp. is not conclusive: Some authors have interpreted the taxon as a grazer (Dantas et al., 2013), others as a browser (Cartelle and De Iuliis, 1995) and still other as an opportunistic C3/C4 mix-feeder (Dantas et al., 2017; Larmon et al., 2019). In the Guatemala sites, *Eremotherium* co-occurs with *Mixotoxodon* and *Cuvieronius* along low-lying river systems with oak-tree dominated vegetation. This is particularly striking for localities along the Motagua-Polochic lateral fault-zone (Fig. 1) which forms a low-level East-West trending morphological depression across central Guatemala and includes the localities of Estanzuela, Ciudad Real and San Rafaelito.

Several authors have postulated cold and dry climatic conditions for the Late Pleistocene in the area, especially for the LGM (Leyden et al., 1993; Metcalfe et al., 2000; Larmon et al., 2019). However, a re-interpretation of the data and new pollen and ^{14}C data from Petén Itzá, have shown that the previous research was only based on a single ^{14}C date which was stratigraphically misplaced (Hodell et al., 2008; Bush et al., 2009).

Our data support the interpretation of Hodell et al. (2008) and Bush et al. (2009), suggesting that the area was likely rich in water during Marine Isotope Stage 3 (Peterson et al., 2000; Pearson, 2005) and during the LGM (MIS 2; 25,000 to 19,000 cal BP; Bush et al., 2009). During these periods large river-systems and open forests dominated by oak trees are evidenced for wide areas in Guatemala (Pearson, 2005; Hodell et al., 2008; Bush et al., 2009).

Evidence for a widespread forest cover comes from imprints of *Quercus* leaves and mineralized wood, suggesting open forest vegetation at Chaqué in Huehuetenango, Chiquimula, Guatemala, San Rafaelito in Santa Rosa and in the Sierra de las Minas in Zacapa (Fig. 8). The *Quercus*-dominated forest from Huehuetenango was likely buried *in situ* during the Late Pleistocene eruption of the Los Chocoyos volcano (Bush et al., 2009), but this needs to be verified. An increase in *Quercus* pollen was also documented during the LGM (23,000 to 19,000 cal BP) in Péten (Hodell et al., 2008; Bush et al., 2009). Open gallery forests would have been the preferred habitat conditions for *Cuvieronius*, *Glyptotherium*, *Neocherus*, *Mixotoxodon* (MacFadden, 2005; Rincón, 2011; Lundelius et al., 2013) and especially the giant browser *Eremotherium*.

Glyptotherium is known to have preferred lake and stream environments with abundant water supply (Gillette and Ray, 1981; McDonald, 2005). Higher temperatures and the presence of river-systems are also endorsed by the presence of turtles at Río la Pasion, Petén. The presence of *Mazama* sp. and *Odocoileus* sp. in some Guatemalan sites also supports open forest conditions. The most northeastern distributions of *Cuvieronius* and *Glyptotherium* reach to Chivacabé near Huehuetenango, which is about 1,500 m above sea-level, while the Sierra de Altos Cuchumantanes
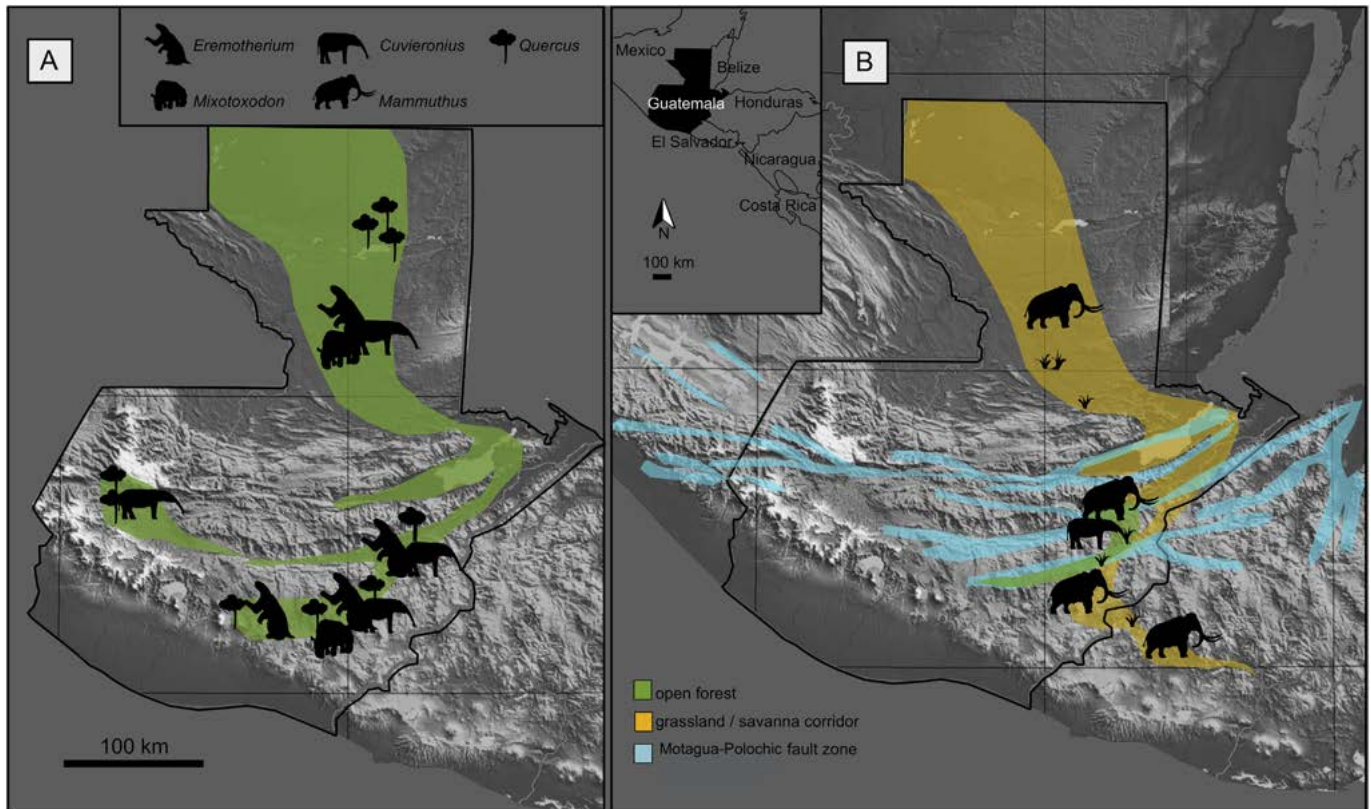
Fig. 8. Interpretative ecological scenario based on the presence of widespread *Quercus* (oak) dominated vegetation tentatively dated to 23,000 to 19,000 cal BP (Bush et al., 2009) and thus MIS 3 and LGM (Peterson et al., 2000). We suggest that *Eremotherium*, *Mixotoxodon* and *Cuvieronius* populated these open forests (A, in green). In Guatemala, *Mammuthus* does not co-occur with *Eremotherium* and *Mixotoxodon* (B) and must therefore represent a different stadial interval with low precipitation and savanna-dominated landscapes, e.g. to post-LGM deglaciation periods (in yellow). Note that *Mammuthus* is limited to a northwest-southeast directed lowland corridor on the east-side of Guatemala and has never been reported in the highland area of central and western Guatemala.

(elevations of >4000 m) at only a few km north of Chivacabé likely formed a geographical barrier.

Pleistocene *Equus* is surprisingly rare in the fossil assemblages of Guatemala. According to mesowear analysis on these Pleistocene fossil horses, their feeding habits may have differed from those of the modern *Equus caballus* in presenting a much wider range of dietary variability (Marín-Leyva et al., 2016). Instead of grazing on silica-rich hard grasses only, they were C_3 to C_4 mix-feeders and therefore substantially more flexible regarding their food than previously expected (Marín-Leyva et al., 2016). This opportunistic feeding behavior may help to explain the wide distribution of *Equus* across Central America, with occurrences in Honduras, El Salvador, Nicaragua, Costa Rica, Panama (Webb and Perrigo, 1984; Lucas and Alvarado, 1991; Lucas et al., 1997; Lucas, 2008b), but it is difficult to understand why horses are only present in a quarter of all Guatemalan sites.

Mixotoxodon larensis has also been interpreted as a C_3 to C_4 mix-feeder (MacFadden, 2005), based on carbon isotope analysis from Panama. Rincón (2011) suggested that the species inhabited woodland, instead of savannas as previously suggested (MacFadden, 2005; Rincón, 2011). This interpretation is also supported by the radiocarbon age of a *Mixotoxodon* specimen from Ciudad Real (27,850 ± 120 BP; 32,368 ± 277 cal BP), indicating co-existence with the giant browser *Eremotherium* in several localities in Guatemala (Table 1). Fossils housed at the La Estanzuela museum (e.g. *Mixotoxodon*, *Glyptotherium*, *Cuvieronius*) range between MIS 3 to 2 (LGM) and indicate wet, open forest conditions. This interpretation is supported by oak (*Quercus*) macrofossils associated with *Mixotoxodon* at San Rafaelito, southern Guatemala

and previously in Texas (Lundelius et al., 2013).

The presence of a specialized forest browser such as *Palaeolama* (Yann et al., 2016) also supports this interpretation. Thurmond reported a camelid, probably *Hemiauchenia*, from Ciudad Real (Woodburne, 1969), but this cannot be confirmed here. However, *Hemiauchenia* has long been regarded as indicative of xeric environments, but recent research suggests that *Hemiauchenia* was rather an opportunistic mix-feeder (Yann et al., 2016). In Central America, *Palaeolama* and *Hemiauchenia* have been reported from El Salvador and Costa Rica.

Our review of the Late Pleistocene megafauna of Guatemala thus shows a dominance of opportunistic mix-feeders and browsers (e.g., *Cuvieronius*, *Eremotherium*, *Equus*, *Palaeolama*, *Mixotoxodon*, *Neocherus*), animals which populated open gallery forests with wide river-systems.

Mammuthus, on the other hand, is regarded to be a grassland-specialized taxon (Pérez-Crespo et al., 2015) that does not fit the above scenario of a forest-covered Guatemala, although some individuals were apparently able to digest C_3 plants (Pérez-Crespo et al., 2012). *Mammuthus* bones have rarely been found associated with the above taxa, e.g. a *Mammuthus* at Chinautla was likely associated with *Euceratherium*. A different age range is therefore interpreted for the *Mammuthus* bones from Guatemala, as well as different environmental conditions (i.e. grassland; see Fig. 8). Even though there is only a single radiocarbon date for *Mammuthus* (from Chinautla) dating to the post-LGM to Younger Dryas stadial (12,340 ± 50 BP; 14,514 ± 339 cal BP), we here suggest that a southern migration of *Mammuthus* into Central America was confined to dry periods (Fig. 8) after the LGM and depended on the

expansion of grassland during these intervals (McDonald and Dávila, 2017). The *Mammuthus* record is generally rare in Central America and based on isolated findings that are not part of a larger faunal assemblage (McDonald and Dávila, 2017). In Guatemala, *Mammuthus* has been found only in the Sayaxché department along Río de la Pasión in the northwestern Petén region and, more abundant, at La Estanzuela along the Motagua-Polochic fault-zone and thus in low-lying regions with abundant water (Table 7; Fig. 8).

The data from Péten suggest dry climatic conditions during the deglaciation period of 18,000 to 11,000 cal BP (Hodell et al., 2008; Bush et al., 2009), which fits the radiocarbon dating of *Mammuthus* from Chinautla (Table 1). The Late Pleistocene age of 12.340 ± 50 uncal BP ($14,514 \pm 339$ cal BP) for the *Mammuthus* from Chinautla (USAC 1075), suggests expansion of grasslands during late deglaciation period through the Younger Dryas epoch, leading to a co-existence of this large proboscidean with *Cuvieronius and Glyptotherium*. Association of *Mammuthus* with *Equus* and *Euceratherium* endorses the interpretation of an expansion of grassland (McDonald and Dávila, 2017). The southern migration of *Mammuthus* may therefore have occurred during drier periods before or after MIS 3 and 2.

Last appearance data from around the Pleistocene-Holocene transition have been reported for *M. columbi* in Mexico (Gonzalez et al., 2014). However, this ^{14}C data compilation suggests that latest Pleistocene refugial areas of small *Mammuthus* populations were located in central Mexico and the Great Lakes in North America (Domingo et al., 2012). The random findings of *Mammuthus* along the Central American corridor (McDonald and Dávila, 2017) may represent small groups of these animals moving south during stadial periods (Fig. 8), since increased precipitation around the Pleistocene-Holocene boundary would have been unfavorable for these animals (Bush et al., 2009).

5. Conclusions

Central America played a crucial role in the distribution of megafauna during the Great American Biotic Interchange (GABI) and since that event. Guatemala is a key area along this Meso-american Corridor which acted as a paleobiogeographic bridge and filter between North- and South America during both the Pliocene and Pleistocene. The present revision of Late Pleistocene fossil assemblages of Guatemala thus adds to the knowledge of faunal distribution in this poorly known region. The most fossiliferous localities in Guatemala, Chivacabé, Estanzuela, Ciudad Real and San Rafaelito, are all associated with reworked volcanic sediments (lahars) and thus provide evidence for high volcanic activity in the Late Pleistocene and Early Holocene.

The Late Pleistocene fossil assemblages of Guatemala mostly consist of random findings of large herbivores, comparable to other fossil sites along the Mesoamerican Corridor. Although many of the fossils have not been dated, due to significant mineralization of the bones and the lack of stratigraphic context, an assignation of most localities to the Middle to Late Pleistocene (Rancholabrean) epoch is tentatively suggested by the faunal assemblages documented here. These are dominated by *Cuvieronius hyodon* and *Eremotherium laurillardi*, while *Glyptotherium* sp. is frequent and other taxa are surprisingly rare. For instance, *Equus* is underrepresented in the faunal assemblages, and *Mammuthus* remains have only been found as isolated fragments along the Motagua-Polochic fault-zone. *Bison*, cats and bears are totally absent to date, as are small faunal elements, although the latter is likely due to collection bias. In consequence, the faunal assemblages mainly consist of large herbivores, principally mesic-adapted browsers, e.g. *Cuvieronius* and *Eremotherium*. Their distribution within Central America is likely a

result of adaptation to semitropical to tropical conditions and forested areas with abundant precipitation. These animals are characteristically absent in Late Pleistocene sites in the arid southwest of North America. The presence of oak forests and *Eremotherium*, *Cuvieronius* and *Mixotoxodon* dating to the MIS 3 and 2, supports this scenario, as also the presence of *Glyptotherium* sp. which is well-known to have lived along water courses in moist, lowland tropical to subtropical habitats. The ages and finding localities of *Glyptotherium* sp. in Guatemala, however, reveal that this genus was highly adaptable and even reached high altitudes. *Mammuthus* findings from Guatemala, on the other side, appear to be stratigraphically unrelated to the above faunal assemblage. As *Mammuthus* is well known to be specialized to *Artemisia*-dominated grassland vegetation, a different stratigraphic interval, before or after MIS 3 and 2, is here suggested for the southward expansion of these large-sized grazers.

The survival of some megafaunal taxa beyond the Pleistocene-Holocene boundary has so far only been discussed for South America. Radiocarbon dates of *Cuvieronius hyodon* presented here for La Estanzuela in southern Guatemala, now suggest survival into the Early Holocene of these large gomphotheres in Central America. Our ^{14}C ages therefore suggest that survival of megafauna depended on refugial areas with suitable conditions. An Early Holocene co-existence in Guatemala of humans and megafauna therefore appears possible.

Appendix A. Supplementary data

Supplementary data to this article can be found online at https://doi.org/10.1016/j.quascirev.2019.07.011.

References

Aeschbach, M., Carrillo, J.D., Sánchez-Villagra, M.R., 2016. On the growth of the largest living rodent: postnatal skull and dental shape changes in capybara species (*Hydrochoerus* spp.). Mamm. Biol. 81, 558–570.

Aguilar, D.H., Laurito, C.A., 2009. El armadillo gigante (Mammalia, Xenarthra, Pampatheriidae) del río Tomayate, Blancoano Tardío - irvingtoniano Temprano, El Salvador, América Central. Rev. Geol. Am. Cent. 41, 25–36.

Alberdi, M.T., Corona, M.,E., 2005. Revisión de los gonfoterios en el Cenozoico tardío de México. Rev. Mex. Ciencias Geol. 22, 246–260.

Breyer, J.A., 1983. The biostratigraphic utility of camel metapodials. J. Paleontol. 57, 302–307.

Bronk Ramsey, C., 2013. OxCal 4.2. Man. https://c14.arch.ox.ac.uk/oxcalhelp/hlp_contents.html. (Accessed 27 March 2013).

Bush, M.B., Correa-Metrio, A., Hodell, D.A., Brenner, M., Anselmetti, F.S., Ariztegui, D., Mueller, A.D., Curtis, J.H., Grzesik, D.A., Burton, C., Gilli, A., 2009. Re-evaluation of climate change in lowland Central America during the Last Glacial Maximum using new sediment cores from Lake Petén Itzá, Guatemala. In: Vimeux, F., Sylvestre, F., Khodri, M. (Eds.), Past Climate Variability in South

America and Surrounding Regions. Springer, Dordrecht, pp. 113—128.

Cano, E.B., Schuster, J.C., 1993. Fosiles Pleistocenicos De Chivacabe, Huehuetenango, Guatemala: Expedicion UVG-1993, vol. 5. Rev. la Univ. del Val. Guatemala, pp. 11—14.

Carbot-Chanona, G., 2010. The first record of *Dasypus* (Xenarthra: Cingulata: Dasypodidae) in the late Pleistocene of Mexico. Curr. Res. Pleistocene 27, 164—166.

Carlini, A.A., Zurita, A.E., Aguilera, O.A., 2008. North American glyptodontines (Xenartha, Mammalia) in the upper Pleistocene of northern South America. Paläontol. Z. 82, 125—138.

Carranza-Castañeda, Ó., Miller, W.E., 1995. Development of vertebrate paleontology at the state University of Hidalgo, Mexico. J. Vertebr. Paleontol. 15, 530.

Cartelle, C., De Iuliis, G., 1995. *Eremotherium laurillardi*: the Panamerican late Pleistocene megatheriid sloth. J. Vertebr. Paleontol. 15, 830—841.

Chatters, J.C., Kennett, D.J., Asmerom, Y., Kemp, B.M., Polyak, V., Blank, A.N., Beddows, P.A., Reinhardt, E., Arroyo-Cabrales, J., Bolnick, D.A., Malhi, R.S., Culleton, B.J., Erreguerena, P.L., Rissolo, D., Morell-Hart, S., Stafford, T.W., 2014. Late Pleistocene human skeleton and mtDNA link Paleoamericans and modern Native Americans. Science 344 (80), 750—754.

Cherkinsky, A., 2009. Can we get a good radiocarbon age from "bad bone"? Determining the reliability of radiocarbon age from bioapatite. Radiocarbon 51 (2), 647—655.

Cisneros, J.C., 2005. New Pleistocene vertebrate fauna from El Salvador. Rev. Bras. Palaontol. 8, 239—255.

Dantas, M.A.T., Cherkinsky, A., Bocherens, H., Drefahl, M., Bernardes, C., França, L. de M., 2017. Isotopic paleoecology of the Pleistocene megamammals from the Brazilian Intertropical Region: feeding ecology (δ 13C), niche breadth and overlap. Quat. Sci. Rev. 170, 152—163.

Dantas, M.A.T., Dutra, R.P., Cherkinsky, A., Fortier, D.C., Kamino, L.H.Y., Cozzuol, M.A., Ribeiro, A. de S., Vieira, F.S., 2013. Paleoecology and radiocarbon dating of the Pleistocene megafauna of the Brazilian intertropical region. Quat. Res. 79, 61—65.

De Iuliis, G., Cartelle, C., 1999. A new giant megatheriine ground sloth (Mammalia: Xenarthra: Megatheriidae) from the late Blancan to early Irvingtonian of Florida. Zool. J. Linn. Soc. 127, 495—515.

De Iuliis, G., McDonald, H.G., Stanchly, N., Spenard, J., Powis, T.G., 2015. *Nothrotheriops shastensis* (Sinclair) from Actun Lak: first record of Nothrotheriidae (Mammalia, Xenarthra, pilosa) from Belize. Ameghiniana 52, 153—171.

Domingo, L., Prado, J.L., Alberdi, M.T., 2012. The effect of paleoecology and paleobiogeography on stable isotopes of Quaternary mammals from South America. Quat. Sci. Rev. 55, 103—113.

Downing, K., White, R., 1995. The cingulates (Xenarthra) of Leisey shell pit local fauna (irvingtonian), Hillborough county, Florida. Bull. Florida Museum Nat. Hist. 37, 375—396.

Ferretti, M.P., 2008. Enamel structure of *Cuvieronius hyodon* (proboscidea, gomphotheriidae) with a discussion on enamel evolution in elephantoids. J. Mamm. Evol. 15, 37—58.

García García, V., Ericastilla Gody, S., 1995. Descubrimientos paleontológicos en Rosario-ipala, Chiquimula, Oriente de Guatemala. In: Laporte, J.P., Escobedo, H. (Eds.), VIII Simposio de Investigaciones Arqueolóicas en Guatemala. Museo Nacional de Arqueología y Etnología, Guatemala, pp. 113—128.

Gaudin, T.J., Lyon, L.M., 2017. Cranial osteology of the pampathere Holmesina floridanus (Xenarthra: Cingulata; Blancan NALMA), including a description of an isolated petrosal bone. PeerJ, e4022.

Gazin, C.L., 1956. Exploration for the mains of giant ground sloths in Panama. Smithson. Inst. Annu. Rep. 4772, 344—354.

Gillette, D.D., Carranza-Castañeda, Ó., White, R.S., Morgan, G.S., Thrasher, L.C., McCord, R., McCullough, G., 2016. Ontogeny and sexual dimorphism of *Glyptotherium texanum* (Xenarthra, Cingulata) from the Pliocene and Pleistocene (blancan and irvingtonian NALMA) of Arizona, New Mexico, and Mexico. J. Mamm. Evol. 23, 133—154.

Gillette, D.D., Ray, C.E., 1981. Glyptodonts of North America, Smithsonian Contributions to Paleobiology. Smithsonian Institution Press, Washington D. C.

González González, A.H., Rojas Sandoval, C., Terrazas Mata, A., Benavente Sanvicente, M., Stinnesbeck, W., Aviles Olguín, J., De los Ríos, M., Acevez Nuñez, E., 2008. The arrival of humans on the Yucatan Peninsula: evidence from submerged Caves in the state of Quintana Roo, Mexico. Curr. Res. Pleistocene 25, 1—24.

González González, A.H., Terrazas Mata, A., Stinnesbeck, W., Benavente, M., Avilés Olguín, J., Rojas Sandoval, C., Padilla, J.M., Velázquez Morlet, A., Acevez Nuñez, E., Frey, E., González González, A.H., Terrazas, A., Stinnesbeck, W., Benavente, M.E., Avíles, J., Padilla, J.M., Velásquez, A., Aceves, E., Frey, E., 2013. The first human settlers on the Yucatan Peninsula: evidence from drowned Caves in the state of Quintana Roo (south Mexico). In: Graf, K.E., Ketron, C.V., Waters, M. (Eds.), Paleoamerican Odyssey. Texas A&M University, pp. 323—337.

Gonzalez, S., Huddart, D., Israde-Alcántara, I., Dominguez-Vazquez, G., Bischoff, J., 2014. Tocuila mammoths, basin of Mexico: late pleistocene-early Holocene stratigraphy and the geological context of the bone accumulation. Quat. Sci. Rev. 96, 222—239.

Gruhn, R., Bryan, A.L., Nance, J.D., 1977. Los Tapiales: a paleo-Indian campsite in the Guatemalan highlands. Proc. Am. Philos. Soc. 121, 235—273.

Guiomar Vucetich, M., Deschamps, C.M., Encarnación Pérez, M., 2015. The first capybaras (Rodentia, Caviidae, Hydrochoerinae) involved in the Great American biotic interchange. Ameghiniana 52, 324—333.

Hodell, D.A., Anselmetti, F.S., Ariztegui, D., Brenner, M., Curtis, J.H., Gilli, A.,

Grzesik, D.A., Guilderson, T.J., Müller, A.D., Bush, M.B., Correa-Metrio, A., Escobar, J., Kutterolf, S., 2008. An 85-ka record of climate change in lowland Central America. Quat. Sci. Rev. 27, 1152—1165.

Ibarra, J., 1980. Paleontología en Guatemala. José de Pineda Ibarra, Guatemala City.

Koch, P.L., Tuross, N., Fogel, M.L., 1997. The effects of sample treatment and diagenesis on the isotopic integrity of carbonate in biogenic Hydroxylapatite. J. Archaeol. Sci. 24, 417—429.

Kropf, M., Mead, J.I., Scott Anderson, R., 2007. Dung, diet, and the paleoenvironment of the extinct shrub-ox (*Euceratherium collinum*) on the Colorado Plateau, USA. Quat. Res. 67, 143—151.

Kurten, B., Anderson, E., 1980. Pleistocene Mammals of North America, 1st Edition. Cambridge University Press.

Larmon, J.T., McDonald, H.G., Ambrose, S., DeSantis, L.R.G., Lucero, L.J., 2019. A year in the life of a giant ground sloth during the Last Glacial Maximum in Belize. Sci. Adv. 5, eaau1200.

Laurito, C.A., 1993. Análisis topológico y sistemático del Toxodonte de Bajo de los Barrantes, provincia de Alajuela, Costa Rica. Rev. Geol. Am. Cent. 16, 61—68.

Leidy, J., 1886. *Toxodon* and other remains from Nicaragua: Acad. Proc. Acad. Nat. Sci. Phila. 275—276.

Leyden, B.W., Brenner, M., Hodell, D.A., Curtis, J.H., 1993. Late Pleistocene climate in the central American lowlands. Geophys. Monogr. 78, 165—178.

Lindauer, S., Santos, G.M., Steinhof, A., Yousif, E., Phillips, C., Jasim, S.A., Uerpmann, H.-P., Hinderer, M., 2017. The local marine reservoir effect at Kalba (UAE) between the Neolithic and Bronze Age: an indicator of sea level and climate changes. Quat. Geochronol. 42, 105—116.

Lohse, J.C., Paiz, L., 2010. Final Project Report: Exploring for Clovis Adaptations in Highland Mesoamerica. Washington D. C.

Lucas, S.G., 2014a. Paleontología de vertebrados en América Central: 30 años de progreso. Rev. Geol. Am. Cent. 139—155. https://doi.org/10.15517/rgac.v0i0.16576.

Lucas, S.G., 2014b. Late Pleistocene mammals from el Hatillo, Panama. Rev. Geol. Am. Cent. 50, 139—151.

Lucas, S.G., 2008a. Late Cenozoic fossil mammals from the Chapala rift basin, Jalisco, Mexico. Neogene Mamm. New Mex. USA 39—49.

Lucas, S.G., 2008b. Pleistocene mammals from Yeroconte, Honduras. New Mex. Museum Nat. Hist. Sci. Bull. 44, 403—408.

Lucas, S.G., Alvarado, G.E., 2016. Vertebrate palaeontology in Central America: a narrative and analytical history. In: Mayer, W., Clary, R.M., Azuela, L.F., Mota, T.S., Wołkowicz, S. (Eds.), History Of Geoscience: Celebrating 50 Years of INHIGEO. Geological Society, London, pp. 155—169.

Lucas, S.G., Alvarado, G.E., 2010. Fossil proboscidea from the upper Cenozoic of Central America: taxonomy, evolutionary and paleobiogeographic significance. Rev. Geol. Am. Cent. 42, 9—42.

Lucas, S.G., Alvarado, G.E., 1995. El proboscideo *Rhynchotherium blicki* (Mioceno Tardio) del Oriente de Guatemala. Rev. Geol. Am. Cent. 18.

Lucas, S.G., Alvarado, G.E., Vega, E., 1997. The Pleistocene mammals of Costa Rica. J. Vertebr. Paleontol. 17, 413—427.

Lucas, S.G., Alvarado, G.I., 1991. El Hallazgo mas austral de un *Mammut americanum*, el caso del mastodonte de San Pedro Sula, Honduras. Rev. Geol. Am. Cent. 13.

Lucas, S.G., Morgan, G.S., Estep, J.W., Mack, G.H., Hawley, J.W., 1999. Co-occurrence of the proboscideans *Cuvieronius, stegomastodon*, and *Mammuthus* in the lower Pleistocene of southern New Mexico. J. Vertebr. Paleontol. 19, 595—597.

Lundelius, E.L., Bryant, V.M., Mandel, R., Thies, K.J., Thoms, A., 2013. The first occurrence of a *toxodont* (Mammalia , Notoungulata) in the United States. J. Vertebr. Paleontol. 33, 229—232.

MacFadden, B.J., 2005. Diet and habitat of toxodont megaherbivores (Mammalia, Notoungulata) from the late quaternary of South and Central America. Quat. Res. 64, 113—124.

Marín-Leyva, A.H., DeMiguel, D., García-Zepeda, M.L., Ponce-Saavedra, J., Arroyo-Cabrales, J., Schaaf, P., Alberdi, M.T., 2016. Dietary adaptability of late Pleistocene *Equus* from west Central Mexico. Palaeogeogr. Palaeoclimatol. Palaeoecol. 441, 748—757.

Mayorga, R., Cáceres, A., Toriello, C., Gutiérrez, G., Alvarez, O., Ramírez, M.E., Mariat, F., 1979. Investigación de Una zona Endémica de esporotricosis en La region de La Laguna de Ayarza, Guatemala. Bol. Sanit. Panam. 87, 20—34.

McAfee, R.K., 2009. Reassessment of the cranial characters of *Glossotherium* and *Paramylodon* (Mammalia: Xenarthra: Mylodontidae). Zool. J. Linn. Soc. 155, 885—903.

McAfee, R.K., 2007. Reassessing the Taxonomy and Affinities of the Mylodontinae Sloths, *Glossotherium* and *Paramylodon* (Mammalia: Xenarthra: Tardigrada). Northern Illinois University.

McDonald, H.G., 2006. Sexual dimorphism in the skull of Harlan's ground sloth. Contrib. Sci. Nat. Hist. Museum Los Angeles City 510, 1—9.

McDonald, H.G., 2005. Paleoecology of extinct xenarthrans and the Great American biotic interchange. Bull. Florida Museum Nat. Hist. 45, 313—333.

McDonald, H.G., 2002. Fossil Xenarthra of Mexico: a review. In: Avances En Los Estudios Paleomastozoológicos: México. Instituto Nacional de Antropología e Historia, DF, pp. 227—248.

McDonald, H.G., Chatters, J.C., Gaudin, T.J., 2017. A new genus of megalonychid ground sloth (Mammalia, Xenarthra) from the late Pleistocene of Quintana Roo, Mexico. J. Vertebr. Paleontol. 37.

McDonald, H.G., Dávila, S.L., 2017. Mammoths in Central America: new records from Guatemala. Quat. Int. 443, 122—128.

Mead, J.I., Baez, A., Swift, S.L., Lohse, J., Paiz, L., 2012. Late Pleistocene mammals from Chivacabé, Huehuetenango, Guatemala. Rev. Mex. Ciencias Geol. 29, 319—329.

Menegaz, A.N., Ortiz Jaureguizar, E., 1995. Los Artiodtiloács. In: Alberdi, M.T., Leone, G., Tonni, E.P. (Eds.), Evolución climática y biolgicóa de la region Pampeana durante los últimos cinco milliones de anos.Un ensayo de correlaci óncon el Mediterrnáneo occidental, 12. Museo Nacional de Ciencias Naturales, Monografías, pp. 311—337.

Metcalfe, S.E., O'Hara, S.L., Caballero, M., Davies, S.J., 2000. Records of Late Pleistocene-Holocene climatic change in Mexico - a review. Quat. Sci. Rev. 19, 699—721.

Mones, A., 1984. Estudios sobre la familia Hydrochoeridae, XIV. Revision sistemática (Mammalia: Rodentia). Senckenberg. Biol. 65, 1—17.

Moreira, J.R., Ferraz, K.M.P.M.B., Herrera, E.A., Macdonald, D.W., 2012. Capybara: biology, use and conservation of an exceptional neotropical species. Capybara Biol. Use Conserv. Except. Neotrop. Species 1—419.

Morgan, G.S., 2008. Vertebrate fauna and geochronology of the Great American biotic interchange in Northamerica. Neogene Mamm. Bull. 44, 93.

Morgan, G.S., Harris, A.H., 2015. Pliocene and Pleistocene vertebrates of New Mexico. In: Lucas, S.G., Sullivan, R.M. (Eds.), Vertebrate Paleontology in New Mexico. New Mexico Museum of Natural History and Science, Albuquerque, pp. 233—428.

Mothé, D., Avilla, L., 2015. Mythbusting evolutionary issues on south American gomphotheriidae (Mammalia: proboscidea). Quat. Sci. Rev. 110, 23—35.

Mothé, D., Avilla, L.S., Cozzuol, M.A., 2013. the South American gomphotheres (Mammalia, proboscidea, gomphotheriidae): taxonomy, phylogeny, and biogeography. J. Mamm. Evol. 20, 23—32.

Oliveira, É.V., Porpino, K.O., Barreto, A.F., 2010. On the presence of *Glyptotherium* in the late Pleistocene of northeastern Brazil, and the status of *Glyptodon* and *Chlamydotherium*. Paleobiogeographic implications. Neues Jahrb. Geol. Palaontol. Abh. 258, 353—363.

Osborn, H.F., 1923. New subfamily, generic, and specific stages in the evolution of the Proboscidea. Am. Mus. Novit. 99, 1—4.

Page, W.D., 1978. The geology of el Bosque archaeological site, Nicaragua. In: Bryan, A.L. (Ed.), Early Man in America from a Circum-PacificPerspective. University of Alberta, Alberta, pp. 231—260.

Pearson, G.A., 2005. Late Pleistocene megafaunal deposits on the isthmus of Panama and their paleoenvironmental implications. Caribb. J. Sci. 41, 1—13.

Pérez-Crespo, V.A., Arroyo-Cabrales, J., Benammi, M., Johnson, E., Polaco, O.J., Santos-Moreno, A., Morales-Puente, P., Cienfuegos-Alvarado, E., 2012. Geographic variation of diet and habitat of the Mexican populations of Columbian Mammoth (*Mammuthus columbi*). Quat. Int. 276—277, 8—16.

Pérez-Crespo, V.A., Carbot-Chanona, G., Morales-Puente, P., Cienfuegos-Alvarado, E., Otero, F.J., 2015. Paleoambiente de la Depresión Central de Chiapas, con base en isótopos estables de carbono y oxígeno. Rev. Mex. Ciencias Geol. 32, 273—282.

Perini, F.A., Oliveira, J.A., Salles, L.O., Moraes Neto, C.R., Guedes, P.G., Oliveira, L.F.B., Weksler, M., 2011. New fossil records of *Tapirus* (Mammalia, Perissodactyla) from Brazil, with a critical analysis of intra-generic diversity assessments based on lower molar size variability. Geobios 44, 609—619.

Peterson, L.C., Haug, G.H., Hughen, K.A., Röhl, U., 2000. Rapid changes in the Hydrologic Cycle of the tropical Atlantic during the last glacial. Science 290 (80), 1947—1952.

Pocock, R.I., 1933. Homologies between the branches of the antlers of the Cervidae based on the theory of dichotomous growth. Proc. Zool. Soc. Lond. 377—406.

Polaco, O.J., Guzmán, A.F., Tapia, R.G., 2004. Occurrence of toxodonts in the Pleistocene of México. Curr. Res. Pleistocene 21, 113—114.

Prado, J.L., Alberdi, M.T., Azanza, B., Sánchez, B., Frassinetti, D., 2005. The Pleistocene gomphotheriidae (proboscidea) from south America. Quat. Geochronol. 21—30.

Prado, J.L., Alberdi, M.T., Sánchez, B., Azanza, B., 2003. Diversity of the Pleistocene gomphotheres (gomphotheriidae, proboscidea) from south America. Adv. Mammoth Res. 1—18.

Pujos, F., Salas, R., 2004. A systematic reassessment and paleogeographic review of fossil Xenarthra from Peru. Bull. l'Institut français d'études Andin. 33, 331—377.

Ramírez-Cruz, G.A., Montellano-Ballesteros, M., 2014. Two new glyptodont records (Mammalia: Cingulata) from the late Pleistocene of Tamaulipas and Tlaxcala, Mexico: implications for the taxonomy of the genus *Glyptotherium*. Southwest. Nat. 59, 522—530.

Reimer, P.J., Bard, E., Bayliss, A., Beck, J.W., Blackwell, P.G., Ramsey, C.B., Buck, C.E., Cheng, H., Edwards, R.L., Friedrich, M., Grootes, P.M., Guilderson, T.P., Haflidason, H., Hajdas, I., Hatté, C., Heaton, T.J., Hoffmann, D.L., Hogg, A.G., Hughen, K.A., Kaiser, K.F., Kromer, B., Manning, S.W., Niu, M., Reimer, R.W.,

Richards, D.A., Scott, E.M., Southon, J.R., Staff, R.A., Turney, C.S.M., van der Plicht, J., 2013. IntCal13 and Marine13 radiocarbon age calibration curves 0—50,000 Years cal BP. Radiocarbon 55, 1869—1887.

Rincón, A.D., 2011. New remains of *Mixotoxodon larensis* van Frank 1957 (Mammalia: Notoungulata) from Mene de Inciarte tar pit, north-western Venezuela. Interciencia 36, 894—899.

Rincón, A.D., White, R., 2007. Los Xenarthra Cingulata del Pleistoceno tardío (Lujanense) de Cerro Misión, Estado de Falcón, Venezuela. Bol. la Soc. Venez. Espeleol. 41, 2—12.

Rincón, A.D., White, R., McDonald, H.G., 2008. Late Pleistocene cingulates (Mammalia: Xenarthra) from Mene de Inciarte tar pits, Sierra de Perijá, western Venezuela. J. Vertebr. Paleontol. 28, 197—207.

Sánchez, B., Prado, J.L., Alberdi, M.T., 2004. Feeding ecology, dispersal, and extinction of South American Pleistocene gomphotheres. Paleobiology 30, 146—161.

Scillato-Yané, G.J., Carlini, A.A., Tonni, E.P., Noriega, J.I., 2005. Paleobiogeography of the late Pleistocene pampatheres of South America. J. South Am. Earth Sci. 20, 131—138.

Simpson, G.G., 1950. History of the fauna of Latin America. Am. Sci. 38, 361—389.

Simpson, G.G., 1929. Pleistocene mammalian fauna of the seminole field, pinellas county, Florida. Bull. Am. Mus. Nat. Hist. 56, 561—599.

Stinnesbeck, S.R., Frey, E., Olguín, J.A., Stinnesbeck, W., Zell, P., Mallison, H., González González, A., Aceves Núñez, E., Velázquez Morlet, A., Terrazas Mata, A., Benavente Sanvicente, M., Hering, F., Rojas Sandoval, C., 2017. *Xibalbaonyx oviceps*, a new megalonychid ground sloth (Folivora, Xenarthra) from the Late Pleistocene of the Yucatán Peninsula, Mexico, and its paleobiogeographic significance. Paläontol. Z. 91, 245—271.

Stinnesbeck, S.R., Frey, E., Stinnesbeck, W., 2018. New insights on the paleogeographic distribution of the Late Pleistocene ground sloth genus *Xibalbaonyx* along the Mesoamerican Corridor. J. South Am. Earth Sci. 85, 108—120.

Stirton, R.A., Gealey, W.K., 1949. Reconnaissance geology and vertebrate paleontology of El Salvador, Central America. Bull. Geol. Soc. Am. 60, 1731—1764.

Thurmond, J.T., 1973. The Ciudad real fauna of Pleistocene mammals from the highlands of Guatemala. Geol. Soc. Am. Abstr. Progr. 5, 445.

Valerio, A.L., Laurito, C.A., 2011. Nuevos hallazgos de Mammalia, Xenarthra (Cingulata) y confirmaciòn del registro de *Pachyarmatherium leiseyi* Downing & White, 1995 en la localidad de Buenos Aires de Palmares, provincia de Alajuela, Costa Rica. Rev. Geol. Am. Cent. 44, 131—139.

van Frank, R., 1957. A fossil collection from northern Venezuela. 1. Toxodontidae (Mammalia, Notoungulata). Am. Mus. Novit. 1850, 1—38.

Webb, S.D., 2006. The Great American biotic Interchange : patterns and processes. Ann. Mo. Bot. Gard. 93, 245—257.

Webb, S.D., 2000. Evolutionary history of new world Cervidae. In: Vrba, E., Schaller, G. (Eds.), Antelopes, Deer, and Relatives. Fossil Record, Behavioral Ecology Systematics, and Conservation. Yale University, pp. 38—64.

Webb, S.D., Perrigo, S., 2018. Late Cenozoic vertebrates from Honduras and El Salvador. J. Vertebr. Paleontol. 4, 237—254.

Webb, S.D., Perrigo, S., 1985. New megalonychid sloths from El Salvador. In: Montgomery, G.G. (Ed.), The Evolution and Ecology of Armadillos, Sloths, and Vermilinguas. Smithsonian Institution Press, Washington & London, pp. 113—120.

Webb, S.D., Perrigo, S.C., 1984. Late Cenozoic vertebrates from Honduras and El Salvador. J. Vertebr. Paleontol. 4, 237—254.

Webb S.D. and Stehli S. Selenodont artiodactyla (Camelidae and Cervidae) from the Leisey Shell Pits, Hillsborough County, Florida. Bulletin of the Florida Museum of Natural History 37, Part 2(19), 621—643.

Woodburne, M.O., 2010. The Great American Biotic Interchange: dispersals, tectonics, climate, sea level and holding pens. J. Mamm. Evol. 17, 245—264.

Woodburne, M.O., 1969. A late Pleistocene occurrence of the Collared peccary, *Dicotyles tajacu*, in Guatemala. Am. Soc. 50, 121—125.

Yann, L.T., DeSantis, L.R.G., Koch, P.L., Ludelius, E.L., 2016. Dietary ecology of Pleistocene camelids: Influences of climate, environment, and sympatric taxa. Palaeogeography, Palaeoclimatology, Palaeoecology 461, 389—400.

Yelacic, D.M., 2010. Proyecto Arqueologico Y Paleontologico Chivacabe: A Geomorphic and Geoarchaeological Investigation of Late Quaternary Environments in Northwesten Highland Guatemala. Texas State University.

Yelacic, D.M., Lohse, J.C., Frederick, C.D., 2018. Sitio Chivacabe, an early paleoindian site in western highland Guatemala. In: Society for American Archaeology. Unpublished Abstract, Albuquerque.
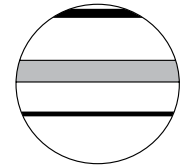
The Muknal cave near Tulum, Mexico: An early-Holocene funeral site on the Yucatán peninsula

Sarah R Stinnesbeck,[1,2] Wolfgang Stinnesbeck,[3]
Alejandro Terrazas Mata,[4] Jerónimo Avilés Olguín,[5]
Martha Benavente Sanvicente,[4] Patrick Zell,[6] Eberhard Frey,[1,2]
Susanne Lindauer,[7] Carmen Rojas Sandoval,[8]
Adriana Velázquez Morlet,[8] Eugenio Acevez Nuñez[5]
and Arturo González González[5]

Abstract

Here, we report on an incomplete human skeleton, soot patches related to anthropogenic fireplaces, and cut marks on the mandible of an extinct peccary, from the submerged Muknal cave southwest of Tulum on the Mexican Yucatán peninsula. The human individual, here named 'Muknal Grandfather', was identified as a male based on cranial parameters. The age at the time of death was estimated to be between 40 and 45 years. We propose that the human bones have been brought to the cave during the latest Pleistocene or early Holocene, but not later than 8600 $_{14}$C yr BP (ca. 9600 cal BP), as a secondary burial of a partial skeleton. The peccary mandible was placed close to the burial site, possibly as part of the same ritual. The Muknal cave therefore served as a place for funeral rituals.

Introduction

Ongoing investigations on the Yucatán peninsula reveal one of the largest assemblages of late Pleistocene to early Holocene human skeletons in the Americas. Nine almost complete (>80%) human skeletons have been identified to date in the submerged caves in the Tulum area of Quintana Roo in southern Mexico (Chatters et al., 2014; González González et al., 2008a, 2013; Stinnesbeck et al., 2017c), some in association with hearths (Hering et al., 2018) and other archeological evidence such as anthropogenic cut marks on Pleistocene mammal bones (González González et al., 2008a, 2008b, 2013).

A diverse faunal assemblage was also discovered, including peccaries (*Muknalia minima*), tapirs (*Tapirus* sp.), camels (*Hemiauchenia* sp.), ground sloths (*Nothrotheriops shastensis, Xibalbaonyx oviceps, Nohochichak xibalbakah*), proboscideans (*Cuvieronius hyodon*), giant armadillos (*Glyptotherium* sp.), and horses (*Equus* sp.) of late Pleistocene and early Holocene ages (e.g. peccaries and tapirs; Chatters et al., 2014; González González et al., 2008b; McDonald et al., 2017; Stinnesbeck et al., 2017a, 2017b, 2017c).

Here, we report on new anthropogenic and paleontological evidence from the cave system located southwest of Tulum. These findings inside the submerged Muknal cave allow for a glimpse into the life and death of the early settlers of the Yucatán peninsula and add new evidence to the importance of the Tulum system of submerged caves as a potential place of ritual importance for these people.

The Karst System in the Tulum area

The Yucatán peninsula is characterized by limestone bedrock with a submerged karst system of >7000 km of caves, of which about 1000 km are currently explored (Bauer-Gottwein et al., 2011; Quintana Roo Speleological Society (QRSS), 2018). During the Late Glacial Maximum (LGM) of the Wisconsin Glacial, from 25,000 to 18,000 BP, sea level was about 120 m below present sea

[1]Geowissenschaftliche Abteilung, Staatliches Museum für Naturkunde Karlsruhe, Germany
[2]Institut für Geographie und Geoökologie, Karlsruher Institut für Technologie (KIT), Germany
[3]Institut für Geowissenschaften, Universität Heidelberg, Germany
[4]Área de Prehistoria y Evolución del Instituto 21 de Investigaciones Antropológicas de la Universidad Nacional Autónoma de México, Investigación Científica, Mexico
[5]Museo del Desierto, Carlos Abedrop Dávila 3745, Nuevo Centro Metropolitano de Saltillo, Mexico
[6]Welterbe Grube Messel gGmbH, Germany
[7]Klaus-Tschira-Laboratory for Radiometric Dating Method, Curt-Engelhorn-Zentrum Archäometrie gGmbH, Germany
[8]Instituto Nacional de Antropología e Historia, Mexico

Corresponding author:
Sarah R Stinnesbeck, Geowissenschaftliche Abteilung, Staatliches Museum für Naturkunde Karlsruhe, Erbprinzenstraße 13, 76133 Karlsruhe, Germany.
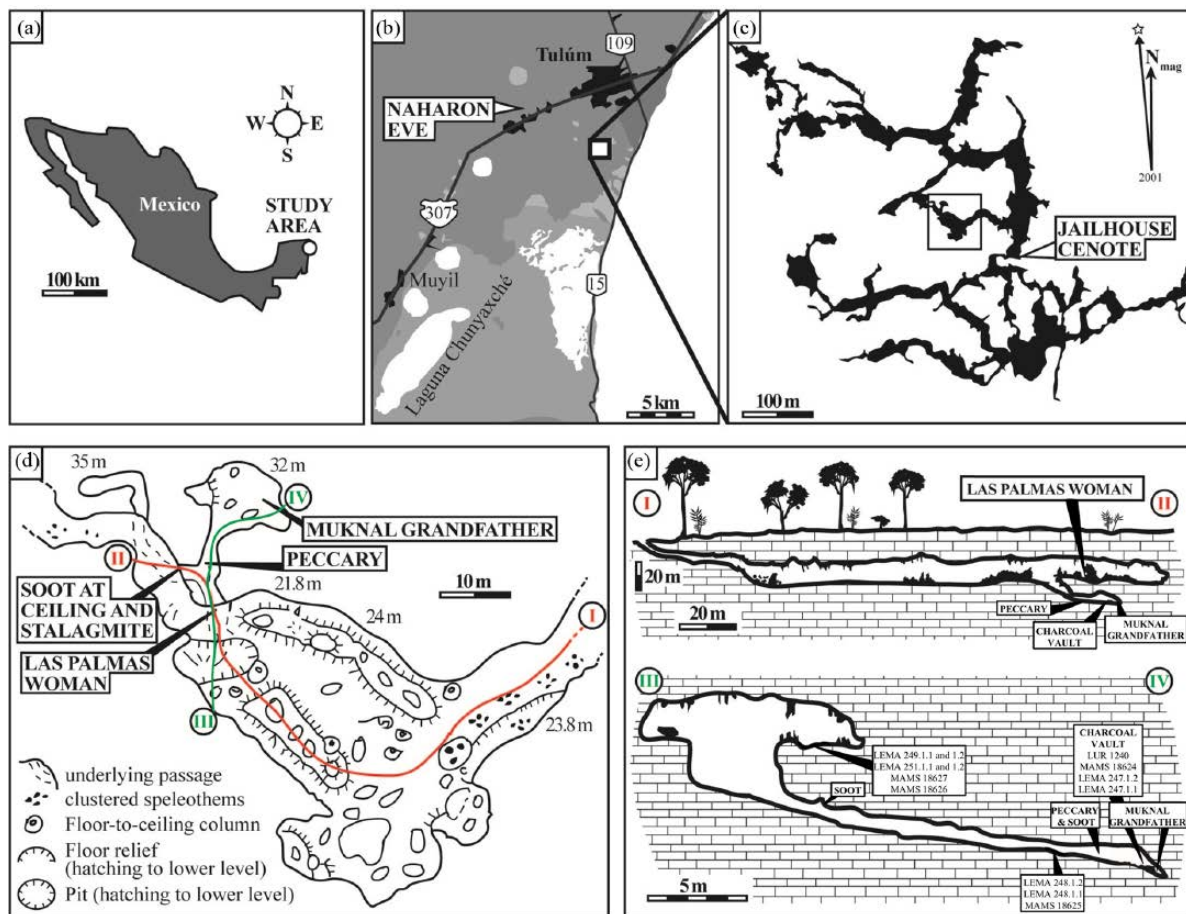Email: sarah.stinnesbeck@kit.edu

Figure 1. Study area near Tulum on the Yucatán peninsula of southeast Mexico (a and b) and location of the Muknal cave within the Remote Muknal Siphon area of the extended and complex Ox Bel Ha cave system (c). The box in the upper right figure is detailed in (d) and illustrates the cave near the Las Palmas and Muknal anthropological sites. Access is via Jailhouse cenote (c). (e) Cross sections through the Muknal cave. For position of sections I-II and III-IV, see (d). The deepest part of the cave is 34 m below sea level and was measured at the Muknal human site.

levels (bpsl) and large parts of this enormous cave system were exposed and accessible (Blanchon and Shaw, 1995; Moseley et al., 2015). The cave system was flooded during sea-level rise across the Pleistocene–Holocene transition from 12,000 to 8000 BP (Moseley et al., 2015; Smart et al., 2006), preserving paleontological and archeological evidence inside the caves.

The Muknal cave forms part of the Naranjal subsystem within the Ox Bel Ha system of connected caves and sinkholes, locally called *cenotes*, and it is located southwest of Tulum (Figure 1). Ox Bel Ha ranks among the most extended cave systems in the area, and globally, with 270 km of explored length and >140 cenotes proven to conform the system (QRSS, 2018). Name and connections of the cave system are presently as confusing as the multiple connections between the subsystems; here we only refer to the Naranjal subsystem known by local cave divers as the Muknal remote siphon (Figure 1). It is connected to the Jailhouse cenote, also called Las Palmas (QRSS, 2018), which is the entrance to both the Muknal and Las Palmas submerged caves from which anthropological sites are documented here (Figure 1).

Pre-ceramic evidence from the Naranjal system

Three pre-ceramic human skeletons have been reported from the Naranjal subsystem and are described briefly in González González et al. (2008b, 2013).

The 'Naharon Eve', a woman aged 18–20 years, was discovered mainly articulated, indicating an in situ decay in a dry cave. The skeleton was located at 23 m water depth and 368 m from the nearest entrance, Jailhouse cenote (González González et al., 2008a, 2008b).

The 'Las Palmas Lady', a female between 44 and 50 years old, was found at about 2 km distance south of the 'Naharon Eve' in the same cave system (Figure 1b). This site is located within the Muknal remote siphon area, at 24 m water depth and 59 m distance from the nearest entrance, the Jailhouse cenote (Figure 1c). The skeleton was documented as articulated, with arms and legs flexed and adducted to the body. This position of the body likely represents an intentional deposition, a crouch funeral with the corpse probably bundled with skins or strings (González González et al., 2013). This funeral ritual must then have taken place prior to cave flooding, which is consistent with ^{14}C ages measurements assigning both skeletons to the late Pleistocene–early Holocene transition, with 11,570 ± 65 ^{14}C BP (13,454 ± 117 cal BP) for the 'Naharon Eve' and 8050 ± 130 ^{14}C BP (8937 ± 203 cal BP) for the 'Las Palmas Lady' (González González et al., 2013). However, radiocarbon dating of human and animal bones from the submerged caves of Quintana Roo is a controversial issue (Taylor, 2009) due to long-term post-depositional dissolution of bones in the water-filled caves. These processes modified not only cortex and spongiosa of the bone tissue but also led to an almost complete degradation of collagen (Chatters et al., 2014; González González et al., 2013; Stinnesbeck et al., 2017c; Taylor, 2009).

After the discovery of the 'Naharon Eve' and the 'Las Palmas Lady', a third skeleton was found at only 60 m distance from the Las Palmas site and thus also within the Muknal remote siphon, at a depth of 34 m (Figure 1d and e). Access to this new site is also via Jailhouse cenote, passing the finding place of the 'Las Palmas Lady' (Figure 1d). The human skeleton was briefly documented by González González et al. (2013) and was referred to by these authors as the 'Muknal Grandfather'. Water temperature at the
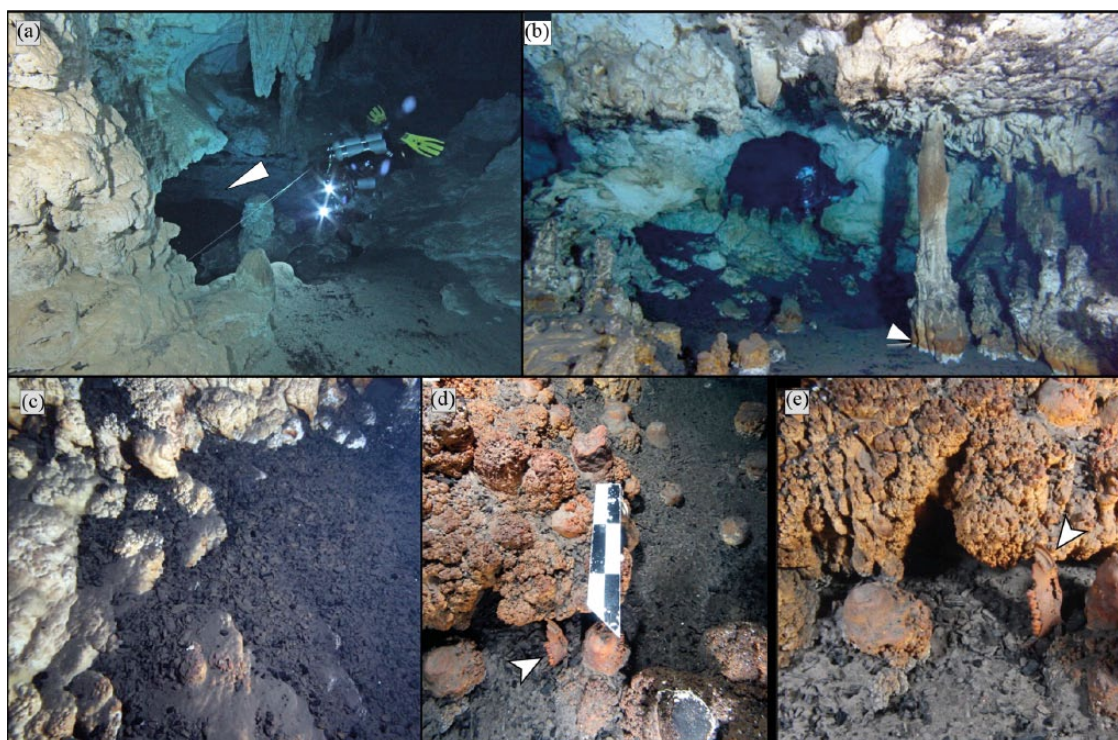
Figure 2. (a-e) Underwater photographs from the Muknal cave; for approximate location, see Figure 1. (a) Details of the internal pit at 25 m water depth, leading to the Muknal anthropological site. The arrow in (a) points toward the deepening tunnel. (b) From about 29 m water depth and illustrates the entrance to the tunnel deepening to the north and leading to the Muknal human site. Note the ancient watermark level, here pointed out by the white arrow. (c) Ash and charcoal coverage within the 'Charcoal Vault' chamber, at 34 m depth. (d) and (e) show the original upright position of the peccary mandibular ramus inside the cave.

site is about 27°C. The halocline was detected at around 16 m depth.

Location of the Muknal site and access

The partial skeleton of the 'Muknal Grandfather' was discovered by one of us (JAO) in 2012 (Figure 1). It can only be accessed from Jailhouse cenote (Figure 1c), which is located at about 210 m to the east of the finding site documented here. Inside the cave a wide east-west trending tunnel connects the cenote with the White River cave located to the northwest (Figure 1d). At about half way distance, an internal pit at about 25 m water depth marks the entrance into a 30-m-long tunnel trending to the north and deepening from 25 to about 35 m maximum water depth (Figures 1 and 2a and b). This tunnel, only 0.5–1.5 m high (Figures 1e and 2a), has abundant speleothems and represents a restrictive (bottleneck) situation even for experienced cave divers. A peccary mandible was found on the western side of the tunnel at 13 m distance from the internal sinkhole, while the 'Muknal Grandfather' was discovered at the end of the tunnel in a 3 m × 5 m wide dead-end chamber (Figures 1d and e and 2d and e). The site, also known as the 'Charcoal Vault' (Figure 2b and c) by the local cave diving community, was measured to 28–34 m water depth and corresponds to the deepest part of the Muknal cave.

Materials and methods

Diving campaigns into the cave system were initiated in 2004. Subsequent visits to the site were performed from 2006 to 2014. The 'Muknal Grandfather' and peccary mandible were discovered and collected in 2012. Both the Muknal human and the peccary mandible were found in the saltwater unit of the submerged Muknal cave. For collection methodologies and equipment used during the dives, see González González et al. (2008b).

Photographs were made with an Olympus E 620 SLR camera with a Zuiko digital lens, 14–42 mm, 1:3.5–5.8. The peccary mandibular ramus has been described in detail and assigned to an extinct genus and species of peccary, *Muknalia minima*, by Stinnesbeck et al. (2017a). The peccary mandible was scanned with an Artec three-dimensional (3D) scanner. A colored 3D print is housed in the State Museum of Natural History in Karlsruhe, Germany.

The human skeletal material with the registration number PQR2011-PALMAS-H-2 and the peccary mandible PQR2011-PALMAS-V-1 are housed in the Laboratorio Arqueológico of the Dirección del Registro Público de Monumentos y Zonas Arqueológicos E Históricos (INAH) Tulum and Mexico City. All necessary permits were obtained from the Consejo de Arqueología (INAH) No. C.A.401-36/0960.

Osteological analysis

Morphometric analysis of the skull and mandible of the 'Muknal Grandfather' is based on a set of linear measurements of anatomical landmark points in the skull (Howells, 1973; Hubbe et al., 2011; Jantz and Owsley, 2001; Owsley and Jantz, 1999). Characters that are missing due to insufficient preservation were estimated by average geometric values of the sample (Hubbe et al., 2011) for a 3D reconstruction of the cranium. Osteological methods related to age and sexual interpretation of the Muknal individual are based on standard anthropological manuals (Buikstra and Ubelaker, 1994; Comas, 1966; Terrazas Mata and Benavente Sanvicente, 2006; White and Folkens, 2000).

Microscopical analysis

The surface modifications on the peccary mandibular ramus were analyzed and photographed with a Keyence digital microscope VHX-5000. Cut marks on the peccary mandible were examined
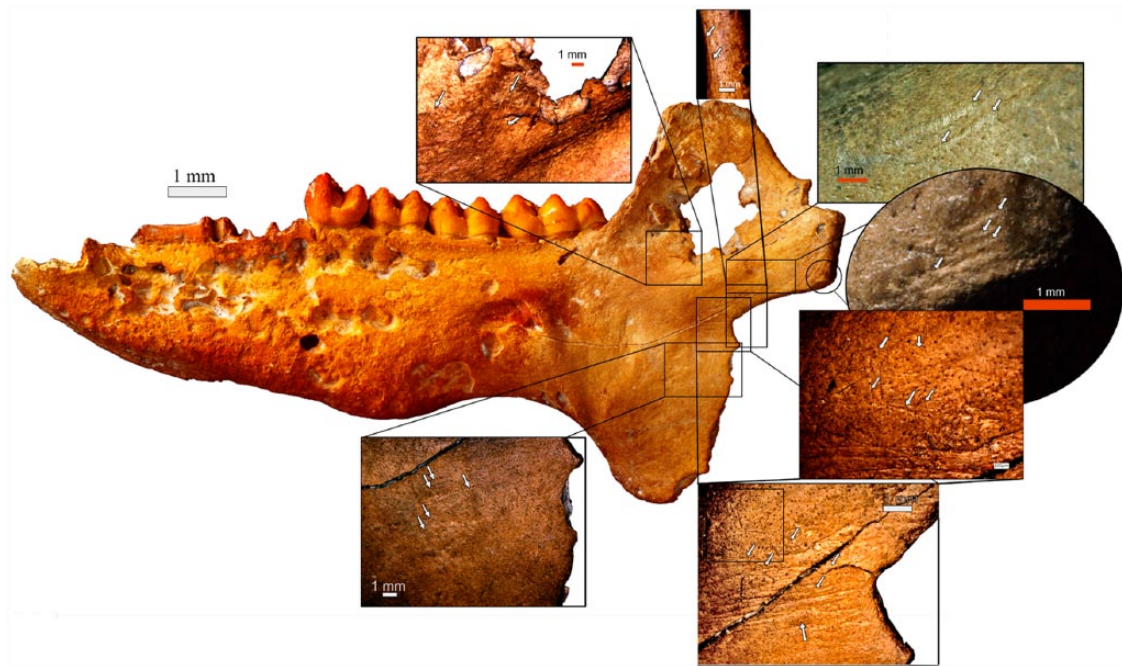
Figure 3. *Muknalia minima* (PQR2011-PALMAS-V-1): left mandibular ramus with details of cut marks (white arrows), in lateral view.
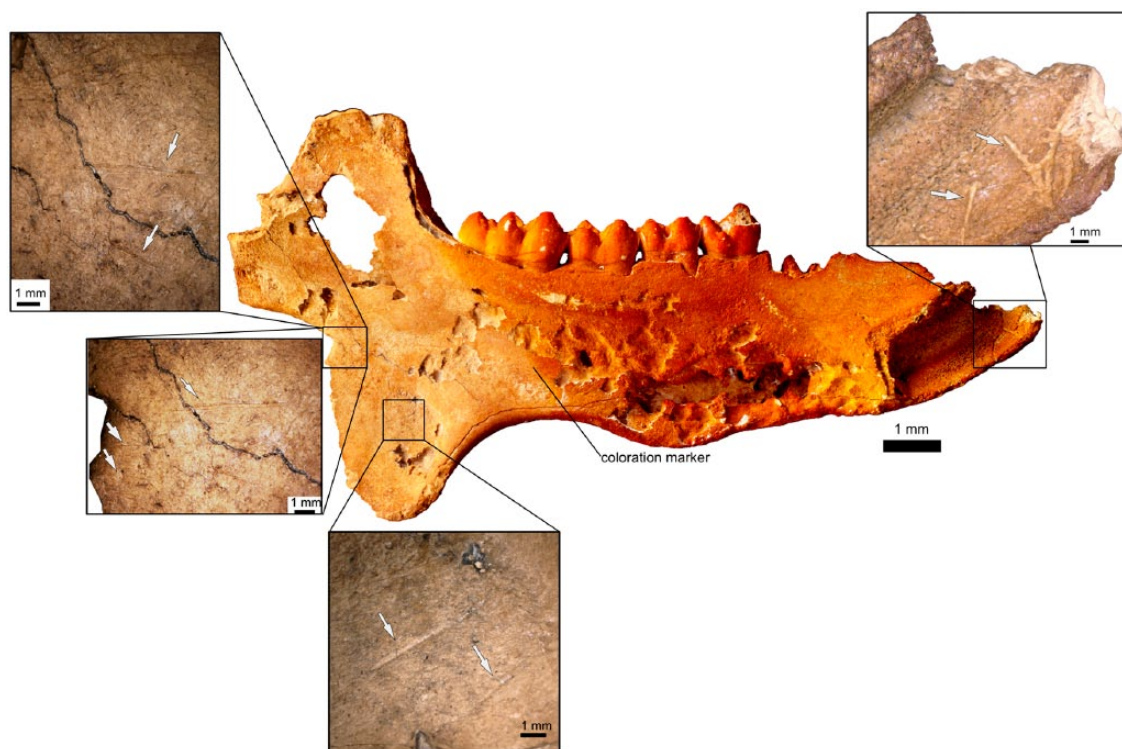

Figure 4. *Muknalia minima* (PQR2011-PALMAS-V-1) left mandibular ramus of peccary with details of cut and scratch marks in medial view.

under optical magnification (15×–100×) and were then mapped and numbered consecutively (Figure 3; Supplementary 1, available online).

All modifications were examined under magnifications of 5×–50× and 15×–200× using a VH-Z20R/W lens. Additional photographs were taken with a resolution of 3200 × 2400 pixels (Figures 3 and 4). A high-resolution 3D model of each mark was created by the scan software of the Keyence VHX-5000, thus accurately representing the micromorphology of these modifications (Bello et al., 2009; Courtenay et al., 2017). Relief and depth of the cross-sections of the marks were measured perpendicular to

the longitudinal axis of the modification and interpreted according to the attributes developed by Bello and Soligo (2008), Domínguez-Rodrigo et al. (2009), and Bello et al. (2011). They include cut mark length and depth, opening angle of the mark, the shoulder height index, and floor radius. The following abbreviations are used slightly modified after Bello et al. (2011) and Waltenberger and Schutkowski (2017):

Cut mark depth (CMD): The deepest point of the cut mark floor measured perpendicularly from the connection line of both shoulder margins.

Table 1. ^{14}C Radiocarbon dating of charcoal and soot associated with the 'Muknal Grandfather' underwater cave system.

	Sample depth (m)	Material	Labcode	^{14}C years BP	cal yr BP (1σ)	Mean (cal yr BP)
Las Palmas site	24	Charcoal	LEMA 249.1.2	8.737 ± 30	9.623–9.765	9.705 ± 62
Las Palmas site	24	Charcoal	LEMA 249.1.1	8.836 ± 30	9.780–10.119	9.957 ± 139
Las Palmas site	24	Charcoal	LEMA 251.1.1.	8.854 ± 55	9.820–10.153	9.965 ± 144
Las Palmas site	24	Charcoal	LEMA 251.1.2	8.824 ± 30	9.769–10.114	9.934 ± 138
Las Palmas site	24	Charcoal	MAMS 18627	8.963 ± 35	9.982–10.196	10.089 ± 107
Las Palmas site	24	Charcoal	MAMS 18626	8.908 ± 34	9.959–10.146	10.053 ± 93
Muknal Tunnel	27	Soot	MAMS 30421	8.605 ± 34	9.583–9.530	9.564 ± 33
Peccary site	28	Soot	MAMS 30420	8.749 ± 44	9.628–9.886	9.747 ± 109
Muknal Tunnel	28	Charcoal	LEMA 248.1.2	9.301 ± 50	10.422–10.575	10.495 ± 72
Muknal Tunnel	28	Charcoal	LEMA 248.1.1	9.375 ± 45	10.525–10.670	10.607 ± 57
Muknal Tunnel	30	Charcoal	MAMS 18625	9.430 ± 36	10.610–10.706	10.658 ± 48
'Charcoal Vault'	33	Charcoal	LUR 1240, UNAM	8.890 ± 100	9.797–10.139	9.968 ± 171
'Charcoal Vault'	33	Charcoal	MAMS 18624	9.589 ± 36	10.823–11.063	10.943 ± 120
'Charcoal Vault'	33	Charcoal	LEMA 247.1.2	9.588 ± 55	10.786–11.092	10.945 ± 132
'Charcoal Vault'	33	Charcoal	LEMA 247.1.1	9.646 ± 45	10.869–11.175	11.011 ± 133

For location of the samples within the cave, see Figure 1.

Shoulder height right side (SHR): Right side slope of the cut mark.

Shoulder height left side (SHL): Left side slope of the cut mark.

Maximum shoulder height (MSH): Height between the deepest point of the cut mark floor and the top level of the shoulder margin.

Cut mark width (CMV): The width between the top shoulder margins of the cut mark measured perpendicular to cut mark direction.

Cut mark length (CML): The maximum length of the cut mark measured at the cut mark floor.

Opening angle (OA): The angle between the two cut mark walls or slopes (Bello et al., 2009).

Floor radius (FR): The radius of a circle connects the transverse endpoints of the cut mark floor, where it is angled against the slopes. FR only applies to marks with a through-shaped cross-section.

Floor angles (FA): The angle between the slopes and the cut mark floor marks a trough-shaped cross-section, measured on the left (FAL) and right side (FAR) ignoring the actual orientation of the mark.

Radiocarbon dating

The charcoal and soot samples (Table 1) were radiocarbon dated at the Curt-Engelhorn-Center Archaeometry gGmbH (CEZA) at Mannheim, Germany, with a MICADAS (Mini Carbon Dating System) AMS system. Both charcoal and soot samples were prepared using a standard protocol including acid and base treatments to remove contaminants such as carbonate and humic acids (Lindauer et al., 2017). The BP Radiocarbon years were calibrated with OxCal version 4.2.4. The calibrated ages are given as weighted mean and 1-sigma standard deviations. No ^{14}C age could be obtained from the peccary mandibular ramus (Stinnesbeck et al., 2017). The sample treatment then included steps to remove the conservation chemicals using organic solvents, but no collagen was detected. Initial radiocarbon ages of the Muknal skeleton and of charcoal collected from the interior of the skull were published by González González et al. (2013) and were

dated by the Laboratorio Universitario de Radiocarbono (LUR) del Laboratorio Nacional de Geoquímica y Mineralogía of the UNAM/CONACYT, México. Further charcoal samples were dated by the Laboratorio de Espectrometría de Masas con Aceleradores (LEMA) of the Instituto de Física of the UNAM. All radiocarbon dates were calibrated using Oxcal 4.2.4 with the IntCal13 dataset (Reimer et al., 2013).

Results

'Muknal Grandfather'

The bones of the 'Muknal Grandfather' (PQR2011-PALMAS-H-2) laid scattered but clustered, across an area of about 1 m^2 on a limestone rock shelf, about 0.5 m above the cave floor and thus above the charcoal layer (Figure 5). Only the right humerus and right tibia were leaning obliquely against the socket of the rock shelf (Figure 5). Bones lying on the rock shelf were mostly devoid of charcoal coverage but a few charcoal flakes were found inside the calvarium, although the bones do not show any signs that they were exposed to heat.

Bone preservation is good, but the long bones show erosion pits reaching into the spongiosa. These are due to chemical dissolution that also destroyed the collagen during the long exposure in the water. The bones do not show any rolling wear, transport fractures, or marks, suggesting that they were deposited on the shelf and may only have moved slightly during the flooding of the cave. The bone color is mostly pale yellow to light buff, but irregular black-colored patches are present on the external surface and likely result from temporary contact with local charcoal flakes.

Osteology of the 'Muknal Grandfather'. Skull (Figure 6a): Resulting from post-mortem fractures and superficial dissolution of the ethmoid and the internal portion of the orbits, only part of the greater wings and spines of the sphenoid are preserved. A post-mortem fracture is identified in the ventral portion of the malar. The zygomatic arches are fractured with sharp margins, suggesting that the fractures are recent. In ventral view, the entire caudal fourth of the maxilla adjacent to the sphenoid is lost, including the posterior alveolar region of the first molar of the right side and all teeth anterior to the third molar on the left side. The anterodorsal portion of the right maxilla is also missing, as well as the plate of the ethmoid, the infraorbital margin, and ventral margin of the maxilla. Almost the entire basicranium is lost. Only the posterior
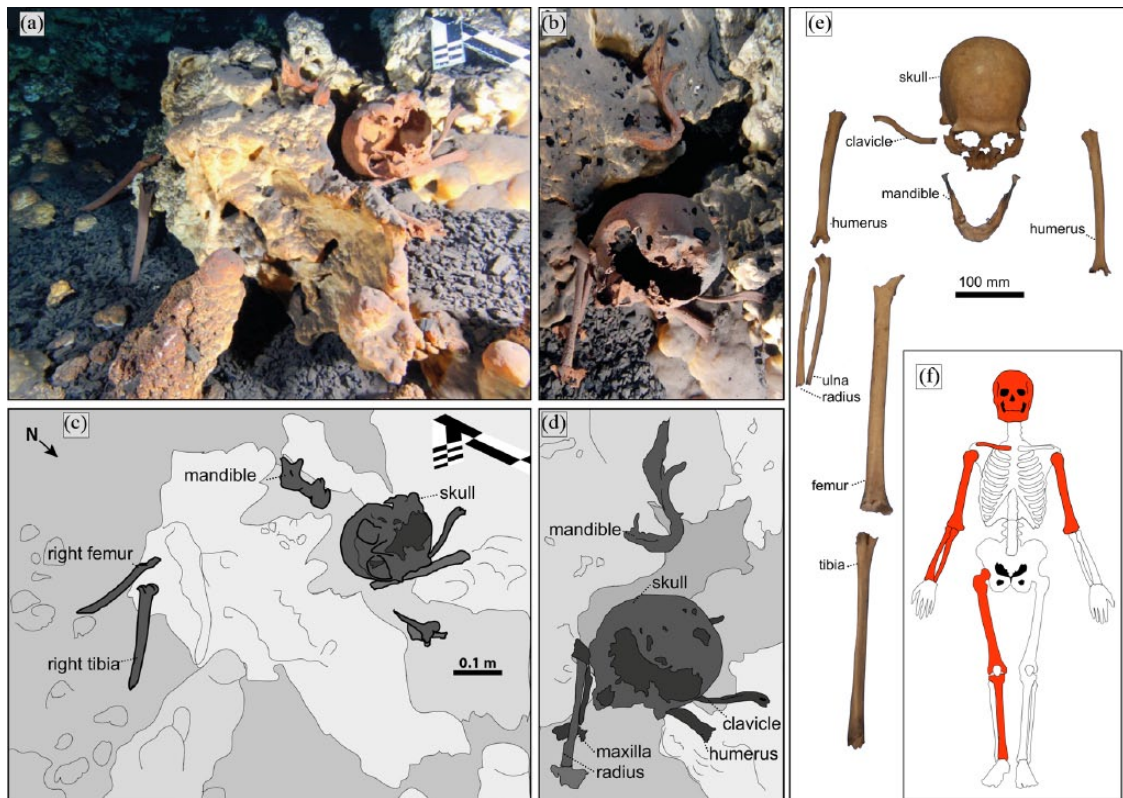
Figure 5. (a and b) Location and bone distribution of the 'Muknal Grandfather' at 34 m water depth in the 'Charcoal Vault' of the Muknal cave. (a) and (b) Underwater photographs of the skeleton in situ; (c) and (d)) interpretative line drawings of the different elements of the skeleton found in situ, (e) the Muknal skeleton, and (f) illustration of a human skeleton, the red colored bones are the equivalent that have been found at the Muknal anthropological side.

margin of the foramen magnum is preserved. Black rims on the break edges on the cranial base indicate that they are considerably older than the facial fractures. Most teeth (Figure 6b and c) must have been lost *ante mortem*, among them the right second incisor, the second right premolar, the left canine, the first left premolar, and first left molar. A possible left premolar and some badly preserved roots detached on the respective alveolar cavities of the maxilla were too abraded during life of the individual to allow a secure identification. The skull roof and the right orbit are complete, part of the left malar and the central portion of the maxilla are broken, but were reconstructed in the laboratory to their original anatomical position (see Figure 6).

The identification of the sex of the 'Muknal Grandfather' follows the method of Buikstra and Ubelaker (1994). The superciliar arches are medially prominent. They merge with the glabella forming a robust bulge reaching grade 4 in the scale of Buikstra and Ubelaker (1994). The nuchal crest reaches grade 3 in this scale. The mastoid process is medium-sized, anteriorly inclined, and identified as grade 3. The supraorbital margin is delicate, slightly rounded, and elevated to grade 4 (Buikstra and Ubelaker, 1994). The chin is deformed due to alveolar resorption caused by the loss of teeth. Still, a marked triangular chin of grades 3 to 4 is present. According to the Buikstra and Ubelaker (1994) scale of grades, the Muknal skeleton represents a male individual. Even though the individual has lost all molars during life, the eruption of the third mandibular and maxillary molars was completed. The few teeth that are preserved in the mandible show extreme abrasion (Figure 6b and c), reaching grade I of dental attrition (White and Folkens, 2000), whereas the maxillary tooth abrasion reaches grade H. This suggests that the age of the individual may range between 45 and 55 years considering the abrasion grade of the mandibular teeth and between 40 and 50 based on the abrasion grade of the maxillary teeth.

According to Lovejoy and Mendl (in White and Folkens, 2000), the fusion stage of the cranial sutures suggest an age of 48.5 (SD 10.5) for the first group of sutures and 56 (SD 8.5) for the second. However, these standard techniques are known to present a wide range of error and the Muknal individual shows little bone-tissue degeneration. The age at death may therefore have been lower than suggested by the index-based data above and may range between 40 and 45 years, as it is suggested by the analysis of the mandible.

Charcoal samples and soot patches on the cave ceiling

The Muknal anthropological site is characterized by extensive but patchy accumulations of charcoal and ash covering the cave floor of the north-south directed tunnel deepening from 25 to 35 m, and the 'Charcoal Vault' chamber at the dead end of this tunnel (Figure 2). The charcoal and ash coverage extends over an area of 60 m². It is 30 m long and 2 m wide and reaches a thickness of up to 1.0 m. Charcoal flakes and ashes accumulated in cave floor depressions and reached maximum thickness in the 'Charcoal Vault', where the bones of the 'Muknal Grandfather' were deposited.

Several charcoal samples were taken along the tunnel (see Figure 1 and Table 1 for exact location). A charcoal sample taken from below the Muknal skeleton was dated by the LUR lab of the UNAM to 8890 ± 100 ^{14}C yr BP, δ^{13}C –26.63, ±1σ (9968 ± 171 cal BP; UNAM-1240), while three samples analyzed by LEMA and MICADAS from charcoal collected in the charcoal vault, in a radius of 1–2 m (Figures 1e and 2c) to the skeleton resulted in ages between 9589 ± 36 and 9646 ± 45 BP (10,943–11,011 cal BP; Table 1). Further samples were taken from locations between the cave entrance at Jailhouse cenote and the 'Muknal Grandfather' (Figure 1 for locations and Table 1 for lab details and ages).
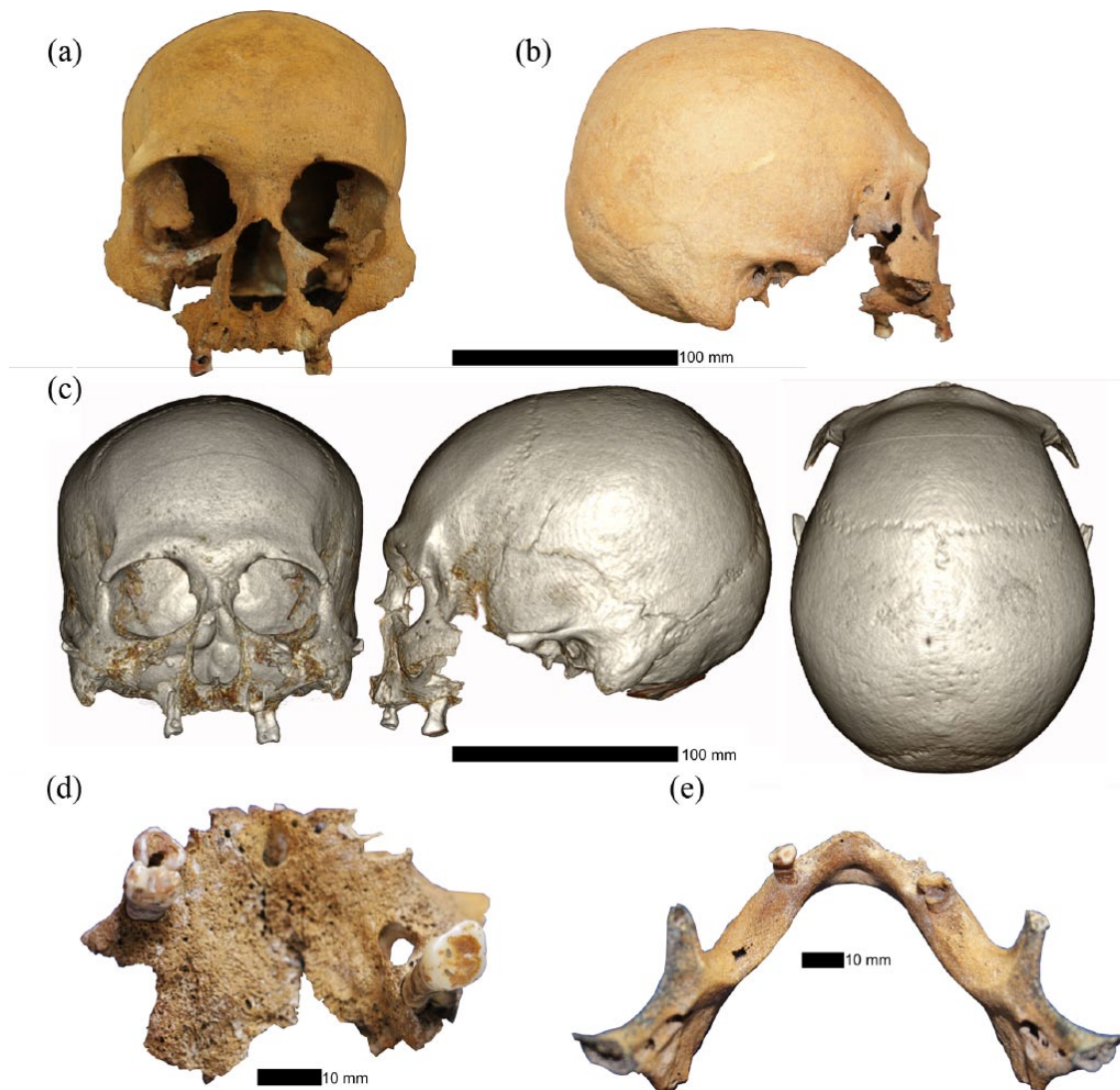
Figure 6. 'Muknal Grandfather' skull in (a) rostral view and (b) lateral view. (c) 'Muknal Grandfather' cranium 3D reconstruction in rostral, lateral, and dorsal view; (d) ventral view of the maxilla and (e) dorsal view of the mandible.

Several irregular patches of soot were detected on the ceiling of the north-south directing cave tunnel descending toward the 'Charcoal Vault' (Figures 1 and 7). We collected samples of this soot at about 13 m south of the partial human skeleton at 2.5 m above the peccary mandibular ramus (Figures 1 and 7a), and a second sample at about 6 m to the west (Figures 1 and 7b). The 'peccary site' sample was dated to 8605 ± 34 ^{14}C years BP (9583–9530 cal BP; MAMS 30421, 1σ) at CEZA, while the second sample, located 6 m to the west, was dated to 8749 ± 49 BP years (9886–9628 cal BP, MAMS 30420, 1σ).

Peccary mandibular ramus (PQR2011-PALMAS-V-1)

A left mandibular ramus of the peccary *Muknalia minima*, Stinnesbeck et al. (2017a), was discovered in the Muknal remote siphon in 2012 by JAO and EAN and collected in the same year. The mandibular ramus was found at about 197 m distance from the Jailhouse cenote entrance and <13 m south of the 'Muknal Grandfather' in the cave tunnel terminating in the 'Charcoal Vault' (Figure 1), at a water depth of 30 m. The mandibular ramus was found in a vertical position, with the rostral end up and the articular part sticking in a charcoal accumulation at about 1.0–1.5 m distance from four prominent stalagmites (Figure 1d and e). The mandibular ramus does not present evidence for carbonization by burning.

The red-brown color of the mandibular ramus is due to mineralization by Fe-hydroxides (Figures 3 and 4). The bone surface is perforated by numerous irregular dissolution pits resulting from long-lasting exposure to saltwater. These pits occur on the medial and lateral surface and reach to between 0.5 and 20 mm in diameter. The surface of the coronoid process exhibits a hole of 10 mm diameter. The rostral end of the mandibular ramus is strongly eroded and lacks the incisor part.

Manipulation of the peccary mandibular ramus PQR2011-PALMAS-V-1 by man prior to deposition is suggested by a total of 112 cut and scratch marks, approximately 87 on the lateral (Figure 8) and 25 on the medial face of the ramus (Figure 8; Supplementary, available online). The cut and scratch marks are of the same color as the bone, indicating that processes leading to the coloration of the mandibular ramus must have followed the cutting or scratching processes (Figures 3, 4, and 8). Recent marks would be distinguished by a lighter color of the bone. The marks are therefore regarded to be ancient, man-made, but cannot have been caused by recent vandalism of the site or inappropriate treatment. V-shaped microscopical grooves have been interpreted as cut marks, based on experimental archeology (Bello, 2011; Braun et al., 2016; Domínguez-Rodrigo et al., 2009), while trough-shaped marks (_/) are here regarded as scratch marks, produced by a blunt tool, but there presently is no positive evidence for this interpretation other than the horizontal floor.
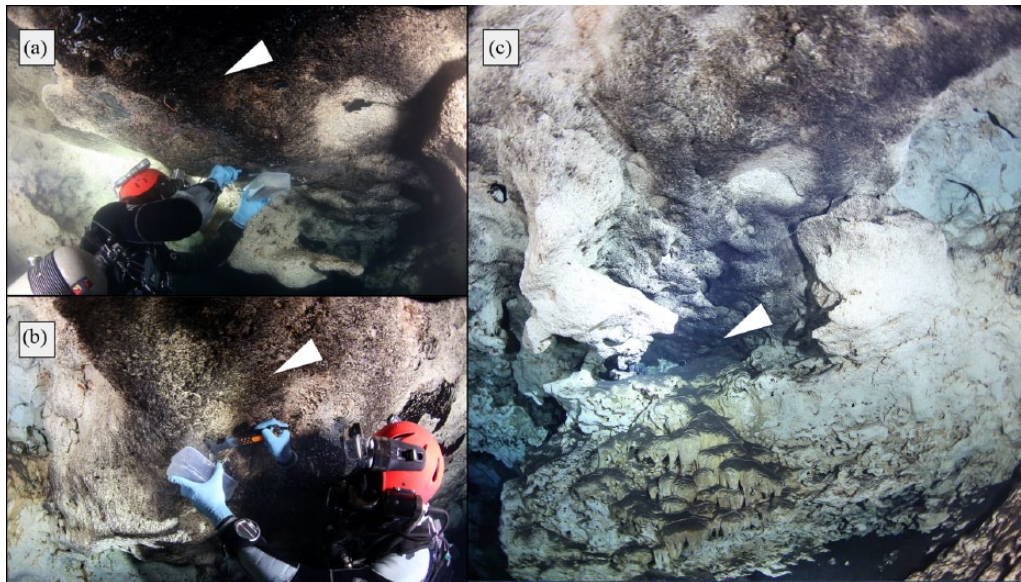
Figure 7. Photographs of soot patches on the cave ceiling leading to the Muknal anthropological site: (a, b) JAO during the sample taking, notice that the remaining area (c) is light colored.

The cut and scratch marks are accumulated in four areas on the lateral surface (Figure 8a–d) and three on the medial face (Figure 8a–c; for abbreviations see section 'Results').

Lateral face

Area A on the lateral side (Figure 8a–d): Two intersecting groups of cut marks run dorsal of the caudal limit of the masseteric fossa. The dorsal series of 26 marks is similar to the caudal series of 20 marks in running vertically and parallel to each other. The marks of the dorsal series (1–26) show an average length of 367 µm, of which 218 µm is the shortest and 516 µm the longest measured mark. The marks of the caudal series are slightly longer, with an average length of 529 µm. 394 µm represents the shortest and 656 µm the longest mark. The microtopography of individual marks shows an OA of 59.5°, an SHL of 61.57 µm, and an SHR of 72 µm in average. 34 µm is the shortest measured SHL, 101 µm the MSH on the left side, 49 µm the shortest SHR, and 131 µm the MSH on the right side. Two single marks are identified on the mandibular ramus situated rostroventrally to the group of aligned, almost parallel running marks. They are twice the length of the intersected cut marks and run rostroventrally to vertically to each other (Figure 8).

Area B: This area (Figure 8) presents the largest cut marks. The marks diverge fan-like from the caudal-most concavity of the mandibular ramus toward rostrally. Intervals between individual scratches range from 0.5 to 0.8 mm.

A total of 26 marks were counted in area B with an average length of 3.9 mm. 1.97 mm was the shortest and 6.21 mm the longest measured mark. 80% of all marks show a V-shaped cross-section, 20% show a trough-shaped cross-section. The average OA is 63°. The shortest measured SHL is 47 µm, and 41 µm is the shortest SHR. The MSH is 308 µm on the left and 226 µm on the right side.

A large scratch mark runs from the mandibular ramus across the dorsal half of the mandibular angle to rostrally, terminating on the mandibular body level with m3.

Area C: This area lies caudal to area B. A total of 12 marks are accumulated on the lateral surface of the mandibular angle (Figure 8). Area C is divided into two opposing clusters of marks: the first cluster is characterized by marks running diagonally from dorsally to caudoventrally, while the opposite cluster consists of diagonal marks running from caudally to rostroventrally. All marks run subparallel to each other at distances ranging between 0.23 and 0.32 mm and have an average length of 2.54 mm. The shortest mark detected in the rostral cluster of area C reaches a length of 1.28 mm. The longest mark, reaching a length of 6.32 mm, belongs to the caudal cluster. The microtopography of the marks shows a V-shaped cross-section with an OA of 35° to 46°, an average SHL of 346 µm and an average SHR of 266 µm. The lowest SH measured here is 344 µm on the left and 210 µm on the right side. The left MSH measures up to 348 µm, and the right MSH is 266 µm.

Area D: This area consists of three single marks and is located ventral to m2 on the lateral surface of the mandibular body (Figure 8). The marks run diagonally from dorsally to caudoventrally and are 2.73–3.8 mm long.

Medial face

A total of 27 marks were documented on the medial side of the mandibular ramus (Figure 8b). Area A: 23 marks are located on the ramus and angular process of PQR2011-PALMAS-V-1. The incisions on the median surface show a fan-like distribution, initiating near the caudal margin of the ramus and diverging rostrally with intervals of 350–550 µm between each other. The largest cluster is identified on the medial side of the mandibular ramus (Area A, medial side). These marks reach an average length of 2.63 mm, with 0.92 mm measured for the shortest and 6.56 mm for the longest mark. The OA measures 34° in average, with 84 µm as the shortest SHL and 80 µm as the shortest SHR. The MSH on the left side reaches 126 µm and the MSH on the right side 167 µm.

Area B: Two single marks are located on the mandibular angle running diagonally (Figure 8b) from caudoventrally to rostrodorsally. Area C: Two additional marks are located rostroventrally of the alveolus of the canine, diverging from each other from dorsally to ventrally.

Overall, 114 cut marks were measured, their cross-sections evaluated at approximately 400 µm distance between each other. On average, a cut mark is 2 mm long, 150 µm deep, and 35 µm wide, with OAs of 62°, SAs of 122° to 133°, and
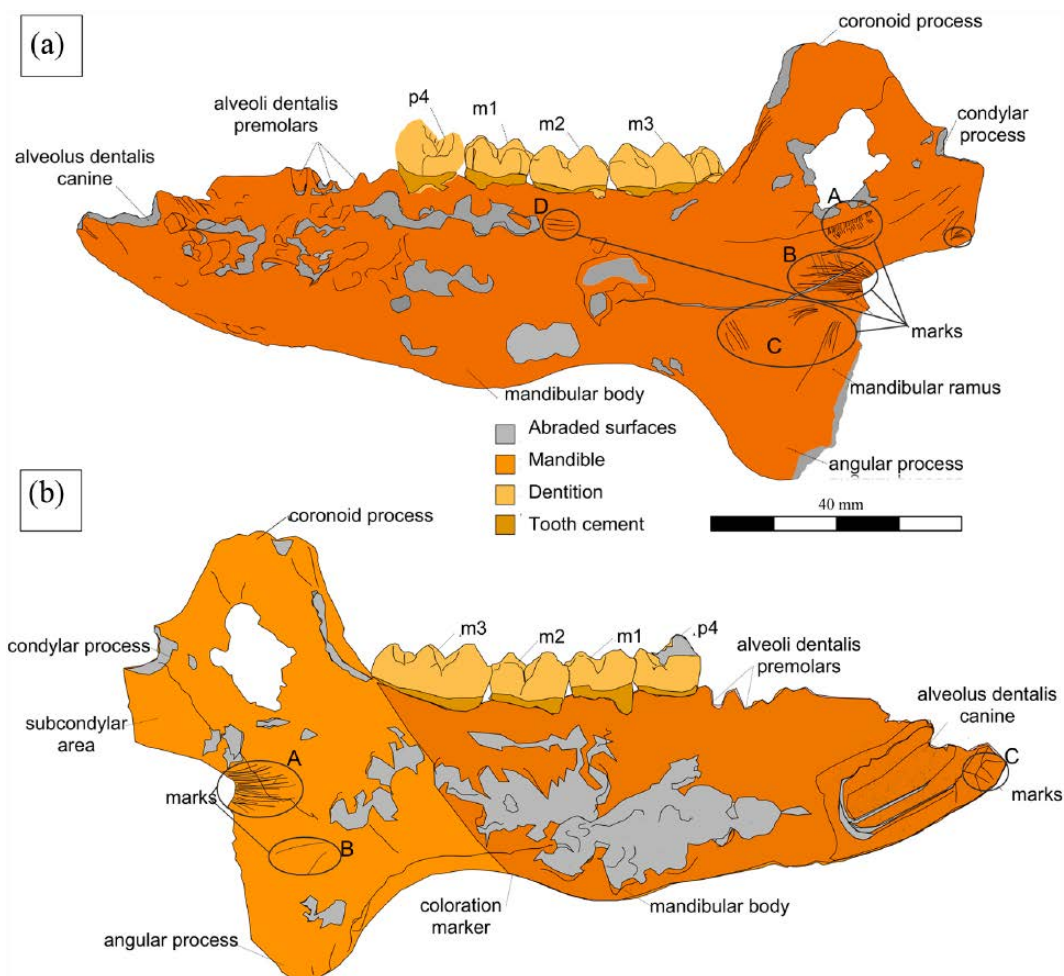
Figure 8. *Muknalia minima* (PQR2011-PALMAS-V-1), interpretative line drawing of the left mandibular ramus: (a) lateral view and (b) medial view.
Note that *several* sets of approximately parallel cut marks are identified in both views and are concentrated on the mandibular ramus and angular process (black lines).

22° for FAs. The average FR is 32 μm. These small values of the V-shaped mark indicate the sharpness of the cutting edge (Bello et al., 2011). The oblique cutting angles of the mark with respect to the bone surface result in a different height of the slope and suggest a usage of the tool to remove meat (Bello et al., 2011).

Discussion

The 'Muknal Grandfather'

Five out of nine preceramic human individuals reported to date (Chatters et al., 2014; González González et al., 2013, 2008b; Stinnesbeck et al., 2017) from the submerged cave system north and south of Tulum are virtually complete, with >80% of the respective skeletons present, and even including the preservation of tiny, delicate bones such as auditory ossicles and sesamoid bones (González González et al., 2008b, 2013; Stinnesbeck et al., 2017). The skeletons discovered in Naharon, Las Palmas, El Templo, Chan Hol I and II were close to be articulated. The overall preservation status of the human skeletons and their completeness suggests that these humans died or were placed in the caves while these were dry. Their arrival at the sites must thus have occurred prior to the early–middle Holocene sea-level rise resulting in flooding of the caves (González González et al., 2013; Stinnesbeck et al., 2017). The flooding of the cave systems was very slow, since in the Muknal cave of fossils remained at their original place, for example at the Las Palmas funeral site.

The 'Muknal Grandfather' does not belong to the group of virtually complete skeletons, because only the skull, mandible, clavicle, and a few long bones were present. Ribs, vertebrae, girdle bones, and small bones such as phalanges and tarsals are missing. All bones discovered by us laid clustered in a radius of about 1 m. When compared to other similarly old human skeletons found in the submerged cave system of the Tulum area, only two individuals from El Pit are comparably incomplete (González González et al., 2013). These skeletons were discovered on the debris mount of the El Pit sinkhole below the cenote opening (González González et al., 2013). In consequence, they may have fallen into the deep El Pit sinkhole and their corpses could have disintegrated while floating in the water, or bones could have been displaced gravitationally on the steep and rocky slopes of the debris mount.

Taphonomical circumstances indicate that this scenario does not hold true for the Muknal individual as is indicated by the following characteristics of preservation:

1. The site of the 'Muknal Grandfather' is located 210 m away from the nearest entrance, the Jailhouse cenote, and thus in a remote part of the cave. The latter is a complex system of tunnels, halls, and galleries with abundant speleothem development and rock falls (Figures 1 and 2), especially in the declining tunnel leading to the 'Charcoal Vault'. If the 'Muknal Grandfather' had fallen into Jailhouse cenote and died, the corpse would have disintegrated there. Even if there had been a water current

facilitating the transport of the corpse into the cave tunnel, it is physically impossible that this body would have made its way through the labyrinth of stalactites and stalagmites. It is further unlikely that it would have passed through the internal pit and sunk through the deepening tunnel ending in the 'Charcoal Vault' (Figure 1). In addition, in the case of drift and slow decay, the skull and extremities would have been among the first parts to disintegrate from the body and fall off (Sorg and Haglund, 2002). However, the skull and long bones are present at the Muknal site but not the torso (Figure 5).

2. The bone concentration, clustered on 1 m², precludes a long-distance water transport of a decomposed carcass, even if the bones discovered in the 'Charcoal Vault' are scattered. This scenario is supported by the complete absence of rolling traces or fractures caused by water transport through a rocky tunnel, as well as by the location of these bones 0.5 m above the cave floor on top of a rock shelf. In addition, the anthropological material comprises right side long bones and the skull. These bones must have been pre-selected prior to deposition in the cave.

3. Transport by predatory animals or scavenging could explain the presence of a partial skeleton in a cave, with bones scattered and many of them missing. However, none of the preserved bones shows bite marks. A strong argument against scavenging is the remote place of deposition. Predators, even jaguars and bears that are provided with an excellent night vision and known to live in shelters and cave entrances, are unlikely to penetrate a cave for hundreds of meters to hide prey.

With no plausible evidence for a natural transportation process of the 'Muknal Grandfather' to its final burial place, we here argue for handling of the bones by ancient settlers and hypothesize that these people transported and deposited selected bones for a final rest. Two potential scenarios could be put forward to explain the enigmatic taphonomy presented by the partial skeleton:

1. The 'Muknal Grandfather' died on the rock shelf of the cave. In this case, the selective removal of bones must have occurred when the body was largely decomposed. We exclude the option of a modern modification of the locality by unknown cave divers, because cranium and long bones are present at Muknal. In the nearby Chan Hol II site laymen cave divers stole the most interesting skeletal parts such as the cranium and all collectable large bones, but ignored numerous small bones and bone fragments including teeth and auditory ossicles (Stinnesbeck et al., 2017c). It appears similarly unlikely to us that ancient inhabitants would have selectively taken all small bones of the Muknal skeleton, but left the cranium and a few long bones in place.

2. The cranium, the right-side long bones, and the left humerus of the 'Muknal Grandfather' were brought to the cave post-mortem and placed there in a dead-end chamber on an elevated rock shelf. This specific presentation of the bones represents a secondary burial. Manipulation of bones and secondary burials are an ancient practice (Neves et al., 2002; Oliveira et al., 2012; Strauss, 2017; Strauss et al., 2015), also existing in the Maya tradition (*pumoc tradition*; Gómez Cobá, 2011) to present day (Fornaciari et al., 2010; Millaire, 2004; Schroeder, 2001; Strauss et al., 2015). In this scenario, the body of the 'Muknal Grandfather' was originally buried elsewhere on the surface of the Yucatán peninsula or in another part of the dry cave system of Tulum. Due to the lack of soil on

the karst surface, the burial was superficial and decomposition rapid. Alternatively, the corpse could have been placed on a scaffold and exposed to surface decay, but this is also a hypothetical scenario. However, the corpse could have been accessible to scavengers at an early stage of decay. When the bones were clean, the remainders not scavenged by predators, or washed away by rain, were collected and brought into the cave for a secondary burial. Such a manipulation and secondary intentional placement of specific bones would best explain the location of bones on a rock shelf in a deep and remote site inside the cave, the exclusive presence of selective unarticulated bones (e.g. skull, mandible, long bones), and their clustered distribution. The long bones leaning to the shelf may have moved and fallen down the shelf during flooding of the cave. Due to the air-filled spongiosa, these bones were extremely light-weighted when dry and could have been lifted then, drifting over the edge of the shelf during flooding.

Soot patches and charcoal in the cave

Convincing evidence for anthropogenic fires comes from local soot patches found on the ceiling of the Muknal cave, including stalactites. These soot patches were identified at the uppermost end of the diagonal tunnel leading to the 'Muknal Grandfather' above the peccary mandible (Figures 1 and 7), and a few meters to the northwest, but not inside the 'Charcoal Vault'. These patches are well identified on the otherwise gray to white cave ceiling by their dark gray-black color (Figure 7). Tips of stalactites are coated by an evenly distributed dark stain from all directions. This is consistent with a staining from below and opposes coverage by flowing water containing soot particles. The presence of soot was discovered by JAO and two ^{14}C ages were determined: 8605 ± 34 ^{14}C years BP (9583–9530 cal BP MAMS 30421) and 8749 ± 49 BP (9886–9628 cal BP MAMS 30420). These ages are roughly consistent with the sea-level rise and flooding of the caves based on isotope analysis on speleothem and radiocarbon dating on hearths and fires (Hering et al., 2018; Khan et al., 2017; Moseley et al., 2015; Smart et al., 2006) and indicate one or several human visits to this part of the cave (Figure 9).

In order to reach the deep and most remote part of the lightless and dangerous Muknal cave, the people depositing the bones must have lit fires to artificially illuminate their path or used torches. While the soot at the ceiling thus provides evidence for these human-made illumination fires, the charcoal accumulations discovered by us variously on the cave floor is not considered here to be unequivocal prove for an anthropogenic origin (Scott and Damblon, 2010). Rather, the wide coverage of the area of 30 m × 2 m, the concentration of charcoal and ash in depressions of the floor, the absence of clearly defined hearths, and the accumulation of charcoal in an explicitly deep location suggest a natural origin of most of the Muknal charcoal and wash-in by the raising water. This is evidenced by the fact that the Muknal charcoal contains burned and unburned wood and unburned leafs (e.g. Fabaceae), grasses (Graminacea), seeds (Fabaceae, Apocynaceae, Sapotaceae), as well as unidentified fruits and root fragments, indicating that the area was already forested and exposed to wildfires around 9500 BP (10,943 cal BP). Charcoal accumulation is not restricted to the chamber containing the 'Muknal Grandfather', but is present inside the cave all the way between the Las Palmas and Muknal sites, with increasing quantities in the tunnel descending to the 'Charcoal Vault', the deepest part of the local cave system. This situation suggests charcoal and plant debris intake by massive rainfalls that likely alternated with dry seasons during which the wildfires may have broken out. Because this forest existed at a time, when the groundwater level was
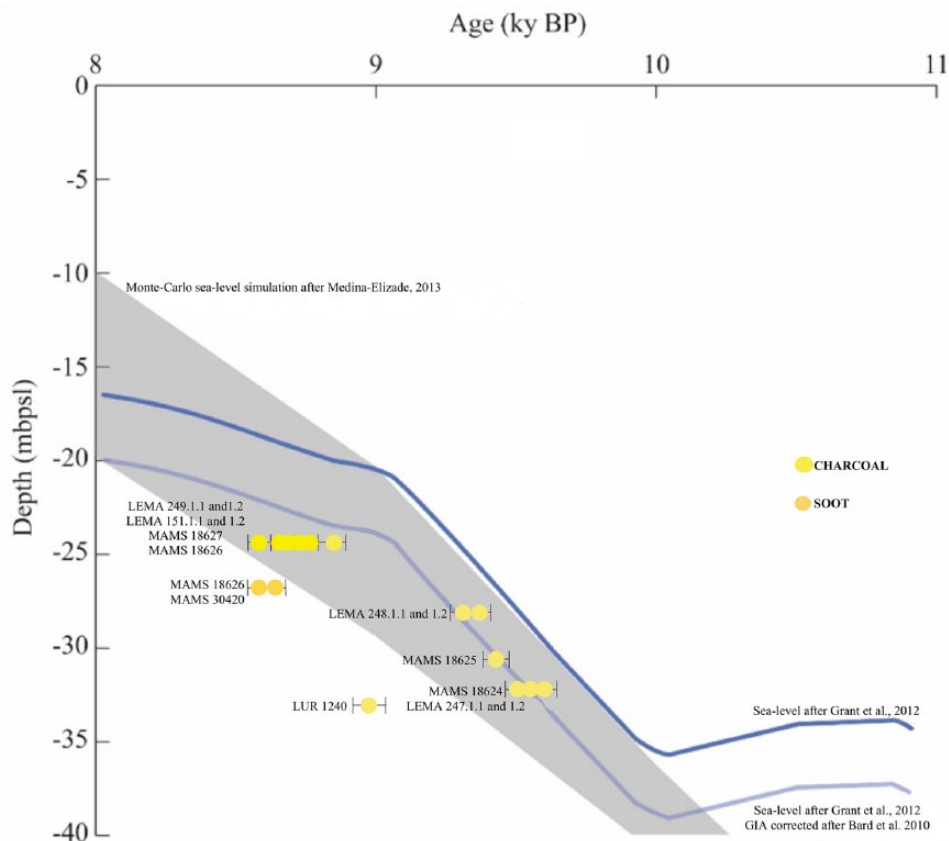
Figure 9. Muknal charcoal and soot data plotted on top of the Yucatán relative sea level curve.

some 30 m below today, such heavy seasonal rains must have soaked the limestone in a way that the development of a forest in the Yucatán peninsula was possible. Our initial evidence clearly favors such a scenario, but this needs to be substantiated by further investigations.

Small clusters of ash and charcoal that would provide unequivocal evidence for hearths, or black-stained patches interpreted as burned cave floor, are not identified to date in the Muknal cave, in contrast to the nearby Chan Hol cave, where an early Holocene use of the cave is evidenced by numerous hearths dating from 8110 $_{14}$C yr BP (9122–8999 cal BP) to 7177 $_{14}$C yr BP (8027–7951 cal yr BP; Hering et al., 2018). However, if the 'Charcoal Vault' was artificially illuminated by man during the secondary burial process, these fires did not leave soot at the cave ceiling, probably because the ceiling was higher than in the descending tunnel or because a different kind of burning material was used. If there were hearth fires in 'Charcoal Vault', their leftovers were mixed with charcoal, ash and plant debris washed in at a later stage, which is also suggested by the thick accumulation of charcoal.

In dry caves, cell wall reflectance analysis is frequently used for an evaluation of temperatures reached during burning, which occasionally allows for a distinction between wild- and anthropological fires (e.g. in metallurgical processes; McParland et al., 2009). Due to the underwater location, however, reflectance parameters are not preserved in the Muknal charcoal.

Peccary mandibular ramus

We hypothesize that the peccary mandible was deposited by man. This is indicated by the following lines of evidence:

1. The upright position of the mandibular ramus suggests placement on purpose in the dry cave and precludes an

allochthonous deposition by water transport. Recent placement of the bone by cave divers is objected by the differential coloration observed in the mandibular ramus (Figures 3, 4, and 8). The caudal end of the bone that was stuck in the charcoal accumulation is brown-colored, while the rostral part that was exposed to saltwater is red-colored. This differential chemical coloration by Fe-hydroxides requires a long-term exposure to water for hundreds, if not thousands, of years. The maintained upright position over many thousands of years was possible only under extremely low energy water current conditions during flooding of the originally dry cave system.

2. The cut marks on the caudal edge of the mandibular ramus are straight, subparallel, with a symmetrical or asymmetrical V-shaped cross-section and extensive shoulder effects, suggesting the use of a simple flake as a tool (Domínguez-Rodrigo et al., 2009). Only 20% of all documented marks show a trough-shaped cross-section (_/), especially the ones on the rostral part of the ramus. Experimental studies now interpreted these types of marks with maximum depths > maximum width as modifications by scraping tools (Domínguez-Rodrigo et al., 2009; Domínguez-Rodrigo and Yravedra, 2009; Reynard, 2014). These marks are arranged in sets of parallel striations identified on both the lateral and medial surfaces of the mandible, and they were likely caused by a scraping tool to separate the soft tissue from the bone. Due to the upright position of the mandible on the cave floor, we speculate that the ramus was intentionally deposited there. Whether or not the peccary mandibular ramus was placed there in the context of the funeral of the 'Muknal Grandfather' cannot be said, because the soot remains above the mandibular ramus are slightly younger than the charcoal found in the deepest part of 'Charcoal Vault'. This means that the

'Charcoal Vault' may already have been flooded when people returned to the site where the *Muknalia* mandibular ramus was placed. Still, a depositional context between the peccary bone and the bones of 'Muknal Grandfather' cannot be positively precluded.

The concentration of cut marks on the mandibular ramus is consistent with the removal of the principal masticatory musculature and possibly the canine as well (Figure 8).

1. *Muknalia minima* (Stinnesbeck et al., 2017; UNAM PQR2011-PALMAS-V-1) represents an extinct new genus and species of peccary. This taxon from the Muknal cave formed part of the American mammal fauna that went extinct at, or near, the Pleistocene–Holocene boundary, during a short period of time between 11,400 and 10,800 BP (e.g. Barnosky et al., 2004; Haynes, 2013). Last appearance data (LADs) of other extinct Tayassuids from North America also date to this time interval (e.g. LAD of *Mylohyus* is 11,860 ± 40 BP and that of *Platygonus* is 11,060 ± 60 BP; Haynes, 2013, 2016). The peccary was intentionally placed by humans inside the cave before the flooding of the cave systems (>8000 BP), or even prior to the continent-wide megafauna extinction in the latest Pleistocene.

The Muknal burial under the aspect of early Holocene sea-level rise

The bones of the 'Muknal Grandfather' must have been actively deposited in the dry Muknal cave prior to the flooding of the 35 m deep dead-end chamber at about 9900 BP (Collins et al., 2015; Hering et al., 2018; Khan et al., 2017; Moseley et al., 2015; Smart et al., 2006). Ages determined for the soot patches on the cave ceiling of the tunnel leading to the 'Charcoal Vault' suggest the use of artificial illumination, but possibly not in the context the deposition event, but later. The absence of evident autochthonous charcoal concentrations such as unequivocal hearths at the burial site inside the 'Charcoal Vault', unlike in other caves in the region (Hering et al., 2018), may be a taphonomic artifact due to a wash-in of younger charcoal that mixed up with possible hearth or illumination charcoal. The random, extensive, and fan-shaped distribution of charcoal in the Muknal cave suggests such a later wash-in, probably by several flooding events. The bathymetric distribution of charcoal is correlated to the early Holocene rise of sea level and successive flooding of cave floors. This interpretation is suggested by a weak correlation between radiometric ^{14}C charcoal ages and their depth positions. Even though the charcoal ages range from 8890 to 9589 BP (9968 to 10,943 cal BP; Table 1), oldest ages were measured in the deepest sector of the cave (33–34 m), near the 'Muknal Grandfather', which may be a result of a mix-up of 'funeral charcoal' with early wild-fire charcoal. Successively younger ages are identified in lower bathymetric levels (Figure 9). ^{14}C ages measured from the 24–25 m level between Jailhouse cenote and Muknal, for example, near the 'Las Palmas Lady' by us and González González et al. (2008, 2013) cluster to about 8737 ± 30 BP to 8908 ± 34 BP (9000 to 10,100 cal BP). The ^{14}C ages presented here are therefore consistent with their bathymetric sequence and correlate well with ages postulated for the drowning of deep parts of the Yucatán cave system (Khan et al., 2017; Moseley et al., 2015; Smith et al., 2011) and established sea-level curves (Grant et al., 2012). Ancient watermark levels are identified in the cave (e.g. Figure 2b), suggesting that the flooding process was interrupted by temporary standstills, for example, at about 30 m water depth, which corresponds to the deposition time of most of the charcoal and plant debris. Our data show that a placement of the 'Muknal Grandfather' later

than 8600 yr BP (ca. 9600 cal BP) was impossible. This age is also suggested by the soot discovered on the cave ceiling at 27–28 m depth (Figure 7).

The gradual rise of water level and flooding of the cave was a slow and low energy process. Otherwise, the human lower arm bones and the peccary mandible would not have maintained their upright position.

Significance of the Muknal burial site

The Muknal burial site adds new evidence to the interpretation of González González et al. (2008, 2013) that the Tulum caves and particularly the Ox Bel Ha system was an important burial and ritual site for the first settlers of the area. For instance, the unnaturally flexed legs of the nearly complete and mostly articulated 'Las Palmas Lady' and 'Naharon Eve' suggest intentional burial bundles, including wrapping of the corpses in leather, tissue, or vegetable cords (González González et al., 2008, 2013). The 'Las Palmas Lady' was discovered at 24 m water depth at only 58.6 m distance from the 'Muknal Grandfather' inside the same cave, but at a different depth level (Figure 1e), while the 'Naharon Eve' was found at 23 m depth at about 368 m to the north. The nearest sinkhole is the cenote Cristal. The Muknal anthropological site differs from the latter two in representing a potential secondary funeral, previously unknown from the early human settlers in this area of the Yucatán peninsula.

Conclusion

Human remains, faunal assemblages of Pleistocene age and anthropogenic fires dated to about the Pleistocene–Holocene transition, suggest that the Tulum cave system was an area of potential ritual significance for the early human settlers of the Yucatán peninsula.

Taphonomical evidence suggests that the cranium and several long bones of the 'Muknal Grandfather' were intentionally placed in a dead-end chamber of the Muknal cave by early settlers as a secondary burial. We suggest that the bones were not transported by water, cave divers, or animals. A modified mandibular ramus of the extinct peccary *Muknalia minima* was placed at only 13 m distance from the human burial. It exhibits post-mortem cut marks on its medial and lateral surface, indicating removal of the masticatory muscles with a sharp, unretouched tool. The most likely scenario would be that this peccary bone was placed there in the context of the burial. Based on this finding complex we propose that the Muknal cave was a funeral site during the late Pleistocene to early Holocene, in which important members of the community of early settlers of the Yucatán peninsula were laid to rest. Evidence for the early Holocene age of the Muknal burial site comes from soot on the cave ceiling dated to 8600 BP, indicating dry and accessible cave pathways to the 35 m depth level, and from the interpretation that the man-handled peccary mandibular ramus represents an element of the Pleistocene American fauna, which went extinct around the Pleistocene/Holocene boundary.

de los contextos actualmente inundados'. Dr Corina Solís Rosales from the UNAM and Fabio Hering kindly assisted us with the charcoal samples. *Dive-xtras* are acknowledged for their support with units of their diver propulsion vehicles, xscooters 'Piranhas' and 'Cudas 800', as well as the *Me dive center* and *Playa del Carmen diving center, Grupo Xcaret*, and the Rotzinger family. We are grateful to two anonymous reviewers and editor Professor Arlene Rosen for their useful comments and suggestions.

References

Barnosky AD, Koch PL, Feranec RS et al. (2004) Assessing the causes of late Pleistocene extinctions on the continents. *Science* 306: 70–75.

Bauer-Gottwein P, Gondwe BRN, Charvet G et al. (2011) Review: The Yucatán Peninsula Karst aquifer, Mexico. *Hydrogeology Journal* 19: 507–524.

Bello SM (2011) New results from the examination of cut-marks using three-dimensional imaging. *Developments in Quaternary Science* 14: 249–262.

Bello SM and Soligo C (2008) A new method for the quantitative analysis of cutmark micromorphology. *Journal of Archaeological Science* 35: 1542–1552.

Bello SM, Parfitt SA and Stringer C (2009) Quantitative micromorphological analyses of cut marks produced by ancient and modern handaxes. *Journal of Archaeological Science* 36: 1869–1880.

Bello SM, Verveniotou E, Cornish L et al. (2011) 3-dimensional microscope analysis of bone and tooth surface modifications: Comparisons of fossil specimens and replicas. *Scanning* 33: 316–324.

Blanchon P and Shaw J (1995) Reef drowning during the last deglaciation: Evidence for catastrophic sea-level rise and ice-sheet collapse. *Geology* 23: 4–8.

Braun DR, Pante M and Archer W (2016) Cut marks on bone surfaces: Influences on variation in the form of traces of ancient behaviour. *Interface Focus* 6: 20160006.

Buikstra JE and Ubelaker DH (1994) *Standards for Data Collection from Human Skeletal Remains: Proceedings of a Seminar at the Field Museum of Natural History* (Arkansas Archaeology Research Series 44). Fayetteville, AR: Arkansas Archeological Survey.

Chatters JC, Kennett DJ, Asmerom Y et al. (2014) Late Pleistocene human skeleton and mtDNA link Paleoamericans and modern Native Americans. *Science* 344: 750–754.

Collins SV, Reinhardt EG, Rissolo D et al. (2015) Reconstructing water level in Hoyo Negro, Quintana Roo, Mexico, implications for early Paleoamerican and faunal access. *Quaternary Science Reviews* 124: 68–83.

Comas J (1966) *Manual de antropología física*. Mexico City, Mexico: Instituto de Investigaciones Históricas, Universidad Nacional Autónoma de México.

Courtenay LA, Yvravedra J, Mate-González MA et al. (2017) 3D analysis of cut marks using a new geometric morphometric methodological approach. *Journal of Archaeological Anthropological Sciences*. Epub ahead of print 10 November. DOI: 10.1007/s12520-017-0554-x.

Domínguez-Rodrigo M and Yravedra J (2009) Why are cut mark frequencies in archaeofaunal assemblages so variable? A multivariate analysis. *Journal of Archaeological Science* 36: 884–894.

Domínguez-Rodrigo M, de Juana S, Galán AB et al. (2009) A new protocol to differentiate trampling marks from butchery cut marks. *Journal of Archaeological Science* 36: 2643–2654.

Fornaciari A, Giuffra V and Pezzini F (2010) Secondary burial and mummification practices in the Kingdom of the two Sicilies. *Mortality* 15: 223–249.

Gómez Cobá MJ (2011) Consideraciones arqueológicas sobre contextos mortuorios encontrados en cuevas de Yucatán, México. *Estudios de Antropología Biológica* XV: 195–218.

González González AH, Terrazas A, Stinnesbeck W et al. (2013) The first human settlers on the Yucatan Peninsula: Evidence from drowned caves in the state of Quintana Roo (South Mexico). In: Graf KE, Ketron CV and Waters M (eds) *Paleoamerican Odyssey*. College Station, TX: A&M University, pp. 323–337.

González González AH, Rojas Sandoval C, Acevez Nuñez E et al. (2008a) Evidence of early inhabitants in submerged caves in Yucatan, Mexico. In: Leshikar-Denton ME and Erreguerena PL (eds) *Underwater and Maritime Archaeology in Latin America and the Caribbean*. Walnut Creek, CA: Left Coast Press, pp. 127–142 (in Latin).

González González AH, Rojas Sandoval C, Terrazas Mata A et al. (2008b) The arrival of humans on the Yucatan Peninsula: Evidence from submerged caves in the state of Quintana Roo, Mexico. *Current Research in the Pleistocene* 25: 1–24.

Grant KM, Rohling EJ, Bar-Matthews M et al. (2012) Rapid coupling between ice volume and polar temperature over the past 150,000 years. *Nature* 491(7426): 744.

Haynes G (2013) Extinctions in North America's Late Glacial landscapes. *Quaternary International* 285: 89–98.

Haynes G (2016) North American megafauna extinction: Climate or overhunting? In: Smith C (ed.) *Encyclopedia of Global Archaeology*. New York: Springer, pp. 5382–5390.

Hering F, Stinnesbeck W, Folmeister J et al. (2018) The Chan Hol cave near Tulum (Quintana Roo, Mexico): Evidence for long-lasting human presence during the early to middle Holocene. *Journal of Quaternary Science* 33: 444–454.

Howells WW (1973) *Cranial Variation in Man: A Study by Multivariate Analysis of Patterns of Difference among Recent Human Populations*. Cambridge, MA: Peabody Museum of Archaeology and Ethnology, Harvard University.

Hubbe M, Harvati K and Neves W (2011) Paleoamerican morphology in the context of European and East Asian late Pleistocene variation: Implications for human dispersion into the New World. *American Journal of Physical Anthropology* 144: 442–453.

Jantz RL and Owsley DW (2001) Variation among early North American Crania. *American Journal of Physical Anthropology* 114: 146–155.

Khan NS, Ashe E, Horton BP et al. (2017) Drivers of Holocene sea-level change in the Caribbean. *Quaternary Science Reviews* 155: 13–36.

Lindauer S, Santos GM, Steinhof A et al. (2017) The local marine reservoir effect at Kalba (UAE) between the Neolithic and Bronze Age: An indicator of sea level and climate changes. *Quaternary Geochronology*. 42: 105–116.

McDonald HG, Chatters JC and Gaudin TJ (2017) A new genus of megalonychid ground sloth (Mammalia, Xenarthra) from the late Pleistocene of Quintana Roo, Mexico. *Journal of Vertebrate Paleontology* 37(3): e1307206.

McParland LC, Collinson ME, Scott AC et al. (2009) The use of reflectance values for the interpretation of natural and anthropogenic charcoal assemblages. *Archaeological and Anthropological Sciences* 1: 249–261.

Millaire JF (2004) The manipulation of human remains in Moche society: Delayed burials, grave reopening, and secondary offerings of human bones on the Peruvian North Coast. *Latin American Antiquity* 15: 371–388.

Moseley GE, Richards DA, Smart PL et al. (2015) Early–middle Holocene relative sea-level oscillation events recorded in a submerged speleothem from the Yucatán Peninsula, Mexico. *The Holocene* 25: 1511–1521.

Neves WA, Hubbe M and Araujo AGM (2002) A late paleoindian secondary ritual burial from Lagoa Santa, Minas Gerais, Brazil. *Current Research in the Pleistocene* 19: 83–85.

Oliveira RE, Strauss A, Da Gloria PT et al. (2012) Secondary ritual or peri-mortem body manipulation during early Holocene in South America: The case of Burial 21 from the site of Lapa do Santo, Lagoa Santa region, Brazil. *American Journal of Physical Anthropology* 147: 229.

Owsley DW and Jantz RL (1999) Databases for Paleo-American skeletal biology research. In: Graf K, Ketron C and Waters M (eds) *Who Were the First Americans*. Corvallis, OR: Center for the Study of the First Americans, pp. 79–96.

Quintana Roo Speleological Society (QRSS) (2018) 2000–2018, 6 May. Available at: https://caves.org/project/qrss/qrlong.htm.

Reimer PJ, Bard E, Bayliss A et al. (2013) IntCal13 and Marine13 radiocarbon age calibration curves 0–50,000 years cal BP. *Radiocarbon* 55: 1869–1887.

Reynard JP (2014) Trampling in coastal sites: An experimental study on the effects of shell on bone in coastal sediment. *Quaternary International* 330: 156–170.

Schroeder S (2001) Secondary disposal of the dead: Cross-cultural codes. *World Cultures* 12: 77–93.

Scott AC and Damblon F (2010) Charcoal: Taphonomy and significance in geology, botany and archaeology. *Palaeogeography, Palaeoclimatology, Palaeoecology* 291: 1–10.

Smart PL, Beddows P, Coke J et al. (2006) Cave development on the Caribbean coast of the Peninsula, Yucatan Roo, Quintana. *Special Paper of the Geological Society of America* 404: 105–128.

Smith DE, Harrison S, Firth CR et al. (2011) The early Holocene sea level rise. *Quaternary Science Reviews* 30 (15–16): 1846–1860.

Sorg M and Haglund W (2002) *Advancing Forensic Taphonomy: Purpose, Theory, and Process*. New York: CRC Press (Taylor & Francis Group).

Stinnesbeck SR, Frey E, Olguín JA et al. (2017a) *Xibalbaonyx oviceps*, a new megalonychid ground sloth (Folivora, Xenarthra) from the Late Pleistocene of the Yucatán Peninsula, Mexico, and its paleobiogeographic significance. *Palaontologische Zeitschrift* 91: 245–271.

Stinnesbeck SR, Frey E, Stinnesbeck W et al. (2017b) A new fossil peccary from the Pleistocene-Holocene boundary of the eastern Yucatán Peninsula, Mexico. *Journal of South American Earth Sciences* 77: 341–349.

Stinnesbeck W, Becker J, Hering F et al. (2017c) The earliest settlers of Mesoamerica date back to the late Pleistocene. *PLoS ONE* 12: 16–18.

Strauss A (2017) Burial practices in the Lagoa Santa region. In: Da-Gloria P, Neves WA and Hubbe M (eds) *Archaeological and Paleontological Research in Lagoa Santa*. Cham: Springer, pp. 275–295.

Strauss A, Oliveira RE, Bernardo DV et al. (2015) The oldest case of decapitation in the new world (Lapa do Santo, East-Central Brazil). *PLoS ONE* 10: e0137456.

Taylor RE (2009) Six decades of radiocarbon dating in new world archaeology. *Radiocarbon* 51: 173–212.

Terrazas Mata A and Benavente Sanvicente ME (2006) Estudio preliminar de tres cráneos tempranos. procedentes de cuevas sumergidas de la costa este de Quintana Roo. In: Jiménez López CJ, Polaco OJ, Martínez Sosa G et al. (eds) *II Simposio Internacional El Hombre Temprano En América*. México City, Mexico: Instituto Nacional de Antropología e Historia, pp. 189–197.

Waltenberger L and Schutkowski H (2017) Effects of heat on cut mark characteristics. *Forensic Science International* 271: 49–58.

White TD and Folkens PA (2000) *Human Osteology*. 2nd Edition. San Diego, CA: Academic Press.

JQS   **Journal of Quaternary Science**   QRA

The Chan Hol cave near Tulum (Quintana Roo, Mexico): evidence for long-lasting human presence during the early to middle Holocene

FABIO HERING,[1] WOLFGANG STINNESBECK,[1]* JENS FOLMEISTER,[2] EBERHARD FREY,[3] SARAH STINNESBECK,[3] JERÓNIMO AVILÉS,[4] EUGENIO ACEVES NÚÑEZ,[4] ARTURO GONZÁLEZ,[5] ALEJANDRO TERRAZAS MATA,[6] MARTHA ELENA BENAVENTE,[6] CARMEN ROJAS,[7] ADRIANA VELÁZQUEZ MORLET,[7] NORBERT FRANK,[8] PATRICK ZELL[9] and JULIA BECKER[3]

[1]Institut für Geowissenschaften, Universität Heidelberg, Heidelberg, Germany
[2]Institute für Erd- und Umweltwissenschaften, Universität Potsdam, Potsdam-Golm, Germany
[3]Staatliches Museum für Naturkunde Karlsruhe, Karlsruhe, Germany
[4]Instituto de la Prehistoria de America, Carretera Chetumal-Puerto Juárez, Solidaridad, Mexico
[5]Museo del Desierto, Saltillo, Coahuila, Mexico
[6]Área de Prehistoria y Evolución del Instituto de Investigaciones Antropológicas de la Universidad Nacional Autónoma de México, Mexico
[7]Instituto Nacional de Antropología y Historia, Tulum, Quintana Roo, Mexico
[8]Institut für Umweltphysik, Universität Heidelberg, Heidelberg, Germany
[9]Hessisches Landesmuseum Darmstadt, Darmstadt, Germany

ABSTRACT: Numerous charcoal accumulations discovered in the submerged Chan Hol cave near Tulum, Quintana Roo, Mexico, have been ^{14}C-dated revealing ages between 8110 ± 28 ^{14}C a BP (9122–8999 cal a BP) and 7177 ± 27 ^{14}C a BP (8027–7951 cal a BP). These charcoal concentrations, interpreted here as ancient illumination sites, provide strong evidence that the Chan Hol cave was dry and accessible during that time interval. Humans used the cave for at least 1200 years during the early and middle Holocene, before access was successively interrupted by global sea level rise and flooding of the cave system. Our data thus narrow the gap between an early settlement in the Tulum area reaching from the late Pleistocene ($\sim$13 000 a) to middle Holocene (e.g. 7177 ^{14}C a BP), and the Maya Formative period at approximately 3000 a bp. Yet, no evidence has been presented to date for human settlement during the $\sim$4000-year interval between 7000 and 3000 a. This is remarkable as settlement in other areas of south-eastern Mexico (e.g. Chiapas, Tabasco) and in Guatemala was apparently continuous. Copyright © 2018 John Wiley & Sons, Ltd.

KEYWORDS: charcoal; early Holocene; human settlement; pre-Maya settlement; sea level rise; submerged cave; Yucatán Peninsula.

Introduction

During the past decade, seven human skeletal remains dating back to the latest Pleistocene and earliest Holocene, 13–8 ka bp, were discovered during diving activities in the submerged cave system and sinkholes (cenotes) on the north-eastern Yucatán Peninsula (YP; González González *et al.*, 2008, 2013; Chatters *et al.*, 2014; Stinnesbeck *et al.*, 2017). In addition, fossil bones and complete and articulated skeletons of coeval mammals were reported (González González *et al.*, 2008; Chatters *et al.*, 2014; McDonald *et al.*, 2017; Stinnesbeck *et al.*, 2017a, 2017b). These discoveries have been made in Quintana Roo, Mexico, in a 20-km-long and up to 11-km-wide coastal band between Tulum in the south and Playa del Carmen in the north (Fig. 1). The Quintana Roo cave system thus preserves a unique archive for the early history of human settlement in the Americas.

Some of the human individuals in deep parts of the submerged cave system (>20 m) were almost complete (>80%) and articulated to a major extent, indicating an *in situ* decay of the bodies at times when these parts of the caves were still dry (González González *et al.*, 2008, 2013; Stinnesbeck *et al.*, 2017). The evidence also indicates that humans deliberately accessed the caves.

While fossil bones, especially human remains, have attracted immediate interest (González González *et al.*, 2008, 2013; Chatters *et al.*, 2014; Stinnesbeck *et al.*, 2017), charcoal concentrations in the cave system have received little attention, even though these patches and clusters may evidently represent ancient fire sites and hence present important evidence for human activity, long before Maya times (González González *et al.*, 2008, 2013). Underwater bone material from the area is difficult to date accurately, due to extreme loss of organic carbon. Charcoal, on the other hand, preserves the original carbon even when exposed to water and can precisely be dated using ^{14}C techniques (Taylor, 2009).

Here we concentrate on anthropogenic charcoal deposits from the Chan Hol underwater cave near Tulum, Quintana Roo. We evaluate the age of these charcoal deposits and provide new data regarding the timing and mode of use of the caves by the early inhabitants of the Tulum area.

Regional setting

With a presumed total extension of 7000 km, the Yucatán subterranean karst cave system is among the most extensive active cave systems worldwide, with an explored length of >1000 km (Bauer-Gottwein *et al.*, 2011; Kambesis and Coke, 2013; Quintana Roo Speleological

*Correspondence: Wolfgang Stinnesbeck, as above.
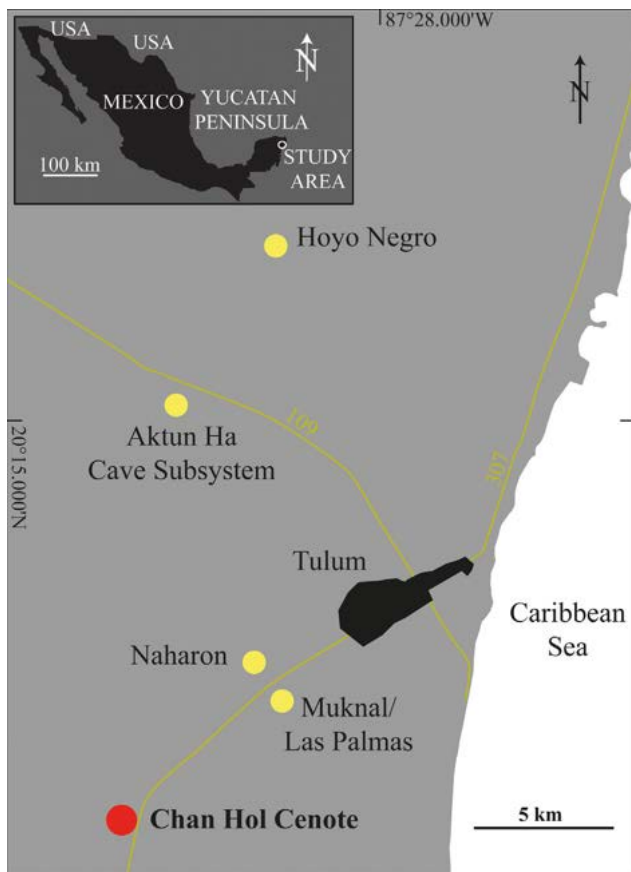E-mail: wolfgang.stinnesbeck@geow.uni-heidelberg.de

Figure 1. The Tulúm area in the Mexican state of Quintana Roo, with locations of Chan Hol cenote and the Aktun Ha cave subsystem as well as Hoyo Negro sinkhole, the Las Palmas skeleton and Naharon subsystem. Distance between the caves is about 15 km (modified after González González *et al.*, 2008).

Society, 2014). The system perforates almost horizontally layered, thick-bedded, shallow-water carbonate bedrock that developed during the Mio-, Plio- and Pleistocene (Weidie, 1985; Lefticariu *et al.*, 2006). Karstification maxima existed during Pleistocene glacial stages (Ward, 1985) when sea level was more than 100 m below present-day sea level (bpsl; Blanchon and Shaw, 1995; Moseley *et al.*, 2013). During these stadials large parts of the cave system were exposed, drained and became accessible for animals and humans. During interglacial stages of the Pleistocene and during the early–middle Holocene (13 000–7600 a bp), the caves were repeatedly flooded (Smart *et al.*, 2006; Gabriel *et al.*, 2009; van Hengstum *et al.*, 2010; Collins *et al.*, 2015; Medina-Elizalde *et al.*, 2016). Modern water levels were reached at about 4500 a bp (van Hengstum *et al.*, 2010; Grant *et al.*, 2012; Khan *et al.*, 2017), although oscillations of up to a few meters must still have occurred during Maya times (Curtis *et al.*, 1996; Kennett *et al.*, 2012; Medina-Elizalde *et al.*, 2016). Today, the YP contains a coastal density-stratified aquifer with a freshwater lens of mete-oric groundwater overlying a saline groundwater generated from penetrating seawater. The elevation of the halocline depends on the global sea level, on the thickness of the freshwater lens and on the distance to the coast (Stoessell *et al.*, 1995; Beddows *et al.*, 2007). Strong weathering and erosion across the halocline resulted in an enlargement of conduits during phases of flooding (Back *et al.*, 1986; Myloire and Carew, 2003; Smart *et al.*, 2006; Collins *et al.*, 2015).

Paleontological and anthropological sites in the submerged cave system are often tens or even hundreds of meters from the entrance. Such remote locations impeded *post-mortem* destruction by scavengers, when the cave was dry and, in recent years, protected the sites from raiding and destruction by layman divers. This latter threat has developed with the recent increase in cave diving tourism worldwide.

Chan Hol cave site

The Chan Hol cave forms part of the Toh Ha system, which is at least 32 km long and linked with the Caribbean Sea via a system of subterraneous conduits. It was first explored by Kim Davidson in 2005 (Quintana Roo Speleological Society, 2014) and is now explored to a length of about 5000 m. The main entrance, the Chan Hol cenote, is located adjacent to highway 307 connecting Tulum with Chetumal, at approximately 15 km south of Tulum, at 20°9.467′N, 87°34.165′W and 11.6 km west of the coastline (Fig. 1). The 3–4-m-wide entrance is about 5 m above sea level and is partially covered by a natural roof of limestone. The maximum depth of the Chan Hol cave is about 13 m bpsl. The water level mostly equals mean sea level, because the hydraulic gradient across the peninsula is only between five and 100 mm km^{-1} (Back and Hanshaw, 1970; Mar̀n, 1990; Moore *et al.*, 1992; Beddows, 2004). The mean water temperature at the site is about 25 °C. The halocline is only visible in one small part of the cave, about 30 m north-west of the Chan Hol I site, from which a presumably pre-Maya human skeleton was reported by González González *et al.* (2013), at a depth of about 9 m bpsl. During long-lasting heavy rain, the halocline lowers by about 0.5 m and rises by about the same magnitude when the seawater is pressed into the system by upland storms.

Diving campaigns to Chan Hol were initiated in 2006 and extended through 2014. During the campaigns abundant animal bone material and numerous charcoal accumulations were discovered. The assemblage includes isolated bones of a fossil megalonychid ground sloth, and of extant pacas (*Dasyprocta punctata*), spider monkeys (*Ateles geoffroyi*), peccaries (cf. *Tayassu tajacu*) and white-tailed deer (*Odocoileus virginianus*). These findings are presently undated and have not been osteologically revised in detail.

Two human skeletons of preceramic age were also discovered. A preliminary documentation of these individuals, termed Chan Hol I and Chan Hol II, is presented by González González *et al.* (2013), while Stinnesbeck *et al.* (2017) discussed the age of the Chan Hol II skeleton. These latter authors used U-series techniques to date a stalagmite over-growing the pelvis of the Chan Hol II human. The oldest closed system U/Th age from around 21 mm above the pelvis defined the terminus ante quem for the pelvis to 11 311 ± 370 a. However, the skeleton might even be as old as 13 000 a as indicated by stable isotope data preserved in the speleothem.

Material and methods

Material

Charcoal samples for ^{14}C dating were collected from 18 distinct accumulation sites scattered throughout the cave (Fig. 2). This includes charcoal patches near the Chan Hol cenote entrance to nearly the Chan Hol I human site (Fig. 2). One piece of charcoal associated with the Chan Hol I human
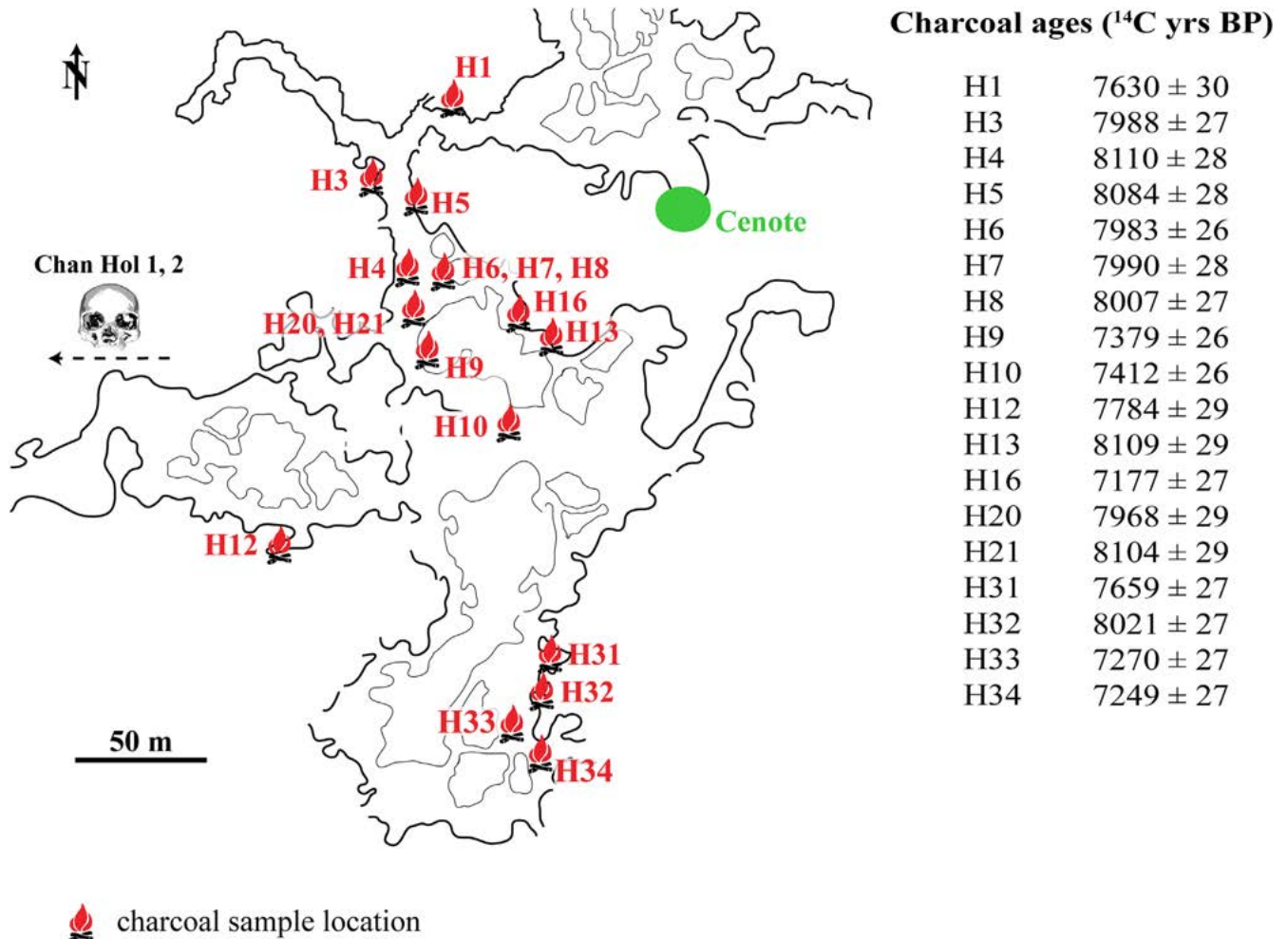
Figure 2. Charcoal sample locations in the Chan Hol cave. ¹⁴C ages are given on the right-0hand side. Chan Hol cenote is marked by the green ellipse. Individual sites are illustrated in Figs 3–7 and are discussed in the text.

was previously used for indirect dating of the skeleton and yielded an age of 9589 ± 49 ^{14}C a BP (11 144–10 742 cal a BP, González González *et al.*, 2008); no other charcoal samples from Chan Hol have been dated before this study. The samples dated here are listed in Table 1 and are presently housed at the Instituto de la Prehistoria de America (IPA) at

Solidaridad, Quintana Roo (collection numbers: H1, H3–H10, H12–H14, H20, H21, H31–H34).

All necessary permits were obtained for this study, which complied with all relevant regulations from Instituto Nacional de Antropología e Historia, Mexico (INAH permit number: C.A. 401.B (4)19.2011/36/1723).

Table 1. ^{14}C charcoal age measurements from the Chan Hol cave. Calibrated ages are given as a weighted mean and 2-sigma standard deviations. δ^{13}C data are part of the accelerator mass spectrometry measurement.

Sample ID	^{14}C age	$\pm$	^{13}C (‰)	Calibrated age (cal a BP)	Sample depth (m bpsl)	Distance from entrance (m)
H1	7630	30	-38.2	8514–8379	-9.4	85
H3	7988	27	-28.3	8999–8729	-10.3	141
H4	8110	28	-26.1	9122–8999	-10.2	151
H5	8084	28	-29.5	9113–8982	-10.2	152
H6	7983	26	-25.7	8997–8727	-10.3	180
H7	7990	28	-30.1	9000–8728	-10.8	199
H8	8007	27	-29.7	9006–8775	-10.8	203
H9	7379	26	-27.7	8317–8066	-10.5	217
H10	7412	26	-26.3	8322–8181	-8.8	258
H12	7784	29	-26.3	8628–8463	-10.6	352
H13	8109	29	-24.9	9123–8998	-7.7	225
H16	7177	27	-29	8027–7951	-8	220
H20	7968	29	-28.7	8993–8662	-9.3	190
H21	8104	29	-22.5	9122–8996	-9.3	191
H31	7659	27	-27.2	8538–8399	-9.5	329
H32	8021	27	-29.3	9010–8778	-9.8	357
H33	7270	27	-30.1	8165–8018	-10.1	360
H34	7249	27	-33.2	8162–8004	-10	365

Radiocarbon dating

The charcoal samples were dried and a common acid–base–acid method was used to remove possible carbonaceous contaminants (cf. Higham *et al.*, 2009). The samples were then combusted in an elemental analyzer (Microcube, Elementar, Hanau, Germany), connected to a 10-reactor graphitization system. Carbon dioxide is cryogenically trapped and converted to graphite at 575 °C using Fe (Merck, 10 µm) as catalyst (Kromer *et al.*, 2013). The samples were measured at the Klaus-Tschira-Archäometrie-Zentrum in Mannheim using a Mini RadioCarbon Dating System (MICADAS) (Kromer *et al.*, 2013).

Radiocarbon ages were calibrated with OxCal version 4.2.4 (Bronk Ramsey, 2009) using the IntCal13 dataset (Reimer *et al.*, 2013). Calibrated ages are given as a weighted mean and 2-sigma standard deviation. The reference year for all ages given in the study is 1950 AD.

Results

A total of 18 charcoal samples have been collected from concentrations discovered at various locations in the Chan Hol cave, most of them along the submerged cave tunnels connecting Chan Hol cenote with the Chan Hol I skeleton (Fig. 2). Charcoal fragments range from 3 to 25 mm in diameter and are dark grey to black. Most are exceedingly porous and fragile, due to their long-lasting exposure to freshwater. At each sample location, charcoal and ash was concentrated to less than ∼0.4 m² of the cave floor. The underlying carbonate bedrock revealed dark gray to black-
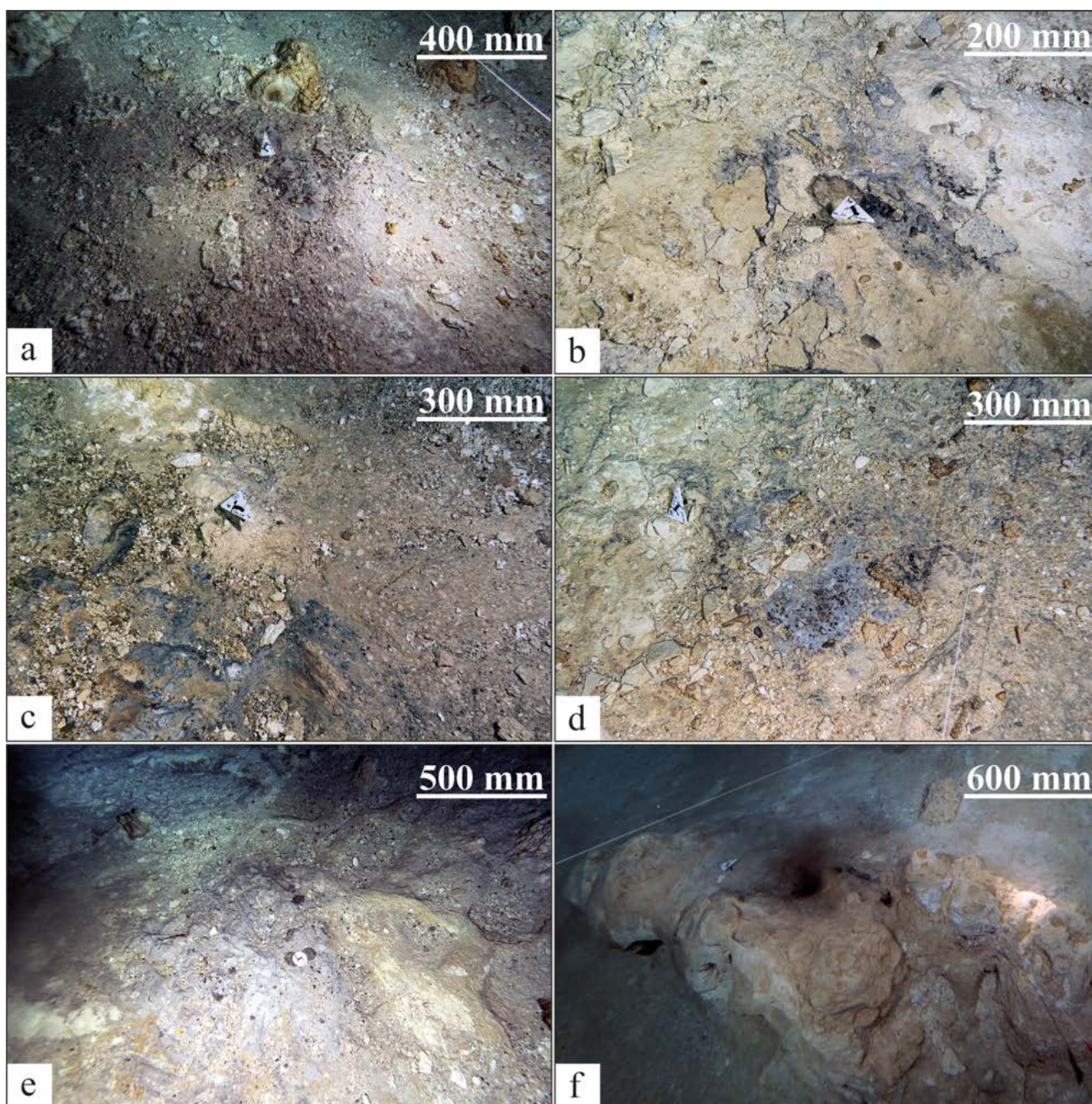
Figure 3. Selected hearths with charcoal and ash concentrations. a. H1. Poorly defined oval accumulation of charcoal (black) and ash (gray). Millimeter-thick calcite rafts are present indicating *in situ* deposition of the charcoal. b. H3. Oval-shaped charcoal and ash accumulation partially covered by floor carbonate. c. H4. Major charcoal and ash accumulation south of the marker point. d. H5. Poorly defined oval structure that is partially covered by floor-calcite. e. H6. Oval feature with dense ash accumulation that dispersed southward (bottom of the picture), due to water flow from the north. f. H16. Charcoal accumulation on a slightly elevated plateau of the cave floor. Ash is rare; charcoal chips are dispersed.

stained burning traces, thus indicating that the cave floor was dry and that wood fragments producing the charcoal were burned in place. Millimeter layers of lime mud (calcite rafts) and even solid floor calcite frequently overlie the charcoal and ash and have thus been accumulated posteriorly (e.g. Fig. 3). [14]C ages of the charcoal concentrations are given in Table 1.

Documentation of charcoal and ash accumulations of anthropogenic origin

Here we describe and illustrate the most representative charcoal and ash concentrations from the Chan Hol cave. These concentrations have oval to rounded outlines and reach diameters of between 0.2 and 0.6 m; they are occasionally contained between rocks, in individual shallow morphological depressions on the cave floor. They are here interpreted as hearths and illumination sites of anthropogenic origin (for locations of the sites see Fig. 2). Cardinal directions (magnetic north) in the photographs are indicated by the pointed tip of the scale.

H1: 7630 ± 30 [14]C a BP (8514–8379 cal a BP)

H1 is located at about 85 m from Chan Hol cenote at a depth of 9.4 m (bpsl). It is an oval accumulation of charcoal and ash covering an area of 200×300 mm. The highest density of charcoal particles is preserved south-east of the marker point (Fig. 3a). Ash is mostly accumulated north of the marker point and has probably drifted westwards. Millimeter-thick calcite rafts overlie the charcoal and ash (Fig. 3a), which indicates that this accumulation has been generated inside the dry cave and has not been washed in.

H3: 7988 ± 27 [14]C a BP (8999–8729 cal a BP)

H3 is located 141 m from the Chan Hol cenote at 10.3 m depth (bpsl). The ash and charcoal accumulation is triangular in shape and extends over at least 200×300 mm. The total expansion of the site is not seen as it is partly covered by floor carbonate (Fig. 3b). The latter has formed in a dry cave.

H4: 8110 ± 28 [14]C a BP (9122–8999 cal a BP)

H4 is situated 151 m from the Chan Hol cenote at 10.2 m depth (bpsl). Major charcoal and ash accumulations are seen south of the marker point (Fig. 3c). The area covered by ash and charcoal extends to about 200×200 mm.

H5: 8084 ± 28 [14]C a BP (9113–8982 cal a BP)

H5 is positioned at about 152 m from the Chan Hol cenote at 10.2 m depth (bpsl). It consists of a poorly defined oval structure of about 200×300 mm that is partially covered by floor-carbonate. Charcoal and ash accumulation is strongest south-west of the marker point (Fig. 3d).

H6: 7983 ± 26 [14]C a BP (8977–8727 cal a BP)

CH-15 is located at about 180 m distance from the Chan Hol cenote at 10.3 m depth (bpsl). This extensive oval-shaped and dense ash accumulation of 600×300 mm may represent the original hearth area (Fig. 3e).

H7: 7990 ± 28 [14]C a BP (9000–8728 cal a BP)

H7 is located at about 199 m from the Chan Hol cenote at 10.8 m depth (bpsl). The feature comprises a well-defined oval outline of 700×600 mm with prominent margins to the south and west (Fig. 4). The accumulation of charcoal is thickest south-west of the scale bar in the center between four rocks of 100–200 mm diameter each, which are here interpreted as draped (Fig. 4). Ash is slightly dispersed to the north-west. A stalactite 0.2 m length fell down on the accumulation.

H8: 8007 ± 27 [14]C a BP (9006–8775 cal a BP)

Figure 4. H7. Hearth with well-defined oval outline and prominent margins to the south and west. Three bigger rocks (middle and lower middle quadrant) may have been draped. Ash is slightly dispersed to the north-west (middle and lower left quadrant). Note the stalactite visible in the middle and lower left squares (grid width 500 mm).

H8 is located at 203 m distance from the Chan Hol cenote at 10.8 m depth (bpsl) and at only 1.5–2 m distance from H7. This well-defined oval feature of 400 × 300 mm reveals a prominent accumulation of ash and charcoal (Fig. 5). Three rocks have potentially been draped to limit the hearth. Four small boulders are aligned next to the marker point in the central area of Fig. 5, while a fifth isolated stone is present to the south-southeast. Ash is slightly dispersed to the north-west and north-east quadrants revealing a maximum expanse of 600 mm diameter.

H9: 7379 ± 26 [14]C a BP (8317–8066 cal a BP)

This ash and charcoal accumulation extends to a diameter of approximately 1000 mm; it is located on a limestone block 400 mm above the cave floor.

H10: 7412 ± 26 [14]C a BP (8322–8181 cal a BP)

H10 is located at 258 m from the Chan Hol cenote at 8.8 m depth (bpsl). The site is characterized by a prominent charcoal accumulation of 200 × 260 mm in a shallow morphological depression on top of a flowstone plateau, about 1.5 m above the cave floor (center-top of Fig. 6). Black-colored ash is abundant in the cavity and the cave bedrock shows evidence of burning. An accumulation of charcoal was also identified on the slope of the plateau (lower and middle left and lower middle quadrant) and either drifted laterally from the plateau top, or originated from another unidentified hearth (Fig. 6). The unusual location of H10 suggests that this feature may not have resulted from a hearth but, instead, its elevated position suggests an elucidation site.

H12: 7784 ± 29 [14]C a BP (8628–8463 cal a BP)

H12 is located 352 m from the Chan Hol cenote at 10.6 m depth (bpsl). It comprises two clearly defined structures; one (middle left quadrant) consists of a dense charcoal accumulation with partially burned wood fragments. Ash is abundant and slightly dispersed. The structure is confined by speleothems to the east. The second structure (middle and middle right quadrant) contains two big (~200 mm) partially burned wood fragments with associated charcoal pieces. These appear to be draped. Part of the structure is covered by floor calcite (Fig. 7). H12 is located on a flat limestone block about 200 mm above the cave floor.

H13: 8109 ± 29 [14]C a BP (9123–8998 cal a BP)

H13 is identified at 8 m depth. This red–brown charcoal accumulation is overlain by a calcite crust which does not allow us to reconstruct the complete extent of the site.

H16: 7177 ± 27 [14]C a BP (8027–7951 cal a BP)

H16 is situated 220 m away from the Chan Hol cenote at 8 m depth (bpsl). The hearth is placed on an elevated part of the cave adjacent to the wall. Elevation is about 0.7 m with respect to the floor. The site is surrounded by speleothems to the south and east, thus providing a natural restriction. A black charcoal accumulation of 250 × 100 mm occurs east-south-east of the marker point placed in Fig. 3(f). Ash is dispersed to the north-west (Fig. 3f). The elevated burned portion of the cave floor is gray.

Sites H31–H34 are clustered in the same tunnel to the south of the cave system documented here (Fig. 2); they are located at only a few meters between each other. Distance from the cenote entrance of the Chan Hol cave is about
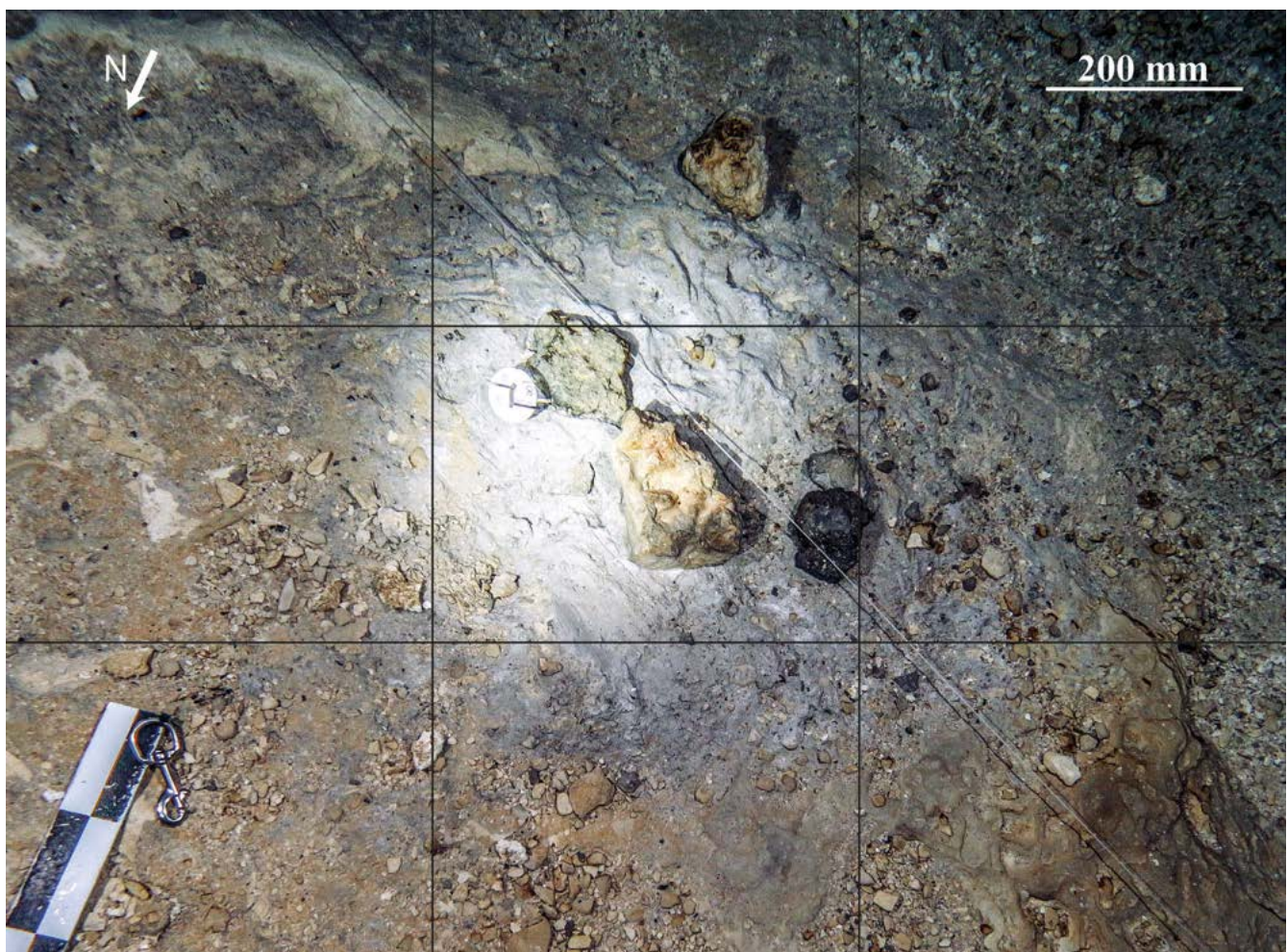
Figure 5. H8. Strong accumulation of charcoal and ash. Rocks in the middle and upper middle quadrant may have been draped to limit the hearth. Ash is slightly dispersed to the north-northeast (lower left quadrants, grid width 500 mm).

420 m and from the nearest other site, H12, about 60 m. H31–H34 are circular ash accumulations, each about 600–1000 mm in diameter, with charcoal particles of up to 200 mm, including burned wood.

Discussion

The numerous charcoal accumulations discovered by us in the Chan Hol cave are here interpreted to represent ancient hearths and illumination sites of anthropogenic origin, which result from times before the flooding of the system. Our interpretation is supported (i) by the nature of the charcoal accumulations, which point to designed arrangements rather than coincidental accumulations, and (ii) by the ages of the charcoal which all fall into the time before the anticipated flooding of the cave. We will elaborate these two points and show that humans have been active in the caves for about 1200 years during the early to middle Holocene.

It is important to note that the cave floor is consistently formed by hard limestone bedrock, while soil, or soft sediment coverage, is absent. Ash and charcoal patches are therefore easily identified, as this is the only organic material on the hard cave floor. At each sample location, the concentration of charcoal is restricted to well-defined areas of 0.04–0.25 m^2 that are independent from the cave floor morphology (e.g. depressions). Wash-in of wood fragments burned by natural processes, such as forest fires, or eolian transport of ash, would have resulted in a randomly dispersed distribution of charcoal on the Chan Hol cave floor, with a concentration gradient declining with increasing distance from the cave entrance. Instead, the charcoal

and ash accumulations are refined to isolated patches with distinct shape, well separated from each other. The stained cave floor underlying most charcoal accumulations provides strong evidence for an *in situ* burning of wood fragments. Calcareous crusts covering some fire places (i.e. H1, H3, H5) and the elevated position of others (i.e. H10, H16) also suggest an *in situ* accumulation of these light and mobile particles before cave flooding and thus confirm this interpretation.

The charcoal samples yield ^{14}C ages ranging from 8110 ^{14}C a BP (9122–8999 cal a BP, CH-13) to 7177 ^{14}C a BP (8027–7951 cal a BP, CH-31; Table 1, Fig. 8), thereby covering a time interval of nearly 1200 years. The results indicate that the cave must have been dry and accessible down to the maximum sampling depth of 10.8 m bpsl at 7990 ^{14}C a BP (9000–8728 cal a BP) (H7), to 10 m bpsl at 7249 cal a (8162–8004 cal a B) (H34), and to 8 m at 7177 ^{14}C a BP (8027–7951 cal a BP; H16; Table 1, Fig. 8). These data agree with global and regional sea level curves (Coke *et al.*, 1991; Waelbroeck *et al.*, 2002; Muhs *et al.*, 2011; Grant *et al.*, 2012; Moseley *et al.*, 2015; Khan *et al.*, 2017).

Three periods of cave usage are distinguished (Figs 8 and 9), with clusters at about 8000 a (Fig. 9a), at about 7700 a (Fig. 9b) and at about 7300 ^{14}C a BP (Fig. 9c). The oldest episode is the most distinct and evidenced by most data points, while the other two clusters suggest extended use of the cave to about 7300 ^{14}C a BP. The oldest accumulations are clustered at close distance to each other (Fig. 9a), whereas subsequent younger charcoal ages (Fig. 9b,c) are distributed over a wider area in the cave and vary in distance from the cenote entrance. The proximity of sites H31–34 (Figs 2 and 9)

Figure 6. H10. Charcoal accumulation in a morphological depression on top of a flowstone plateau (middle, upper middle and upper left quadrant). No ash is present in the immediate surrounding of the charcoal. On the slope of the plateau (middle and lower left and lower middle quadrants) another accumulation of charcoal has either been dispersed from the top of the plateau or it originated from another unknown source (grid width 450 mm).

Figure 7. H12. Two clearly defined charcoal clusters here interpreted as hearths. The dense charcoal accumulation in the middle left quadrant contains partially burned wood fragments. Ash is abundant and slightly dispersed. The structure is confined by speleothems to the east. The second structure, located in the middle and middle right quadrant of the figure, contains two larger (~200 mm) partially burned wood fragments with associated charcoal pieces. These have probably been draped. Part of the charcoal accumulation in the middle right quadrant is covered by floor carbonate.

may suggest the existence of another yet unknown entrance to the cave, at least in ancient times. Ceramics of Maya origin have been found by us (J.A., E.A.) close to the Chan Hol I site. This also hints to another unknown entrance which allowed for access to this portion of the cave to at least Maya times, but there is no geologic evidence yet to substantiate this interpretation.

Most charcoal sites are relatively small, covering areas of only about 0.06 m^2. This is far too small for a cooking site. Also, no fragmented, burned or unburned animal bones, or
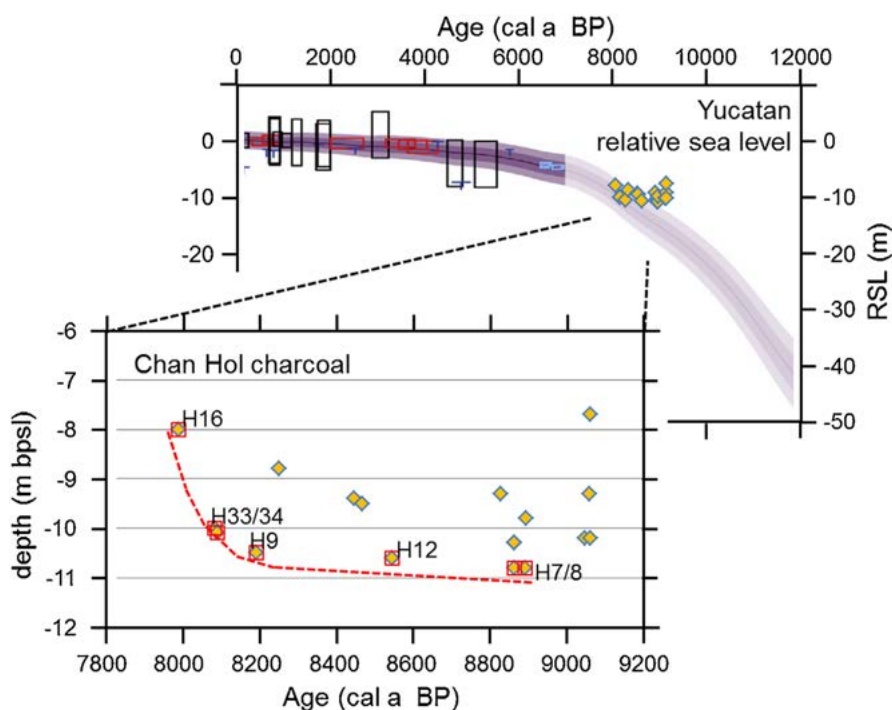
Figure 8. Bottom: depth (m bpsl; below present sea level) of Chan Hol charcoal (yellow diamonds) plotted versus age (cal a bp). Red boxes mark deepest locations through time; red stipple line marks lower depth limit of charcoal samples. Top: Chan Hol charcoal data (yellow diamonds) plotted on top of the Yucatan relative sea level (RLS in m) curve taken from Khan et al. (2017).
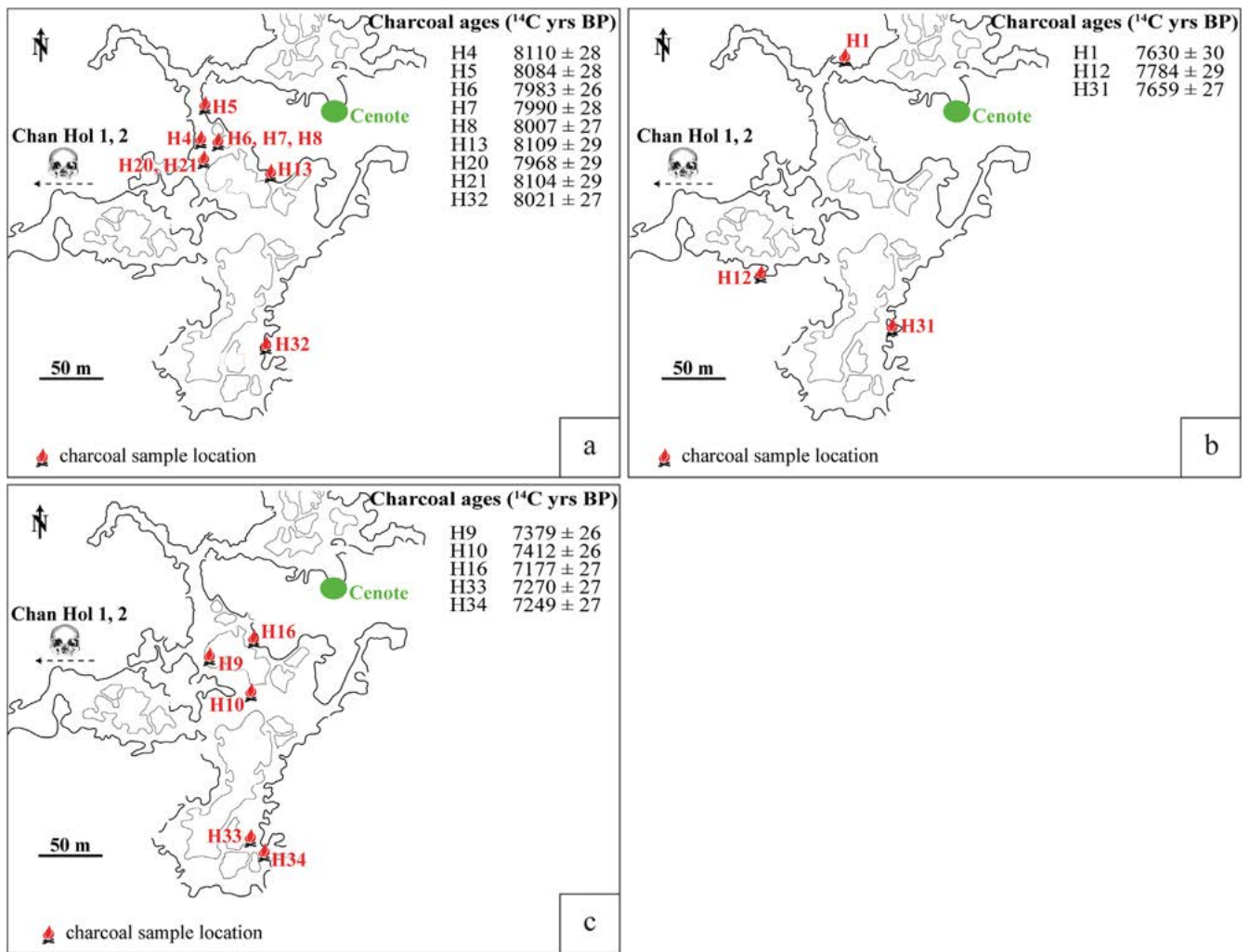
Figure 9. Three charcoal age clusters plotted on the map of the Chan Hol cave. a. Cluster of ^{14}C ages between 7968 ± 29 and 8110 ± 28 a BP. This is the most prominent cluster and consists of nine data points. B. A second less well-defined cluster groups at about 7700 a BP. C. The youngest charcoal ages range between 7177 ± 27 and 7412 ± 26 a BP. Fire place locations of the oldest cluster (a) are closely assembled and at short distance to the entrance (except for H32), whereas fire place locations of the two younger clusters (b, c) spread throughout the cave.

lithics, have been found at or near the Chan Hol charcoal accumulations. This suggests that these fire sites may have served for illumination, rather than representing everyday gathering places or cooking sites. This hypothesis is supported by the distance of the sites, of many tens to several hundreds of meters from the Chan Hol cenote; this indicates a deep penetration and thus excludes use of the cave as a temporary shelter, as an everyday fire place or campsite, which typically would have been located closer to the entrance area. We assume that humans visited and probably explored the cave system using small fires for illumination during their stay and to light branches (torches) on their way. This is also suggested by the elevated position of numerous sites above the cave floor, mostly on limestone rocks. This also contradicts an interpretation as cooking places or campsites, but rather supports our scenario that these sites served for illumination and orientation in a lightless environment. Based on the charcoal accumulations, the Chan Hol humans penetrated as far as 360 m into the cave (Fig. 8).

Interestingly, sites H6, H7 and H8 are larger (0.6–0.8 m in diameter) and are also refined by rocks. The sites are of about equal age (8000 ^{14}C a BP) and located close to each other at an intersection of cave passages at about 200 m from the cenote. They could mark a place of particular importance, *e.g.* for orientation or as a meeting point.

Approximately coeval charcoal concentrations of probable cultural origin have been reported from other sites in the Tulum area (e.g. Muknal, Aktun Ha). They were ^{14}C dated by González González *et al.* (2008) to 7740 ± 39 ^{14}C a BP (8600–8430 cal a BP) at Las Palmas, 8890 ± 100 ^{14}C a BP (10 234–9670 cal a BP) at Muknal, and 9524 ± 84 ^{14}C a BP (11 150–10 550 cal a BP) at Aktun Ha (see Table 1 for calibrated dates of bone and associated charcoal). The charcoal accumulation at Aktun Ha (Figs 1 and 10) was found in a niche 0.6 m above the cave floor near the cave center, and provides the strongest evidence for an anthropogenic site (González González *et al.*, 2008).

The ^{14}C charcoal ages from Las Palmas, Muknal and Aktun Ha concur with the ^{14}C ages determined for the Chan Hol fire places and provide independent evidence for an early Holocene human use of the caves in the Tulum area, which evidently was not limited to Chan Hol. Human visits to caves in the area, including Chan Hol, started earlier, probably during the late Pleistocene, as is indicated by ^{14}C and U/Th ages of skeletons in the Tulum cave system (e.g. Hoyo Negro, Naharon, Chan Hol II; González González *et al.*, 2008, 2013; Chatters *et al.*, 2014; Stinnesbeck *et al.*, 2017). Although the early human settlers in the Tulum area may have used the cave system as a burial ground (González González *et al.*, 2008, 2013), there is no positive evidence to
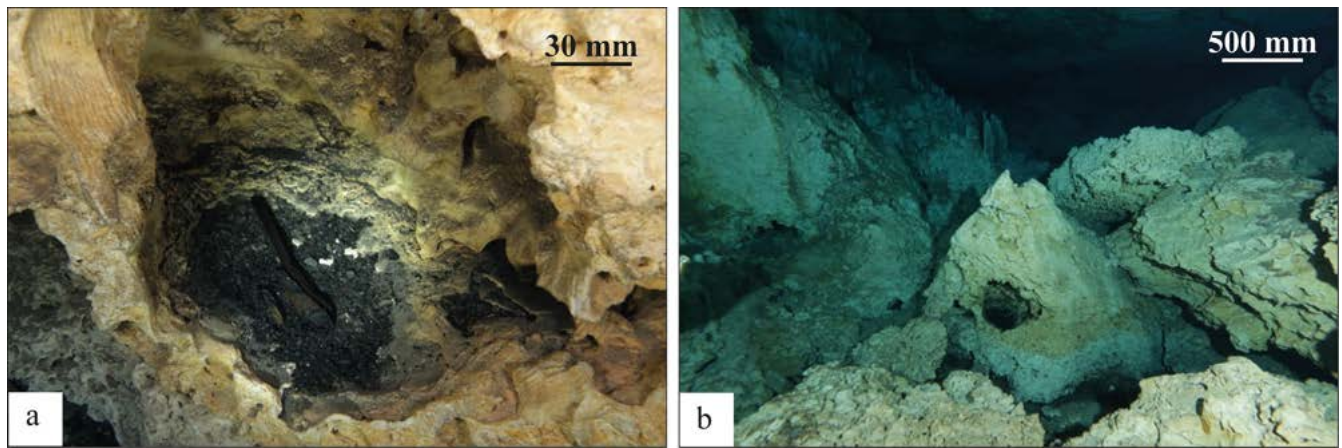
Figure 10. Charcoal concentration of probable anthropogenic origin at Aktun Ha cave. The accumulation was found in a deep erosional depression in a limestone boulder, at 0.6 m above the cave floor. a. Close-up view of the niche from above, with associated charcoal and burned wood fragments. b. Overview of the Aktun Ha cave chamber, with charcoal-filled erosional niche in the pyramidal rock in the center.

support this scenario for the two human skeletons discovered at Chan Hol (Chan Hol I and II). Rather, their death in the caves may have been accidental (González González et al., 2013; Stinnesbeck et al., 2017). Therefore, the use of these distant locations is presently unknown.

Visits to the Chan Hol cave ended at about 7950 cal a BP, as indicated by the youngest charcoal age. Presumably, most of the cave pathways were then already flooded with seawater. This flooding hindered human access to these passages. For Outland cave, which is part of the Sac Actun cave system and contains the Hoyo Negro cenote (Chatters et al., 2014), Collins et al. (2015) postulate flooding of upper cave passages after about 8100 cal a BP, and complete inundation at around 6000 cal a BP; this is in agreement with the results provided here.

Our youngest datum of 7951 cal a BP (7177 ± 27 [14]C a BP) for anthropogenic charcoal at Chan Hol represents the last evidence for the presence of humans in the Tulum area for roughly 4000 years, until about 3000 a, when archeological evidence of the Preclassic Period of Maya settlers is reported by Hammond (1992). The reason for this remarkable gap in the human settlement history of north-eastern Yucatán is presently unknown. It is striking, as settlement in other areas of south-eastern Mexico (e.g. Chiapas, Tabasco) and in Guatemala was apparently continuous. With the new results presented here we narrow this gap and add a few more pieces to the settlement history of the Tulum area.

Conclusions

Charcoal accumulation sites from Chan Hol cave are here interpreted as anthropogenic in origin and to represent illumination sites used by humans during cave exploration. The sites are ^{14}C age-dated by us to 9122–7951 cal a BP, indicating that the Chan Hol cave was repeatedly visited by humans during at least 1200 years, from the early Holocene to about the beginning of the middle Holocene. At the time of our youngest charcoal datum, 7951 cal a BP (7177 ± 27 [14]C a BP), the cave was dry to 8 m bpsl, which concurs with global and regional sea level curves. Our charcoal data extend the use of the Chan Hol cave from 13 ka to 7177 [14]C a BP, and thus a period of 6000 years. Moreover, they significantly narrow the present gap in the settlement history of the area, between this early phase of human settlement, and the Preclassic Period of Maya settlement at about 3000 a.

References

Back W, Hanshaw BB. 1970. Comparison of chemical hydrogeology of the carbonate peninsulas of Florida and Yucatan. *Journal of Hydrology* **10**: 330–368.

Back W, Hanshaw BB, Herman JS et al. 1986. Differential dissolution of a Pleistocene reef in the ground-water mixing zone of coastal Yucatan, Mexico. *Geology* **14**: 137–140.

Bauer-Gottwein P, Gondwe BRN, Charvet G et al. 2011. The Yucatán Peninsula karst aquifer, Mexico. *Hydrogeology Journal* **19**: 507–524.

Beddows PA. 2004. *Groundwater hydrology of a coastal Conduit carbonate aquifer: Caribbean Coast of the Yucatán Peninsula, México.* PhD Dissertation, University of Bristol.

Beddows PA, Smart PL, Whitaker FF, Smith SL. 2007. Decoupled fresh-saline groundwater circulation of a coastal carbonate aquifer: spatial patterns of temperature and specific electrical conductivity. *Journal of Hydrology* **346**: 18–32.

Blanchon P, Shaw J. 1995. Reef drowning during the last deglaciation: evidence for catastrophic sea-level rise and ice-sheet collapse; *Geology* **23**: 4–8.

Bronk Ramsey C. 2009. Bayesian analysis of radiocarbon dates. *Radiocarbon* **51**: 337–360.

Chatters JC, Kennett DJ, Asmerom Y et al. 2014. Late Pleistocene human skeleton and mtDNA link Paleoamericans and modern Native Americans. *Science* **344**: 750–754.

Coke JG, Perry EC, Long A. 1991. Sea-level curve. *Nature* **353**: 25.

Collins SV, Reinhardt EG, Rissolo D et al. 2015. Reconstructing water level in Hoyo Negro, Quintana Roo, Mexico, implications for early Paleoamerican and faunal access. *Quaternary Science Reviews* **124**: 68–83.

Curtis JH, Hodell DA, Brenner M. 1996. Climate Variability on the Yucatan Peninsula (Mexico) during the Past 3500 Years, and implications for Maya Cultural Evolution. *Quaternary Research* **46**: 37–47.

Gabriel JJ, Reinhardt EG, Peros MC *et al.* 2009. Palaeoenvironmental evolution of Cenote Aktun Ha (Carwash) on the Yucatan Peninsula, Mexico and its response to Holocene sea-level rise. *Journal of Paleolimnology* **42**: 199–213.

González González AH, Sandoval CR, Terrazas Mata A *et al.* 2008. The arrival of humans on the Yucatan Peninsula: evidence from Submerged Caves in the State of Quintana Roo, Mexico. *Current Research in the Pleistocene* **25**: 1–24.

González González AH, Terrazas Mata A, Stinnesbeck W *et al.* 2013. The first human settlers on the Yucatan Peninsula: evidence from Drowned Caves in the State of Quintana Roo (South Mexico). In *Paleoamerican Odyssey*, Graf KE, Ketron CV, Waters M (eds). A&M University: College Station; 399–413.

Grant KM, Rohling EJ, Bar-Matthews M *et al.* 2012. Rapid coupling between ice volume and polar temperature over the past 150,000 years. *Nature* **491**: 744–747.

Hammond N. 1992. Preclassic Maya civilisation. In *New Theories on the Ancient Maya*, Danien EC, Sharer RJ (eds). Symposium Series III, University Museum Monograph, **77**. University of Pennsylvania Museum of Archeology and Anthropology: Pennsylvania; 137–144.

Higham TFG, Barton H, Turney CSM *et al.* 2009. Radiocarbon dating of charcoal from tropical sequences: results from the Niah Great Cave, Sarawak, and their broader implications. *Journal of Quaternary Science* **24**: 189–197.

Kambesis PN, Coke JG. 2013. Overview of the controls of eogenetic cave and karst development in Quintana Roo, Mexico. In *Coastal Karst Landforms*, Lace MJ, Mylroie JE (eds). Springer: Dordrecht; 347–373.

Kennett DJ, Breitenbach SF, Aquino VV *et al.* 2012. Development and disintegration of Maya political systems in response to climate change. *Science* **338**: 788–791.

Khan NS, Ashe E, Horton bp *et al.* 2017. Drivers of Holocene sea-level change in the Caribbean. *Quaternary Science Reviews* **155**: 13–36.

Kromer B, Lindauer S, Synal HA *et al.* 2013. MAMS − A new AMS facility at the Curt-Engelhorn-Centre for Achaeometry, Mannheim, Germany. *Nuclear Instruments and Methods in Physics Research Section B: Beam Interactions with Materials and Atoms* **294**: 11–13.

Lefticariu M, Perry EC, Ward WC *et al.* 2006. Post-Chicxulub depositional and diagenetic history of the northwestern Yucatan Peninsula, Mexico. *Sedimentary Geology* **183**: 51–69.

Maràn LE. 1990. *Field Investigations and numerical simulation of groundwater flow in the karstic aquifer of northwestern Yucatan, Mexico*. PhD Dissertation, Northern Illinois University.

McDonald HG, Chatters JC, Gaudin TJ. 2017. A new genus of megalonychid ground sloth (Mammalia, Xenarthra) from the late Pleistocene of Quintana Roo, Mexico. *Journal of Vertebrate Paleontology* **37**: e1307206.

Medina-Elizalde M, Burns SJ, Polanco-Martínez JM *et al.* 2016. High-resolution speleothem record of precipitation from the Yucatan Peninsula spanning the Maya Preclassic Period. *Global and Planetary Change* **138**: 93–102.

Moore YH, Stoessell RK, Easley DH. 1992. Fresh-water sea-water relationship within a groundwater-flow system, northeastern coast of the Yucatan Peninsula. *Ground Water* **30**: 343–350.

Moseley GE, Richards DA, Smart PL *et al.* 2015. Early-middle Holocene relative sea-level oscillation events recorded in a submerged speleothem from the Yucatan Peninsula, Mexico. *The Holocene* **25**: 1511–1521.

Moseley GE, Smart PL, Richards DA *et al.* 2013. Speleothem constraints on marine isotope stage (MIS) 5 relative sea levels, Yucatan Peninsula, Mexico. *Journal of Quaternary Science* **28**: 293–300.

Muhs DR, Simmons KR, Schumann RR *et al.* 2011. Sea-level history of the past two interglacial periods: new evidence from U-series dating of reef corals from south Florida. *Quaternary Science Reviews* **30**: 570–590.

Myloire JE, Carew JL. 2003. Karst development on carbonate islands. *Speleogenesis and Evolution of Karst Aquifers* **1**: 1–21.

Quintana Roo Speleological Society, 2014. 2014. *List of Long Underwater Caves in Quintana Roo Mexico*. Quintana Roo Speleological Society.

Reimer PJ, Bard E, Bayliss A *et al.* 2013. IntCal13 and MARINE13 Radiocarbon age calibration curves 0-50,000 years cal bp. *Radiocarbon* **55**: 1869–1887.

Smart PL, Beddows PA, Coke J *et al.* 2006. Cave Development on the Caribbean coast of the Yucatan Peninsula, Quintana Roo, Mexico. *Geological Society of America Special Paper* **404**; 105–128.

Stinnesbeck SR, Frey E, Olguín JA *et al.* 2017. Xibalbaonyx oviceps, a new megalonychid ground sloth (Folivora, Xenarthra) from the Late Pleistocene of the Yucatán Peninsula, Mexico, and its paleobiogeographic significance. *Paläontologische Zeitschrift* **91**: 245–271.

Stinnesbeck SR, Frey E, Stinnesbeck W *et al.* 2017. A new fossil peccary from the Pleistocene-Holocene boundary of the eastern Yucatán Peninsula, Mexico. *Journal of South American Earth Sciences* **77**: 341–349.

Stinnesbeck W, Becker J, Hering F *et al.* 2017. The earliest settlers of Mesoamerica date back to the late Pleistocene. *PLoS One* **12**: e0183345.

Stoessell RK. 1995. Dampening of transverse dispersion in the halocline in karst limestone in the northeastern Yucatan Peninsula. *Ground Water* **32**: 366–371.

Taylor RE. 2009. Six decades of radiocarbon dating in new world archaeology. *Radiocarbon* **51**: 173–212.

van Hengstum PJ, Reinhardt EG, Beddows PA *et al.* 2010. Linkages between Holocene paleoclimate and paleohydrogeology preserved in a Yucatan underwater cave. *Quaternary Science Reviews* **29**: 2788–2798.

Waelbroeck C, Labeyrie L, Michel E *et al.* 2002. Sea-level and deep water temperature changes derived from benthic foraminifera isotopic records. *Quaternary Science Reviews* **21**: 295–305.

Ward WC. 1985. Quaternary geology of Northeastern Yucatan peninsula. In *Geology and Hydrogeology of the Yucatan and Quaternary Geology of Northeastern Yucatan Peninsula*, Ward WC, Weidie AE, Back W (eds). NOGS Publication: New Orleans; 23–91.

Weidie AE. 1985. Geology of the Yucatan platform. In *Geology and Hydrogeology of the Yucatan and Quaternary Geology of Northeastern Yucatan Peninsula*, Ward WC, Weidie AE, Back W (eds). NOGS Publication: New Orleans; 1–19.
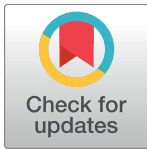
The earliest settlers of Mesoamerica date back to the late Pleistocene

Wolfgang Stinnesbeck[1]*, **Julia Becker[2]**, **Fabio Hering[1]**, **Eberhard Frey[3]**, **Arturo González González[4]**, **Jens Fohlmeister[5]**, **Sarah Stinnesbeck[3]**, **Norbert Frank[6]**, **Alejandro Terrazas Mata[7]**, **Martha Elena Benavente[7]**, **Jerónimo Avilés Olguín[8]**, **Eugenio Aceves Núñez[8]**, **Patrick Zell[9]**, **Michael Deininger[10]**

1 Institut für Geowissenschaften, Universität Heidelberg, Im Neuenheimer Feld 234, Heidelberg, Germany, **2** Institut für Meteorologie und Klimaforschung, Karlsruher Institut für Technologie, H.-v.-Helmholtz-Platz 1, Leopoldshafen, Germany, **3** Staatliches Museum für Naturkunde Karlsruhe, Geowissenschaftliche Abteilung, Erbprinzstrasse 13, Karlsuhe, **4** Museo del Desierto, Carlos Abedrop Dávila 3745, Nuevo Centro Metropolitano de Saltillo, Saltillo, Coahuila, Mexico, **5** Institut für Erd- und Umweltwissenschaften, Universität Potsdam, Karl-Liebknecht-Str. 24, Potsdam, Germany, **6** Institut für Umweltphysik, Universität Heidelberg, Im Neuenheimer Feld 229, Heidelberg, Germany, **7** Área de Prehistoria y Evolución del Instituto de Investigaciones Antropológicas de la Universidad Nacional Autónoma de México (UNAM), Mexico, **8** Instituto de la Prehistoria de América, Carretera federal 307, Solidaridad, Solidaridad, Quintana Roo, Mexico, **9** Hessisches Landesmuseum Darmstadt, Friedensplatz 1, Darmstadt, Germany, **10** UCD School of Earth Sciences, University College Dublin, Belfield, Dublin 4, Ireland

* wolfgang.stinnesbeck@geow.uni-heidelberg.de

Abstract

Preceramic human skeletal remains preserved in submerged caves near Tulum in the Mexican state of Quintana Roo, Mexico, reveal conflicting results regarding ^{14}C dating. Here we use U-series techniques for dating a stalagmite overgrowing the pelvis of a human skeleton discovered in the submerged Chan Hol cave. The oldest closed system U/Th age comes from around 21 mm above the pelvis defining the terminus *ante quem* for the pelvis to 11311 ±370 y BP. However, the skeleton might be considerable older, probably as old as 13 ky BP as indicated by the speleothem stable isotope data. The Chan Hol individual confirms a late Pleistocene settling of Mesoamerica and represents one of the oldest human osteological remains in America.

Introduction

The early settlement of the Americas is a controversial subject. While genetic evidence suggests a Beringian origin of the earliest inhabitants of the continent [1–5], migration routes used for the southward spread of these humans and the timing of human arrival across the Americas are presently reevaluated [6–11]. The hypothesis of a routing across the exposed Bering land bridge through an ice-free corridor between retreating North American glaciers, at about 12.6 thousand years (ky) ago [12], is increasingly challenged by the discovery of evidence predating the earliest North American widespread archaeological complex, the Clovis culture [13–15]. Based on new sites in both North and South America this emerging consensus suggests that people must have arrived in North America as early as 22 ky ago (e.g. [2, 6, 10, 16–18]).

Osteological evidence for early American settlers is scarce and majorly fragmentary, with at present only a few individuals, from North-, Central- and South America, securely predating 11 ky BP [19–24]. Recently, Chatters et al. [25] documented a well-preserved prehistoric skull of a young girl from the submerged Hoyo Negro (Black Hole) sinkhole of the Tulum area, southern Mexico. The individual was ^{14}C-dated to 10976±20 y BP (12910–11750 cal y BP) based on bioapatite from tooth enamel [25]. Previously, González González et al. [20, 21] published a similar ^{14}C age for a human skeleton from the nearby Naharon cave, also located close to Tulum (11670±60 ^{14}C y BP; 13721–13354 y cal BP). These two skeletons belong to the oldest ^{14}C-dated New World *Homo sapiens*. They emphasize the enormous potential of the Tulum system of submerged caves as an archive for the human settlement history in America.

Nevertheless, ^{14}C data from the Tulum submerged caves must be considered with extreme caution because the amount of collagen in both bones and teeth of these individuals is extremely low. This lack of collagen is the result of the exposure of the osteological remains for thousands of years to alternating salt- and fresh water environments [21, 25–27]. In addition, bioapatite is highly susceptible to contamination with fossil carbon resulting in false, mostly older ages [25], apart from a general problem with radiocarbon ages in the tropics [26]. Here we use U-series techniques to date a human skeleton that was discovered in the Chan Hol cave near Tulum (here referred to as Chan Hol II, because there are other prehistoric human skeletons in this cave [21]. The pelvis of this skeleton, previously documented briefly by [21], is overgrown by a stalagmite (CH-7; Fig 1).

Regional setting

The Tulum submerged cave system developed in almost horizontally layered, thick-bedded, shallow-water carbonate bedrock of Neogene ages [28, 29] and is the result of intensive karstification during the Pleistocene [30], caused by a series of sea-level oscillations and changes in the overall hydrology of the area. During Pleistocene stadials, sea-level was more than 100 m below the recent level [31, 32], thus leaving large parts of the cave system dry and accessible. In contrast, during interstadials of the Pleistocene and the early Holocene, between 13 and 7.6 ky BP [33], the karst labyrinth was flooded preserving both archaeological and climate archives. Recent water levels were reached at approximately 4500 y BP [34], although oscillations of up to a few meters are known to have occurred during Maya times [35–37]. The Tulum cave system contains a coastal density stratified aquifer with a freshwater layer overlying penetrating seawater. The depth of the halocline depends on the global sea-level as well as on the thickness of the superimposed freshwater layer and is controlled by the distance to the coastline as well as the amount of precipitation, with a hydraulic gradient across the Yucatan Peninsula (YP) of between 0.5 and 100 mm km^{-1} [38–40]. Water level in the Tulum area is thus approximately equivalent to mean sea-level. Sea-level rise on the YP was predominantly controlled by eustasy, because the peninsula is tectonically stable and glacial isostatic adjustments in this tropical area were minor (e.g. [32, 40, 41]).

The Chan Hol II site and the skeleton

The Chan Hol II skeleton was located at 20˚9.467' N, 87˚34.165' W, 15 km southwest of Tulum, Quintana Roo, southern Mexico, and about 11.5 km from the coast line (Fig 1). It was discovered in a low cave tunnel approximately 1240 m southwest of the Chan Hol sinkhole, at about 8.5 m water depth. The maximum depth of the Chan Hol cave is about 13 m below present day sea-level. The halocline is at a depth of about 9 m. Contrary to most other preceramic human skeletons discovered so far in the submerged caves of Tulum, which have been located at water depths of 20 to >30 m [20, 21, 25], the shallow Chan Hol cave must have been accessible up to
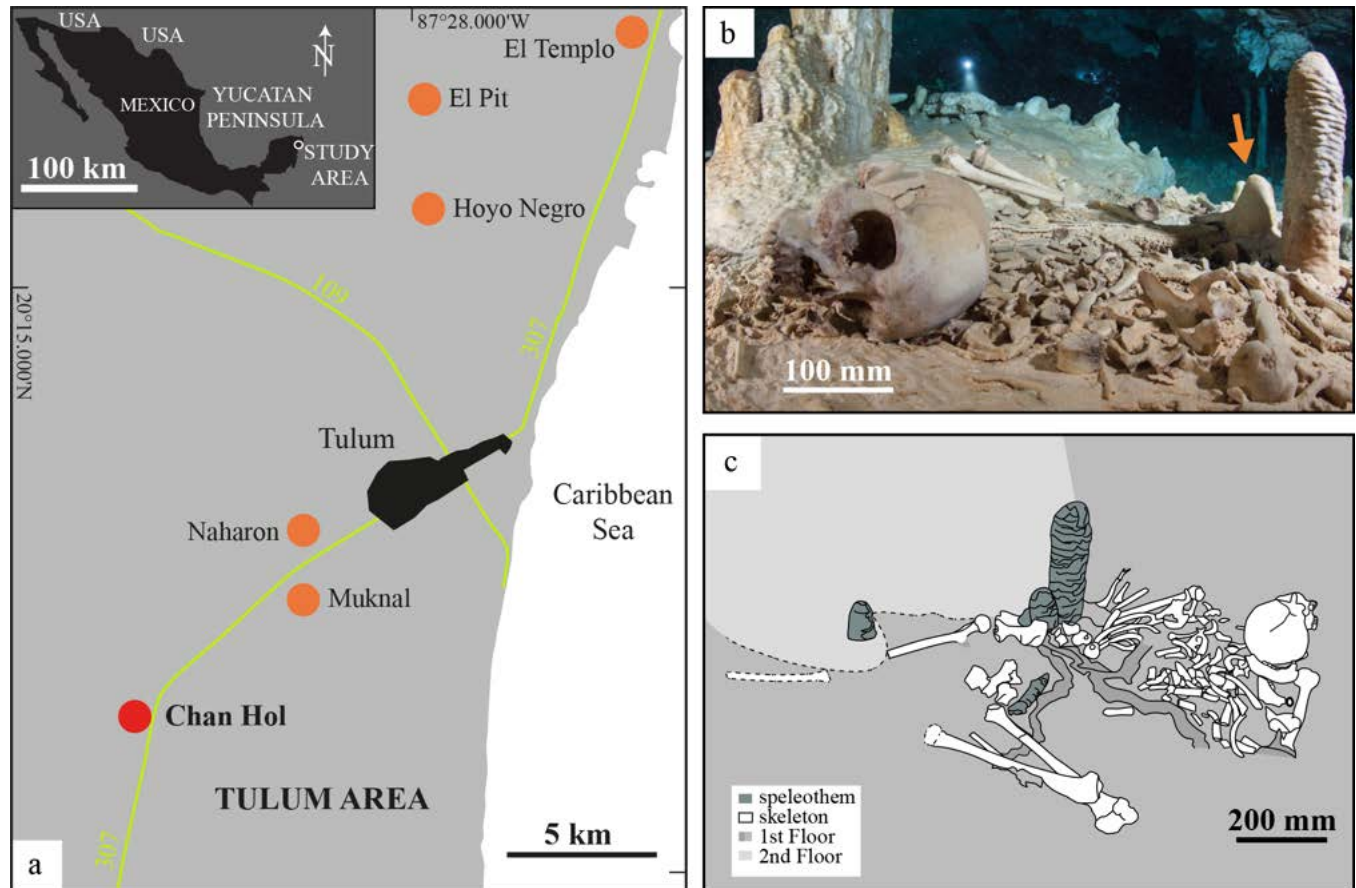
Fig 1. Geographical position and site of the Chan Hol skeleton. *a*: Location of submerged caves containing human skeletal remains dating to >8000 BP in the Tulum area of Quintana Roo, Mexico. Orange dots refer to human remains [20, 21, 25]. The red dot marks Chan Hol II. *b*: The Chan Hol II archaeological site prior to looting. The arrow points to the CH-7 stalagmite analyzed here. (*c*) Reconstruction of the skeleton based on photographs of the site prior to looting. Note that the skeleton was originally complete and almost articulated (Photo courtesy Nick Poole and Thomas Spamberg).

https://doi.org/10.1371/journal.pone.0183345.g001

the middle Holocene [33, 34]. This interpretation is supported by an U/Th age of 5700 y BP of a stalagmite tip from the 8.5 m depth level at Chan Hol. For the nearby Outland cave, [42] postulate a flooding initiating from 8100 cal y BP to a complete inundation at around 6000 cal y BP, which agrees with the results provided here.

Fossil remains were also discovered by us in the extended Chan Hol cave system, though not close to the Chan Hol II skeleton. They include isolated bones of a megalonychid ground sloth, and of extant pacas (*Dasyprocta punctata*), spider monkeys (*Ateles geoffroyi*), peccaries (cf. *Tayassu tajacu*) and white-tailed deer (*Odocoileus virginianus*).

The Chan Hol II skeleton was brought to our knowledge (JAO) in February 2012 through photos in social media. Soon after, the site was vandalized between the 16th and 23rd of March 2012 and all easily collectable bones were stolen. Photographs of the Chan Hol II skeleton prior to this vandalism provide strong evidence that the skeleton must have been more than 80% complete with the skull excellently preserved (Figs 1B, 1C and 2).

The photographs also allow us to reconstruct the original position of the skeleton and indicate that it was preserved nearly articulated (Fig 1B), with the corpse lying on its back. This is concluded from the ribs covering the vertebral column (Figs 1B and 2A) and the position of the left angled femur showing its caudal face (Fig 2B$_1$ and 2C$_1$). The head was inclined slightly
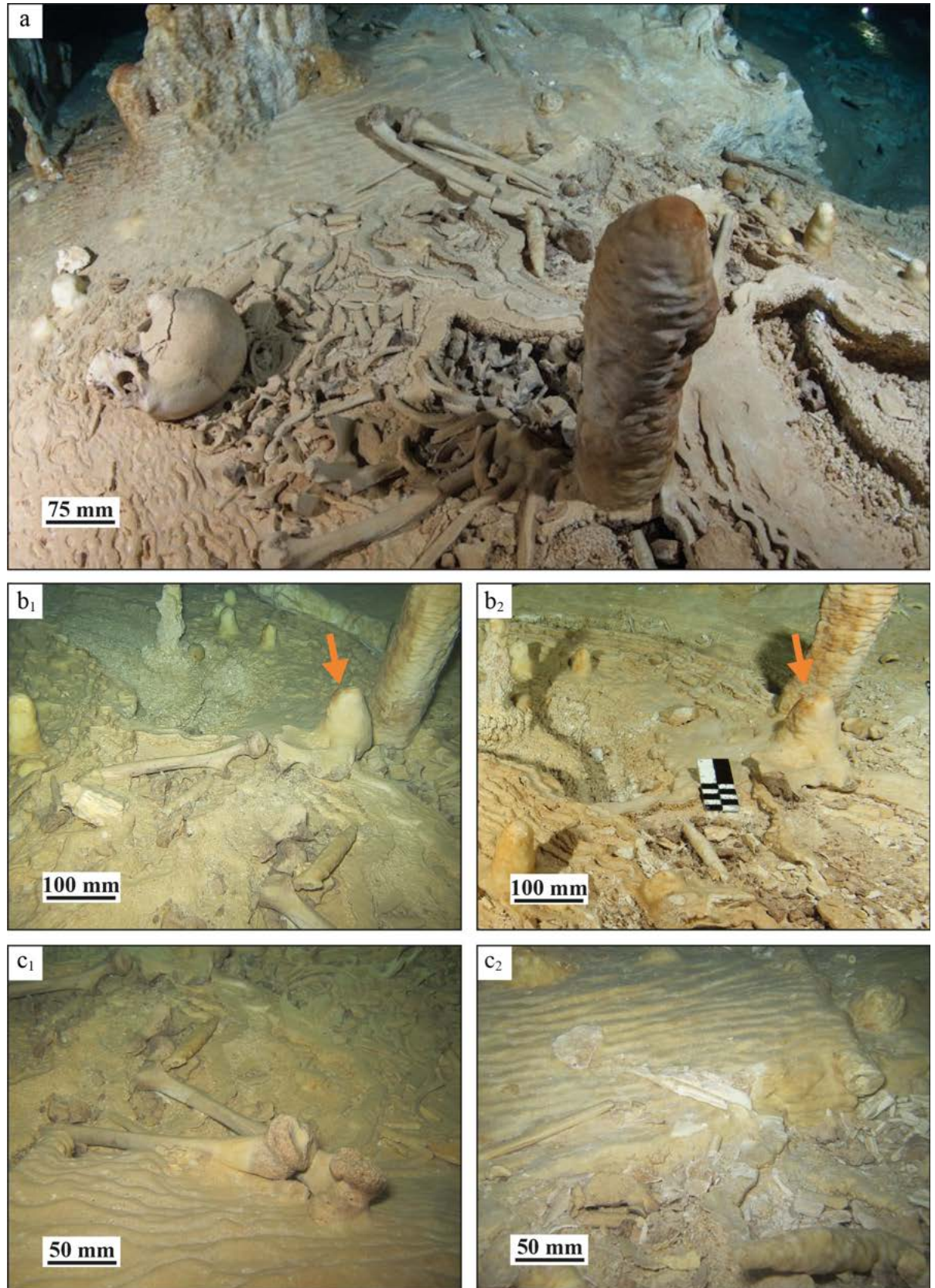
Fig 2. The original Chan Hol II skeleton. Chan Hol II site prior to (*a*, *b₁*.*c₁*) and after (*b₂*, *c₂*) looting. About 10% of the skeleton remained on site, including the pelvis covered by stalagmite CH-7 (red arrows in Figs *b₁* and *b₂*).

https://doi.org/10.1371/journal.pone.0183345.g002

to the right. The right leg was fully extended, while the left leg was flexed at the knee at an angle of 20˚ (Fig 1C). The right femur was still in an articulated position with the pelvis. Based on these data we speculate that the Chan Hol II human died in the cave and that it was not intentionally buried, but there is no positive evidence for this interpretation. Also, no artifacts were identified close to the skeleton on the photographs of the original site or during our collection.

After the looting of Chan Hol II only about 10% of the skeleton remained on site (Fig 2). Among the 155 bone fragments collected there are two auditive labyrinths, an incus, fragments of the temporal, the occipital condyle, four teeth (two incisors, two molars), a mandibular fragment, the hyoid, numerous ribs, carpals and metacarpals, the right pelvis, a patella, tarsals and metatarsals. Embedding of the pelvis in a stalagmite (CH-7) likely prevented this bone from being stolen (Fig 3). Interpretation of sex and age of the Chan Hol II human is speculative, given that our collection only consists of highly fragmentary bones and a few photographs from the original site. We suggest that the individual was a young adult based on the osteophytes in the vertebral bodies, eruption of the third molar in the right half of the mandible, and an epiphysis that was completely fused. Based on the sciatic notch, it was likely a male.

Results

The CH-7 stalagmite

Stalagmite CH-7 is 107 mm high with a mean diameter of ~70 mm (Figs 3 and 4). It encloses the human pelvis of the Chan Hol II skeleton at ~95 mm below the top of the stalagmite. The bone is under- and overlain by brown-colored calcareous stalagmite layers, which are each between 1 and 3 mm thick. The internal section of the stalagmite exhibits a succession of milky white with less frequent dark brown calcitic laminae along its long axis. Layers underlying the 3–5 mm thick solid layers below the bone show a wide range of porosity, resembling lime tufa, and they are thus distinct from the dense overlying layers. In addition, the underlying layers are irregularly flexed and bent, which is not seen directly below and above the pelvic fragment, where the lime layers are substantially more homogenous.

U/Th analysis

17 samples were taken along the growth axis of stalagmite CH-7 and were dated using mass spectrometric measurements of the natural disequilibrium isotope ratios of U and Th [43]. U concentrations of these samples are variable with values ranging between 0.2605 and 12.78 ppm. Initial δ^{234}U values are close to the secular equilibrium with values ranging between -33.7‰ and +23.4‰ (Table 1).

Contamination of the samples with non-carbonate particles is mostly insignificant. This is indicated by ^{232}Th concentrations of <10 ng g-1, introducing only minor age corrections when using the bulk Earth ^{230}Th/^{232}Th ratio as a correlate [43]. Thus, corrected U/Th ages for CH-7 are variable, ranging between 7.82 ky BP and 12.09 ky BP with most data, however, clustering between 9.8 and 12.1 ky (Fig 4A, Table 1).

Only the calculated U-Th ages of samples taken from the stalagmite growth axis above 72 mm can be interpreted as in stratigraphic order and reflecting a closed system behavior. The U-Th ages of samples below the 72 mm cluster reveal much younger ages than those above. This contradicts a quasi linear growth model for the stalagmite. Furthermore, the U-Th age of
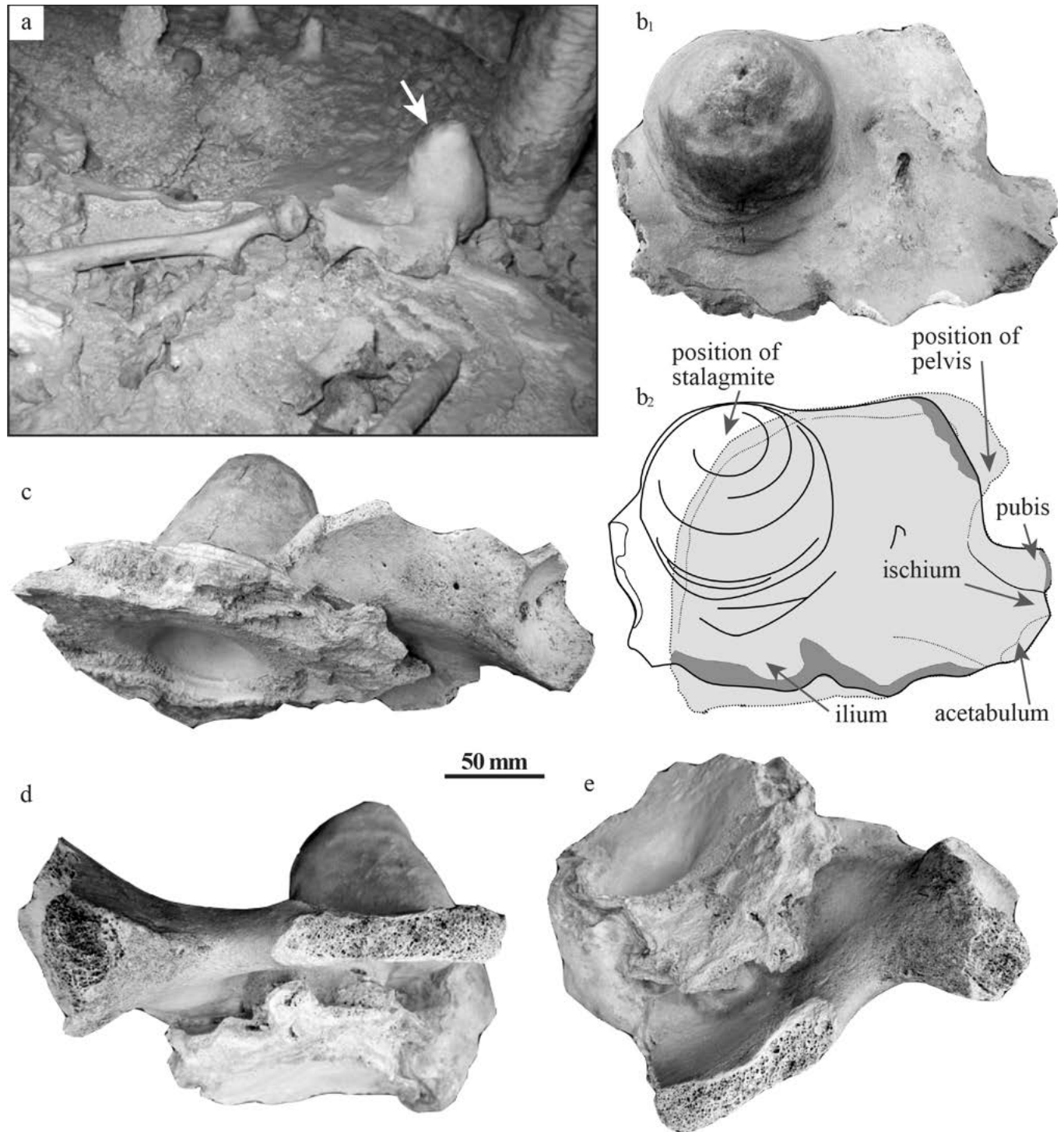
Fig 3. The Chan Hol II pelvis. Different views of the Chan Hol II pelvis within the CH-7 stalagmite. Arrow in Fig 3A points to the CH-7 stalagmite prior to the robbery of the skeleton. Note that the pelvis was then articulated to the right femur. Extraction of collagen and thus ^{14}C age determination failed on the bones of the Chan Hol II individual due to the complete dissolution of organic matter, specifically collagen.

a sample at the left flank of CH-7 at 45 mm distance from top (dft) is much older compared to this linear age-depth relationship (Fig 4B). The relationship between the U concentration and
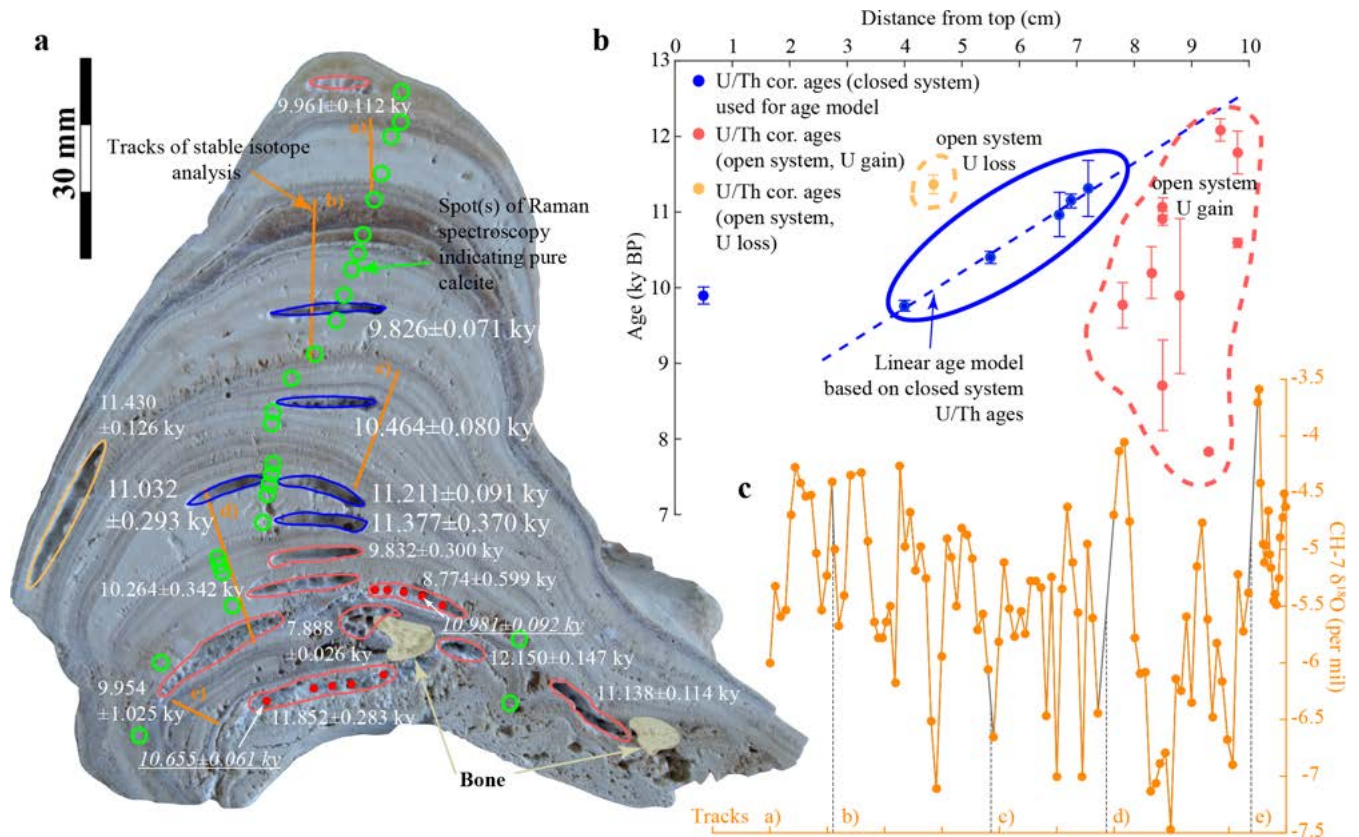
Fig 4. Cross-section of CH-7 and results of U/Th age measurements. Samples for U/Th age measurements are taken along growth layers and are highlighted by coloured frames; red dots within red frames and underlined ages indicate replicates that were drilled into CH-7. Green circles indicate the location where the mineralogy of CH-7 was tested by Raman spectroscopy. Orange lines indicate the location of points, where samples for isotope analysis where taken. (*a*) U/Th ages (y before 2016) above 72 mm from the top (blue) are most likely unaffected by the presence of the encrusted bone and infiltrating seawater, whereas U/Th ages below (red) are likely affected by a re-mineralization processes, infiltrating of the porous encrusted bone, possibly leading to an open-system U series. The orange circle highlights one sample from the steeply sloped and porous edge of the stalagmite, which has been taken to test the possible influence of stalagmite—sea water interactions through time. Please note that ages are given as age before the year of measurement, which is 2016. Ages thus appear older by 66 years than ages given in years BP (i.e. before 1950) as used in Fig 4b and all other figures and text. (*b*) Based on most probable closed-system U/Th ages (see text) it is concluded that the pelvis of the Chan Hol II skeleton dates to a minimum age of 11311±370 y BP. Underlined ages are from samples drilled into the CH-7 stalagmite. All other ages are from samples taken from stalagmite growth layers. (*c*) Stable oxygen isotope profile of CH-7. The labelled section a) to e) corresponds to the isotope tracks shown in (*a*).

https://doi.org/10.1371/journal.pone.0183345.g004

the initial $\delta^{234}U$ isotopy is asymptotic between these two parameters, indicating that $\delta^{234}U$ decreases for higher U concentrations and proximity to the pelvis. The highest U concentrations, which reach 12.8 ppm, and smallest $\delta^{234}U$ values are measured for samples that are adjacent to the pelvis (Fig 5).

It is a matter of fact that the U concentration increases in bones post mortem to as high as 100 ppm (e.g. [44]). This is due to the "soaking up effect" of U into the bone due to diffusion (e.g. [44]). One approach to date a bone or tooth by U-series is to use this effect and to determine the U-isotopes of subsamples across the bone by application of an adsorption-diffusion (D-A) model (e.g. [45, 46]). Because of the porous structure of the pelvis, which makes it likely that pore water in the spongiosa disturbed the original D-A relationship, this approach was not adopted here. Instead, we identified the *termini ante quem* and *post quem*, by using the reliable closed system U/Th ages of carbonate above and below the pelvis from the overgrowing

Table 1. U/Th measurements of the CH-7 stalagmite from Chan Hol cave. Errors are 2σ analytical errors. Corrected [230]Th ages assume an initial [230]Th/[232]Th concentration ratio of 3.8 ± 1.9. Please note that corrected ages are given as age (ka) before the year of measurement, which is 2016. Ages thus appear older by 66 years than ages given in years BP (i.e. before 1950) used in all other figures and text.

Lab. Nr.	238U	Error	232Th	Error	230Th/238U	Error	230Th/232Th	Error	d234U corr.	Error 2σ	Age (uncorr.)	Error	Age (corr.)	Error	d234U (initial)	Error 2σ	dft
	(ng/g)	(abso.)	(ng/g)	(abso.)	(Act.rat.)	(abso.)	(Act.rat.)	(abso.)	(‰)	(abso.) ‰	(ka)	(ka)	(ka)	(ka)	(‰)	(abso.) ‰	cm
7413	411,598	0,044	1,5958	0,0031	0,08787	0,00084	69,50	0,57	-2,7	4,4	10,073	0,096	9,961	0,112	-2,8	4,5	0,5
7412	538,268	0,038	1,6539	0,0032	0,08650	0,00059	86,45	0,49	-3,4	1,5	9,915	0,058	9,826	0,071	-3,4	1,5	4
7411	494,252	0,027	2,0906	0,0034	0,09294	0,00065	67,48	0,31	6,0	1,4	10,585	0,051	10,464	0,080	6,2	1,4	5,5
7295	590,553	0,037	4,6726	0,0086	0,10091	0,00102	39,17	0,17	-3,4	1,2	11,659	0,050	11,430	0,126	-3,6	1,2	4,5
7707	301,23	0,22	1,263	0,025	0,0979	0,0023	71,7	2,2	8,8	5,1	11,151	0,279	11,032	0,293	9,1	5,3	6,7
7410	353,658	0,021	1,2969	0,0030	0,09989	0,00075	83,65	0,54	14,6	1,5	11,315	0,074	11,211	0,091	15,1	1,5	6,9
7708	260,51	0,12	1,205	0,022	0,1011	0,0030	69,3	2,3	10,9	4,7	11,509	0,349	11,377	0,370	11,2	4,9	7,2
7709	331,185	0,089	0,4032	0,0082	0,0877	0,0026	226,0	8,0	15,5	3,2	9,867	0,304	9,832	0,300	15,9	3,3	7,8
7710	344,57	0,14	0,806	0,016	0,0922	0,0029	121,9	4,4	21,7	4,8	10,330	0,340	10,264	0,342	22,3	4,9	8,3
6331	273,543	0,470	0,4578	0,0081	0,15666	0,01037	144,84	9,87	19,9	6,1	8,821	0,613	8,774	0,599	20,4	6,2	8,5
7408	385,346	0,026	1,2234	0,0022	0,09791	0,00073	94,96	0,62	15,3	2,1	11,071	0,078	10,981	0,092	15,8	2,2	8,5
6282	288,507	0,433	0,3907	0,0043	0,08857	0,00854	200,61	19,39	16,3	14,3	9,992	0,996	9,954	1,025	16,8	15,0	8,8
7296	1386,210	0,070	10,3090	0,0159	0,09703	0,00093	40,07	0,13	-17,4	0,6	11,356	0,034	11,138	0,114	-18,0	0,6	8,5
7409	12779,036	0,703	9,4110	0,0209	0,06755	0,00021	282,14	1,01	-32,9	0,4	7,910	0,023	7,888	0,026	-33,7	0,4	9,3
6321	706,188	1,202	0,6430	0,0062	0,10457	0,00233	349,33	8,43	16,6	3,9	11,877	0,280	11,852	0,283	17,2	4,0	9,8
7407	1800,994	0,102	5,6876	0,0109	0,09248	0,00051	90,00	0,37	-13,1	0,5	10,747	0,043	10,655	0,061	-13,5	0,6	9,8
6396	712,213	1,135	2,2923	0,0107	0,10764	0,00112	103,66	1,16	22,7	3,9	12,240	0,139	12,150	0,147	23,4	4,0	9,5

https://doi.org/10.1371/journal.pone.0183345.t001

stalagmite, respectively. While the stalagmite base around the pelvic bone fragment is characterized by a complex morphological texture, as well as age which complicate the determination of the terminus *post quem* and the use of these ages, determination of the terminus *ante quem* is possible from ages above the pelvis. These show a linear age-depth model and likely no influence on the U- and Th-system (Fig 5).

The exceedingly porous carbonate texture adjacent to and below the pelvis is likely influenced by U diffusion, as indicated by extremely high U concentrations. These high U concentrations result from an opening of the uptake series system, for which the source of U is unlikely seawater because the δ^{234}U values stay in close ranges. Hence, it could be that U is redistributed from the very local environment resulting in variable ages, such as the very young age of the sample in direct contact with the bone. Most likely, this effect is restricted to the lowermost section of the stalagmite below 72 mm (dft). We cannot exclude the possibility that samples above 72 mm (dft) are also influenced by U-exchange, but the low variability and quasi linear age-depth relationship suggests that this effect is likely negligible and within ranges of standard age-uncertainty. Based on U/Th ages above 72 mm of the CH-7 stalagmite the minimum *terminus ante quem* of the pelvis is 11311±370 y BP.

Regarding the significantly older age of the sample at the flank of CH-7, one must assume U loss possibly due to the mineralogical change from presumably aragonite to calcite, as is indicated by the needle like texture and present day calcite configuration.

Stable isotope analysis

Stable oxygen and carbon isotope values, δ^{18}O and δ^{13}C (expressed in the δ-notation relative to V-PDB), vary from -3.59‰ to -7.47‰ and from -5.22‰ to -11.61‰, respectively (Fig 6; S1 Table).

A significant change in the δ^{18}O profile of CH-7 occurs in the lower part of CH-7 between 100 mm and 70 mm dft of CH-7. The δ^{18}O values vary by as much as 3.87‰ and show a w-
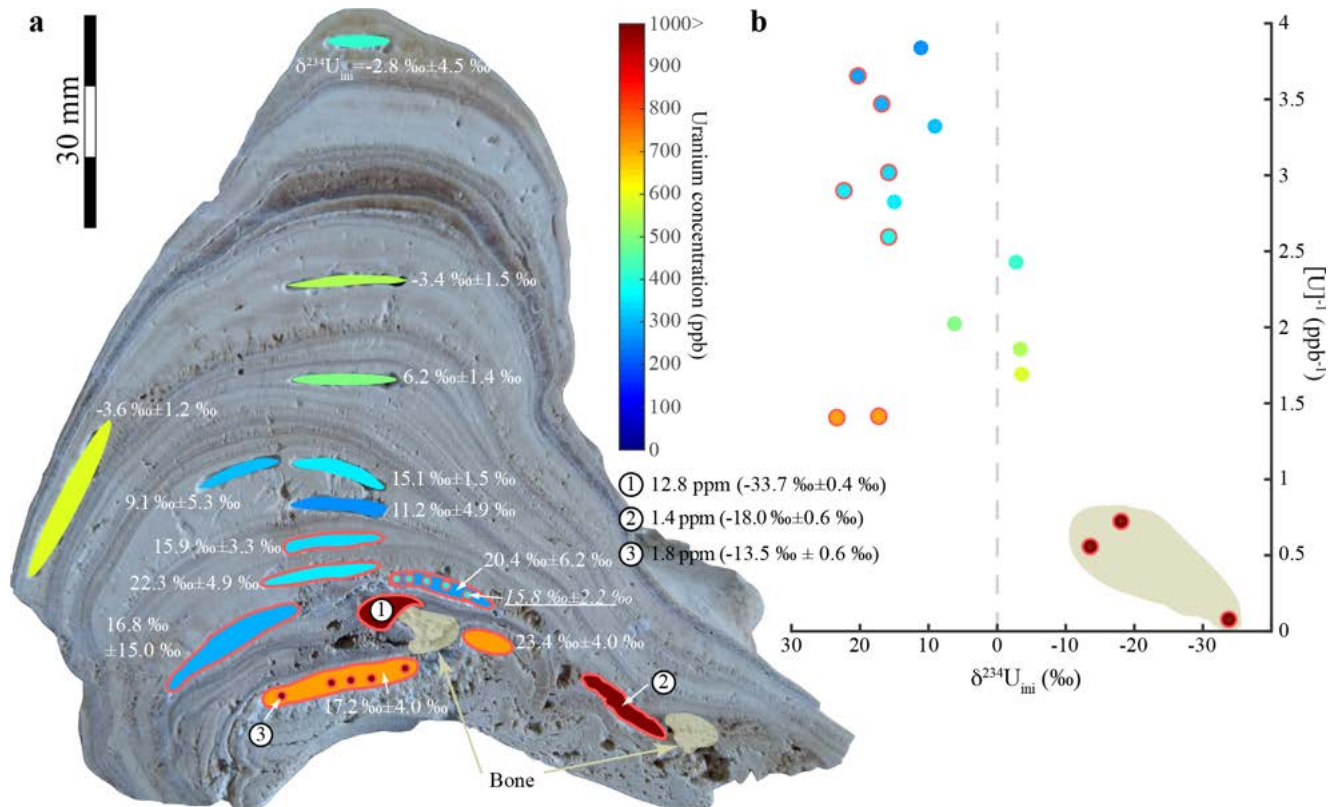
Fig 5. Uranium concentrations and initial δ²³⁴U values of CH-7. The U concentration of samples analysed by us is illustrated by warm/cool coloured frames indicating higher/lower U concentrations (a) Samples 1–3 present the highest U concentrations and lowest initial δ²³⁴U values. (b) The relationship between the U concentrations and the initial δ²³⁴U values show that samples with highest U concentrations are generally low in initial δ²³⁴U. This is likely caused by the influence of the pelvic bone, causing a U gain and at the same time a decrease in ²³⁴U/²³⁸U.

shape in this section. Above 70 mm dft, the δ¹⁸O profile of CH-7 is more variable but a trend towards higher values is identified towards the top of CH-7 being -5.41‰ on average, with a 1-sigma standard deviation of 0.69‰. Internal δ¹³C variability is less compared to that of the δ¹⁸O. Heaviest δ¹³C values occur at the bottom and top-most isotope tracks, with lighter δ¹³C values in between.

Age assessment

Our Chan Hol (CH-7) isotope record indicates a very pronounced 4‰ shift across tracks c and d (Fig 6), from the most positive (-3.5‰) δ¹⁸O values at 95 mm to the most negative (-7.5‰) δ¹⁸O values at 80 mm and back to -4‰ at around 11.3 ky BP, the oldest open system U-Th date. This near 4‰ excursion presents a significant shift in the isotopic signal.

Our oldest open system U/Th date of 11311±370 y BP coincides with the end of the Younger Dryas (YD), a time episode characterized by a brief return to near glacial conditions interrupting the general amelioration of climate conditions at the last deglaciation [47–50]. The ~ 4‰ shift in our CH-7 δ¹⁸O record occurs across a 21 mm interval below this last U/Th date, and hence potentially falls into the time interval of the YD. Seen the amplitude and signature of the CH-7 δ¹⁸O signal, it seems likely that the YD, or part of the YD time interval, is displayed in our Chan Hol speleothem. As we do not have an absolute (U/Th) date in this lower part of the speleothem we can only, as a first guess, assume a continuous growth rate for the CH-7 stalagmite in the interval below our last independent U/Th date and linearly extrapolate
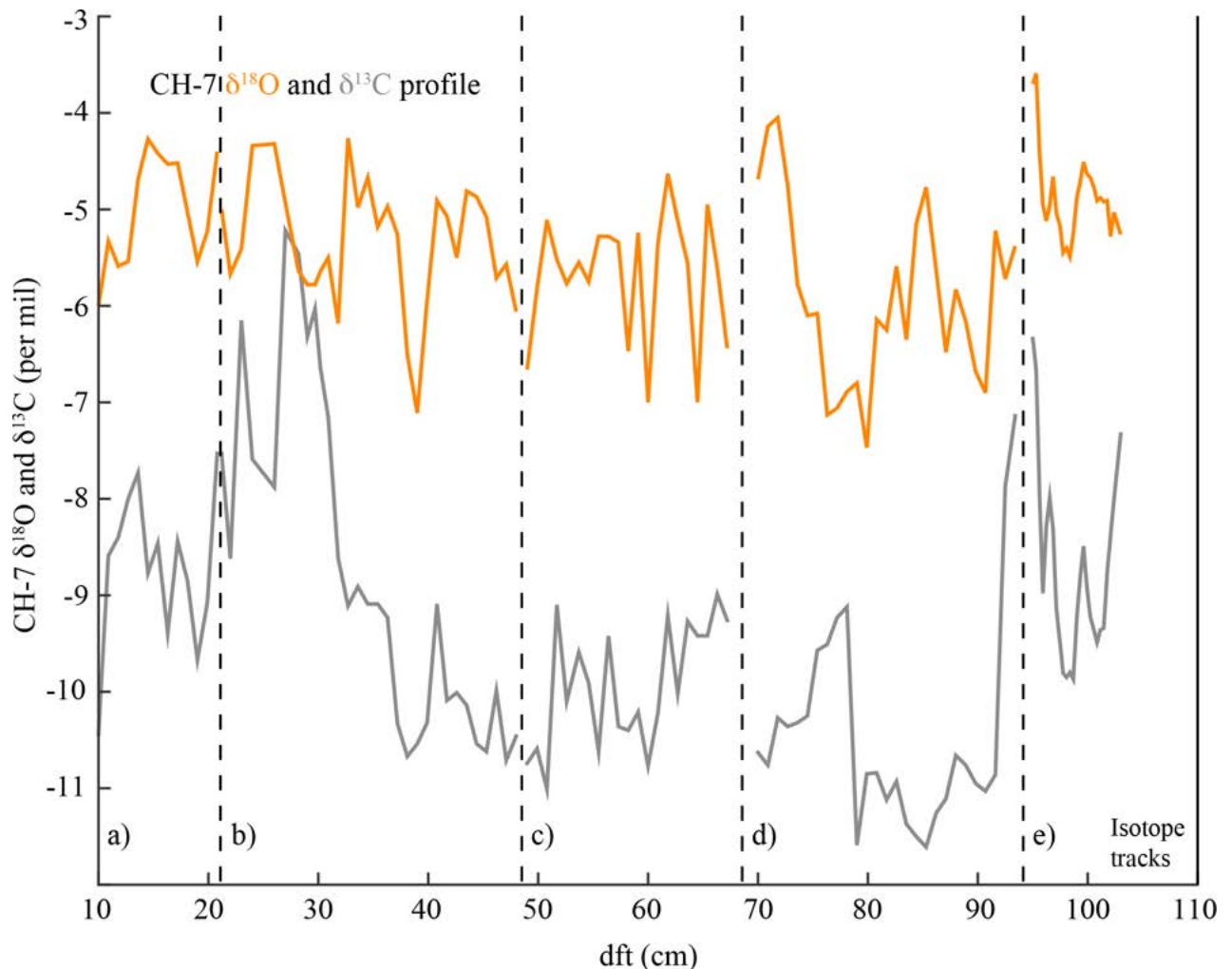
Fig 6. Stable isotope profile. Stable oxygen and carbon isotope profile of CH-7 (δ^{18}O and δ^{13}C, orange and grey curve, respectively).

our age model back in time. We can then compare our stable isotope record of CH-7 to other well-known independently dated climate archives from a similar time interval and area.

Unfortunately, speleothem records covering the YD interval are rare from the wider Caribbean region. The closest records come from New Mexico and Arizona (Fig 7A) and have been discussed in detail by [51–53]. These precipitation sensitive speleothem records have been U/Th dated and interpreted to reflect changes in the intensity of the North American monsoon region during the YD time interval, in concert with global climate as recorded in Greenland Ice cores [54, 55], Asian speleothems (Fig 7B; [56]), or Cariaco Basin (off Venezuela) Ti % (Fig 7C; [57]). In terms of signature, absolute values and amplitude our Yucatan δ^{18}O record resembles the American speleothem records and hence reflects a similar climate signal. It further resembles the global climate signal during the YD time interval as reflected in the Yamen speleothem (China) δ^{18}O and Caricao Basin Ti % records (Fig 7B and 7C). Therefore, we are confident that the Chan Hol stalagmite has indeed grown throughout the YD time interval.

Confirmation for this age assessment comes from the comparison of the CH-7 carbon isotope record with radio carbon dated Lake Peten Itza (Guatemala) magnetic susceptibility [58] (Fig 7D). Variations in the Lake Peten Itza magnetic susceptibility record reflect changes in

the sediment lithology, with high values associated with clay-rich horizons and low values associated with gypsum deposits, thereby representing episodes of high and low lake levels, respectively [61].

Speleothem carbon isotope values depend on the amount of local rainfall and infiltration of vegetation cover. During the late Pleistocene, the Tulum area was dominated by 'steppe' and possibly looked like the Irish Burren today [62]. The dense tropical forest that dominates the present-day landscape only developed around 9000 years ago [63–65]. Due to the low sea-level, local rainfall at the time of CH-7 growth would have immediately infiltrated the epikarst, with water level in the karst caves dependent on the amount of rainfall. Consequently, the CH-7 δ^{13}C record should reflect the availability of CO_2 (δ^{13}C$\approx$-10 per mil) during the dissolution of limestone in the epikarst (δ^{13}C$\approx$0 per mil), with decreasing (increasing) δ^{13}C of CH-7 reflecting lower (higher) infiltration, respectively. In this way, both the Peten Itza and CH-7 records reflect changes in water runoff into the lake and cave, respectively, with lowest run off signals during the early YD. This is also similar to the Cariaco Basin Ti % record, where low Ti percentages reflect low river runoff into the basin at that time (Fig 7C; [57]).

Although the proxy signals of both Peten Itza and CH-7 contain a certain portion of nonlinear response to vegetation cover retaining water and CO_2 dissolution levels in the epikarst and lake water, respectively, the agreement between the two different records is good. Both records show coeval episodes of low lake stand (Peten Itza) and infiltration (CH-7), and high lakes stand and infiltration, respectively, across the growth interval of CH-7.

A last confirmation for our age assessment comes from comparison of the CH-7 oxygen isotope record with the detrended residual Δ^{14}C data [59–60]. This comparison, presented in Fig 7E, is inspired by [51] who showed a correlation between the δ^{18}O variability of Pink Panther cave and the detrended residual Δ^{14}C data, postulating a linkage of North American monsoonal precipitation and solar forcing through modulation in the Walker circulation, and the tropical Pacific Decadal Oscillation and El Niño–Southern Oscillation systems [51]. From the visual inspection, CH-7 δ^{18}O and detrended residual Δ^{14}C data show a remarkable similarity, with episodes of increased solar activity expressed as negative Δ^{14}C, well correlated with positive δ^{18}O anomalies in CH-7. Correlation is reasonably high (0.48 for inversed δ^{18}O) considering the different nature of the proxies and the independence of the age models.

To summarize, we are confident that our age assessment is reasonably correct and that the YD time interval is indeed recorded in our CH-7 speleothem. This rises the age of the pelvis from the U/Th derived *terminus ante quem* of 11311 y BP to an age as old as 13 kyr BP (Fig 7F).

Discussion

The Chan Hol II individual was discovered at about 1240 meters away from the nearest modern entrance, the Chan Hol sinkhole. The skeleton disarticulated slightly during the final stages of decomposition and, probably again, during the early to middle Holocene flooding of the cave, but most bones still lie close to their original anatomical position. Even small bones, like auditory ossicles, hyoid, or ungual phalanges are present. The person must thus have died in the cave at a time when the cave floor was dry [21]. The decay of the carcass occurred *in-situ*. Growth of the CH-7 stalagmite began after the decay of the Chan Hol II individual was complete. This interpretation is consistent with the macroscopic sequence of basal-most stalagmite laminae. At that time, the drip point was located near the margin of the pelvis (Fig 5). The calcite layer precipitated by the lateral run-off dripping water embraced the pelvic bone from laterally to ventrally, with its ventral surface coalescent with the stalagmite, due to flow extension below the pelvis. This close overgrowth could not have taken place with bones covered by soft
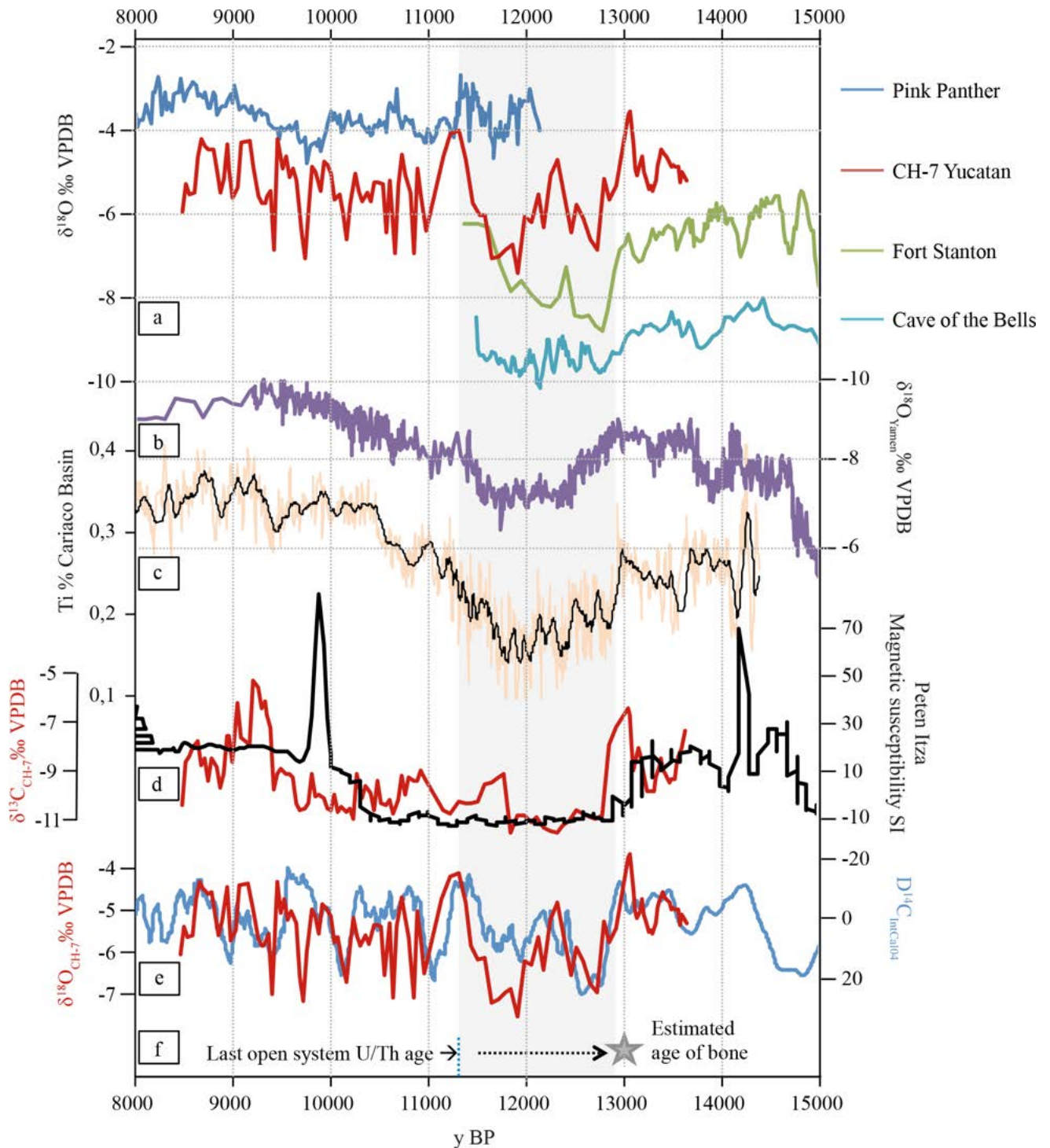
Fig 7. Comparison of oxygen isotope and other environmental data across the Pleistocene-Holocene boundary. a) Speleothem $\delta^{18}O$ data (blue, red, green and light blue curve, respectively) of Pink Panther cave, Guadalupe Mountains, New Mexico, USA [51], Chan Hol cave (this study), Fort Stanton cave, New Mexico, USA [52] and Cave of the Bells, Arizona, USA [53]. b) China deglacial speleothem oxygen isotope data from Yamen Cave, Guizhou Province, China, [56] on a reversed scale; c) Cariaco Basin, Venezuela, Ti % (orange curve) overlain by moving average (black curve) [57]; d) comparison of Peten Itza magnetic susceptibility (black curve) [58] and CH-7 $\delta^{13}C$ data (red curve); e) Covariation of CH-7 $\delta^{18}O$ record (red line) and residual $\Delta^{14}C$ (blue line) 1000 year moving average of IntCal04 [58–60]. Scales for two records are in opposite direction to each other to show negative correlation. Note that age models of both records are completely independent from each other; f) last closed system U/Th date (blue vertical stippled line). Extrapolation (black stippled arrow) of age model by assuming constant speleothem growth rate and interpretation of CH-7 climate signal estimates the age of the bone to around 12.8 ky (grey asterisk). All data are presented in years BP. Grey shaded interval indicates the Younger Dryas time episode.

https://doi.org/10.1371/journal.pone.0183345.g007

tissue. The porous tufa-like layer conforming the basis of the stalagmite must therefore have formed at that time, when the cave was dry and the pelvis completely exposed on the cave floor for an unknown amount of time.

No data are at hand to define the amount of time that elapsed between the death of the individual and initial growth of the CH-7 stalagmite, nor the lapse needed for maceration and decay of this individual under the environmental conditions prevailing in the cave during the YD. Corpses decaying in caves are mostly decomposed by fungi and insects. Both are not able to move bones [66]. According to [66], a 25 kg kangaroo carcass, deposited in a cave in southern Australia, is completely decayed after a little more than 1000 days. For the complete decay of a human carcass with a body mass of 60 kg one would expect a minimum decay time of 2000 days as an estimate. Our U/Th datum of 11311±370 y BP at 72 mm of the CH-7 stalagmite and even the 13 ky BP age assignment resulting from the speleothem stable isotope record must therefore be regarded as minimum ages of the Chan Hol II skeleton.

Validation of our age assessment has been done by comparison of our CH-7 stable isotope data with different independently dated climate records (Fig 7). We stress, that no age correlation or wiggle matching has been carried out to any of the records. All we did was to apply the linear age model from the closed system U/Th dates to the lower part of the stalagmite.

The comparison of our CH-7 stable isotope record with other climate records indicates that the Chan Hol speleothem indeed covers the Younger Dryas time interval (Fig 7). In terms of amplitude and absolute value, the Yucatan $\delta^{18}O$ record fits well the $\delta^{18}O$ signal of speleothem records of New Mexico [51–52] and Arizona [53] that have been demonstrated to record the global climate signal of the YD. The American speleothem $\delta^{18}O$ records have further been interpreted to reflect changes in the contribution, intensity and source of winter versus summer precipitation, the latter being fed from the Caribbean, and these changes have been linked to changes in the positioning of the polar jet stream related to the still northerly expansion of ice sheets causing modulation of winter storm tracks across the continent [52–53]. On the other hand, the relationship between the Pink Panther cave oxygen isotope record and solar forcing has been explained through changes in the Walker circulation and the Pacific Decadal Oscillation and El Niño–Southern Oscillation systems [51] but shows a significant similarity to Northern Hemisphere records. Finally, the climate signals at Peten Itza and Cariaco Basin have been discussed to reflect swings in the position of the ITCZ [57, 58].

In the end, these climate components are all linked to a complex system [67] and likely influenced our Chan Hol record. However, it is beyond the scope of this paper to disentangle the different components of this complex climate system. This deserves a thorough discussion in a separate paper. The focus of the current paper is on the dating of the Chan Hol II skeleton and we can confidently state that with the U/Th dates and the stable isotope record at hand we can approximate the age of the Chan Hol II individual to ~13 ky BP.

Conclusions

Speleothem (U/Th) age data indicate that the Chan Hol underwater cave south of Tulum, state of Quintana Roo, Mexico, was accessed by humans during the Younger Dryas period, i.e. during the late Pleistocene. This is indicated by a minimum speleothem age of 11311±370 y BP of a stalagmite encrusting and overgrowing the pelvic bone of an almost articulated human individual in this cave. The age was measured at 72 mm depth from the top of the CH-7 stalagmite, at about 21 mm above the pelvis and 33 mm above the base of the stalagmite, while ages in the immediate bone vicinity are altered due to uranium dissolution. 11311±370 y BP is thus a minimum age for the skeleton. Based on a linear growth model and extension of growth rates from the well-dated upper part of the CH-7 stalagmite to its lower portion and base, the age of the

Chan Hol II human rises to ~13 ky BP. The Chan Hol II skeleton thus represents one of the oldest directly dated osteological heritage of a human from the American continent. Age of the Chan Hol II human equals that of other skeletons in the Tulum cave system (e.g. Naia, Najaron), thus emphasizing the importance of these caves for early human settlement in the Americas [20, 21, 25].

Methods

The CH-7 stalagmite consists of only calcite (no aragonite was detected), as was confirmed by 25 measurements using Raman spectroscopy techniques at the Institute of Earth Sciences at Mainz University, Germany (Figs 5 and 8). For Raman spectroscopy a Horiba Jobin Yvon was used that was connected to an Olympus BX41 microscope using a Nd-YAK laser at a wavelength of 532.12 nm (hole = 400 μm; slit = 100 μm).

U/Th dating

Samples for U/Th-dating were drilled from stalagmite CH-7 using a Dremel Fortifex precision tool, 1 mm in diameter. The samples were taken along laminar growth layers to minimize mixing of material of different age and thus age uncertainties. Individual sample thickness is typically 2 mm (in growth direction), with an individual sample weight of between 100 and 150 μg. All samples (carbonate powder) were prepared for measurements in the clean laboratories at the Institute of Earth Sciences and Institute of Environmental Physics, both Heidelberg University, by wet-column chemistry using UETVA® resin. All samples were spiked using a Th-U multi-spike. U- and Th-isotopes were analyzed using ICP-MS (Thermo Finnigan Neptune Plus and iCAP (RQ), respectively) at the Institute of Environmental Physics at Heidelberg University. Details for sample preparation and U- and Th-isotope analysis are documented in [69]. Ages were calculated using the half-lives of both elements as determined by [70]. Detrital correction was performed using a bulk Earth value of 3.8 ± 1.9. Age uncertainties are quoted at the 2-σ level and do not include half-life uncertainties. The reference year for all ages given in the study is 1950 AD (i.e. 0 BP).

U/Th ages and the growth of the CH-7 stalagmite

U/Th ages in the upper 72 mm of the CH-7 stalagmite are approximately consistent with the macroscopic sequence of individual laminae growing onto each other (Fig 4). The basal-most layer was dated to 11363±304 y BP. In this layer, the drip point (the highest point of each stalagmite layer) is located at about 20 mm lateral to the pelvis (Fig 4). The layer embraces the bone from lateral to ventral and its ventral surface is coalescent with the stalagmite. The dripping water accumulated lateral of the bone and ran off diffusing laterally, with the flow expanding below the pelvis. To do so, the body must then have been completely decayed already. In a second step, calcium carbonate-rich water, dripping from the ceiling, accumulated next to the pelvis and enclosed the bone completely. The porous tufa-like layer conforming the base of the stalagmite and dated to >11363 y BP, must therefore have formed when the cave was dry and the carcass already completely skeletonized. This is concluded from the spongy carbonate crust that formed beneath the pelvis, at a time when this bone blank of soft tissue.

C and O isotope analysis of CH-7 stalagmite

Stable oxygen and carbon isotope samples were micro-milled and measured at the Institute for Earth Sciences (GeoZentrum Nordbayern), Friedrich-Albert-Universität Erlangen,
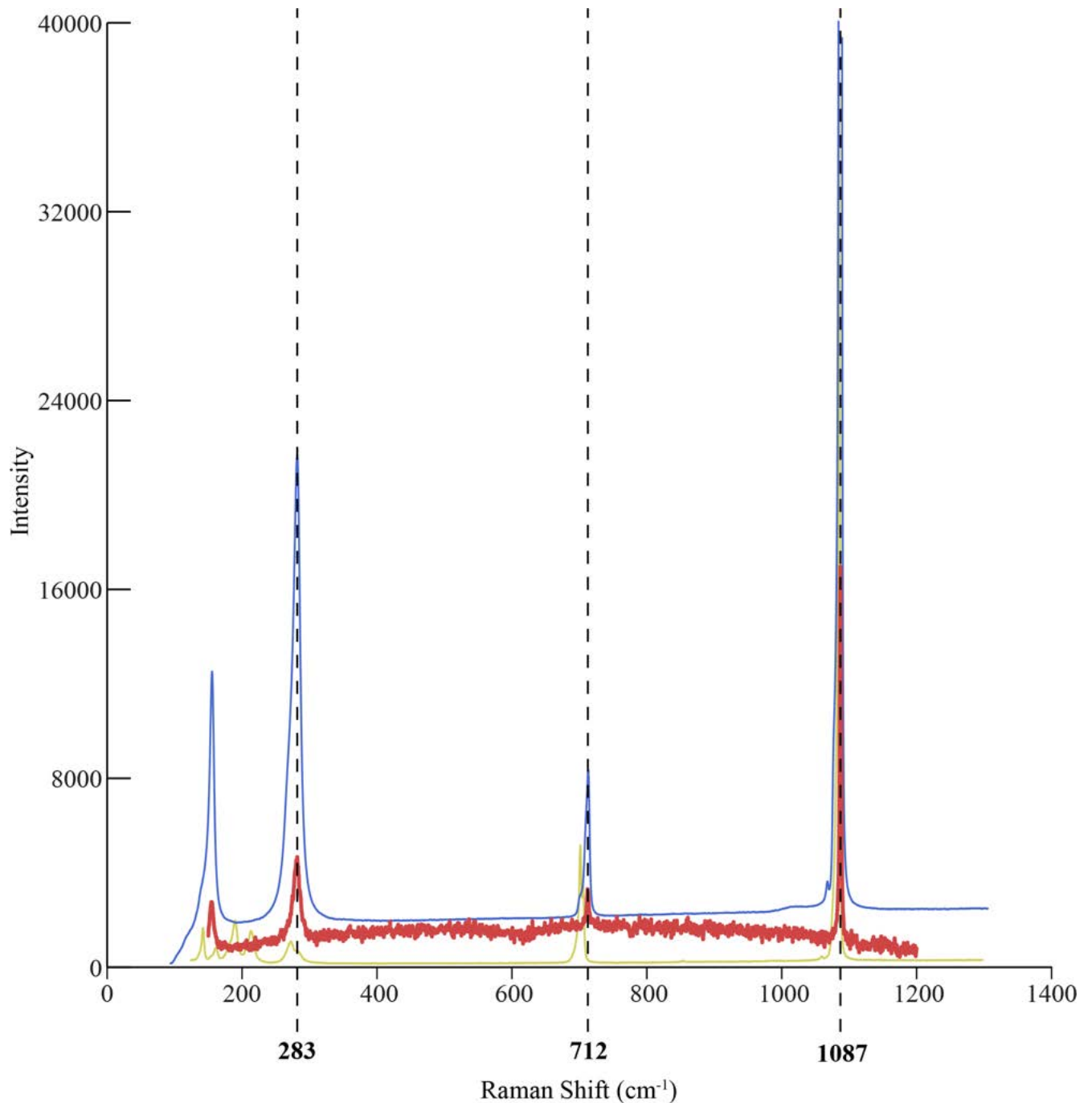
Fig 8. Raman spectrum of CH-7. Values measured are compared to Raman spectra of reference calcite and aragonite (RRUFF database; [68]). Comparison shows that CH-7 consists of calcite.

Germany. A total of 117 data points was sampled along five transects, each along the growth axis of stalagmite CH-7 (Figs 4 and 6). A minimum of 0.05 to 0.1 mg CaCO$_3$ was analyzed to ensure precise measurement. Carbonate powders were reacted with 100% phosphoric acid at 70˚C, using a Gasbench II connected to a ThermoFisher Delta V Plus mass spectrometer All values are reported in per mil relative to V-PDB through international standard

NBS19. Reproducibility was monitored by international and in house laboratory standards and was 0.5‰ and 0.8‰ for δ^{13}C and δ^{18}O, respectively.

Supporting information

S1 Table. Stable isotope (δ^{13}O, δ^{18}O) measurements of the CH-7 stalagmite from Chan Hol cave.
(DOCX)

Acknowledgments

Material

The Chan Hol II osteological material, including the CH-7 stalagmite encrusting pelvic remains, is housed at the Área de Prehistoria y Evolución of the Instituto de Investigaciones Antropológicas at the Universidad Nacional Autónoma de México (UNAM), in Mexico City. Here the material is publicly deposited and accessible by others in a permanent repository. Specimen numbers: Chan Hol II human: PQR2012-CHAN HOL-2; the Chan Hol stalagmite is housed under the number CH-7. The material was recovered from the Chan Hol cave sytem at 20˚9.467' N, 87˚34.165' W, 15 km southwest of Tulum, Quintana Roo, southern Mexico, and about 11.5 km from the coast line (Fig 1).

Permits

All necessary permits were obtained for the described study, which complied with all relevant regulations from Instituto Nacional de Antropología e Historia, Mexico (INAH permit number: C.A. 401.B (4)19.2011/36/1723).

Author Contributions

Conceptualization: Eberhard Frey, Arturo González González.

Data curation: Fabio Hering, Sarah Stinnesbeck, Norbert Frank, Alejandro Terrazas Mata, Martha Elena Benavente, Jerónimo Avilés Olguín, Eugenio Aceves Núñez.

Formal analysis: Julia Becker, Fabio Hering, Jens Fohlmeister, Norbert Frank, Michael Deininger.

Funding acquisition: Wolfgang Stinnesbeck, Eberhard Frey, Arturo González González, Jens Fohlmeister.

Investigation: Wolfgang Stinnesbeck, Arturo González González, Jens Fohlmeister, Sarah Stinnesbeck, Alejandro Terrazas Mata, Martha Elena Benavente, Jerónimo Avilés Olguín, Eugenio Aceves Núñez.

Methodology: Julia Becker, Fabio Hering, Jens Fohlmeister, Norbert Frank, Alejandro Terrazas Mata, Martha Elena Benavente, Eugenio Aceves Núñez, Michael Deininger.

Supervision: Wolfgang Stinnesbeck, Norbert Frank.

Visualization: Fabio Hering, Sarah Stinnesbeck, Patrick Zell.

Writing – original draft: Wolfgang Stinnesbeck, Julia Becker, Fabio Hering, Eberhard Frey, Sarah Stinnesbeck, Michael Deininger.

Writing – review & editing: Wolfgang Stinnesbeck, Julia Becker, Patrick Zell, Michael Deininger.

References

1. Kemp BM, Malhi RS, McDonough J, Bolnick DA, Eshleman JA, Rickards O, et al. Genetic Analysis of Early Holocene Skeletal Remains from Alaska and its Implications for the Settlement of the Americas. Am J Phys Anthropology.2007; 32: 605–621.

2. Jenkins DL, Davis LG, Stafford TW, Campos PF, Connolly TJ, Cummings LS, et al. Geochronology, archaeological context, and DNA at the Paisley Caves. In: Graf KE, Ketron CV, Waters M, editors. Paleoamerican Odyssey, Texas, A&M University, Center for the Study of the First Americans; 2013. pp. 485–510.

3. Rasmussen M, Anzick SL, Waters MR, Skoglund P, DeGiorgio M, et al. The genome of a late Pleistocene human from a Clovis burial site in western Montana. Nature. 2014; 506: 225–229. https://doi.org/10.1038/nature13025 PMID: 24522598

4. Raghavan M, Steinrücken M, Harris K, Schiffels S, Rasmussen S, DeGiogio M, et al. Genomic evidence for the Pleistocene and recent population history of Native Americans. Science.2015; 349: aab3884. https://doi.org/10.1126/science.aab3884 PMID: 26198033

5. Hoffecker JF, Elias SA, O'Rourke DH, Scott GR, Bigelow NH. Beringia and the global dispersal of modern humans. Evolutionary Anthropology: Issues, News, and Reviews.2016; 25(2): 64–78.

6. Goebel T, Waters MR, O'Rourke DH. The Late Pleistocene Dispersal of Modern Humans in the Americas. Science.2008; 319: 1497–1502. https://doi.org/10.1126/science.1153569 PMID: 18339930

7. Stanford DJ, Bradley DA. Across Atlantic Ice: The Origin of America's Clovis Culture. U California Press, Berkeley; 2012. 336 pp.

8. Erlandson JM, Rick TC, Braje TJ. Paleoindian seafaring, maritime technologies, and coastal foraging on California's Channel Islands. Science.2011; 33: 1181–1185.

9. Erlandson JM, Braje TJ, McGill KM, Graham MH. Ecology of the Kelp Highway: Did Marine Resources Facilitate Human Dispersal From Northeast Asia to the Americas? J I Coast Archaeol.2015; 10(3): 392–411.

10. Dillehay TD, Ocampo C, Saavedra J, Oliveira Sawakuchi A, Vega RM, Pino M, et al. New archaeological evidence for an early human presence at Monte Verde, Chile. PLoSOne.2015; 10, e0141923 (2015).

11. Pedersen MW, Ruter A, Schweger C, Friebe H, Staff RA, Kjeldsen KK, et al. Postglacial viability and colonization in North America's ice-free corridor. Nature.2016; 537. https://doi.org/10.1038/nature19085 PMID: 27509852

12. Heintzman PD, Froese D, Ives JW, Soares AE, Zazula GD, Letts B, et al. Bison phylogeography constrains dispersal and viability of the Ice Free Corridor in western Canada. Proceedings of the National Academy of Sciences.2016; 113(29), 8057–8063.

13. Fiedel SJ. The Peopling of the New World: Present Evidence, New Theories, and Future Directions. J Archaeological Res.2000; 8(1): 39–103.

14. Ferring CR. The Archaeology and Paleoecology of the Aubrey Clovis Site (41DN479) Denton County, Texas. University of North Texas.2001; 1–276.

15. Sanchez G, Holliday VT, Gaines EP, Arroyo Cabrales J, Martinez-Taqüeña N, Kowler A, et al. Human (Clovis)-gomphothere (*Cuvieronius* sp.) association ~13,390 calibrated y BP in Sonora, Mexico. Proc Nac Acad Sci.2014; 111: 10972–10977.

16. Waters MR, Stafford TW. The first Americans: a review of the evidence for the Late-Pleistocene peopling of the Americas. In: Graf KE, Ketron CV, Waters M, editors. Paleoamerican Odyssey, Texas, A&M University, Center for the Study of the First Americans; 2014. pp. 541–560.

17. Joyce DJ. Pre-Clovis megafauna butchery sites in the Western Great Lakes Region. In: Graf KE, Ketron CV, Waters M, editors. Paleoamerican Odyssey, Texas, A&M University, Center for the Study of the First Americans;2013. pp. 467–483.

18. Halligan JJ, Waters MR, Perrotti A, Owens IJ, Feinberg JM, Bourne MD, et al. Pre-Clovis occupation 14,550 years ago at the Page-Ladson site, Florida, and the peopling of the Americas. Sci Adv. 2016; 2: e1600375. https://doi.org/10.1126/sciadv.1600375 PMID: 27386553

19. Lessa A, Guidon N. Osteobiographic analysis of skeleton I, Sítio Toca dos Coqueiros, Serra da Capivara National Park, Brazil, 11,060 BP: First results. American Journal of Physical Anthropology.2002; 118(2): 99–110. https://doi.org/10.1002/ajpa.10084 PMID: 12012362

20. González González AH, Sandoval CR, Terrazas Mata A, Benavente Sanvicente M, Stinnesbeck W, Aviles OJ, et al. The Arrival of Humans on the Yucatan Peninsula: Evidence from Submerged Caves in the State of Quintana Roo, Mexico. Current Res in the Pleistocene.2008; 25: 1–24.

21. González González AH, Terrazas Mata A, Stinnesbeck W, Benavente Sanvicente M, Aviles OJ, Rojas C, et al. The First Human Settlers on the Yucatan Peninsula: Evidence from Drowned Caves in the State of Quintana Roo (South Mexico). In: Graf KE, Ketron CV, Waters M, editors. Paleoamerican Odyssey, Texas, A&M University, Center for the Study of the First Americans; 2013. pp 399–413.

22. Bueno L, Schmidt Dias A, Steele J. The late Pleistocene/early Holocene archaeological record in Brazil: A geo-referenced database. Quaternary International.2013; 301: 74–93.

23. Neves WA, Hubbe M, Bernardo D, Strauss A, Araujo A, Kipnis R. Early Human Occupation of Lagoa Santa Eastern Central Brazil: Craniometric Variation of the Initial Settlers of South America. In: Graf KE, Ketron CV, Waters M, editors. Paleoamerican Odyssey, Texas, A&M University, Center for the Study of the First Americans; 2013. pp. 397–412.

24. Jackson D, Méndez C, de Saint Pierre M, Aspillaga E, Politis G. Direct Dates and mtDNA of Late Pleistocene Human Skeletons from South America: A Comment on Chatters et al. (2014). PaleoAmerica.2015; 1(3): 213–216.

25. Chatters JC, Kennett DJ, Asmerom Y, Kemp BM, Polyak V, Blank AN, et al. Late Pleistocene human skeleton and mtDNA link Paleoamericans and modern Native Americans. Science.2014; 344(6185): 750–754. https://doi.org/10.1126/science.1252619 PMID: 24833392

26. Taylor RE. Six decades of radiocarbon dating in New World Archaeology. Radiocarbon.2009; 51(1): 173–212.

27. Prüfer K, Meyer M. Anthropology. Comment on "Late Pleistocene human skeleton and mtDNA link Paleoamericans and modern Native Americans". Science.2015; 347: 835–835.

28. Weidie AE. Geology of the Yucatan Platform. In: Ward WC, Weidie AE, Back W, editors. Geology and Hydrogeology of the Yucatan and Quaternary Geology of Northeastern Yucatan Peninsula, New Orleans, NOGS Publication; 1985. pp. 1–19.

29. Lefticariu M, Perry EC, Ward WC, Lefticariu L. Post-Chicxulub depositional and diagenetic history of the northwestern Yucatan Peninsula, Mexico. Sed Geol.2006; 183(1–2): 51–69.

30. Ward WC. Quaternary Geology of Northeastern Yucatan Peninsula. In: Ward WC, Weidie AE, Back W, editors. Geology and Hydrogeology of the Yucatan and Quaternary Geology of Northeastern Yucatan Peninsula, New Orleans, NOGS Publication; 1985. pp. 23–91.

31. Blanchon P, Shaw J. Reef drowning during the last deglaciation: Evidence for catastrophic sea-level rise and ice-sheet collapse. Geology.1995; 23(1): 4–8.

32. Moseley GE, Richards DA, Smart PL, Standish CD, Hoffmann DL, ten Hove H, et al. Early-middle Holocene relative sea-level oscillation events recorded in a submerged speleothem from the Yucatan Peninsula, Mexico. The Holocene.2015; 25(9): 1–11.

33. Smart PL, Beddows P, Coke J, Doerr S, Whitaker FF. Cave Development on the Caribbean coast of the Yucatan Peninsula, Quintana Roo, Mexico. Geol Soc America Spec Pap.2006; 404: 105–128.

34. Grant KM, Rohling EJ, Bar-Matthews M, Ayalon A, Medina-Elizalde M, Ramsey CB, et al. Rapid coupling between ice volume and polar temperature over the past 150,000 years. Nature.2012; 491 (7246):744–747.

35. Curtis J, Hodell D, Brenner M. Climate Variability on the Yucatan Peninsula (Mexico) during the Past 3500 Years, and implications for Maya Cultural Evolution. Quat Res.1996; 46: 37–47.

36. Kennett DJ, Breitenbach S, Aquino V, Asmerom Y, Awe J, Baldini J, et al. Development and Disintegration of Maya Political Systems in Response to Climate Change. Science.2012; 338: 788–791. https://doi.org/10.1126/science.1226299 PMID: 23139330

37. Douglas PM, Pagani M, Canuto MA, Brenner M, Hodell DA, Eglinton TI, Curtis JH. Drought, agricultural adaptation, and sociopolitical collapse in the Maya Lowlands. Proc Nac Acad Sci.2015; 112(18): 5607–5612.

38. Marín LE. Field investigations and numerical simulation of the karstic aquifer of northwest Yucatan, Mexico. Ph.D. thesis, Northern Illinois University, DeKalb, IL; 1990. 183 p.

39. Moore YH, Stoessell RK, Easley DH. Fresh-water/sea-water relationship within a ground-water flow system, northeastern coast of the Yucatan Peninsula. Ground Water.1992, 30(3): 343–350.

40. Beddows PA. Groundwater hydrology of a coastal Conduit carbonate aquifer: Caribbean Coast of the Yucatán Peninsula México. Ph.D. thesis, University of Bristol, UK; 2004.

41. Blanchon P, Eisenhauer A, Fietzke J, Liebetrau V. Rapid sea-level rise and reef back-stepping at the close of the last interglacial highstand. Nature. 2009; 458: 881–884. https://doi.org/10.1038/nature07933 PMID: 19370032

42. Collins SV, Reinhardt EG, Rissolo D, Chatters JC, Nava Blank A, Luna Erreguerena P. Reconstructing water level in Hoyo Negro, Quintana Roo, Mexico, implications for early Paleoamerican and faunal access. Quat Sci Rev 2015; 124: 68–83.

43. Fontugne M, Shao Q, Frank N, Thil F, Guidon N, Boeda E. Cross-dating (Th/U-C-14) of calcite covering prehistoric paintings at Sierra Da Capivara National Park, Piaui, Brazil. Radiocarbon. 2013; 55: 1191–1198.

44. Pike AWG, Pettitt PB. U-series Dating and Human Evolution. Rev Mineral Geochem.2003; 52: 607–629.

45. Millard AR, Hedges REM. A diffusion–adsorption model of uranium uptake by archaeological bone. Geochim Cosmochim Acta.1996; 60: 2139–2152.

46. Sambridge M, Grün R, Eggins S. U-series dating of bone in an open system: The diffusion-adsorption-decay model. Quat Geochron.2012; 9: 42–53.

47. Haug GH, Gunther D, Peterson LC, Sigman DM, Hughen KA, Aeschlimann B. Climate and the collapse of Maya civilization. Science.2003; 299: 1731–1735. https://doi.org/10.1126/science.1080444 PMID: 12637744

48. Dansgaard W. Stable isotopes in precipitation. Tellus.1964; 16: 436–468.

49. Stuiver M, Grootes PM, Braziunas TF. The GISP2 δ^{18}O climate record of the past 16,500 years and the role of the sun, ocean and volcanoes. Quat Res.1995; 44: 341–354

50. Carlson AE. The Younger Dryas Climate Event. In: Elias SA, editor. The Encyclopedia of Quaternary Science, Amsterdam, Elsevier; 2013. 3, pp. 126–134.

51. Asmerom Y, Polyak V, Burns S, Rasmussen J. Solar forcing of Holocene climate: New insights from a speleothem record, Southwestern United States. Geology.2007; 35: 1–4.

52. Asmerom Y, Polyak VJ, Burns SJ. Variable winter moisture in the southwestern United States linked to rapid glacial climate shifts. Nature Geoscience.2010; 3: 114–117.

53. Wagner JDM, Cole JE, Beck JW, Patchett PJ, Henderson GM, Barnett HR. Moisture variability in the southwestern United States linked to abrupt glacial climate change. Nature Geoscience.2010; 3: 110–113.

54. Alley RB. The Younger Dryas cold interval as viewed from central Greenland. Quat Sci Rev.2000; 19: 213–226.

55. Rasmussen SO, Andersen KK, Svensson AM, Steffensen JP, Vinther BM, Clausen HB, et al. A new Greenland ice core chronology for the last glacial termination. Jl Geophys Res.2006; 111: D6.

56. Yang Y, Yuan DX, Cheng H, Zhang ML, Qin JM, Lin YS, et al. Precise dating of abrupt shifts in the Asian Monsoon during the last deglaciation based on stalagmite data from Yamen Cave, Guizhou Province, Science China. Earth Sci.2010; 53: 633–641.

57. Haug GH, Hughen KA, Sigman DM, Peterson LC, Röhl U. Southward migration of the Intertropical Convergence Zone through the Holocene. Science.2001; 293: 1304–1308. https://doi.org/10.1126/science.1059725 PMID: 11509727

58. Escobar J, Hodell DA, Mark Brenner M, Curtis JH, Gilli A, Mueller AD, et al. 43-ka record of paleoenvironmental change in the Central American lowlands inferred from stable isotopes of lacustrine ostracods. Quat Sci Rev.2012; 37: 92–104.

59. Reimer PJ, Baillie MGL, Bard E, Bayliss A, Beck JW, Bertrand C, et al. Radiocarbon.2004; 46:1029–1058.

60. IntCal04. Calibration Issue of Radiocarbon (Volume 46, 3, 2004)

61. Hodell DA, Anselmetti FS, Arizegui D, Brenner M, Curtis JH, Gilli A, et al. An 85-ka record of climate change in lowland Central America. Quat Sc Rev.2008; 27: 1152–1165.

62. Feehan J. The Rocks and Landforms of the Burren. In: O'Connell JW, Korff A, editors. The Book of the Burren, Tir Eolas; 2001. pp. 14–23.

63. Leyden BW, Brenner M, Hodell DA, Curtis JH. Late Pleistocene climate in the Central American lowlands. In: Climate Change in Continental Isotopic Records, Swart PK, Lohmann KC, McKenzie J, Savin S, editors. Geophysical Monograph 78, American Geophysical Union, Washington, DC; 1993. pp. 165–178.

64. Leyden BW. Evidence of the Younger Dryas in Central America? Quat Sci Rev.1995; 14: 833–839.

65. Brenner M, Rosenmeier MF, Hodell DA, Curtis JH. Paleolimnology of the Maya Lowlands. Long-term perspectives on the interactions among climate, environment, and humans. Ancient Mesoamerica.2002; 13: 141–157.

66. Reed E. Decomposition and Disarticulation of Kangaroo Carcasses in Caves at Naracoorte, South Australia. J Taph.2009; 7(4): 265–284.

67. Felis T, Scholz D, Lohmann G, Giry C, Fensterer C, Wei W, Mangini A. Control of Seasonality and Interannual to Centennial Climate Variability in the Caribbean During the Holocene Combining Coral Records, Stalagmite Records and Climate Models. In: Schulz M, Paul A, editors. Integrated Analysis of Interglacial Climate Dynamics (INTERDYNAMIC), SpringerBriefs in Earth System Sciences;2015. pp. 69–75.

68. Lafuente B, Downs RT, Yang H, Stone N. The power of databases: the RRUFF project. In: Armbruster T, Danisi RM, editors. Highlights in Mineralogical Crystallography, Berlin, Germany, W. De Gruyter;2015. pp. 1–30.

69. Douville E, Sallé E, Frank N, Eisele M, Pons-Branchu E, Ayrault S. Rapid and accurate U-Th dating of ancient carbonates using inductively coupled plasma-quadrupole mass spectrometry. Chem Geol.2010; 272: 1–11.

70. Cheng H, Edwards RL, Hoff J, Gallup CD, Richards DA, Asmerom Y. The half-lives of uranium-234 and thorium-230. Chem Geol.2000; 169: 17–33.
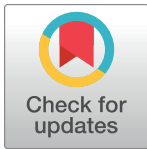
New evidence for an early settlement of the Yucatán Peninsula, Mexico: The Chan Hol 3 woman and her meaning for the Peopling of the Americas

Wolfgang Stinnesbeck[1]*, Samuel R. Rennie[2,3], Jerónimo Avilés Olguín[4], Sarah R. Stinnesbeck[5], Silvia Gonzalez[2], Norbert Frank[1,6], Sophie Warken[1,6], Nils Schorndorf[1], Thomas Krengel[1,6], Adriana Velázquez Morlet[7], Arturo González González[4]

1 Institut für Geowissenschaften, Universität Heidelberg, Im Neuenheimer Feld, Heidelberg, Germany, 2 School of Biological and Environmental Sciences, Liverpool John Moores University, Liverpool, United Kingdom, 3 Department of Archaeology and Anthropology, Bournemouth University, Poole, United Kingdom, 4 Museo del Desierto, Carlos Abedrop Dávila, Nuevo Centro Metropolitano de Saltillo, Saltillo, Coahuila, Mexico, 5 Staatliches Museum für Naturkunde Karlsruhe, Geowissenschaftliche Abteilung, Erbprinzstrasse, Karlsuhe, Germany, 6 Institut für Umweltphysik, Universität Heidelberg, Im Neuenheimer Feld, Heidelberg, Germany, 7 Instituto Nacional de Antropología e Historia, CINAH Campeche, Campeche, Mexico

* wolfgang.stinnesbeck@geow.uni-heidelberg.de

Abstract

Human presence on the Yucatán Peninsula reaches back to the Late Pleistocene. Osteological evidence comes from submerged caves and sinkholes (cenotes) near Tulum in the Mexican state of Quintana Roo. Here we report on a new skeleton discovered by us in the Chan Hol underwater cave, dating to a minimum age of 9.9±0.1 ky BP based on ^{230}Th/U-dating of flowstone overlying and encrusting human phalanges. This is the third Paleoindian human skeleton with mesocephalic cranial characteristics documented by us in the cave, of which a male individual named Chan Hol 2 described recently is one of the oldest human skeletons found on the American continent. The new discovery emphasizes the importance of the Chan Hol cave and other systems in the Tulum area for understanding the early peopling of the Americas. The new individual, here named Chan Hol 3, is a woman of about 30 years of age with three cranial traumas. There is also evidence for a possible trepanomal bacterial disease that caused severe alteration of the posterior parietal and occipital bones of the cranium. This is the first time that the presence of such disease is reported in a Paleoindian skeleton in the Americas. All ten early skeletons found so far in the submerged caves from the Yucatán Peninsula have mesocephalic cranial morphology, different to the dolicocephalic morphology for Paleoindians from Central Mexico with equivalent dates. This supports the presence of two morphologically different Paleoindian populations for Mexico, coexisting in different geographical areas during the Late Pleistocene-Early Holocene.

1. Introduction

Osteological evidence for early American settlers is scarce and usually fragmentary, with only a few individuals known from both North and South America securely predating 10 thousand years (ky) ago ([1] and references therein). Mexico has long played a minor role in the discussion of the early settlement of the continent because researchers interested in the theme were majorly not aware of the wealth of Paleoindian skeletons found in this large geographical area of the Americas. Nevertheless, this situation is slowly changing [2]; today scientific interest particularly focuses on the Yucatán Peninsula (YP) in southern Mexico where a total of nine well-preserved human skeletons have been discovered during the past decade in submerged caves of the Tulum area and have been dated to between 13–9 ky BP ([1, 3–6]; S1 Table).

The caves are located within a few kilometers distance from the Caribbean coast and were dry and accessible during most of the period of interest of this study (13–9 ky BP), as they were not flooded until the worldwide sea-level rise that happened during the early Holocene (e.g. [4, 7–9]). The discovery of a well-preserved Paleoindian skull of a young girl from the submerged Hoyo Negro (Black Hole) sinkhole (Fig 1A) has received special interest. The individual was ^{14}C-dated to 10,976±20 y BP (12,910–11,750 cal y BP; 95.4% probability using CalPal) by Chatters et al. [1] based on bioapatite from tooth enamel. Previously, a similar ^{14}C age was already published for a human skeleton from Naharon cave (Fig 1A), also located close to Tulum, with an age of 11,570±65 [14]C y BP (13,571–13,337 cal y BP; 68% probability using CalPal) [3, 6]. It is, however, difficult to exactly determine the ^{14}C age of these two humans using conventional radiocarbon dating, because the amount of collagen found in their bones and teeth is extremely low. This is due to a general lack of collagen preservation in human and faunal remains found underwater in the Tulum caves (e.g. [4, 5]), which has been interpreted as the result of exposure of the osteological remains for thousands of years to alternating salt- and fresh water environments [5]. In addition, bioapatite is highly susceptible to contamination with fossil carbon resulting in false, mostly older ages [1]. Therefore, Stinnesbeck et al. [5] dated a stalagmite that had precipitated on top of a human pelvis earlier discovered in the Chan Hol cave system [3]. The analysis of uranium-thorium isotopes of the stalagmite precipitated on the Chan Hol 2 skeleton resulted in a minimum age of 11.3 ky BP for this human skeleton. However, the correlation of oxygen and carbon isotope ratios in the speleothem with other regional, independently dated paleoclimate records, indicates a much earlier onset of speleothem growth, suggesting an older age of about 13 ky BP for the Chan Hol 2 individual [5]. This implies that Chan Hol 2 is one of the oldest known skeletons of the American continent [5].

We here report on a new skeleton from the Chan Hol cave, named Chan Hol 3, which is the third human skeleton discovered from the Chan Hol system [3, 5]. The cave also preserves evidence for early to mid-Holocene human usage in the form of numerous charcoal accumulations with radiocarbon dates between 8110 ± 28 [14]C y BP (9122–8999 cal y BP) to 7177 ± 27 [14]C y BP (8027–7951 cal y BP) [9].

2. Geological setting

The Tulum submerged cave system on the northeastern YP in the Mexican state of Quintana Roo, is among the most extensive active underwater cave systems worldwide, with a presumed total length of 7,000 km, but only 1,500 km have currently been explored [10]. Karst developed in almost horizontally layered, thick-bedded, shallow-water carbonate bedrock of Neogene ages and is the result of intensive development during the Pleistocene, caused by a series of sea-level oscillations and changes in the overall hydrology of the area [11, 12]. Sea-level rise on
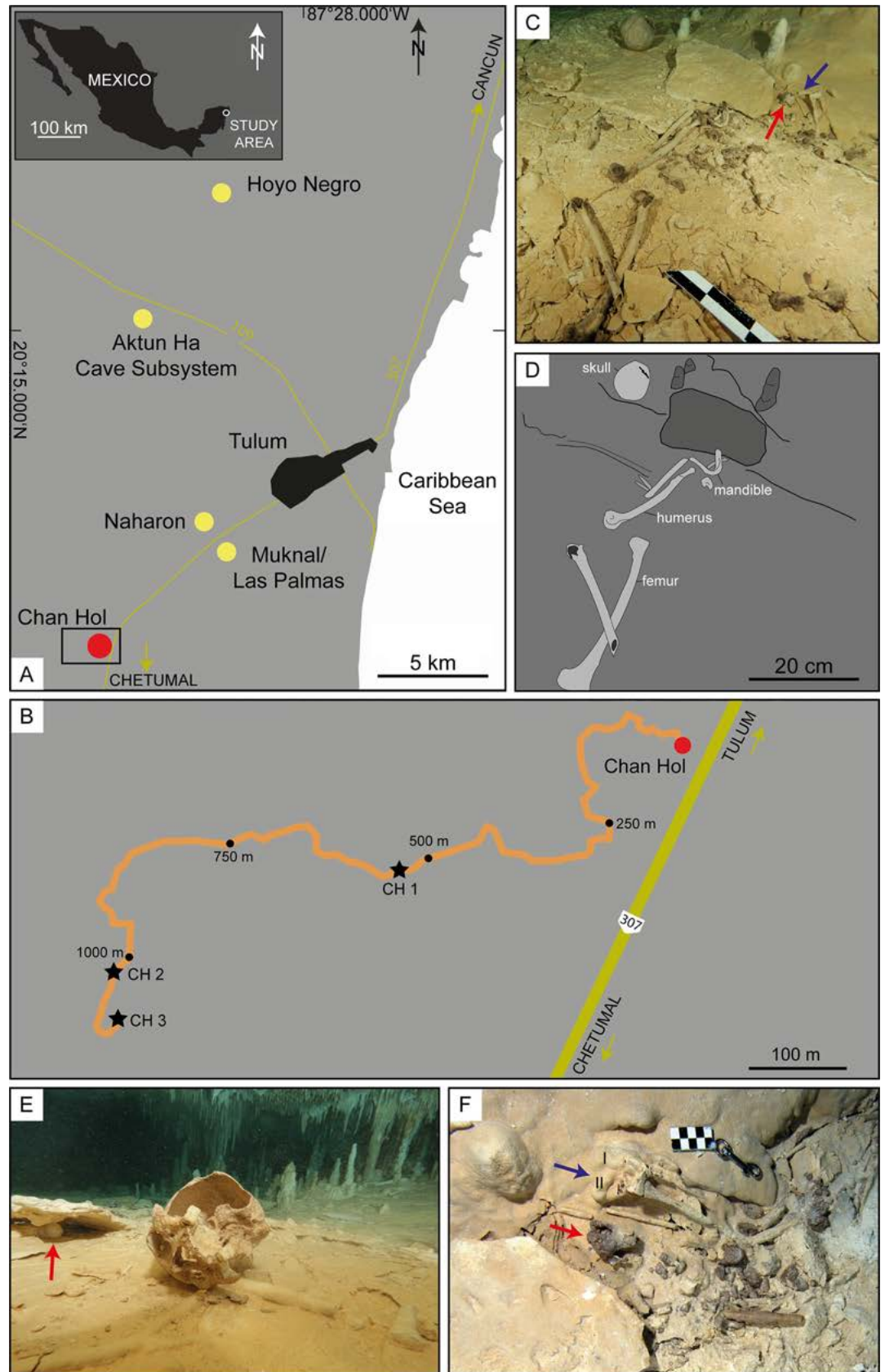
Fig 1. Geographical location of the Chan Hol 3 anthropological site. (A) Location of submerged caves containing human skeletal remains dating to >9 ky BP in the Tulum area of Quintana Roo, Mexico. Yellow dots refer to anthropological sites mentioned in the text with presence of human remains [1, 3–6]. The red dot marks the Chan Hol cave described previously by González González et al. [3, 6] and Stinnesbeck et al. [5]. (B) Close-up of the black box seen in Fig 1A with location of the three human skeletons found within the Chan Hol cave. (C) The Chan Hol 3 anthropological site. Note that human bones are spread over an area of 3 x 1 m. The original anatomical position of the skeleton is thus not preserved. The red arrow points to distal radius fragment while the blue arrow indicates position of finger bones (metacarpals, phalanges) depicted in Fig 2. A prominent flat limestone rock 0.3 wide and 0.2 m long and 50 mm in thickness is seen in the upper right quadrant of the photo, and the mandible immediately in front of this rock slab. (D) Interpretative drawing of the site. (E) The skull rotated upside down. It is likely this was water-transported and rolled for about 0.5 m to this position. The red arrow points to a broken stalagmite below the limestone slab seen in Fig 1C and 1D. (F) Flowstone encrusting phalangeal bones used for ^{230}Th/U-dating of the Chan Hol 3 skeleton (see Fig 2 for details).

https://doi.org/10.1371/journal.pone.0227984.g001

the YP was predominantly controlled by eustasy, as the peninsula has been tectonically stable in the recent past and glacial isostatic adjustments are negligible in this tropical area [12–14].

During the Last Glacial Maximum (25 to 19 ky BP) sea-level was more than 100 m below the present day sea-level and large parts of the Tulum cave system were dry and accessible for animals and humans. During the last deglaciation, between 13 and 7.6 ky BP, sea-level rose again and modern water levels were reached at approximately 4.5 ky BP [7–9], although oscillations of up to a few meters are known to have occurred during Mayan times, and later [15]. Today, the Tulum cave system contains a coastal, density stratified aquifer, i.e. a freshwater layer overlying penetrating seawater. The depth of the halocline depends on the global sea-level as well as on the thickness of the superimposed freshwater layer. It is controlled by the distance to the coastline as well as the amount of precipitation, with a hydraulic gradient across the YP of between 0.5 and 100 mm/km. As most of the Tulum caves are hydrologically open-systems, groundwater flows through the porous limestone karst directly towards the ocean. In consequence, water level near the coast (e.g. in the Tulum area) is approximately equivalent to mean sea-level ([15] and references therein).

2.1. The Chan Hol 3 Site and the Human Skeleton

The Chan Hol 3 skeleton was found in September 2016 by cave explorers Vicente Fito and Ivan Hernández during a systematic survey led by Jeronimo Avilés in Chan Hol cave. The entrance to the cave is at Chan Hol cenote (sinkhole), located at 20˚9.467' N, 87˚34.165 W, about 15 km southwest of Tulum, and about 11.5 km from the coastline (Fig 1). The skeleton was discovered in a low cave tunnel in fresh water at 8 m water depth, at 1141 m diving distance from the cenote (Fig 1). During the dive, the sites of the Chan Hol 1 [3] and Chan Hol 2 [5] human skeletons were passed at 541 m (Chan Hol 1) and 1027 m (Chan Hol 2) from the cenote entrance. The maximum depth of the Chan Hol cave is about 13 m below present day sea-level and the halocline is located at about 9 m water depth. Due to its shallow position, this part of the Chan Hol cave must have been accessible until early stages of the middle Holocene [5, 9]. Anthropogenic charcoal accumulations in the cave have been dated to between 8,110 ±28 ^{14}C y BP (9,122–8,999 cal y BP) and 7,177±27 ^{14}C y BP (8,027–7,951 cal y BP) [9].

3. Material and methods

Underwater registration and documentation of skeletal remains in the Tulum underwater caves has been described in detail [6]. The underwater documentation has been executed by J. A.O., Vicente Fito, Eugenio Acévez and Ivan Hernández. After collection, the skeleton was treated with distilled water for eight months and slowly dried. Underwater photographs were taken with an Eos rebel Ti4 with a 10–20 mm zoom lens inside an ikelite housing. Laboratory photography was taken with a Canon D5 Mark III with 50 mm and 100 mm macro lenses.

3.1. Human osteology

The cranium is well preserved allowing for the execution of detailed craniometric measurements of Howells [16] and Buikstra and Ubelaker [17]. Cranial and femoral measurements are listed in S2 Table. Paleopathological analysis and documentation follow definitions made by Ortner and Putschar [18] and Aufderheide et al. [19]. Sex, age, and stature assessments were completed following procedures established by Buikstra and Ubelaker [17], Genovés [20], and Walker [21]. Stature equation was chosen because the parent sample was from Mexico [20].

Cranial Indices and Upper Facial Indices were calculated to make overall comparisons between crania across North, Central, and South America. We excluded the Hoyo Negro skull as there are no data published currently for this individual. For other individuals, a full Principal Components Analysis (PCA) was calculated using samples from the Howell's cranial database [16, 21–23] and other open source cranial data [24–28]. A total of 452 human skulls from ten different samples were included for analysis (S3 Table). Twelve variables were used and were all collected from peer-reviewed articles and books [16, 21, 22, 24–28]. The 12 variables were chosen because they were most frequently available from all specimens. For individuals that were missing these variables, a k Nearest Neighbor analysis was used to compute what the missing variables would be [29]. Each sample's missing values were computed separately to allow for a better portrayal of that sample variation. S3 Table lists the variables used for analysis. From these 12 cranial variables (S3 Table), PCA was computed (S4 Table).

3.2. ^{230}Th/U-dating

Samples for mass spectrometer ^{230}Th/U-dating were taken from a flowstone up to 10 mm thick overlying and encrusting phalanges of the Chan Hol 3 skeleton (Fig 2). As the carbonate encrustation of the bone and cave floor itself has a very heterogeneous structure, our sampling strategy concentrated on this laminar layered flowstone from which a sequence of three subsequent samples was cut using a diamond wired band saw (Fig 2). This strategy ensured that samples were taken to minimize mixing of material of possibly different ages. Individual sample thickness is typically 2 mm (in growth direction), with an individual sample weight ranging between 60 and 90 mg. All samples were pre-cleaned through a weak acid leach and dried prior to dissolution in 7 N HNO$_3$. The chemical preparation for mass spectrometric U and Th isotope measurements was conducted at the Institute of Environmental Physics at Heidelberg University using wet-column chemistry (resin: UTEVA$^{®}$) to purify U and Th from the flowstone samples. The chemical protocol follows the one of Wefing et al. [30]. The natural isotopes of uranium (^{238}U-^{235}U-^{234}U) and thorium (^{232}Th- and ^{230}Th) and the artificial isotopes of the triple-spike (^{233}U-^{236}U-^{229}Th) were quasi-simultaneously analyzed using a multi-collector, inductively coupled, plasma source mass spectrometer (MC-ICP-MS) (Thermo Finnigan Neptune^{Plus}) coupled to a desolvator (CETAC—ARIDUS) at the Institute of Environmental Physics, Heidelberg University [30, 31]. The 3 sample measurements of the Chan Hol 3 flowstone samples were bracketed with measurements of HU-1 reference material and prior to each standard a blank sample was analyzed. The detector yield and abundance sensitivity were independently assessed before and after the sample analysis and the data was corrected for instrumental biases, abundance sensitivity, detector yield and peak tailing. The raw data treatment is conducted using an in-house Matlab Script [31]. Ages were calculated using the half-lives of both elements [32]. Using the more recent values of Cheng et al. [33] does not influence the results.

Due to the complete dissolution of organic matter, specifically collagen, we refrained from the extraction of collagen and thus ^{14}C age determination of the Chan Hol 3 individual.
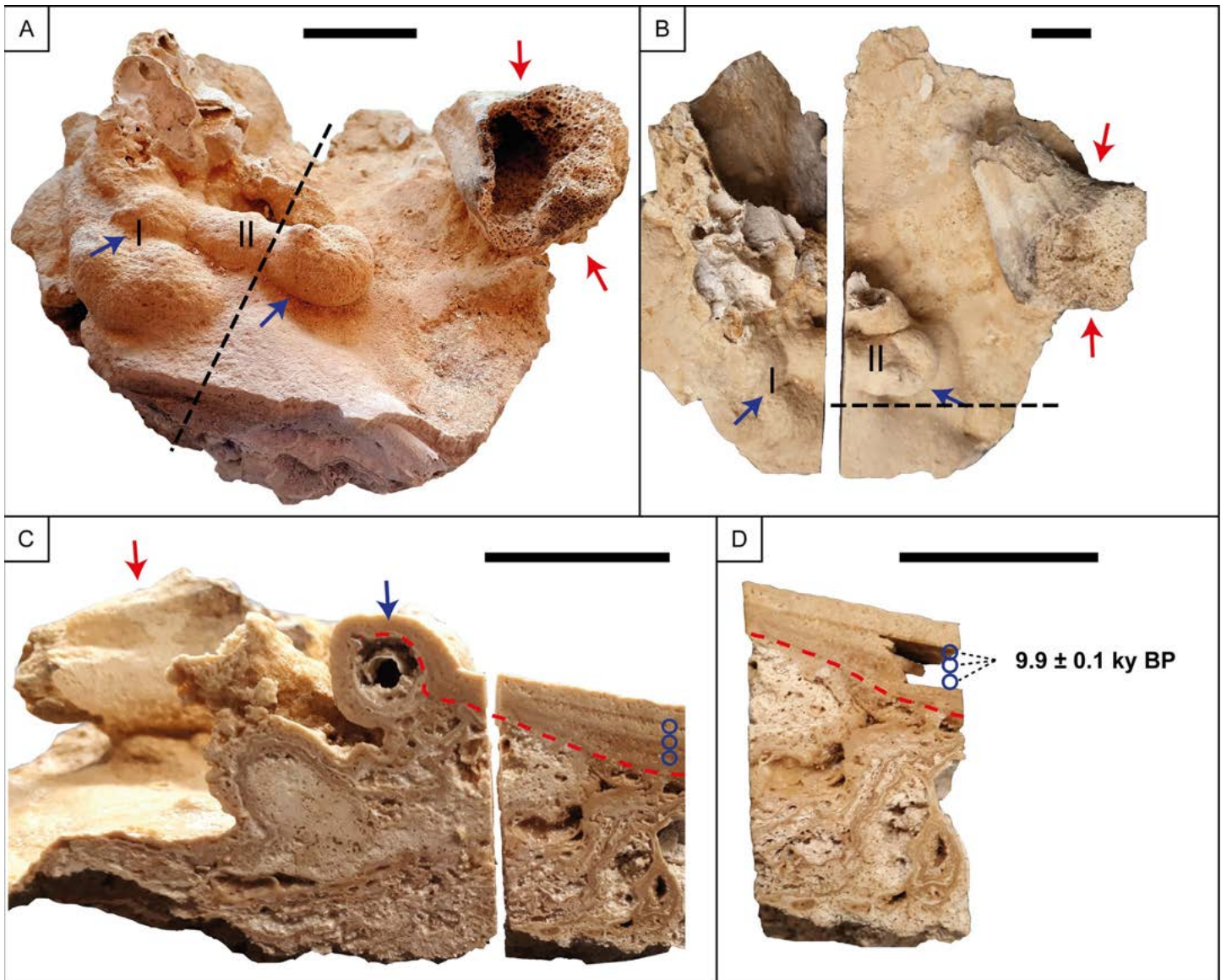
Fig 2. Flowstone encrusting phalangeal bones of the Chan Hol 3 human individual. For the original position of the sample on the cave floor see Fig 1C and 1F. Red arrows point to the position of distal radius and blue arrows to carpal and metacarpal bones, and blue circles to the position of samples used for ^{230}Th/U-dating. (A) Sample seen from above. The dotted line indicates the position in which the sample was vertically cut. Note lateral view of distal radius fragment. The covered bone to the left is a carpal (I) and the one next to it is a metacarpal (II). (B) view of distal radius shown in (A) from above. (C) Vertical cross section of the sample. Note that the blue arrow points to the spherical aperture which originally represented the metacarpal and is now dissolved. (D) Magnification of the slab shown on the right side of (C), with the position of the three ^{230}Th/U-dating samples with approximately coeval ages of 9.9±0.1 ky. A contaminating ^{230}Th/^{232}Th activity ratio of 3.96±0.09 is estimated from the Osmond isochron. Scale used in all figures is 20 mm.

https://doi.org/10.1371/journal.pone.0227984.g002

3.3. Strontium Isotope analysis

Due to availability and preservation we selected the third left mandibular molar from Chan Hol 3 for Sr-isotope analysis. Third molar enamel forms during adolescence, between 7 and 16 years of age (e.g. [34]).

We sampled 2 to 5 mg chips of tooth enamel using a 0.2 mm diamond-coated cutting disc to minimize material loss of the valuable sample. We carefully avoided dentine components in the samples, because dentine is known to be sensitive to diagenesis and, unlike enamel, easily

takes up mobile geogenic strontium components from the surrounding rocks and sediments [35].

The enamel pieces were cleaned by repeated washing with ultrapure water. After drying the enamel grains were digested using nitric acid. Strontium was purified through wet-column extraction chemistry using an EiChrom SrResin® column [36]. The protocol applied at the Institute of Earth Sciences, Heidelberg University was adopted after Kober et al. [37]. A 1 ml column was filled with SrResin (TRISKEM) and washed with 6 column volumes (CV) H_2O. Next the columns were loaded with 3 ml 7N HNO_3. The samples were dried and re-dissolved in 1 ml nitric acid added onto the columns. The columns were then washed with 6 CV 7 N HNO_3. To elute Sr from the resin the columns were rinsed with 3 CV H_2O. The samples were evaporated on a hot plate until a small barely visible drop remained at the bottom of the beaker. The column chemistry was repeated to further purify Sr from the sample matrix and the final Sr solution was evaporated to dryness. The sample was re-dissolved in a drop of concentrated HNO_3 and a drop of H_2O_2 to ensure dissolution of remains of the resin and it was then again evaporated to dryness. Finally, samples were dissolved in 10 μl 7N HNO_3 and were transferred onto a preheated rhenium filament. Isotopic measurements (10 sequences of each 10 measurements) were conducted on a thermal ionization mass spectrometer (Finnigan MAT-262) using a dynamic multi-collection method normalized to the Nier value of $^{86}Sr/^{88}Sr$ = 0.1194 using an exponential fractionation law. All isotopes were measured on Faraday cups with minimum ^{86}Sr intensities of 0.5 V. Each measurement was checked for ^{85}Rb. Isotope ratios were corrected for internal mass fractionation assuming a stable $^{88}Sr/^{86}Sr$ ratio of 8.375209. The NIST isotope standard SRM-987 was used for routine monitoring and correction of instrumental bias and to assess reproducibility. Replicate SRM-987 analysis of the $^{87}Sr/^{86}Sr$ ratio yields 0.710261 ± 0.000006 (2σ, N = 4).

4. Results

4.1. The Chan Hol 3 site and skeleton

At the Chan Hol 3 anthropological site, human bones are spread over an area of 3 x 1 m and the original anatomical position of the skeleton is thus not preserved (Fig 1C and 1D). The skull is seen at about 0.5 m north of the rest of the skeleton (Fig 1C–1E), while forearm (radius, ulna) and finger bones (metacarpals, phalanges) are identified to one side of a rectangular shaped limestone slab 0.3 x 0.2 m wide and 50 mm in thickness, while a humerus and metacarpals are identified on the opposite side, along with the mandible. Both legs are fully extended and located in the south quadrant (Fig 1C and 1D), but the original position of these bones is disturbed.

The Chan Hol 3 individual is only about 30% complete which indicates that many bones may either have been water-transported and carried away, were lost due to decomposition, or are still in the cave covered by flowstone. Bones collected include the cranium, mandible, both clavicles, manubrium, the left humerus, both femora, both tibiae, three fragments of the pelvis (ilium and ischium), two ulnae and one radial shaft fragment, seven fragments of vertebrae (thoracic and lumbar), seven fragments of ribs, and three phalanges (Fig 3).

The cranium is largely preserved but post-mortem fractures have occurred. Most internal cranial bones (ethmoid, vomer, and large amounts of the sphenoid etc.) are lost. Portions of the occipital bone, especially near the *foramen magnum*, are also missing. A small wormian bone was located alongside the right lambdoidal suture. The left parietal has been fractured post-mortem but remains present. The fracture margins remain sharp, suggesting that the fracture was recent. Zygomatic arches on both sides are no longer present.
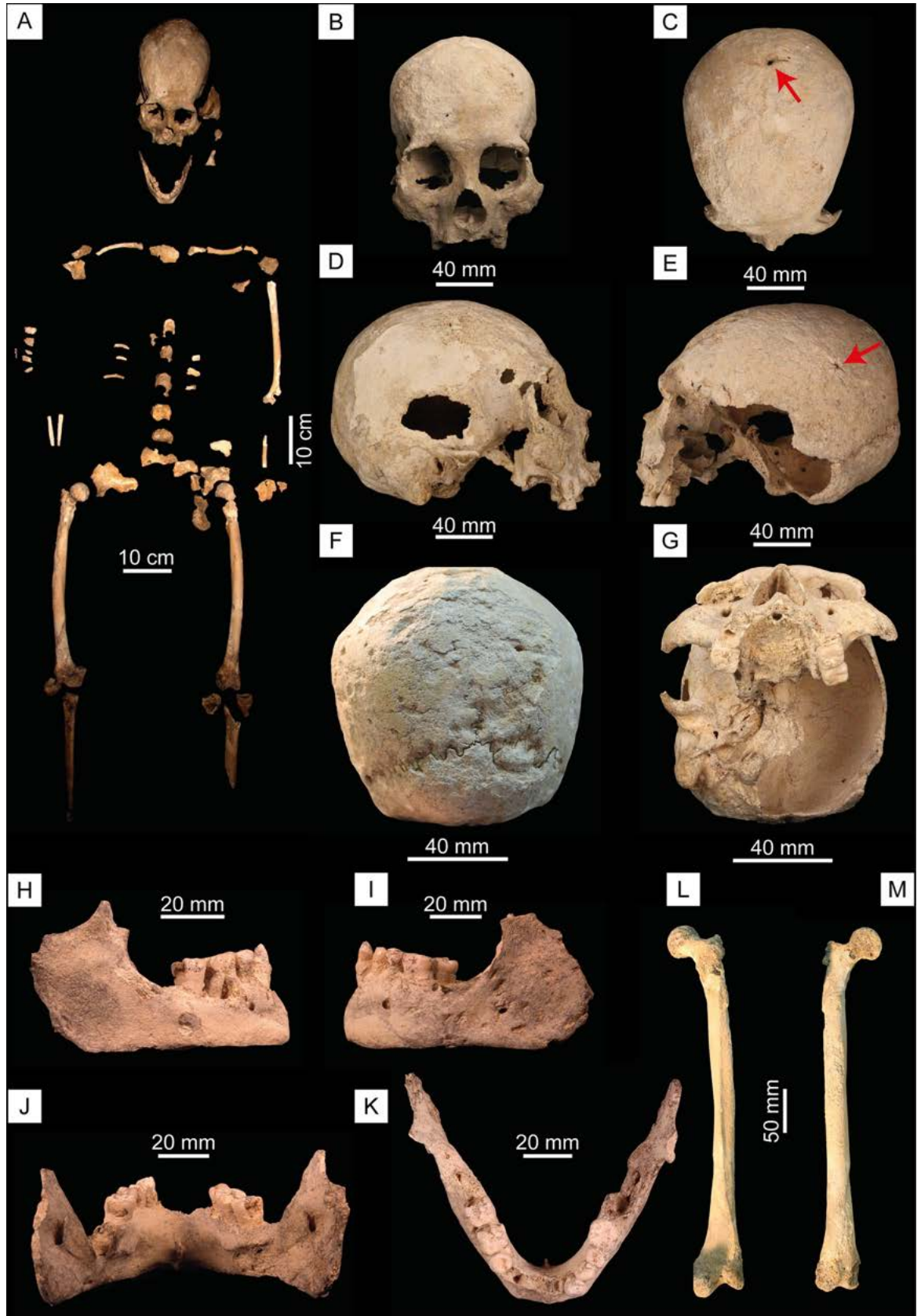
Fig 3. The Chan Hol 3 skeleton. (A) Bone map of the Chan Hol 3 skeleton. (B) Cranium in rostral view. (C) Cranium in dorsal view. Arrow points to a trauma on the posterior portion of the parietal. (D) Cranium in right lateral view. (E) Cranium in left lateral view. The red arrow points to trauma on the parietal bone. (F) Cranium in caudal view. Note extensive bone destruction on the occipital bone here interpreted to result from treponemal bacterial disease. (G) Cranium in ventral view. (H) Mandible in right lateral view. (I) Mandible in left lateral view. (J) Mandible in caudal view. (K) Mandible in dorsal view. (L) Right femur in frontal and (M) posterior view.

The only teeth that are still present in the maxilla are the left and right 1st molars and the left 2nd molar (Fig 3G). There is post-mortem breakage on the right canine with the root still present in the maxilla. The four incisors have complete resorption indicating that they were lost ante-mortem alongside the right upper canine, left, and right premolars. The 2nd and 3rd molars on the upper right side have been lost, most likely ante-mortem due to dental abscess (Fig 3G).

The mandible is mostly complete, apart from the mandibular condyles being broken post-mortem (Fig 3H–3K). Central and medial incisors are no longer present showing ante-mortem loss with complete resorption of the alveolar bone alongside the loss of the right lower canine and 1st premolar. The 2nd and 3rd molars from the left side and the 3rd molar on the right are not present.

Postcranially, both clavicles are present alongside the manubrium which presents a recent post-mortem break running superior-inferiorly. The left humerus is presented as two main fragments, the humeral head and the diaphyses, and the distal portion (trochlea and capitulum). Several pieces of vertebral bodies and arches belong to thoracic and lumbar regions. The left *os coxa* has fragments from the ilium and ischium, with the right side only preserves the ilium. Both femora are present with only the right side preserving the femoral head (Fig 3L and 3M). The tibial diaphysis has been preserved for both left and right sides but shows more fragmentation on the left.

4.2. Biological profile

The Chan Hol 3 individual represents an adult female. Sex determination followed morphognostic traits of the skull [38] and of the greater sciatic notch [39]. Using Walker's method for the assessment of the Greater Sciatic Notch [39], a score of 2 was given which is more indicative of a female individual. For sex diagnosis using the skull, Walker's methodology [38] was used alongside that of Buikstra and Ubelaker [17]. The Glabella was scored to 2, Mastoid Process scored 2, Nuchal Crest scored 1, and the Mental Eminence scored 4. Sadly, the Supra-Orbital Margins could not be scored with confidence due to insufficient preservation. The femoral head diameter was taken and compared to the sectioning points laid out by Iscan and Steyn [40]; page 174. Musculoskeletal markings on the long bones are all weakly developed and overall present as gracile.

Chan Hol 3 is a fully mature adult showing complete fusion of all long bones and the medial clavicle suggesting an age of 21+ years. Due to fragmentation, the pubic symphysis and the auricular surface of the pelvis were not present for further age assessment following cranial suture closure. Due to slight erosion of the external surface of the skull, ectocranial suture closure techniques could not be fully implemented [41]. From what was available, the mid-lambdoidal and lambda sutures show signs of non-closure whilst the rest shows either significant closure or complete obliteration of the suture. All permanent dentition had erupted resulting in an age of >18 years. With the addition of using Brothwell's method for aging using dental attrition [42], slight wear is identified on the occlusal surfaces of the 1st and 2nd mandibular molars. This puts Chan Hol 3 at the later phase of the first stage which provides an approximate age of 25 years. With this information, the Chan Hol 3 woman was a young adult (30±11 years old) at the time of death, but this assessment is to be taken with caution. Stature was

calculated using the regression equation by Genovés using maximum femoral length [20]. With this, a stature of 1.635±0.035 m was calculated. Overall, Chan Hol 3 is therefore an adult female, approximately 30±11 years of age, with a height of 1.64 m.

4.3. Craniomorphology

Cranial Index was calculated to 76.00 and resulted in Chan Hol 3 being classified as mesocephalic. This result fits in with the other three individuals from Yucatan: Hoyo Negro, Muknal and Las Palmas (Fig 4; S5 Table). However, this cannot be said for the large proportion of other crania in a similar age range (Late Pleistocene-Early Holocene), most of them being dolicocephalic (Fig 4; S5 Table). Chan Hol 3 has an upper/superior facial index of 51 which places the skull as having a medium face, neither broad nor narrow. This is slightly different to the other crania from Yucatan which have slightly broader faces (Fig 4; S5 Table). In general terms, however, our data indicate that two distinct morphologies were present in Mexico as early as 12 ky BP, with the individuals from Yucatan being the only sample present with mesocephalic skulls.

For the PCA study, a total of 452 individuals were analyzed when pooling both males and females (Males: 241 & Females: 211; S3 Table). This data set included all specimens currently present from the YP, with the newly discovered Chan Hol 3 plotted separately to highlight its association with the rest of the Yucatan individuals. Two Principal Components (PCs) were extracted resulting in 29.95% of the variation being explained by PC1 and 15.83% being explained by PC2 (Fig 5). The main differences are seen along the second principal component where the three 'younger' samples (Arikara, Peru, and Santa Cruz) occupy space within the positive Y-axis, whereas older samples all have negative PC2 scores (Fig 5). This difference is primarily explained by the variation seen in five cranial measurements (S4 Table). The larger Maximum Cranial Length (GOL) and Basion—Bregma Height (BBH) are more associated with the older samples (Mexico and South America), whilst Maximum Cranial and Facial Breadths (XCB and XFB), and Nasio–Occipital Length (NOL) are greater in the younger samples. Focusing on the negative PC2 space, we see three main clusters among the South American, Mexican, and Californian samples. This variation is primarily driven by three measurements on the mid-facial skull. The three individuals from the YP differ from the other two clusters by smaller Bizygomatic Breadths (ZYB), Nasion-Prosthion Heights (NPH) and Nasal Heights (NHL) (Fig 5; S4 Table). We further identify a cluster containing the other two Mexican samples and the one from California; the three samples exhibit much larger ZYB, NPH, and NHL, alongside the South Americans, as compared to the sister Yucatan sample (Fig 5). These differences highlight some of the main differences found between a dolicocephalic skull from Central Mexico and a mesocephalic skull from Yucatan.

4.4. Pathologies

Caries were identified on the first and second molars on the right side of the mandibular ramus (Fig 6E). Also, the interproximal spaces between the molars are affected. The third mandibular molar on the right has been completely resorbed. The third premolar on the right and left sides and the second molars present plaque. The mandibular ramus on the left side presents a heavy abscess and a loss of the third molar (Fig 3I). The abscess goes deep into the bone, which must have caused severe pain. An abscess is seen on the middle and right part of the mandible leading to a loss of all incisors and canines as well as the first premolar (Fig 3J and 3K).

The Chan Hol 3 presents arthritis on the humeral head and some vertebrae are showing signs of eburnation (Fig 6C). Schmorl's nodes are present on two of the vertebral bodies and can be described as vertical disk hernias due to their position on the vertebral bodies.
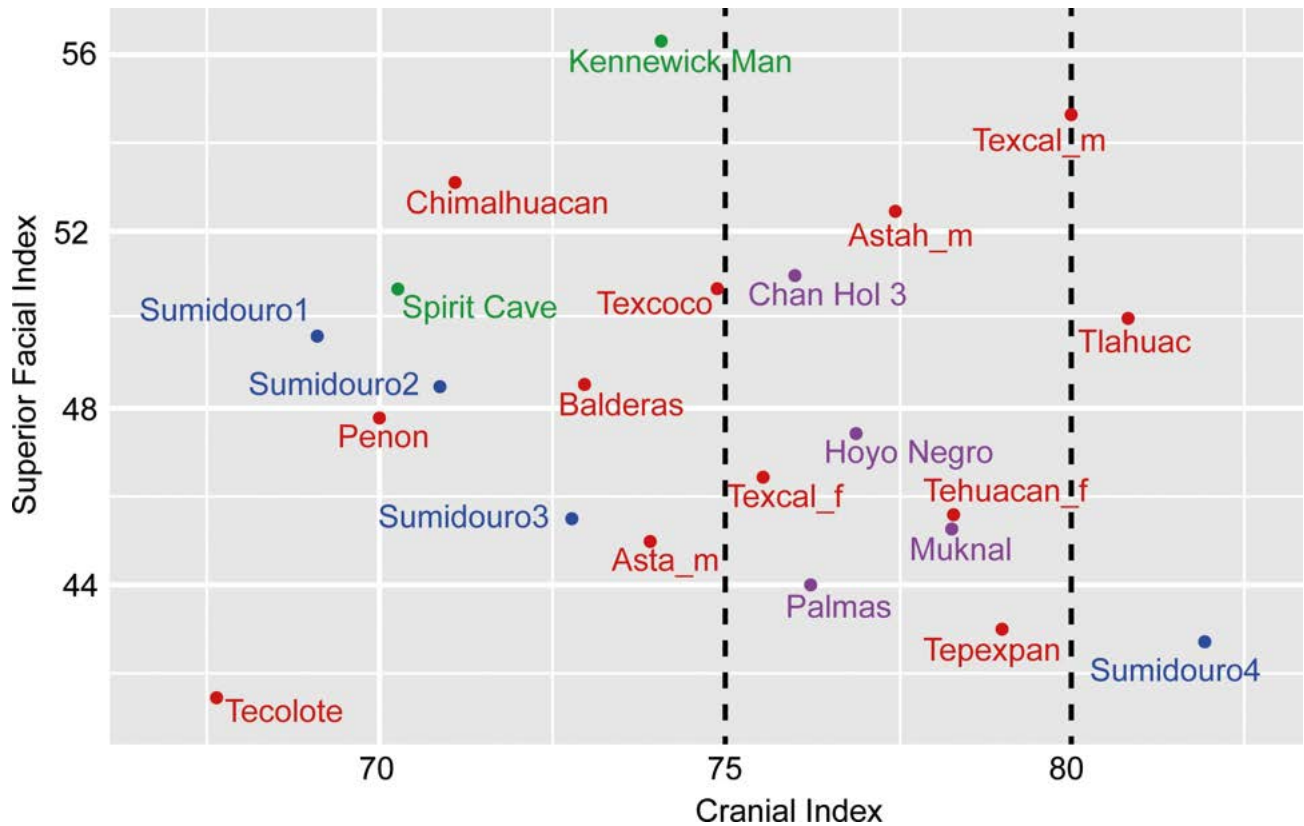
Fig 4. Cranial index of the Chan Hol 3 woman in comparison with other North and South American skeletons ranging in age to >9 ky BP. For numerical values of cranial index and for Superior Facies Index see S5 Table. Purple color: skeletons from the YP. Red color: skeletons from Central Mexico. Green color: skeletons from North America. Blue color: Skeletons from Lagoa Santa (Sumidouro Cave), Brazil. The data indicate that the Paleoindians from the YP are all in the mesocephalic index range (75–80), contrasting with the individuals from Central Mexico and North America with dates older than 9 ky BP which are in general dolicocephalic (68–75). Graph modified from Hernández Flores [43].

https://doi.org/10.1371/journal.pone.0227984.g004

The posterior portion of the cranial vault surface exhibits dents and crater-like deformations. These deformations appear to be pathological in nature, especially surrounding the lambdoidal suture (Fig 3F). The affected bone tissue has signs of a potential infection which may have been caused by the healing trauma to the cranial vault (Fig 3F). The facial skeleton is not affected. Possible differential diagnoses of the pathological lesions would be *Treponema peritonitis* alongside osteitis, or severe periostitis resulting from a trauma to the skull [18, 19, 44]. The lesions observed in Chan Hol 3 show similarities to a pre-Colombian South American male skull exhibiting *Treponema peritonitis* from 1650 y BP [22]. Other treponemal diseases such as Syphilis and Yaws are less likely because they typically manifest in the skeleton differently (facial skeleton not affected etc.) and there is a lack of *caries sicca*.

The Chan Hol 3 individual shows signs of three traumas to the posterior and lateral portion of the skull resulting in bone loss and remodeling. Two traumas are visible on the posterior portion of the right parietal bone along the sagittal and lambdoidal sutures and are caused by a potential sharp object (Figs 3C, 3F, 6A and 6B). The injuries resemble an isolated incisive trepanation which produces a fusiform groove (a.k.a. Indian canoe), which is normally caused by scraping [45]. A differential assessment would be a healed sharp force trauma that has signs of healing, with the perforations and slight irregular borders being caused by post-mortem taphonomic processes. Neither of the possible two sharp force traumas show signs of radiating/concentric fractures at the macro level due to the sharpness of the object hitting the skull and there
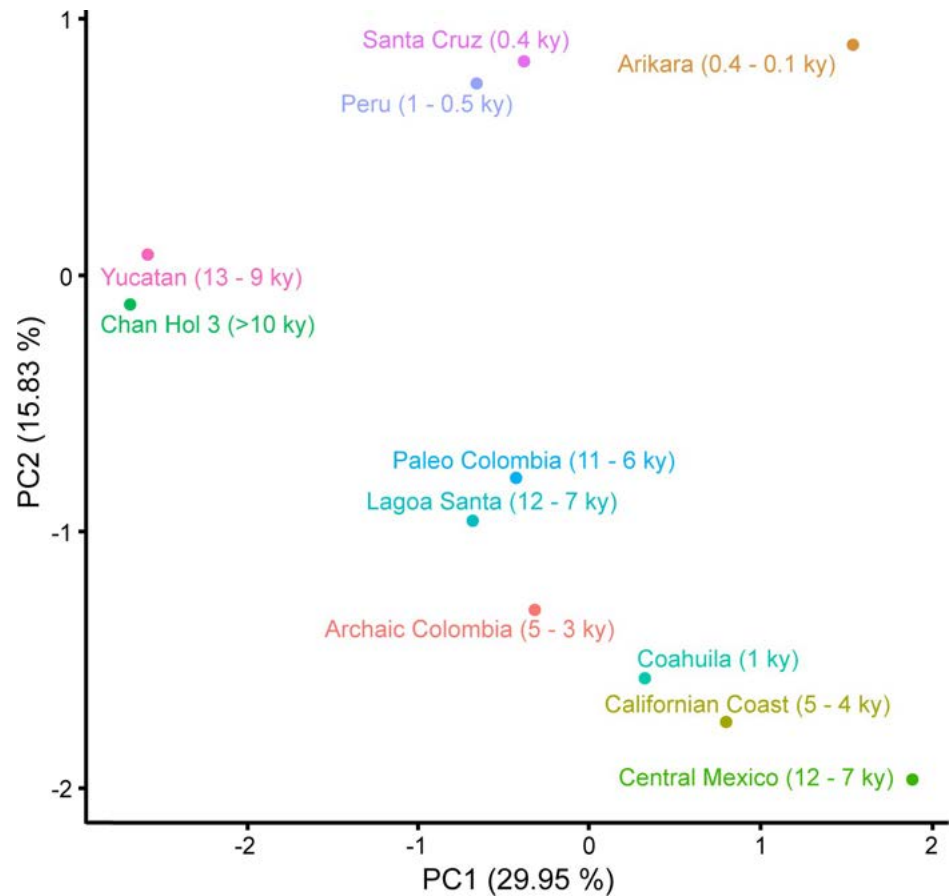
Fig 5. Principal Components Analysis based on crania from the Americas with PC1 explaining 29.95% and PC2 explaining 15.83% of the total variation seen within the samples. See S4 Table for PC1 and PC2 loadings for each variable.

https://doi.org/10.1371/journal.pone.0227984.g005

creating an incised wound. As mentioned before, the slight irregular border/margins could have been caused by healing and post-mortem taphonomic processes. The third potential trauma is identified on the left parietal bone. This shows a circular perforation surrounded by a raised area of new bone which could be signs of healing (Figs 3E and 6A). The cause of this third trauma is unknown due to the new bone formation. Two small cut marks (20 mm) have also been identified on the right caudal side of the temporal lobe (Fig 6D). To help fully understand the pathologies and trauma seen on the cranium further analysis using medical imaging (computerized tomography/CT) would help with the diagnoses of such lesions.

4.5. Dating

The preservation of the Chan Hol 3 bone material is good from the outside, but the internal bone consistency is fragile due to the complete dissolution of collagen. We therefore refrained from the application of ^{14}C age analysis. Rather, we conducted ^{230}Th/U-analysis of a flowstone encrusting and embedding phalangeal bones of the Chan Hol 3 skeleton (Fig 2). In a previous study, open-system behavior of U isotopes has been observed in speleothem calcite within 2 cm distance to the bone material [5]. To avoid similarly affected material, we therefore sampled at sufficient distance of > 2 cm to the bone material (Fig 2). The analysis yielded low U concentrations of 140 to 157 ng/g and low ^{232}Th concentrations of 0.59 to 1.31 ng/g (Table 1).
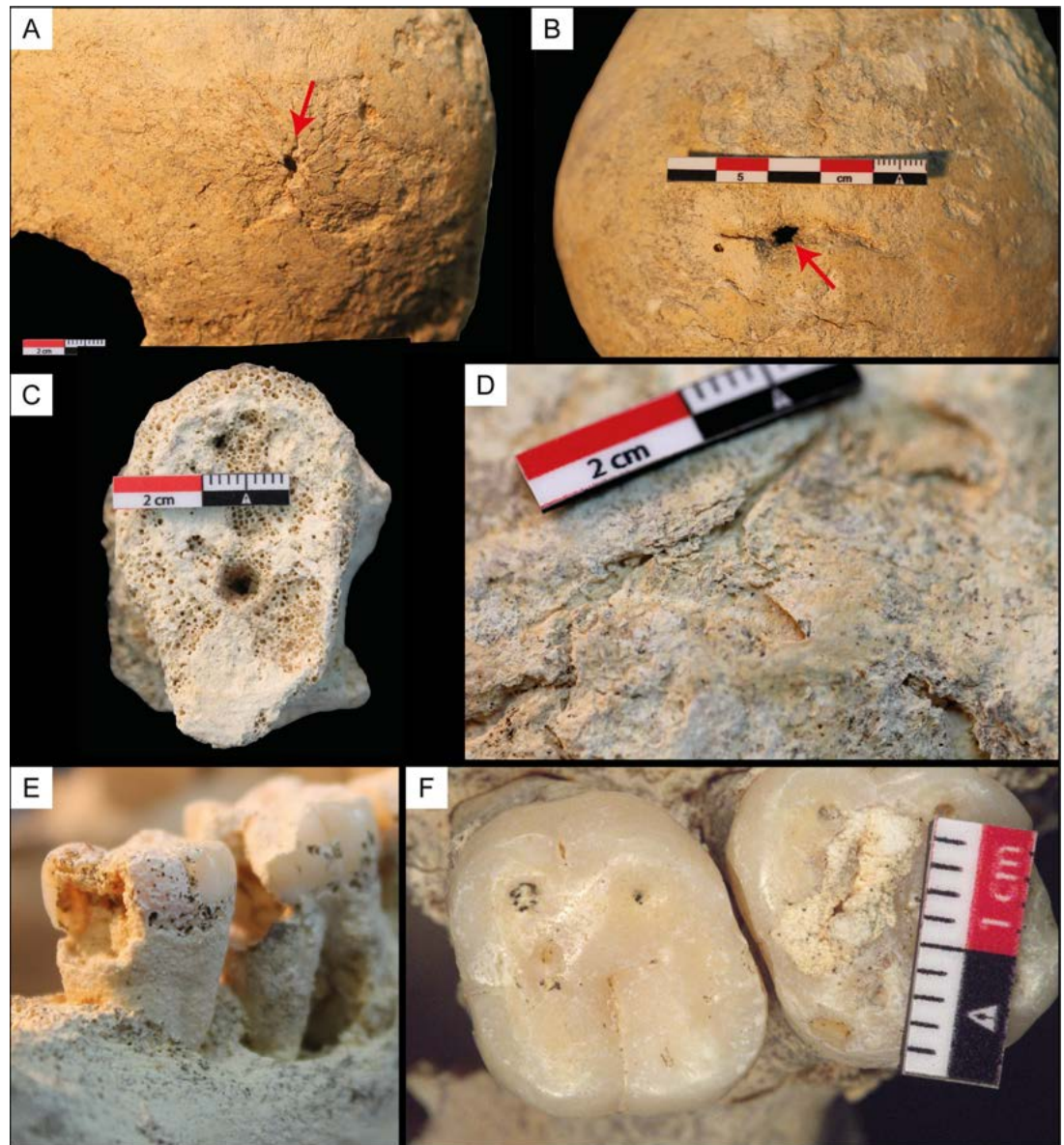
Fig 6. Pathologies detected in the Chan Hol 3 female. (A) The red arrow points to trauma on the left parietal bone. (B) The red arrow points to trauma on the parietal bone in caudal view. (C) Eburnation on the vertebrae. (D) Cut mark on the right temporal bone. (E) Caries in molars 2 and 3 in the right mandible in buccal view. (F) Plaque and caries in molars of the left maxilla in occlusal view.

https://doi.org/10.1371/journal.pone.0227984.g006

Table 1. ^{230}Th/U measurements of the flowstone crust embedding a phalange of the Chan Hol skeleton.

N°	^{238}U (ng/g)	^{232}Th (ng/g)	^{230}Th/^{238}U (Act. rat.)	^{230}Th/^{232}Th (Act. rat.)	δ^{234}U corr. (‰)	Age uncorr. (ky)	Age* corr. (ky)	Age** corr. (ky)	δ^{234}U$_{initial}$ (‰)	Depth [mm]
9770	139.862 ±0.040	0.8527 ±0.0026	0.0969 ±0.0013	49.06±0.68	35.23±2.47	10.66±0.15	10.50±0.17	**9.83±0.16**	36.3±2.5	3.5
9771	157.01±0.11	1.3132 ±0.0043	0.1007 ±0.0016	37.13±0.59	36.77±2.47	11.08±0.18	10.87±0.22	**9.94±0.18**	37.9±2.5	4.5
9769	144.952 ±0.024	0.5874 ±0.0053	0.0952 ±0.0016	72.29±1.41	36.14±2.28	10.45±0.21	10.35±0.20	**9.90±0.19**	37.2±2.3	5.5

https://doi.org/10.1371/journal.pone.0227984.t001

The U-isotopic composition, i.e. the ^{234}U/^{238}U activity ratio (expressed as ‰-deviation from secular radioactive equilibrium δ^{234}U), is moderately positive and identical in all three samples with 37.1±1.1 ‰. To estimate the influence of initial ^{230}Th on the ^{230}Th/U age, e.g. by detrital contamination, our first order model is based on the conventionally used bulk Earth (^{230}Th/^{232}Th) activity ratio of 0.76±0.2, which further assumes radioactive equilibrium within the U-series decay chain. Using this assumption, calculated ages range from 10.35±0.2 ky BP to 10.87±0.22 ky BP, with uncertainties quoted as 2σ uncertainty of the mean (Table 1). The reference year for all ages given in the study is 1950 AD.

Given the minor traces of ^{232}Th (< 1.3 ng), the conventional detrital corrections are small (< 200 years) and lie within the uncertainty of the uncorrected ages. Ages are identical within 2σ uncertainty, except for the central sample which shows a moderate age inversion of 360 to 520 years outside the 2σ uncertainty of individual ages of 220 years. For stratigraphic reasons, we tested the assumption that this age inversion is related to an elevated ^{230}Th/^{232}Th activity ratio of the contaminating non-carbonate material, or an additional source of seepage water-derived ^{230}Th. For this purpose, we presumed the three samples as coeval within an uncertainty of ±200 years; this assumption is based on the short period of carbonate growth (~520 years) and allows us to test the detrital ^{230}Th model using an Osmond isochron [46]. From the Osmond isochron (S1 Fig) a contaminating ^{230}Th/^{232}Th activity ratio of 3.96±0.2 can be estimated leading to significant age corrections of up to -1100 years for the central-most contaminated carbonate. Assuming such a high ^{230}Th contribution from cave seepage water or non-carbonate contamination leads to an average age of the three samples of 9.9±0.1 ky BP with no remaining age inversion, thus representing a minimum age of the carbonate. Given the small number of analyses, it remains difficult to privilege one over the other correction models. Consequently, we suggest that the layered carbonate embedding of the already present skeletal remains formed between 9.9±0.1 and 10.57±0.11 ky BP, reflecting the weighted mean age of both ^{232}Th-correction models.

See Fig 2 for the position of samples. Errors are 2σ analytical errors. Corrected ^{230}Th ages assume (1) an initial (^{230}Th/^{232}Th) activity ratio of 0.76 ± 0.2 (*); and (2) 3.96 ± 0.2 (**) derived from the Osmond isochrones approach assuming the three sub-samples as coeval.

4.6. Strontium Isotope analysis

The normalized ^{87}Sr/^{86}Sr ratio for the third right molar of Chan Hol 3 is 0.708878±0.000042 (2σ) and is given together with the SRM-987 standard values in S6 Table. Previous studies have mapped the Sr-isotopic composition of modern local fauna samples (e.g. mice, deer, peccary, rock, water, soils) and show increasing ^{87}Sr/^{86}Sr ratios from 0.704–0.706 in the southern part, to higher ratios of 0.707–0.709 in the northern part of the YP (e.g. [47–49]). The highest ratios (0.711–0.712) in Mesoamerica are associated with old plutonic and metamorphic rocks in the Maya Mountains of Belize [49]. Hodell et al. [49] grouped the strontium baseline values in five clusters that broadly match major geologic provinces (S2 Fig). Our measurement is well in the range of values expected for the northern YP and corresponds to cluster 1 defined by Hodell et al. [49] (S2 Fig).

5. Discussion

5.1. The Chan Hol 3 site

The Chan Hol 3 human skeletal remains were spread around a limestone slab, which nevertheless was not covered by bones, neither were bones detected by us below this rock (Fig 1C). The limestone is inclined by about 15˚ from the horizontal as it is positioned on top of a horizontally lying stalagmite (Fig 1E). We tentatively suggest that the flat limestone was intentionally

placed by humans, perhaps serving as a "head rest" for the Chan Hol 3 individual. This interpretation is based on the following pieces of circumstantial evidence: the rock shelf is lithologically identical to other limestone slabs that cover the cave floor forming an *in situ* broken layer, but it partially overlies smaller fragments of this rock as well a broken stalagmite which also appears to be out of place. Transport of the heavy limestone slab and its elevated position above the cave floor are difficult to explain by water transport, nor does the slab correspond to limestone from the ceiling that would have fallen to the ground, there knocking down the stalagmite below the slab. As no human bones were detected below the limestone shelf, the skeleton must be younger than the placement of the slab.

Some bones were water-transported from their original position. While the mandible and long bones only moved down gravitationally and were slightly moved by the water, the round and air-filled skull was water-transported and rolled for about half a meter, where it rotated upside down (Fig 1E). The original position of the skeleton is therefore difficult to determine, but we tentatively suggest that it was preserved in a dorsal position.

At the time of decay and skeletonization, the cave was still dry and the Chan Hol 3 individual completely exposed on the cave floor. Water dripping from the cave ceiling resulted in the deposition of flowstone encrusting some of the bones, e.g. a solid calcite crust of up to 10 mm thickness covered the phalanges and fragmentary distal forearm epiphyses (Fig 2). From the shape of this flowstone it appears that the cave floor was sloping, so that the bones caused the water to be dammed. The flow around the bones caused those to be encrusted and resulted in a nearly laminar layered crust. Below these bones, a porous tufa-like flowstone is present.

Millimeter-thin crusts of calcite crystals covered several other bones, e.g. metacarpals, ulna, radius, maxillae. These crusts on the upward-directed surfaces of the long bones are caused by humidity and vapor within a dry cave. The lower cave floor-directed portion of these bones lack the crusts. Desiccation cracks on the cave floor further suggest a dry cave environment alternating with episodes of precipitation.

5.2. Skeleton age assessment

Based on the ^{230}Th/U analyses of the layered flowstone crust overlying the phalangeal bones (Figs 2 and 7) the minimum *terminus ante quem* of the Chan Hol 3 skeleton is 9.9±0.1 ky BP.

Tufa-like flowstone immediately underlying the bone was not dated due to its porous texture and due to the potential effects of open-system behavior by U diffusion (e.g. [5]). In consequence, no data are available to define the amount of time that elapsed between the death of the individual and initial growth of the overlying carbonate, nor the time lapse needed for maceration and decay of this individual. Consequently, the precise age of the Chan Hol 3 skeleton within the Pleistocene-Holocene transition remains uncertain.

Clearly, flooding of the Chan Hol 3 site was significantly later, during the final middle Holocene rise of sea-level. This interpretation is supported by numerous charcoal concentrations of cultural origin located at various sites of the Chan Hol cave system in depth levels equivalent to those of the Chan Hol 3 site. These charcoal hearths ^{14}C-dated to between 8,110 ±28 [14]C y BP (9,122–8,999 cal y BP) and 7,177±27 [14]C y BP (8,027–7,951 cal y BP) are therefore younger than both the Chan Hol 2 and 3 individuals [3, 6]. The Chan Hol 1 skeleton has been dated to 9,589±49 [14]C y BP (11,073–10,817 cal y BP) [3, 6].

5.3. Assignation of the Chan Hol 3 individual

We originally expected that the skeleton documented here as Chan Hol 3 would have constituted the Chan Hol 2 skeleton, discovered in 2012 at only 140 m distance north of the one described here but stolen by unknown cave divers a few weeks after discovery [5]. However,

after a closer inspection and comparison of the present osteological material from the Chan Hol 3 locality with photos taken prior to the looting of the Chan Hol 2 site, we are now positive that the two must represent different individuals. This interpretation results from the fact that several bones present in the material documented from Chan Hol 2 by Stinnesbeck et al. [5], are also present at Chan Hol 3. Among this replicated material is a complete mandible at Chan Hol 3, but fragmentary mandible at Chan Hol 2, upper lateral incisors, and complete right and left femora in both skeletons. In addition, two perforations are clearly seen in the right parietal of the Chan Hol 3 cranium, which are absent in the one documented for Chan Hol 2. Even though the prominent chin of the Chan Hol 3 mandible is usually considered to be a male feature, the femur size along with the gracile skull indicates a female individual, whereas Chan Hol 2 has been interpreted as a male [5].

5.4. Pathologies

Chan Hol 3 represents the fourth early female skeleton from the submerged caves of Tulum, together with the Naharon, Las Palmas and Hoyo Negro individuals. The right and left femora show strong anterior convexity (Fig 3L and 3M) which suggests high mobility, a feature often seen in hunter-gatherer populations [50]. Arthritis has been documented in the Chan Hol 3 skeleton, as in those from Hoyo Negro, Naharon, Muknal, Las Palmas and El Templo [1, 3, 6].

5.4.1. Traumas.   The Chan Hol 3 female survived three potential cranial traumas. The one identified on the left parietal bone was caused by a potential blunt impact, leading to a rounded opening of 2 mm diameter (Figs 3E and 6A). The cracks spread out in a circular manner around the impact and are due to a strong swelling. The second and third trauma on the parietal and occipital were caused by a hit, or heavy blow, on the back of the head with a sharp object (Figs 3C, 3E, 3F, 6A and 6B). The turning angle of 15˚ indicates a lateral impact. However, these traumas show signs of healing, suggesting that the Chan Hol 3 female survived all three.

5.4.2. Potential treponemal bacterial disease.   In addition to traumas, the skull of the Chan Hol 3 female exhibits irregular dents and crater-like deformations on the posterior parietal and occipital bones of the cranium. These are here interpreted as evidence for an infection (Fig 3F). The argument for infection is based on the interaction of these deformations with the lambdoidal suture. A taphonomical issue of bone preservation can be excluded, as neither the facial area of the skull, the mandible, nor postcranial elements, are affected by this form of bone alteration. Furthermore, the osteological remains of Chan Hol 1 and 2 from the same cave system, as also all other human and megafauna [51] remains from nearby caves in the area, are extremely well preserved and their bone surfaces are smooth. They allow for a reliable comparison of bone preservation levels based on the different find localities and from both fresh- and salt-water (e.g. Chan Hol 1 to 3 skeletons were contained in fresh-water, most other sites are salt-water). This excludes disintegration of bones by chemical reaction, producing holes, as seen for example on the dorsal surface of the cranium of the ground sloth *Xibalbaonyx* from the El Zapote cenote [51]. However, even at El Zapote where bones are extremely fragile due to heavy dissolution, the bone texture and surface are not deformed. Different to these bones collected from salt-water, the cortex of the Chan Hol 3 cranium is thick, especially the occipital area, indicating the absence of chemical dissolution. The morphological deformation on the skull in the Chan Hol 3 skeleton is more than likely to be a pathological pattern and not a preservation issue.

Pathological skull deformation as seen in the Chan Hol 3 female has not been documented for other early skeletons in the area and we here propose that it is possibly related to a treponemal bacterial disease (*Treponema peritonitis)* with subsequent osteitis/periostitis. The

evolutionary history of treponemal diseases includes the origin of syphilis and is therefore the subject of on-going debate. As this would be the first evidence for *Treponema peritonitis* in an early Holocene skeleton in the New World, the Chan Hol 3 skeleton may potentially help to settle the debate. Today, the only other cases of these lesions in pre-Columbian skeletons are associated with the Atacameña culture of Chile, Argentina and southern Bolivia, from a specimen dating to 1650 BP [44], and a second dating to 2160 BP [52]. At this current stage, it is impossible to say which came first, the trauma to the skull or the bacterial infection. However, it makes more sense to say that the bacterial infection is a result of the trauma seen on the skull.

5.4.3. Dental diseases. All pre-Mayan skeletons discovered to date in caves of the Tulum area present extraordinary light dental attrition for a hunter and gatherer society, but extremely high percentages of caries, aggressive periodontal diseases and dental abscesses (e.g. 53% of teeth affected in the 16–18 years old Naia female [53], but also see [3, 4, 54]. This pathological pattern is also evident in the Chan Hol 3 female that lost most of her teeth during life, and the remaining few show occlusal caries extending into the pulp cavity. Dental caries is an oral infectious bacterial disease, causing demineralization of the enamel and underlying dentine [55]. The disease is multifactorial, but usually related to buccal microflora, enamel composition, dental surface irregularities and fluorine contents of the ground water [56–58], as well as diet (e.g. carbon hydrate and sugar consumption) and body immunological responses [56–58]. Dental caries and abscess prevalence in the Yucatan skeletons are thus significantly higher than observed among other hunter-gatherers, except for a series of early Holocene skeletal remains from Lagoa Santa, Brazil [59]. The unexpected record of poor oral health, especially among females in this tropical South American locality, was attributed to a diet based on a highly cariogenic combination of wild tubers and fruits [59]. Elsewhere, caries is rare in coeval Paleoamerican skeletons of hunter-gatherer societies. In these latter individuals, e.g. from the Basin of Mexico, strong crown attrition is attributed to the consumption of hard fibrous foods ([2]; OTHERS), as is also interpreted for coeval groups from Europe [60]. Attrition is surprisingly light in the Chan Hol 3 female, but also in all other pre-Mayan skeletons known to date from the Tulum area, including Naia [53].

We therefore hypothesize that the paleodiet of the Tulum pre-Mayan humans must have differed significantly from that of other late Paleolithic hunter-gatherer societies, e.g. from Europe and the Basin of Mexico. We agree with the interpretation of Cucina et al. [53] that the Yucatan group depended on a nonabrasive diet that was at least seasonally rich in carbohydrates. As there is no evidence for early Holocene cultivation of plants on the YP, the unusually high amount of caries observed in the Tulum skeletons suggests a high consumption of tubercles and sweet (maltodextrine and sugar-rich) fruits, sweet cactus fruits, or honey from native stingless bees (*Meliposa* sp.) as part of the daily diet.

5.5. Provenance of early Yucatan settlers

The isotopic composition of tooth enamel is based on food and liquids consumed during infancy and does not change chemically during the life of the individual, and rather little during death. Therefore, the tooth enamel composition measured here should provide a fingerprint on the provenance (place of birth/youth) of the individual [48, 61, 62]. The value of $^{87}Sr/^{86}Sr$ of 0.708878 is close to the ones previously determined for areas located within 40 km distance to Tulum (0.7087 to 0.7091) [49, 63] and is also close to the one of modern seawater. Nevertheless, this value also fits to localities in the Northwestern part of the peninsula where identical values of 0.7089 to 0.7087 have repeatedly been observed [47, 49]. Consequently, we cannot say whether the female studied here continuously lived in the Tulum area, or whether she spent part of her life (esp. during adolescence) in the northwestern part of the peninsula.

5.6. Usage of the Chan Hol cave

Interpretation of the Chan Hol 3 site as a burial, as previously documented for Las Palmas, Muknal and Naharon skeletons [3, 4, 6], is inconclusive, even though the head and torso of the female individual may have been intentionally placed on a limestone slab moved from its original position. As in the Chan Hol 1 and 2 individuals, the legs of the Chan Hol 3 skeleton were outstretched, suggesting that the individual was lying on its back. However, the anatomical position is difficult to assess, since the female torso was disintegrated.

The *terminus ante quem* age of 9.9±0.1 ky of the Chan Hol 3 skeleton provides new supporting evidence for an early human use of the caves in the Tulum area. Human visits to caves in the area, including Chan Hol Cave, started during the Late Pleistocene, as is indicated by ^{14}C ages of bones and by ^{230}Th/U dating of limestone crusts and stalagmites encrusting bones (e.g. Hoyo Negro, Naharon, Chan Hol 2) [1, 3, 5, 6]. Although the early human settlers may have used the cave system as a burial ground or cult place [3, 4, 6], there is no positive evidence yet to support this scenario for the three human skeletons discovered at Chan Hol Cave. Rather, the death of the Chan Hol 1 to 3 individuals may have been accidental (e.g. treatment of the infection by trepanning) [3, 5]. Alternatively, the traumas discovered on the skull of the Chan Hol 3 female indicate potential personal violence. This interpretation is supported by the sharp incised (healing) wounds, rather than crushing or blunt force trauma which would have been caused by more rugged and larger objects (e.g. falling debris). In any case, it appears unlikely that visits to the Tulum cave system were routine procedures that were executed frequently.

5.7. Cranial morphology studies and the settlement of the Americas

The Chan Hol 3 woman has a mesocranial morphology (Fig 4; S5 Table), characterized by a flat forehead with wide cheekbones. These morphological traits have been detected in all pre-Mayan skeletons discovered in the Tulum cave system [1, 3–6] (Fig 1A). Their cranial morphology thus differs significantly from that of coeval Paleoindian skeletons from Central Mexico, e.g. Peñon III Woman, Tlapacoya Man, Metro Man, Chimalhuacan Man [3], which have been dated to between 12 to 7 ky BP (S1 Table) and all present dolicocephalic morphologies [3] (Figs 4 and 5; S5 Table). Based on these important morphometric differences among the skulls from Central Mexico and Tulum we suggest that at least two morphologically different Paleoindian human groups inhabited Mexico during the late Pleistocene-Early Holocene.

There are two potential hypotheses to explain the origin of these two different human groups: (1) They are derived from human populations from different geographical points of origin, or (2) They are the result of local micro-evolutionary processes such as genetic isolation, habitat preference, survival strategies, or even diet, that may have resulted in an *in situ* differentiation of the mesocranial morphologies identified in the skeletons of the Tulum area. They may thus have been a substantial factor in the evolutionary development of the subsequent Mayan populations from Mesoamerica. Clearly, however, the two scenarios are exclusively based on the morphometric aspects of these two populations and does not refer to their phylogenetic relationships, or genetic data. Full genome data from these populations is required to decide which hypothesis is correct because there are currently no data available.

6. Conclusions

The pre-Mayan skeleton here described from the Chan Hol cave near Tulum, Mexico, belongs to a woman of about 30 years with three severe cranial traumas, in addition to evidence for a possible treponemal bacterial disease. As seen in two other skeletons previously found in the same cave system, the new Chan Hol 3 woman decayed *in situ* at times when these shallow

parts of the cave were still dry. After skeletonization, some of the bones were cemented to the cave floor by flowstone precipitated from calcite-saturated water (e.g. phalanges), while others were water-transported and dispersed over a small area of three square meters, either during heavy precipitation events or during the middle Holocene flooding of the cave. ^{230}Th/U dating of the calcite crusts overlying a phalange indicate a minimum age of the skeleton of 9.9±0.1 ky BP.

The ten ate Pleistocene-Early Holocene individuals discovered and described so far in the submerged caves of Tulum, Yucatán, indicate a mobile group, eating sugary foods as indicated by the ubiquitous presence of caries. Their mesocranial skull morphologies are different to the dolicocephalic morphologies found in equivalent Paleoindian age human populations from Central Mexico that had strong teeth attrition indicating the consumption of hard foods. Our data thus support the presence of two morphologically different human groups with different subsistence strategies in Mexico during the Pleistocene-Holocene boundary transition.

Supporting information

S1 Fig. Osmond Isochron, assuming the three samples as coeval. This allows to test the detrital ^{230}Th model [46]. The slope of the regression line yields a (^{230}Th/^{232}Th) activity ratio of the contaminating non-carbonate material of 3.96 ±0.2.
(TIF)

S2 Fig. Simplified geologic map of the Maya region showing the age of exposed bedrock and results of cluster analysis based on ^{87}Sr/^{86}Sr measurements of water, bedrock, soils and plant [49]. Yellow star shows position of the Chan Hol cave and skeleton. Slightly modified figure taken from Hodell et al. [49].
(TIF)

S1 Table. Radiometric dating of human bones, speleothem and charcoal associated with early skeletons from submerged caves in the Tulum area and from other North- and South America sites.
(PDF)

S2 Table. Osteometric measurements taken according to Buikstra and Ubelaker [17] and Howells [16]. Abbreviations are explained there.
(PDF)

S3 Table. Breakdown of osteometric variables and cranial samples used for the PCA. Summary of Chronologies and Location of each Sample used for the PCA.
(PDF)

S4 Table. The PC loadings for the first two Principal Components extracted from the PCA. For definition of the cranial variables see S3 Table.
(PDF)

S5 Table. Cranial index and Superior Facial Index of skeletons from Mexico, North and South America presented in Fig 4.
(PDF)

S6 Table. Results of ^{87}Sr/^{86}Sr analyses of tooth enamel of the third left mandibular molar of the Chan Hol 3 skeleton found in the submerged Chan Hol cave at Tulum, Quintana Roo, Mexico. The data are normalized to standard SRM987.
(PDF)

Acknowledgments

Author Contributions

Conceptualization: Sarah R. Stinnesbeck, Nils Schorndorf, Arturo González González.

Data curation: Jerónimo Avilés Olguín, Norbert Frank, Sophie Warken, Thomas Krengel, Adriana Velázquez Morlet.

Formal analysis: Samuel R. Rennie, Sarah R. Stinnesbeck, Silvia Gonzalez, Norbert Frank, Sophie Warken, Nils Schorndorf, Thomas Krengel.

Funding acquisition: Wolfgang Stinnesbeck, Arturo González González.

Investigation: Wolfgang Stinnesbeck, Samuel R. Rennie, Jerónimo Avilés Olguín, Sarah R. Stinnesbeck, Silvia Gonzalez, Norbert Frank, Sophie Warken, Nils Schorndorf, Thomas Krengel, Arturo González González.

Methodology: Samuel R. Rennie, Jerónimo Avilés Olguín, Sarah R. Stinnesbeck, Silvia Gonzalez, Norbert Frank, Sophie Warken, Nils Schorndorf, Thomas Krengel.

Project administration: Wolfgang Stinnesbeck, Adriana Velázquez Morlet.

Supervision: Wolfgang Stinnesbeck, Jerónimo Avilés Olguín, Silvia Gonzalez, Norbert Frank, Adriana Velázquez Morlet, Arturo González González.

Validation: Wolfgang Stinnesbeck, Jerónimo Avilés Olguín, Adriana Velázquez Morlet, Arturo González González.

Visualization: Sarah R. Stinnesbeck, Norbert Frank, Nils Schorndorf, Thomas Krengel.

Writing – original draft: Wolfgang Stinnesbeck, Samuel R. Rennie, Sarah R. Stinnesbeck, Silvia Gonzalez, Norbert Frank, Sophie Warken, Nils Schorndorf, Thomas Krengel.

Writing – review & editing: Wolfgang Stinnesbeck, Samuel R. Rennie, Silvia Gonzalez, Norbert Frank, Sophie Warken, Nils Schorndorf.

References

1. Chatters JC, Kennett DJ, Asmerom Y, Kemp BM, Polyak V, Blank AN, et al. Late Pleistocene human skeleton and mtDNA link Paleoamericans and modern Native Americans. Science. 2014; 344 (6185):750–4. Epub 2014/05/17. https://doi.org/10.1126/science.1252619 PMID: 24833392.

2. González S, Jimenez-López JC, Hedges R, Huddart D, Ohman JC, Turner A, et al. Earliest humans in the Americas: new evidence from México. J Hum Evol. 2003; 44(3):379–87. Epub 2003/04/04. https://doi.org/10.1016/s0047-2484(03)00004-6 PMID: 12674097.

3. González González A, Terrazas A, Stinnesbeck W, Benavente ME, Avilés J, Rojas C, et al. The First Human Settlers on the Yucatán Peninsula: Evidence from Drowned Caves in the State of Quintana Roo (South Mexico). In: Graf K, Ketron C, Waters M, editors. Paleomarican Odyssey. Texas A&M University: Center for the Study of the First Americans; 2013. p. 323–38.

4. Stinnesbeck SR, Stinnesbeck W, Terrazas Mata A, Avilés Olguín J, Benavente Sanvicente M, Zell P, et al. The Muknal cave near Tulum, Mexico: An early-Holocene funeral site on the Yucatán peninsula. Holocene. 2018; 28(12):1992–2005. https://doi.org/10.1177/0959683618798124

5. Stinnesbeck W, Becker J, Hering F, Frey E, Gonzalez AG, Fohlmeister J, et al. The earliest settlers of Mesoamerica date back to the late Pleistocene. PLoS One. 2017; 12:16–8. Epub 2017/08/31. https://doi.org/10.1371/journal.pone.0183345 PMID: 28854194; PubMed Central PMCID: PMC5576649.

6. González González AH, Sandoval CR, Mata AT, Sanvicente MB, Stinnesbeck W, Aviles O, et al. The arrival of humans on the Yucatan Peninsula: Evidence from submerged caves in the state of Quintana Roo, Mexico. Curr Res Pleistocene. 2008; 25:1–24.

7. Collins SV, Reinhardt EG, Rissolo D, Chatters JC, Nava Blank A, Luna Erreguerena P. Reconstructing water level in Hoyo Negro, Quintana Roo, Mexico, implications for early Paleoamerican and faunal access. Quat Sci Rev. 2015; 124:68–83. https://doi.org/10.1016/j.quascirev.2015.06.024 WOS:000361258000004.

8. Khan NS, Ashe E, Horton BP, Dutton A, Kopp RE, Brocard G, et al. Drivers of Holocene sea-level change in the Caribbean. Quat Sci Rev. 2017; 155:13–36. https://doi.org/10.1016/j.quascirev.2016.08.032 WOS:000390626700002.

9. Hering F, Stinnesbeck W, Folmeister J, Frey E, Stinnesbeck S, Avilés J, et al. The Chan Hol cave near Tulum (Quintana Roo, Mexico): evidence for long-lasting human presence during the early to middle Holocene. J Quaternary Sci. 2018; 33(4):444–54. https://doi.org/10.1002/jqs.3025 WOS:000431658900007.

10. QRSS. [QRSS], Quintana Roo Speleological Society. 2018. Survey and cartography of the underwater caves of Quintana Roo Mexico. 2018 [cited 2019 Apr 08]. Available from: http://caves.org/project/qrss/qrss.htm.

11. Blanchon P, Shaw J. Reef drowning during the last deglaciation: evidence for catastrophic sea-level rise and ice-sheet collapse. Geology. 1995; 23(1):4–8.

12. Moseley GE, Richards DA, Smart PL, Standish CD, Hoffmann DL, ten Hove H, et al. Early–middle Holocene relative sea-level oscillation events recorded in a submerged speleothem from the Yucatán Peninsula, Mexico. Holocene. 2015; 25(9):1511–21. https://doi.org/10.1177/0959683615585832

13. Blanchon P, Eisenhauer A, Fietzke J, Liebetrau V. Rapid sea-level rise and reef back-stepping at the close of the last interglacial highstand. Nature. 2009; 458(7240):881–4. Epub 2009/04/17. https://doi.org/10.1038/nature07933 PMID: 19370032.

14. Beddows PA. Groundwater hydrology of a coastal conduit carbonate aquifer: Caribbean coast of the Yucatán Peninsula [thesis]: University of Bristol, UK; 2004.

15. Ritter SM, Isenbeck-Schroter M, Scholz C, Keppler F, Gescher J, Klose L, et al. Subaqueous speleothems (Hells Bells) formed by the interplay of pelagic redoxcline biogeochemistry and specific hydraulic conditions in the El Zapote sinkhole, Yucatan Peninsula, Mexico. Biogeosciences. 2019; 16 (11):2285–305. https://doi.org/10.5194/bg-16-2285-2019 WOS:000470702100003.

16. Howells WW. Cranial variation in man: A Study by Multivariate Analysis of Patterns of Difference Among Recent Human Populations: Harvard University Press; 1973.

17. Buikstra J, Ubelaker D. Standards for data collection from human skeletal remains: proceedings of a seminar at the field museum of natural history. Documentation of sex differences and age changes in adults. Ark Archeol. 1994;44.

18. Ortner D, Putschar W. Identification of Pathological Conditions in Human Skeletal Remains: Smithsonian Contributions to Anthropology; 1981. 1–488 p.

19. Aufderheide AC, Rodríguez-Martín C, Langsjoen O. The Cambridge encyclopedia of human paleopathology: Cambridge University Press, US; 1998.

20. Genovés S. Proportionality of the long bones and their relation to stature among Mesoamericans. Am J Phys Anthropol. 1967; 26(1):67–77. https://doi.org/10.1002/ajpa.1330260109 PMID: 5633729

21. Howells WW. Skull shapes and the map: craniometric analyses in the dispersion of modern Homo. Papers of the Peabody Museum of Archaeology and Ethnology. 1989; 79.

22. Howells WW. Who's who in skulls: ethnic identification of crania from measurements. Papers of the Peabody Museum of Archaeology and Ethnology. 1995; 82.

23. Howells WW. Howells' craniometric data on the internet. Am J Phys Anthropol. 1996; 101(3):441–2. Epub 1996/11/01. https://doi.org/10.1002/ajpa.1331010302 PMID: 8922187.

24. Gonzalez-Jose R, Neves W, Lahr MM, Gonzalez S, Pucciarelli H, Hernandez Martinez M, et al. Late Pleistocene/Holocene craniofacial morphology in Mesoamerican Paleoindians: implications for the peopling of the New World. Am J Phys Anthropol. 2005; 128(4):772–80. Epub 2005/07/20. https://doi.org/10.1002/ajpa.20165 PMID: 16028226.

25. Hubbe M, Strauss A, Hubbe A, Neves WA. Early South Americans cranial morphological variation and the origin of American biological diversity. PLoS One. 2015; 10(10):e0138090. Epub 2015/10/16. https://doi.org/10.1371/journal.pone.0138090 PMID: 26465141; PubMed Central PMCID: PMC4605489.

26. Neves WA, Hubbe M. Cranial morphology of early Americans from Lagoa Santa, Brazil: implications for the settlement of the New World. Proc Natl Acad Sci U S A. 2005; 102(51):18309–14. Epub 2005/12/14. https://doi.org/10.1073/pnas.0507185102 PMID: 16344464; PubMed Central PMCID: PMC1317934.

27. Pacheco AR. Los restos óseos humanos de la Cueva de La Candelaria, Coahuila: craneología: Instituto Nacional de Antropología e Historia; 2005.

28. Terrazas Mata A, Benavente Sanvicente M. Estudio preliminar de tres cráneos tempranos. procedentes de cuevas sumergidas de la costa este de Quintana Roo. In: López JCJ, editor. 2° Simposio Internacional el Hombre Temprano en América: Instituto Nacional de Antropologia e Historia, México; 2006. p. 198 pp.

29. Kenyhercz MW, Passalacqua NV. Chapter 9—Missing Data Imputation Methods and Their Performance With Biodistance Analyses. In: Pilloud MA, Hefner JT, editors. Biological Distance Analysis. San Diego: Academic Press; 2016. p. 181–94.

30. Wefing AM, Arps J, Blaser P, Wienberg C, Hebbeln D, Frank N. High precision U-series dating of scleractinian cold-water corals using an automated chromatographic U and Th extraction. Chem Geol. 2017; 475:140–8. https://doi.org/10.1016/j.chemgeo.2017.10.036 WOS:000415947400012.

31. Arps J. Towards ε-Precision of U-series Age Determinations of Secondary Carbonates [thesis]: University of Heidelberg; 2017.

32. Cheng H, Edwards RL, Hoff J, Gallup CD, Richards DA, Asmerom Y. The half-lives of uranium-234 and thorium-230. Chem Geol. 2000; 169(1–2):17–33. https://doi.org/10.1016/s0009-2541(99)00157-6 WOS:000088941300003.

33. Cheng H, Lawrence Edwards R, Shen C-C, Polyak VJ, Asmerom Y, Woodhead J, et al. Improvements in ^{230}Th dating, ^{230}Th and ^{234}U half-life values, and U–Th isotopic measurements by multi-collector inductively coupled plasma mass spectrometry. Earth Planet Sci Lett. 2013; 371:82–91. https://doi.org/10.1016/j.epsl.2013.04.006

34. Nelson SJ. Wheeler's Dental Anatomy, Physiology and Occlusion-E-Book: Elsevier Health Sciences; 2014.

35. Kohn MJ, Schoeninger MJ, Barker WW. Altered states: effects of diagenesis on fossil tooth chemistry. Geochim Cosmochim Acta. 1999; 63(18):2737–47. https://doi.org/10.1016/S0016-7037(99)00208-2. WOS:000083013500004.

36. Horwitz EP, Chiarizia R, Dietz ML. A Novel Strontium-Selective Extraction Chromatographic Resin. Solvent Extr Ion Exc. 1992; 10(2):313–36. https://doi.org/10.1080/07366299208918107 WOS: A1992HJ66300008.

37. Kober B, Schwalb A, Schettler G, Wessels M. Constraints on paleowater dissolved loads and on catchment weathering over the past 16 ka from ^{87}Sr/^{86}Sr ratios and Ca/Mg/Sr chemistry of freshwater ostracode tests in sediments of Lake Constance, Central Europe. Chem Geol. 2007; 240(3):361–76. https://doi.org/10.1016/j.chemgeo.2007.03.005.

38. Walker PL. Sexing skulls using discriminant function analysis of visually assessed traits. Am J Phys Anthropol. 2008; 136(1):39–50. Epub 2008/03/08. https://doi.org/10.1002/ajpa.20776 WOS:000255067500005. PMID: 18324631

39. Walker PL. Greater sciatic notch morphology: sex, age, and population differences. Am J Phys Anthropol. 2005; 127(4):385–91. Epub 2005/02/05. https://doi.org/10.1002/ajpa.10422 PMID: 15693026.

40. Iscan MY, Steyn M. The human skeleton in forensic medicine: Charles C Thomas Publisher; 2013.

41. Meindl RS, Lovejoy CO. Ectocranial suture closure: a revised method for the determination of skeletal age at death based on the lateral-anterior sutures. Am J Phys Anthropol. 1985; 68(1):57–66. https://doi.org/10.1002/ajpa.1330680106 PMID: 4061602

42. Brothwell DR, Brothwell DR. Digging up bones: the excavation, treatment, and study of human skeletal remains: Cornell University Press; 1981.

43. Hernández Flores R. Analisis de la variación craneofacial en los primeros pobladores de México y su implicación en el poblamiento de América [thesis]: Universidad Nacional Autónoma de México; 2018.

44. Gerszten PC, Gerszten E, Allison MJ. Diseases of the skull in pre-Columbian South American mummies. Neurosurgery. 1998; 42(5):1145–51. Epub 1998/05/20. https://doi.org/10.1097/00006123-199805000-00114 PMID: 9588561.

45. Kaufman MH, Whitaker D, McTavish J. Differential Diagnosis of Holes in the Calvarium: Application of Modern Clinical Data to Palaeopathology. J Archaeol Sci. 1997; 24(3):193–218. https://doi.org/10.1006/jasc.1995.0104. WOS:A1997WP41200001.

46. Ludwig KR, Titterington DM. Calculation of ^{230}Th/U isochrons, ages, and errors. Geochim Cosmochim Acta. 1994; 58(22):5031–42. https://doi.org/10.1016/0016-7037(94)90229-1.

47. Price TD, Burton JH, Fullagar PD, Wright LE, Buikstra JE, Tiesler V. Strontium Isotopes and the Study of Human Mobility in Ancient Mesoamerica. Latin American Antiquity. 2008; 19(2):167–80. https://doi.org/10.2307/25478222

48. Price TD, Burton JH, Sharer RJ, Buikstra JE, Wright LE, Traxler LP, et al. Kings and commoners at Copan: Isotopic evidence for origins and movement in the Classic Maya period. J Anthropol Archaeol. 2010; 29(1):15–32. https://doi.org/10.1016/j.jaa.2009.10.001.

49. Hodell DA, Quinn RL, Brenner M, Kamenov G. Spatial variation of strontium isotopes (87Sr/86Sr) in the Maya region: a tool for tracking ancient human migration. J Archaeol Sci. 2004; 31(5):585–601. https://doi.org/10.1016/j.jas.2003.10.009.

50. De Groote I. Femoral curvature in Neanderthals and modern humans: A 3D geometric morphometric analysis. J Hum Evol. 2011; 60(5):540–8. Epub 2011/03/18. https://doi.org/10.1016/j.jhevol.2010.09.009 PMID: 21411122.

51. Stinnesbeck SR, Frey E, Olguín JA, Stinnesbeck W, Zell P, Mallison H, et al. Xibalbaonyx oviceps, a new megalonychid ground sloth (Folivora, Xenarthra) from the Late Pleistocene of the Yucatán Peninsula, Mexico, and its paleobiogeographic significance. Palaontol Z. 2017; 91(2):245–71. https://doi.org/10.1007/s12542-017-0349-5 WOS:000404260000009.

52. Castro MM, Benavente MA, Ortega J, Acuña R, Montero C, Thomas C, et al. Thoracic aortic aneurysm in a pre-Columbian (210 BC) inhabitant of Northern Chile: Implications for the origins of syphilis. Int J Paleopathol. 2016; 13:20–6. Epub 2016/06/01. https://doi.org/10.1016/j.ijpp.2016.01.002 PMID: 29539505.

53. Cucina A, Herrera Atoche R, Chatters JC. Oral health and diet of a young Late Pleistocene woman from Quintana Roo, Mexico. Am J Phys Anthropol. 2019;0(0). Epub 2019/06/22. https://doi.org/10.1002/ajpa.23884 PMID: 31222724.

54. González González AH, Sandoval CR, Núñez EA, Olguín JA, Ramírez SA, Del Río Lara O, et al. Evidence of early inhabitants in submerged caves in Yucatan, Mexico. In: Leshikar-Denton ME, Luna Erreguerena P, editors. Underwater and maritime archaeology in Latin America and the Caribbean. Walnut Creek, CA: Left Coast Press; 2008. p. 127–42.

55. Larsen CS. The agricultural revolution as environmental catastrophe: Implications for health and lifestyle in the Holocene. Quat Int. 2006; 150(1):12–20. https://doi.org/10.1016/j.quaint.2006.01.004. WOS:000238405700003.

56. Sheiham A. Dental Caries in Underdeveloped Countries. In: Guggenheim B, editor. Cariology Today. Basel: Karger; 1984. p. 33–9.

57. Cohen MN, Armelagos GJ. Paleopathology at the origins of agriculture: Editors summation. In: Cohen MN, Armelagos GJ, editors. Paleopathology at the Origins of Agriculture. Orlando, FL: Academic Press; 1984. p. 585–601.

58. Larsen T. Occurrence of doxycycline resistant bacteria in the oral cavity after local administration of doxycycline in patients with periodontal disease. Scand J Infect Dis. 1991; 23(1):89–95. Epub 1991/01/01. https://doi.org/10.3109/00365549109023379 PMID: 2028232.

59. Da-Gloria P, Larsen CS. Oral health of the Paleoamericans of Lagoa Santa, central Brazil. Am J Phys Anthropol. 2014; 154(1):11–26. https://doi.org/10.1002/ajpa.22467 PMID: 24449259

60. Tillier A-M, Arensburg B, Rak Y, Vandermeersch B. Middle Palaeolithic dental caries: new evidence from Kebara (Mount Carmel, Israel). J Hum Evol. 1995; 2(29):189–92.

61. Price TD, Nakamura S, Suzuki S, Burton JH, Tiesler V. New isotope data on Maya mobility and enclaves at Classic Copan, Honduras. J Anthropol Archaeol. 2014; 36:32–47. https://doi.org/10.1016/j.jaa.2014.02.003. WOS:000346460000004.

62. Freiwald C. Maya migration networks: Reconstructing population movement in the Belize River valley during the Late and Terminal Classic [thesis]: University of Wisconsin-Madison; 2011.

63. Ortega-Muñoz A, Price TD, Burton JH, Cucina A. Population movements and identity in Postclassic Yucatan. Bioarchaeological analysis of human remains from the East Coast of the Yucatan peninsula. J Archaeol Sci Rep. 2019; 23:490–500. https://doi.org/10.1016/j.jasrep.2018.11.013.